frontiers | Research Topics

Immunovirology in aquatic animals

Edited by
Elena Chaves-Pozo, Carolina Johnstone,
Iddya Karunasagar and Indrani Karunasagar

Published in
Frontiers in Immunology
Frontiers in Aquaculture

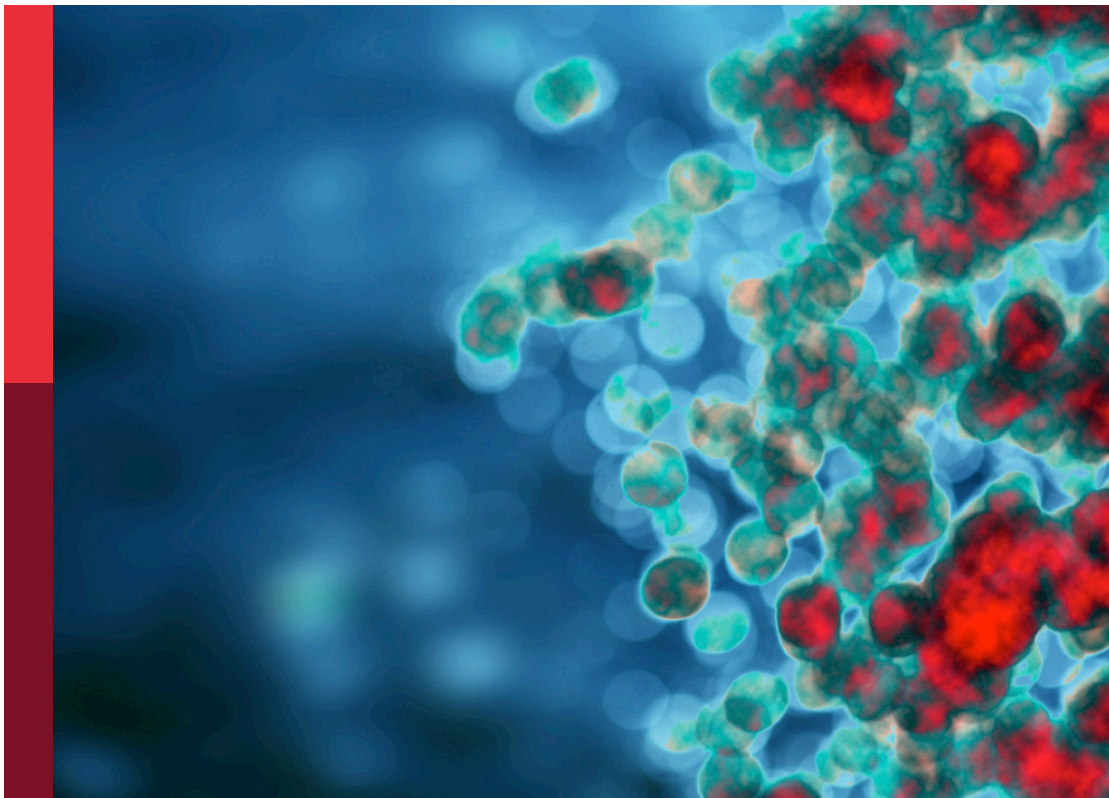

ISSN 1664-8714
ISBN 978-2-8325-6821-7
DOI 10.3389/978-2-8325-6821-7

Generative AI statement
Any alternative text (Alt text) provided alongside figures in the articles in this ebook has been generated by Frontiers with the support of artificial intelligence and reasonable efforts have been made to ensure accuracy, including review by the authors wherever possible. If you identify any issues, please contact us.

About Frontiers

Frontiers is more than just an open access publisher of scholarly articles: it is a pioneering approach to the world of academia, radically improving the way scholarly research is managed. The grand vision of Frontiers is a world where all people have an equal opportunity to seek, share and generate knowledge. Frontiers provides immediate and permanent online open access to all its publications, but this alone is not enough to realize our grand goals.

Frontiers journal series

The Frontiers journal series is a multi-tier and interdisciplinary set of open-access, online journals, promising a paradigm shift from the current review, selection and dissemination processes in academic publishing. All Frontiers journals are driven by researchers for researchers; therefore, they constitute a service to the scholarly community. At the same time, the *Frontiers journal series* operates on a revolutionary invention, the tiered publishing system, initially addressing specific communities of scholars, and gradually climbing up to broader public understanding, thus serving the interests of the lay society, too.

Dedication to quality

Each Frontiers article is a landmark of the highest quality, thanks to genuinely collaborative interactions between authors and review editors, who include some of the world's best academicians. Research must be certified by peers before entering a stream of knowledge that may eventually reach the public - and shape society; therefore, Frontiers only applies the most rigorous and unbiased reviews. Frontiers revolutionizes research publishing by freely delivering the most outstanding research, evaluated with no bias from both the academic and social point of view. By applying the most advanced information technologies, Frontiers is catapulting scholarly publishing into a new generation.

What are Frontiers Research Topics?

Frontiers Research Topics are very popular trademarks of the *Frontiers journals series*: they are collections of at least ten articles, all centered on a particular subject. With their unique mix of varied contributions from Original Research to Review Articles, Frontiers Research Topics unify the most influential researchers, the latest key findings and historical advances in a hot research area.

Find out more on how to host your own Frontiers Research Topic or contribute to one as an author by contacting the Frontiers editorial office: frontiersin.org/about/contact

Immunovirology in aquatic animals

Topic editors

Elena Chaves-Pozo — Oceanographic Center of Murcia, Spanish Institute of Oceanography, Spain

Carolina Johnstone — Centro Oceanográfico de Málaga, IEO-CSIC, Spain

Iddya Karunasagar — Nitte University, India

Indrani Karunasagar — Nitte University, India

Citation

Chaves-Pozo, E., Johnstone, C., Karunasagar, I., Karunasagar, I., eds. (2025). *Immunovirology in aquatic animals*. Lausanne: Frontiers Media SA.

doi: 10.3389/978-2-8325-6821-7

Table of contents

frontiers | Frontiers in Immunology

TYPE Editorial
PUBLISHED 26 August 2025
DOI 10.3389/fimmu.2025.1655117

OPEN ACCESS

EDITED AND REVIEWED BY
Li-Shang Dai,
Wenzhou Medical University, China

*CORRESPONDENCE
Elena Chaves-Pozo
elena.chaves@ieo.csic.es
Carolina Johnstone
carolina.johnstone@ieo.csic.es

RECEIVED 27 June 2025
ACCEPTED 14 July 2025
PUBLISHED 26 August 2025

CITATION
Johnstone C and Chaves-Pozo E (2025) Editorial: Immunovirology in aquatic animals. *Front. Immunol.* 16:1655117. doi: 10.3389/fimmu.2025.1655117

Editorial: Immunovirology in aquatic animals

Carolina Johnstone[1]* and Elena Chaves-Pozo[2]*

[1]Physiology and Welfare of Marine Species Group (PHYSIS), Centro Oceanográfico de Málaga, Instituto Español de Oceanografía (COMA-IEO), Consejo Superior de Investigaciones Científicas (CSIC), Málaga, Spain, [2]Physiology and Welfare of Marine Species Group (PHYSIS), Centro Oceanográfico de Murcia, Instituto Español de Oceanografía (COMU-IEO), Consejo Superior de Investigaciones Científicas (CSIC), Murcia, Spain

KEYWORDS

viral infectious disease, marine virus, viral zoonosis, antiviral, aquaculture, viral immunity

Editorial on the Research Topic
Immunovirology in aquatic animals

Aquatic ecosystems are home to invertebrate and vertebrate animal species and they provide important natural resources, including food. Protein-rich aquatic animal foods contribute to global food security and nutrition. Over the last decades the production of fish food through aquaculture has surpassed that of fisheries (1). One of the challenges currently faced by aquaculture is viral infectious diseases, which can affect product quality and cause harvest losses. This Research Topic collects in its first volume part of the current knowledge on viral immunology in freshwater and marine fish species, from high commercial value species to species of interest for aquaculture diversification.

Global warming in aquatic ecosystems alters the distribution of species contributing to the spread and emergence of new viruses. The stress response triggered in all living specimens by environmental changes, including pollution, pushes viral emergence to its peak. In this sense, mitigation tools will be needed in the near future and are worth investigating as in the case of iron nanoparticles, which have been found to modulate gene expression in fish (Kumar et al.). In addition, a soluble recombinant glycoprotein nanoparticle of IHNV was constructed and proved to be stable and immunogenic *in vitro* (Ahmadivand et al.), opening the possibility of using self-assembling ferritin nanocages as vaccine platforms for fish viral antigens. This volume also presents foundational research on viral diseases that affect global salmonid aquaculture. Extensive cell surface modulation in infectious salmon anemia virus (ISAV)-infected erythrocytes of Atlantic salmon was found to be directly linked to the viral surface glycoprotein hemagglutinin esterase, which binds to sialic acid, acting as a viral receptor-destroying enzyme (Fosse et al.). Infectious hematopoietic necrosis virus (IHNV) is another lethal viral pathogen that affects the global trout and salmon aquaculture industry, for which no commercial vaccine is available. A transcriptomic approach in salmonid red blood cells was performed to assess differentially expressed genes that may affect the viral propagation during the early phases of infection with piscine orthoreovirus 1 (PRV-1), which causes heart and skeletal muscle inflammation (HSMI) (Tsoulia et al.). Transcriptomics were also employed to assess the physiological status of a species of interest for Mediterranean aquaculture diversification: the Shi drum. This study established that high culture densities

could hinder the control of nervous necrosis virus (NNV) outbreaks (Garcia-Beltran et al.). Since having an overview of the immune response is interesting for compiling knowledge on specific fish viral pathogens, this volume also presents a review of the recent advances in the immune response to Tilapia lake virus (TiLV) (Kembou-Ringert et al.), a novel lethal RNA virus that represents a threat to tilapia aquaculture, one of the top ten products of fisheries and aquaculture (1). Also, viral infectious diseases can affect global aquaculture production when they compromise meat quality or cause secondary infections. This is the case of the self-limiting chronic Lymphocystis disease, which is characterized by the growth of papilloma-like nodules on the skin and fins of infected fish. The differentially expressed genes in the infected skin nodules associated with the lymphocystis disease virus (LCDV) were investigated through transcriptomics in flounder (*Paralichthys olivaceus*), a species of economic importance in Asian countries (Zhang et al.). In gilthead seabream (*Sparus aurata*), a species of economic importance for Mediterranean aquaculture, the immune genes involved in the protection induced by a DNA vaccine based on the major capsid protein of an LCDV were investigated through an array platform (Leiva-Rebollo et al.). Acipenserid herpesvirus 2 (AciHV-2), another DNA virus, causes a fatal disease in juvenile white sturgeons (*Acipenser transmontanus*) and was found to affect the outcome of secondary bacterial infections (Quijano Cardé et al.). Finally, poly(I:C) (polyriboinosinic polyribocytidylic acid), an analogue of double stranded viral RNA that is used as an adjuvant and is known to induce viral immune responses in fish, was employed to assess the antiviral response in species such as lumpfish, a species that is important for the control of sea lice in salmon aquaculture, or the gadiform species *Lota lota*, whose population is decreasing.

The prevention and treatment of aquatic animal viral diseases requires basic research in comparative immunology to understand the host response in fish, a group of animals with evolutionary diversification. Our knowledge of viral immunology is essential for developing treatments and vaccines against infectious viral diseases in fish, which cause high mortality rates and significant economic losses for aquaculture producers. This first volume provides a foundation of knowledge on the cellular and molecular mechanisms underlying fish innate and adaptive immunity to different infectious viral diseases and explores novel treatments.

Author contributions

CJ: Writing – review & editing, Writing – original draft. EC-P: Writing – review & editing.

Conflict of interest

The authors declare that the research was conducted in the absence of any commercial or financial relationships that could be construed as a potential conflict of interest.

The author(s) declared that they were an editorial board member of Frontiers, at the time of submission. This had no impact on the peer review process and the final decision.

Generative AI statement

The author(s) declare that no Generative AI was used in the creation of this manuscript.

Any alternative text (alt text) provided alongside figures in this article has been generated by Frontiers with the support of artificial intelligence and reasonable efforts have been made to ensure accuracy, including review by the authors wherever possible. If you identify any issues, please contact us.

Publisher's note

Reference

1. FAO. *The State of World Fisheries and Aquaculture 2024 – Blue Transformation in action*. Rome: FAO. (2024). Available online at: https://doi.org/10.4060/cd0683en (Accessed August 25, 2025).

frontiers | Frontiers in Immunology

TYPE Original Research
PUBLISHED 25 April 2023
DOI 10.3389/fimmu.2023.1158077

OPEN ACCESS

EDITED BY
Elena Chaves-Pozo,
Spanish Institute of Oceanography, Spain

REVIEWED BY
Ivan Nombela,
Charité University Medicine Berlin, Germany
Delia Vanessa Lopez-Guerrero,
Autonomous University of the State of Morelos, Mexico

*CORRESPONDENCE
Johanna Hol Fosse
johanna.hol.fosse@vetinst.no

SPECIALTY SECTION
This article was submitted to Viral Immunology, a section of the journal Frontiers in Immunology

RECEIVED 03 February 2023
ACCEPTED 03 April 2023
PUBLISHED 25 April 2023

CITATION
Fosse JH, Andresen AMS, Ploss FB, Weli SC, Heffernan IA, Sapkota S, Lundgård K, Kuiper RV, Solhaug A and Falk K (2023) The infectious salmon anemia virus esterase prunes erythrocyte surfaces in infected Atlantic salmon and exposes terminal sialic acids to lectin recognition. *Front. Immunol.* 14:1158077. doi: 10.3389/fimmu.2023.1158077

The infectious salmon anemia virus esterase prunes erythrocyte surfaces in infected Atlantic salmon and exposes terminal sialic acids to lectin recognition

Johanna Hol Fosse*, Adriana Magalhaes Santos Andresen, Frieda Betty Ploss, Simon Chioma Weli, Inger Austrheim Heffernan, Subash Sapkota, Krister Lundgård, Raoul Valentin Kuiper, Anita Solhaug and Knut Falk

Norwegian Veterinary Institute, Ås, Norway

Many sialic acid-binding viruses express a receptor-destroying enzyme (RDE) that removes the virus-targeted receptor and limits viral interactions with the host cell surface. Despite a growing appreciation of how the viral RDE promotes viral fitness, little is known about its direct effects on the host. Infectious salmon anemia virus (ISAV) attaches to 4-*O*-acetylated sialic acids on Atlantic salmon epithelial, endothelial, and red blood cell surfaces. ISAV receptor binding and destruction are effectuated by the same molecule, the haemagglutinin esterase (HE). We recently discovered a global loss of vascular 4-*O*-acetylated sialic acids in ISAV-infected fish. The loss correlated with the expression of viral proteins, giving rise to the hypothesis that it was mediated by the HE. Here, we report that the ISAV receptor is also progressively lost from circulating erythrocytes in infected fish. Furthermore, salmon erythrocytes exposed to ISAV *ex vivo* lost their capacity to bind new ISAV particles. The loss of ISAV binding was not associated with receptor saturation. Moreover, upon loss of the ISAV receptor, erythrocyte surfaces became more available to the lectin wheat germ agglutinin, suggesting a potential to alter interactions with endogenous lectins of similar specificity. The pruning of erythrocyte surfaces was inhibited by an antibody that prevented ISAV attachment. Furthermore, recombinant HE, but not an esterase-silenced mutant, was sufficient to induce the observed surface modulation. This links the ISAV-induced erythrocyte modulation to the hydrolytic activity of the HE and shows that the observed effects are not mediated by endogenous esterases. Our findings are the first to directly link a viral RDE to extensive cell surface modulation in infected individuals. This raises the questions of whether other sialic acid-binding viruses that express RDEs affect host cells to a similar extent, and if such RDE-mediated cell surface modulation influences host biological functions with relevance to viral disease.

KEYWORDS

receptor destroying enzyme (RDE), *Orthomyxoviridae*, infectious salmon anemia (ISA) virus, red blood cells (erythrocytes), sialic acid, *Salmo salar* (L.)

Introduction

Sialic acids are highly diverse (>80 derivatives known to date) and typically present on the outermost ends of glycans attached to plasma membrane-anchored proteins or lipids (1). Many sialic acid-binding viruses express a receptor-destroying enzyme (RDE) that removes the virus-targeted receptor and limits viral host cell attachment (2). An appropriate balance between viral receptor-binding and receptor-destroying activities promotes viral fitness. The RDE supports both early and late steps in the infectious cycle: First, RDE activity destroys decoy receptors in mucus and reduces the cell surface density of virus-targeted sialic acids; this appears to help virus particles reach sites on the plasma membrane that favor viral entry (3–6). Second, when new virus particles bud from the plasma membrane, RDE activity is required to prevent aggregation of viral particles and allow their release (7). The importance of viral receptor destruction can be exemplified by the strong reduction of influenza virus replication by compounds that inhibit its RDE, the neuraminidase (6). In addition, viral receptor destruction mediates attachment interference that limits host cell superinfection (8–11).

Despite the growing appreciation of the role of the viral RDE in the infectious cycle, little is known about its direct effects on the host. First, how extensive is the RDE-mediated modulation of target cell surfaces in an infected individual? Second, considering that cell surface sialic acids modulate a range of cellular functions, including the activation of immune responses (12–14), could the loss of sialic acid viral receptors influence host biological functions with relevance to viral disease?

Infectious salmon anemia virus (*Isavirus salaris*, ISAV) is an enveloped, segmented, single-stranded, negative sense RNA virus of the *Orthomyxoviridae* family. ISAV contains eight genomic segments that encode at least 10 proteins (15–17). Amongst these is the dual-function surface glycoprotein haemagglutinin esterase (HE) that is responsible for both binding to and hydrolysis of 4-*O*-acetylated sialic acids, identified as the ISAV receptor (18, 19). Infection with pathogenic ISAV variants causes disease (infectious salmon anemia, ISA) in farmed Atlantic salmon (*Salmo salar* L.) (20), and has led to vast economic losses in all major salmon-producing countries.

Vascular endothelial cells are the main target cells of pathogenic ISAV and support the generation of new virus particles that are released into the blood stream (21, 22). Moreover, clinical signs of ISA are compatible with a viral sepsis-like breakdown of central vascular functions, including petechial bleeds, vascular leakage, and focal necrosis (20). We recently revealed a global loss of vascular 4-*O*-acetylated sialic acids in ISAV-infected fish that correlated with the expression of viral proteins (23). While this suggested that the esterase activity of the HE could be involved in the host cell surface modulation, we could not exclude the involvement of endogenous host esterases.

Several lines of reasoning made us curious if erythrocyte surfaces in infected fish were modulated in a similar manner: First, nucleated fish erythrocytes are targeted by ISAV, but show limited, if any, permissiveness to infection (24). Consequently, any surface modulation would be independent of the cellular expression of viral proteins. Second, prior to the onset of sepsis-like clinical signs and mortality, ISAV-infected fish typically develop anemia (24, 25). In general, sialic acids and their 9-*O*-acetylation are involved in regulating the circulating half-life of erythroid-lineage cells in other species (26–29); hence, a modulation of erythrocyte sialic acids could potentially contribute to the pathogenesis of ISA. Finally, erythrocytes are accessible to sampling and *ex vivo* manipulation, facilitating exploration of underlying mechanisms.

We found that erythrocytes in infected fish, similar to endothelial cells, progressively lost the ability to bind new ISAV particles. By exposing erythrocytes from non-infected fish to ISAV and recombinant proteins *ex vivo*, we further revealed that the loss of ISAV binding was not due to saturation of the receptor, but associated with pruning of surface sialic acids by the ISAV esterase. These findings expand on our recent observation of loss of vascular 4-*O*-acetylated sialic acids in infected fish, as we provide direct mechanistic evidence that the surface modulation is caused by ISAV esterase activity, rather than endogenous host esterases. Moreover, we demonstrate that cells can be extensively modulated by RDE activity despite not permitting viral replication. Our observations raise the questions of whether RDEs of other sialic acid-binding viruses modulate target cell populations to the same extent, and if such surface modulations influence biological processes in infected hosts.

Results

Disease and viraemia in experimentally infected fish

Atlantic salmon (n = 47, median body weight 115 g) were challenged by immersion for two hours with ISAV (Glesvaer/2/90, $10^{3.75}$ $TCID_{50}$/mL) and subsequently maintained in a fresh water flow-through system at 12°C for the duration of the trial (Figure 1A). The first mortality in the infected fish group occurred 15 days post infection (dpi), with mortality rapidly increasing over the next days (Figure 1B). The trial was terminated 18 dpi, upon reaching its pre-determined end point of 40% cumulative mortality. No fish in the non-infected group (n = 26) died during the trial. Infected fish developed anemia 12 dpi (Figure 1C), prior to other clinical signs. Histological examination of hematoxylin & eosin-stained sections of formalin-fixed paraffin-embedded tissues revealed increased erythrophagocytosis in head kidney and spleen of infected fish that coincided with the onset of anemia (Figures S1A–C), suggesting that erythrocytes were removed from the circulation at an increased rate. Viraemia, measured by ISAV segment 8 RNA and infective particles in the blood, was detected in 3 out of 4 fish at the earliest sampling point (4 dpi) and all infected fish at subsequent samplings. Blood viral loads peaked and plateaued 14 dpi (Figure 1D), with no significant decline within the trial period (Table S1). Levels of viral RNA in the head kidney peaked and plateaued earlier, 10 dpi (Figure S1D), in line with the assumption that circulating ISAV particles originate from extensive replication in vascular endothelial cells (21, 22).

Erythrocyte-associated ISAV was first evaluated by manual counting of immunostained blood smears, detecting ISAV-positive erythrocytes in 2 out of 4 fish 6 dpi and all fish at subsequent samplings (Figures 1E, F, black dots). Blood smears obtained at 16 and 18 dpi were not of sufficient technical quality for analysis. Flow cytometry provided a more objective method for

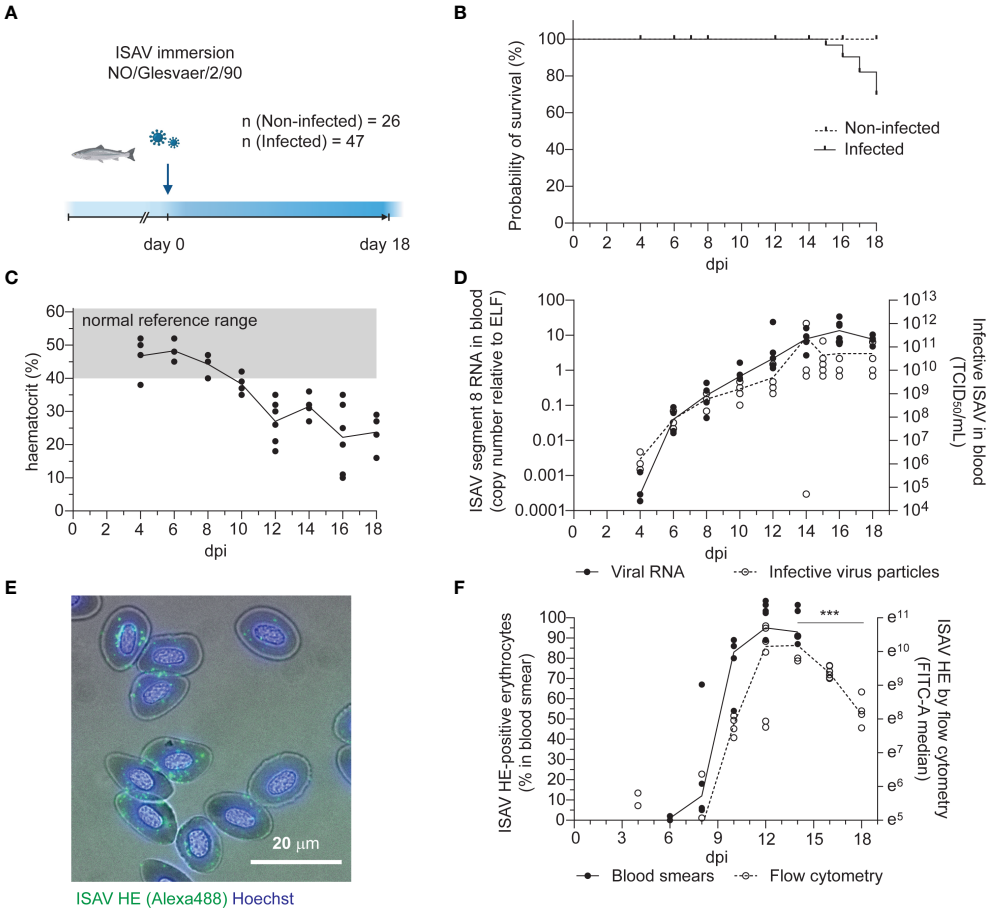

FIGURE 1
Disease and viraemia in experimentally infected fish. **(A)** Outline of the infection trial. Atlantic salmon were challenged with ISAV (NO/Glesvaer/2/90, 2 hours immersion) and followed for 18 days. The illustration was created in BioRender.com. **(B)** Cumulative mortality in the infected fish group. No deaths occurred in the non-infected group. **(C)** Hematocrits (HCT) of infected fish. Data points represent individual fish, and the line connects median values. The reference range (grey shading) is based on blood samples from 25 non-infected fish (mean +/- 2 standard deviation). **(D)** Viral RNA and infective particles in blood were measured by qPCR targeting ISAV segment 8 (left y-axis, black dots and line) and titration on ASK cells (right y-axis, open circles, stippled line). Data points represent individual fish, lines connect median values. **(E)** Representative micrograph of an acetone-fixed blood smear from an infected fish (12 dpi) immunostained for HE (clone 3H6F8, green/Alexa488). Nuclei are counterstained with Hoechst 33342 (blue), and bright field contrast shows the outline of the cells. The scale bar measures 20 µm. **(F)** The percentage of HE-positive cells in acetone-fixed blood smears were counted manually (black dots and line). PFA-fixed blood cells from infected fish were immunostained for HE, and the signal was measured by flow cytometry (open circles, stippled line). Data points represent individual fish. Lines connects median values. ***p<0.001: flow cytometry data from 14, 16, and 18 dpi were compared by Kruskall-Wallis test and Dunn's multiple comparison (Table S1).

quantifying the erythrocyte-associated ISAV, and was performed at day 4, 8, 10, 12, 14, 16, and 18 dpi (Figure 1F, open circles, stippled line, Figure S1E). A decline in ISAV-positive cells was detected from 14 to 18 dpi (Figure 1F and Table S1). Both the percentage of ISAV-positive cells assessed by immunostaining of blood smears (Spearman r = 0.8302, p < 0.001, Table S1) and the flow cytometry-measured ISAV HE signal (Spearman r = 0.6774, p < 0.0001, Table S1) correlated with infective titers.

The ISAV receptor is lost from circulating erythrocytes in infected fish

Next, we assessed the distribution of the ISAV receptor in tissue sections and membrane-enriched fractions of erythrocytes from infected fish. We performed a virus binding assay where ISAV antigen produced in infected cells was used as the primary probe (21) (Figure 2A). Consistent with our recent observations (23), heart vascular endothelial cells lost their capacity to bind new ISAV particles 10 dpi and did not recover (Figures 2B, C). Despite ISAV remaining attached to circulating erythrocytes throughout the course of infection (Figure 1F), a similar loss of the capacity to bind new ISAV particles was observed 10 dpi onwards (Figures 2D–F). New ISAV binding to heart sections and erythrocyte membranes correlated in individual fish (Spearman's correlation coefficient = 0.7494, p < 0.0001, Table S1). These findings reveal that erythrocytes in ISAV-infected fish lose the ability to bind new ISAV particles as the infection progresses in a similar manner to vascular endothelial cells (23), suggesting loss of the host cell surface receptor.

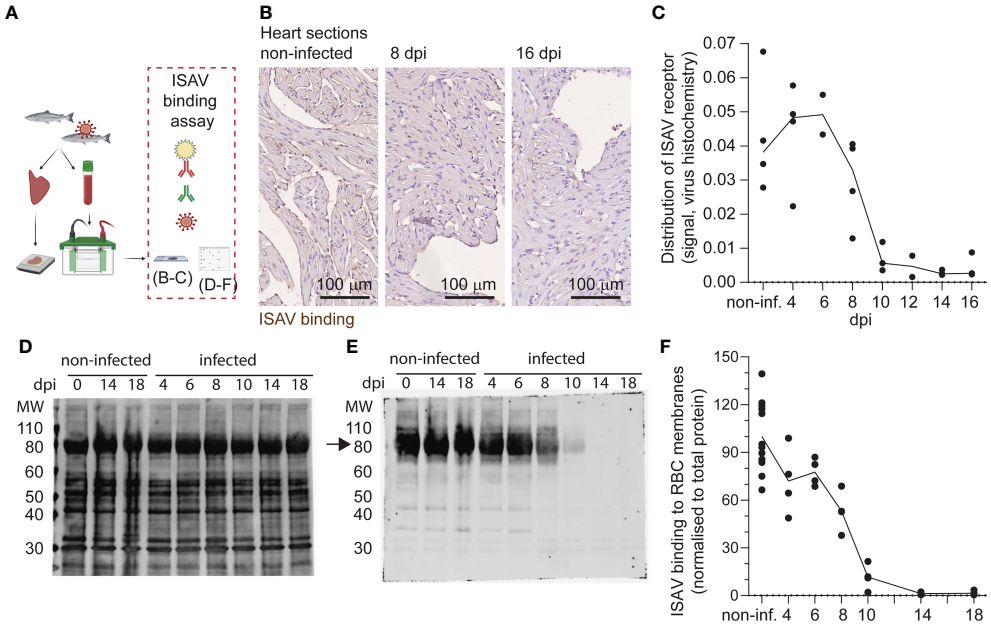

FIGURE 2
Like vascular endothelium, circulating erythrocytes in infected fish lose the ability to bind new ISAV. **(A)** The distribution of the ISAV receptor in heart tissues and membrane-enriched erythrocyte fractions was evaluated by serial incubation with ISAV antigen, mouse IgG_1 targeting HE (clone 3H6F8), fluorescence- or HRP-conjugated secondary antibodies, and substrate if relevant. The illustration was created in Biorender.com. **(B)** Representative micrographs showing the ISAV receptor (brown) in hearts of non-infected and infected fish (8 and 16 dpi). Sections are counterstained with hematoxylin. Scale bars measure 100 µm. **(C)** Quantification of ISAV receptor signal in scanned heart sections. **(D, E)** Membrane-enriched erythrocyte lysates were separated by SDS-PAGE and blotted to nitrocellulose membranes, before evaluation of ISAV binding as described above. Representative blots show **(D)** total protein and **(E)** ISAV binding (arrow) to samples from non-infected fish harvested 0, 14, and 18 dpi and infected fish harvested 4, 6, 8, 10, 14, and 18 dpi. **(F)** Quantification of signal (4 fish per time point) normalized to total protein. **(C, F)** Data points represent individual fish. Lines connect median values.

The erythrocyte loss of ISAV binding is not mediated by saturation of the ISAV receptor

To understand the mechanisms behind the observed loss of the ISAV receptor in infected fish, we next exposed density-purified erythrocytes from non-infected fish to supernatants from ISAV-infected cells. After identifying a virus dose that did not saturate the ISAV binding capacity (10^5 $TCID_{50}$ per 2×10^7 cells, Figure 3A), we evaluated ISAV binding in cells exposed to this non-saturating dose for 20 hours. Reflecting the situation in infected fish, we found that prior exposure to ISAV abolished subsequent ISAV binding to the membrane-enriched fractions (Figures 3B, C).

This illustrates that exposure to ISAV-containing supernatants is sufficient to reproduce the loss of ISAV binding observed in infected fish, and that the loss of binding is not due to receptor saturation.

The loss of ISAV binding is accompanied by increased availability to sialic acid-binding lectins

Loss of 9-*O*-acetylation can make sialic acids more available to endogenous sialic acid-binding immunoglobulin-like lectins (siglecs), probably by reducing steric hindrance (29–31). Similarly, 4-*O*-acetylation prevents binding of the plant lectin wheat germ agglutinin (WGA) to a range of α2,3-linked sialic acids (32). Four members of the siglec family (siglec 1, 2, 4, and 15) are conserved in all vertebrates, including Atlantic salmon (33). As the binding specificities of Atlantic salmon siglecs have not been characterized, we here used WGA as a proxy for testing if the loss of the ISAV receptor could modulate interactions between lectins and Atlantic salmon erythrocytes.

We found that exposure to both low (10^5 $TCID_{50}$ per 2×10^7 cells) and high (10^6 $TCID_{50}$ per 2×10^7 cells) doses of ISAV increased the binding of WGA to erythrocytes (Figure 4A). The effect was evident as soon as 60 min after exposure. At this time, the low-dose effect was less prominent, but after 20 hours, the low and high doses of virus increased WGA binding to a similar extent (Figure 4A and Table S1). Only the high dose of ISAV increased binding of the sambucus nigra lectin (SNA), which specifically targets α2,6-linked sialic acids (32) (Figure 4B).

Erythrocytes of infected fish (12-18 dpi) also bound WGA more efficiently than cells from non-infected individuals harvested at the same time (Figures 4C, D), confirming the *in vivo* relevance of our finding. Finally, incubation of erythrocytes from healthy fish with plasma from infected fish increased their binding to WGA (Figure 4E). Due to the limited amount of sample available, SNA-binding was not tested in samples from infected fish.

10.3389/fimmu.2023.1158077

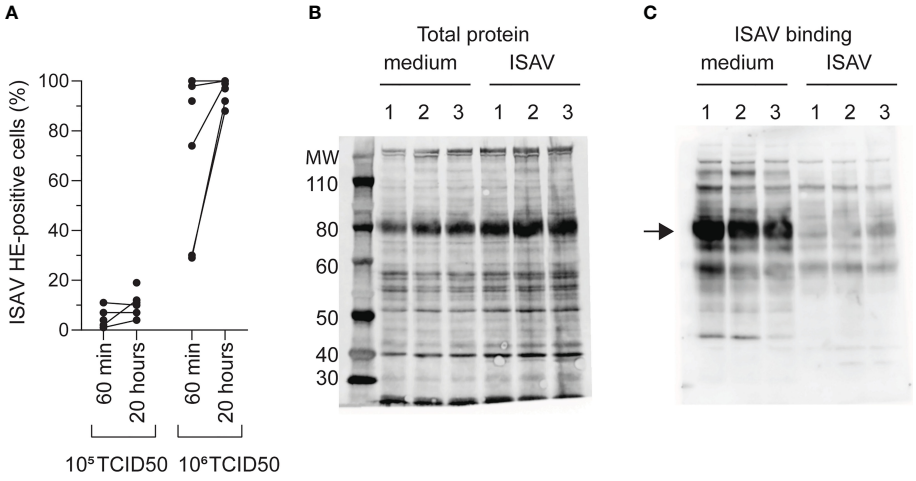

FIGURE 3
Loss of ISAV binding is not mediated by saturation of its cellular receptor. **(A)** Density-purified erythrocytes isolated from non-infected fish were incubated with ISAV at the indicated dose (per 20 million cells) and given duration, and the percentage of HE-positive cells was quantified by flow cytometry. Data points show measurements in cells from individual fish, with lines connecting values from the same fish when relevant. **(B, C)** Membrane-enriched erythrocyte lysates from three fish (1, 2, 3) exposed to medium or ISAV (10^5 $TCID_{50}$ per 20 million cells, 20 hours) were separated by SDS-PAGE and blotted to nitrocellulose membranes. **(B)** Blots were stained for total protein by Revert700 Total Protein Stain, **(C)** and the level of ISAV receptor was evaluated by serial incubation with ISAV antigen, mouse IgG_1 targeting HE (clone 3H6F8), HRP-conjugated secondary antibody, and substrate. The assay was repeated twice with identical results. The arrow points to the band representing ISAV binding in medium-treated erythrocytes.

The modulation of erythrocyte surfaces is mediated by the ISAV esterase

A monoclonal antibody (mouse IgG_1 clone 9G1F10A) that inhibited cellular ISAV attachment and hemagglutination (Figure S2) prevented the increase in WGA and SNA binding (Figures 5A–C). Similarly, the increase in WGA-binding observed when erythrocytes were incubated with plasma from infected fish, was strongly reduced when the plasma samples were pre-incubated with this neutralizing antibody (Figure 5D). Finally, incubating erythrocytes with recombinant HE showed that HE was sufficient to induce an increase in WGA-binding (Figures 5E, F). However, when the HE esterase activity was silenced by alanine mutation of its catalytic serine (S32) (34), the HE-mediated increase in WGA was abolished (Figures 5E, F).

Together, these findings suggest that ISAV-exposure renders erythrocyte sialic acids more available to lectin binding; that the attachment of ISAV to the cellular surface is required for this effect to take place; and that the ISAV-induced surface modulation at least in part is mediated by the hydrolytic activity of the viral RDE.

Our collected results support the conclusion that the ISAV RDE extensively removes 4-*O*-acetylated sialic acids from target cell surfaces in infected Atlantic salmon and suggest that this activity has potential to influence interactions with endogenous lectins.

Discussion

We recently discovered that the ISAV receptor disappears from the vascular surface of ISAV-infected Atlantic salmon (23). Here, we confirm and expand on that observation, by showing that circulating erythrocytes in infected fish also lose the ability to bind new ISAV particles, and that the viral esterase has a key role in this process. Our findings support a model where the HE first attaches to cell surface 4-*O*-acetylated sialic acids and then causes extensive hydrolysis of adjacent non-bound 4-*O*-acetylated sialic acids. The RDE-mediated loss of cell surface 4-*O*-acetylated sialic acids limits further ISAV binding and makes cell surface sialic acids more available to lectins, but does not affect already-bound ISAV particles.

Despite being nucleated, and in contrast to endothelial cells (21), only a minor fraction of Atlantic salmon erythrocytes supports ISAV protein production (24). Our findings therefore illustrate that the loss of viral receptor does not depend on viral replication and suggest that the cell surface is modulated at an early stage of the infectious cycle.

The loss of erythrocyte ISAV binding was attributed to the hydrolytic activity of HE: First, the effect was not associated with receptor saturation; suggesting that it was mediated by hydrolysis of 4-*O*-acetyl sialic acids, like in endothelial cells (23). Second, the loss of ISAV receptor from vascular endothelial cells and erythrocytes correlated in individual fish, indicating a common denominator. Third, exposing normal erythrocytes to plasma from infected fish reproduced the surface modulation, suggesting that this denominator was present in plasma. The plasma-induced surface modulation was inhibited by an antibody that prevented ISAV receptor engagement, strengthening the assumption that circulating ISAV particles were responsible for the effect, rather than secreted host esterases. ISAV-dependent surface modulation was also observed when erythrocytes from non-infected fish were exposed to supernatants from infected cells. Finally, exposure to recombinant HE was sufficient to induce the same surface

10.3389/fimmu.2023.1158077

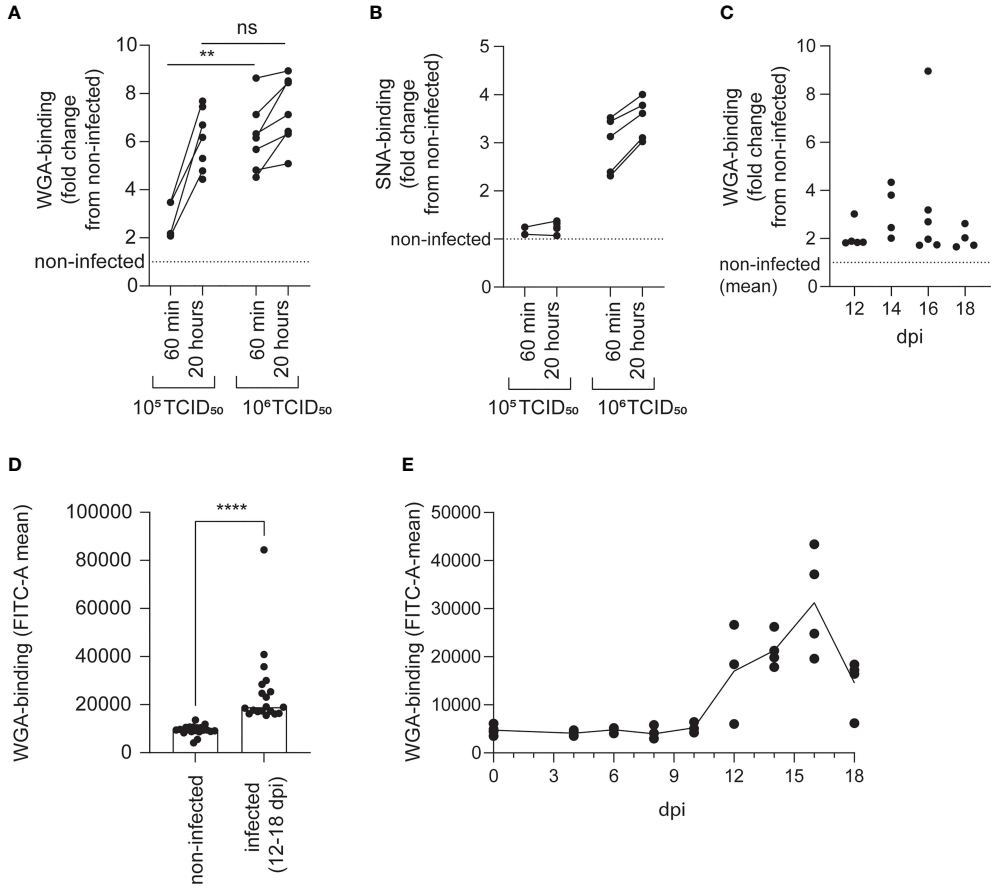

FIGURE 4
The loss of ISAV binding is accompanied by increased availability to sialic acid-binding lectins. The lectin-binding capacity of erythrocytes was evaluated by flow cytometry. **(A, B)** Density-purified erythrocytes isolated from non-infected fish were incubated with ISAV at the indicated dose (per 20 million cells) and given duration, and WGA-binding **(A)** and SNA-binding **(B)** was quantified in live cells by flow cytometry. Data points show measurements in cells from individual fish, with lines connecting values from the same fish. ** $p < 0.01$, Mann-Whitney U, ns, non-significant. **(C, D)** WGA-binding to PFA-fixed blood cells from infected fish was quantified by flow cytometry. Data points show values in individual fish. **** $p < 0.0001$, Mann-Whitney U. **(E)** Density-purified erythrocytes were incubated with plasma from infected fish harvested at the indicated time points (10 µL/10^6 cells) and incubated overnight before quantification of WGA-binding by flow cytometry. Data points show cells incubated with plasma from individual fish (4 per time point). The line connects medians.

modulation in normal erythrocytes, but only when the HE hydrolytic activity was preserved.

Even though erythrocytes from infected fish no longer supported the attachment of new virus particles, ISAV remained associated with erythrocytes throughout the trial, with only a small decline over the last four days. The antibody used to quantify erythrocyte-associated ISAV specifically binds the ISAV surface protein HE (35); hence, it will not detect virus proteins after their release to the cytoplasm. However, it is possible that pre-fusion virus particles in endosomes could account for part of the observed signal. Nevertheless, several studies have suggested that the dissociation of ISAV from Atlantic salmon erythrocytes is limited. The isolate used in the current study, Glesvaer/2/90, was the first ISAV isolate propagated (36) and has since been used in many of the key publications that characterize ISAV proteins, including HE (16–19, 34). The isolate efficiently hydrolyses both free and glycosidically bound 4-*O*-acetylated sialic acids (18), and both horse, rabbit, rainbow trout, cod, and crucian carp erythrocytes elute in the expected manner after Glesvaer/2/90-mediated agglutination (16, 17). Yet, the virus does not permit elution of agglutinated Atlantic salmon erythrocytes (16, 17). Interestingly, the same lack of elution is seen when Atlantic salmon erythrocytes are agglutinated with influenza C virus (17), which binds and hydrolyses 9-*O*-acetylated sialic acids (37, 38). This suggests that the lack of virus dissociation might be due to specific properties of Atlantic salmon erythrocytes.

The discrepancy between hydrolytic activity and virus dissociation indicates that the release of ISAV from the cell surface depends more on the on-off rate of the initial receptor engagement than the viral esterase hydrolytic activity. In other words, the ISAV esterase appears to limit the initiation of new attachments, rather than inducing the dissociation of already-bound ISAV particles. Nevertheless, the hydrolysis of adjacent receptors will reduce the local receptor density around the site initially bound by the virus, limiting the possibility to reattach to the cellular surface after release of the initial attachment (3, 4).

The erythrocyte surface modulation in infected fish that abrogated further ISAV attachment also increased the binding of

10.3389/fimmu.2023.1158077

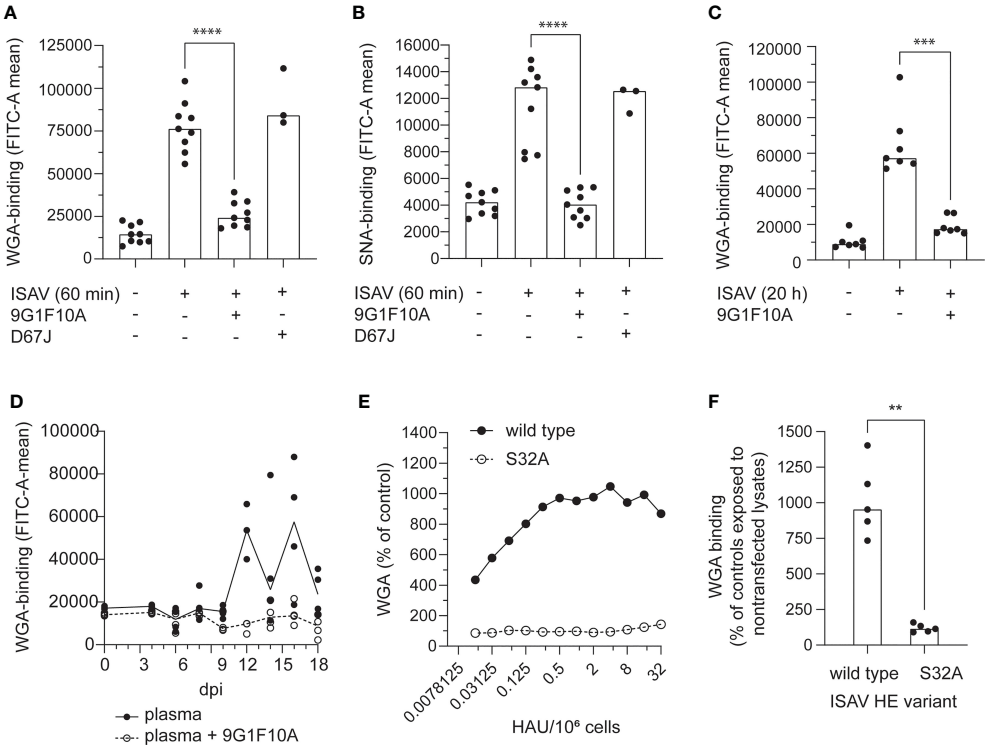

FIGURE 5
The pruning of erythrocyte surface is mediated by the ISAV esterase. **(A–C)** Virus supernatants were pre-incubated with antibodies targeting HE (9G1F10A) or the influenza A virus nucleoprotein (D67J) as a negative control (both: 5 µg/mL, 30 min, RT) before inoculation with erythrocytes (**A-B**: 10^6 $TCID_{50}$ per 20 million cells, 60 min; **C**: 10^5 $TCID_{50}$ per 20 million cells, 20 hours). Flow cytometry was used to evaluate **(A, C)** WGA-binding and **(B)** SNA-binding. **(D)** Plasma from infected fish harvested at the indicated time points was added to erythrocytes (10 µL/10^6 cells) either alone (black dots and line) or pre-incubated with the antibody 9G1F10A (open circles, stippled line). Samples were incubated overnight before quantification of WGA-binding by flow cytometry. Data points show cells incubated with plasma from individual fish (4 per time point). The lines connect medians. **(E, F)** WGA-binding to erythrocytes exposed to wild type or esterase-silenced (S32A) HE at 1 HAU per 10^6 cells for 20 hours. **(A-D, F)** Each data point represents blood cells isolated from one fish. Bars and line show median values. **p < 0.01, ***p < 0.001, ****p < 0.0001, Mann Whitney U.

the plant lectin WGA. The hydroxyl-group of sialic acid carbon 4 contributes to determining the specificity of WGA (39). Also, the binding of WGA to a range of α2,3-linked sialic acids is inhibited by 4-*O*-acetylation (32). It is therefore not surprising that the ability to bind WGA increases when the ISAV receptor is lost. The effect on SNA-binding was less expected. SNA is highly specific to α2,6-linked sialic acids, and its binding is not inhibited by 9-*O*-acetylation (32). While we have not identified any previous studies of how 4-*O*-acetylation influences SNA-binding, our findings suggest that this modulation could limit interactions between SNA and its ligand on Atlantic salmon erythrocytes, presumably α2,6-linked sialic acids.

In addition to increasing the knowledge of how ISAV interacts with target cell surfaces in the early phase of the infectious cycle, our observations raise two important questions:

First, does the RDE-induced cell surface-modulation influence biological functions in the host? In viral infection, it is essential for a successful outcome that the immune response is powerful enough to eliminate the viral infection, yet controlled and specific enough to avoid unsustainable collateral damage to the host. In addition to being exploited by numerous microbes for attachment (2), sialic acids regulate host tolerance and immune activation by interacting with siglec-expressing immune cells (12–14, 40). These interactions can be modulated by sialic acid *O*-acetylation (41–43). Sialic acid de-acetylation, which we have identified on erythrocyte and vascular surfaces in ISAV-infected fish, typically enhances siglec interactions (41), and the biological end-result will depend on the specific siglec and cell type involved. ISA is characterized by a severe reduction in the number of circulating erythrocytes and circulatory collapse, but surprisingly low levels of perivascular inflammation, despite a strong vascular endothelial expression of viral proteins (20, 21). Amongst several interesting observations that may be relevant to ISA pathogenesis is that loss of 9-*O*-acetylation enhanced interactions between murine erythroid leukemia cells and siglec-1 and promoted erythroid cell retention in the spleen and liver (29). Furthermore, loss of *O*-acetylated sialic acids promoted the activation of natural killer cell inhibitory siglecs and protected human cancer cell lines from cytotoxicity (42). Atlantic salmon siglecs and other sialic acid-binding molecules remain poorly characterized. Hence, it is difficult to predict the effects of the ISAV RDE-induced loss of vascular and erythrocyte 4-*O*-acetylated sialic acids. Nevertheless, in the light of ISA pathogenesis, it is reasonable to ask if this virus-mediated cell surface modulation could play a role in the premature removal of erythrocytes from circulation or a possible inhibition of cytotoxic immune responses in infectious salmon anemia.

Second, do other viral RDEs modulate target cell surfaces to a similar extent? A range of viruses targets different host sialic acid derivatives as highly specific attachment receptors, and many of these also express a RDE (2). The influenza A virus neuraminidase promotes viral fitness (6, 44), but little is known about its direct effects on host cells during infection. The same is true for other viral RDEs. Evidence for destruction of the human erythrocyte influenza virus receptor was provided in hemagglutination reactions more than 70 years ago (45). Still, we have not identified any studies that address possible modulations of erythrocyte surfaces in influenza virus-infected hostss. Two studies have documented loss of host sialic acids in lung tissues of influenza A virus (H1N1, H1N2, and H4N6)- and highly pathogenic avian influenza A virus (HPAIV) (H5N1)-infected animals, as well as *ex vivo* HPAIV (H5N1)-infected human lung biopsies (46, 47). These studies support the assumption that influenza A virus, similar to ISAV, modulates target cell surfaces during infection. Interestingly, in contrast to the ISAV esterase that appears to make host cell surfaces more available to lectins that target de-acetylated sialic acids, the influenza A virus neuraminidase removes the virus-targeted sialic acid from the cell surface (48). Hence, it is possible that RDE activity could reduce interactions with immune-modulatory lectins and contribute to the dysregulated inflammation characteristic of severe human influenza (49, 50). While most influenza A strains rarely cause viraemia in humans, HPAIV (H5N1) is an exception (51). Considering the zoonotic and even pandemic potential of HPAIV (52), we suggest that the consequences of a widespread loss of virus-targeted sialic acids in the context of this infection should be addressed by future studies.

Materials and methods

Fish and experimental infection

Atlantic salmon (AquaGen, Trondheim, Norway) were hatched, reared, and kept at the aquaculture research station: Center for Sustainable Aquaculture (Norwegian University of Life Sciences [NMBU], Ås, Norway). Fish were maintained on a 24 hour light photoperiod in circular tanks in a temperature-controlled (14 ± 1°C) fresh water recirculatory aquaculture system and fed a standard salmon diet in excess, using automatic belt feeders. Blood for use in *ex vivo* experiments was collected in heparinized containers by terminal blood sampling from the caudal veins of fish (body weight 100-300 g) anesthetized by Tricaine methanesulfonate immersion (100-200 mg/L). Prior to the infection trial, the relevant fish group was tested by qPCR and found negative for infectious salmon anemia virus (gills/heart/kidney), salmon pox gill virus (gills), infectious pancreatic necrosis virus, piscine rheovirus-1, piscine myocarditis virus, and salmonid alphavirus (all heart/kidney) by the diagnostic services at the Norwegian Veterinary Institute.

A total of 73 fish (median body weight 115 g) were transferred to the NMBU infection Aquarium (Ås, Norway) for use in the infection trial. The unit uses a fresh water flow-through aquaculture system at 12°C. After acclimatization, one group (n=47) was infected by 2-hour immersion in water containing the high-virulent Norwegian ISAV isolate NO/Glesvaer/2/90 (36) ($10^{3.75}$ $TCID_{50}$/mL), as previously described (53). This protocol reliably infects all fish in a synchronized manner, but the severity of disease varies between trials (53, 54). Infected fish were sampled 4, 6, 8, 10, 12, 14, 16, and 18 dpi (n=4-6 fish per time point). A group of non-infected fish from the same batch (n=26) served as controls and was sampled 0, 12, 14, 16, and 18 dpi (n=4-6 fish per time point). At sampling, fish were anesthetized by immersion in benzocaine (40 mg/L), weighed and measured, and blood was collected from the caudal vein into heparinized containers. After blood sampling, the exterior of the fish was examined, fish were killed by cervical sectioning, the midline was incised, and organs were inspected and harvested. Hematocrits were measured within 90 min after sampling, by measuring the cell fraction of centrifuged blood (75 mm capillary tubes, 1200 rpm, 3 min, room temperature [RT]).

Cells

Atlantic salmon kidney (ASK) cells (55) were maintained in L-15 medium (Lonza) supplemented with fetal bovine serum (FBS, 10%, Lonza), L-glutamine (Lonza, 4mM), and penicillin/streptomycin/amphotericin (Lonza, 1%) or gentamicin (50 µg/mL). The cells were cultured in closed cap tissue culture flasks at 20°C and were split 1:2 every 14 days.

Erythrocytes for *ex vivo* experiments were isolated from heparinized blood from non-infected Atlantic salmon by density gradient centrifugation. Briefly, 0.25 mL blood was diluted in 5 mL phosphate-buffered isotonic saline (PBS), layered on top of 7.5 mL 51% Percoll Plus (Sigma-Aldrich), and centrifuged without breaks (500x *g*, 20 min, 10°C). The erythrocyte pellets were extensively washed in PBS and resuspended 2×10^7 cells/mL in the same culture medium as the ASK cells. Erythrocyte suspensions were maintained in 6-well cell culture plates on a microplate shaker (IKA-Werke, 150-200 rpm, 15°C) for up to 10 days. ISAV exposure was performed by resuspending erythrocytes in medium containing ISAV, plasma from infected fish, or recombinant HE (serial dilutions), followed by incubation in 24- or 48-well cell culture plates on a microplate shaker. Where relevant, ISAV or plasma from infected fish was pre-incubated with a mouse IgG_1 targeting ISAV HE (clone 9G1F10A, generated by Knut Falk in the late 1990s) or mouse IgG_{2a} targeting influenza virus NP (clone D67J, Thermo Fisher Scientific) (both: 5 µg/mL, 30 min, RT).

Virus and titer determination

ISAV was propagated in ASK cells at 15°C, and supernatants were harvested when cytopathic effects were close to complete, 14-28 dpi. Infective titers were determined by inoculating serial dilutions of supernatants or blood (10 µL heparinized blood was added to 500 µL L-15 medium and kept at -80°C until titration) in quadruplicate wells of ASK cells cultured in 96-well microtiter plates. Acetone-fixed cells were incubated with IgG_1 against the ISAV nucleoprotein (P10, Aquatic Diagnostics Ltd, 0.4 µg/mL, 60 min, RT), washed (PBS × 3), and incubated with Alexa488-

labelled goat anti-mouse IgG (A11001, Thermo Fisher Scientific, 5 µg/mL, 45 min, RT), and titers were calculated by the modified Kärber method, as previously described (17).

RNA extraction and qPCR

20 µL heparinized blood was added to 400 µL MagNA Pure LC RNA Isolation Tissue Lysis buffer (Roche). Head kidney pieces (15-30 mm^3) were collected in RNA later (Thermo Fisher Scientific), transferred to 500 µL MagNA Pure LC RNA Isolation Tissue Lysis buffer, and homogenized with 3-5 mm steel beads in a TissueLyser II (Qiagen, 24 Hz, 2 × 3 min). 350 µL lysed blood or 200 µL lysed head kidney were transferred to a Magna Pure 96 Processing Cartridge (Roche), and the total volume of head kidney samples was adjusted to 350 µL by adding MagNA Pure LC RNA Isolation Tissue Lysis buffer. RNA was extracted on a MagNA Pure 96 instrument (Roche) with the MagNA Pure 96 Cellular RNA Large Volume Kit (Roche), using the RNA tissue FF standard cellular RNA protocol with an elution volume of 50 µL per sample. RNA yield and purity was determined by a Multiskan Sky spectrophotometer (Thermo Fisher Scientific). The QuantiTect reverse transcription kit (Qiagen) was used for cDNA synthesis. Real time PCR was carried out with the TaqMan fast Advanced kit (Applied Biosystems) using the following protocol: TaqMan Fast advanced master mix (1x), TaqMan assay probe (0.2 µM), forward and reverse primers (0.5 µM), and cDNA template (0.5 ng/µl) final concentrations. Thermocycling was performed on a CFX384 Bio-Rad) and CFX-manager (software version 3.1, Bio-rad) under the following conditions: 2 min at 50 °C, 20 seconds at 95 °C, 40 cycles of 3 seconds each at 95 °C, and 30 seconds at 60 °C. Standard curves of a synthetic DNA fragment containing the relevant target sequences (Integrated DNA Technologies) were used for calculation of copy number per µg RNA. Sequences for primer/probes/DNA: ISAV segment 8: FW 5′-CGAAAGCCCTGGAAACTTTAGA-3′; REV 5′-GATGCCGGAAGTCGATGAACT-3′; probe FAM-aaggccatcgtcgct-NFQ. ELF-1α (for normalization): FW 5′-GGCTGGTTCAAGGGATGGA-3′; REV 5′-CAGAGTCACACCATTGGCGTTA-3′; probe FAM-tcgagcgtaaggatg-NFQ. DNA fragment: CATGCTGGAGGCTAGCGCCAACATGGGCTGGTTCAAGGGATGGAAGGTCGAGCGTAAGGATGGTAACGCCAATGGTGTGACTCTGCTGGAAGCCCTGGACGATGCAGATGTATGCTCTAGGAGCGAGTTCGAAAGCCCTGGAAACTTTAGAAAAGGCCATCGTCGCTGCAGTTCATCGACTTCCGGCATCCTGCTCGACAGAGAAGATGGTGCCAGGGTTGTATCCATGGTTGAAATGGACAGAGACGGCGTATCATTCATCTACGAGAAGCCTAGCATCTACCATAGTGATGGGTGCACTGGGACAGCATCGAGGGTCTGGAGACGGGATCACAATGAGAGAGCTGGAGTTGAGCTTAGGGCTGGACTTCACTTCAGAA.

Flow cytometry

100 µL heparinized blood from each fish in the infection trial was collected in PBS, washed, and fixed (3% paraformaldehyde, 10 min, RT) before staining (RT). Erythrocytes from *ex vivo* experiments were stained live (4°C). Cells were labelled with Alexa488-labelled WGA (1 µg/mL, Thermo Fisher Scientific, 60 min), FITC-labelled SNA (10 µg/mL, Thermo Fisher Scientific, 60 min), or mouse IgG_1 specific to the ISAV hemagglutinin esterase (clone 3H6F8 (35), hybridoma supernatants diluted 1:10 for fixed and 1:100 for live cells, 60 min), washed (PBS × 3), and (for detection of ISAV only) incubated with Alexa488-labelled goat anti-mouse IgG (A11001, Thermo Fisher Scientific, 5 µg/mL, 45 min). Signal was detected by a NovoCyte flow cytometer (Agilent), recording 25 000 events per sample.

Immunostaining of blood smears

Blood smears were made and fixed (80% acetone, 15 min, RT) within 120 min of sampling, dried, and stored at -80°C until staining. Thawed and dried smears were incubated with 1x clear milk block (Thermo Fisher Scientific, 30 min, RT), mouse IgG_1 specific to the ISAV HE (clone 3H6F8 (35), hybridoma supernatant diluted 1:100, 60 min, RT), washed (PBS × 3), and incubated with Alexa488-labelled goat anti-mouse IgG (A11001, Thermo Fisher Scientific, 5 µg/mL) together with Alexa594-labelled phalloidin (Thermo Fisher Scientific, 2 units/mL, 45 min, RT). Nuclei were counterstained by Hoechst 33342 (Thermo Fisher Scientific, 2 µg/mL, 5 min, RT), and slides were mounted in ProLong Gold antifade mountant (Thermo Fisher Scientific). Wide-field microscopy was performed by a Nikon Ti-2e inverted microscope, using a Plan Apo lambda DIC N2 63x oil objective (NA 1.4). The percentage of ISAV-positive cells in individual fish was quantified in ImageJ (version 1.53c) (56): Total cell numbers were determined using the *Analyze particles* function on thresholded images generated from the Hoechst channel. Next, the number of ISAV-positive cells were counted manually in the channel containing signal from the HE-staining, assessing a minimum of 99 cells per fish.

Histology

An organ panel including heart, spleen, and head kidney was collected from each fish, fixed in 10% formalin for at least 24 hours, dehydrated, and embedded in paraffin. Thin tissue sections were heat treated (60-70°C, 20 min), deparaffinized, and either stained with hematoxylin & eosin for histological evaluation or subjected to a virus binding assay, as described below.

Preparation and blotting of membrane-enriched lysates

Cell pellets were prepared from full blood or density-purified erythrocytes and stored at -80°C before preparation of membrane-enriched fractions as previously described (24). Briefly, 100 µL cell pellets were lysed by 1:10 dilution in ice cold water with 1% protease inhibitor (P8340, Sigma-Aldrich, 10 min, on ice). The cells were homogenized with a tight-fitting Dounce homogenization (20

strokes), 1000 µL buffer A (75 mM Tris pH 7.5, 12.5 mM MgCl, 15 mM EDTA) was added, and the homogenization was repeated. To remove nuclei and organelles, the suspension was centrifuged (5000× *g*, 5 min), and the supernatant was collected on ice. The homogenization procedure was repeated three times with the cell pellet in buffer A diluted 1:1 with water, pooled supernatant fractions were centrifuged (40,000× *g*, 30 min), the membrane-enriched pellets were resuspended in 50 µL buffer B (20 mM Tris, 2 mM EDTA, pH 7.5), and samples were stored at -80°C. After thawing, 10 µL sample, 3.88 µL NuPage LDS sample buffer, and 1.55 µL NuPage sample reducing agent (both from Thermo Fisher Scientific) was mixed and homogenized by centrifugation in QiaShredder columns (Qiagen), heat-treated (10 min, 70°C), and loaded to gels (8 µL/well) for SDS-PAGE and Western blotting (NuPage Novex system, Thermo Fisher Scientific) to 0.45 µm nitrocellulose membranes (BioRad laboratories).

Production of antigen for virus binding assays

Antigens for virus histochemistry and virus binding assays were prepared by collecting membrane fractions of infected ASK cells, as previously described (21). Briefly, cells in 75 cm^2 tissue culture flasks were harvested when cytopathic effects were evident but most cells remained attached, typically 3-7 dpi. Cells were washed and scraped on ice, and cell pellets containing cellular-expressed viral membrane glycoproteins were washed, resuspended in 0.5 mL PBS, and subjected to three rounds of freeze-thawing. Hemagglutination titers were determined by incubating serial dilutions of antigen preparations with 1% Atlantic salmon erythrocyte suspensions in 96-well V-bottom microtiter plates.

Virus binding assays

To map virus-binding sites in Atlantic salmon tissues and membrane-enriched cell fractions, we used virus antigen preparations as primary probes as previously described (21, 23, 24).

Deparaffinized formalin-fixed tissue sections were incubated with 100 µL ISAV antigen (512 HAU/mL, 60 min, RT), washed (PBS × 3), quenched with peroxidase block (5 min, RT), treated with blocking buffer (Background sniper, Biocare Medical, 30 min, RT), incubated with mouse IgG_1 specific to ISAV HE (clone 3H6F8 (35), hybridoma supernatants diluted 1:100, 60 min, RT), washed (PBS × 3), and signal was visualized by the MACH2 HRP polymer-DAB (Biocare Medical) system, following manufacturer's instructions. Signal was analyzed as described in the section *Quantification of virus histochemistry signal*.

Blotted membrane-enriched cell lysates (prepared as described above) were stained for total protein using Revert700 Total Protein Stain as recommended by the manufacturer (Licor Biosciences), treated with dry milk (5% in Tris-buffered saline [TBS], 60 min, RT), washed (TBS 0.1% Tween [TBST] × 2), incubated with ISAV antigen (256 HAU/mL diluted in TBS, 60 min, RT), washed (TBST × 3), incubated with mouse IgG_1 specific to ISAV HE (clone 3H6F8 (35), hybridoma supernatants diluted 1:250 in TBST with 5% dry milk, 60 min, RT), and washed (TBST × 3). Bound primary antibody was detected either by incubation with IRDye800-labelled goat anti-mouse IgG (Li-Cor Biosciences, 1:10,000 in TBST with 5% dry milk, 60 min, RT), or by incubation with HRP-conjugated horse anti-mouse IgG (Cell Signaling, 1:1000, 60 min, RT), wash (TBST x 3), and incubation with Super Signal West pico substrate (Thermo Fisher scientific). Chemiluminescent or fluorescent signal was visualized by an Azure imager C500 (Azure Biosystems). For quantification, fluorescent signal was normalized to total protein signal, using Azure spot software (Azure Biosystems, version 2.2.167).

Quantification of virus histochemistry signal

Images of tissue sections subjected to virus binding assays were digitized using a Hamamatsu Nanozoomer digital slide scanner with 40x objective (114932 pixels per inch, 221 nm/pixel, JPEG compression at 80%). The virus histochemistry signal was analyzed using Visiopharm, v2022.2. For region of interest (= organ) detection and area measurement, a generic analysis protocol package using artificial intelligence (DeepLab V3) trained in our lab on collections of slides containing Atlantic salmon liver, heart, kidney, spleen and adipose tissue, was retrained on the full set of stained sections from the present study. Signal detection was performed at 20x magnification: The image pixel value was inverted, multiplied by 5, and combined with their red-green contrast values using a maximum pixel value filter. Pixels with resulting values above a threshold of 50 were considered positive. The total area covered by positive pixels per organ was divided by organ area to yield the fraction of positive signal relative to area of the organ in the section.

Generation of recombinant ISAV HE

Codon optimized sequences of the open reading frame encoding ISAV HE, corresponding to isolate NO/Finnmark/NVI-70-1250/2020 (Genbank accession UGL76651.1), as well as a variant where serine 32 was mutated to alanine to abolish catalytic activity (S32A), was synthesized and inserted in the pcDNA3.1 (+) vector commercially and delivered transfection-ready (GeneCust). Monolayers of CHSE-214 cells were cultured until 90-100% confluent and detached by Trypsin EDTA (Lonza). 4 transfection reactions, each with 10^6 cells and 10 µg plasmid DNA, were performed, using the Neon 100 µL Transfection System (Invitrogen, Waltham, MA, USA, three pulses at 1600 V and 10 ms width). Non-transfected cells were used as controls. The transfected cells were pooled and incubated 24 hours in antibiotic free medium, then another 24 hours in culture medium. Membrane fractions were collected as described for infected cells and previously (21).

Statistics

Statistics were performed in Graph Pad Prism 8 for Windows 64-bits, v.8.4.3.

Data availability statement

The original contributions presented in the study are included in the article/Supplementary Material. Further inquiries can be directed to the corresponding author.

Ethics statement

Protocols for harvesting material from healthy fish and experimental infection and their implementation were approved prior to the studies by the Norwegian Food Safety Authority (FOTS24382, FOTS28403). All facilities were operated in compliance with Organization for Economic Co-operation and Development principles of Good Laboratory Practice and Guidelines to Good Manufacturing Practice issued by the European Commission.

Author contributions

Conceptualization: JF, KF; Design, planning, and supervision: JF, AA, KF; Experimentation: JF, AA, FP, SW, IH, SS, KL, AS; Analysis and interpretation: JF, AA, FP, SW, AS; Initial draft and figures: JF. Revision of initial draft: All authors. Funding: KF. All authors contributed to the article and approved the submitted version.

Funding

The work was funded by the Research Council of Norway (Grant 254876, obtained by KF). The funders had no role in study design, data collection and analysis, decision to publish, or preparation of the manuscript.

Acknowledgments

The authors would like to thank: Eirill Aager-Wick and Hetron Mweemba Munang'andu (the NMBU infection aquarium for salmonids, Ås, Norway) for administrative and technical support for the infection trial; Ricardo Tavares Benicio and Bjørn-Reidar Hansen (the aquaculture research station, NMBU, Ås, Norway) for providing fish and technical assistance; Torfinn Moldal (Norwegian Veterinary Institute) for organizing the pre-trial screening for infectious agents; Marit Måsøy Amundsen, Randi Faller, Randi Terland, Britt Saure, Lone Engerdahl, and Ingebjørg Modahl (Norwegian Veterinary Institute) for technical assistance; and Maria Aamelfot (Norwegian Institute for Public Health) for fruitful discussions. The authors would also like to acknowledge two research projects funded by the Research Council of Norway (grant 302551) and strategic base-funding at the Norwegian Veterinary institute (BIODIRECT: Biomarkers and bioassays for future research and diagnostics) for methodological support and refinement.

Conflict of interest

The authors declare that the research was conducted in the absence of any commercial or financial relationships that could be construed as a potential conflict of interest.

Publisher's note

Supplementary material

The Supplementary Material for this article can be found online at: https://www.frontiersin.org/articles/10.3389/fimmu.2023.1158077/full#supplementary-material

SUPPLEMENTARY TABLE 1
Numericals and statistics used to generate the figures.

SUPPLEMENTARY FIGURE 1
Supplemental to Figure 1 : **(A, B)** Manual scoring and **(C)** example micrograph of erythrophagocytosis in **(A)** head kidney and **(B, C)** spleen in hematoxylin and eosin-stained formalin-fixed, paraffin-embedded tissue sections of individual fish. Arrows point to examples of frequent erythrophagocytosis and pigmentation in spleen of an infected fish harvested 16 dpi, indicating breakdown of hemoglobin. **(D)** Viral RNA in head kidney was measured by qPCR targeting ISAV segment 8. Data points show values in individual fish, the line connects median values. **(E)** Gating strategy and examples of histograms showing HE-staining in PFA-fixed erythrocytes from non-infected (black) and infected (red) fish, harvested 12 dpi.

SUPPLEMENTARY FIGURE 2
Supplemental to Figure 5: **(A)** ISAV was pre-incubated with monoclonal antibodies as indicated (5 µg/mL, 30 min, RT), before inoculation with density-purified erythrocytes isolated from non-infected fish (10^6 $TCID_{50}$ per 2 x10^7 cells, 60 min) and quantification of HE by flow cytometry. Data points show measurements in cells from individual fish. **p<0.01, Kruskal-Wallis with Dunn's multiple comparisons test (Table S1). **(B)** Hemagglutination inhibition assay testing the ability of 9G1F10A to inhibit ISAV-induced agglutination (4 HAU ISAV antigen and 10^6 erythrocytes per well). The boxed area indicates the concentration range of the antibody that completely inhibited agglutination.

References

1. Lewis AL, Chen X, Schnaar RL, Varki A. Sialic acids and other nonulosonic acids. In: Varki A, Cummings RD, Esko JD, Stanley P, Hart GW, et al, editors. *Essentials of glycobiology*. Cold Spring Harbor (NY (2022). p. 185–204.

2. Matrosovich M, Herrler G, Klenk HD. Sialic acid receptors of viruses. *Top Curr Chem* (2015) 367:1–28. doi: 10.1007/128_2013_466

3. Guo H, Rabouw H, Slomp A, Dai M, van der Vegt F, van Lent JWM, et al. Kinetic analysis of the influenza a virus HA/NA balance reveals contribution of NA to virus-receptor binding and NA-dependent rolling on receptor-containing surfaces. *PLoS Pathog* (2018) 14(8):e1007233. doi: 10.1371/journal.ppat.1007233

4. Sakai T, Nishimura SI, Naito T, Saito M. Influenza a virus hemagglutinin and neuraminidase act as novel motile machinery. *Sci Rep* (2017) 7:45043. doi: 10.1038/srep45043

5. Strobl B, Vlasak R. The receptor-destroying enzyme of influenza c virus is required for entry into target cells. *Virology* (1993) 192(2):679–82. doi: 10.1006/viro.1993.1087

6. Matrosovich MN, Matrosovich TY, Gray T, Roberts NA, Klenk HD. Neuraminidase is important for the initiation of influenza virus infection in human airway epithelium. *J Virol* (2004) 78(22):12665–7. doi: 10.1128/JVI.78.22.12665-12667.2004

7. Palese P, Tobita K, Ueda M, Compans RW. Characterization of temperature sensitive influenza virus mutants defective in neuraminidase. *Virology* (1974) 61(2):397–410. doi: 10.1016/0042-6822(74)90276-1

8. Horga MA, Gusella GL, Greengard O, Poltoratskaia N, Porotto M, Moscona A. Mechanism of interference mediated by human parainfluenza virus type 3 infection. *J Virol* (2000) 74(24):11792–9. doi: 10.1128/jvi.74.24.11792-11799.2000

9. Huang IC, Li W, Sui J, Marasco W, Choe H, Farzan M. Influenza a virus neuraminidase limits viral superinfection. *J Virol* (2008) 82(10):4834–43. doi: 10.1128/JVI.00079-08

10. Goto H, Ohta K, Matsumoto Y, Yumine N, Nishio M. Evidence that receptor destruction by the Sendai virus hemagglutinin-neuraminidase protein is responsible for homologous interference. *J Virol* (2016) 90(17):7640–6. doi: 10.1128/JVI.01087-16

11. Morrison TG, McGinnes LW. Avian cells expressing the Newcastle disease virus hemagglutinin-neuraminidase protein are resistant to Newcastle disease virus infection. *Virology* (1989) 171(1):10–7. doi: 10.1016/0042-6822(89)90505-9

12. Saini P, Adeniji OS, Abdel-Mohsen M. Inhibitory siglec-sialic acid interactions in balancing immunological activation and tolerance during viral infections. *EBioMedicine* (2022) 86:104354. doi: 10.1016/j.ebiom.2022.104354

13. Laubli H, Varki A. Sialic acid-binding immunoglobulin-like lectins (Siglecs) detect self-associated molecular patterns to regulate immune responses. *Cell Mol Life Sci* (2020) 77(4):593–605. doi: 10.1007/s00018-019-03288-x

14. Macauley MS, Crocker PR, Paulson JC. Siglec-mediated regulation of immune cell function in disease. *Nat Rev Immunol* (2014) 14(10):653–66. doi: 10.1038/nri3737

15. Mjaaland S, Rimstad E, Falk K, Dannevig BH. Genomic characterization of the virus causing infectious salmon anemia in Atlantic salmon (*Salmo salar* l.): an orthomyxo-like virus in a teleost. *J Virol* (1997) 71(10):7681–6. doi: 10.1128/JVI.71.10.7681-7686.1997

16. Falk K, Aspehaug V, Vlasak R, Endresen C. Identification and characterization of viral structural proteins of infectious salmon anemia virus. *J Virol* (2004) 78(6):3063–71. doi: 10.1128/jvi.78.6.3063-3071.2004

17. Falk K, Namork E, Rimstad E, Mjaaland S, Dannevig BH. Characterization of infectious salmon anemia virus, an orthomyxo-like virus isolated from Atlantic salmon (*Salmo salar* l.) *J Virol* (1997) 71(12):9016–23. doi: 10.1128/JVI.71.12.9016-9023.1997

18. Hellebo A, Vilas U, Falk K, Vlasak R. Infectious salmon anemia virus specifically binds to and hydrolyzes 4-*O*-acetylated sialic acids. *J Virol* (2004) 78(6):3055–62. doi: 10.1128/jvi.78.6.3055-3062.2004

19. Cook JD, Sultana A, Lee JE. Structure of the infectious salmon anemia virus receptor complex illustrates a unique binding strategy for attachment. *Proc Natl Acad Sci U S A* (2017) 114(14):E2929–E36. doi: 10.1073/pnas.1617993114

20. Falk K, Aamelfot M. Infectious salmon anaemia. In: *Fish viruses and bacteria: pathobiology and protection* (2017). p. 68–78. CABI (Oxfordhire, UK).

21. Aamelfot M, Dale OB, Weli SC, Koppang EO, Falk K. Expression of the infectious salmon anemia virus receptor on Atlantic salmon endothelial cells correlates with the cell tropism of the virus. *J Virol* (2012) 86(19):10571–8. doi: 10.1128/JVI.00047-12

22. Koren CWR, Nylund A. Morphology and morphogenesis of infectious salmon anaemia virus replicating in the endothelium of Atlantic salmon salmo salar. *Dis Aquat Organisms* (1997) 29:99–109. doi: 10.3354/dao029099

23. Aamelfot M, Fosse JH, Viljugrein H, Ploss FB, Benestad SL, McBeath A, et al. Destruction of the vascular viral receptor in infectious salmon anaemia provides *in vivo* evidence of homologous attachment interference. *PLoS Pathog* (2022) 18(10):e1010905. doi: 10.1371/journal.ppat.1010905

24. Fosse JH, Aamelfot M, Sønstevold T, Weli SC, Vendramin N, Petersen PE, et al. Salmon erythrocytes sequester active virus particles in infectious salmon anaemia. *Viruses* (2022) 14. doi: 10.3390/v14020310

25. Thorud KE. *Infectious salmon anaemia: transmission trial: haematological, clinical, chemical and morphological investigations*. Oslo: Norwegian Veterinary College (1991).

26. Jancik J, Schauer R. Sialic acid–a determinant of the life-time of rabbit erythrocytes. *Hoppe Seylers Z Physiol Chem* (1974) 355(4):395–400. doi: 10.1515/bchm2.1974.355.1.395

27. Durocher JR, Payne RC, Conrad ME. Role of sialic acid in erythrocyte survival. *Blood* (1975) 45(1):11–20. doi: 10.1182/blood.V45.1.11.11

28. Bratosin D, Mazurier J, Debray H, Lecocq M, Boilly B, Alonso C, et al. Flow cytofluorimetric analysis of young and senescent human erythrocytes probed with lectins. evidence that sialic acids control their life span. *Glycoconj J* (1995) 12(3):258–67. doi: 10.1007/BF00731328

29. Shi WX, Chammas R, Varki NM, Powell L, Varki A. Sialic acid 9-o-acetylation on murine erythroleukemia cells affects complement activation, binding to I-type lectins, and tissue homing. *J Biol Chem* (1996) 271(49):31526–32. doi: 10.1074/jbc.271.49.31526

30. Sjoberg ER, Powell LD, Klein A, Varki A. Natural ligands of the b cell adhesion molecule CD22 beta can be masked by 9-o-acetylation of sialic acids. *J Cell Biol* (1994) 126(2):549–62. doi: 10.1083/jcb.126.2.549

31. Cariappa A, Takematsu H, Liu H, Diaz S, Haider K, Boboila C, et al. B cell antigen receptor signal strength and peripheral b cell development are regulated by a 9-o-acetyl sialic acid esterase. *J Exp Med* (2009) 206(1):125–38. doi: 10.1084/jem.20081399

32. Srivastava S, Verhagen A, Sasmal A, Wasik BR, Diaz S, Yu H, et al. Development and applications of sialoglycan-recognizing probes (SGRPs) with defined specificities: exploring the dynamic mammalian sialoglycome. *Glycobiology* (2022) 32(12):1116–1136. doi: 10.1093/glycob/cwac050

33. Bornhofft KF, Goldammer T, Rebl A, Galuska SP. Siglecs: a journey through the evolution of sialic acid-binding immunoglobulin-type lectins. *Dev Comp Immunol* (2018) 86:219–31. doi: 10.1016/j.dci.2018.05.008

34. Muller A, Markussen T, Drablos F, Gjoen T, Jorgensen TO, Solem ST, et al. Structural and functional analysis of the hemagglutinin-esterase of infectious salmon anaemia virus. *Virus Res* (2010) 151(2):131–41. doi: 10.1016/j.virusres.2010.03.020

35. Falk K, Namork E, Dannevig BH. Characterization and applications of a monoclonal antibody against infectious salmon anaemia virus. *Dis Aquat Organ* (1998) 34(2):77–85. doi: 10.3354/dao034077

36. Dannevig BH, Falk K, Namork E. Isolation of the causal virus of infectious salmon anaemia (ISA) in a long-term cell line from Atlantic salmon head kidney. *J Gen Virol* (1995) 76:1353–9. doi: 10.1099/0022-1317-76-6-1353

37. Rogers GN, Herrler G, Paulson JC, Klenk HD. Influenza c virus uses 9-O-acetyl-N-acetylneuraminic acid as a high affinity receptor determinant for attachment to cells. *J Biol Chem* (1986) 261(13):5947–51. doi: 10.1016/s0021-9258(17)38475-2

38. Herrler G, Rott R, Klenk HD, Müller HP, Shukla AK, Schauer R. The receptor-destroying enzyme of influenza c virus is neuraminate-o-acetylesterase. *EMBO J* (1985) 4(6):1503–6. doi: 10.1002/j.1460-2075.1985.tb03809.x

39. Sharon N. Lectin-carbohydrate complexes of plants and animals: an atomic view. *Trends Biochem Sci* (1993) 18(6):221–6. doi: 10.1016/0968-0004(93)90193-q

40. Lubbers J, Rodriguez E, van Kooyk Y. Modulation of immune tolerance *via* siglec-sialic acid interactions. *Front Immunol* (2018) 9:2807. doi: 10.3389/fimmu.2018.02807

41. Visser EA, Moons SJ, Timmermans S, de Jong H, Boltje TJ, Bull C. Sialic acid *O*-acetylation: from biosynthesis to roles in health and disease. *J Biol Chem* (2021) 297(2):100906. doi: 10.1016/j.jbc.2021.100906

42. Grabenstein S, Barnard KN, Anim M, Armoo A, Weichert WS, Bertozzi CR, et al. Deacetylated sialic acids modulates immune mediated cytotoxicity *via* the sialic acid-siglec pathway. *Glycobiology* (2021) 31(10):1279–94. doi: 10.1093/glycob/cwab068

43. Schauer R, Srinivasan GV, Wipfler D, Kniep B, Schwartz-Albiez R. O-Acetylated sialic acids and their role in immune defense. *Adv Exp Med Biol* (2011) 705:525–48. doi: 10.1007/978-1-4419-7877-6_28

44. Yang J, Liu S, Du L, Jiang S. A new role of neuraminidase (NA) in the influenza virus life cycle: implication for developing NA inhibitors with novel mechanism of action. *Rev Med Virol* (2016) 26(4):242–50. doi: 10.1002/rmv.1879

45. Hirst GK. Adsorption of influenza hemagglutinins and virus by red blood cells. *J Exp Med* (1942) 76(2):195–209. doi: 10.1084/jem.76.2.195

46. van Riel D, Leijten LM, Kochs G, Osterhaus A, Kuiken T. Decrease of virus receptors during highly pathogenic H5N1 virus infection in humans and other mammals. *Am J Pathol* (2013) 183(5):1382–9. doi: 10.1016/j.ajpath.2013.07.004

47. Trebbien R, Larsen LE, Viuff BM. Distribution of sialic acid receptors and influenza a virus of avian and swine origin in experimentally infected pigs. *Virol J* (2011) 8:434. doi: 10.1186/1743-422X-8-434

48. Lai JCC, Karunarathna H, Wong HH, Peiris JSM, Nicholls JM. Neuraminidase activity and specificity of influenza a virus are influenced by haemagglutinin-receptor binding. *Emerg Microbes Infect* (2019) 8(1):327–38. doi: 10.1080/22221751.2019.1581034

49. Kalil AC, Thomas PG. Influenza virus-related critical illness: pathophysiology and epidemiology. *Crit Care* (2019) 23(1):258. doi: 10.1186/s13054-019-2539-x

50. Liu Q, Liu DY, Yang ZQ. Characteristics of human infection with avian influenza viruses and development of new antiviral agents. *Acta Pharmacol Sin* (2013) 34(10):1257–69. doi: 10.1038/aps.2013.121

51. Kuiken T, van den Brand J, van Riel D, Pantin-Jackwood M, Swayne DE. Comparative pathology of select agent influenza a virus infections. *Vet Pathol* (2010) 47 (5):893–914. doi: 10.1177/0300985810378651

52. Yamaji R, Saad MD, Davis CT, Swayne DE, Wang D, Wong FYK, et al. Pandemic potential of highly pathogenic avian influenza clade 2.3.4.4 A(H5) viruses. *Rev Med Virol* (2020) 30(3):e2099. doi: 10.1002/rmv.2099

53. McBeath A, Aamelfot M, Christiansen DH, Matejusova I, Markussen T, Kaldhusdal M, et al. Immersion challenge with low and highly virulent infectious salmon anaemia virus reveals different pathogenesis in Atlantic salmon, *Salmo salar* l. *J Fish Dis* (2015) 38(1):3–15. doi: 10.1111/jfd.12253

54. Fosse JH, Haraldsen G, Falk K, Edelmann R. Endothelial cells in emerging viral infections. *Front Cardiovasc Med* (2021) 8:619690. doi: 10.3389/fcvm.2021.619690

55. Devold M, Krossoy B, Aspehaug V, Nylund A. Use of RT-PCR for diagnosis of infectious salmon anaemia virus (ISAV) in carrier sea trout *Salmo trutta* after experimental infection. *Dis Aquat Organ* (2000) 40(1):9–18. doi: 10.3354/dao040009

56. Schindelin J, Arganda-Carreras I, Frise E, Kaynig V, Longair M, Pietzsch T, et al. Fiji: An open-source platform for biological-image analysis. *Nat Methods* (2012) 9 (7):676–82. doi: 10.1038/nmeth.2019

frontiers | Frontiers in Immunology

TYPE Original Research
PUBLISHED 06 June 2023
DOI 10.3389/fimmu.2023.1209926

OPEN ACCESS

EDITED BY
Elena Chaves-Pozo,
Spanish Institute of Oceanography, Spain

REVIEWED BY
Xiuzhen Sheng,
Ocean University of China, China
Sonia Dios,
Spanish National Research Council (CSIC), Spain

*CORRESPONDENCE
Alejandro M. Labella
amlabella@uma.es

RECEIVED 21 April 2023
ACCEPTED 22 May 2023
PUBLISHED 06 June 2023

CITATION
Leiva-Rebollo R, Gémez-Mata J, Castro D, Borrego JJ and Labella AM (2023) Immune response of DNA vaccinated-gilthead seabream (*Sparus aurata*) against LCDV-Sa infection: relevance of the inflammatory process.
Front. Immunol. 14:1209926.
doi: 10.3389/fimmu.2023.1209926

Immune response of DNA vaccinated-gilthead seabream (*Sparus aurata*) against LCDV-Sa infection: relevance of the inflammatory process

Rocio Leiva-Rebollo, Juan Gémez-Mata, Dolores Castro, Juan J. Borrego and Alejandro M. Labella*

Department of Microbiology, Faculty of Sciences, University of Malaga, Malaga, Spain

Lymphocystis disease is one of the main viral pathologies affecting cultured gilthead seabream (*Sparus aurata*) in the Mediterranean region. Recently, we have developed a DNA vaccine based on the major capsid protein (MCP) of the *Lymphocystis disease virus 3* (LCDV-Sa). The immune response triggered by either LCDV-Sa infection or vaccination have been previously studied and seem to be highly related to the modulation of the inflammatory and the IFN response. However, a comprehensive evaluation of immune-related gene expression in vaccinated fish after viral infection to identify immunogenes involved in vaccine-induced protection have not been carried out to date. The present study aimed to fulfill this objective by analyzing samples of head-kidney, spleen, intestine, and caudal fin from fish using an OpenArray® platform containing targets related to the immune response of gilthead seabream. The results obtained showed an increase of deregulated genes in the hematopoietic organs between vaccinated and non-vaccinated fish. However, in the intestine and fin, the results showed the opposite trend. The global effect of fish vaccination was a significant decrease ($p<0.05$) of viral replication in groups of fish previously vaccinated, and the expression of the following immune genes related to viral recognition (*tlr9*), humoral and cellular response (*rag1* and *cd48*), inflammation (*csf1r*, *elam*, *il1β*, and *il6*), antiviral response (*isg15*, *mx1*, *mx2*, *mx3*), cell-mediated cytotoxicity (*nccrp1*), and apoptosis (*prf1*). The exclusive modulation of the immune response provoked by the vaccination seems to control the progression of the infection in the experimentally challenged gilthead seabream.

KEYWORDS

LCDV-Sa, innate immune response, inflammation, DNA-vaccine, gilthead seabream, OpenArray®, DEGs

1 Introduction

Self-limited chronic Lymphocystis disease (LCD) is a well-known viral infection in fish that is characterized by the growth of small pearl-like nodules, with papilloma-like appearance, on the skin and fins of affected fish (1, 2). It has an incidence rate that can be as high as 70%, meaning it causes significant economic losses in the aquaculture sector due to the appearance of external lesions and the difficult commercialization of specimens with signs of the disease (3). This viral disease affects a wide variety of freshwater, brackish, and marine fish species, with *Lymphocystis disease virus 3* (LCDV-3, also named LCDV-Sa) being the main causative agent of LCD in gilthead seabream (*Sparus aurata*), and Senegalese sole (*Solea senegalensis*) in the Mediterranean and European South-Atlantic marine aquaculture (4–7). That said, recently LCDV belonging to genotype I, associated with LCD in Northern European countries, has also been reported to affect this fish species in Egypt (8). LCD lesions usually resolve one month after their appearance and are significantly influenced by water temperature. However, an asymptomatic carrier state is frequently detected in both gilthead seabream and Senegalese sole, with the detection of viral DNA and transcripts in a systemic distribution in fish tissues and organs. Asymptomatic infections are frequently detected in these fish species in fish farms, even when no sign of the disease or outbreaks are registered (4).

The genus *Lymphocystivirus* (Family *Iridoviridae*, subfamily *Alphairidovirinae*) has to date comprised four species: *Lymphocystis disease virus 1* (LCDV-1), isolated from European flounder (*Platichthys flesus*) and plaice (*Pleuronectes platessa*) in Europe; *Lymphocystis disease virus 2* (LCDV-2), isolated from Japanese flounder (*Paralichthys olivaceus*) in China; *Lymphocystis disease virus 3* (LCDV-3), isolated from gilthead seabream (*S. aurata*) in Spain; and *Lymphocystis disease virus 4* (LCDV-4), isolated from whitemouth croaker (*Micropogonias furnieri*) in Uruguay (9–13). These viruses have double-stranded DNA genomes, with icosahedral particles ranging from 130 to 300 nm in diameter, and nucleocytoplasmic replication (14).

The immune response of gilthead seabream against LCDV-3 involved in natural or experimental infections has been under-studied to date. In naturally infected fish, an impairment of the innate and adaptive immune response has been described, characterized by the presence of granular cells containing interleukin-1 beta (IL-1β) in perivascular sites and within capillaries, and also surrounding the lymphocysts, but with intense degranulation of acidophilic granulocytes or with no regulation of the transcript, diminished expression of antiviral genes *ifn*, *irf3*, and *mx*, a detriment of macrophages with down-regulation of *csf1r*, and also *mhcIIα*, *tcrα*, and *ighm* genes of antigen presentation cells (APC), and the main receptors of T and B cells, respectively (15, 16). Only a positive role in killing infected cells has been described for non-specific cytotoxic cells (NCCs) by the up-regulation of *nccrp1* (16). Regarding the immune response of gilthead seabream after experimental infection, a partial response of the type I interferon system in head-kidney and intestine and a lack of genes related to the inflammatory process in both organs have also been observed, results that agree with those obtained in naturally infected fish and that could favor the establishment of asymptomatic chronic infection. In addition, *nccrp1* was also up-regulated as it was described previously and postulated the NCCs as the main defensive mechanism of this fish species against this viral pathogen (17).

At present, there are no commercialized treatments or vaccines to prevent LCD, and the unique practices in hatcheries consist of controlling asymptomatic fish and/or food carriers, disinfectant procedures, and stocking density (18, 19). Recently, a plasmid DNA vaccine against LCDV-Sa has been developed by cloning the *mcp* (major capsid protein) gene into pcDNA3.1/NT-GFP-TOPO vector, and the protection conferred by the vaccine and the immune response induced in vaccinated fish was evaluated. The vaccine persists for at least 20 days with systemic distribution and *mcp* transcripts mostly detected in the head-kidney. In contrast to the results described during LCDV-Sa natural or experimental infections, the vaccine induced an inflammatory process by the overexpression of pro-inflammatory genes (*il1β*, *il6*, *casp1*, *ck3*, and *ck10*), and the down-regulation of the anti-inflammatory interleukin 10 (*il10*), also driving the production of specific neutralizing antibodies, conferring a possible protective state against LCDV-Sa. However, the type I interferon genes were not induced after the vaccination trials (20).

The relevance of the inflammatory response to control LCDV infection has been described in Japanese flounder and Senegalese sole as being critical to an effective innate and adaptive immune response to viral infections (21–23). It seems that in LCDV-infected gilthead seabreams, the opposite trend occurs, as inflammation was inhibited and early activation of *il10* was observed, which could be related to the development of persistent infection in this important cultured fish species (17, 24).

The present study aimed to evaluate the immune response of vaccinated-gilthead seabream juveniles after LCDV-Sa infection, analyzing the hematopoietic organs (head-kidney and spleen), the mucosal immunity (intestine), and the target organ/tissue of viral replication (fin) using an OpenArray® platform consisting of 49 genes related to gilthead seabream immune response, with special emphasis on the inflammatory process as a potential marker of protection against LCD in this fish species.

2 Materials and methods

2.1 Fish maintenance

Gilthead seabream specimens (5-10 g weight) were obtained from a fish farm (Predomar SL, Almeria, Spain) and belonged to a single cohort. Fish were acclimated for two weeks before starting the experiment. The fish were maintained under natural photoperiod conditions and fed with a commercial pellet at a rate of 1% of the fish biomass administrated once per day. Water temperature and salinity conditions were 22 ± 1°C and 35–37 g L^{-1}, respectively. During the acclimation stage, 10 fish were randomly analyzed by real-time PCR (qPCR) (25) to confirm a negative result for LCDV.

2.2 Vaccine preparation

The DNA vaccine used in the vaccination trial is based on the viral gene *mcp* (ORF LCDVSa062R, GenBank accession number KX643370.1) cloned into the eukaryotic expression vector pcDNA3.1/NT-GFP-TOPO (named pcDNA-MCP), following the manufacturer`s instructions (Invitrogen, Life Technologies Cop., Carlsbad, CA, USA). *Escherichia coli* One Shot TOP10 cells (Invitrogen) were transformed with pcDNA-MCP, and then the insert was confirmed by PCR and sequenced using primers and protocols previously described (20). For mock-vaccination trials, a re-ligated empty pcDNA3.1/NT-GFP-TOPO plasmid (pcDNA) was used.

E. coli containing pcDNA-MCP or pcDNA plasmids were conserved at -80 °C in LB broth, supplemented with ampicillin (100 μg mL^{-1}), and glycerol (20%, vol/vol) as cryopreservant. The EndoFree Plasmid Mega Kit (Qiagen, Hilden, Germany) was used for plasmid purification, measuring its concentration by spectrophotometry using NanoDrop 1000 (Thermo Scientific, Life Technologies Co., Carlsbad, CA, USA). Purified plasmids were conserved at -20 °C until used.

2.3 Cell culture and viral isolate

SAF-1 cells were cultured in 25 cm^2 flasks (Nunc) (Thermo Scientific) using growth medium (Leibovitz L-15 medium) (Gibco, Life Technologies Co., Carlsbad, CA, USA) supplemented with 1% penicillin-streptomycin (Sigma-Aldrich, Merck, Darmstadt, Germany), 2% L-glutamine (Sigma-Aldrich) and 10% fetal bovine serum (FBS) (Gibco).

The LCDV-Sa isolate used in this study was obtained from skin and fin lesions of diseased gilthead seabream specimens collected from a local farm (Southwestern Spain). Samples were homogenized (20% w/v) in an L-15 medium (Gibco). The cell suspension was sonicated at 40 W for 20 min and centrifuged (1000 x *g*, 5 min, 4 °C). The supernatant recovered was incubated with 10% penicillin-streptomycin overnight at 4 °C and stored at -80 °C. Viral titration was performed by end-point assays using SAF-1 cells grown on a 24-well plate. Cells were inoculated in triplicated with 200 μL per well of the appropriated viral dilution and incubated at 20 °C for 2 hours to ensure adsorption. The virus suspension was then replaced with 1 mL of maintenance medium (L-15 medium with 2% FBS and 1% penicillin-streptomycin). The cells were incubated at 20 °C and maintained for up to 14 days to observe CPE. The 50% cell culture infectious dose ($TCID_{50}$) values were determined using the Reed and Muench method (26).

2.4 Experimental design

Gilthead seabream specimens (5 g mean weight) were separated into three experimental conditions and maintained in 100 L-capacity aquariums with independent water recirculation systems: 30 vaccinated fish (0.1 μg pcDNA-MCP/g fish dose), 30 mock-vaccinated specimens (same dose using pcDNA), and 60 fish were used as a control group (PBS, 100 μL). Animals were anesthetized with MS-222 (50 mg L^{-1}) (Sigma-Aldrich) prior to the experiment being performed by intramuscular injection. Thirty days post-vaccination, the control group was divided into two groups, one injected with 100 μL of L-15 medium (negative control group), and the other one inoculated with the virus, establishing the non-vaccinated group. Vaccinated, mock-vaccinated, and non-vaccinated groups were inoculated with 100 μL of LCDV-Sa stock diluted in L-15 (10^6 $TCID_{50}$ per fish). Six fish per group were randomly selected at 24, 48, and 72 hours post-inoculation (pi). Prior to sampling, all fish were euthanized by MS-222 overdose (400 mg L^{-1}). Samples from the caudal fin, intestine, head-kidney, and spleen were aseptically collected and stored at -80 °C until used.

All procedures were carried out under the Guidelines of the European Union Council (Directive 2010/63/EU) and the Spanish directive (RD 53/2013) for the protection of animals used in scientific experiments and authorized by the Spanish authorities for the regulation of animal care and experimentation (registration number 10-06-2016-102).

2.5 DNA-RNA extractions and cDNA synthesis

Samples of the selected organs were homogenized with Tri Reagent® (Sigma-Aldrich), suspending the tissue (50-100 mg) in 1 mL and using the MM400 (Retsch, Haan, Germany) homogenizer. Afterward, 100 μL of 1-bromo-3-chloropropane (AppliChem, Darmstadt, Germany) was added and samples were centrifuged at 12.000 x *g* at 4 °C for 5 min. The aqueous phase was recovered and an equal volume of 75% ethanol was added. RNA extraction was carried out using the RNeasy Mini Kit (Qiagen) following the manufacturer's instructions. RNA samples were quantified by spectrophotometry (NanoDrop 1000) ensuring their quality and integrity.

cDNA synthesis was carried out using MicroAmp Optical 96-well reaction plates (Applied Biosystems, Life Technologies Co., Carlsbad, CA, USA) and the High-Capacity cDNA Reverse Transcription Kit (Applied Biosystems). Each reaction contained 2 μg RNA, 2 μL of 10X RT Buffer, 2 μL of 10X RT Random Primers, 1 μL of 25X dNTPs, 1 μL of MultiScribe™ Reverse Transcriptase and 4 μL of RNase-free water. The synthesis profile was 10 min at 25 °C, 2 hours at 37 °C, 5 min at 85 °C, and during the final step, it was 4 °C.

DNA extractions were carried out using the E.Z.N.A. Tissue DNA Kit (Omega Bio-Tek Inc., Norcross, GA, USA) following the manufacturer's instructions. DNA samples were suspended in DNase-free buffer, quantified spectrophotometrically, and stored at -20 °C until used.

2.6 LCDV-Sa detection and gene expression

Viral DNA quantification was carried out from caudal fin samples by qPCR in triplicate according to the procedure previously described (20), targeting a viral structural protein gene

alternative to the *mcp* gene contained in the vaccine. The putative myristoylated membrane protein (*mmp*) gene (ORF LCDVSa074R, GenBank accession number KX643370.1) was used for qPCR assays. Amplification was performed using a 20-μL final volume reaction containing 12.5 μL of FastStart Essential DNA Green Master (Roche Diagnostics), 2 μL of each primer (10 pmol μL^{-1}) (Table 1), and 200 ng of DNA. PCR amplifications were performed in a LighCycler® 96 Instrument (Roche Diagnostics). The amplification profile was: initial denaturation at 95 °C for 10 min, followed by 40 cycles at 95 °C for 10 s, 60 °C for 10 s, and 72 °C for 10 s. Nonspecific amplification products were discarded by dissociation curve analyses following the thermal profile: 95 °C for 10 s, 65 °C for 60 s, and 97 °C for 1 s. LCDV-Sa DNA copy number was calculated by interpolation on a standard curve (20), and viral loads were expressed as *mmp* copies per microgram of DNA.

LCDV-Sa expression in caudal fin samples was quantified by real-time PCR from viral *mmp*. Viral RNA was extracted using the E.Z.N.A. total RNA kit, treated with RNase-free DNase I (Roche Diagnostics), and reverse-transcribed with the Transcription First Strand cDNA Synthesis Kit (Roche Diagnostics) following the manufacturer's instructions and stored at -20 °C until used. Amplification was performed using a 20-μL final volume reaction according to the above-described conditions.

2.7 Gilthead seabream immune response after LCDV-Sa infection

To analyse the immune response in gilthead seabream after LCDV-Sa infection, qPCR reactions based on TaqMan™ probes were performed using an OpenArray® platform (ThermoFisher Scientific). The array includes 49 target genes, which were included based on their important role in the fish immune response against viral infections and, in some of them, for their activity against LCDV-Sa infections (17). There were viral recognition-related genes (*tlr9, tlr5*, *cd209)*, inflammatory-related and cytokine genes (*c3*, *il1β, il6, il8, il10*, *tnfα, ck3, ck7, ck8, ck10, cox2, csf1r, ncf4, ccr3*, and *elam*), regulation of innate and adaptive immune response (*clec10a*, *tgfβ1*), antigen processing and presentation (*mhc1α*, *mhcIIα*, *iclp* and *mrc1*), type I IFN trigger genes and genes involved in IFN-1-dependent immune response (*irf1, irf3, irf9, ifn, pkr, isg15, mx1, mx2, mx3* and *ifi30)*, nonspecific cytotoxic cell receptor (*nccrp1)*, proteolysis process (*ctsb*), apoptotic process *(casp1, lgals1, perp, prf1)*, molecular stress response (*hsp70* and *hsp90*) and genes involved in humoral and cellular immune response (*tcrα, tcrβ, ighm, rag1, ilc, cd48* and *cd276*). Four genes have been selected as endogenous (*rps18, ub, actβ*, and *ef1α*). Primers and probes were designed using the Custom TaqMan™ Assay Design Tool with the option TaqMan™ Gene Expression Assays (Life Technologies). Selected transcripts, assay ID, assay sequences, primers, and TaqMan™ probes (Reporter dye FAM) and 3' non-fluorescent quencher (NFQ) are indicated in Supplementary Table S1.

Quantitative PCRs were performed in the OpenArray® system QuantStudio 12K Flex Real-Time PCR System (Applied Biosystems), sited in the Research Central Service of the University of Cordoba (Spain), using the TaqMan™ OpenArray® Real-Time PCR Master Mix kit (Applied Biosystems). Samples were loaded in triplicate into OpenArray® plates. For gene expression analysis, Ct values were obtained using the Thermo Fisher Connect™ (ThermoFisher Scientific) online application, and the Relative Quantification (RQ) software. The setup was adjusted with options Benjamini-Hochberg deactivated, maximum Ct was set up at 28, AMP score was activated and HIGHSD was changed to 0.25. Fold change (FC) values were obtained by the $2^{-\Delta\Delta Ct}$ method (27). Values were normalized with endogenous gene *rps18*, which showed a more stable expression by OpenArray®, according to their score values, which were obtained using the Applied Biosystems™ Relative Quantitation Analysis Module (ThermoFisher cloud dashboard), and indicate how the Ct values for a specific endogenous gene varied between samples compared to the other genes used as endogenous. Samples from the control group (non-infected) were used as the calibrator. To identify the differentially expressed genes (DEGs) involved in gilthead seabream immune response against LCDV-Sa infection, genes with $\log_2$ fold change < -0.5 (down-regulated) or > 0.5 (up-regulated) and $p<0.05$ were considered DEGs. A cluster analysis of the samples, based on the $\log_2$ fold change of the host genes, was conducted using the Expression Heat Map option on the web server Heatmap-per (http://www2.heatmapper.ca/) (28) with Euclidean as distance measurement method, and complete linkage as a clustering method. In addition, the expressed genes were also clustered using the same parameters. The Venn diagram method was used for the comparative analysis of DEG datasets obtained in each experimental group and the timepoint analyzed after the infection with the virus (29).

2.8 Statistical analysis

The qPCR data were log-transformed to get normality and homogeneity of variance, and the normality of the data was analyzed using a Shapiro-Wilk test. To determine significant differences in viral load or gene expression levels between groups and/or time points, a one-way ANOVA followed by Fisher's LSD test was used. Differences were considered significant when $p<0.05$. The statistical tests were performed using GraphPad Prism version 8.0.0 for Windows, GraphPad Software, Sand Diego, California USA, www.graphpad.com.

TABLE 1 Primers used for gene expression analysis by real-time PCR.

Abbreviation	Gene name	Sequence (5'-3')	Amplicon size (bp)	Reference
mmp	Myristoylated membrane protein	F: TTGCCCCACTTCCTATTGTC	122	(20)
		R: CCGGTTTTTCAGACTTGGAA		

3 Results

3.1 Viral load and gene expression in gilthead seabream

To study the course of LCDV-Sa infection in gilthead seabream, viral load and *mmp* gene expression in caudal fin samples were analyzed by qPCR at 24, 48, and 72 hours pi for vaccinated, mock-vaccinated, and non-vaccinated animals inoculated with the virus by intramuscular injection (Figure 1). No signs of LCD were observed in any group at any time analyzed. LCDV-Sa was detected in all samples and timepoints in the infected groups, whereas no amplification was registered in the control group (L-15). Viral load in caudal fin samples at different times pi is shown in Figure 1A. Through the experiment, significant differences in viral load were observed between the non-vaccinated and vaccinated fish at all timepoints ($1.1 \pm 0.69 \times 10^3$, $1.97 \pm 1.20 \times 10^3$, $3.15 \pm 1.49 \times 10^2$, and $1.24 \pm 0.26 \times 10^2$, $4.84 \pm 0.65 \times 10^1$, $1.76 \pm 0.52 \times 10^1$ copies of viral DNA μg^{-1} of tissue, respectively) ($p<0.05$ at 24- and 48-hours pi, $p<0.01$ at 72 hours pi). Regarding mock-vaccinated animals, significant differences were observed with the vaccinated animals at 48- and 72-hours pi ($p<0.05$) ($2.97 \pm 1.22 \times 10^2$ and $9.83 \pm 2.97 \times 10^1$ copies of viral DNA μg^{-1} of tissue, respectively), and with the non-vaccinated animals only at 48 hours pi ($p<0.05$) where the highest viral load was detected. In all cases, the viral load in the vaccinated group had the lowest values at any timepoint analyzed, and also significant differences were observed within the group from 24 to 48 hours pi ($p<0.0113$) and 24 to 72 hours pi ($p<0.0008$), with a constant decrease in the viral load. The *mmp* gene expression in caudal fin samples is shown in Figure 1B. Significant differences were detected between vaccinated fish and the other groups at 48 and 72 hours pi ($p<0.0001$ and $p<0.05$ for mock-vaccinated, and $p<0.05$ for non-vaccinated animals, respectively). No expression of the *mmp* gene was detected in the vaccinated animals at 24 hours pi.

3.2 Immune response of gilthead seabream infected with LCDV-Sa

In the present study, we evaluated the immune response in gilthead seabream juveniles after infection with LCDV-Sa using an OpenArray® carrying 49 different assays related to the immune system. Only 4 out of the 49 genes were not differentially expressed during the experiment in any group; those genes were involved in the inflammatory process (*c3* and *ck7*), the interferon response (*ifn*), and antigen processing and presentation (*mhcIα*). Differentially expressed genes (DEGs) were analyzed in 4 different organs (head-kidney, spleen, intestine, and caudal fin) at 24, 48, and 72 hours pi. Regarding vaccinated animals, the number of DEGs detected was higher in the head-kidney and intestine (26 and 27, respectively) than in the spleen and caudal fin (14 and 16, respectively). A similar profile was detected in mock-vaccinated animals being 21 and 19 DEGs detected in the head-kidney and intestine, and 13 and 14 in the spleen and caudal fin. However, in the non-vaccinated group, a different profile of DEGs was detected, with the intestine and caudal fin being the organs where the highest number of DEGs was observed (42 and 28, respectively). Moreover, in the hematopoietic organs, the number of DEGs detected was lower than that observed in vaccinated and mock-vaccinated animals (18 and 9, for head-kidney and spleen) (Figure 2).

Attending to the type of gene regulation, down-regulation of genes was the major event in the head-kidney, intestine, and caudal fin for all the experimental groups analyzed (66.7, 66.7, and 78.6%, respectively in non-vaccinated animals) (57.7, 77.8, and 68.7%, respectively in vaccinated animals) (52.4, 94.7, and 64.3%, respectively in mock-vaccinated animals), with the exception of spleens where a different trend was detected with major up-regulation of genes (88.9% in non-vaccinated animals) (85.7% in vaccinated animals) (92.3% in mock-vaccinated animals) (Table 2). Regarding the tendency of gene regulation between experimental groups, organs, and timepoints analyzed, there was a change of regulation observed exclusively in vaccinated animals compared to the other groups, registered in the intestine, head-kidney, and caudal fin at 24, 48- and 72-hours pi, respectively, shifting from down- to up-regulation of DEGs. In this experimental group, the opposite trend (up- to down-regulation) was also denoted in the caudal fin and intestine at 24 and 72 hours pi with respect to non-vaccinated animals, but in this case, these profiles of regulation were also identified in the mock-vaccinated group (Table 2). Specific genes that were differentially expressed in the organs analyzed are discussed in detail below. Fold change (FC) values will be shown as Log_2 FC to clearly explain the type of gene regulation (negative values for down-regulation and positive values for up-regulation).

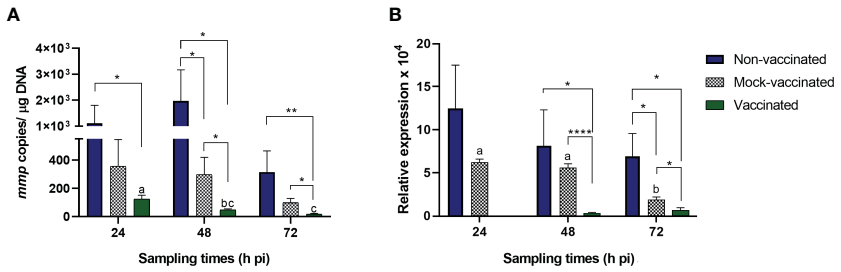

FIGURE 1
(A) Viral load (mmp copies/µg DNA) and **(B)** *mmp* gene relative expression in LCDV-Sa-infected gilthead seabreams analyzed by qPCR. Data are expressed as mean ± SEM (n = 6). Asterisks denote significant differences between experimental groups at a timepoint (*$p<0.05$, **$p<0.01$, ****$p<0.0001$). Letters establish significant differences through timepoint analyzed in a specific group.

10.3389/fimmu.2023.1209926

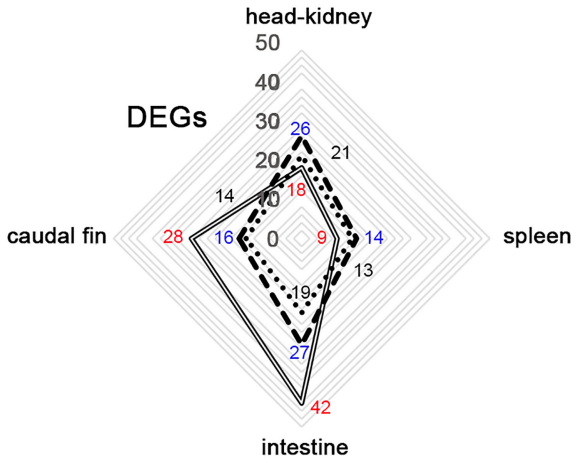

FIGURE 2
Distribution of differential expressed genes (DEGs) between organs from gilthead seabream infected with LCDV-Sa in non-vaccinated (full-line), vaccinated (segmented-line), and mock-vaccinated (dotted-line) animals through the whole experiment. Number of DEGs detected in the different experimental groups: in blue (vaccinated), black (Mock-vaccinated), and red (non-vaccinated).

3.2.1 DEGs in head-kidney

In the head-kidney samples of infected gilthead seabreams, 33 DEGs were detected between experimental groups and timepoints analyzed (Figure 3A). Regarding samples, the different experimental groups clustered to the timepoint of analysis, showing a general change of gene regulation from 24 h to 48- and 72-hours pi (down- to up-regulation of genes). The interferon regulatory factor 9 (*irf9*) gene had a strong modulation in this organ (FC of -2.62 in mock-vaccinated fish at 48 hours pi to 2.92 in non-vaccinated animals at 24 hours pi) (Supplementary Tables S2-4).

In non-vaccinated animals at 24 hours pi 9 DEGs were detected, all down-regulated and related to different processes of the immune response as viral recognition (*tlr9* with FC of -1.60), regulation of innate and adaptive immune response (*tgfβ1* with FC of -0.71), the type I interferon system (*irf1* with FC of -0.58), inflammation (*ck3* and *ck8*, with FC values of -1.60 and -1.18, respectively), antigen processing and presentation (*iclp* with FC of -0.86), apoptosis (*casp1* and *lgals1*, with FC values of -0.60 and -2.25, respectively), and molecular stress response (*hsp90* with FC of -0.51). On the other hand, only 3 DEGs were up-regulated and related to viral recognition (*tlr5* with FC of 1.05) and the interferon response (*irf9* and *mx2*, with FC values of 2.92 and 0.58, respectively). At 48 hours pi, the down-regulation of genes continued being predominant, with the detection of 3 DEGs related to inflammation (*ck3* with FC of -0.985) and cell-mediated response (*tcrβ* and *cd276* with FC values of -1.32 and -0.68, respectively). When infection progressed, up-regulation of the following genes were detected exclusively in *isg15* (FC of 0.93), *rag1* (FC of 1.21), and *perp* (FC of 0.6), indicating a change of tendency and slight promotion of antiviral response (Supplementary Table S2).

Regarding vaccinated animals, at 24 hours pi a major down-regulation of genes was also recorded related to viral recognition (*tlr9* and *cd209* with FC values of -1.32 and -0.97, respectively), the regulation of innate and adaptive immune response (*tgfβ1* with FC of -0.74), type I interferon system (*irf1* and *ifi30* with FC of -0.74 and -0.92, respectively), inflammatory process (*ck3*, *ccr3*, *ck8* and *csf1r* with FC of -2.12, -1.15, -0.94, and -0.6, respectively), antigen processing and presentation (*mrc1* with FC of -1.18), cellular-mediated response (*tcrα* and *cd48* with FC values of -0.54 and -0.86, respectively), proteolysis and apoptosis (*ctsb* and *lgals1* with FC values of -0.79 and -1.89, respectively), and stress response (*hsp90* with FC of -0.51). However, the recombination-activating gene 1 (*rag1* with FC of 0.93) was the only gene up-regulated at this timepoint indicating an early cell-mediated response in comparison with the non-vaccinated animals (Supplementary Table S3). At this timepoint, 7 DEGs were exclusively detected in this group (*cd209*, *ifi30*, *csf1r*, *tcrα*, *cd48*, *ctsb*, and *rag1*). At 48 hours pi, a clear change of expression profile was recorded with up-regulation of genes related to the regulation of the innate and adaptive immune response (*clec10a* with FC of 1.48), inflammation (*il1β* and *il6* with FC values of 2.05 and 0.86, respectively), and cell-mediated response (*cd48* and *nccrp1* with FC values of 0.71 and 1.12, respectively) (Supplementary Table S3). Comparatively, the non-vaccinated animals showed a stronger antiviral response mediated by the interferon-related genes at 72 hours pi with the detection of *isg15*, *irf3*, *mx1*, *mx2*, and *mx3*, all of which were up-regulated with FC values of 0.86, 0.72, 1.92, 1.89, and 2.01, respectively (Figure 4A1-3, Table 3, Supplementary Tables S2-3).

Regarding the mock-vaccinated group, DEGs were mainly shared with the other experimental groups at 24- and 72-hours pi. However, the exclusive down-regulation of genes related to viral

TABLE 2 Differentially expressed genes (DEGs) detected in gilthead seabream post-infection (pi) with LCDV-Sa.

Experimental group	DEGs	Head-kidney			Spleen			Intestine			Caudal-fin		
		24h	48h	72h	24h	48h	72h	24h	48h	72h	24h	48h	72h
Non-vaccinated	Up-regulated	3	0	3	5	1	2	5	0	9	6	0	0
	Down-regulated	9	3	0	1	0	0	9	15	4	1	14	7
Vaccinated	Up-regulated	1	5	5	4	3	5	4	1	1	0	1	4
	Down-regulated	15	0	0	2	0	0	3	15	3	6	4	1
Mock-vaccinated	Up-regulated	2	0	8	0	3	9	1	0	0	2	3	0
	Down-regulated	8	2	1	1	0	0	2	12	4	3	5	1

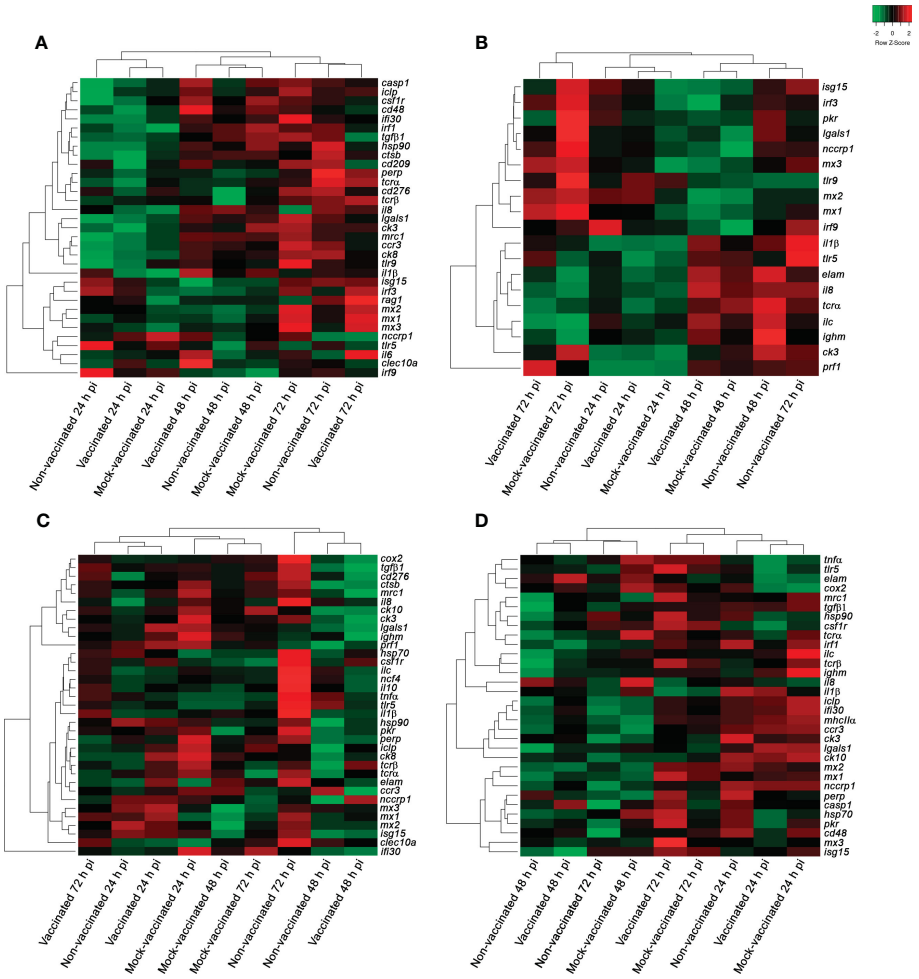

FIGURE 3
Hierarchical clustering analysis of samples from non-vaccinated, vaccinated, and mock-vaccinated LCDV-Sa infected gilthead seabreams at 24, 48, and 72 h pi. **(A)** Head-kidney, **(B)** spleen, **(C)** intestine, and **(D)** caudal fin samples. Green and red colors indicate down- and up-regulation of genes according to the scale shown [Log_2 (FC)].

recognition (*tlr9* with FC of -0.775 at 48 hours pi), inflammation (*il8* with FC values of -1.25 and -1.18 at 24- and 72-hours pi), and regulation of interferon response (*irf9* with FC of -2.62 at 48 hours pi) was detected. In addition, up-regulation of genes related to interferon induced proteins (*ifi30* with FC of 1.07), non-specific cell-mediated response (*nccrp1* with FC of 1.12), and apoptosis (*lgals1* with FC of 0.91) were detected at 72 hours pi (Figure 4A1-3, Table 3, Supplementary Tables S-4).

3.2.2 DEGs in spleen

In spleen samples, 19 DEGs were detected between experimental groups and the timepoints analyzed (Figure 3B). In this organ, the lowest modulation of differential gene expression was detected in the entire experiment. Regarding samples, three clusters of gene expression profiles were obtained, where all the samples of the different experimental groups clustered together at 24 hours pi. However, a clear distinction between groups was obtained at 48- and 72-hours pi, establishing a separate cluster for vaccinated and mock-vaccinated fish at the last timepoint of analysis (Figure 3B). The chemokine 3 (*ck3*) gene registered the lowest fold change value (-1.24 in mock-vaccinated fish at 24 hours pi) in this organ. On the contrary, the perforin 1 (*prf1*) gene had strong up-regulation in the vaccinated group (6.28 at 72 hours pi) (Supplementary Tables S5-7).

In non-vaccinated animals, a higher antiviral interferon-related response was only detected early on in the infection (24 hours pi), with the up-regulation of *irf9*, *pkr*, *isg15*, *mx1*, and *mx2* (FC values of 2.15, 0.81, 0.89, 1.29, and 1.74, respectively) in comparison to vaccinated and mock-vaccinated groups. In vaccinated fish, only *mx1* and *mx2* were up-regulated at 24 hours pi (FC values of 1.18 and 1.82, respectively). However, later on during the infection (72 hours pi) the three Mx were detected (FC values of 2.62, 2.08, and 1.65, respectively), indicating sustained interferon response during the infection. In contrast, in mock-vaccinated animals, the interferon pathway was only up-regulated at 72 hours pi but with a more complete gene profile (*irf3*, *pkr*, *mx1*, *mx2*, and *mx3*, with FC values of 1.14, 1.55, 3.07, 2.38, and 1.83) (Figure B1-3, Table 3, Supplementary Tables S5-7).

Regarding inflammation, early down-regulation of genes was observed in all the groups, with chemokine 3 (*ck3*) most commonly

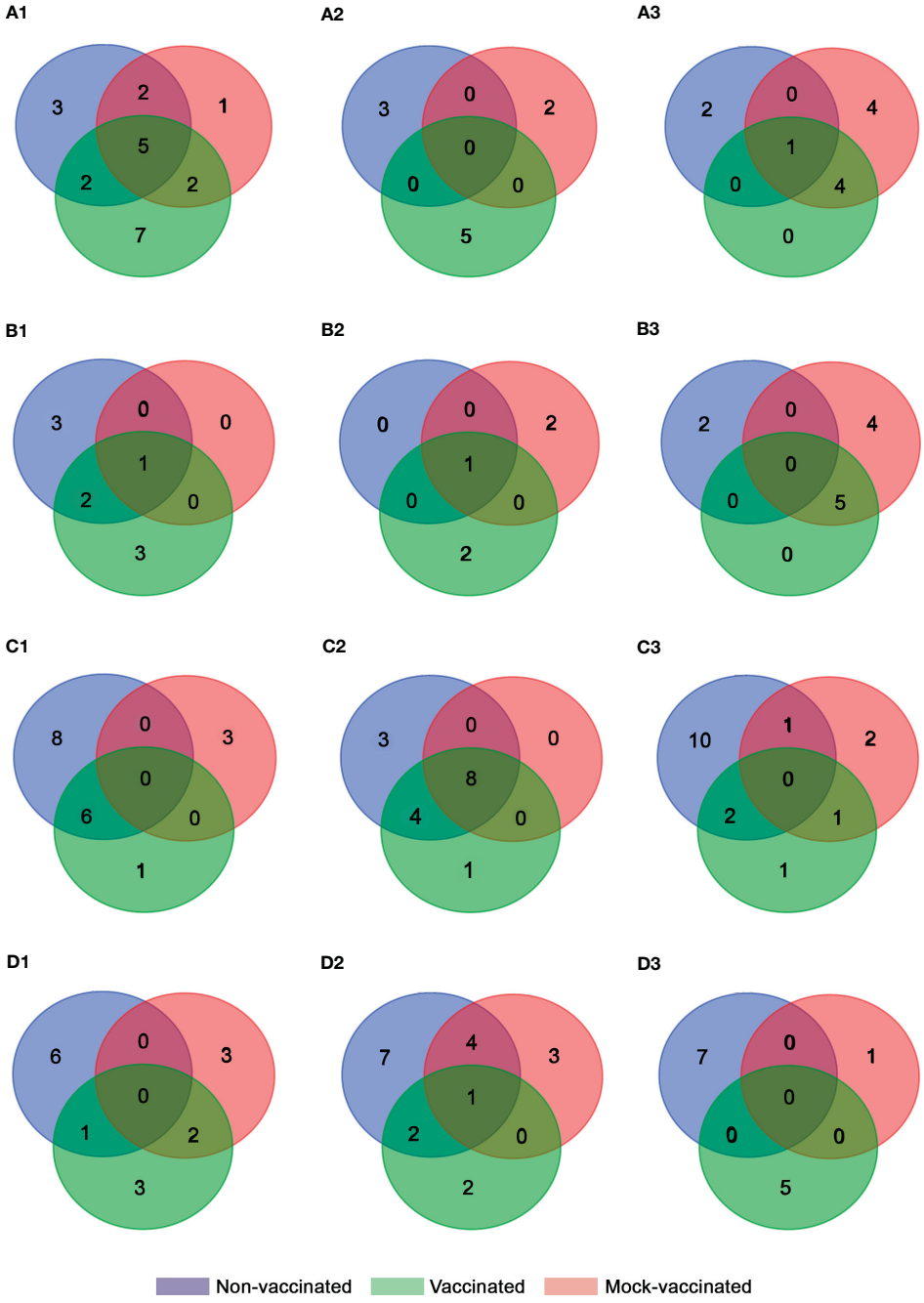

FIGURE 4
Venn diagram analysis of DEGs obtained for each experimental group from **(A)** head-kidney, **(B)** spleen, **(C)** intestine, and **(D)** caudal fin samples at (1) 24 (2), 48, and (3) 72 h pi.

detected (Figure 4B1). Only in vaccinated animals, the endothelial leukocyte adhesion molecule (*elam*) was initially down-regulated (FC of -0.85 at 24 hours pi). However, at 48 hours pi the modulation of this gene changed and was up-regulated in these fish (FC of 1.71), promoting inflammation. In mock-vaccinated fish, the promotion of inflammation occurred at the same timepoint as in vaccinated fish with the up-regulation of the interleukin 8 (*il8*) gene (FC of 0.93). This is contrary to the pro-inflammatory response in non-vaccinated fish, which was not detected until 72 hours pi mediated by the up-regulation of interleukin 1 subunit beta (*il1β*) gene (FC of 2.06) (Table 3, Supplementary Tables S5-7).

In addition, in non-vaccinated animals, genes related to the humoral response (*ighm* with FC of 1.06) and viral recognition (*tlr5* with FC of 1.94) were detected at 48- and 72-hours pi, respectively. Interestingly, in vaccinated and mock-vaccinated animals, the toll-like receptor 9 (*tlr9*) was the nucleic acid sensor up-regulated, with an earlier modulation in vaccinated fish (FC of 1.03 at 24 hours pi) compared to the mock group (FC of 1.78 at 72 hours pi). Non-

10.3389/fimmu.2023.1209926

TABLE 3 DEGs commonly or exclusively detected between non-vaccinated, vaccinated, and mock-vaccinated fish after infection with LCDV-Sa.

Shared DEGs	24 h pi	48 h pi	72 h pi
Head-kidney			
Non-vaccinated, vaccinated, mock-vaccinated	*tgfβ1, irf1, ck3, ck8, lgals1*	ND[a]	*isg15*
Non-vaccinated, vaccinated	*tlr9, hsp90*	ND	ND
Non-vaccinated, mock-vaccinated	*tlr5, irf9*	ND	ND
Vaccinated, mock-vaccinated	*ccr3, mrc1*	ND	*irf3, mx1, mx2, mx3*
Non-vaccinated	*mx2, iclp, casp1*	*ck3, tcrβ, cd276*	*rag1, perp*
Vaccinated	*cd209, ifi30, csf1r, tcrα, rag1, cd48, ctsb*	*clec10a, il1β, il6, cd48, nccrp1*	ND
Mock-vaccinated	*il8*	*tlr9, irf9*	*ifi30, il8, nccrp1, lgals1*
Spleen			
Non-vaccinated, vaccinated, mock-vaccinated	*ck3*	*ighm*	ND
Non-vaccinated, vaccinated	*mx1, mx2*	ND	ND
Vaccinated, mock-vaccinated	ND	ND	*mx1, mx2, mx3, nccrp1, prf1*
Non-vaccinated	*irf9, pkr, isg15*	ND	*tlr5, il1β*
Vaccinated	*tlr9, elam, nccrp1*	*elam, ilc*	ND
Mock-vaccinated	ND	*il8, tcrα*	*tlr9, irf3, pkr, lgals1*
Intestine			
Non-vaccinated, vaccinated, mock-vaccinated	ND	*tgfβ1, ck3, ck10, mrc1, cd276, ctsb, lgals1, hsp90*	ND
Non-vaccinated, vaccinated	*isg15, mx1, ifi30, il8, ck3, nccrp1*	*ifi30, ck8, nccrp1, prf1*	*ifi30, il1β,*
Non-vaccinated, mock-vaccinated	ND	ND	*lgals1*
Vaccinated, mock-vaccinated	ND	ND	*il8*
Non-vaccinated	*tgfβ1, mx2, mx3, ccr3, ck10, mrc1, cd276, lgals1*	*iclp, tcrα, tcrβ,*	*tlr5, clec10a, isg15, il10, ck10, csf1r, ncf4, ilc, prf1, hsp70*
Vaccinated	*csf1r*	*perp*	*ck3*
Mock-vaccinated	*tnfα, elam, perp*	ND	*ccr3, ighm*
Caudal fin			
Non-vaccinated, vaccinated, mock-vaccinated	ND	*mhcIIα*	ND
Non-vaccinated, vaccinated	*tcrβ,*	*tcrβ, ilc*	ND
Non-vaccinated, mock-vaccinated	ND	*ifi30, ccr3, ck10, iclp*	ND
Vaccinated, mock-vaccinated	*cox2, elam,*	ND	ND
Non-vaccinated	*pkr, il1β, cd48, nccrp1, casp1, perp*	*tgfβ1, csf1r, mrc1, tcrα, ighm, lgals1, hsp90*	*tlr5, ifi30, ck3, ccr3, ck10, mhcIIα, iclp*
Vaccinated	*tnfα, csf1r, tcrα*	*irf1, casp1*	*isg15, mx1, mx2, mx3, il8*
Mock-vaccinated	*tlr5, ccr3, ck10,*	*isg15, il8, hsp70*	*ilc*

[a]ND, non-detected.

specific cell mediated response, humoral immune markers, and apoptosis were also promoted in these fish (vaccinated and mock), with the up-regulation gene profile of *ighm* and *ilc* (FC values of 1.34 and 1.25 at 48 hours pi), *nccrp1* (FC values of 0.7 and 0.87 at 24 and 72 hours pi, respectively), and strong modulation of *prf1* (FC of 6.28 at 72 hours pi) in vaccinated fish, and *tcrα* and *ighm* (FC values of 0.86 and 0.94 at 48 hours pi), *nccrp1* (FC of 1.42 at 72 hours pi), *lgals1* and *prf1* (FC values of 1.4 and 2.38 at 72 hours pi,

respectively) in the mock animals (Table 3, Supplementary Tables S5-7).

3.2.3 DEGs in the intestine

In intestine samples 35 DEGs were detected between experimental groups and the timepoints analyzed (Figure 3C). In this organ, samples of the different experimental groups constituted 3 clusters, where all the samples of the mock-vaccinated fish clustered together at the three timepoints analyzed. Although gene expression profiles of samples from vaccinated and non-vaccinated fish were more similar, establishing two clusters at 24- and 48-hours pi, a clear distinction of gene profiles between them was observed at 72 hours pi (Figure 3C). The genes with strong modulation in this organ were the interferon-gamma-inducible protein 30 (*ifi30*) gene (-5.44 at 48 h pi in vaccinated fish) and interleukine-1β (*il1β*) (2.41 at 72 hours pi in non-vaccinated fish) (Supplementary Tables S8-10).

In this organ modulation of gene expression was higher in the non-vaccinated animals (Figure 4C1-3). Regarding antiviral response mediated by type I interferon, a higher number of genes were up-regulated in this group (*isg15* with FC values of 0.94 and 0.97 at 24 and 72 hours pi, respectively, and *mx1*, *mx2*, and *mx3* with FC values of 1.38, 1.42, and 1.11 at 24 hours pi) compared to the vaccinated fish (*isg15* and *mx1* with FC values of 0.78 and 1.87 at 24 hours pi). Interestingly, in both groups, a strong down-regulation of *ifi30* was detected throughout the experiment. Contrary to this, in mock-vaccinated animals, no up-regulation of genes related to this pathway was observed. Moreover, a down-regulation of *pkr*, *mx2*, and *mx3* was registered at 48 hours pi pointing out an inhibited antiviral response in this fish group (FC values of -0.55, -1.59, and -0.98, respectively) (Supplementary Tables S8-10).

Regarding inflammatory process, major down-regulation of genes was detected (*il8*, *ck3*, *ck8*, and *ck10* in the non-vaccinated; *il8*, *ck3*, *ccr3*, *ck10*, and *cox2* in the vaccinated fish; *il8*, *tnfα*, *ck3*, *ccr3*, *ck10*, and *elam* in the mock-vaccinated group) (Table 3), although at 72 hours pi in non-vaccinated animals up-regulation of *il1β*, *il10*, *csf1r*, and *ncf4* (FC values of 2.41, 1.48, 0.96, and 1.04, respectively) was registered. Interestingly, in vaccinated fish, the detection of *csf1r* (FC of 0.58), related to macrophages and inflammatory process, was also detected but early on in the infection (24 hours pi). In addition, *il1β* was also up-regulated in vaccinated fish at the same timepoint as the non-vaccinated fish (FC of 1.06) (Supplementary Tables S8-10). No gene related to inflammation was up-regulated in the mock-vaccinated fish in this organ.

In non-vaccinated animals, an exclusive up-regulation of *tlr5* (FC of 2.17) was detected at 72 hours pi, as described previously in the spleen samples. At the same timepoint genes coding for c-type lectin 10a (*clec10a*), related to modulation of the immune response, the humoral marker *ilc*, and *hsp70*, related to molecular stress response, were also up-regulated (FC values of 2.3, 1.28, and 0.69, respectively). Regarding non-specific cellular-mediated response, early on in the infection, the up-regulation of *nccrp1* (FC of 0.59) was observed. However, the expression of the *nccrp1* was inhibited later on (FC of -0.84) at 48 hours pi. This profile of expression changes in the vaccinated fish where the up-regulation remained from 24 to 48 hours pi (FC values of 0.58 and 0.82, respectively). In contrast, no modulation of this gene was observed in the mock group. However, an exclusive up-regulation of *perp*, related to cellular apoptosis, was detected at 24 hours pi (FC of 0.7) in mock-vaccinated fish (Supplementary Tables S8-10).

3.2.4 DEGs in caudal fin

In caudal fin samples, 32 DEGs were identified through the experiment. The clustering analysis of the different samples showed the same profile that was obtained in the spleen, with samples of all experimental groups establishing a cluster at 24 hours pi, and the differentiation of samples for the vaccinated and mock-vaccinated fish at 72 hours pi (Figure 3D). Chemokine 10 (*ck10*) gene registered the lowest fold change value in this organ in non-vaccinated animals (-1.88 at 72 hours pi). In contrast, the MX dynamin Like GTPase 3 (*mx3*) gene had the highest fold change value in vaccinated fish (2.28 at 72 hours pi) (Supplementary Tables S11-13).

In non-vaccinated animals, the up-regulation of genes related to type I IFN (*pkr*, with FC of 0.5), inflammation (*il1β*, with FC of 0.95), B-cell markers (*cd48*, with FC of 0.54), non-specific cell-mediated response (*nccrp1*, with FC of 1.09), and cellular apoptosis (*casp1* and *perp*, with FC values of 0.56 and 0.7, respectively) were detected at 24 hours pi. In ulterior times post-infection, all DEGs were down-regulated in this fish group (Figure 4D1-3, Table 3, Supplementary Table S11). In contrast, in vaccinated fish a clearly different profile of expression was observed, with major down-regulation at 24 hours pi. Regarding type I IFN response, the exclusive up-regulation of *isg15*, *mx1*, *mx2*, and *mx3* (FC values of 1.27, 1.06, 1.03, and 2.28, respectively) at 72 hours pi was remarkable. In addition, cellular apoptosis was mediated by *casp1* up-regulation, which occurred in non-vaccinated fish, but at a later point in time (48 hours pi) (Figure 4D1-3, Table 3, Supplementary Table S12). The immune response studied in the mock group revealed a different profile of expression compared to the other groups and was characterized by the induction of *isg15* (FC of 0.81), and the pro-inflammatory interleukin 8 (*il8*, FC of 0.97) at 48 hours pi. Chemokine 3 receptor (*ccr3*) and chemokine 10 (*ck10*) were also up-regulated (FC values of 0.6 and 1.02, respectively) at 24 hours pi; however at 48 hours pi their tendency of expression changed to down-regulation (FC values of -1.58 and-1.41, respectively). At the same timepoint, *hsp70*, which is related to the stress response, was also induced (FC of 0.53) in this group but only where the expression of this gene was modulated during the experiment in caudal fin samples (Figure 4D1-3, Table 3, Supplementary Table S13).

4 Discussion

The study demonstrated that the DNA vaccine (pcDNA-MCP) when administrated to gilthead seabream juveniles one-month before experimental challenge, was able to significantly reduce

($p<0.05$) the viral load and expression of LCDV-Sa in the target site of viral replication (caudal fin) in vaccinated fish compared to that of fish who were not vaccinated or inoculated with an empty plasmid (pcDNA). Both, vaccine and viral inoculation were performed by intramuscular injection. The efficacy of this route of administration was previously reported for vaccine and viral dissemination in fish species (17, 20, 30). Other studies have verified the remarkable efficacy of protection against viral diseases for DNA vaccines administered intramuscularly (31–33).

The immune response of gilthead seabream against LCDV-Sa infection and after a vaccination trial with the pcDNA-MCP has been previously described in head-kidney and intestine samples (17, 20). The profile of the gene expression was different in the infection and vaccination trial groups. Inhibition of the inflammatory process, antigen processing and presentation, humoral and cellular response and a slight activation of the type I interferon route characterized the host response against the viral infection, which was proposed as the cause of LCDV-Sa chronic infection in aquaculture facilities (17). By contrast, for the vaccination trial, an up-regulation of genes related to inflammation was postulated as being responsible for the reduction of viral replication, acting as a marker of vaccine protection efficacy (20). In the present study, we evaluated the immune response in infected-gilthead seabream juveniles that were vaccinated one month prior to the challenge. Head-kidney, spleen, intestine, and caudal fin samples were analyzed, covering a wider spectrum of immune organs and the target tissue for the virus.

Viral infections trigger local and systemic inflammatory responses in the host, recruiting immune cells for adaptive (lymphocytes) and innate immunity (neutrophils, monocytes, and NK cells). Virus recognition by cellular sensors initiates the transcription of pro-inflammatory cytokines, including type I IFN, inducing the synthesis of ISGs as antiviral effector proteins and regulators of immunity (34). In addition, the transcription of toll-like receptors *tlr5* and *tlr9*, and the c-type lectin *cd209* genes were analyzed to evaluate its implication in LCDV-Sa, vaccine, or plasmid recognition by immune cells. It is well known that both, TLR5 and TLR9, have similar functions to the mammalian TLRs (35). Interestingly, different profiles of expression were observed for the different nucleic acid sensors analyzed in the different samples. Regarding TLR9, it has been described as having a higher presence in the spleen compared to other fish organs of different fish, such as zebrafish (*Danio rerio*), Atlantic salmon (*Salmo salar*), rainbow trout (*Oncorhynchus mykiss*), and cobia (*Rachycentron canadum*) (36–39). Up-regulation of *tlr9* only occurred in the spleen of vaccinated (24 hours pi) and mock-vaccinated (72 hours pi) gilthead seabream, while up-regulation of *tlr5* was observed in head-kidney, spleen, and intestine samples of non-vaccinated fish and the head-kidney of mock animals. Similar results were obtained in a previous study using the same model of pathogen-host interaction, where *tlr9* was not differentially expressed in the head-kidney and, on the contrary, *tlr5* was upregulated in head-kidney and intestine of LCDV-Sa-infected gilthead seabreams (17). However, in vaccinated fish no modulation (up or down-regulation) of *tlr5* was detected in any sample analyzed, indicating specific immune induction of toll-like receptors for the different experimental groups. TLR9 has been previously associated with the recognition of different dsDNA viruses (40), including the human cytomegalovirus whose promoter is present in the vaccine vector (pcDNA). Regarding TLR5, it was primarily associated with the detection of bacterial flagellin, however different studies have described the role of this receptor in the reactivation of persisting ranavirus infection through bacterial coinfections (41). Therefore, overexpression of the *mcp* gene in vaccinated fish appears to cause differential expression of pathogen recognition-related genes and could indicate an mcp-independent mechanism of LCDV-Sa entry and recognition through TLR5 regulation. A down-regulation of the expression of CD209, a c-type lectin receptor found specifically in dendritic cells (DC), was observed only in the head-kidney of vaccinated animals early on infection in addition to the *tlr9* inhibition. It has been described that viral recognition by c-type lectin receptors (CTLRs) could favor infection by different viruses (42), therefore its inhibition in vaccinated fish could have a protective role for gilthead seabreams during LCDV-Sa infection.

Regarding inflammation related-gene regulation and IFN response, the specific profiles of gene expression were obtained for the non-vaccinated, vaccinated, and mock fish in an organ-dependant manner. In the head-kidney samples of non-vaccinated animals, inhibition of the inflammatory process and slight IFN response was recorded with the down-regulation of *ck3* (24 and 72 hours pi) and *ck8* (24 hours pi), and only the up-regulation of *irf9*, *mx2* (24 h pi), and *isg15* (72 hours pi). In contrast, in vaccinated fish from 48 hours pi a high pro-inflammatory response mediated by the up-regulation of *il1β* and *il6* transcripts was detected. At the same timepoint, the up-regulation of the c-type lectin domain family 10 member A (*clec10a*) transcript was detected. This receptor was related to the regulation of adaptive and innate immune responses and the induction of the synthesis of several pro-inflammatory cytokines in rainbow trout macrophages and fibroblast-like cells (43). Moreover, at 72 hours pi a higher IFN response was registered through the up-regulation of *irf3*, *isg15*, *mx1*, *mx2*, and *mx3* genes. Nevertheless, the induction of IFN genes was also detected in the mock fish, without the up-regulation of *clec10a* and pro-inflammatory interleukins, establishing a possible role for the vector (pcDNA) as an adjuvant of IFN response induction in this organ. In mammals, it has been described as a "built-in" adjuvant effect derived from CpG-motifs and double-strand DNA for DNA plasmids which are detected by toll-like receptor 9 (TLR9), stimulating IFN-γ-secreting cells in TLR9 +/+ mice but also in TLR9 -/-, suggesting that DNA vaccines induce immune responses by multiple mechanisms different from TLR9 following DNA immunization (44). In the head-kidney samples of mock fish, the *tlr9* transcript was down-regulated. Moreover, the adjuvant properties of the backbone plasmid pcDNA3.3 compared to the plasmid encoding the envelope glycoprotein, hemagglutinin esterase (pHE), of ISAV was able to induce IFN-I response at a higher level in cells (45). In addition, it has been described to have an adjuvant effect of the CpG-enriched plasmid DNA pcDNA3.1 (used in this study) co-administrated with the inactivated grass carp reovirus (GCRV) vaccine in grass carp fingerlings, providing increased levels of IgM in serum, spleen, and head-kidney, as well as up-regulation of *tlr9* and *mx2* expression, inhibiting GCRV

proliferation (46). In spleen samples, inflammation and IFN response took place in all experimental groups. However, the timepoint of IFN response diverged between them and different effectors were recorded regarding inflammation. In non-vaccinated animals, high IFN-related transcripts were up-regulated at 24 hours pi, and only *il1β* was up-regulated at 72 hours pi. In vaccinated fish, although the IFN response was less intense, it was prolonged in time. In turn, the only gene associated with inflammation that was overregulated was *elam*. The cytokine TNF-α and il1β released by resident cells are known to induce E-selectin and other chemokines in teleost (47). Endothelial cell leukocyte adhesion molecule-1 (ELAM-1) or E-selectin has been described as an inducible endothelial cell-adhesion molecule for neutrophils and memory T-cells, related to extravasation of these cells at sites of acute inflammation (48). In mammals, leucocytes are maturated in the secondary lymphoid organs, waiting to be recruited by the immune system. In gilthead seabream, the head-kidney has been described as a major hematopoietic and lymphoid organ, with a role in the migration of leucocytes to injured locations (49). Therefore, the up-regulation of *elam* in the present study could indicate a role for the spleen, the secondary lymphoid organ, in the recruitment of leucocytes in this fish species. On the other hand, in mock fish, the IFN response was only observed at 72 hours pi and the unique inflammatory effector detected was interleukin 8 (*il8*). The DEGs detected in the intestinal samples showed the opposite expression trend to that described for the head-kidney, as part of which the interferon response was more intense and took place earlier in the non-vaccinated fish compared to other groups that received the vaccine or the empty plasmid. In addition, the profile of upregulated genes related to inflammation was broader (*il1β*, *il10*, *csf1r*, and *ncf4*) compared to fish inoculated with the DNA plasmid (*csf1r* and *il1β*). This establishes the differential function of the immune organs. However, it is interesting to note that in vaccinated fish the inflammation-related gene *csf1r* was up-regulated early (24 hours pi) compared to non-vaccinated fish (72 hours pi). Furthermore, in the latter, up-regulation of the anti-inflammatory interleukin il10 was detected at 72 hours pi. The kinase receptor CSF-1R is the receptor found in macrophages for the colony-stimulating factor-1 (CSF-1). These have an important role in homeostasis, providing early defense against pathogens, regulation of immune responses and tissue repair (50). Related to inflammation in teleost, it has been described as playing a direct role in promoting the expression of several cytokines including IL-1, Il-6, IL-8, Il-18, TNFα, and IFN (51, 52). Even though the early expression of this genetic marker for macrophage proliferation was detected in vaccinated fish, no significant differences were detected in comparison with the non-vaccinated fish related to cytokine production in the intestine samples. The possible implication of this early expression of *csf1r* in the intestine and the exclusive pro-inflammatory response detected in the head-kidney of vaccinated fish 24 hours later remains uncertain. However, it has been identified as a soluble form of CSF-1R in goldfish (*Carassius auratus* L.), which regulates the CSF-1 activity (53), and promotes the proliferation of kidney primary macrophages (54). In addition, this soluble factor was found in the serum of goldfish giving it a role in systemic regulation of this activity (53). Finally, in caudal fin samples, it is worth noting the exclusive induction in vaccinated fish of the interferon-mediated antiviral response at 72 hours pi (*isg15*, *mx1*, *mx2*, and *mx3*), which was very scarce in non-vaccinated fish and those inoculated with the empty plasmid (*pkr* at 24 hours pi and *isg15* at 48 hours pi, respectively). The differential expression of the pro-inflammatory caspase-1 (*casp1*) and the no-modulation of the expression of the different chemokines analyzed could be the crucial factor that differentiates the results obtained from those of the non-vaccinated group, where a strong anti-inflammatory response by down-regulation of *ccr3*, *ck3*, and *ck10* was detected at 48 and 72 hours pi. This down-regulation of chemokines could inhibit the early inflammatory response mediated by the up-regulation of *casp1* and *perp* detected in the same group at 24 hours pi. In the mock fish, this kind of inflammation-related response was observed by the early up-regulation of *ccr3* and *ck10* and subsequent up-regulation of *isg15* and *il8* 24 h later (48 hours pi). At 48 hours pi, chemokines were down-regulated and no inflammatory or interferon responses were observed later on. The antiviral role of the inflammatory response mediated by chemokines in gilthead seabream has been studied under nodavirus infection in the target site (brain) of viral replication, and a strong up-regulation of CK3, CK8, and CK10, among others chemokines, was correlated with antiviral defense in seabream (55). It seems that the infection by LCDV-Sa in gilthead seabream triggers a different profile of chemokine expression that could be related to the immune evasion mechanisms of the virus at the target site of replication. However, the administration of the vaccine seems to compensate for the lack of chemokine-mediated inflammation through the caspase-1 pathway, triggering an efficient antiviral interferon response.

In terms of antigen presentation and humoral and cellular responses, a major trend in gene dysregulation was detected in the different experimental groups. Regarding hematopoietic organs, in vaccinated gilthead seabream, early expression of recombination activating gene 1 (*rag1*) (24 hours pi), compared to non-vaccinated fish (72 hours pi), and a cluster of differentiation 48 (*cd48*) genes (48 hours pi) were detected in head-kidneys. The *rag1* gene encodes a protein with endonuclease activity related to the assembly of the diversity of immunoglobulins and T cell receptor genes (56) and serves as a marker for the development of the adaptive immune response. It has been postulated that the expression of *rag* genes is crucial to the maturation of B cells and the production of Ig, and its expression within a lymphoid organ can be used as a developmental marker to assess immunological competence (57). Moreover, the cell-surface receptor CD48 is a lipid-anchored protein expressed on all antigen-presenting cells and T cells that contributes to maintaining the inflammatory response (58). As described earlier, at 48 hours pi the up-regulation of *il1β* and *il6* was observed exclusively in the head-kidney of vaccinated fish. Therefore, based on the early expression of these genes in the vaccinated animals, an immunocompetent state provoked by the DNA vaccine could be postulated. In addition, in spleen samples, the markers of humoral response *ighm* (also detected in the other experimental groups) and the immunoglobulin light chain (*ilc*) gene were differentially expressed at 48 hours pi. However, no up-regulation of genes was observed in the intestine and caudal fin, defining an organ-specific

immune response in gilthead seabream. Interestingly, in these latter organs, in the non-vaccinated group, the *ilc* (intestine) and *cd48* (caudal fin) genes were detected. The expression of the T-cell receptor (*tcrα*) was only detected in the mock fish. This impaired T-specific cell immunity in contrast to the promotion of humoral response and has been previously described in gilthead seabream infected with LCDV-Sa (17).

Regarding the elimination of infected cells by cell-mediated response, two main genes were detected, the non-specific cytotoxic cell receptor (*nccrp1*) and perforin (*prf1*), which are previously described as crucial effectors for virus clearance. Major differences were observed regarding the non-specific cytotoxic response mediated by the *nccrp1* gene in the different experimental groups. In non-vaccinated fish no modulation of the gene was recorded in hematopoietic organ samples and an up-regulation was detected in vaccinated and mock fish; however, it was only present in vaccinated fish early on in infection. In contrast, in intestine samples, this gene was up-regulated in non-vaccinated and vaccinated fish exclusively, but in the latter, its up-regulation was maintained for a longer period. However, in caudal fin samples, *nccrp1* gene was exclusively up-regulated in non-vaccinated fish. The importance of the innate immune response of this cytotoxic cell effector has been described in gilthead seabream against LCDV (16) and nodavirus (59) infection, as it mediates the leucocyte killing of virus-infected cells. Genes related to apoptosis were scarcely modulated through the experiment. Only in spleen samples, *prf1* gene up-regulation was remarkable, especially in vaccinated fish at 72 hours pi, which was the transcript with the highest fold change values registered in the experiment, although it was also detected in mock fish at the same timepoint but with lower expression. Perforin gene has been identified in several teleost fish, including zebrafish (60), Japanese flounder (*Paralichthys olivaceus*) (61), rainbow trout (62), rock bream (*Oplegnathus fasciatus*) (63), ginbuna crucian carp (*Carassius auratus langsdorfii*) (64), and common carp (*Cyprinus carpio*) (65). Similar to mammals, perforin is involved in the immune defense against virus infections in teleosts. Perforin, a pore-forming glycoprotein, has been demonstrated to play key roles in clearing virus-infected cells, also playing indispensable roles in CD8+T cell-mediated cytotoxicity (64). This is the first study to analyse the involvement of perforin in the immune response of gilthead seabream after infection with LCDV. Interestingly, in the head-kidney samples, the main immune organ in teleost fish (66), no differential expression of *prf1* was detected. The up-regulation of perforin genes has been described after infection with different viruses (60, 63, 65, 67, 68) and has mainly been studied in kidney samples where the modulation occurred several days after infection, which could explain the results of this study, establishing specific immune roles in a time-dependant manner against pathogens between the two hematopoietic organs analyzed.

In conclusion, our data suggest that the administration of the DNA vaccine (pcDNA-MCP) in gilthead seabream juveniles reduces the viral replication after inoculation of fish with LCDV-Sa. In addition, specific immune determinants have been detected exclusively in vaccinated fish that could be related to this control of viral multiplication. The specific role of the immune response of each of the organs analyzed has been denoted. An early humoral and cellular response mediated by *rag1* and *cd48*, and a pro-inflammatory response mediated by *il1β* and *il6* in head-kidney were also observed. This could be related to the possible presence of a soluble form of macrophage receptor (CSF-1R) found in intestine samples. In addition to a specific modulation of toll-like receptor 9 (*tlr9*), a recruitment of leukocytes by overexpression of *elam* and a cell-mediated cytotoxic response controlled by *nccrp1* and *prf1* was detected in the spleen. Moreover, an efficient antiviral response was detected through the interferon effectors *isg15*, *mx1*, *mx2*, and *mx3* in the target site of viral replication in the context of lymphocystis disease. More comparative studies examining the route of administration by oral chitosan beads containing the vaccine will be carried out. This study furthers understanding of the immune determinants modulated in vaccinated gilthead seabream following infection with LCDV-Sa, outlining which could confer protection against this viral disease for the aquaculture sector.

Data availability statement

The original contributions presented in the study are included in the article/Supplementary Material, further inquiries can be directed to the corresponding author/s.

Ethics statement

The animal study was reviewed and approved by Spanish authorities for the regulation of animal care and experimentation.

Author contributions

AL, RL-R, JB, and DC conceived and designed the study. RL-R and AL performed the experimental trials. AL, RL-R, and JG-M carried out all gene expression experiments and data analyses. AL and RL-R wrote the manuscript. JB and DC revised the manuscript. All authors contributed to the article and approved the submitted version.

Funding

This research was funded by the Junta de Andalucía and FEDER under Grants P12-RNM-2261 and UMA20-FEDERJA-076.

Acknowledgments

The authors thank Laura Redondo from the University of Cordoba (Servicio Central de Apoyo a la Investigación, Unidad de Genómica) for assistance with OpenArray® analysis.

Conflict of interest

The authors declare that the research was conducted in the absence of any commercial or financial relationships that could be construed as a potential conflict of interest.

Publisher's note

All claims expressed in this article are solely those of the authors and do not necessarily represent those of their affiliated organizations, or those of the publisher, the editors and the reviewers. Any product that may be evaluated in this article, or claim that may be made by its manufacturer, is not guaranteed or endorsed by the publisher.

Supplementary material

The Supplementary Material for this article can be found online at: https://www.frontiersin.org/articles/10.3389/fimmu.2023.1209926/full#supplementary-material

References

1. Anders K. Lymphocystis disease of fishes. In: Anhe W, Kurstak K, editors. *Viruses of lower vertebrates*. Berlin, GER: Springer, Heidelberg (1989). p. 141–60.

2. Sarasquete C, González de Canales ML, Arellano J, Pérez-Prieto SI, García-Rosado E, Borrego JJ. Histochemical study of lymphocystis in skin of gilthead seabream, *Sparus aurata*, from the south Atlantic coast of Spain. *Histol Histopathol* (1998) 13:37–45. doi: 10.14670/HH-13.37

3. Masoero L, Ercolini C, Caggiano M, Rossa A. Osservazioni preliminary sulla linfocisti in una maricoltura intensive italiana. *Riv Ital Piscic Ittiopatologia* (1986) 21:70–4.

4. Borrego JJ, Valverde EJ, Labella AM, Castro D. Lymphocystis disease virus: its importance in aquaculture. *Rev Aquacult* (2017) 9:179–93. doi: 10.1111/raq.12131

5. Paperna I, Sabnai HI. An outbreak of lymphocystis in *Sparus aurata* l. in the gulf of aqaba, red Sea. *J Fish Dis* (1982) 5:433–7. doi: 10.1111/j.1365-2761.1982.tb00500.x

6. Menezes J, Ramos MA, Pereira TG. Lymphocystis disease: an outbreak in *Sparus aurata* from ria Formosa, south coast of Portugal. *Aquaculture* (1987) 67:222–5. doi: 10.1016/0044-8486(87)90037-8

7. Basurco B, Marcotegui MA, Rueda A, Tiana A, Castellanos A, Tarazona J, et al. First report of lymphocystis disease in *Sparus aurata* (Linnaeus) in Spain. *Bull Eur Assoc Fish Pathol* (1990) 10:71–3.

8. Shawky M, Taha E, Ahmed B, Mahmoud MA, Abdelaziz M, Faisal M, et al. Initial evidence that gilthead seabream (*Sparus aurata* l.) is a host for lymphocystis disease virus genotype I. *Animals* (2021) 11:3032. doi: 10.3390/ani11113032

9. Perretta A, Doszpoly A, Puentes R, Bessonart M. Diagnosis of lymphocystis disease in a novel host, the whitemouth croaker *Micropogonias furnieri*, associated with a putatively novel lymphocystivirus species (LCDV-WC). *Dis Aquat Organ* (2020) 137:185–93. doi: 10.1007/s00705-020-04570-1

10. Doszpoly A, Kaján GL, Puentes R, Perretta A. Complete genome sequence and analysis of a novel lymphocystivirus detected in whitemouth croaker (*Micropogonias furnieri*): lymphocystis disease virus 4. *Arch Virol* (2020) 165:1215–8. doi: 10.1007/s00705-020-04570-1

11. Tidona CA, Darai G. The complete DNA sequence of lymphocystis disease virus. *Virology* (1997) 230:207–16. doi: 10.1006/viro.1997.8456

12. Zhang QY, Xiao F, Xie J, Li ZQ, Gui JF. Complete genome sequence of *lymphocystis disease virus* isolated from China. *J Virol* (2004) 78:6982–94. doi: 10.1128/JVI.78.13.6982-6994.2004

13. López-Bueno A, Mavian C, Labella AM, Castro D, Borrego JJ, Alcami A, et al. Concurrence of iridovirus, polyomavirus, and a unique member of a new group of fish papillomaviruses in lymphocystis disease-affected gilthead sea bream. *J Virol* (2016) 90:8768–79. doi: 10.1128/JVI.01369-16

14. Chinchar VG, Yu KH, Jancovich JK. The molecular biology of frog virus 3 and other iridoviruses infecting cold-blooded vertebrates. *Viruses* (2011) 3:1959–85. doi: 10.3390/v3101959

15. Dezfuli BS, Lui A, Giari L, Castaldelli G, Mulero V, Noga EJ. Infiltration and activation of acidophilic granulocytes in skin lesions of gilthead seabream, *Sparus aurata*, naturally infected with lymphocystis disease virus. *Dev Comp Immunol* (2012) 36:174–82. doi: 10.1016/j.dci.2011.06.017

16. Cordero H, Cuesta A, Meseguer J, Esteban MA. Characterization of the gilthead seabream (*Sparus aurata* l.) immune response under a natural lymphocystis disease virus outbreak. *J Fish Dis* (2016) 39:1467–76. doi: 10.1111/jfd.12481

17. Leiva-Rebollo R, Labella AM, Borrego JJ, Castro D. Immune gene expression in gilthead seabream (*Sparus aurata*) after lymphocystis disease virus (LCDV-sa) challenge resulting in asymptomatic infection. *J Appl Microbiol* (2019) 128:41–53. doi: 10.1111/jam.14454

18. Cano I, Valverde EJ, García-Rosado E, Alonso MC, López-Jimena B, Ortiz-Delgado JB, et al. Transmission of lymphocystis disease virus to cultured gilthead seabream, *Sparus aurata* l., larvae. *J Fish Dis* (2013) 36:569–76. doi: 10.1111/jfd.12011

19. Valverde EJ, Labella AM, Borrego JJ, Castro D. *Artemia* spp., a susceptible host and vector for lymphocystis disease virus. *Viruses* (2019) 11:506. doi: 10.3390/v11060506

20. Leiva-Rebollo R, Castro D, Moreno P, Borrego JJ, Labella AM. Evaluation of gilthead seabream (*Sparus aurata*) immune response after LCDV-sa DNA vaccination. *Animals* (2021) 11:1613. doi: 10.3390/ani11061613

21. Wu R, Sheng X, Tang X, Xing J, Zhan W. Transcriptome analysis of flounder (*Paralichthys olivaceus*) gill in response to lymphocystis disease virus (LCDV) infection: novel insights into fish defense mechanisms. *Int J Mol Sci* (2018) 19:160. doi: 10.3390/ijms19010160

22. Carballo C, Castro D, Borrego JJ, Manchado M. Gene expression profiles associated with lymphocystis disease virus (LCDV) in experimentally infected Senegalese sole (*Solea senegalensis*). *Fish Shellfish Immunol* (2017) 66:129–39. doi: 10.1016/j.fsi.2017.04.028

23. Hussell T, Goulding J. Structured regulation of inflammation during respiratory viral infection. *Lancet Infect Dis* (2010) 10:360–6. doi: 10.1016/S1473-3099(10)70067-0

24. Wilson EB, Brooks DG. The role of IL-10 in regulating immunity to persistent viral infections. *Curr Top Microbiol Immunol* (2011) 350:39–65. doi: 10.1007/82_2010_96

25. Valverde EJ, Cano I, Labella A, Borrego JJ, Castro D. Application of a new real-time polymerase chain reaction assay for surveillance studies of lymphocystis disease virus in farmed gilthead seabream. *BMC Vet Res* (2016) 12:71. doi: 10.1186/s12917-016-0696-6

26. Reed LJ, Muench H. A simple method of estimating fifty per cent endpoints. *Am J Hyg* (1938) 27:493–7. doi: 10.1093/oxfordjournals.aje.a118408

27. Livak KJ, Schmittgen TD. Analysis of relative gene expression data using real-time quantitative PCR and the $2^{-\Delta\Delta Ct}$ method. *Methods* (2001) 25:402–8. doi: 10.1006/meth.2001.1262

28. Babicki S, Arndt D, Marcu A, Liang Y, Grant JR, Maciejewski A, et al. Heatmapper: web-enabled heat mapping for all. *Nucleic Acids Res* (2016) 44:W147–53. doi: 10.1093/nar/gkw419

29. Bioinformatics and Evolutionary Genomics. (2022). Available at: http://bioinformatics.psb.ugent.be/webtools/Venn/ (Accessed July 15, 2022).

30. Garver KA, Conway CM, Elliott DG, Kurath G. Analysis of DNA-vaccinated fish reveals viral antigen in muscle, kidney and thymus, and transient histopathologic changes. *Mar Biotechnol* (2005) 7:540–53. doi: 10.1007/s10126-004-5129-z

31. Lorenzen E, Einer-Jensen K, Martinussen T, Lapatra SE, Lorenzen N. Feature DNA vaccination of rainbow trout against viral hemorrhagic septicemia virus: a dose–response and time-course study. *J Aquat Anim Health* (2000) 12:167–80. doi: 10.1577/1548-8667(2000)012<0167:FVORTA>2.0.CO;2

32. Evensen O, Leong JA. DNA Vaccines against viral diseases of farmed fish. *Fish Shellfish Immunol* (2013) 35:1751–8. doi: 10.1016/j.fsi.2013.10.021

33. Collins C, Lorenzen N, Collet B. DNA Vaccination for finfish aquaculture. *Fish Shellfish Immunol* (2019) 85:106–25. doi: 10.1016/j.fsi.2018.07.012

34. Langevin C, Boudinot P, Collet B. IFN signalling in inflammation and viral infections: new insights from fish models. *Viruses* (2019) 11:302. doi: 10.3390/v11030302

35. Palti Y. Toll-like receptors in bony fish: from genomics to function. *Dev Comp Immunol* (2011) 35:1263–72. doi: 10.1016/j.dci.2011.03.006

36. Yeh DW, Liu YL, Lo YC, Yuh CH, Yu GY, Lo JF, et al. Toll-like receptor 9 and 21 have different ligand recognition profiles and cooperatively mediate activity of CpG-oligodeoxynucleotides in zebrafish. *Proc Natl Acad Sci U. S. A.* (2013) 110:20711–6. doi: 10.1073/pnas.1305273110

37. Skjaeveland I, Iliev DB, Zou J, Jorgensen T, Jorgensen JB. A TLR9 homolog that is up-regulated by IFN-gamma in Atlantic salmon (*Salmo salar*). *Dev Comp Immunol* (2008) 32:603–7. doi: 10.1016/j.dci.2007.10.011

38. Ortega-Villaizan M, Chico V, Falco A, Perez L, Coll JM, Estepa A. The rainbow trout TLR9 gene and its role in the immune responses elicited by a plasmid encoding the glycoprotein G of the viral haemorrhagic septicaemia rhabdovirus (VHSV). *Mol Immunol* (2009) 46:1710–7. doi: 10.1016/j.molimm.2009.02.006

39. Byadgi O, Puteri D, Lee YH, Lee JW, Cheng TC. Identification and expression analysis of cobia (*Rachycentron canadum*) toll-like receptor 9 gene. *Fish Shellfish Immunol* (2014) 36:417–27. doi: 10.1016/j.fsi.2013.12.017

40. Zahid A, Ismail H, Li B, Jin T. Molecular and structural basis of DNA sensors in antiviral innate immunity. *Front Immunol* (2020) 11:613039. doi: 10.3389/fimmu.2020.613039

41. Samanta M, Yim J, De Jesus Andino F, Paiola M, Robert J. TLR5-mediated reactivation of quiescent ranavirus FV3 in *Xenopus* peritoneal macrophages. *J Virol* (2021) 95:e00215–21. doi: 10.1128/JVI.00215-21

42. Ojeda N, Salazar C, Cardenas C, Marshall SH. Expression of DC-SIGN-like c-type lectin receptors in salmo salar. *Dev Comp Immunol* (2020) 113:103806. doi: 10.1016/j.dci.2020.103806

43. Perez-Sanchez J, Benedito-Palos L, Estensoro I, Petropoulos Y, Calduch-Giner JA, Browdy CL, et al. Effects of dietary NEXT ENHANCE(R)150 on growth performance and expression of immune and intestinal integrity related genes in gilthead sea bream (*Sparus aurata* l.). *Fish Shellfish Immunol* (2015) 44:117–28. doi: 10.1016/j.fsi.2015.01.039

44. Babiuk S, Mookherjee N, Pontarollo R, Griebel P, Van Drunen Littel-Van Den Hurk S, Hecker R. TLR9-/- and TLR9+/+ mice display similar immune responses to a DNA vaccine. *Immunology* (2004) 113:114–20. doi: 10.1111/j.1365-2567.2004.01938.x

45. Mehrdad S, Aleksej K, Chia Jung C, Børre R. Transcriptome analysis of plasmid-induced genes sheds light on the role of type I IFN as adjuvant in DNA vaccine against infectious salmon anemia virus. *PloS One* (2017) 12:e0188456. doi: 10.1371/journal.pone.0188456

46. Su H, Liao Z, Yuan G, Su J. A plasmid containing CpG ODN as vaccine adjuvant against grass carp reovirus in grass carp *Ctenopharyngodon idella*. *Oncotarget* (2017) 8:86576–91. doi: 10.18632/oncotarget.21245

47. Campos-Sanchez JC, Esteban MA. Review of inflammation in fish and value of the zebrafish model. *J Fish Dis* (2020) 44:123–39. doi: 10.1111/jfd.13310

48. Picker LJ, Kishimoto TK, Smith CW, Warnock RA, Butcher EC. ELAM-1 is an adhesion molecule for skin-homing T cells. *Nature* (1991) 349:796–9. doi: 10.1038/349796a0

49. Meseguer J, Lopez A, Garcia A. Reticuloendothelial stroma of the head-kidney from the seawater teleost gilthead seabream (*Sparus aurata* l.): an ultrastructural and cytochemical study. *Anat Rec* (1995) . 241:303–9. doi: 10.1002/ar.1092410303

50. Rieger AM, Hanington PC, Belosevic M, Barreda DR. Control of CSF-1 induced inflammation in teleost fish by a soluble from of the CSF-1 receptor. *Fish Shellfish Immunol* (2014) 41:45–51. doi: 10.1016/j.fsi.2014.03.035

51. Moore RN, Oppenheim JJ, Farrar JJ, Carter CSJr., Waheed A, Shadduck RK. Production of lymphocyte-activating factor (Interleukin 1) by macrophages activated with colony stimulating factors. *J Immunol* (1980) 125:1302–5. doi: 10.4049/jimmunol.125.3.1302

52. Evans R, Kamdar SJ, Fuller JA, Kruple DM. The potential role of the macrophage colony-stimulating factor, CSF-1, in inflammatory responses: characterization of macrophage cytokine gene expression. *J Leukoc Biol* (1995) 58:99–107. doi: 10.1002/jlb.58.1.99

53. Daniel R, Barreda PC, Hanington JL, Stafford MB. A novel soluble form of the CSF-1 receptor inhibits proliferation of self-renewing macrophages of goldfish (*Carassius auratus* l.). *Dev Comp Immunol* (2005) 29:879–94. doi: 10.1016/j.dci.2005.02.006

54. Barreda DR, Belosevic M. Characterisation of growth enhancing factor production in different phases of *in vitro* fish macrophage development. *Fish Shellfish Immunol* (2001) 11:169–85. doi: 10.1006/fsim.2000.0305

55. Cuesta A, Dios S, Figueras A, Novoa B, Esteban MA, Meseguer J, et al. Identification of six novel CC chemokines in gilthead seabream (*Sparus aurata*) implicated in the antiviral immune response. *Mol Immunol* (2010) 47:1235–43. doi: 10.1016/j.molimm.2009.12.014

56. Bassing CH, Swat W, Alt FW. The mechanism and regulation of chromosomal V(D)J recombination. *Cell* (2002) 109:S45–55. doi: 10.1016/S0092-8674(02)00675-X

57. Willett CE, Cherry JJ, Steiner LA. Characterization and expression of the recombination activating genes (*rag1* and *rag2*) of zebrafish. *Immunogenetics* (1997) 45:394–404. doi: 10.1007/s002510050221

58. Abadia-Molina A, Ji H, Faubion W, Julien A, Latchman Y, Yagita H, et al. CD48 controls T-cell and antigen-presenting cell functions in experimental colitis. *Gastroenterology.* (2006) 130:424–34. doi: 10.1053/j.gastro.2005.12.009

59. Chaves-Pozo E, Guardiola FA, Meseguer J, Esteban MA, Cuesta A. Nodavirus infection induces a great innate cell-mediated cytotoxic activity in resistant, gilthead seabream, and susceptible, European sea bass, teleost fish. *Fish Shellfish Immunol* (2012) 33:1159–66. doi: 10.1016/j.fsi.2012.09.002

60. Varela M, Forn-Cuni G, Dios S, Figueras A, Novoa B. Proinflammatory caspase a activation and an antiviral state are induced by a zebrafish perforin after possible cellular and functional diversification from a myeloid ancestor. *J Innate Immun* (2016) 8:43–56. doi: 10.1159/000431287

61. Hwang JY, Ohira T, Hirono I, Aoki T. A pore-forming protein, perforin, from a non-mammalian organism, Japanese flounder, *Paralichthys olivaceus*. *Immunogenetics* (2004) 56:360–7. doi: 10.1007/s00251-004-0688-8

62. Taylor EB, Moulana M, Stuge TB, Quiniou SMA, Bengten E, Wilson M. A leukocyte immune type receptor subset is a marker of antiviral cytotoxic cells in channel catfish, ictalurus punctatus. *J Immunol* (2016) 196:2677. doi: 10.4049/jimmunol.1502166

63. Jung MH, Nikapitiya C, Song JY, Lee JH, Lee J, Oh MJ, et al. Gene expression of pro and anti-apoptotic proteins in rock bream (*Oplegnathus fasciatus*) infected with megalocytivirus (family *Iridoviridae*). *Fish Shellfish Immunol* (2014) 37:122–30. doi: 10.1016/j.fsi.2014.01.012

64. Toda H, Araki K, Moritomo T, Nakanishi T. Perforin-dependent cytotoxic mechanism in killing by CD8 positive T cells in ginbuna crucian carp, carassius auratus langsdorfii. *Dev Comp Immunol* (2011) 35:88–93. doi: 10.1016/j.dci.2010.08.010

65. Li T, Wang L, Zhang Y, Guo X, Chen X, Zhang F, et al. Molecular characterization of three novel perforins in common carp (*Cyprinus carpio* l.) and their expression patterns during larvae ontogeny and in response to immune challenges. *BMC Vet Res* (2018) 14:299. doi: 10.1186/s12917-018-1613-y

66. Zwollo P, Cole S, Bromage E, Kaattari S. B cell heterogeneity in the teleost kidney: evidence for a maturation gradient from anterior to posterior kidney. *J Immunol* (2005) 174:6608–6616. doi: 10.4049/jimmunol.174.11.6608

67. Jung MH, Jung SJ. CpG ODN 1668 induce innate and adaptive immune responses in rock bream (*Oplegnathus fasciatus*) against rock bream iridovirus (RBIV) infection. *Fish Shellfish Immunol* (2017) 69:247–57. doi: 10.1016/j.fsi.2017.08.030

68. Ordas MC, Cuesta A, Mercado L, Bols NC, Tafalla C. Viral hemorrhagic septicaemia virus (VHSV) up-regulates the cytotoxic activity and the perforin/granzyme pathway in the rainbow trout RTS11 cell line. *Fish Shellfish Immunol* (2011) 31:252–9. doi: 10.1016/j.fsi.2011.05.010

frontiers | Frontiers in Immunology

TYPE Review
PUBLISHED 09 August 2023
DOI 10.3389/fimmu.2023.1240094

OPEN ACCESS

EDITED BY
Carolina Johnstone,
Spanish Institute of Oceanography (IEO), Spain

REVIEWED BY
Pamela Nicholson,
University of Bern, Switzerland
Mehmet Arif Zoral,
Okinawa Institute of Science and Technology Graduate University, Japan

*CORRESPONDENCE
Japhette E. Kembou-Ringert
kjaphette@yahoo.fr
Mikolaj Adamek
mikolaj.adamek@tiho-hannover.de

RECEIVED 14 June 2023
ACCEPTED 20 July 2023
PUBLISHED 09 August 2023

CITATION
Kembou-Ringert JE, Steinhagen D, Thompson KD, Daly JM and Adamek M (2023) Immune responses to Tilapia lake virus infection: what we know and what we don't know.
Front. Immunol. 14:1240094.
doi: 10.3389/fimmu.2023.1240094

Immune responses to Tilapia lake virus infection: what we know and what we don't know

Japhette E. Kembou-Ringert[1*], Dieter Steinhagen[2], Kim D. Thompson[3], Janet M. Daly[4] and Mikolaj Adamek[2*]

[1]Department of Infection, Immunity and Inflammation, Great Ormond Street Institute of Child Health, University College London, London, United Kingdom, [2]Fish Disease Research Unit, Institute for Parasitology, University of Veterinary Medicine Hannover, Hannover, Germany, [3]Moredun Research Institute, Pentlands Science Park, Penicuik, United Kingdom, [4]School of Veterinary Medicine and Science, University of Nottingham, Sutton Bonington, United Kingdom

Tilapia lake virus (TiLV) is a novel contagious pathogen associated with a lethal disease affecting and decimating tilapia populations on several continents across the globe. Fish viral diseases, such as Tilapia lake virus disease (TiLVD), represent a serious threat to tilapia aquaculture. Therefore, a better understanding of the innate immune responses involved in establishing an antiviral state can help shed light on TiLV disease pathogenesis. Moreover, understanding the adaptive immune mechanisms involved in mounting protection against TiLV could greatly assist in the development of vaccination strategies aimed at controlling TiLVD. This review summarizes the current state of knowledge on the immune responses following TiLV infection. After describing the main pathological findings associated with TiLVD, both the innate and adaptive immune responses and mechanisms to TiLV infection are discussed, in both disease infection models and *in vitro* studies. In addition, our work, highlights research questions, knowledge gaps and research areas in the immunology of TiLV infection where further studies are needed to better understand how disease protection against TiLV is established.

KEYWORDS

Tilapia lake virus, immunity, innate immunity, adaptive immunity, antiviral response, host immune resistance, immune subversion

1 Introduction

Tilapia lake virus (TiLV) or *Tilapia tilapinevirus* is an enveloped icosahedral virus of 55–75 nm (1), belonging to the *Amnoonviridae* family, and is characterized by a 10,323 kb segmented, negative sense, and single-stranded RNA (ssRNA) genome (2). TiLV is currently the sole representative member of this virus family (3), although recent meta-transcriptomic and data mining studies have identified several viral segments and transcripts related to TiLV PB1 gene (4, 5), that probably belong to novel divergently TiLV-related viruses. The TiLV genome is composed of ten ribonucleoproteins (RNP)

units and encodes at least 14 predicted proteins (6), including the recently identified NP protein encoded by segment 4 (7).

TiLV primarily infects tilapia species [particularly Nile tilapia *Oreochromis niloticus*, Mozambique tilapia *O. mossambicus*, Gray tilapia (*Oreochromis niloticus x O. aureus*) and Red tilapia *Oreochromis* spp.)], although other fish species such as tinfoil barbs (*Barbonymus schwanenfeldii*) (8, 9), giant gourami *Osphronemus* (10), angelfish (*Pterophyllum scalare*) and firemouth cichlid (*Thorichthys meeki*) (11) have also shown susceptibility to TiLV infection and could be experimentally infected with the virus. TiLV clinical infection has also been experimentally recapitulated through intraperitoneal (IP) injection of adult zebrafish (*Danio rerio*) (12, 13), zebrafish larvae (14), juvenile rainbow trout (*Oncorhynchus mykiss*) and brown trout (*Salmo trutta*) (15).

Cases of co-infection of TiLV with *Aeromonas hydrophila* and *Streptococcus agalactiae* in farmed red hybrid tilapia have also been reported (16). In general, co-infections with TiLV and *Aeromonas* spp. seem to be frequent, and infection with TiLV appears to promote secondary bacterial infections, especially with *Aeromonas veronii* (17) and *Aeromonas hydrophila* (18). Together with sporadic *Streptococcus agalactiae* co-infections, these bacteria co-infections can synergistically increase fish mortality and worsen disease severity in affected tilapia (16–18). Indeed, TiLVD can cause mortalities as high as 90% in affected fish populations (19), even though a few cases of inapparent infection have also been documented (20).

The virus has a broad tissue tropism and can induce a systemic infection. Tissue tropism studies have shown the presence of the virus in multiple organs, including the brain, liver, kidney, muscles, gills, fins, spleen, intestines, eye, heart, ovaries and testis (21). Moreover, all the life stages of tilapia, including fertilized eggs, yolk-sac larvae, fries, fingerlings, and adults appear to be susceptible to TiLV (21–24) and vertical transmission from broodstock to progeny can also occur (25, 26), altogether making TiLV a significantly lethal pathogen.

The elimination of virus pathogens such as TiLV during infection largely depends on the presence of a functional immune system. In bony fish such as tilapia, the host innate immune system, which is at the forefront of fish immune defenses, activates and triggers antiviral and pro-inflammatory responses early during infection (27). The adaptive immune response, although often delayed, also plays a critical role in the clearance of viral pathogens during the later stages of infection and is essential for long-lasting immunity and a key factor in successful vaccination (28).

It has been shown that tilapia mount a protective immune response following exposure to TiLV (29), as around 200 differently expressed microRNAs regulating genes involved in the immune response have been identified in tilapia fish infected with TiLV (30). Moreover, over 4640 genes, some of which are involved in antigen processing and presentation, nuclear factor kappa-light-chain-enhancer of activated B-cells (NF-κB), interferon (IFN) and chemokine signaling, were found to be differentially expressed in the liver of tilapia experimentally infected with TiLV (31), all suggestive of an attempt to establish an antiviral state.

However, it has also been shown that TiLV can downplay the innate immune response, especially during the early stages of infection (32), suggesting the existence of yet to be discovered viral effector proteins involved in and associated with immune response modulation.

The development of effective therapeutics and prevention strategies against viral diseases certainly requires an understanding of the various immunopathogenesis processes and mechanisms occurring during viral infections and contributing to disease establishment and persistence. Although also associated with the damages caused by viral replication (viral related factors), disease pathogenesis following viral infections often appears to result from an abnormal host response or overreaction of the immune system (host-related factors) to resolve the infection. Given that several studies aimed at elucidating the immune responses occurring during TiLV infection have recently emerged, it is timely to review our current understanding of the mechanisms governing the antiviral response to TiLV infection as it is important for the development of novel drugs and antiviral treatment strategies for controlling TiLV infection.

2 Pathology of TiLV disease

The pathogenesis of TiLV is not yet fully defined and understood, partly because the cellular receptor for this virus has not yet been identified and its mode of entry is not yet fully resolved. From what is currently known, TiLV enters endothelial TmB cells via a dynamin-mediated endocytic pathway largely dependent on cholesterol rich lipid-rafts and cytoskeleton but not on clathrin (33). In addition, endosomal acidification seems to not be required for TiLV endosomal escape during virus entry (33).

2.1 TiLV tissue tropism

As previously mentioned, TiLV appears to exhibit a very broad tissue tropism as the virus is capable of replicating in the brain, liver, kidney, muscles, gills, fins, spleen, intestines, eye, heart, ovaries and testis (13, 34) of both infected tilapia and zebrafish, and immunohistochemical detection of TiLV using a TiLV immunoglobulin G antibody has revealed the presence of the virus in the endothelial cells of various organs (liver, pancreas, kidney, gills, intestines, brain, and spleen) as well as in the circulating leukocytes in the blood vessels (34).

Syncytia formation is a major pathological change reported by several studies during TiLVD (1, 17, 19, 24, 35–37). Although the mechanisms underlying this pathological finding have not yet been elucidated in the specific case of TiLV, several viruses are known to produce proteins capable of fusogenic activity (38, 39), and membrane fusion during infection with such viruses is a crucial step during virus entry of target cells. Although the fusion protein of TiLV remains to be identified and its fusogenic activity demonstrated, similar underlying fusion mechanisms as the ones described for some parainfluenza virus lineages (for which membrane fusion does not require low-pH) could be at play during TiLV infection. Moreover, the gene for RhoA, whose signaling has been associated with cell-to-cell fusion and syncytium formation during respiratory syncytial virus (RSV)

infection (40), is upregulated in the liver during TiLV infection (31), suggesting that this small GTPase may play a role in initiating cell-to-cell fusion during TiLV infection. Further studies are thus required to shed some light on TiLV syncytia formation and the specific role of RhoA during this event.

2.2 Routes of infection and infection models

TiLV seems to have a relatively narrow host range with tilapia species being the canonical host for the virus. Therefore, the immune responses to TiLV infection have mainly been measured in Nile and red hybrid tilapia. Apart from the limited number of results obtained from infection performed by cohabitation, most results from experimental infections have been obtained following IP injection. This type of infection route does not allow the elucidation of the key antiviral responses at virus entry sites. Infection models based on IP injections of the canonical host often lead to a very fast onset of disease and mortality. In addition, TiLVD has also been modelled using an intragastric challenge model (35, 37). However, the low mortality rates observed with this route of infection (40% mortality after 10 days as opposed to 70% mortality in IP injected tilapia) may suggest a lack of systemic absorption from the digestive tract and raises the possibility that this route of infection is not the principal entry route of the virus in natural infection.

Other than tilapia, immune responses during TiLV infection have also been modelled in zebrafish which were also infected by IP injection (12, 13), or injection via duct of Cuvier of zebrafish larvae (14). In the zebrafish model, the virus has the ability to spread to several tissues of the body although it does not lead to high mortality (12, 13). Both zebrafish and tilapia are ray-finned fish and can tolerate tropical to sub-tropical water temperatures. Although most fish immune related genes are well-annotated in zebrafish (due to extensive studies conducted with zebrafish as an animal model) and can significantly inform our understanding of immune responses and pathways activated during TiLV infection, the zebrafish model remains limited by the requirement for IP-injection to initiate viral infection. Moreover, cases of natural infection of zebrafish with TiLV have not yet been reported suggesting the existence of factors restricting TiLV infection at virus entry sites in zebrafish, further emphasising that zebrafish is not a natural host for TiLV. As such, antigen recognition, disease establishment and progression, and immune responses and modulation might be different in this model.

3 Innate immune response

TiLV seems to be well recognized by pattern recognition receptors (PRRs) which elicit several key host immune responses such as increasing the release of antiviral factors important in restricting viral replication and spreading.

It is generally accepted that upon viral infection, the pathogen-associated molecular patterns (PAMPs) of viruses, either non-capped double or single stranded RNA (dsRNA or ssRNA) are sensed by cellular pattern recognition receptors (PRRs) located at the cell surface, in endosomes or in the cytosol. Sensing of viruses by PRRs such as Toll-like receptors (TLRs) and retinoic acid inducible gene I (RIG-I)-like receptors (RLRs) leads to the activation of several signaling pathways and transcription factors such as the interferon regulatory factors (IRFs) and NF-κB (41), both subsequently inducing the transcription of type I IFNs, crucial for the establishment of an antiviral state.

3.1 Activation of innate immune signaling upon intracellular detection of TiLV infection

It has been demonstrated that during TiLV infection, there is a significant upregulation of the PRR sensors TLR3 and TLR7 in the brain of TiLV-infected tilapia (31, 42). In contrast, upregulation of TLR3 as well as the fish-specific TLR22 (a cell surface TLR sensor) was observed in the spleen and kidney of TiLV-infected adult zebrafish and larvae (12–14). The upregulation of TLR3, normally present in cellular endocytic compartments, suggests its possible interaction with TIR-domain-containing adapter inducing interferon β (TRIF) to mediate the activation of NF-κB and the Interferon regulatory factor 3 (IRF3), leading mainly to the promotion of both inflammatory and IFN-β-mediated antiviral responses. Indeed, an abundant and upregulated expression of the gene transcripts encoding IRF3, a key transcriptional regulator of type I interferon (IFN)-dependent immune responses which plays a critical role in the innate immune response against DNA and RNA viruses, has been observed in the liver, spleen, intestine, gills and kidney of both tilapia and zebrafish infected with TiLV (12–14, 35).

In addition, a significant increase in IRF1 gene expression early during infection was observed in the liver of TiLV-infected tilapia (43). Similarly to IRF3, IRF1 is a member of the IRF family. Although it seems to not be essential for the induction of type I IFNs, IRF1 has nevertheless been found to play a significant role in IFN-mediated signaling, in TNF-mediated type I IFN signaling and in IFN-dependent inflammation (44). IRF1 protein can induce the expression of type I IFNs downstream of RLRs (45), and although IRF3 and IRF7 have always been assumed to be the predominant transcriptional regulators in the canonical TLR signaling, IRF1 has also nevertheless been shown to also participate in the transcriptional responses involving the engagement of some TLRs (such as TLR9, TLR7, TLR2, TLR3 and TLR4) or involving the myeloid differentiation primary response 88 (MYD88) protein. Increases in IRF1 expression induced by viral infections in most cases primarily result from NF-κB and STAT1-mediated transcriptional activation. IRF1 expression is usually induced rapidly following virus infection and there is evidence that IRF1 effector genes can suppress the replication of a variety of RNA viruses (46). Moreover, IRF1 can regulate basal antiviral states that restrict both positive- and negative-stranded RNA viruses in various cell types.

Likewise, IRF7 has also been found to be upregulated in both adult zebrafish and larvae (12–14). Both IRF7 and IRF3 promote the

expression of genes encoding type I IFNs. IRF5 involved in the activation of the expression of type I IFNs and inflammatory cytokines downstream of endolysosomal toll-like receptors TLR7, TLR8 and TLR9 was also found to be upregulated (31), as well as the gene transcripts encoding for other interferon regulatory factors such as IRF4 and IRF8 (primarily involved in the adaptive immune response). Their possible role in adaptive immunity is discussed later in the section "*Activation and modulation of the T-cell adaptive immune response*".

A significant upregulation of the PRR sensor RIG-I has also been reported in both adult zebrafish and larvae infected with TiLV (12–14). The signaling pathway triggered when RIG-I is activated is well characterised in mammals. After binding its nucleic acid ligands (RNA with a 5' triphosphate moiety, uncapped short ssRNA or dsRNA), RIG-I signals via interaction of its caspase activation and recruitment domain (CARD) with an adapter protein associated with the outer mitochondrial membrane known as MAVS (mitochondrial antiviral signaling protein or IFN-β promoter stimulator (IPS)-1 protein) (47, 48). This CARD-dependent association of RIG-I and MAVS triggers a downstream transduction signaling cascade subsequently leading to the activation of IRF3 and IRF7 as well as NF-κB, thus causing the expression of a variety of type I IFNs and cytokines aimed at inhibiting viral replication (49). These mechanisms are also very likely to take place in teleost fish such as tilapia, especially when considering that RIG-I and MAVS (IPS) also exist in teleost fish (50–52), and their salmonid orthologues also have the same domain structures as seen in mammals (27).

In fact, MAVS (or IPS-1) has been found to be upregulated in the kidney and brain of tilapia fish during late stages (96 hours post-infection) of TiLV infection (42). In Atlantic salmon, a MAVS homologue protein (AsMAVS) has been found to mediate the activation of the salmon IFN-a1 promoter (53) although possessing the CARD, proline-rich and transmembrane domains found in mammalian MAVS. The observation that MAVS is also induced and upregulated during TiLV infection, indicates that MAVS may play a significant role in the RIG-I innate immune processes occurring during TiLV infection.

It has been shown that over-expression of MAVS in teleost fish protects cells from infection by both DNA and RNA viruses by inducing IFN stimulated genes (ISGs), such as IRF3 and the myxovirus resistance (Mx) as well as type I IFN (54, 55). The overexpression of MAVS protein could thus represent a potential therapeutic approach (56), for the treatment and prevention of TiLVD. Overall, PRRs sensors of the innate immune system and their adaptor proteins are activated during TiLV infection (Figure 1).

3.2 Antiviral molecules involved in innate immunity against TiLV infection

The activation of transcription factors such as NF-κB, IRF1, IRF3 and IRF7 during TiLV infection results in their translocation into the nucleus, where they initiate the transcription of genes encoding type I IFNs, inflammatory cytokines such as tumour

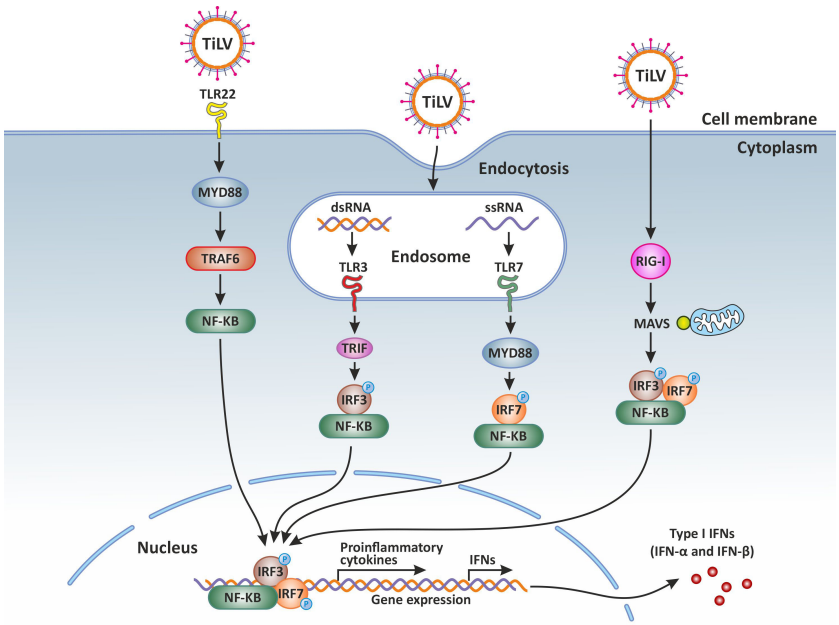

FIGURE 1
Innate immune response against Tilapia lake virus (TiLV) infection. Intracellular detection of TiLV infection by the host pathogen recognition receptors (PRRs) activates the transcription factors nuclear factor kappa-light-chain-enhancer of activated B-cells (NF-κB), interferon regulatory factor 3 (IRF3), and IRF7. The PRRs involved include toll-like receptors (3, 7 and 22) and retinoic acid-inducible gene-I protein (RIG-I). By signaling through the adaptor proteins MYD88 and TRIF, the activated transcription factors translocate to the nucleus and trigger the expression of type I and type III interferons (IFNs) which are crucial for the establishment of the antiviral state. Original image realized with CorelDRAW graphics suite 2020.

necrosis factor (TNF)α, interleukins (IL-8, IL-1β and IFNγ1-2), and proinflammatory gene products such as cyclooxygenase-2 (COX-2) (31). Although the specific activation of NF-κB during TiLV infection has not yet been demonstrated, upregulation of both the tumour necrosis factor receptor associated factor 3 (TRAF3) and the nuclear factor-kappa-B-inhibitor alpha (NFKBIA) gene has been observed in the liver of TiLV-infected tilapia (31). TRAF3 is an adaptor protein that functions both independently as a negative regulator of the NF-κB pathway and as a positive regulator of type I IFN production. It is therefore at the intersection between the IFN-I and NF-κB pathways (57). The NFKBIA gene on the other hand, encodes for the alpha subunit of the IκB kinase (IKK) protein complex, which is a group of related proteins regulating the activity of NF-κB. The specific upregulation of these 2 factors regulating NF-κB function suggests the modulation of NF-κB downstream of the RIG-I sensing signaling pathway during TiLV infection. It will thus be interesting to determine how NF-κB is regulated during TiLV infection and if TiLV also induces an upregulation of the melanoma differentiation-associated protein (MDA5).

The significant upregulation of type I IFNs (*ifnϕ1*) during TiLV infection has been demonstrated in adult zebrafish and larvae (12–14). Moreover, treatment with exogenous recombinant zebrafish IFNϕ1 (zfIFNϕ1) has been shown to significantly decrease both the mortality and the viral load at 48 hours post-infection in TiLV-infected zebrafish larvae (14), suggesting the early administration of exogenous IFN as a therapeutic strategy. Indeed, it was recently shown that human IFN-α2a both completely prevented and inhibited TiLV infection (by more than 80%) when administered before the infection (58). Similarly, the fish IFNc significantly reduced TiLV-induced CPE and viral loads in a dose-dependent manner; further demonstrating the protective role of type I IFNs in preventing TiLV infection (58).

It is well known that type I IFNs act in autocrine and paracrine ways to induce the transcription of several ISGs, some of which encode antiviral proteins such as Mx (59, 60). The expression of genes encoding for Mx is controlled by type I interferons (61). Indeed abundant and significantly upregulated *mx* genes transcripts were detected in the brain, liver, spleen, intestine, and gills of TiLV-infected tilapia (31, 32, 35), and in adult and zebrafish larvae infected with TiLV (12–14) as well as brown and rainbow trout (15). Moreover, the administration of exogenous recombinant zfIFNϕ1 was found to up-regulate Mxa expression in zebrafish larvae infected with TiLV, which coincided with the observation of a significant reduction of TiLV viral load in zfIFNϕ1 pre-treated zebrafish larvae (14). Mx proteins are key components of the antiviral state induced by interferons. One unique property of some Mx GTPases is their antiviral activity (illustrated in Figure 2) against a wide range of RNA viruses, including orthomyxoviruses, paramyxoviruses, rhabdoviruses and members of the bunyavirus family. It has been shown for instance that the constitutive expression of Atlantic salmon (*Salmo salar*) Mx1 protein in CHSE-214 cells (fibroblastic cells deriving from Chinook Salmon - *Oncorhynchus tshawytscha* - embryo) conferred resistance to the cells against cytopathic infectious salmon anemia virus (ISAV) strain NBISA01. A resistance characterized by a delayed development of cytopathic effect

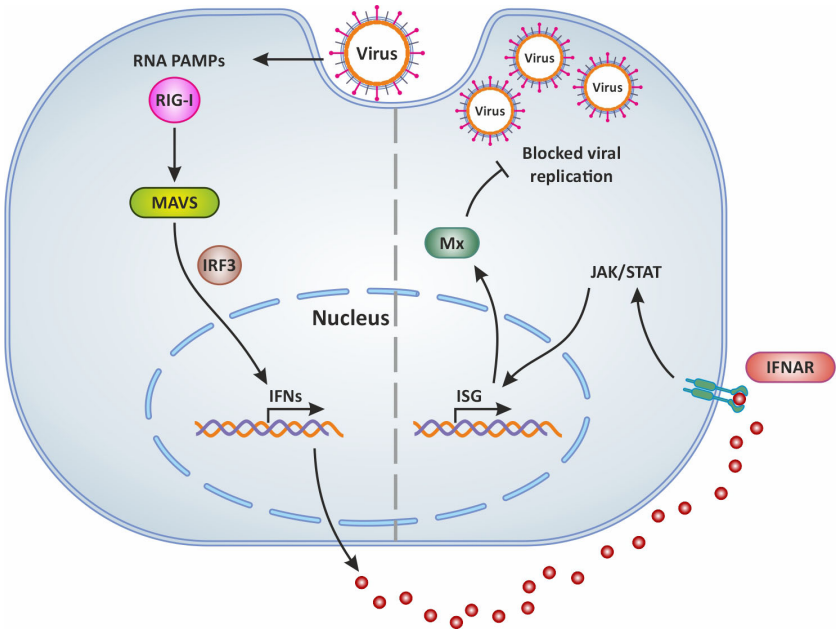

FIGURE 2
Mx production following virus infection and antiviral activity. In general, following virus infection, the RNA PAMPs of viruses activate RIG-I (which then activates the adaptor molecule MAVS downstream of RIG-I). This PRR signaling leads to the subsequent activation of the transcription factor IRF-3 for the induction of IFN. Secreted IFNs dock onto their receptor IFNAR and thus mediate the expression of antiviral ISGs via the JAK/STAT signaling pathway. This results in the production of Mx which blocks viral replication and is involved in IFN-mediated inhibition of viruses. Original image realized with CorelDRAW graphics suite 2020.

(CPE), a significant reduction in the severity of CPE, and a 10-fold reduction in virus yield (62). An open question is thus whether or not TiLV is sensitive to the antiviral action of Mx.

Interestingly, the *rsad2* gene encoding for radical s-adenosyl methionine domain containing 2 protein, (also known as viperin), a multifunctional IFN-inducible protein, is also significantly highly upregulated in the liver of TiLV-infected tilapia (43). Although this IFN-inducible protein is constitutively highly expressed in the liver, its significant upregulation in liver cells of TiLV-infected tilapia suggests that viperin could be playing an important role in the regulation of TiLV infection cycle as this protein has been shown to inhibit a broad spectrum of DNA and RNA viruses, including herpesviruses, flaviviruses (Hepacivirus C [HCV], West Nile virus, and dengue virus), paramyxoviruses (Sendai virus and measles virus), a rhabdovirus (vesicular stomatitis virus), an alphavirus (Sindbis virus), a retrovirus (human immunodeficiency virus type 1, HIV-1) and an orthomyxovirus (Influenza A virus) (63). As an IFN-inducible protein, viperin is produced in a variety of cell types by stimulation with all types of IFNs and by infection with multiple viruses. Viperin induction by viruses is mediated by the classical ISG induction pathways involving the engagement of TLR3, TLR4 and RIG-1, which in turn activates IRF3 and IRF7. Alternatively, viperin can also be upregulated independently of IFNs by a number of viruses including human cytomegalovirus (HCMV), vesicular stomatitis virus, Japanese encephalitis virus, and Chikungunya virus (63).

In fact, the direct stimulation of viperin expression can occur through the activation of MAVS following the downstream activation of IRF1 and IRF3. In this case, the stimulation of RLRs by dsRNA leads to the activation of the adaptor protein MAVS (or IPS-1) either residing on the peroxisome or at the mitochondrial membrane through an IRF1- and IRF3-dependent gene induction [illustrated in Figure 3 and reviewed in (64)]. Thus, it appears that the significant upregulation of both IRF1 (43) and IRF3 (35) during TiLV infection, especially in the liver, could be leading to their translocation into the nucleus and their subsequent binding to the *rsad2* promoter (which contains functional binding sites for both IRF1 and IRF3). This in turn, leads to the induction of viperin in an IFN-independent manner; although the significant upregulation of type I IFNs [in adult zebrafish and larvae (12–14)] also raises the possibility that this protein might also be induced in an IFN-dependent manner.

The full antiviral mechanisms at play and associated with viperin antiviral functions against a wide range of viruses remain somewhat elusive, but overall range from inhibition of viral RNA replication, direct binding to viral proteins, to blocking of viral particles release (viral budding) by disruption of lipid rafts (65). However, some DNA viruses (notably the dsDNA herpesviruses

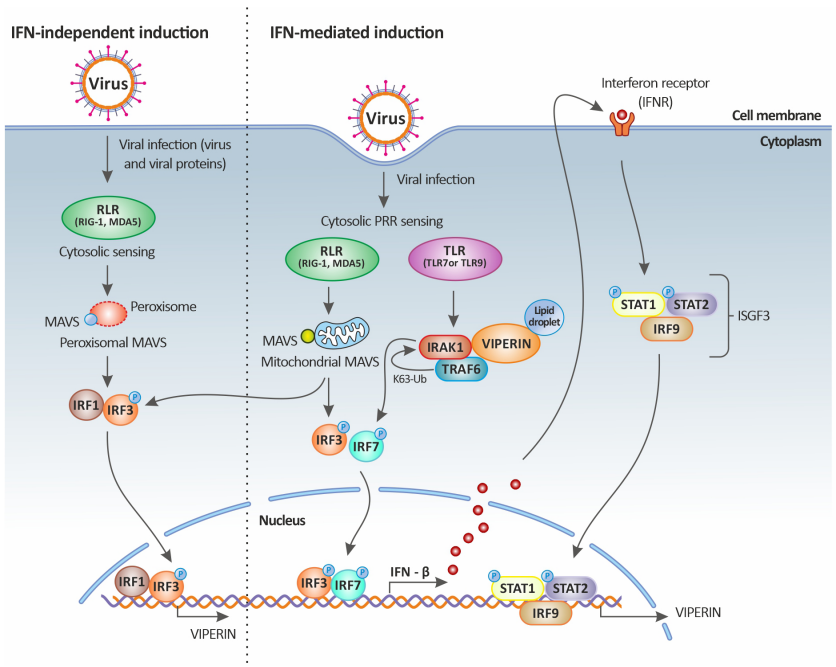

FIGURE 3
Viperin induction upon viral infection. Viperin expression is mediated by both the classical IFN-stimulated gene induction pathway (right panel) and the IFN-independent pathway (left panel). In the IFN-independent pathway, viperin gene expression is regulated by IRF1 and IRF3, which can be activated by viral factors or by the peroxisomal MAVS signaling pathway. In the IFN-mediated pathway, viperin gene expression is regulated by the ISGF3 complex. Upon viral infection, cytosolic sensing of viral nucleic acids by PRRs leads to the activation of downstream signaling factors including those dependent on endosomal TLRs and mitochondrial MAVS and culminates in the activation of the transcription factors IRF3 and IRF7. IRF3 and IRF7 translocate to the nucleus resulting in the induction of IFNs (more specifically IFN-β). The secreted IFN-β then signals both in autocrine and paracrine manners upon binding to its receptor, leading to the downstream activation of the Jak-STAT pathway. This in turn results in the formation of the heterotrimeric complex ISGF3, which translocates to the nucleus and binds to the promoter of ISGs, including that of viperin. Viperin itself can also increase IFN-β induction by promoting TRAF6-dependent ubiquitination of IRAK1 and phosphorylation of IRF7. Original image realized with CorelDRAW graphics suite 2020.

HCMV and Kaposi's sarcoma-associated herpesvirus - KSHV) appear to have repurposed the cellular roles of viperin to their benefit during viral replication. The first by co-opting viperin (HCMV) and the second by enhancing the activity of its viral protein (KSHV). Indeed, the co-option of viperin by HCMV alters the cellular metabolism which in turns favours HCMV replication. In the case of KSHV, the binding of viperin to the viral helicase protein enhances the stability of the protein and thus promotes viral replication (64). Therefore, can the remarkably high expression profile of viperin in the liver during TiLV infection (43), promote viral infection at this site or is it an attempt by host cells to restrict and inhibit viral replication? The severity of the infection in the liver [one of the main target organs of TiLV, hence the name syncytial hepatitis originally attributed to TiLVD (1, 23)] could make the first case scenario possible. Evidence is needed to draw any conclusions on the possible antiviral effects of viperin on TiLV replication.

It has been observed that TiLV infection induces an up-regulation of the expression of the gene encoding for pro-inflammatory cytokine IL-1β at mucosal sites such as the intestine and gills (35), as well as in the brain and liver of infected tilapia (31, 32, 66, 67). High expression levels of this mediator of inflammatory response have also been reported in both adult zebrafish and larvae experimentally infected with TiLV (12–14). IL-1β acts downstream of the nucleotide-binding domain leucine-rich repeat (NLR) family pyrin domain containing 3 (NLRP3) inflammasome (NLRP3) following binding to the IL-1 receptor (IL-1R). In fact, the activation of NLRP3 inflammasome contributes to the enzymatical maturation of the inactive precursor pro-IL-1β into its active form IL-1β (68). A signaling pathway thought to ensure the efficient secretion of IL-1β for the initiation of host innate immunity, which subsequently leads to the induction of both NF-κB-dependent inflammation and trafficking of neutrophils and T-cells (69). Similarly, an upregulation of the gene encoding for IL-8 was observed in the liver, spleen and head kidney of TiLV-infected tilapia (43, 70), and in both adult zebrafish and larvae infected with TiLV (12–14). IL-8 acts as a chemoattractant cytokine that specifically attracts and activates neutrophils in inflammatory regions (71). Therefore, the concerted action of IL-1β and IL-8 at infection sites may drive the massive infiltration of lymphocytic inflammatory cells that has been consistently observed in multiple organs including the brain, liver, intestines and spleen, during TiLVD (19, 35, 42, 43). The role of the NLRP3 inflammasome during TiLV infection and disease pathogenesis should thus be elucidated.

TNF-α is another inflammatory cytokine for which mRNA expression has been reported to be significantly upregulated during TiLV infection in both tilapia and zebrafish (12–14, 31, 66). TNF-α is produced by epithelial, endothelial and smooth muscle cells, as well as by astrocytes, activated macrophages, T and B lymphocytes, natural killer cells, and some tumour cells (72). It induces endothelial adhesion molecules, which trigger the migration of innate immune cells, such as blood-borne dendritic cells (DCs), natural killer (NK) cells and macrophages, to the site of infection. It is an interesting pro-inflammatory cytokine as it has been shown to inhibit the replication of viruses such as vesicular stomatitis virus, encephalomyocarditis virus, herpes simplex virus, influenza virus and HIV-1 in specific cell lines (72–74), but also stimulates HIV-1 replication in chronically infected T-cells and promonocytic cell lines (75–77). TNF-α also plays a crucial role in both the mitogen-activated protein kinases (MAPK) and the necroptosis (programmed necrosis) pathways. In the necroptosis pathway, the binding of TNF-α to membrane receptors TNFR1 activates the intracellular RIP (receptor interacting protein) family kinases. TNFR1 in turn interacts with the death domain of other adapter proteins, ultimately recruiting the receptor-interacting serine/threonine protein kinase 1 (RIPK1). RIPK1 and other proteins form a complex most often consisting of RIPK1, RIPK3, FADD and mixed lineage kinase domain like pseudokinase (MLKL), thereby activating MLKL. Activated MLKL then translocates to cellular membranes, causing their rupture (78).

This "dirty death" of cells i.e. necrosis, could be important in shaping disease evolution and pathogenicity as it enhances inflammatory reactions that may help curtail viral reproduction. Necrosis has been consistently associated with TiLVD pathology in several studies (1, 13, 19, 21, 24, 31, 32, 35, 37, 42). In addition, in TiLV-infected tilapia, several genes namely *tnfa*, *tnfrsf6b*, and *ripk1* all involved in the regulation of necroptosis have also been found to be upregulated (31). It is therefore possible that such a significant upregulation in *tnfa* and in genes involved in the regulation of necroptosis during TILVD progression both drive the development of programmed necrosis as observed in multiple organs, especially in the liver of TiLV-infected fish. It might thus be a host-induced strategy to both inhibit viral replication as previously reported (72–74) and enhance inflammatory reactions to lessen viral reproduction. It will therefore be crucial to elucidate the contribution of necroptosis in TiLVD pathogenesis. Furthermore, it will be interesting to determine if TNF-α inhibits or stimulates TiLV replication as previously described for other viruses and to determine in which specific cells this inhibition occurs, as this might be cell-type specific.

Chemokine genes, encoding for chemotactic key player cytokines controlling the migration of immune cells in tissues during the innate immune response to infections, have also been found to be upregulated in the liver of TiLV-infected tilapia, notably the chemokine (C-C motif) ligand (CCL3) together with its receptor CCR1 (31).

CCL3, produced by macrophages and implicated in macrophage, neutrophil and NK-cell migration as well as in T-cell – dendritic cells interactions, has been reported to be associated with antiviral immunity through the production of IFNγ, meaning that it is almost invariably associated with viral infections (79), although with few exceptions. Of note, the ifnγ1-2 gene was also found to be significantly upregulated in the brain of adult zebrafish during TiLV infection (12). Therefore, together with IFNγ, CCL3 could be driving the inflammatory response and phenotype in affected tissues, through the recruitment of CCR1 as previously described during paramyxovirus infection (80).

Genes coding for CXCR4, the specific receptor for the chemokine CXCL12, a highly potent chemoattractant involved in chronic inflammation (81) was also found to be upregulated in the liver of tilapia during TiLV infection (31). The production of CXCR4, is induced highly in the liver during HCV or Hepatitis B

virus (HBV) infection and has been reported to be involved in directing immune cells from the circulation to the liver, while promoting their retention (81). It is therefore possible that CCL3 (possibly together with CXCL12) participates in driving the infiltration of lymphocytic inflammatory cells consistently observed in the liver during TiLV infection (21, 32, 35, 82). This is even more plausible when considering that genes encoding hematopoietic cell kinase - HCK [associated with enhanced secretion of pro-inflammatory cytokines (83)], and dedicator of cytokinesis - DOCK2 [reported to be critical for migration and activation of leukocytes (84)], both involved in inflammation and leukocytes migration, were also upregulated in the liver during TiLV infection (31).

3.3 Complement activation during TiLV infection

The complement system is a major component of the innate immune system. It consists of several plasma proteins responsible for various innate immune functions such as the elimination of invading pathogens, promotion of inflammatory responses, clearance of apoptotic cells and necrotic cell debris, and modulation of adaptive immune responses (85). Activation of complement leads to proteolytic cascades, terminating in opsonization and lysis of the pathogen as well as in the generation of the classical inflammatory response through the production of potent proinflammatory molecules. Almost all of the mammalian components of the complement system have homologues in teleost fish (27), and activation of complement generally occurs via three main pathways (classical, lectin, and alternative), depending on specific recognition molecules. It was recently found that genes coding for a significant number of components of the complement system such as C3, C4, C1R, CFB, CFD, C8A, C9, C1S, CFI and CFH, belonging to all three complement activation pathways, are upregulated in the liver of tilapia during TiLV infection (31). Moreover, genes encoding opsonins such as C-reactive protein (CRP) and signaling lymphocytic activation molecule (SLAM)-associated protein (SAP) which are involved in complement activation and facilitate the clearance of pathogens through phagocytosis (86) were also found to be upregulated during TiLV infection (31). Similarly, the gene encoding lysozyme LYZ, which is reported to stimulate the cellular and humoral defense mechanisms of fish and to provide protection against viral diseases (87), was also upregulated in addition to phospholipase A2 gene (*pla2s*) (31), which has been reported to block viral entry into cells (88). Furthermore, the gene encoding alpha2-macroglobulin (a2M), which has been reported to be involved in innate immunity against viruses and apoptosis (89), was also upregulated during TiLV infection (31).

3.4 Local innate immune response in the brain: TiLV induces brain inflammation and microglia activation

The consistent reports of TiLV infection and pathology in the brain (12, 16, 19, 32, 35, 42, 66, 82, 90), clearly demonstrate that TiLV exhibits neurotropism. When cells of the brain become infected, the rapid production of type I IFNs is important to ensure host survival, as it has been shown that mice lacking the receptor for these IFNs were more susceptible to fatal disease progression following Sindbis virus infection (91, 92).

As previously mentioned, genes encoding RIG-I, TLR3 and TLR7 are all upregulated during TiLV infection in the brain (12, 47), similarly to IRF3, IRF7 and MAVS (IPS-1) (12, 42). Interestingly, type I IFN genes (infϕ1) are also significantly upregulated in the brain of zebrafish IP-injected with TiLV (12). It is known that in mammals IFN-β is immediately and preferentially produced by neurons and glial cells of the brain during virus infection (93, 94), probably because of its reduced central nervous system (CNS) toxicity compared to IFN-α (93, 94). Moreover, IFN-β might induce the production of neurotrophic factors by astrocytes (95) and might also induce the local production of the anti-inflammatory cytokine IL-10 (96), which all participate in maintaining the integrity of brain cells by dampening the inflammatory response in the brain. In support of this, high levels of the gene encoding the anti-inflammatory cytokine IL-10 were also found in the brain of zebrafish during TiLV infection (12). However, probably in response to brain damage as a result of virus replication and as an attempt of the host to clear the infection, high levels of the genes encoding proinflammatory cytokines such as IL-1β, IFNγ1-2, TNF-α, IL-8 (*cxcl8a*), the enzyme COX2b, and the antiviral effector Mxa were also detected in the brain during TiLV infection (12, 66). This results in the induction of brain inflammation or encephalitis (12) reported during TiLV infection in the brain, probably driven by the concomitant potent inflammatory action of IL-1β and IL-8 cytokines on brain cells (71, 97).

Inflammatory cytokines such as TNF-α, IL-1β, and IFN-γ disrupt the blood-brain barrier (BBB) as well as the tight junction integrity of brain endothelial cells (98–100). These inflammatory cytokines signaling at the BBB during infection facilitate leukocytes trafficking into the CNS, which although essential for virus clearance (100, 101), has multiple consequences, including enhancement of inflammation and activation of microglia as also observed during TiLV infection (12).

Microglia are brain resident antigen presenting cells (APCs) and macrophages. They are involved in first line innate immunity of the CNS and have a large regulatory role in CNS immunity. They play an important role in controlling viral replication and reducing mortality in the early stage of infection (102). Activated microglia

have a direct antiviral effect during viral infection by producing IFN-I after recognition of virus by PRRs, and the IFN produced by microglia exerts an indirect antiviral effect by acting on other cells. In addition, microglia can restrict viral infection by autophagy (103). In fact, microglia also affect the induction of the adaptive immune response in the brain, as it has been shown that the total number and percentage of activated CD4+ T-cells decrease, as well as the frequency and number of T regulatory cells significantly decrease following depletion of microglia (102), indicating that they are crucial for fully activating virus-specific T-cell responses.

Microglia activation during TiLV infection was characterized by a change in their shape from highly ramified cells in their resting state, to ameboid, spherical morphology when activated. Furthermore, genes expressing microglia markers such as *csf1r* and *cd68* in the brain of adult zebrafish and *apoeb* in the larvae were all upregulated further supporting their activation (12). However, phagocytosis or autophagy were not demonstrated. It thus remains to be determined whether such an activation also results in phagocytosis of TiLV-damaged brain cells. The ultimate questions however remain which specific cells of the brain (neurons, microglia, oligodendrocytes, meninges, astrocytes) are targeted by TiLV virus during its neurotropic stage of infection and what is the specific route of entry of TiLV virus into the CNS.

4 Adaptive immunity against TiLV infection

In general, the adaptive immune system recognizes foreign pathogens by means of two types of cellular receptors: the B-cell receptor (BCR) and the T-cell receptor (TCR). B- and T-cells are the main effector cells of the adaptive immune response. The adaptive immune response is regulated by several mechanisms and increases with antigen exposure, producing an immunological memory, which constitutes the basis of vaccine development. The adaptive response is generally established days after infection and can recognize specific foreign antigens, thus leading to a response that increases in both speed and magnitude with subsequent exposures (104). In general, B-cells mediate the antibody (humoral) responses while T-cells are mainly involved in cell-mediated immune responses. However, both the humoral and cell-mediated responses are essential in antiviral defense and the function of both arms occurs in concert.

The relationship between the innate and adaptive immune system occurs via the antigen-presenting cells (APC) such as dendritic cells (DCs) and macrophages which, after processing microorganisms, display the processed antigen molecules on their surface to be presented to T lymphocytes via the major histocompatibility complex (MHC) class 2 receptors, which in turn initiates the adaptive cell mediated immune response.

4.1 Induction of the adaptive immunity by activation of melano-macrophage centres

In teleost fish such as tilapia, antigen trapping and presentation occurs in melano-macrophage centres (MMCs), which often exist as complex discrete centres containing lymphocytes and macrophages (105). As such, they are thought to participate in the adaptive immune response, and they likely perform similar functions as mammalian germinal centers (GCs), although with certain differences (106). These immune-related structures, commonly seen within the reticuloendothelial supporting matrix of hematopoietic tissues, have been found to significantly increase in size and frequency in conditions of environmental stress and during infection (107, 108), and their proliferation is often associated with late stages of chronic infection (109, 110).

Throughout the progression of TiLVD, MMCs have been consistently found to increase in size and number in the liver and the spleen (36, 90), and in the kidney (82) of tilapia exposed to TiLV. Such an increase in MMC abundance is thus likely indicative of the activation of the adaptive immune system as the populations of lymphocytes (and macrophages) capable of mounting an immune response are often situated close to these sites of antigen trapping also associated with accumulations of melano-macrophages (27).

4.2 Cell-mediated adaptive immune response

Histocompatibility molecules are glycoprotein receptors encoded by a gene complex, which are expressed in almost all nucleated cells of the organism. MHC plays an important role for the presentation and recognition of both endogenous and exogenous antigens. In fact, antigen presentation is an important immunological process playing a crucial role in both the detection of viruses and virally infected cells by T-cells and the activation of cell-mediated adaptive immunity (111).

4.2.1 Antigen presentation

As previously mentioned, antigens processed by cells are displayed on their surface via the MHC I and MHC II receptors to be presented to T-cells for cell-mediated immune response activation. MHC class I molecules are ubiquitously expressed while MHC class II molecules are expressed in specialized APCs such as DCs, B-cells and macrophages. While MHC class I molecules are expressed on the surface of all nucleated cells and present peptides to be recognized by the T cell receptor of CD8+ T-cells, MHC class II molecules are expressed by specialized immune cells and present peptides to CD4+ T-cells (111).

During TiLV infection, a couple of genes coding for proteins regulating and modulating MHC class I antigen presentation were

found to be upregulated, especially in the liver of TiLV-infected tilapia fish (31). The *pmse2* gene, involved in altering the cleavage properties of the proteasome thereby enhancing MHC class I antigen presentation (112), was found to be upregulated during TiLV infection. Genes encoding heat shock proteins such as HSPA1s, HSPA4, HSPA5, and HSP90A, reported to serve as post-proteasomal peptide carriers delivering processed antigen peptides to transporters associated with antigen processing (TAPs) thereby preventing the degradation of processed epitopes by cytosolic peptidases (113), were also found to be upregulated during TiLV infection (31).

Similarly, genes encoding molecules involved in MHC class II pathway regulation such as the CD74 (I chain), which facilitates the assembly of alpha and beta subunits of the MHC II molecules within the endoplasmic reticulum (114), as well as GILT and CTSL, involved in reducing protein disulfide bonds formation thereby exposing epitopes for efficient MHC II-restricted binding and subsequent antigen presentation (115) and in the processing of class II-associated invariant chains followed by the loading of antigenic peptides into MHC II molecules (116) respectively, were all found to be upregulated during TiLV infection (31). The upregulation of these genes associated with and involved in MHC I and MHC II antigen presentation suggests that TiLV-deriving antigens and peptides are effectively processed, transported to the cell surface and presented to T-cells for the efficient induction of the cell-mediated adaptive immunity.

4.3 Activation and modulation of the T-cell adaptive immune response

Mature T-cells possess a T-cell receptor (TCR) by which they recognize linear antigens presented by MHC molecules. They express the TCR co-receptor CD8 or CD4 which drives their specificity for MHC class I or MHC class II presented antigens respectively, while also having the potential to form immunological memory in case of future pathogen insult.

There is a clear distinction between CD8 and CD4 expressing T cells, based on the expression of the co-receptors CD8 or CD4 (CD8 + and CD4+ cells respectively). While CD8 marks cytotoxic T lymphocytes (CTLs) that recognize antigenic peptides associated with MHC class I molecules on the surface of antigen presenting cells and whose main function is the direct killing of target cells. CD4 on the other hand, marks T helper cells (Th cells) that recognise peptides associated with MHC class II and which orchestrate several aspects of the adaptive immune response via the release of modulatory cytokines.

The specific activation and cytotoxic actions of CD8+ cells during TiLV infection have not yet been demonstrated. However, at later stages during TiLV infection (at 6 to 14 days post-infection), a significant up-regulation of the expression of CD4 markers *cd4-1* and *cd4-2* was observed in the liver and spleen of TiLV-infected zebrafish (13), suggesting the activation of CD4+ and their cell-mediated antiviral action. The role of CD4+ T-cells in antiviral immunity is highly dependent on the production of pro-inflammatory cytokines such as IFN-γ (79, 117), which has also been found to be significantly upregulated in the spleen and kidney of zebrafish during TiLV infection (13). CTLs are major producers of IFN-γ, which is also the hallmark cytokine of Th1 cells activation. By also producing IFN-γ, Th1 cells, which are crucial for controlling most viral infections, promote CTL-mediated lysis of infected target cells by stimulating the maturation of CTL precursors. In addition, IFN-γ stimulates the production of several other proteins that contribute to enhanced antigen presentation and T-cell activation including MHC molecules.

It is also possible that the significant up-regulation of genes encoding the anti-inflammatory cytokines tumour growth factors (TGF)-β and IL-10 in the intestine, spleen, liver and kidney of TiLV infected tilapia and zebrafish (13, 35, 67) aims at promoting the development of Th17 cells, although IL-6 and IL-1 might also be required; the presence and up-regulation of which have not yet been demonstrated during TiLV infection. Such an upregulation in TGF-β and IL-10 levels might also predict the activation of T-reg cells since these two cytokines are also produced by T-reg cells. Although Th17 differentiation is inhibited by IFN-γ and IL-4, DCs can also efficiently present antigens to Th17 in the presence of TGF-β, thereby promoting Th17 cell differentiation. However, TGF-β and IL-10 remain natural anti-inflammatory cytokines which, together with T-reg cells, can strongly suppress immune responses to pathogens.

Other gene transcripts encoding for other interferon regulatory factors involved in adaptive immunity have also been found to be upregulated in the liver of tilapia fish infected with TiLV. This is for instance the case of IRF4 (31), thought to regulate the maturation and differentiation of immune cells, especially the development of effective cytotoxic T-cell responses during viral infection (118) and IRF8 (31), which is involved in CD8+ dendritic cell differentiation and is required for natural killer (NK)-cell-mediated antiviral immunity by promoting the proliferation of virus-specific NK cells (119). As previously mentioned, the gene transcripts coding for *viperin* (*rsad2*) are also significantly upregulated in the liver during TiLV infection (43). Such an upregulation in the expression of viperin suggests that this IFN-induced protein may also be involved in regulating Th2 cells response (120) during the infection and could thus be modulating anti-TiLV T-cell-mediated immunity.

4.3.1 Adaptive immunity activation in the brain

During most neurotropic viral infections in mammals, the activation of naive T-cells and B-cells occurs in secondary lymphoid tissues outside of the CNS (121–123), although there exist cells that can present antigens to primed T-cells in the CNS. Although the route of entry of TiLV into the CNS remains to be determined, inoculation of neurotropic viruses directly into the cerebrospinal fluid (CSF) tends to elicit a potent immune response characterized by marked antibody responses and priming of cytotoxic $CD8^+$ T-cells (124). Both tight junctions and the relative nonreactivity of cerebral capillary endothelial cells generally restrict the entry of circulating leukocytes into the CNS. However, it has been shown that activated T-cells can routinely cross the blood–brain barrier as part of the normal immunological surveillance of all tissues (125–127) and can be retained in the CNS when the relevant

antigen is present and associated with appropriate MHC molecules (125).

Indeed, infiltration of mononuclear inflammatory immune cells into the CNS can occur days following neurotropic virus infections, with cells first accumulating in the perivascular areas, as also observed during TiLV infection in the brain (16, 90), followed by massive infiltration in the regions of virus infection, which has also been described during TiLV infection (32, 42, 82). Such a massive infiltration can drive the occurrence of lymphocytic meningitis, a condition often associated with brain inflammation, and which has also been described during TiLV infection (19).

It will thus be of interest to elucidate if the local production of chemokines during brain inflammation caused by TiLV infection induces the expression of adhesion molecules by endothelial cells, which could enhance the entry of activated immune cells into the CNS. Of particular interest, the expression profiles of the genes encoding the intercellular adhesion molecule 1 (ICAM1, CD54) and the vascular-cell adhesion molecule 1 (VCAM1) during TiLV infection could be investigated as this could provide insights into the immune cell infiltration observed during TiLV infection, and open avenues for lymphocytic entry blockade using antibodies or ligands binding to these molecules.

Microglia activation has also been reported during brain inflammation following TiLV infection (12), whether such an activation, in turn, leads to brain DCs differentiation remains to be elucidated.

4.4 Humoral (antibody) response during TiLV infection

As previously mentioned, B-cells mediate antibody (humoral) responses. During antibody responses, B-cells are activated to secrete antibodies, which are soluble forms of their surface immunoglobulin (Ig) antigen receptor. The antibodies circulate in the bloodstream, binding specifically to the foreign antigen that stimulates their production. The binding of antibodies to their targets such as viruses, results in their inactivation and the blocking of their ability to bind to their receptors on host cells. In addition, antibody binding also tags invading pathogens for destruction by cells such as phagocytic cells of the innate immune system bearing cell surface receptors for the Ig molecules.

During TiLV infection, it has been shown that tilapia can mount a humoral antibody response reaching high levels within 2 to 4 weeks post primary exposure to the virus (29). This antibody response is characterized by an upregulation of IgM mRNA levels in organs such as the brain, head kidney, liver (in tilapia), spleen and kidney (in zebrafish) of TiLV infected fish (13, 32). In some individuals, circulating antibodies persisted for up to 110 days in TiLV-exposed tilapia; upon re-exposure, an antibody response was shown to develop within 7 to 14 days (Figure 4) (29). Interestingly, some individuals only produce antibodies against TiLV about 12 weeks post-primary exposure to the virus. Moreover, few tilapia have been found to survive both the initial exposure and a

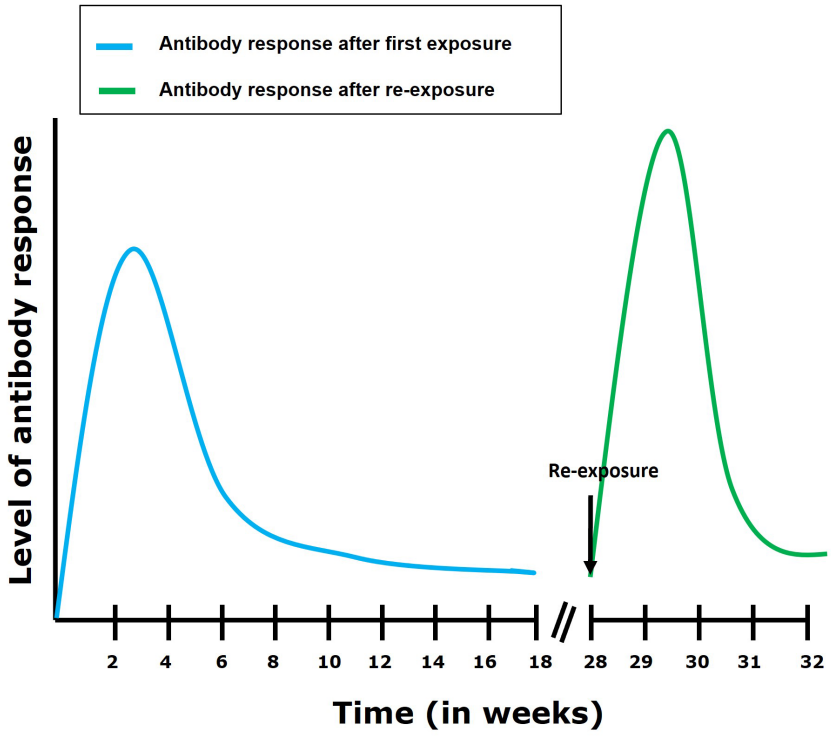

FIGURE 4
Antibody response following first exposure and re-exposure to TiLV infection. It has been shown (29) that the antibody response in most tilapia fish following first exposure to TiLV reaches its highest level within 4 weeks post exposure. The antibody levels then gradually declines but remains maintained till about 16 weeks post-exposure. After re-exposure, an elevated and more rapid (7 to 14 days to establish itself) antibody response can be observed which then gradually declines.

subsequent TiLV virus challenge without generating an antibody response (29). This suggests a great variation in disease susceptibility and probably immune defense mechanisms which could be characterized by the induction of a robust innate immune response which could have resolved the infection without inducing the adaptive immunity in these individuals. Alternatively, it is also possible that these individuals are naturally resistant to TiLV infection. Factors associated with disease resistance are thus also discussed later.

Strikingly, fish specific IgT antibody production, which is associated with mucosal immunity in teleost fish (128, 129), has not yet been reported following TiLV natural infection. Moreover, the gene transcripts encoding this antibody isotype (*igt 1/2*) were downregulated in the liver, gill and brain of TiLV-resistant tilapia fish strains and only slightly upregulated in the brain of a TiLV-susceptible strain later during infection (67). Interestingly, a significant upregulation of this antibody isotype was observed in the head kidney of tilapia fish vaccinated with heat-inactivated whole TiLV virus (130), suggesting that IgT might still be produced at mucosal surfaces during infection with live virus. Moreover, accelerated host responses in mucosa could be related to significantly lower viral loads in a TiLV-resistant tilapia strain (67), probably indicating that mucosal immunity also plays an important role in protection from TiLV infection.

The role of mucosal immunity during TiLV infection should warrant further studies, which will also enable the mechanisms governing specific B-cells activation during TiLV infection to be uncovered. The full spectrum of antibodies produced during infection with TiLV should also be explored as this could reveal a great deal about humoral immunological responses against viral infections in teleost fish such as tilapia in general.

5 Interplay between TiLV and host responses

5.1 Host factors associated with resistance to TiLV infection

Several significant quantitative trait loci (QTL) affecting resistance to TiLV were identified on chromosomes Oni3 and Oni22 of farmed Nile tilapia (*Oreochromis niloticus*). The average mortality rate of tilapia fish homozygous for the resistance allele at the most significant single nucleotide polymorphism (SNP) on these QTLs was 11% compared to 43% for tilapia homozygous for the susceptibility allele. Several candidate genes related to the host response to viral infection were identified within these QTLs, including *cdc42*, *trim21* and *trim29* (131).

In mice, CDC42 appears to be a key regulator of B-cell differentiation required for antiviral humoral immunity (antibody responses), germinal center formation, and formation of plasma cells during influenza virus (PR8 strain) infection (132). Moreover, *cdc42* gene was also mapped to a QTL associated with host resistance to cardiomyopathy syndrome (133) in Atlantic salmon populations. The role of CDC42 as a key regulator of B-cell fate and physiology during TiLV infection should thus be explored.

The ubiquitin ligase tripartite motif containing-21 (TRIM21) antibody receptor provides one of the last lines of defense against invading viruses by acting as a sensor that intercepts antibody-coated viruses (virus neutralization) that have evaded extracellular neutralization and breached the cell membrane (134). TRIM29 on the other hand has been found to negatively control antiviral immune response to DNA viruses (135). Moreover, TRIM29 has been found to inhibit innate immune activation following Epstein-Barr virus infection (136) and to negatively regulate type I IFN production during dsRNA reovirus infection by interacting with MAVS and by inducing its K11-linked ubiquitination and degradation (137).

Interestingly, the gene coding for TRIM21 was found to be significantly upregulated in the liver, gill and brain of TiLV-susceptible tilapia strains but only in the liver and gill of a TiLV-resistant tilapia strain during TiLV infection (67). However, resistance to TiLV disease in this resistant tilapia strain was correlated with lower viral loads both at the mucosa-rich tissue of the gills and internal tissues, once more highlighting the need for studies to understand the role of mucosal immunity during TiLV infection. Moreover, a higher magnitude of Mx-1-based antiviral response possibly limiting virus spread in the initial phase of infection was proposed as a possible mechanism driving such lower viral load as well as the lower pro-inflammatory responses exhibited by the TiLV-resistant strain, which is thought to additionally contribute to its protection from developing pathological changes related to the disease (67).

The resistance of red hybrid tilapia to TiLV infection could also be modulated using probiotic-supplemented diets, which resulted in lower cumulative mortality rate and significantly lower viral load (in the liver, spleen and head kidney), especially in red hybrid tilapia fed with 1% *Bacillus spp* probiotics. In addition, in tilapia fed with 1% *Bacillus spp*, a significant upregulation of the expression of *inf-γ* and *il-8* genes was observed in the liver, spleen, and head kidney subsequently contributing to improving the antiviral response mounted by this group of fish against TiLV (70).

5.2 Possible immune subversion by TiLV virus

It has been shown that TiLV can downplay the innate immune responses during the early stage of infection in Nile tilapia (32). Although the exact mechanisms by which TiLV subverts and modulates the immune response remain to be elucidated, it has been observed that, following TiLV infection, there is a downregulation of genes encoding both the interferon-induced proteins with tetratricopeptide repeats (IFIT1) (in interferons) and TRIM25 (in the NF-kB pathway) in the liver of TiLV-infected tilapia (31), further suggesting that TiLV is capable of modulating the host immune response to its advantage to establish and sustain the infection.

Indeed, IFIT1 is strongly induced downstream of type I IFN signaling. Although the mechanisms underlying the antiviral activity of IFITM proteins in general remain uncertain, IFIT1 could exert one of its antiviral activities by recognizing and potentially sequestering viral triphosphorylated RNA (PPP-RNA), thereby preventing it from being translated by the host machinery (138). In addition, it has been shown that human IFIT1 can suppress IRES-dependent viral RNA translation during HCV infection (139). It has also been shown to directly bind to viral proteins such as the human papillomavirus (HPV) viral helicase E1 protein required for HPV viral replication, leading to E1 sequestration within the cytoplasm, thus preventing it from aiding in viral replication within the nucleus (140, 141).

On the other hand, the E3 ubiquitin ligase TRIM25 has been shown to play a role in the RIG-I pathway, triggering the expression of type I interferons upon viral infection. TRIM25 has been shown to inhibit influenza A virus (IAV) infection by destabilizing IAV viral mRNA, and its direct tethering to an RNA molecule is also sufficient to downregulate the targeted RNA (142). TRIM25 could also inhibit flavivirus and birnavirus replication *in vitro* (143, 144) and in the case of birnavirus infection, by targeting VP3 for ubiquitination and degradation (144).

The downregulation of such antiviral restriction factors suggests possible immune evasion and modulation strategies of TiLV to successfully establish and sustain the infection within its host. Immune evasion and modulation strategies by the virus should therefore warrant further investigations.

6 Discussion

6.1 Knowledge gaps

It is clear that many questions remain to be addressed regarding the immune responses of tilapia to TiLV infection. The exact virus entry site(s) remain to be determined as well as the specific immune responses at those entry sites. The mechanisms by which TiLV escapes the early immune responses at entry sites, and which lead to its systemic dissemination [and systemic infection - (43)] also remain unresolved.

TiLV has been shown to persist in the brain (for up to 90 days) during infection (12). Such a long viral persistence in the brain suggests that the brain is an immune privileged site incapable of clearing the infection. Ideally, the development of antibodies (especially neutralising antibodies) during the infection, should provide sterile immunity against the pathogen. However, the persistent detection of the virus in asymptomatic tilapia could indicate that the virus can hide from the immune system even at late stages of the infection. The immune evasion mechanisms governing this persistence of the virus as well as the lack of virus clearance in the brain also remain largely unknown.

Infection with TiLV is in most cases lethal. However there have been reports of fish surviving the infection (67, 90, 131) suggesting the existence of specific immune mechanisms leading to both favourable (preventing mortality) and unfavourable (immunotoxic) disease outcomes, both of which are still to be established.

TiLVD outbreaks are often detected within complex diseases involving the virus and additional pathogens, most often bacteria and parasites. Moreover, TiLV has been associated with co-infections with other viruses such as tilapia parvovirus (TiPV) (145). Although the synergism between TiLV and TiPV coinfection remains to be determined, this could suggest that TiLV is passively (by disrupting mucosal barriers) or actively (by inducing immunosuppression) promoting superinfections, thus worsening disease severity. However, the mechanisms of mucosa disruption or immune subversion by TiLV infection remain to be clarified.

6.2 Closing remarks

Since the initial reports of TiLV disease and infection in 2014 (23, 90), several studies have been undertaken to elucidate the immune responses occurring during TiLV infection. Although these studies, and the immune response branches they address (all summarized in Table 1), have greatly contributed to our knowledge of the possible immune responses of tilapia to TiLV infection, it remains clear that the specific mechanisms underlying the antiviral response to TiLV infection are still poorly studied and understood. For instance, the nature of the specific cells involved in innate immunity against TiLV infection remains to be determined as well as the exact mechanisms by which TiLV suppresses and subverts the host immune response to establish the infection. The full spectrum of antibodies generated during TiLV infection remains to be established, and the exact mechanisms of TiLV entry into the CNS remain to be uncovered as well as the specific brain cells targeted by the virus.

The presence of TiLV in the intestine (13, 34) raises the notion of TiLV antigen sampling in the intestine, which we believe should also be addressed, since it could significantly improve our knowledge of the development of the adaptive cellular and humoral response in the intestine (which could be one of the main port of entry for the virus).

We have seen that resistance to TiLV disease in some tilapia strains correlates with lower viral loads at the mucosa-rich tissue of the gills (67) and that accelerated host responses in mucosa could be related to such significantly lower viral loads in a TiLV-resistant tilapia strain (67). It thus becomes clear that the extent of the role played by mucosal immunity during TiLV infection control should be further addressed.

The complex network regulating both the innate and adaptive immune responses during TiLV infection remains to be uncovered and explored. It will be interesting to know whether similar mammalian Th1, Th2, Th17 and Treg responses occur during TiLV infection and if these responses are governed by mechanisms similar to those in their mammalian counterparts. Moreover, the T-cell and B-cell interplay should be explored to understand their implications in immunopathogenesis.

TABLE 1 Summary of the different studies addressing the pathology and immune responses to TiLV infection.

Immune component	Immune response	References
Pathogenesis	Syncytia formation	(1, 11, 17, 19, 23, 24, 35–37, 43)
	Necrosis	(1, 13, 19, 21, 24, 31, 32, 35, 37, 42)
	Upregulation of genes involved in the regulation of necroptosis, in inflammation and in leukocyte migration	(31)
	Infiltration of lymphocytic inflammatory cells in the brain, liver, intestines and spleen	(19, 21, 32, 35, 42, 43, 82)
Innate immunity	Upregulation of *tlr3*, *tlr7*, *tlr22* in tilapia and zebrafish	(12–14, 42)
	Upregulated expression of *irf1*, *irf3*, *irf5*, *irf7* in tilapia and zebrafish	(12–14, 31, 35, 43)
	Upregulated expression of *rig-1* in zebrafish	(12–14)
	Upregulated expression of *mavs* (*ips-1*) in tilapia	(42)
	Upregulation of *traf3* and *nfkbia* genes in tilapia	(31)
	Upregulation of type I IFNs (*ifnϕ1*) in zebrafish and antiviral activity of type I IFN against TiLV infection	(12–14)
	Upregulation of *mxa* gene transcripts in tilapia and zebrafish	(12–14, 31, 32, 35)
	Upregulation of genes coding for *mx1* and *rsad2* (viperin) transcripts in brown trout and rainbow trout	(15)
	Upregulation/high levels of IL-1β in tilapia and zebrafish	(12–14, 31, 32, 35, 66, 67)
	Upregulation of *il-8* in tilapia and zebrafish	(12, 43, 70)
	Upregulation of *tnf-α* in tilapia and zebrafish	(12, 13, 31, 66)
	Upregulation of chemokine *ccl3* gene and chemokine receptor *cxcr4* gene/Upregulation of genes coding for components of the complement activation pathways/Upregulation of opsonins genes in tilapia	(31)
	Upregulation of *rsad2* (viperin) expression in tilapia	(43)
	TiLV infection and pathology in the brain	(12, 16, 19, 32, 35, 42, 66, 82, 90)
	Induction of brain inflammation (encephalitis)/Microglia activation	(12)
Adaptive immunity	Activation of MMCs in tilapia	(36, 82, 90)
	Upregulation of genes encoding proteins regulating or modulating MHC class I antigen presentation/Upregulation of genes involved in MHC class II pathway	(31)
	Upregulation of the expression of CD4 markers (*cd 4-1* and *cd 4-2*)/Upregulation of IFN-γ	(13)
	Upregulation of *irf4* and *irf8* in tilapia	(31)
	Accumulation of mononuclear inflammatory immune cells at perivascular areas in the brain	(16, 90)
	Massive infiltration of immune cells in the brain/Lymphocytic meningitis	(19, 32, 42, 82)
	Upregulation of *igm* in tilapia and zebrafish	(13, 32)
	Downregulation of IgT (*igt 1/2*) in resistant tilapia strains and upregulation in susceptible tilapia strain	(67)
	Upregulation of *tgf-β* and *il-10* in tilapia and zebrafish	(13, 35, 67)
	Development of protective immunity including a humoral response after the exposure to TiLV	(29)
Interplay between TiLV and host responses	Downregulation of *ifit1* and *trim25*	(31)
	Host factors located in the vicinity of QTL associated with resistance to TiLV infection (*cdc 42*, *trim21, trim29*)	(131)
	Host factors associated with responses during resistance to TiLV infection (upregulation of *mx1*, downregulation of *il1b*)	(67)

An overall downregulation of genes involved in cellular metabolism has been observed during TiLV infection (31). The implications of such a downregulation on the overall immune profile of the host tilapia during the infection should also thus be explored.

Author contributions

JK-R: Conceptualization, methodology, investigation, resources, writing and review – original draft. DS: review and editing – original draft. KT: review and editing – original draft. JD: supervision, review and editing – original draft. MA: supervision, funding acquisition, resources and review and editing – original draft. All authors contributed to the article and approved the submitted version.

Funding

Author MA was supported by Deutsche Forschungsgemeinschaft (DFG project number 426513195). This Open Access publication was funded by the Deutsche Forschungsgemeinschaft (DFG, German Research Foundation) - 491094227 "Open Access Publication Funding" and the University of Veterinary Medicine Hannover, Foundation.

Acknowledgments

We are grateful to Dr. John Readman (Department of Infection, Immunity & Inflammation, GOS Institute of Child Health (ICH), University College London) for his wonderful assistance in the conceptualization of the manuscript.

Conflicts of interest

The authors declare that the research was conducted without any commercial or financial relationships that could be construed as a potential conflict of interest.

Publisher's note

References

1. del-Pozo J, Mishra N, Kabuusu R, Cheetham S, Eldar A, Bacharach E, et al. Syncytial hepatitis of tilapia (Oreochromis niloticus L.) is associated with orthomyxovirus-like virions in hepatocytes. *Vet Pathol* (2017) 54(1):164–70. doi: 10.1177/0300985816658100

2. Bacharach E, Mishra N, Briese T, Zody MC, Kembou Tsofack JE, Zamostiano R, et al. Characterization of a novel orthomyxo-like virus causing mass die-offs of tilapia. *mBio* (2016) 7(2):e00431–16. doi: 10.1128/mBio.00431-16

3. Adams MJ, Lefkowitz EJ, King AMQ, Harrach B, Harrison RL, Knowles NJ, et al. Changes to taxonomy and the International Code of Virus Classification and Nomenclature ratified by the International Committee on Taxonomy of Viruses (2017). *Arch Virol* (2017) 162(8):2505–38. doi: 10.1007/s00705-017-3358-5

4. Turnbull OMH, Ortiz-Baez AS, Eden J-S, Shi M, Williamson JE, Gaston TF, et al. Meta-transcriptomic identification of divergent amnoonviridae in fish. *Viruses* (2020) 12(11):1254. doi: 10.3390/v12111254

5. Ortiz-Baez AS, Eden JS, Moritz C, Holmes EC. A divergent articulavirus in an Australian gecko identified using meta-transcriptomics and protein structure comparisons. *Viruses* (2020) 12(6):613. doi: 10.3390/v12060613

6. Acharya V, Chakraborty HJ, Rout AK, Balabantaray S, Behera BK, Das BK. Structural characterization of open reading frame-encoded functional genes from Tilapia Lake Virus (TiLV). *Mol Biotechnol* (2019) 61(12):945–57. doi: 10.1007/s12033-019-00217-y

7. Abu Rass R, Kustin T, Zamostiano R, Smorodinsky N, Meir DB, Feder D, et al. Inferring protein function in an emerging virus: detection of the nucleoprotein in tilapia lake virus. *J Virol* (2022) 96(6):e01757–21. doi: 10.1128/jvi.01757-21

8. Abdullah A, Pazai AMM, Ridzuan MSM, Sudirwan F, Hashim S, Abas A, et al. Persistent detection of Tilapia lake virus in wild tilapia and tinfoil barbs. *Vet World* (2022) 15(4):1097–106. doi: 10.14202/vetworld.2022.1097-1106

9. Abdullah A, Ramly R, Mohammad Ridzwan MS, Sudirwan F, Abas A, Ahmad K, et al. First detection of tilapia lake virus (TiLV) in wild river carp (Barbonymus schwanenfeldii) at Timah Tasoh Lake, Malaysia. *J Fish Dis* (2018) 41(9):1459–62. doi: 10.1111/jfd.12843

10. Jaemwimol P, Rawiwan P, Tattiyapong P, Saengnual P, Kamlangdee A, Surachetpong W. Susceptibility of important warm water fish species to tilapia lake virus (TiLV) infection. *Aquaculture* (2018) 497:462–8. doi: 10.1016/j.aquaculture.2018.08.028

11. Paria A, Yadav SC, Verma DK, Mishra A, Rastogi A, Ravindra, et al. Susceptibility of selected tropical non-tilapine ornamental cichlids to Tilapia tilapinevirus following experimental infection. *Aquaculture* (2023) 567:739224. doi: 10.1016/j.aquaculture.2022.739224

12. Mojzesz M, Widziolek M, Adamek M, Orzechowska U, Podlasz P, Prajsnar TK, et al. Tilapia lake virus-induced neuroinflammation in zebrafish: microglia activation and sickness behavior. *Front Immunol* (2021) 12:760882. doi: 10.3389/fimmu.2021.760882

13. Rakus K, Mojzesz M, Widziolek M, Pooranachandran N, Teitge F, Surachetpong W, et al. Antiviral response of adult zebrafish (Danio rerio) during tilapia lake virus (TiLV) infection. *Fish Shellfish Immunol* (2020) 101:1–8. doi: 10.1016/j.fsi.2020.03.040

14. Widziolek M, Janik K, Mojzesz M, Pooranachandran N, Adamek M, Pecio A, et al. Type I interferon-dependent response of zebrafish larvae during tilapia lake virus (TiLV) infection. *Dev Comp Immunol* (2021) 116:103936. doi: 10.1016/j.dci.2020.103936

15. Adamek M, Matras M, Surachetpong W, Rakus K, Stachnik M, Bauer J, et al. How susceptible are rainbow trout and brown trout to infection with tilapia lake virus at increased water temperature – Is there any potential for climate change driven host jump? *Aquaculture* (2023) 571:739469. doi: 10.1016/j.aquaculture.2023.739469

16. Basri L, Nor RM, Salleh A, Md. Yasin IS, Saad MZ, Abd. Rahaman NY, et al. Co-Infections of Tilapia Lake Virus, Aeromonas hydrophila and Streptococcus agalactiae in Farmed Red Hybrid Tilapia. *Animals* (2020) 10(11):2141. doi: 10.3390/ani10112141

17. Amal MNA, Koh CB, Nurliyana M, Suhaiba M, Nor-Amalina Z, Santha S, et al. A case of natural co-infection of Tilapia Lake Virus and Aeromonas veronii in a Malaysian red hybrid tilapia (Oreochromis niloticus×O. mossambicus) farm experiencing high mortality. *Aquaculture* (2018) 485:12–6. doi: 10.1016/j.aquaculture.2017.11.019

18. Nicholson P, Mon-on N, Jaemwimol P, Tattiyapong P, Surachetpong W. Coinfection of tilapia lake virus and Aeromonas hydrophila synergistically increased mortality and worsened the disease severity in tilapia (Oreochromis spp.). *Aquaculture* (2020) 520:734746. doi: 10.1016/j.aquaculture.2019.734746

19. Aich N, Paul A, Choudhury TG, Saha H. Tilapia Lake Virus (TiLV) disease: Current status of understanding. *Aquac Fish* (2022) 7(1):7–17. doi: 10.1016/j.aaf.2021.04.007

20. Senapin S, Shyam KU, Meemetta W, Rattanarojpong T, Dong HT. Inapparent infection cases of tilapia lake virus (TiLV) in farmed tilapia. *Aquaculture* (2018) 487:51–5. doi: 10.1016/j.aquaculture.2018.01.007

21. Dong HT, Siriroob S, Meemetta W, Santimanawong W, Gangnonngiw W, Pirarat N, et al. Emergence of tilapia lake virus in Thailand and an alternative semi-nested RT-PCR for detection. *Aquaculture* (2017) 476:111–8. doi: 10.1016/j.aquaculture.2017.04.019

22. Dong HT, Ataguba GA, Khunrae P, Rattanarojpong T, Senapin S. Evidence of TiLV infection in tilapia hatcheries in Thailand from 2012 to 2017 reveals probable global spread of the disease. *Aquaculture* (2017) 479:579–83. doi: 10.1016/j.aquaculture.2017.06.035

23. Ferguson HW, Kabuusu R, Beltran S, Reyes E, Lince JA, del Pozo J. Syncytial hepatitis of farmed tilapia, Oreochromis niloticus (L.): a case report. *J Fish Dis* (2014) 37 (6):583–9. doi: 10.1111/jfd.12142

24. Surachetpong W, Janetanakit T, Nonthabenjawan N, Tattiyapong P, Sirikanchana K, Amonsin A. Outbreaks of tilapia lake virus infection, Thailand, 2015-2016. *Emerg Infect Dis* (2017) 23(6):1031–3. doi: 10.3201/eid2306.161278

25. Dong HT, Senapin S, Gangnonngiw W, Nguyen VV, Rodkhum C, Debnath PP, et al. Experimental infection reveals transmission of tilapia lake virus (TiLV) from tilapia broodstock to their reproductive organs and fertilized eggs. *Aquaculture* (2020) 515:734541. doi: 10.1016/j.aquaculture.2019.734541

26. Yamkasem J, Tattiyapong P, Kamlangdee A, Surachetpong W. Evidence of potential vertical transmission of tilapia lake virus. *J Fish Dis* (2019) 42(9):1293–300. doi: 10.1111/jfd.13050

27. Secombes CJ, Wang T. The innate and adaptive immune system of fish. In: Austin B, editor. *Infectious Disease in Aquaculture*. Sawston, Cambridge, UK: Woodhead Publishing (2012). p. 3–68.

28. Wang B, Thompson KD, Wangkahart E, Yamkasem J, Bondad-Reantaso MG, Tattiyapong P, et al. Strategies to enhance tilapia immunity to improve their health in aquaculture. *Rev Aquac* (2023) 15(S1):41–56. doi: 10.1111/raq.12731

29. Tattiyapong P, Dechavichitlead W, Waltzek TB, Surachetpong W. Tilapia develop protective immunity including a humoral response following exposure to tilapia lake virus. *Fish Shellfish Immunol* (2020) 106:666–74. doi: 10.1016/j.fsi.2020.08.031

30. Wang Y, Wang Q, Li Y, Yin J, Ren Y, Shi C, et al. Integrated analysis of mRNA-miRNA expression in Tilapia infected with Tilapia lake virus (TiLV) and identifies primarily immuneresponse genes. *Fish Shellfish Immunol* (2020) 99:208–26. doi: 10.1016/j.fsi.2020.01.041

31. Sood N, Verma DK, Paria A, Yadav SC, Yadav MK, Bedekar MK, et al. Transcriptome analysis of liver elucidates key immune-related pathways in Nile tilapia Oreochromis niloticus following infection with tilapia lake virus. *Fish Shellfish Immunol* (2021) 111:208–19. doi: 10.1016/j.fsi.2021.02.005

32. Mugimba KK, Lamkhannat M, Dubey S, Mutoloki S, Munang'andu HM, Evensen Ø. Tilapia lake virus downplays innate immune responses during early stage of infection in Nile tilapia (Oreochromis niloticus). *Sci Rep* (2020) 10(1):20364. doi: 10.1038/s41598-020-73781-y

33. Abu Rass R, Kembou-Ringert JE, Zamostiano R, Eldar A, Ehrlich M, Bacharach E. Mapping of Tilapia Lake Virus entry pathways with inhibitors reveals dependence on dynamin activity and cholesterol but not endosomal acidification. *Front Cell Dev Biol* (2022) 10:1075364. doi: 10.3389/fcell.2022.1075364

34. Piewbang C, Tattiyapong P, Techangamsuwan S, Surachetpong W. Tilapia lake virus immunoglobulin G (TiLV IgG) antibody: Immunohistochemistry application reveals cellular tropism of TiLV infection. *Fish Shellfish Immunol* (2021) 116:115–23. doi: 10.1016/j.fsi.2021.06.017

35. Pierezan F, Yun S, Piewbang C, Surachetpong W, Soto E. Pathogenesis and immune response of Nile tilapia (Oreochromis niloticus) exposed to Tilapia lake virus by intragastric route. *Fish Shellfish Immunol* (2020) 107:289–300. doi: 10.1016/j.fsi.2020.10.019

36. Waiyamitra P, Piewbang C, Techangamsuwan S, Liew WC, Surachetpong W. Infection of Tilapia tilapinevirus in Mozambique Tilapia (Oreochromis mossambicus), a Globally Vulnerable Fish Species. *Viruses* (2021) 13(6):1104. doi: 10.3390/v13061104

37. Pierezan F, Yun S, Surachetpong W, Soto E. Intragastric and intracoelomic injection challenge models of tilapia lake virus infection in Nile tilapia (Oreochromis niloticus L.) fingerlings. *J Fish Dis* (2019) 42(9):1301–7. doi: 10.1111/jfd.13052

38. Skehel JJ, Wiley DC. Receptor binding and membrane fusion in virus entry: the influenza hemagglutinin. *Annu Rev Biochem* (2000) 69:531–69. doi: 10.1146/annurev.biochem.69.1.531

39. Chan DC, Kim PS. HIV entry and its inhibition. *Cell* (1998) 93(5):681–4. doi: 10.1016/s0092-8674(00)81430-0

40. Gower TL, Pastey MK, Peeples ME, Collins PL, McCurdy LH, Hart TK, et al. RhoA signaling is required for respiratory syncytial virus-induced syncytium formation and filamentous virion morphology. *J Virol* (2005) 79(9):5326–36. doi: 10.1128/jvi.79.9.5326-5336.2005

41. Chen X, Liu S, Goraya MU, Maarouf M, Huang S, Chen JL. Host immune response to influenza A virus infection. *Front Immunol* (2018) 9:320. doi: 10.3389/fimmu.2018.00320

42. Haridas L, George MR, John KR, Mansoor MM, Selvamageswaran M, Mageshkumar P. Early innate immune responses of Nile tilapia (Oreochromis niloticus) during tilapia lake virus (TiLV) infection. *Aquaculture* (2023) 563:738962. doi: 10.1016/j.aquaculture.2022.738962

43. Turner JK, Sakulpolwat S, Sukdanon S, Lertwanakarn T, Waiyamitra P, Piewbang C, et al. Tilapia lake virus (TiLV) causes severe anaemia and systemic disease in tilapia. *J Fish Dis* (2023) 43:643–51. doi: 10.1111/jfd.13775

44. Feng H, Zhang YB, Gui JF, Lemon SM, Yamane D. Interferon regulatory factor 1 (IRF1) and anti-pathogen innate immune responses. *PloS Pathog* (2021) 17(1): e1009220. doi: 10.1371/journal.ppat.1009220

45. Feng H, Zhang YB, Zhang QM, Li Z, Zhang QY, Gui JF. Zebrafish IRF1 regulates IFN antiviral response through binding to IFNϕ1 and IFNϕ3 promoters downstream of MyD88 signaling. *J Immunol* (2015) 194(3):1225–38. doi: 10.4049/jimmunol.1402415

46. Carlin AF, Plummer EM, Vizcarra EA, Sheets N, Joo Y, Tang W, et al. An IRF-3-, IRF-5-, and IRF-7-independent pathway of dengue viral resistance utilizes IRF-1 to stimulate type I and II interferon responses. *Cell Rep* (2017) 21(6):1600–12. doi: 10.1016/j.celrep.2017.10.054

47. Yoneyama M, Onomoto K, Jogi M, Akaboshi T, Fujita T. Viral RNA detection by RIG-I-like receptors. *Curr Opin Immunol* (2015) 32:48–53. doi: 10.1016/j.coi.2014.12.012

48. Kumar H, Kawai T, Kato H, Sato S, Takahashi K, Coban C, et al. Essential role of IPS-1 in innate immune responses against RNA viruses. *J Exp Med* (2006) 203(7):1795–803. doi: 10.1084/jem.20060792

49. Hiscott J, Lin R, Nakhaei P, Paz S. MasterCARD: a priceless link to innate immunity. *Trends Mol Med* (2006) 12(2):53–6. doi: 10.1016/j.molmed.2005.12.003

50. Zou J, Bird S, Secombes C. Antiviral sensing in teleost fish. *Curr Pharm Des* (2010) 16(38):4185–93. doi: 10.2174/138161210794519093

51. Chang M, Collet B, Nie P, Lester K, Campbell S, Secombes CJ, et al. Expression and functional characterization of the RIG-I-like receptors MDA5 and LGP2 in Rainbow trout (Oncorhynchus mykiss). *J Virol* (2011) 85(16):8403–12. doi: 10.1128/jvi.00445-10

52. Hansen JD, Vojtech LN, Laing KJ. Sensing disease and danger: A survey of vertebrate PRRs and their origins. *Dev Comp Immunol* (2011) 35(9):886–97. doi: 10.1016/j.dci.2011.01.008

53. Lauksund S, Svingerud T, Bergan V, Robertsen B. Atlantic salmon IPS-1 mediates induction of IFNa1 and activation of NF-κB and localizes to mitochondria. *Dev Comp Immunol* (2009) 33(11):1196–204. doi: 10.1016/j.dci.2009.06.012

54. Biacchesi S, LeBerre M, Lamoureux A, Louise Y, Lauret E, Boudinot P, et al. Mitochondrial antiviral signaling protein plays a major role in induction of the fish innate immune response against RNA and DNA viruses. *J Virol* (2009) 83(16):7815–27. doi: 10.1128/jvi.00404-09

55. Simora RMC, Ohtani M, Hikima J-i, Kondo H, Hirono I, Jung TS, et al. Molecular cloning and antiviral activity of IFN-β promoter stimulator-1 (IPS-1) gene in Japanese flounder, Paralichthys olivaceus. *Fish Shellfish Immunol* (2010) 29(6):979–86. doi: 10.1016/j.fsi.2010.08.012

56. Babajani A, Hosseini-Monfared P, Abbaspour S, Jamshidi E, Niknejad H. Targeted mitochondrial therapy with over-expressed MAVS protein from mesenchymal stem cells: A new therapeutic approach for COVID-19. *Front Cell Dev Biol* (2021) 9:695362. doi: 10.3389/fcell.2021.695362

57. Diani E, Avesani F, Bergamo E, Cremonese G, Bertazzoni U, Romanelli MG. HTLV-1 Tax protein recruitment into IKKϵ and TBK1 kinase complexes enhances IFN-I expression. *Virology* (2015) 476:92–9. doi: 10.1016/j.virol.2014.12.005

58. Wang X, Zeng W, Osterrieder N. Susceptibility of Vero E6 cells to tilapia lake virus (TiLV) and anti-TiLV activity of type I interferon. *Aquaculture* (2023) 574:739598. doi: 10.1016/j.aquaculture.2023.739598

59. Robertsen B. The role of type I interferons in innate and adaptive immunity against viruses in Atlantic salmon. *Dev Comp Immunol* (2018) 80:41–52. doi: 10.1016/j.dci.2017.02.005

60. Zou J, Secombes CJ. Teleost fish interferons and their role in immunity. *Dev Comp Immunol* (2011) 35(12):1376–87. doi: 10.1016/j.dci.2011.07.001

61. Verhelst J, Hulpiau P, Saelens X. Mx proteins: antiviral gatekeepers that restrain the uninvited. *Microbiol Mol Biol Rev* (2013) 77(4):551–66. doi: 10.1128/mmbr.00024-13

62. Kibenge MJ, Munir K, Kibenge FS. Constitutive expression of Atlantic salmon Mx1 protein in CHSE-214 cells confers resistance to infectious salmon anaemia virus. *Virol J* (2005) 2:75. doi: 10.1186/1743-422X-2-75

63. Seo JY, Yaneva R, Cresswell P. Viperin: A multifunctional, interferon-inducible protein that regulates virus replication. *Cell Host Microbe* (2011) 10(6):534–9. doi: 10.1016/j.chom.2011.11.004

64. Rivera-Serrano EE, Gizzi AS, Arnold JJ, Grove TL, Almo SC, Cameron CE. Viperin reveals its true function. *Annu Rev Virol* (2020) 7(1):421–46. doi: 10.1146/annurev-virology-011720-095930

65. Wang X, Hinson ER, Cresswell P. The interferon-inducible protein viperin inhibits influenza virus release by perturbing lipid rafts. *Cell Host Microbe* (2007) 2 (2):96–105. doi: 10.1016/j.chom.2007.06.009

66. Mugimba KK, Tal S, Dubey S, Mutoloki S, Dishon A, Evensen Ø, et al. Gray (Oreochromis niloticus x O. aureus) and Red (Oreochromis spp.) Tilapia Show Equal Susceptibility and Proinflammatory Cytokine Responses to Experimental Tilapia Lake Virus Infection. *Viruses* (2019) 11(10):893. doi: 10.3390/v11100893

67. Adamek M, Rebl A, Matras M, Lodder C, El Rahman S, Stachnik M, et al. Immunological insights into the resistance of Nile tilapia strains to an infection with tilapia lake virus. *Fish Shellfish Immunol* (2022) 124:118–33. doi: 10.1016/j.fsi.2022.03.027

68. Li J-Y, Wang Y-Y, Shao T, Fan D-D, Lin A-F, Xiang L-X, et al. The zebrafish NLRP3 inflammasome has functional roles in ASC-dependent interleukin-1β maturation and gasdermin E–mediated pyroptosis. *J Biol Chem* (2020) 295(4):1120–41. doi: 10.1016/S0021-9258(17)49920-0

69. Bawazeer AO, Rosli S, Harpur CM, Docherty CA, Mansell A, Tate MD. Interleukin-1β exacerbates disease and is a potential therapeutic target to reduce pulmonary inflammation during severe influenza A virus infection. *Immunol Cell Biol* (2021) 99(7):737–48. doi: 10.1111/imcb.12459

70. Waiyamitra P, Zoral MA, Saengtienchai A, Luengnaruemitchai A, Decamp O, Gorgoglione B, et al. Probiotics modulate tilapia resistance and immune response against tilapia lake virus infection. *Pathogens* (2020) 9(11):919. doi: 10.3390/pathogens9110919

71. Bickel M. The role of interleukin-8 in inflammation and mechanisms of regulation. *J Periodontol* (1993) 64(5 Suppl):456–60.

72. Seo SH, Webster RG. Tumor necrosis factor alpha exerts powerful anti-influenza virus effects in lung epithelial cells. *J Virol* (2002) 76(3):1071–6. doi: 10.1128/jvi.76.3.1071-1076.2002

73. Lane BR, Markovitz DM, Woodford NL, Rochford R, Strieter RM, Coffey MJ. TNF-alpha inhibits HIV-1 replication in peripheral blood monocytes and alveolar macrophages by inducing the production of RANTES and decreasing C-C chemokine receptor 5 (CCR5) expression. *J Immunol* (1999) 163(7):3653–61. doi: 10.4049/jimmunol.163.7.3653

74. Mestan J, Digel W, Mittnacht S, Hillen H, Blohm D, Möller A, et al. Antiviral effects of recombinant tumour necrosis factor *in vitro*. *Nature* (1986) 323(6091):816–9. doi: 10.1038/323816a0

75. Duh EJ, Maury WJ, Folks TM, Fauci AS, Rabson AB. Tumor necrosis factor alpha activates human immunodeficiency virus type 1 through induction of nuclear factor binding to the NF-kappa B sites in the long terminal repeat. *Proc Natl Acad Sci U States America* (1989) 86(15):5974–8. doi: 10.1073/pnas.86.15.5974

76. Folks TM, Clouse KA, Justement J, Rabson A, Duh E, Kehrl JH, et al. Tumor necrosis factor alpha induces expression of human immunodeficiency virus in a chronically infected T-cell clone. *Proc Natl Acad Sci U States America* (1989) 86(7):2365–8. doi: 10.1073/pnas.86.7.2365

77. Osborn L, Kunkel S, Nabel GJ. Tumor necrosis factor alpha and interleukin 1 stimulate the human immunodeficiency virus enhancer by activation of the nuclear factor kappa B. *Proc Natl Acad Sci U States America* (1989) 86(7):2336–40. doi: 10.1073/pnas.86.7.2336

78. Han J, Zhong C-Q, Zhang D-W. Programmed necrosis: backup to and competitor with apoptosis in the immune system. *Nat Immunol* (2011) 12(12):1143–9. doi: 10.1038/ni.2159

79. Melchjorsen J, Sørensen LN, Paludan SR. Expression and function of chemokines during viral infections: from molecular mechanisms to *in vivo* function. *J Leuk Biol* (2003) 74(3):331–43. doi: 10.1189/jlb.1102577

80. Domachowske JB, Bonville CA, Gao JL, Murphy PM, Easton AJ, Rosenberg HF. The chemokine macrophage-inflammatory protein-1 alpha and its receptor CCR1 control pulmonary inflammation and antiviral host defense in paramyxovirus infection. *J Immunol* (2000) 165(5):2677–82. doi: 10.4049/jimmunol.165.5.2677

81. Wald O, Pappo O, Safadi R, Dagan-Berger M, Beider K, Wald H, et al. Involvement of the CXCL12/CXCR4 pathway in the advanced liver disease that is associated with hepatitis C virus or hepatitis B virus. *Eur J Immunol* (2004) 34(4):1164–74. doi: 10.1002/eji.200324441

82. Tattiyapong P, Dachavichitlead W, Surachetpong W. Experimental infection of Tilapia Lake Virus (TiLV) in Nile tilapia (Oreochromis niloticus) and red tilapia (Oreochromis spp.). *Vet Microbiol* (2017) 207:170–7. doi: 10.1016/j.vetmic.2017.06.014

83. Poh AR, O'Donoghue RJ, Ernst M. Hematopoietic cell kinase (HCK) as a therapeutic target in immune and cancer cells. *Oncotarget* (2015) 6(18):15752–71. doi: 10.18632/oncotarget.4199

84. Kunimura K, Uruno T, Fukui Y. DOCK family proteins: key players in immune surveillance mechanisms. *Int Immunol* (2020) 32(1):5–15. doi: 10.1093/intimm/dxz067

85. Nakao M, Tsujikura M, Ichiki S, Vo TK, Somamoto T. The complement system in teleost fish: Progress of post-homolog-hunting researches. *Dev Comp Immunol* (2011) 35(12):1296–308. doi: 10.1016/j.dci.2011.03.003

86. Zhou Z, Xu MJ, Gao B. Hepatocytes: a key cell type for innate immunity. *Cell Mol Immunol* (2016) 13(3):301–15. doi: 10.1038/cmi.2015.97

87. Małaczewska J, Kaczorek-Łukowska E, Wójcik R, Siwicki AK. Antiviral effects of nisin, lysozyme, lactoferrin and their mixtures against bovine viral diarrhoea virus. *BMC Vet Res* (2019) 15(1):318. doi: 10.1186/s12917-019-2067-6

88. Fenard D, Lambeau G, Valentin E, Lefebvre JC, Lazdunski M, Doglio A. Secreted phospholipases A(2), a new class of HIV inhibitors that block virus entry into host cells. *J Clin Invest* (1999) 104(5):611–8. doi: 10.1172/jci6915

89. Chen CH, Zhang XQ, Lo CW, Liu PF, Liu YT, Gallo RL, et al. The essentiality of alpha-2-macroglobulin in human salivary innate immunity against new H1N1 swine origin influenza A virus. *Proteomics* (2010) 10(12):2396–401. doi: 10.1002/pmic.200900775

90. Eyngor M, Zamostiano R, Kembou Tsofack JE, Berkowitz A, Bercovier H, Tinman S, et al. Identification of a novel RNA virus lethal to tilapia. *J Clin Microbiol* (2014) 52(12):4137–46. doi: 10.1128/jcm.00827-14

91. Ryman KD, Klimstra WB, Nguyen KB, Biron CA, Johnston RE. Alpha/beta interferon protects adult mice from fatal Sindbis virus infection and is an important determinant of cell and tissue tropism. *J Virol* (2000) 74(7):3366–78. doi: 10.1128/jvi.74.7.3366-3378.2000

92. Byrnes AP, Durbin JE, Griffin DE. Control of Sindbis virus infection by antibody in interferon-deficient mice. *J Virol* (2000) 74(8):3905–8. doi: 10.1128/jvi.74.8.3905-3908.2000

93. Akwa Y, Hassett DE, Eloranta ML, Sandberg K, Masliah E, Powell H, et al. Transgenic expression of IFN-alpha in the central nervous system of mice protects against lethal neurotropic viral infection but induces inflammation and neurodegeneration. *J Immunol* (1998) 161(9):5016–26. doi: 10.4049/jimmunol.161.9.5016

94. McLaurin J, Antel JP, Yong VW. Immune and non-immune actions of interferon-beta-Ib on primary human neural cells. *Mult Scler* (1995) 1(1):10–9. doi: 10.1177/135245859500100103

95. Boutros T, Croze E, Yong VW. Interferon-beta is a potent promoter of nerve growth factor production by astrocytes. *J Neurochem* (1997) 69(3):939–46. doi: 10.1046/j.1471-4159.1997.69030939.x

96. Chabot S, Yong VW. Interferon beta-1b increases interleukin-10 in a model of T cell-microglia interaction: relevance to MS. *Neurology* (2000) 55(10):1497–505. doi: 10.1212/wnl.55.10.1497

97. Lopez-Castejon G, Brough D. Understanding the mechanism of IL-1β secretion. *Cytokine Growth Factor Rev* (2011) 22(4):189–95. doi: 10.1016/j.cytogfr.2011.10.001

98. Pan W, Stone KP, Hsuchou H, Manda VK, Zhang Y, Kastin AJ. Cytokine signaling modulates blood-brain barrier function. *Curr Pharm Des* (2011) 17(33):3729–40. doi: 10.2174/138161211798220918

99. Chai Q, He WQ, Zhou M, Lu H, Fu ZF. Enhancement of blood-brain barrier permeability and reduction of tight junction protein expression are modulated by chemokines/cytokines induced by rabies virus infection. *J Virol* (2014) 88(9):4698–710. doi: 10.1128/jvi.03149-13

100. McCandless EE, Zhang B, Diamond MS, Klein RS. CXCR4 antagonism increases T cell trafficking in the central nervous system and improves survival from West Nile virus encephalitis. *Proc Natl Acad Sci U States America* (2008) 105(32):11270–5. doi: 10.1073/pnas.0800898105

101. Zhao L, Toriumi H, Kuang Y, Chen H, Fu ZF. The roles of chemokines in rabies virus infection: overexpression may not always be beneficial. *J Virol* (2009) 83(22):11808–18. doi: 10.1128/jvi.01346-09

102. Wheeler DL, Sariol A, Meyerholz DK, Perlman S. Microglia are required for protection against lethal coronavirus encephalitis in mice. *J Clin Invest* (2018) 128(3):931–43. doi: 10.1172/jci97229

103. Chen Z, Zhong D, Li G. The role of microglia in viral encephalitis: a review. *J Neuroinflamm* (2019) 16(1):76. doi: 10.1186/s12974-019-1443-2

104. Dixon B, Stet RJM. The relationship between major histocompatibility receptors and innate immunity in teleost fish. *Dev Comp Immunol* (2001) 25(8):683–99. doi: 10.1016/S0145-305X(01)00030-1

105. Press CM, Evensen Ø. The morphology of the immune system in teleost fishes. *Fish Shellfish Immunol* (1999) 9(4):309–18. doi: 10.1006/fsim.1998.0181

106. Steinel NC, Bolnick DI. Melanomacrophage centers as a histological indicator of immune function in fish and other poikilotherms. *Front Immunol* (2017) 8:827. doi: 10.3389/fimmu.2017.00827

107. De Vico G, Cataldi M, Carella F, Marino F, Passantino A. Histological, histochemical and morphometric changes of splenic melanomacrophage centers (SMMCs) in Sparicotyle-infected cultured sea breams (Sparus aurata). *Immunopharmacol Immunotoxicol* (2008) 30(1):27–35. doi: 10.1080/08923970701812290

108. Suresh N. Effect of cadmium chloride on liver, spleen and kidney melano macrophage centres in Tilapia mossambica. *J Environ Biol* (2009) 30(4):505–8.

109. Agius C, Roberts RJ. Melano-macrophage centres and their role in fish pathology. *J Fish Dis* (2003) 26(9):499–509. doi: 10.1046/j.1365-2761.2003.00485.x

110. Wolke RE, Murchelano RA, Dickstein CD, George CJ. Preliminary evaluation of the use of macrophage aggregates (MA) as fish health monitors. *Bull Environ Contamination Toxicol* (1985) 35(1):222–7. doi: 10.1007/BF01636502

111. Traherne JA. Human MHC architecture and evolution: implications for disease association studies. *Int J Immunogenetics* (2008) 35(3):179–92. doi: 10.1111/j.1744-313X.2008.00765.x

112. Kloetzel PM, Soza A, Stohwasser R. The role of the proteasome system and the proteasome activator PA28 complex in the cellular immune response. *Biol Chem* (1999) 380(3):293–7. doi: 10.1515/bc.1999.040

113. Oura J, Tamura Y, Kamiguchi K, Kutomi G, Sahara H, Torigoe T, et al. Extracellular heat shock protein 90 plays a role in translocating chaperoned antigen from endosome to proteasome for generating antigenic peptide to be cross-presented by dendritic cells. *Int Immunol* (2011) 23(4):223–37. doi: 10.1093/intimm/dxq475

114. Landsverk OJB, Bakke O, Gregers TF. MHC II and the endocytic pathway: regulation by invariant chain. *Scand J Immunol* (2009) 70(3):184–93. doi: 10.1111/j.1365-3083.2009.02301.x

115. Nguyen J, Bernert R, In K, Kang P, Sebastiao N, Hu C, et al. Gamma-interferon-inducible lysosomal thiol reductase is upregulated in human melanoma. *Melanoma Res* (2016) 26(2):125–37. doi: 10.1097/cmr.0000000000000230

116. Zhou J, Li L, Cai ZH. Identification of putative cathepsin S in mangrove red snapper Lutjanus argentimaculatus and its role in antigen presentation. *Dev Comp Immunol* (2012) 37(1):28–38. doi: 10.1016/j.dci.2011.12.011

117. Plotnicky-Gilquin H, Cyblat-Chanal D, Aubry JP, Champion T, Beck A, Nguyen T, et al. Gamma interferon-dependent protection of the mouse upper respiratory tract following parenteral immunization with a respiratory syncytial virus G protein fragment. *J Virol* (2002) 76(20):10203–10. doi: 10.1128/jvi.76.20.10203-10210.2002

118. Yao S, Buzo BF, Pham D, Jiang L, Taparowsky EJ, Kaplan MH, et al. Interferon regulatory factor 4 sustains CD8(+) T cell expansion and effector differentiation. *Immunity* (2013) 39(5):833–45. doi: 10.1016/j.immuni.2013.10.007

119. Adams NM, Lau CM, Fan X, Rapp M, Geary CD, Weizman OE, et al. Transcription factor IRF8 orchestrates the adaptive natural killer cell response. *Immunity* (2018) 48(6):1172–82.e6. doi: 10.1016/j.immuni.2018.04.018

120. Helbig KJ, Beard MR. The role of viperin in the innate antiviral response. *J Mol Biol* (2014) 426(6):1210–9. doi: 10.1016/j.jmb.2013.10.019

121. Harling-Berg CJ, Park TJ, Knopf PM. Role of the cervical lymphatics in the Th2-type hierarchy of CNS immune regulation. *J Neuroimmunol* (1999) 101(2):111–27. doi: 10.1016/s0165-5728(99)00130-7

122. Fischer HG, Reichmann G. Brain dendritic cells and macrophages/microglia in central nervous system inflammation. *J Immunol* (2001) 166(4):2717–26. doi: 10.4049/jimmunol.166.4.2717

123. Pope JG, Vanderlugt CL, Rahbe SM, Lipton HL, Miller SD. Characterization of and functional antigen presentation by central nervous system mononuclear cells from mice infected with Theiler's murine encephalomyelitis virus. *J Virol* (1998) 72 (10):7762–71. doi: 10.1128/jvi.72.10.7762-7771.1998

124. Griffin DE. Immune responses to RNA-virus infections of the CNS. *Nat Rev Immunol* (2003) 3(6):493–502. doi: 10.1038/nri1105

125. Irani DN, Griffin DE. Regulation of lymphocyte homing into the brain during viral encephalitis at various stages of infection. *J Immunol* (1996) 156(10):3850–7. doi: 10.4049/jimmunol.156.10.3850

126. Wekerle H, Linington C, Lassmann H, Meyermann R. Cellular immune reactivity within the CNS. *Trends Neurosci* (1986) 9:271–7. doi: 10.1016/0166-2236(86)90077-9

127. Hickey WF, Hsu BL, Kimura H. T-lymphocyte entry into the central nervous system. *J Neurosci Res* (1991) 28(2):254–60. doi: 10.1002/jnr.490280213

128. Zhang YA, Salinas I, Oriol Sunyer J. Recent findings on the structure and function of teleost IgT. *Fish Shellfish Immunol* (2011) 31(5):627–34. doi: 10.1016/j.fsi.2011.03.021

129. Zhang Y-A, Salinas I, Li J, Parra D, Bjork S, Xu Z, et al. IgT, a primitive immunoglobulin class specialized in mucosal immunity. *Nat Immunol* (2010) 11 (9):827–35. doi: 10.1038/ni.1913

130. Mai TT, Kayansamruaj P, Taengphu S, Senapin S, Costa JZ, Del-Pozo J, et al. Efficacy of heat-killed and formalin-killed vaccines against Tilapia tilapinevirus in juvenile Nile tilapia (Oreochromis niloticus). *J Fish Dis* (2021) 44(12):2097–109. doi: 10.1111/jfd.13523

131. Barría A, Tịnh TQ, Mahmuddin M, Peñaloza C, Papadopoulou A, Gervais O, et al. A major quantitative trait locus affecting resistance to Tilapia lake virus in farmed Nile tilapia (Oreochromis niloticus). *Heredity* (2021) 127(3):334–43. doi: 10.1038/s41437-021-00447-4

132. Burbage M, Keppler SJ, Gasparrini F, Martínez-Martín N, Gaya M, Feest C, et al. Cdc42 is a key regulator of B cell differentiation and is required for antiviral humoral immunity. *J Exp Med* (2015) 212(1):53–72. doi: 10.1084/jem.20141143

133. Boison S, Ding J, Leder E, Gjerde B, Bergtun PH, Norris A, et al. QTLs associated with resistance to cardiomyopathy syndrome in Atlantic salmon. *J Hered* (2019) 110(6):727–37. doi: 10.1093/jhered/esz042

134. Foss S, Bottermann M, Jonsson A, Sandlie I, James LC, Andersen JT. TRIM21-from intracellular immunity to therapy. *Front Immunol* (2019) 10:2049. doi: 10.3389/fimmu.2019.02049

135. Li Q, Lin L, Tong Y, Liu Y, Mou J, Wang X, et al. TRIM29 negatively controls antiviral immune response through targeting STING for degradation. *Cell Discovery* (2018) 4(1):13. doi: 10.1038/s41421-018-0010-9

136. Xing J, Zhang A, Zhang H, Wang J, Li XC, Zeng MS, et al. TRIM29 promotes DNA virus infections by inhibiting innate immune response. *Nat Commun* (2017) 8 (1):945. doi: 10.1038/s41467-017-00101-w

137. Xing J, Zhang A, Minze LJ, Li XC, Zhang Z. TRIM29 negatively regulates the type I IFN production in response to RNA virus. *J Immunol* (2018) 201(1):183–92. doi: 10.4049/jimmunol.1701569

138. Vladimer GI, Górna MW, Superti-Furga G. IFITs: emerging roles as key anti-viral proteins. *Front Immunol* (2014) 5:94. doi: 10.3389/fimmu.2014.00094

139. Wang C, Pflugheber J, Sumpter RJr., Sodora DL, Hui D, Sen GC, et al. Alpha interferon induces distinct translational control programs to suppress hepatitis C virus RNA replication. *J Virol* (2003) 77(7):3898–912. doi: 10.1128/jvi.77.7.3898-3912.2003

140. Terenzi F, Saikia P, Sen GC. Interferon-inducible protein, P56, inhibits HPV DNA replication by binding to the viral protein E1. *EMBO J* (2008) 27(24):3311–21. doi: 10.1038/emboj.2008.241

141. Saikia P, Fensterl V, Sen GC. The inhibitory action of P56 on select functions of E1 mediates interferon's effect on human papillomavirus DNA replication. *J Virol* (2010) 84(24):13036–9. doi: 10.1128/jvi.01194-10

142. Choudhury NR, Trus I, Heikel G, Wolczyk M, Szymanski J, Bolembach A, et al. TRIM25 inhibits influenza A virus infection, destabilizes viral mRNA, but is redundant for activating the RIG-I pathway. *Nucleic Acids Res* (2022) 50(12):7097–114. doi: 10.1093/nar/gkac512

143. Kaikai H, Zhao D, Liu Y, Liu Q, Huang X, Yang J, et al. The E3 ubiquitin ligase TRIM25 inhibits tembusu virus replication *in vitro*. *Front Vet Sci* (2021) 8:722113. doi: 10.3389/fvets.2021.722113

144. Wang S, Yu M, Liu A, Bao Y, Qi X, Gao L, et al. TRIM25 inhibits infectious bursal disease virus replication by targeting VP3 for ubiquitination and degradation. *PloS Pathog* (2021) 17(9):e1009900. doi: 10.1371/journal.ppat.1009900

145. Piewbang C, Tattiyapong P, Khemthong M, Lachroje S, Boonrungsiman S, Kasantikul T, et al. Dual infections of tilapia parvovirus (TiPV) and tilapia lake virus (TiLV) in multiple tilapia farms: Their impacts, genetic diversity, viral tropism, and pathological effects. *Aquaculture* (2022) 550:737887. doi: 10.1016/j.aquaculture.2022.737887

frontiers | Frontiers in Immunology

TYPE Original Research
PUBLISHED 05 October 2023
DOI 10.3389/fimmu.2023.1268851

OPEN ACCESS

EDITED BY
Iddya Karunasagar,
Nitte University, India

REVIEWED BY
Subhendu Otta,
Central Institute of Brackishwater Aquaculture (ICAR), India
Jingguang Wei,
South China Agricultural University, China

*CORRESPONDENCE
Xiuzhen Sheng
xzsheng@ouc.edu.cn

RECEIVED 28 July 2023
ACCEPTED 18 September 2023
PUBLISHED 05 October 2023

CITATION
Zhang H, Sheng X, Tang X, Xing J, Chi H and Zhan W (2023) Transcriptome analysis reveals molecular mechanisms of lymphocystis formation caused by lymphocystis disease virus infection in flounder (*Paralichthys olivaceus*). *Front. Immunol.* 14:1268851. doi: 10.3389/fimmu.2023.1268851

Transcriptome analysis reveals molecular mechanisms of lymphocystis formation caused by lymphocystis disease virus infection in flounder (*Paralichthys olivaceus*)

Honghua Zhang[1], Xiuzhen Sheng[1,2]*, Xiaoqian Tang[1,2], Jing Xing[1,2], Heng Chi[1,2] and Wenbin Zhan[1,2]

[1]Laboratory of Pathology and Immunology of Aquatic Animals, Key Laboratory of Mariculture, Ministry of Education (KLMME), Ocean University of China, Qingdao, China, [2]Function Laboratory for Marine Fisheries Science and Food Production Processes, Qingdao National Laboratory for Marine Science and Technology, Qingdao, China

Lymphocystis disease is frequently prevalent and transmissible in various teleost species worldwide due to lymphocystis disease virus (LCDV) infection, causing unsightly growths of benign lymphocystis nodules in fish and resulting in huge economic losses to aquaculture industry. However, the molecular mechanism of lymphocystis formation is unclear. In this study, LCDV was firstly detected in naturally infected flounder (*Paralichthys olivaceus*) by PCR, histopathological, and immunological techniques. To further understand lymphocystis formation, transcriptome sequencing of skin nodule tissue was performed by using healthy flounder skin as a control. In total, RNA-seq produced 99.36%-99.71% clean reads of raw reads, of which 91.11%-92.89% reads were successfully matched to the flounder genome. The transcriptome data showed good reproducibility between samples, with 3781 up-regulated and 2280 down-regulated differentially expressed genes. GSEA analysis revealed activation of Wnt signaling pathway, Hedgehog signaling pathway, Cell cycle, and Basal cell carcinoma associated with nodule formation. These pathways were analyzed to interact with multiple viral infection and tumor formation pathways. Heat map and protein interaction analysis revealed that these pathways regulated the expression of cell cycle-related genes such as *ccnd1* and *ccnd2* through key genes including *ctnnb1*, *lef1*, *tcf3*, *gli2*, and *gli3* to promote cell proliferation. Additionally, cGMP-PKG signaling pathway, Calcium signaling pathway, ECM-receptor interaction, and Cytokine-cytokine receptor interaction associated with nodule formation were significantly down-regulated. Among these pathways, *tnfsf12*, *tnfrsf1a*, and *tnfrsf19*, associated with pro-apoptosis, and *vdac2*, which promotes viral replication by inhibiting apoptosis, were significantly up-regulated. Visual analysis revealed significant down-regulation of *cytc*, which expresses the pro-apoptotic protein cytochrome C, as well as *phb* and *phb2*, which have anti-tumor activity, however, *casp3* was significantly up-regulated. Moreover, *bcl9*, *bcl11a*, and *bcl-xl*, which promote cell proliferation and inhibit apoptosis, were significantly upregulated, as were *fgfr1*, *fgfr2*, and *fgfr3*, which

are related to tumor formation. Furthermore, RNA-seq data were validated by qRT-PCR, and LCDV copy numbers and expression patterns of focused genes in various tissues were also investigated. These results clarified the pathways and differentially expressed genes associated with lymphocystis nodule development caused by LCDV infection in flounder for the first time, providing a new breakthrough in molecular mechanisms of lymphocystis formation in fish.

KEYWORDS

flounder (*Paralichthys olivaceus*), lymphocystis disease virus, RNA-Seq, transcriptome, lymphocystis formation, molecular mechanism

1 Introduction

Lymphocystis disease virus (LCDV) is a member of the genus *lymphocystivirus* of the *Iridoviridae* family and the causative agent of lymphocystis disease (1). LCDV has infected more than 140 species of marine and freshwater fish worldwide, including flounder (*Paralichthys olivaceus*), which is economically important in Asian countries such as Japan, Korea, and China, causing great economic losses (2, 3). Fish with lymphocystis disease develop benign cauliflower-like nodules on the skin, gills, fins, mouth, and some internal organs (4). LCDV mainly infects fibroblasts, and a large number of fibroblasts exist in the connective tissue of the skin, so the skin is the main target tissue where the presence of lymphocystis nodules is usually observed (4). These nodules vary in size, present creamy white or pink (vascularly congested), and are either dispersed or aggregated into clusters. Histopathologically, the nodules contain a large number of hypertrophied cells (i.e., lymphocystis cells) developed from the infected fibroblasts in the connective tissue underlying the epithelium, which may be up to 100 times the size of normal cells in fish, with a thick hyaline capsule outside the cell membrane, expanded and irregular nuclei, and cytoplasm containing a large number of viral particles and inclusion bodies (5–8). Although lymphocystis disease is a self-limiting and rarely fatal disease, and the lesions can heal and the fish may recover after a few weeks, the benign nodules lead to nonmarketability of diseased fish, poor growth, and secondary bacterial infections that can lead to mortality (2, 3). To elucidate the mechanism of LCDV infection and develop effective preventive measures, considerable research has focused on LCDV-host interaction. Remarkably, a 27.8 kDa protein on the cell membrane of flounder gill (FG) cells is identified as the cellular receptor for LCDV entry, which is further confirmed to be voltage-dependent anion channel protein 2 (VDAC2) and receptor of activated protein C kinase 1 (RACK1), and the two receptors mediate LCDV invasion of host cells through interacting with a 32kDa viral adhesion protein (VAP) of LCDV that encoded by LCDV ORF038 gene, using the caveolae/raft mediated endocytosis pathway into FG cells (9–12). In addition to fibroblasts, which are considered to be the main target cells of LCDV, some studies have shown that gilthead seabream (*Sparus aurata*) hepatocytes, macrophages, and *in vitro*-cultured leukocytes are involved in LCDV infection (13, 14). Recently, LCDV has been found to infect peripheral blood IgM^+ B cells of flounder, and IgM^+ B cells also express the 27.8 kDa receptor protein and support LCDV replication, so B cells may be the vector of LCDV transmission among tissues (15). However, the process by which LCDV infects host cells and proliferates intracellularly resulting in hypertrophied cells and then the formation of lymphocytsis nodule, and the underlying mechanism regulating lymphocytsis formation, remains to be clarified.

In mammals, viral infections are a major contributor to nodules and even malignant tumors. Studies have shown that the known viruses, e.g., Epstein–Barr virus (EBV), Merkel cell polyomavirus (MCPyV), hepatitis B virus (HBV), hepatitis C virus (HCV), human T-lymphotropic virus 1 (HTLV-1), human papillomaviruses (HPVs) and Kaposi sarcoma-associated herpesvirus (KSHV), can promote tumorigenesis through common host cellular targets and pathways (16). These viruses have been found to support their proliferation by controlling the cell cycle, apoptosis, autophagy, DNA damage, immune escape (viral protein homologs that regulate immune mechanisms), and biosynthesis and metabolism (17). In fish, few viruses cause nodules but LCDV, so there are fewer studies on the mechanisms of lymphocystis nodule formation. Previously, microarray experiments were used to track the formation of lymphocystis cells, and it was concluded that apoptosis and division were inhibited in the ventral fins of LCDV-infected flounder and further formed lymphocystis cells by cell fusion (5), but the mechanism of nodule formation remains to be systematically investigated.

RNA-Seq is a technique for the detection of transcriptome expression levels in samples by high-throughput sequencing (18) and has become a revolutionary tool for transcriptional and genomic characterization (19, 20). This technique is very sensitive and can accurately detect rare transcripts, with a very wide range of detection and high sensitivity to gene expression at high or very low levels (18). Using RNA-Seq techniques, we have studied gill tissue differentially expressed genes (DEGs) in flounder at one week post LCDV infection, providing preliminary insights into fish defense mechanisms against LCDV (6).

In this study, the flounder (*P. olivaceus*) naturally developed skin and fin nodules for about one month in a fish farm in Rizhao, Shandong province of China. The flounder was first detected for LCDV infection by using polymerase chain reaction (PCR),

quantitative real-time PCR (qRT-PCR), histopathological and indirect immunofluorescence assay (IFA) technique. Subsequently, transcriptomic data of skin nodule tissues of LCDV-infected flounder were obtained by high-throughput sequencing with the skin of healthy flounder as control, the pathways and differentially expressed genes associated with nodule formation were analyzed, and expression patterns of focused genes in various tissues were also analyzed.

2 Materials and methods

2.1 Experimental fish and sampling

Healthy and diseased flounder (250 ± 50 g) were taken from the fish farm, and cultured in a continuous aerated and flow-through seawater system at a temperature of 21 ± 1°C. Before all, flounders were tested by PCR to confirm LCDV-free in the healthy fish and LCDV infection in the diseased fish. For RNA-Seq, skin nodule tissues from four diseased fish and skin tissues from four healthy fish, named LS (LCDV-infected) and CS (control) groups respectively, were randomly selected and placed in liquid nitrogen for rapid freezing. For qRT-PCR, flounder were anesthetized with 100 mg/mL MS-222 (Sigma, MO, USA), and the liver, spleen, head kidney, trunk kidney, hindgut, gills, and skin were taken from these fish. The samples were rapidly immersed in RNAlater (Thermo Scientific, Waltham, Massachusetts, USA) and stored at -80°C.

2.2 Histological preparation and indirect immunofluorescence assay

Skin nodule tissue from diseased fish was aseptically excised, washed with phosphate-buffered saline (PBS), fixed in Bouin's solution, and then washed several times with 70% ethanol. The tissue was subsequently dehydrated in a series of increasing concentrations of ethanol, cleared in xylene, and embedded in paraffin by conventional procedures. The 5 μm-thick sections were cut, and stained with hematoxylin-eosin (H-E) and histologically observed by Zeiss microscope (Oberkochen, Germany).

For IFA, at least three paraffin sections of each fish were subjected to IFA using mouse anti-LCDV 32kDa VAP monoclonal antibody (Mab) 1C8 previously prepared in our laboratory (21). Briefly, the sections were dewaxed using xylene and rehydrated in decreasing concentrations of ethanol, finally washed in PBS. The antigen repair of the sections was carried out by using modified sodium citrate antigen repair solution (50×) (1:50, Beyotime, Shanghai, China) at 95°C for 20 min, followed by incubation with 4% bovine serum albumin (BSA) in PBS at 37°C for 1 h. Mouse anti-LCDV 32kDa VAP Mab 1C8 (1:200 diluted in PBS) was incubated as primary antibody at 37°C for 1 h. After three washes with PBST (PBS containing 0.05% Tween-20) for 5 min each, FITC-conjugated goat-anti-mouse Ig (1:1000 diluted in PBS, Sigma, MO, USA) was incubated as secondary antibody for 45 min at 37°C. Subsequently, DAPI (1:1000 diluted in PBS, Thermo Scientific, Waltham, Massachusetts, USA) was stained for 15 min at room temperature in the dark to visualize the cell nucleus. Non-immune mouse serum replacing primary antibody was used as a negative control. Finally, slides were mounted with extended glass mounting medium (Thermo Scientific, Waltham, Massachusetts, USA) and fluorescence imaging was performed under an immunofluorescence microscope (Zeiss, Oberkochen, Germany).

2.3 Transmission electron microscopy

Skin lymphocystis nodule tissue less than 1 mm^3 in volume was excised, rinsed with PBS to remove blood and mucus, and then fixed with 2.5% glutaraldehyde in 0.1 mol/L PBS (pH 7.4) for 2 h and post-fixed with 1% osmium acid in PBS at 4°C. The samples were dehydrated in gradient alcohol, embedded in Epon812 embedding agent, and sectioned on an ultrathin microtome. Finally, the ultra-thin sections were stained with uranyl acetate-lead citrate and observed by transmission electron microscope.

2.4 Genetic level detection of LCDV

Total DNA was extracted from the skin nodule tissues of LS groups and the skin of CS groups. LCDV ORF038 gene encoding the LCDV 32 kDa VAP was used for PCR amplification (F: 5'-ATGTCTGTCATAGGATTTACTCTACAA-3', R: 5'-AAAAG TCAAATAAAATATTAAAATCATT-3'). 20 μL PCR reaction system: DNA template 1 μL, each primer 1 μL, Ex Taq DNA polymerase 0.5 μL (TaKaRa, Japan), Ex Taq buffer 2.5 μL, dNTPs 2 μL, ddH_2O 12 μL. Reaction procedure: 95°C for 5 min, 35 amplification cycles (95°C for 30 sec, 60°C for 30 sec, 72°C for 1 min), 72°C for 10 min. The PCR product size was detected by 1.0% agarose gel electrophoresis.

To determine the replication of LCDV in various tissues of the diseased flounder, total DNA was extracted from liver, spleen, head kidney, trunk kidney, hindgut, gill and skin tissues, followed by 50 ng DNA as template with a pair of specific primers (F: 5'- TCTT GTTCAGCATTTACTTCTCGGC -3 ' and R: 5'- TCTTCT CCTTTAGATGATTTCCC -3') (11) for qPCR amplification of the LCDV ORF038 gene fragment. Each sample was tested four times, and non-infected samples served as negative controls. After amplification, a melting curve analysis was undertaken to guarantee that there was no non-specific amplification. Finally, the LCDV copy number was determined by calculating the Ct value from the previously established standard curve (11). The data was expressed as mean $\log_{10}$ copies/50 ng DNA.

2.5 cDNA library construction and sequencing

Total RNA was isolated from flounder skin nodule tissue according to the manufacturer's protocol using the Trizol kit (Invitrogen, Carlsbad, CA, USA). The quality of the RNA was determined using an Agilent 2100 Bioanalyzer (Agilent

Technologies, Palo Alto, CA, USA) and RNase-free agarose gel electrophoresis. Afterward, the mRNA was enriched by magnetic beads with Oligo(dT) and then interrupted with First Strand Synthesis Reaction Buffer. To synthesize the first strand of cDNA in the M-MuLV reverse transcriptase system, the fragmented mRNA was used as a template, and random oligonucleotides were used as primers. The RNA strand was then degraded with RnaseH, and the cDNA second strand was synthesized with dNTPs under the DNA polymerase I system. Sequencing connectors were ligated and poly(A) was added. The purified double-stranded cDNA was end-repaired. Approximately 200 bp cDNAs were screened with AMPure XP beads, amplified by PCR, and then sequenced using Illumina HiSeq2500 in Gene Denovo Biotechnology Co (Guangzhou, China).

2.6 Filtering and alignment of clean reads

Reads obtained from the sequencing machines include raw reads containing adapters or low-quality bases. These raw reads will affect the following assembly and analysis. Reads were therefore further filtered using fastp (version 0.18.0) to obtain high-quality clean reads (22). The criteria were as follows: eliminating adapter-containing reads, reads with more than 10% of unknown nucleotides (N), and reads with more than 50% of low-quality (Q-value ≤ 20) bases.

The ribosomal RNA (rRNA) database was mapped using the short reads alignment program Bowtie2 (version 2.2.8) (23) before the rRNA-mapped reads were eliminated. The remaining clean reads were then used for gene abundance estimation and assembly. Using HISAT (version 2.2.4) with "-rna-strandness RF" and other default options, paired-end clean reads were mapped to the reference genome after creating an index of the reference genome (24).

2.7 Differentially expressed genes and gene set enrichment analysis

Differential gene expression between the CS and LS groups was analyzed using DESeq2 software (25). Genes with false discovery rate (FDR) < 0.05 and absolute fold change (FC) ≥ 2 were differentially expressed genes (DEGs). To determine whether a collection of genes in particular KEGG pathways had significant differences in the two groups, gene set enrichment analysis (GSEA) was carried out using the tools GSEA and MSigDB (26). In a nutshell, the SinaltoNoise normalization method was used to input the gene expression matrix and rank genes, and enrichment scores and p-value were calculated in default parameters.

2.8 Protein-protein interaction and pathway visualization

A protein-protein interaction (PPI) network was identified using String (version 10) (27), which determined genes as nodes and interactions as lines in a network. A core and hub gene biological interaction was shown using Cytoscape (version 3.7.1) software by visualizing the network file (28). Pathway visualization and data integration of genes based on gene expression using PATHVIEW (https://pathview.uncc.edu/, accessed on 30 May 2023) (29, 30).

2.9 Quantitative real-time PCR

Briefly, 1 μg of total RNA was extracted from liver, spleen, head kidney, trunk kidney, hindgut, gill, and skin tissues and reverse transcribed into cDNA in a 20 μL reaction system. 2 μL of cDNA was then used as a template. Primer Premier 5 was used to design specific primers for the pathway-related genes in focus. Expression levels were normalized using flounder *β-actin* as an internal reference. The qRT-PCR was performed using SYBR green Master Mix (Roche, Switzerland) in a LightCycler® 480 II Real Time System (Roche, Switzerland). The $2^{-\triangle\triangle Ct}$ method was used to analyze the expression levels of the selected genes. The primers used in this section are shown in Table 1. Each sample was run in quadruplicate.

2.10 Statistical analysis

Statistical Products and Services Solutions (SPSS) software (version 20.0, IBM, BY, USA) was used to analyze the obtained data. One-way analysis of variance (ANOVA) was used to analyze the results of viral proliferation, and the expression levels of genes in each tissue. Values were deemed significant at $p < 0.05$.

3 Results

3.1 Infection characteristics of LCDV in flounder

The healthy and naturally diseased flounder were tested for LCDV. Cauliflower-like nodules were evident on the skin and fins of the diseased flounder (Figure 1A), and a specific LCDV ORF038 gene band of 933 bp was amplified from the diseased fish but not in the healthy fish skin (Figure 1B). The lymphocystis cells within skin connective tissue had hypertrophic features with basophilic inclusion bodies in the cytoplasm by H-E staining (Figure 1D), and a large number of viral particles were observed in the cytoplasm by transmission electron microscopy (Figure 1E). Moreover, the cytoplasm of lymphocystis cells was positive for LCDV as shown by IFA (Figure 1F). The qRT-PCR results indicated that LCDV copy number was detected in all tested tissues of the affected fish, with the highest copy number of 3.0×10^7/50 ng DNA in the skin, followed by the gills (4.5×10^4), trunk kidney (1.5×10^4), hindgut (1.1×10^4), spleen (6.7×10^2) and liver (3.0×10^2), and the lowest in the head kidney (9.0×10^1), while the controls had no LCDV proliferation (Figure 1C). All these results confirmed that the healthy fish were not infected by LCDV, while the diseased fish were naturally infected with LCDV, so they could be used for the next experiment.

10.3389/fimmu.2023.1268851

TABLE 1 Sequence information for primers used in this study.

Gene	Accession No.	Primer Sequence (5'->3')	Length (bp)
β-actin	XM_020109620.1	F: GTCCCTGTATGCCTCTGGTC	215
		R: TGTCACGCACGATTTCCCTC	
wnt5a	XM_020096312.1	F: ACTTCCGCAAGGTGGGTGAT	178
		R: GAGCCCGTGCTTTGGTTCTT	
ctnnb1	XM_020090668.1	F: AGAAACGTCTGTCGGTGGA	161
		R: GCCGTAGGCTGATGGGTAT	
lef1	XM_020101320.1	F: ACTAAACGCCTTCATGCTC	160
		R: TTCCTTGCGGGCTAACT	
tcf3	XM_020107767.1	F: CCTGGATTTCAGTGCGATGT	109
		R: GCCGCTACGCTCGTCTATT	
gli2	XM_020109184.1	F: TTTACGAGACCAACTGCCACTG	147
		R: GCTTCTGCTCCCGAGAACACT	
ccnd1	XM_020080206.1	F: TACTGTGCTGCGAGGTGGACT	116
		R: GTTGGGAGACGGTAGGTAGGTTT	
ccnd2	XM_020078448.1	F: CATGTTCCTCGCATCCAAAT	114
		R: ACCACCAGTTCCCATTCCAG	
bcl9	XM_020089951.1	F: GGAATCCTGTTCCTGGCTCAA	181
		R: GCCTCCGTCTTCGGTTTAG	
bcl11a	XM_020088700.1	F: ACCACCCGAGTGCCTTTGA	182
		R: TGTCTGGAATGGCTGGAGTAA	
bcl-xl	XM_020111495.1	F: TGGTGGAGTTCTTTATCAGTTACA	133
		R: TTGACCAGCAAGCCATTACT	
fgfr1a	XM_020107117.1	F: CTGAAGGAAGGTCACCGTATG	194
		R: GAGTATTGGTCCAGAGGCAC	
fgfr3	XM_020108467.1	F: TCCTATGGTGTGTTGTTGTGG	138
		R: GTACAGCTCATGTGTGCAGTTTG	
fzd2	XM_020113633.1	F: CGATATGCTCAGCGGCGT	108
		R: AGGAACGAGGTCCCGATGAA	
fzd8	XM_020113464.1	F: ACAACTGCTCCAACTGTTTACTG	138
		R: ACGAGTCCAGGGTCTTGCC	
pik3r1	XM_020082241.1	F: TAGAGCCCTTGCCGAGAT	136
		R: TGGAGCAGCCTGACTTTCAC	
fgfr2	XM_020088824.1	F: GATCCACGCTGGGAGTTT	128
		R: TCACGGCTTCCTTAGGTTT	
mtor	XM_020088845.1	F: CAGCGTCAGAACAACCAAGCA	169
		R: AGCAGTGAAGGTGTCCCCA	
fzd9	XM_020095313.1	F: CGAAGCCCACAGCAACTAC	136
		R: CCCAGAGTCCATACTCCCTAC	
lrp5	XM_020104881.1	F: CATTGACTATGTAGACCATCGAC	150

(Continued)

TABLE 1 Continued

Gene	Accession No.	Primer Sequence (5'->3')	Length (bp)
		R: CAGTAGATAAAATCTTGGTATTGTG	
tcf7l2	XM_020083352.1	F: ACGAGACAACTATGCGGCTAAC	167
		R: GCCCGAACAAGGCACGAC	
mdm4	XM_020086872.1	F: ACAGAGGCAGCACATAGTCCA	140
		R: CAGCGTCAGAACAACCAAGCA	
ruvbl1	XM_020086807.1	F: AGGTGCCCTTCTGTCCTAT	117
		R: CCTTGGTTTCTTTGATACGC	

3.2 Transcriptome sequencing quality

Clean reads with 40994192, 46893012, 40908092, and 49650708 were obtained from the CS group, and 52683364, 42481640, 47979600, and 39471322 were obtained from the LS group, respectively. Sequence data for CS-1, CS-2, CS-3, CS-4, LS-1, LS-2, LS-3, and LS-4 have been submitted to the NCBI database under accession numbers SAMN36345915, SAMN36345916, SAMN36345917, SAMN36345918, SAMN36345919, SAMN36345920, SAMN36345921, and SAMN36345922, respectively. The (guanine and cytosine) GC percentages for all samples ranged from 47.52%-49.46%, with reads over 96.0% for Q20 and 91.0% for Q30 for each sample, indicating high sequencing quality. Also, 91.11%-92.89% of the sequence reads were successfully localized to the flounder genome (Table 2).

3.3 Differentially expressed genes after LCDV infection

When we analyzed the expression of different genes in LCDV-infected flounder versus healthy fish, a total of 6061 DEGs were observed. Hierarchical clustering of differential gene expression patterns was performed, and a heat map was used to present the clustering results. The heat map results showed that four biological replicates were clustered together in each group, indicating good concordance (Figure 2A). The volcano map results demonstrated that 3781 DEGs were significantly up-regulated and 2280 DEGs were significantly down-regulated after LCDV infection (FDR < 0.05, FC ≥ 2) (Figure 2B).

The qRT-PCR of random 10 DEGs validated these RNA-Seq results. The qRT-PCR results for the tested genes showed similar expression patterns as observed in the RNA-Seq data (Figure 3), indicating that the RNA-seq results were reliable.

3.4 Lymphocystis nodule-related activated pathways and genes in response to LCDV infection

The KEGG pathways that hosted the gene set of flounder after LCDV infection were analyzed using the GSEA method. In total, 32 active signaling pathways were found (Figure 4A). Among them, those related to nodule formation mainly included Wnt signaling pathway (Figure 4B) and Hedgehog signaling pathway (Figure 4C) in Signal transduction, Cell cycle (Figure 4D) in Cell growth and death, and Basal cell carcinoma (Figure 4E) in Diseases. In the four pathways, *prkcg*, *smad4*, *fzd2*, *ccne1*, *wnt5a*, *gli2*, *fzd8*, *axin1*, *ccna2*, *e2f3*, *plcb4*, *ctbp2*, *prkcb*, *porcn*, *ccnd2*, *plk1*, *ccne2*, *cdkn2b*, *ptch1*, *mcm6*, *lef1*, *ccnb1*, *osa*, *camk2a*, *ccnd1*, *ccnb2*, *cdkn1b*, *e2f1*, *lrp5*, *gli3*, *fzd9*, *smo*, *tcf7l2*, *camk2b*, *tfdp1*, *axin2*, *abl1*, *ctnnb1*, and *tcf3* had significantly upregulated levels of gene expression as compared with healthy groups, while *myc*, *gadd45b*, *cdkn1*, *gadd45g*, *mdm2*, *dvl3*, *bmp2*, and *ap-1* were significantly downregulated, and there were some shared DEGs between these four pathways (FDR < 0.05, FC ≥ 2) (Figure 4F). Details of these genes are listed in Table S1.

3.5 Analysis of protein and KEGG pathway interaction networks

In order to identify the key genes, PPI analysis of the appeal genes showed that *ctnnb1*, *ccnd1*, *lef1*, *ccnd2*, and *wnt5a* played key roles as hub genes (Figures 5A, B), and details of the PPI were listed in Table S2. In addition to the four pathways in Figure 4, KEGG pathway enrichment analysis of PPI results revealed that pathways associated with nodule formation included Pathways in cancer and Viral carcinogenesis; pathways associated with viral infection included Human T-cell leukemia virus 1 infection, Human papillomavirus infection, Epstein-Barr virus infection, Kaposi sarcoma-associated herpesvirus infection, and Human cytomegalovirus infection; pathways associated with multiple cellular processes including p53 signaling pathway were also enriched (Figure 5A). The four pathways analyzed by GSEA (Figure 4) were subjected to KEGG pathway relationship analysis (Figure 5C), which indicated that the four pathways were associated with nodule formation included Gastric cancer, Hepatocellular carcinoma, Proteoglycans in cancer, Breast cancer, Endometrial cancer, and Colorectal cancer, pathways associated with multiple cellular processes included MAPK signaling pathway and TGF-beta signaling pathway in addition to the pathways analyzed in Figure 5A.

10.3389/fimmu.2023.1268851

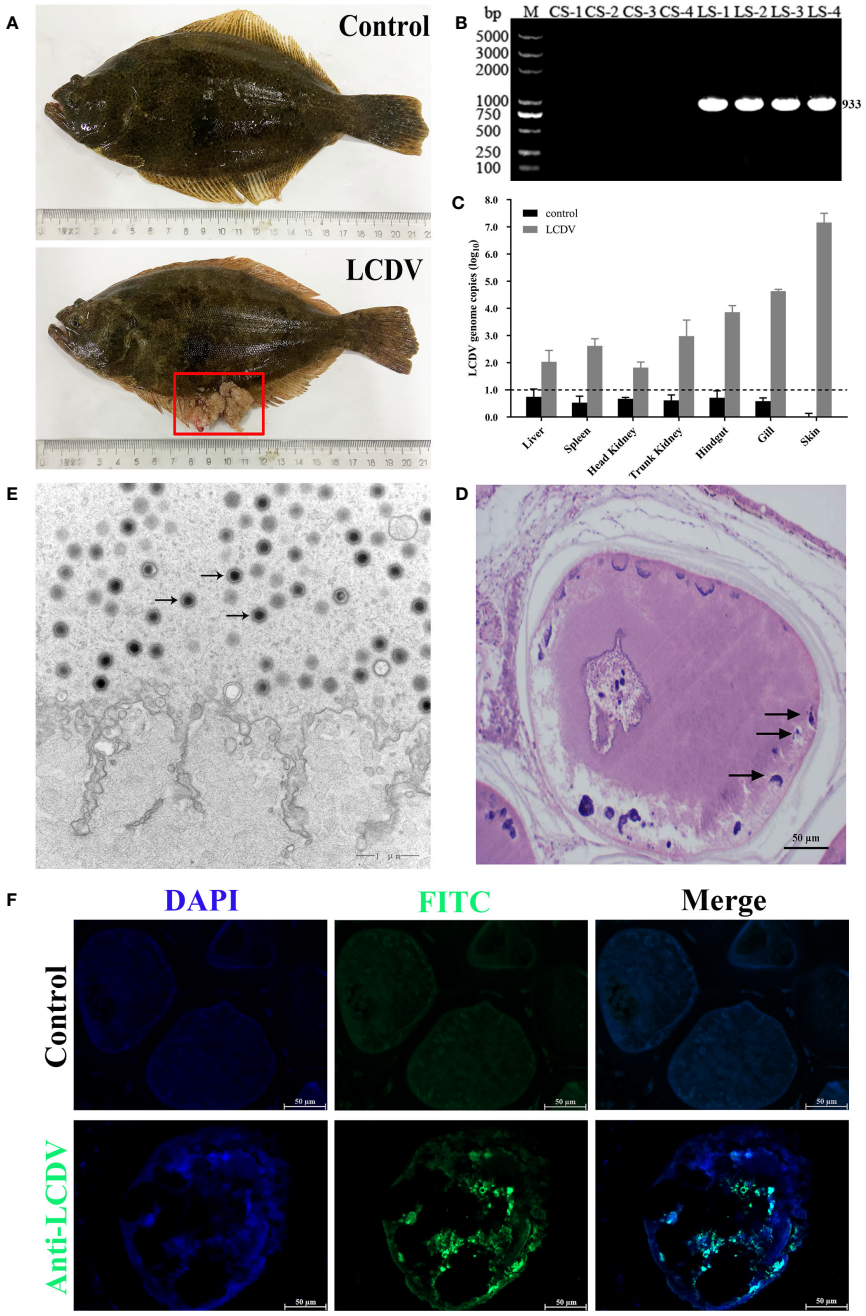

FIGURE 1
LCDV detection in flounder. **(A)** Clinical symptoms of naturally LCDV-infected flounder, and the healthy fish as control. The diseased fish showed obvious nodules on skin and fin (red box). **(B)** PCR assay of the skin of four healthy and diseased flounder, respectively. 933bp LCDV specific band was amplified in all LCDV-infected (LS) groups but not in control (CS) groups. M: DL5000 DNA Marker. **(C)** Copy numbers of LCDV in different tissues of the diseased flounder and control fish. Mean viral copy numbers were represented in the $\log_{10}$ scale. **(D)** H-E staining of skin nodule tissue of diseased fish. Basophilic inclusion bodies (black arrows) were present in the hypertrophic lymphocystis cells. Scale bar = 50μm. **(E)** Transmission electron microscope observation of skin nodule tissue. A large number of viral particles appeared in the cytoplasm (black arrows) of lymphocystis cells. Scale bar = 1μm. **(F)** skin nodule tissue fluorescently stained with mouse anti-LCDV 32kDa VAP Mab. Positive green signal was observed in the cytoplasm; non-immune mouse serum as negative control showing no green signal; cell nucleus stained with DAPI (blue); Scale bar = 50μm.

3.6 GSEA analysis of differential gene expression profiles

In total, there were 27 down-regulated pathways (Figure 6A), of which the main ones associated with nodule formation included the cGMP-PKG signaling pathway (Figure 6B) and Calcium signaling pathway (Figure 6C) in Signal transduction; ECM-receptor interaction (Figure 6D) and Cytokine-cytokine receptor interaction (Figure 6E) in Signaling molecules and interactions. Genes, including *prkcg*, *lamc3*, *col4a5*, *tnfsf12*, *col4a6*, *plcb4*, *xmrk*, *prkcb*, *tnfrsf19*, *csf1r2*, *lamb2*, *camk2a*, *ifnar2*, *tnfrsf1a*, *ptger1*, *gna11*, *adcy7*, *vdac2*, *plcg1*, and *camk2b*, were all significantly

10.3389/fimmu.2023.1268851

TABLE 2 Summary of sequencing and assembly statistics for the transcriptome data.

Samples	Raw reads	Clean reads (%)	Q20 (%)	Q30 (%)	GC (%)	Total mapped (%)
CS-1	41131938	40994192 (99.67%)	97.90%	94.08%	47.93%	37936874 (92.84%)
CS-2	47039530	46893012 (99.69%)	97.94%	94.17%	49.08%	43447661 (92.86%)
CS-3	41052022	40908092 (99.65%)	97.91%	94.09%	48.85%	37935490 (92.89%)
CS-4	49796204	49650708 (99.71%)	96.92%	91.48%	48.33%	45105990 (91.25%)
LS-1	52959048	52683364 (99.48%)	97.34%	92.83%	49.46%	48216058 (91.85%)
LS-2	42753138	42481640 (99.36%)	97.15%	92.35%	47.52%	38516818 (91.11%)
LS-3	48225006	47979600 (99.49%)	97.35%	92.83%	48.58%	43851911 (91.71%)
LS-4	39663740	39471322 (99.51%)	97.36%	92.83%	49.00%	36186336 (92.00%)

upregulated, while *f2r*, *egfr*, *il6r*, *pdgfra*, *rock2*, *col4a2*, *tgfbr2*, *ednrb*, *cxcl12*, *lama3*, *itga6*, *ll2rg*, *lamc2*, *csf1r1*, *gnai2*, *lamb3*, *agtr1*, *il13ra*, *pdgfrb*, *fn1*, *cxcr4*, *bdkrb2*, *ednra*, *bmp2*, and *adcy1*, were all significantly downregulated (FDR < 0.05, FC ≥ 2) (Figure 6F). Details of these genes are listed in Table S1.

3.7 Visualization of pathways in cancer

Enrichment of DEGs in Figures 4F and 6F into Pathways in cancer showed that these genes were involved in different signaling pathways, ultimately leading to cellular processes including Evading apoptosis and Proliferation, further suggesting that the pathways analyzed in Figures 4 and 6 synergistically promote nodule formation (Figure 7A).

In addition, the DEGs in Pathways in cancer were visualized and the heat map was analyzed. Among them, except for the DEGs analyzed in Figures 4 and 6, *fgf12*, *bcl-xl*, *bcl11a*, *pik3r2*, *traf2*, *fgfr1*, *fgf18*, *fgfr1a*, *araf*, *fgfr3*, *fgfr2*, *fgf14*, *pik3r1*, *elk3*, *crk*, *pik3r3*, *max*, *casp3*, and *bcl9* were significantly upregulated (FDR < 0.05, FC ≥ 2). In contrast, *rasgrp2*, *phb2*, *fgf2*, *phb*, *rasgrp1*, *vegfb*, *kitlg*, *pik3ca*, *ets1*, *fos*, *vegfc*, *tchh*, *flt4*, *fgf16*, *rasgrp3*, *fgf6*, *cytc*, *hgf*, *epgn*, *fgf7*, and *fgf1* were significantly downregulated (FDR < 0.05, FC ≥ 2) (Figure 7B).

3.8 Tissue expression patterns of focused genes

The tissue expression patterns of several aforementioned key genes were examined by qRT-PCR, including ligand *wnt5a*, cell cycle-associated *ccnd1* and *ccnd2*, transcription factors *ctnnb1*, *lef1*, *tcf3*, and *gli2*, B-cell lymphoma/leukemia (BCL) family members *bcl9*, *bcl11a*, and *bcl-xl*, cytokine receptors *fgfr1a* and *fgfr3*. In comparison to the LCDV-uninfected group, *wnt5a* expression levels were considerably higher in the head kidney, trunk kidney, hindgut, gills, and skin ($p < 0.05$). The cell cycle-related *ccnd1* and *ccnd2* all had significantly higher levels in the liver, head kidney, trunk kidney, and skin, and *ccnd1* was also significantly overexpressed in the gills ($p < 0.05$). All transcription factors were significantly more highly expressed in liver and skin ($p < 0.05$). In addition, *ctnnb1* and *tcf3* in the head kidney, *ctnnb1*, *lef1*, and *gli2* in the trunk kidney, *lef1* and *gli2* in the hindgut, and *ctnnb1*, *tcf3*, *gli2* in the gills were strongly expressed ($p < 0.05$). BCL family members *bcl9*, *bcl11a*, and *bcl-xl* shared a similar expression pattern that all considerably overexpressed in liver, trunk kidney, gills, and skin ($p < 0.05$). The cytokine receptors *fgfr1a* and *fgfr3* were all significantly highly expressed in the liver, spleen, trunk kidney, and skin, while *fgfr3* was also significantly overexpressed in the gills ($p < 0.05$) (Figure 8).

4 Discussion

The main target tissues for LCDV include the skin and fin where lymphocystis nodules usually develop. In recent searches, LCDV has been detected in internal organs such as brain, liver, kidney, spleen, and gut in addition to fins and skin (31–33). According to several genetic studies, LCDV primarily affects the skin, gut, liver, and kidney (15, 34–36). In gilthead seabream (*Sparus aurata*), the LCDV genome has been detected in the caudal fin, gut, liver, spleen, kidney, and brain, with the highest viral loads in the caudal fin, followed by the kidney and brain (36). In *Amphiprion ocellaris*, LCDV is detected in the fin and spleen, while in Senegalese sole (*Solea senegalensis*), LCDV MCP gene transcripts are detected in the liver, kidney, brain, gut, and skin/fin at 5-7 dpi (8, 34). Previously, we found that the target tissues of LCDV were skin, liver, spleen, kidney, gills, stomach, heart, and gut in flounder (37). In this study, obvious skin and fin nodules developed in flounder for about one month, and typical hypertrophic cells were present in skin nodules and LCDV particles were observed in the cytoplasm of these cells, while LCDV copy number detection showed the highest viral load in the skin, next in the gills, trunk kidney, hindgut, spleen and liver, and the lowest in the head kidney. Combining our previous study that showed flounder immunized with formalin-inactivated LCDV produced the most powerful immune responses at 21°C in the spleen and head kidney (38), we suggested that the naturally infected flounder in this study had a long course of disease, strong immune responses in the spleen and head kidney might limit viral replication, whereas high viral loads remained in tissues with particularly pronounced foci, especially in the skin nodules. Moreover, studies on Senegalese sole (*Solea senegalensis*) and

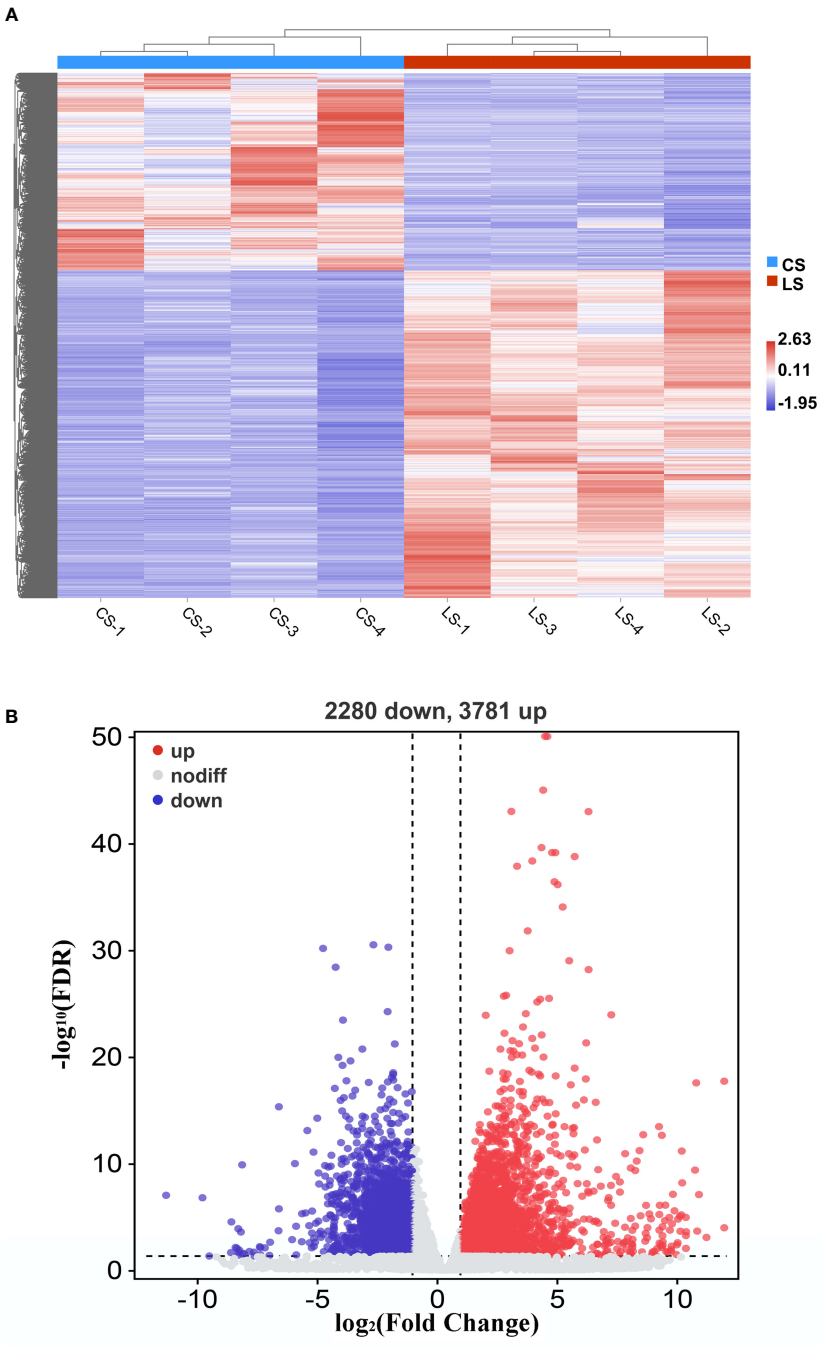

FIGURE 2
DEGs in flounder after LCDV infection. **(A)** The heat map represented the expression levels of those genes that were differentially expressed, as well as the normalization of gene expression using the z-score to construct hierarchical clusters of different samples. Two highly differential clusters were observed: one for genes that were inhibited following LCDV infection and the other for genes that were overexpressed following infection. **(B)** Volcano map of differentially expressed genes. Red represented up-regulated genes, blue represented down-regulated genes, and grey represented no differences.

turbot (*Scophthalmus maximus*) have suggested that LCDV can spread to various tissues by infecting peripheral blood cells (34, 39), and our study has found that LCDV can infect peripheral blood IgM^+ B cells that support viral replication through a 27.8kDa receptor-mediated mechanism (15), these results provide a rationalization for the detection of LCDV in all tissues of the flounder in this study.

The mechanism of lymphocystis cell formation in fish is less well studied. To date, significant alterations in genes related to cell cycle regulation have been found in flounder with lymphocystis cell formation by using microarray experiments, suggesting that LCDV infection leads to cell cycle arrest (5). In human prostate cancer cells, PHB and PHB2 have tumor suppressor functions, and they interact with the E2F transcription factor family in the nucleus to

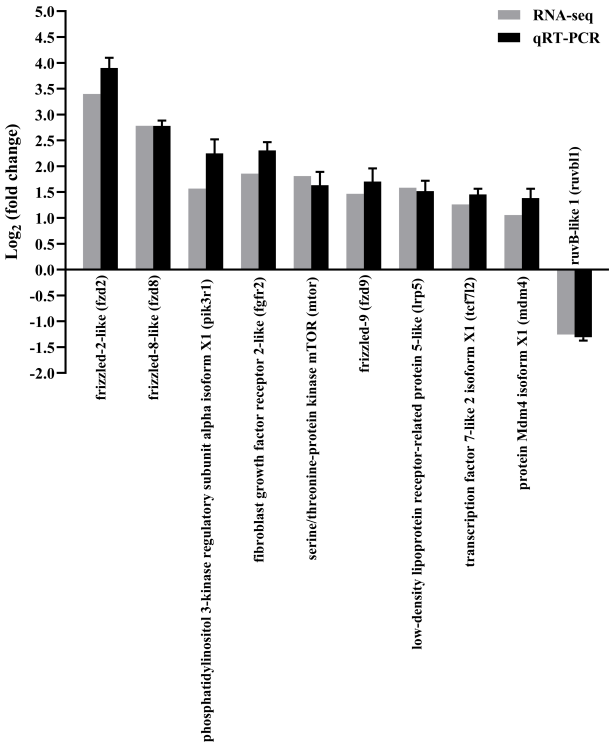

FIGURE 3
Confirmation of RNA-seq data by qRT-PCR. The results were presented as the means ± SEM of four individuals.

reduce E2F function, causing cell cycle arrest in the G1/S phase (40, 41). In this study, transcriptome sequencing analysis of skin nodule tissue indicated that the cell cycle was activated with an up-regulation trend of cell cycle protein-related genes, differing from the significant down-regulation of *phb* and *phb2*, which might lead to rapid cell passage through the cycle checkpoint in favor of viral proliferation. Cell cycle is regulated by the upstream pathways, i.e., Wnt signaling pathway and Hedgehog signaling pathway, in which Wnt signaling pathway regulates various physiological processes such as growth control, stem cell renewal, embryonic development, and tissue differentiation (42). β-catenin (*ctnnb1*), the core transcription factor in Wnt signaling pathway, is normally located on the surface of the cell membrane, mostly involved in homotypic cell adhesion, and to a lesser extent in the cytoplasm, but it cannot enter the nucleus. Nevertheless, when mutations in β-catenin occur, β-catenin can accumulate in the cytoplasm and enter the nucleus where it binds to LEF/TCF to cause transcription of target genes, including the cell growth cycle-related genes *ccnd1* and *ccnd2*, causing pathological changes in cell growth, including tumor formation (43). In mammals, several viruses regulate β-catenin through their proteins to promote cell proliferation and tumorigenesis. As oncogenic viruses, KSHV using the LANA protein and EBV using LMP2A activate and stabilize β-catenin, allowing β-catenin to aggregate into the nucleus to regulate the upregulated expression of target genes including *ccnd1* and *myc*, ultimately leading to cell proliferation and even tumorigenesis (44, 45). Similarly, HBV encodes HBx and hepatitis B surface antigen (HBsAg) proteins that silence antagonists of Wnt/β-catenin signaling pathway or upregulate and stabilize its key components, such as β-catenin, causing aberrant transcription of target genes, which drive cell proliferation and ultimately hepatocarcinogenesis (46). PHB can influence the role of WNT family members in cancer. For instance, overexpression of *phb* in human prostate cancer cells decreases the expression of several members of WNT family and reduces the motility and invasiveness of cancer cells, and *phb* plays an important role in the inter-regulation of *wnt7b*, *wnt9a*, and *wnt10b* with the cell cycle (40). In the present study, we found that Wnt signaling pathway was activated and the gene levels of *ctnnb1*, *lef1*, *tcf3*, *ccnd1*, and *ccnd2* were significantly upregulated, while *ctnnb1* was significantly co-expressed with *ccnd1* and *ccnd2* as hub genes in LCDV-infected skin, gills, head kidney, trunk kidney, and liver tissues. Wnt signaling pathway was also found to interact with multiple tumor pathways. These results suggested that LCDV activated Wnt signaling pathway as well as promoted cell proliferation and nodule formation by regulating *ctnnb1* which in turn leads to overexpression of cell cycle proteins. In addition, Wnt signaling pathway is reported to play an important role in the replication of several viruses. Activation of this pathway can promote avian leukosis virus subgroup J (ALV-J) gene expression and virus production in chicken embryonic fibroblasts cells, while inhibition of this pathway limits virus production in chicken embryonic fibroblasts cells and chicken hepatoma cells (47). Wnt/β-catenin signaling pathway is also thought to act in concert with the Bovine herpesvirus type1 latent gene product to maintain latent Bovine herpesvirus type1 infection, with β-catenin playing a central role (48). In this study, we also found that activated Wnt signaling

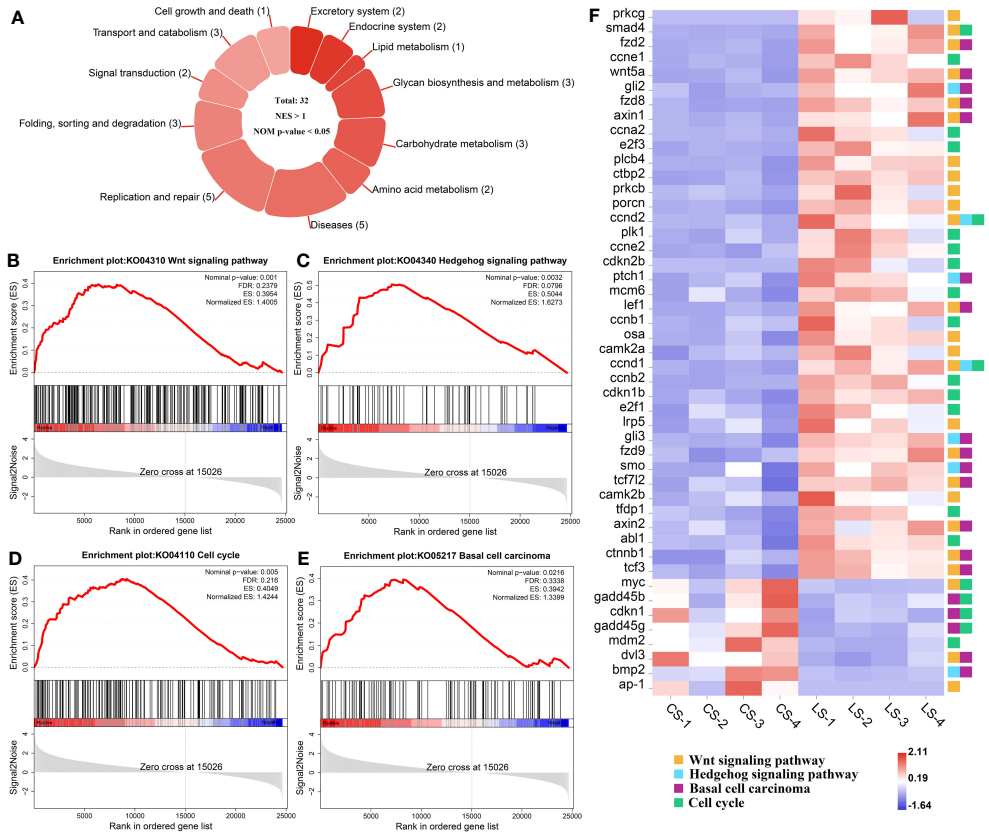

FIGURE 4
GSEA analysis of activated pathways and related genes that are associated with lymphocystis nodule formation after LCDV infection of flounder. **(A)** The number of activated pathways. **(B-E)** KEGG pathways associated with nodule formation including Wnt signaling pathway **(B)**, Hedgehog signaling pathway **(C)**, Cell cycle **(D)**, and Basal cell carcinoma **(E)**. **(F)** The heatmap of DEGs. GSEA was used to analyze the signaling pathway enrichment in different groups. Normalized enrichment score (NES) indicated the analysis results across gene sets. Nominal p-value presented if a set was significantly enriched.

pathway was associated with multiple viral infection pathways, including Human papillomavirus infection and Kaposi sarcoma-associated herpesvirus infection. These findings provided new insights into LCDV virus-host interaction and offered some potential antiviral strategies to control LCDV infection. However, the exact mechanism of which will require later in-depth studies.

The hedgehog signaling pathway was also activated in this study, and based on the KEGG database, we found that there was not only a reciprocal relationship between it and Wnt signaling pathway, but also a link to the tumor formation pathways. In this pathway, when the protein hedgehog (HH) ligand binds to the protein patched homolog (PTCH), smoothened homolog (SMO) repression is removed, and zinc-finger (ZF) transcription factor GLI activity is enhanced, which then enters the nucleus and activates transcription of genes that control cell proliferation, survival and differentiation (49, 50). In this study, *gli2* and *gli3*, members of the GLI family, were significantly upregulated, and they could control cell cycle progression, regulate gene expression levels of cell cycle proteins including *ccnd1* and *ccne2*, and even promote tumourigenesis. It has been reported that silencing of *gli2* leads to cell cycle arrest in G0/G1 phase in human vascular smooth muscle cells and myofibroblasts (51, 52). Similar studies in osteosarcoma, cervical cancer, hepatocellular carcinoma, and hepatocellular carcinogenesis have been conducted to control cell cycle progression (53–56). In cervical cancer, *gli2* overexpression is found to promote cell proliferation, while knockdown of *gli2* causes a stalling effect in G0/G1 phase and a reduction in *ccnd1* gene expression and upregulation of *p21* and *p27* levels (54). In hepatocellular carcinoma, the knockdown of *gli2* gene results in G1 phase arrest, accompanied by downregulation of *ccnd1* and *ccne2* gene expression and upregulation of *p21* levels (55). Additionally, the oncogenic virus HBV is confirmed to contribute to hepatocellular carcinogenesis by regulating members of the GLI family, mainly due to the ability of HBx proteins to stabilize and activate the transcriptional activity of *gli1* and *gli2* (56). In osteosarcoma studies, silencing of *gli2* is found to cause upregulation of *p21*, inhibition of cyclin D1, SKP2, and phosphorylated Rb, thus inducing G1 phase arrest and ultimately preventing the growth of osteosarcoma (53). Basal cell carcinoma is one of the most common types of skin cancer, and Wnt signaling pathway and Hedgehog signaling pathway have been reported to play important roles in this cancer formation (57). Similarly, the present study analyzed a trend of up-regulation in Basal cell carcinoma, which shared the same DEGs with Wnt signaling pathway and Hedgehog signaling pathway, reinforcing the importance of the two pathways in lymphocystis nodule

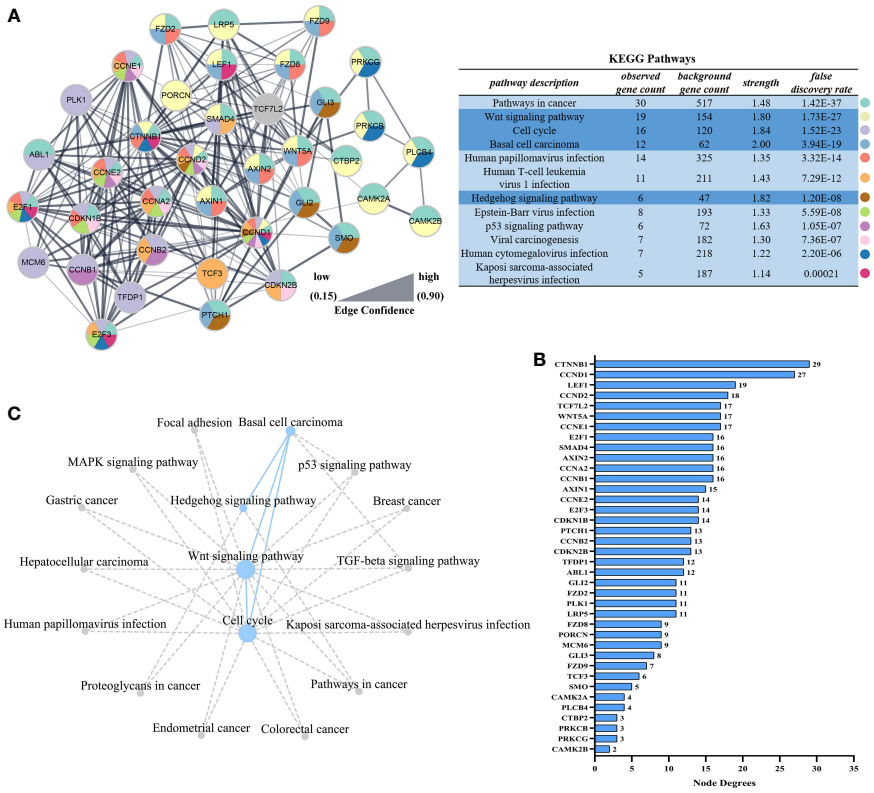

FIGURE 5
Interaction networks based on STRING analysis after LCDV infection of flounder. **(A)** Protein interaction network of up-regulated genes in Figure 4F. The table showed the KEGG analysis of the protein interaction network, dark blue was the pathway analyzed in Figures 4B–E. **(B)** Node degrees of protein interaction network. **(C)** The KEGG database was used to construct the pathway network in Figures 4B–E. The dotted line represented the presence of a relationship and the dot size represented the degree of connectivity.

formation. Considering that *gli2* was expressed in a consistent pattern with *ccnd1* and *ccnd2* in skin, gill, trunk kidney, and liver tissues infected by LCDV in our study, we speculated that the Hedgehog signaling pathway might act in concert with Wnt signaling pathway to control the cell cycle and cause the formation of lymphocystis in fish.

Inhibition of apoptosis is thought to be a major factor in lymphocystis cell formation. By using microarray assay, the reference has investigated gene expression changes in the fins of LCDV-infected flounders and concluded that lymphocystis cell formation was mainly due to inhibition of apoptosis, including the down-regulation of caspase-3 precursor (*casp3*), caspase-6 precursor (*casp6*), caspase-8 precursor (*casp8*) and many other apoptosis-inducing genes (5). Unlike these results, *casp3* was found to be significantly up-regulated in the present study, while some members of the BCL family associated with cell proliferation and inhibition of apoptosis, including *bcl9*, *bcl11a*, and *bcl-xl*, were also considerably up-regulated in LCDV-infected skin, gill, trunk kidney, and liver tissues. BCL9/BCL9L binding to β-catenin can significantly affect tumor growth, suggesting that BCL9/BCL9L interacting with β-catenin plays a key role in tumor progression (58). Bcl11 gene family includes *bcl11a* and *bcl11b*, of which *bcl11a* is a proto-oncogene. In patients with Hodgkin lymphoma, *bcl11a* expression is found to be elevated and associated with EBV infection (59). Bcl-xl is an important member of the BCL-2 family and plays a crucial role in the inhibition of apoptosis (60). A study on HIV shows that β-catenin protects HIV-infected lymphocytes from apoptosis by directly activating the *bcl-xl* promoter activity to induce its expression (61). Therefore, up-regulation of *bcl9*, *bcl11a*, *bcl-xl*, and aforementioned *ctnnb1* in this study revealed that LCDV might regulate the BCL family through β-catenin to promote cell proliferation and inhibit apoptosis. Nevertheless, previous transcriptome analysis of flounder gills infected with LCDV indicates that genes associated with apoptosis including TNF ligand superfamily member 13B and TNF receptor-1 were up-regulated (6). Similarly, the present study found significant upregulation of *tnfsf12*, *tnfrsf1a*, and *tnfrsf19*, these genes might exert a pro-apoptotic effect which appeared to be detrimental to lymphocystis cell formation. But some studies have also found that LCDV can create cytoplasmic TNF receptor-like proteins after *in vivo* infection which react with multiple apoptotic or proliferative signaling proteins, thus inhibiting the apoptotic cascade downstream of the TNFR superfamily (62). In addition, the transcriptome results from flounder gills also demonstrate a downregulation of the apoptosis inhibitor *bcl-2* (6), which shows an opposite expression pattern to the BCL family members that inhibit apoptosis in this study. Combining these results, we suggested that skin cells infected by LCDV might initiate apoptosis to prevent the spread of the virus, while LCDV relied on its own proteins to interfere with apoptosis to facilitate

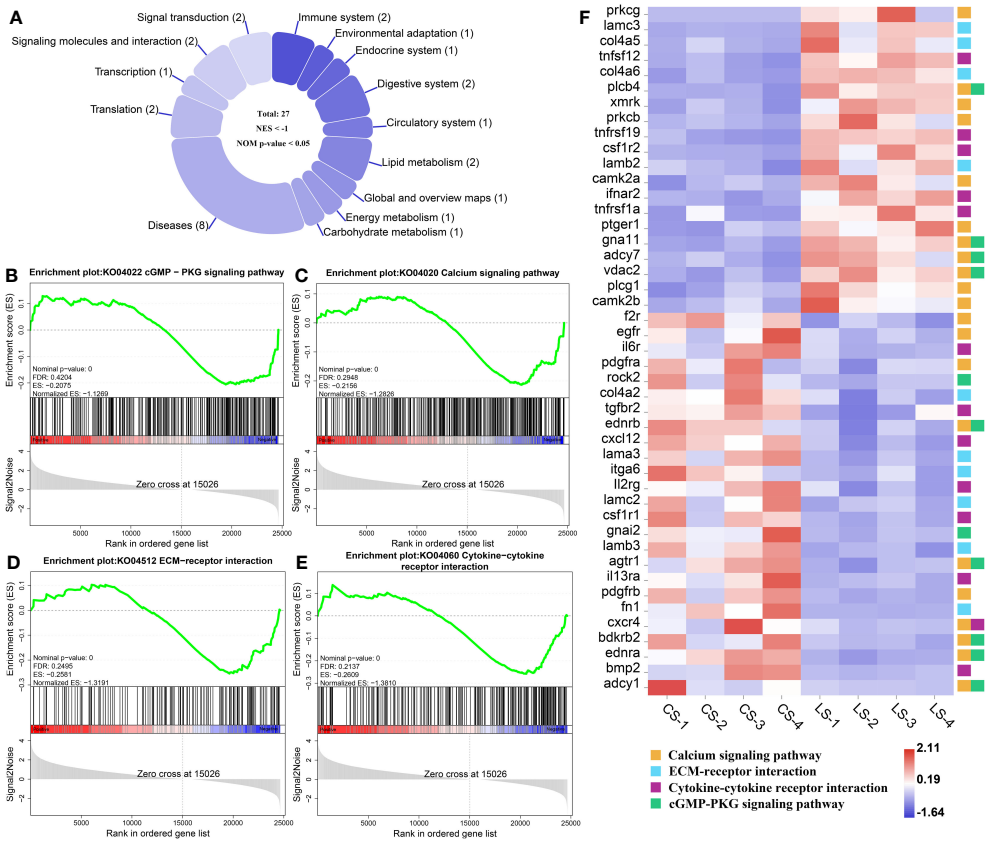

FIGURE 6
GSEA analysis of down-regulated pathways and related genes associated with nodule formation after LCDV infection of flounder. **(A)** The number of down-regulated pathways. **(B–E)** KEGG pathways associated with nodule formation including cGMP-PKG signaling pathway **(B)**, Calcium signaling pathway **(C)**, ECM-receptor interaction **(D)**, and Cytokine-cytokine receptor interaction **(E)**. **(F)** The heatmap of DEGs. GSEA was used to analyze the signaling pathways enrichment in different groups. Normalized enrichment score (NES) indicated the analysis results across gene sets. Nominal p-value presented if a set was significantly enriched.

proliferation, which was more like a competition between the virus and the host cells. VDAC2 was confirmed in our previous study to act as a functional receptor mediating the entry of LCDV into flounder gill (FG) cells (12). In the present study, *vdac2* was significantly upregulated, and we believe that it contributes to lymphocystis formation mainly because it also plays an important role in endogenous apoptosis. VDAC is responsible for the release of apoptosis-inducing proteins such as cytochrome C from the mitochondria into the cytoplasm to induce apoptosis, a process that is influenced by the competitive interactions of pro-apoptotic and anti-apoptotic factors with VDAC isoforms (63, 64). The anti-apoptotic factors Bcl-2, Bcl-xL, or hexokinases block the binding of VDAC to pro-apoptotic proteins by interacting with VDAC to close the pore and thus prevent the release of cytochrome C (63). Additionally, at the gene level, we found that *cytc* was significantly down-regulated, suggesting that cytochrome C was inhibited at both the protein and gene levels thereby failing to exert its pro-apoptotic role. References have shown that effective pro-apoptotic factor bax-mediated apoptosis is dependent on vdac2 (65), whereas the anti-apoptotic factor bcl-xl exerts an anti-apoptotic effect by blocking bax damage to the outer mitochondrial membrane (66). Moreover, LCDV produces the TNF receptor analog and VDAC can be oligomerized by TNF-α, which may contribute to the inhibition of apoptosis by LCDV (3). VDAC can interact with viral proteins to reduce apoptosis in infected cells, as shown in Infectious Bursal Disease Virus whose VP5 formed a complex with RACK1 and VDAC2 to inhibit apoptosis (67). RACK1 is also a receptor for LCDV entry into FG cells together with VDAC2, and not only that, the gene expression levels of RACK1 reach a peak later than VDAC2 after LCDV infection (12). In this study, RACK1 showed an up-regulation trend although it was not significant (Table S1), this might due to the difference in the expression time of the two receptors. Therefore, RACK1 as a receptor for LCDV entry might also play a role in lymphocystis formation. However, whether LCDV proteins forming a complex with VDAC2/RACK1 can inhibit host cell apoptosis, and whether VDAC2/RACK1 determines the balance between cell death and survival (that is, apoptosis and lymphocystis cell formation), need to be further investigated.

Fibroblast growth factors (FGFs) bind to their receptors, fibroblast growth factor receptors (FGFRs), and activate the downstream signaling pathways they regulate, playing an

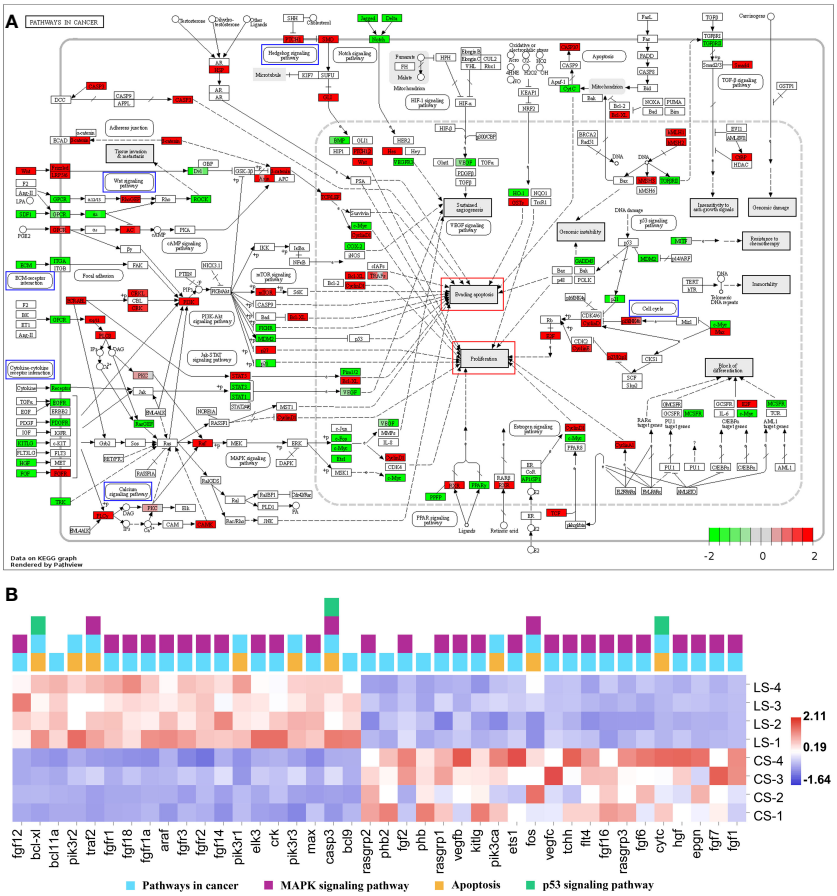

FIGURE 7
Pathways in cancer from KEGG. **(A)** Visualization of DEGs expression. Blue boxes represented pathways analyzed in Figures 4B–E and 6B–E; red boxes represented cellular effects; DEGs were filled in with color, with red representing up-regulation, green representing down-regulation and shades representing expression size. **(B)** The heatmap of DEGs.

important role in both pro-mitotic (embryogenesis, growth, and development) and non-mitotic (neuromodulation, metabolic regulation) biological processes. Among these pathways, high expression and mutations of fgfr lead to abnormal activation of the signaling pathway, resulting in uncontrolled pro-division and subsequent tumor production (68), for example, significant expression of *fgfr2* has been detected in cervical cancer (69). In addition, it is shown that the addition of the pan FGFR inhibitor AZD4547 alone inhibits the growth of cells associated with E2/E4/E5 in HPV positive tumor (70). In the present study, the FGFR family members, *fgfr1*, *fgfr2*, and *fgfr3*, were significantly upregulated in the skin nodule tissue of LCDV-infected flounder. *Fgfr3* is the first member of the FGFR family, which undergoes somatic mutations in tumors and is expressed at elevated levels in cell lines through repeated translocations to and from immunoglobulin heavy chain (IGH) sites (71, 72). *Fgfr1* is thought to be similar to *fgfr3* in recurrent translocations in some tumors (73), but little functional validation has been reported except that it promotes tumorigenesis through gene amplification and overexpression (74). FGFRs also play a role in viral infection, and fgfr1 acts as a co-receptor for adeno-associated virus type 3 (AAV-3) strain H (75). So, it is reasonable to infer that FGFRs might play a similar role in lymphocystis formation after LCDV infection, but more evidence is required to clarify this.

The P53 signaling pathway is involved in several cellular processes and is particularly important in suppressing tumor formation. Several oncogenic viruses promote tumor formation by modulating the p53 signaling pathway. For example, HBV inhibits p53-induced apoptosis by suppressing p53 activity through its HBx protein (17, 76). HCV affects the DNA-binding function of p53 through its NS5A protein (17). While HPV E6/E7 proteins and MCPyV tumor antigen inhibit and degrade p53 and affect other pathways closely associated with cancer including the Notch signaling pathway and TGF-beta signaling pathway (77–80). In addition, oncogenic viruses often manipulate the MAPK signaling pathway to promote host cell proliferation and cause cell metastasis. EBV activates the MAPK signaling pathway through the LMP1 protein to contribute to nasopharyngeal carcinoma cell invasion (81). KSHV activates the MK2 kinase, an effector of the MAPK signaling pathway, through the kaposin B protein to promote tumor formation (82). In this study, although there was no significant trend of up- and down-regulation of the p53 signaling pathway, TGF-beta signaling pathway, and MAPK signaling pathway, we found that there was a linkage of these pathways

10.3389/fimmu.2023.1268851

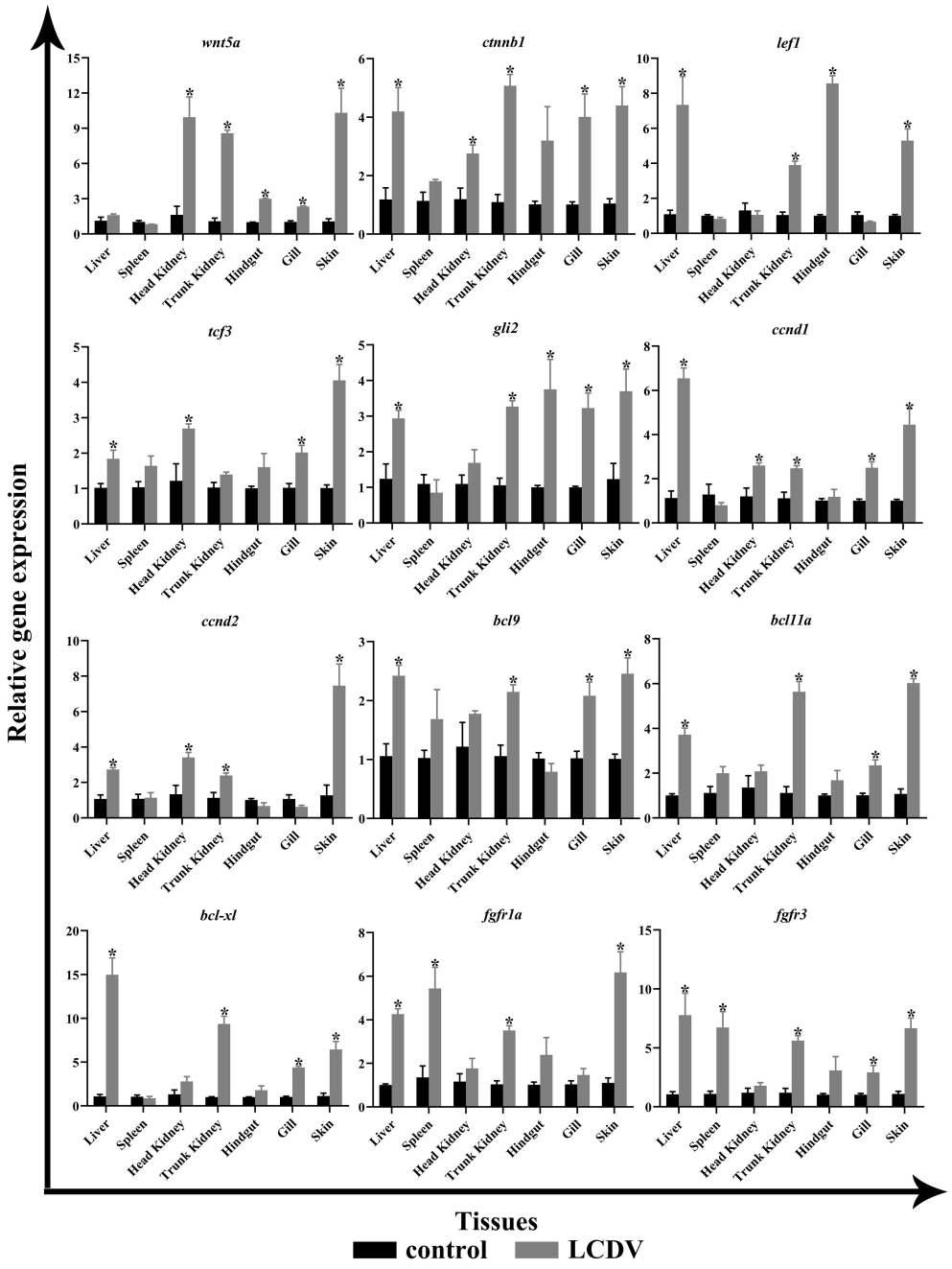

FIGURE 8
qRT-PCR of key genes of the focal pathway in various tissues of LCDV-infected flounder. The results were presented as the means ± SEM of four individuals. Asterisk indicated significant difference ($p < 0.05$).

with Wnt signaling pathway and Cell cycle, implying that there were common DEGs of these pathways that promoted the formation of lymphocystis cells.

In summary, we performed RNA-seq on skin nodule tissues of naturally LCDV-infected flounder using high-throughput sequencing technology and analyzed transcriptome data, and found that Wnt signaling pathway, Hedgehog signaling pathway, Cell cycle, and Basal cell carcinoma associated with lymphocystis formation were activated. These pathways regulated cell cycle-related genes such as *ccnd1* and *ccnd2* through key genes such as *ctnnb1* and *gli2* to promote cell proliferation, which has been shown to interact with several viral infection and tumor formation pathways, and therefore they are considered to be an important cause of lymphocystis formation. *Bcl9*, *bcl11a*, and *bcl-xl*, members of the BCL family that promote cell proliferation and inhibit apoptosis, were significantly upregulated, as were *fgfr1*, *fgfr2*, and *fgfr3*, which are closely related to tumor formation. *Tnfsf12*, *tnfrsf1a*, and *tnfrsf19*, which are associated with pro-apoptosis, as well as *vdac2*, which promotes viral replication by inhibiting apoptosis, also acts as a receptor for LCDV entry, were significantly upregulated.

Pro-apoptotic *cytc* and anti-tumor *phb* and *phb2* were significantly down-regulated. These results are expected to explain the molecular basis of lymphocystis formation after LCDV infection of flounder. For the first time, we have analyzed the pathways and differentially expressed genes associated with lymphocystis formation using high-throughput sequencing technology, providing a new breakthrough in the study of lymphocystis formation in fish.

Data availability statement

The datasets presented in this study can be found in online repositories. The names of the repository/repositories and accession number(s) can be found below: https://www.ncbi.nlm.nih.gov/, SAMN36345915; https://www.ncbi.nlm.nih.gov/, SAMN36345916; https://www.ncbi.nlm.nih.gov/, SAMN36345917; https://www.ncbi.nlm.nih.gov/, SAMN36345918; https://www.ncbi.nlm.nih.gov/, SAMN36345919; https://www.ncbi.nlm.nih.gov/, SAMN36345920; https://www.ncbi.nlm.nih.gov/, SAMN36345921; https://www.ncbi.nlm.nih.gov/, SAMN36345922.

Ethics statement

The animal study was approved by the Animal Care and Use Committee of Ocean University of China (permit number: OUC-AE-2022-071). The study was conducted in accordance with the local legislation and institutional requirements.

Author contributions

HZ: Data curation, Formal Analysis, Investigation, Writing – original draft, Methodology, Validation. XS: Conceptualization, Formal Analysis, Funding acquisition, Writing – original draft, Writing – review & editing, Project administration. XT: Formal Analysis, Resources, Writing – review & editing, Methodology, Validation. JX: Formal Analysis, Writing – review & editing, Resources, Validation. HC: Formal Analysis, Resources, Writing – review & editing, Validation. WZ: Conceptualization, Funding acquisition, Writing – review & editing, Supervision.

Funding

The authors declare financial support was received for the research, authorship, and/or publication of this article. This study was supported by the National Natural Science Foundation of China (Grant numbers: 32273163, 31872599, and 31730101).

Conflict of interest

The authors declare that the research was conducted in the absence of any commercial or financial relationships that could be construed as a potential conflict of interest.

The author(s) declared that they were an editorial board member of Frontiers, at the time of submission. This had no impact on the peer review process and the final decision.

Publisher's note

Supplementary material

The Supplementary Material for this article can be found online at: https://www.frontiersin.org/articles/10.3389/fimmu.2023.1268851/full#supplementary-material

References

1. Leiva-Rebollo R, Gémez-Mata J, Castro D, Borrego JJ, Labella AM. Immune response of DNA vaccinated-gilthead seabream (*Sparus aurata*) against LCDV-Sa infection: relevance of the inflammatory process. *Front Immunol* (2023) 14:1209926. doi: 10.3389/fimmu.2023.1209926

2. Cheng SF, Zhan WB, Xing J, Sheng XZ. Development and characterization of monoclonal antibody to the lymphocystis disease virus of Japanese flounder *Paralichthys olivaceus* isolated from China. *J Virol Methods* (2006) 135:173–80. doi: 10.1016/j.jviromet.2006.03.016

3. Pontejo SM, Sánchez C, Martín R, Mulero V, Alcami A, Alejo A. An orphan viral TNF receptor superfamily member identified in lymphocystis disease virus. *Virol J* (2013) 10:188. doi: 10.1186/1743-422X-10-188

4. Ross N, Ruggieri GD. Studies on virus diseases of fishes, spontaneous and experimentally induced cellular hypertrophy (lymphocystis disease) in fishes of the New York aquarium, with a report of new cases and an annotated bibliography (1874–1965). *Deep-Sea Res Oceanogr Abstr* (1965) 50:83–95. doi: 10.1016/0011-7471(76)91096-2

5. Iwakiri S, Song JY, Nakayama K, Oh MJ, Ishida M, Kitamura SI. Host responses of Japanese flounder *Paralichthys olivaceus* with lymphocystis cell formation. *Fish Shellfish Immunol* (2014) 38:406–11. doi: 10.1016/j.fsi.2014.03.028

6. Wu RH, Sheng XZ, Tang XQ, Xing J, Zhan WB. Transcriptome Analysis of Flounder (*Paralichthys olivaceus*) Gill in Response to Lymphocystis Disease Virus (LCDV) Infection: Novel Insights into Fish Defense Mechanisms. *Int J Mol Sci* (2018) 19:160. doi: 10.3390/ijms19010160

7. López-Bueno A, Mavian C, Labella AM, Castro D, Borrego JJ, Alcami A, et al. Concurrence of iridovirus, polyomavirus, and a unique member of a new group of fish papillomaviruses in lymphocystis disease-affected gilthead sea bream. *J Virol* (2016) 90:8768–79. doi: 10.1128/JVI.01369-16

8. Cheng MC, See MS, Wang PC, Kuo YT, Ho YS, Chen SC, et al. Lymphocystis disease virus infection in clownfish *Amphiprion ocellaris* and *Amphiprion clarkii* in Taiwan. *Animals* (2022) 13:153. doi: 10.3390/ani13010153

9. Sheng XZ, Zhong Y, Zeng J, Tang XQ, Xing J, Chi H, et al. Lymphocystis disease virus (*Iridoviridae*) enters flounder (*Paralichthys olivaceus*) gill cells via a caveolae-mediated endocytosis mechanism facilitated by viral receptors. *Int J Mol Sci* (2020) 21:4722. doi: 10.3390/ijms21134722

10. Wu RH, Tang XQ, Sheng XZ, Zhan WB. Relationship between expression of cellular receptor-27.8kDa and lymphocystis disease virus (LCDV) infection. *PloS One* (2015) 10:e0127940. doi: 10.1371/journal.pone.0127940

11. Zhong Y, Fei CJ, Tang XQ, Zhan WB, Sheng XZ. A 32 kDa viral attachment protein of lymphocystis disease virus (LCDV) specifically interacts with a 27.8 kDa cellular receptor from flounder (*Paralichthys olivaceus*). *J Gen Virol* (2017) 98:1477–88. doi: 10.1099/jgv.0.000805

12. Zhong Y, Tang XQ, Sheng XZ, Xing J, Zhan WB. Voltage-dependent anion channel protein 2 (VDAC2) and receptor of activated protein c kinase 1 (RACK1) act as functional receptors for lymphocystis disease virus infection. *J Virol* (2019) 93: e00122–19. doi: 10.1128/JVI.00122-19

13. García-Rosado E. Serological techniques for detection of lymphocystis virus in fish. *Aquat Living Resour* (2002) 15:179–85. doi: 10.1016/S0990-7440(02)01174-9

14. Cano I, Ferro P, Alonso MC, Sarasquete C, Garcia-Rosado E, Borrego JJ, et al. Application of in *situ* detection techniques to determine the systemic condition of lymphocystis disease virus infection in cultured gilt-head seabream, *Sparus aurata* L. *J Fish Dis* (2009) 32:143–50. doi: 10.1111/j.1365-2761.2008.00970.x

15. Sheng XZ, Zeng J, Zhong Y, Tang XQ, Xing J, Chi H, et al. Peripheral blood B-lymphocytes are involved in lymphocystis disease virus infection in flounder (*Paralichthys olivaceus*) via cellular receptor-mediated mechanism. *Int J Mol Sci* (2022) 23:9225. doi: 10.3390/ijms23169225

16. Moore PS, Chang Y. Why do viruses cause cancer? Highlights of the first century of human tumour virology. *Nat Rev Cancer* (2010) 10:878–89. doi: 10.1038/nrc2961

17. Akram N, Imran M, Noreen M, Ahmed F, Atif M, Fatima Z, et al. Oncogenic role of tumor viruses in humans. *Viral Immunol* (2017) 30:20–7. doi: 10.1089/vim.2016.0109

18. Wang Z, Gerstein M, Snyder M. RNA-Seq: a revolutionary tool for transcriptomics. *Nat Rev Genet* (2009) 10:57–63. doi: 10.1038/nrg2484

19. Kozarewa I, Ning Z, Quail MA, Sanders MJ, Berriman M, Turner DJ. Amplification-free Illumina sequencing-library preparation facilitates improved mapping and assembly of (G+C)-biased genomes. *Nat Methods* (2009) 6:291–5. doi: 10.1038/nmeth.1311

20. Martin JA, Wang Z. Next-generation transcriptome assembly. *Nat Rev Genet* (2011) 12:671–82. doi: 10.1038/nrg3068

21. Zhong Y, Tang XQ, Sheng XZ, Xing J, Zhan WB. Development and characterization of monoclonal antibodies to the 32 kDa viral attachment protein of lymphocystis disease virus and their neutralizing ability *in vitro*. *Int J Mol Sci* (2018) 19:2536. doi: 10.3390/ijms19092536

22. Chen SF, Zhou YQ, Chen YR, Gu J. fastp: an ultra-fast all-in-one FASTQ preprocessor. *Bioinformatics* (2018) 34:i884–90. doi: 10.1093/bioinformatics/bty560

23. Langmead B, Salzberg SL. Fast gapped-read alignment with Bowtie 2. *Nat Methods* (2012) 9:357–9. doi: 10.1038/nmeth.1923

24. Kim D, Langmead B, Salzberg SL. HISAT: a fast spliced aligner with low memory requirements. *Nat Methods* (2015) 12:357–60. doi: 10.1038/nmeth.3317

25. Love MI, Huber W, Anders S. Moderated estimation of fold change and dispersion for RNA-seq data with DESeq2. *Genome Biol* (2014) 15:550. doi: 10.1186/s13059-014-0550-8

26. Subramanian A, Tamayo P, Mootha VK, Mukherjee S, Ebert BL, Gillette MA, et al. Gene set enrichment analysis: A knowledge-based approach for interpreting genome-wide expression profiles. *Proc Natl Acad Sci U.S.A* (2005) 102:15545–50. doi: 10.1073/pnas.0506580102

27. Auwera GA, Carneiro MO, Hartl C, Poplin R, del Angel G, Levy-Moonshine A, et al. From FastQ data to high-confidence variant calls: the genome analysis toolkit best practices pipeline. *Curr Protoc Bioinf* (2013) 43(1110):11.10.1–11.10.33. doi: 10.1002/0471250953.bi1110s43

28. Szklarczyk D, Franceschini A, Wyder S, Forslund K, Heller D, Huerta-Cepas J, et al. STRING v10: protein–protein interaction networks, integrated over the tree of life. *Nucleic Acids Res* (2015) 43:D447–52. doi: 10.1093/nar/gku1003

29. Luo WJ, Pant G, Bhavnasi YK, Blanchard SG, Brouwer C. Pathview Web: user friendly pathway visualization and data integration. *Nucleic Acids Res* (2017) 45:W501–8. doi: 10.1093/nar/gkx372

30. Luo WJ, Brouwer C. Pathview: an R/Bioconductor package for pathway-based data integration and visualization. *Bioinformatics* (2013) 29:1830–1. doi: 10.1093/bioinformatics/btt285

31. Rahmati-Holasoo H, Ahmadivand S, Marandi A, Shokrpoor S, Palić D, Jahangard A. Identification and characterization of lymphocystis disease virus (LCDV) from Indian glassy fish (*Parambassis ranga Hamilton*, 1822) in Iran. *Aquacult Int* (2022) 30:2593–602. doi: 10.1007/s10499-022-00922-7

32. Rahmati-Holasoo H, Ghalyanchilangeroudi A, Ziafati Kafi Z, Marandi A, Shokrpoor S, Imantalab B, et al. Detection of lymphocystis disease virus (LCDV) from yellowbar angelfish (*Pomacanthus maculosus* Forsskål, 1775) in Iran: Histopathological and phylogenetic analysis. *Aquaculture* (2023) 562:738862. doi: 10.1016/j.aquaculture.2022.738862

33. Kvitt H, Heinisch G, Diamant A. Detection and phylogeny of *Lymphocystivirus* in sea bream *Sparus aurata* based on the DNA polymerase gene and major capsid protein sequences. *Aquaculture* (2008) 275:58–63. doi: 10.1016/j.aquaculture.2008.01.007

34. Carballo C, Castro D, Borrego JJ, ManChado M. Gene expression profiles associated with lymphocystis disease virus (LCDV) in experimentally infected Senegalese sole (*Solea Senegalensis*). *Fish Shellfish Immunol* (2017) 66:129–39. doi: 10.1016/j.fsi.2017.04.028

35. Hu GB, Lou HM, Dong XZ, Liu QM, Zhang SC. Characteristics of the interferon regulatory factor 5 (IRF5) and its expression in response to LCDV and poly I:C challenges in Japanese flounder, *Paralichthys olivaceus*. *Dev Comp Immunol* (2012) 38:377–82. doi: 10.1016/j.dci.2012.06.001

36. Valverde EJ, Borrego JJ, Sarasquete MC, Ortiz-Delgado JB, Castro D. Target organs for lymphocystis disease virus replication in gilthead seabream (*Sparus aurata*). *Vet Res* (2017) 48:21. doi: 10.1186/s13567-017-0428-3

37. Zhan WB, Li YQ, Sheng XZ, Xing J, Tang XQ. Detection of lymphocystis disease virus in Japanese flounder *Paralichthys olivaceus* and other marine teleosts from northern China. *Chin J Ocean Limnol* (2010) 28:1213–20. doi: 10.1007/s00343-010-9934-0

38. Xu GJ, Sheng XZ, Xing J, Zhan WB. Effect of temperature on immune response of Japanese flounder (*Paralichthys olivaceus*) to inactivated lymphocystis disease virus (LCDV). *Fish Shellfish Immunol* (2011) 30:525–31. doi: 10.1016/j.fsi.2010.11.026

39. Sheng XZ, Wu RH, Tang XQ, Xing J, Zhan WB. Tissue localization of lymphocystis disease virus (LCDV) receptor-27.8 kDa and its expression kinetics induced by the viral infection in turbot (*Scophthalmus maximus*). *Int J Mol Sci* (2015) 16:26506–19. doi: 10.3390/ijms161125974

40. Koushyar S, Uysal-Onganer P, Jiang WG, Dart DA. Prohibitin links cell cycle, motility and invasion in prostate cancer cells. *Int J Mol Sci* (2023) 24:9919. doi: 10.3390/ijms24129919

41. Koushyar S, Economides G, Zaat S, Jiang W, Bevan CL, Dart DA. The prohibitin-repressive interaction with E2F1 is rapidly inhibited by androgen signalling in prostate cancer cells. *Oncogenesis* (2017) 6:e333–3. doi: 10.1038/oncsis.2017.32

42. Nusse R, Clevers H. Wnt/β-catenin signaling, disease, and emerging therapeutic modalities. *Cell* (2017) 169:985–99. doi: 10.1016/j.cell.2017.05.016

43. Li VSW, Ng SS, Boersema PJ, Low TY, Karthaus WR, Gerlach JP, et al. Wnt signaling through inhibition of β-catenin degradation in an intact axin1 complex. *Cell* (2012) 149:1245–56. doi: 10.1016/j.cell.2012.05.002

44. Fujimuro M, Hayward SD. The latency-associated nuclear antigen of kaposi's sarcoma-associated herpesvirus manipulates the activity of glycogen synthase kinase-3β. *J Virol* (2003) 77:8019–30. doi: 10.1128/JVI.77.14.8019–8030.2003

45. Morrison JA, Klingelhutz AJ, Raab-Traub N. Epstein-Barr virus latent membrane protein 2a activates β-catenin signaling in epithelial cells. *J Virol* (2003) 77:12276–84. doi: 10.1128/JVI.77.22.12276-12284.2003

46. Daud M, Rana MA, Husnain T, Ijaz B. Modulation of Wnt signaling pathway by hepatitis B virus. *Arch Virol* (2017) 162:2937–47. doi: 10.1007/s00705-017-3462-6

47. Qiao DD, He Q, Cheng XW, Yao YX, Nair V, Shao HX, et al. Regulation of avian leukosis virus subgroup J replication by Wnt/β-catenin signaling pathway. *Viruses* (2021) 13:1968. doi: 10.3390/v13101968

48. Zhu LQ, Thunuguntla P, Liu YL, Hancock M, Jones C. The β-catenin signaling pathway stimulates bovine herpesvirus 1 productive infection. *Virology* (2017) 500:91–5. doi: 10.1016/j.virol.2016.10.014

49. Taipale J, Beachy PA. The Hedgehog and Wnt signalling pathways in cancer. *Nature* (2001) 411:349–54. doi: 10.1038/35077219

50. Wickström M, Dyberg C, Shimokawa T, Milosevic J, Baryawno N, Fuskevåg OM, et al. Targeting the hedgehog signal transduction pathway at the level of GLI inhibits neuroblastoma cell growth in *vitro* and in *vivo*. *Int J Cancer* (2013) 132:1516–24. doi: 10.1002/ijc.27820

51. Li FH, Duman-Scheel M, Yang D, Du W, Zhang J, Zhao CC, et al. Sonic hedgehog signaling induces vascular smooth muscle cell proliferation via induction of the G_1 cyclin-retinoblastoma axis. *Arterioscler Thromb Vasc Biol* (2010) 30:1787–94. doi: 10.1161/ATVBAHA.110.208520

52. Kramann R, Fleig SV, Schneider RK, Fabian SL, DiRocco DP, Maarouf O, et al. Pharmacological GLI2 inhibition prevents myofibroblast cell-cycle progression and reduces kidney fibrosis. *J Clin Invest* (2015) 125:2935–51. doi: 10.1172/JCI74929

53. Nagao H, Ijiri K, Hirotsu M, Ishidou Y, Yamamoto T, Nagano S, et al. Role of GLI2 in the growth of human osteosarcoma: GLI2 in osteosarcoma. *J Pathol* (2011) 224:169–79. doi: 10.1002/path.2880

54. Zhu HY, Xia L, Shen Q, Zhao MH, Gu X, Bouamar H, et al. Differential effects of GLI2 and GLI3 in regulating cervical cancer Malignancy in *vitro* and in *vivo*. *Lab Invest* (2018) 98:1384–96. doi: 10.1038/s41374-018-0089-5

55. Zhang DW, Liu JP, Wang Y, Chen J, Chen T. shRNA-mediated silencing of Gli2 gene inhibits proliferation and sensitizes human hepatocellular carcinoma cells towards TRAIL-induced apoptosis. *J Cell Biochem* (2011) 112:3140–50. doi: 10.1002/jcb.23240

56. Kim HY, Cho HK, Hong SP, Cheong J. Hepatitis B virus X protein stimulates the Hedgehog–Gli activation through protein stabilization and nuclear localization of Gli1 in liver cancer cells. *Cancer Lett* (2011) 309:176–84. doi: 10.1016/j.canlet.2011.05.033

57. Jaiswal A, Singh R. Homeostases of epidermis and hair follicle, and development of basal cell carcinoma. *Biochim Biophys Acta Rev Cancer* (2022) 1877:188795. doi: 10.1016/j.bbcan.2022.188795

58. Vafaizadeh V, Buechel D, Rubinstein N, Kalathur RKR, Bazzani L, Saxena M, et al. The interactions of Bcl9/Bcl9L with β-catenin and Pygopus promote breast cancer growth, invasion, and metastasis. *Oncogene* (2021) 40:6195–209. doi: 10.1038/s41388-021-02016-9

59. Chetaille B, Bertucci F, Finetti P, Esterni B, Stamatoullas A, Picquenot JM, et al. Molecular profiling of classical Hodgkin lymphoma tissues uncovers variations in the

tumor microenvironment and correlations with EBV infection and outcome. *Blood* (2009) 113:2765–3775. doi: 10.1182/blood-2008-07-168096

60. Kirkin V, Joos S, Zörnig M. The role of Bcl-2 family members in tumorigenesis. *Biochim Biophys Acta* (2004) 1644:229–49. doi: 10.1016/j.bbamcr.2003.08.009

61. Albalawi YA, Narasipura SD, Al-Harthi L. Wnt/β-catenin protects lymphocytes from HIV-mediated apoptosis via induction of Bcl-xL. *Viruses* (2022) 14:1469. doi: 10.3390/v140714699

62. Essbauer S, Fischer U, Bergmann S, Ahne W. Investigations on the ORF 167L of lymphocystis disease virus (*Iridoviridae*). *Virus Genes* (2004) 28:19–39. doi: 10.1023/B:VIRU.0000012261.96217.fe

63. Najbauer EE, Becker S, Giller K, Zweckstetter M, Lange A, Steinem C, et al. Structure, gating and interactions of the voltage-dependent anion channel. *Eur Biophys J* (2021) 50:159–72. doi: 10.1007/s00249-021-01515-7

64. Saadawy AH, Khalil AM, Sidarous LR, Ibrahim MS, Salem TZ. Voltage-dependent anion channels: key players in viral infection. *Rev Med Virol* (2023) 33: e2453. doi: 10.1002/rmv.2453

65. Chin HS, Li MX, Tan IKL, Ninnis RL, Reljic B, Scicluna K, et al. VDAC2 enables BAX to mediate apoptosis and limit tumor development. *Nat Commun* (2018) 9:4976. doi: 10.1038/s41467-018-07309-4

66. Breckenridge DG, Xue D. Regulation of mitochondrial membrane permeabilization by BCL-2 family proteins and caspases. *Curr Opin Cell Biol* (2004) 16:647–52. doi: 10.1016/j.ceb.2004.09.009

67. Lin WC, Zhang ZQ, Xu ZC, Wang B, Li XQ, Cao H, et al. The association of receptor of activated protein kinase c 1(RACK1) with infectious bursal disease virus viral protein VP5 and voltage-dependent anion channel 2 (VDAC2) inhibits apoptosis and enhances viral replication. *J Biol Chem* (2015) 290:8500–10. doi: 10.1074/jbc.M114.585687

68. Wesche J, Haglund K, Haugsten EM. Fibroblast growth factors and their receptors in cancer. *Biochem J* (2011) 437:199–213. doi: 10.1042/BJ20101603

69. Kawase R, Ishiwata T, Matsuda Y, Onda M, Kudo M, Takeshita T, et al. Expression of fibroblast growth factor receptor 2 IIIc in human uterine cervical intraepithelial neoplasia and cervical cancer. *Int J Oncol* (2009) 36:331–40. doi: 10.3892/ijo_00000504

70. Ren SL, Gaykalova DA, Guo T, Favorov AV, Fertig EJ, Tamayo P, et al. HPV E2, E4, E5 drive alternative carcinogenic pathways in HPV positive cancers. *Oncogene* (2020) 39:6327–39. doi: 10.1038/s41388-020-01431-8

71. Chesi M, Nardini E, Brents LA, Schröck E, Ried T, Kuehl WM, et al. Frequent translocation t(4, 14)(p16.3; q32.3) in multiple myeloma is associated with increased expression and activating mutations of fibroblast growth factor receptor 3. *Nat Genet* (1997) 16:260–4. doi: 10.1038/ng0797-260

72. Richelda R, Ronchetti D, Baldini L, Cro L, Viggiano L, Marzella R, et al. A novel chromosomal translocation t(4, 14)(p16.3; q32) in multiple myeloma involves the fibroblast growth-factor receptor 3 gene. *Blood* (1997) 90:4062–70. doi: 10.1182/blood.V90.10.4062

73. Jha HC, Banerjee S, Robertson E. The role of gammaherpesviruses in cancer pathogenesis. *Pathogens* (2016) 5:18. doi: 10.3390/pathogens5010018

74. Goradia A, Bayerl M, Cornfield D. The 8p11 Myeloproliferative syndrome: review of literature and an illustrative case report. *Int J Clin Exp Pathol* (2008) 1:448–56. doi: 10.1080/14992020802286202

75. Blackburn SD, Steadman RA, Johnson FB. Attachment of adeno-associated virus type 3H to fibroblast growth factor receptor 1. *Arch Virol* (2006) 151:617–23. doi: 10.1007/s00705-005-0650-6

76. Bréchot C. Pathogenesis of hepatitis B virus—related hepatocellular carcinoma: old and new paradigms. *Gastroenterology* (2004) 127:S56–61. doi: 10.1053/j.gastro.2004.09.016

77. Becker JC, Stang A, DeCaprio JA, Cerroni L, Lebbé C, Veness M, et al. Merkel cell carcinoma. *Nat Rev Dis Primers* (2017) 3:17077. doi: 10.1038/nrdp.2017.77

78. Wendzicki JA, Moore PS, Chang Y. Large T and small T antigens of Merkel cell polyomavirus. *Curr Opin Virol* (2015) 11:38–43. doi: 10.1016/j.coviro.2015.01.009

79. Vande Pol SB, Klingelhutz AJ. Papillomavirus E6 oncoproteins. *Virology* (2013) 445:115–37. doi: 10.1016/j.virol.2013.04.026

80. Roman A, Munger K. The papillomavirus E7 proteins. *Virology* (2013) 445:138–68. doi: 10.1016/j.virol.2013.04.013

81. Dawson CW, Laverick L, Morris MA, Tramoutanis G, Young LS. Epstein-Barr virus-encoded LMP1 regulates epithelial cell motility and invasion via the ERK-MAPK pathway. *J Virol* (2008) 82:3654–64. doi: 10.1128/JVI.01888-07

82. McCormick C, Ganem D. The Kaposin B protein of KSHV activates the p38/MK2 pathway and stabilizes cytokine mRNAs. *Science* (2005) 307:739–41. doi: 10.1126/science.1105779

frontiers | Frontiers in Immunology

TYPE Original Research
PUBLISHED 13 October 2023
DOI 10.3389/fimmu.2023.1272393

OPEN ACCESS

EDITED BY
Carolina Johnstone,
Spanish Institute of Oceanography (IEO), Spain

REVIEWED BY
Tor Gjøen,
University of Oslo, Norway
Sebastian Reyes-Cerpa,
Major University, Chile

*CORRESPONDENCE
Tianxiang Gao
gaotianxiang0611@163.com

RECEIVED 04 August 2023
ACCEPTED 26 September 2023
PUBLISHED 13 October 2023

CITATION
Lou F, Zhang Y, Xu A and Gao T (2023) Transcriptional responses of liver and spleen in *Lota lota* to polyriboinosinic polyribocytidylic acid.
Front. Immunol. 14:1272393.
doi: 10.3389/fimmu.2023.1272393

Transcriptional responses of liver and spleen in *Lota lota* to polyriboinosinic polyribocytidylic acid

Fangrui Lou[1], Yuan Zhang[2], Anle Xu[3] and Tianxiang Gao[3]*

[1]School of Ocean, Yantai University, Yantai, Shandong, China, [2]CAS Key Laboratory of Tropical Marine Bio-resources and Ecology, South China Sea Institute of Oceanology Chinese Academy of Sciences, Guangzhou, China, [3]Fishery College, Zhejiang Ocean University, Zhoushan, Zhejiang, China

Introduction: The cultured *Lota lota* can meet the market demand in the context of the decline of wild resources, but the disease in the high-density culture process also deserves attention. Therefore, understanding the immune regulation mechanisms of *L. lota* will be the basis for obtaining high benefits in artificial culture.

Methods: To explore the viral response mechanism of *L. lota*, RNA-seq was applied to identify the transcriptomic changes of the liver and spleen in *L. lota* by poly (I:C) stress.

Results: The DEGs (liver: 2186 to 3123; spleen 1542 to 2622) and up-regulated genes (liver: 1231 to 1776; spleen 769 to 1502) in the liver and spleen increased with the prolongation (12h to 48h) of poly (I:C)-stimulation time. This means *L. lota* needs to mobilize more functional genes in response to longer periods of poly (I:C)-stimulation. Despite the responses of *L. lota* to poly (I:C) showed tissue-specificity, we hypothesized that both liver and spleen of *L. lota* can respond to poly (I:C) challenge may be through promoting apoptosis of DNA-damaged cells, increasing the activity of immune-enhancing enzymes, and increasing energy supply based on DEGs annotation information.

Conclusions: Our results demonstrate the transcriptional responses of *L. lota* to poly (I:C)-stimulation, and these data provide the first resource on the genetic regulation mechanisms of *L. lota* against viruses. Furthermore, the present study can provide basic information for the prevention of viral diseases in *L. lota* artificial culture process.

KEYWORDS

Lota lota, liver, spleen, transcriptome, poly (I:C), viral response mechanism

1 Introduction

Viruses are transmitted horizontally into aquatic fish mainly through the gills and intestine, causing oxidative damage, dysfunction, inflammation, and even death (1, 2). Because aquatic fish do not have perfect antiviral capacity (3), the outbreak of the virus will lead to loss of control of aquatic fish management (4).

The immune organs of aquatic fish are mainly composed of head-kidney, liver, spleen, and so on (5, 6). Among them, the head-kidney can produce red blood cells and B lymphocyte without relying on antigen stimulation, and thus has the dual function of central and peripheral immune organ. Meanwhile, the head-kidney can not only store, destroy, and detoxify various foreign matter, but also participate in the inflammatory response and humoral immune process as the primary center of memory cells (5, 7). The liver has been shown to contain a variety of natural immune cells that can induce immune tolerance or inflammatory responses and produce various cytokines and chemokines (8, 9). Previous studies have suggested that the liver can also synthesize complement (10, 11). Tafalla et al. (12) revealed that the spleen of aquatic fish also had immune function, and its role in non-specific and specific immune systems was only weaker than that of the head-kidney. Although the functions of melano-macrophages in the spleen have not been determined, the virus-clearing function of melano-macrophages is well established and they may be the lymphocyte germinal center (13). Consequently, investigating the immune responses of the immune organs to invading viruses can demonstrate how the fish cope with viral infection.

Lota lota is the only freshwater Gadiformes and is widely distributed in inland lakes and bays of Europe, Asia, and North America north of latitude 45°N (14). Climate warming caused by human activities and other factors is assumed to have resulted in a rapid decrease of *L. lota* resources, which are ecologically dependent on low temperature (15, 16), and *L. lota* has been listed in the Rare Aquatic Wildlife of China. The gradual development of artificial culture can meet the market demand for aquatic food under the background of the decline of *L. lota* resources (17). Parasitic and viral infections have seriously limited the health and sustainable development of *L. lota* aquaculture (18), but there is little research on how to deal with these problems.

Transcriptional processes usually represent the complex dynamics of biological internal regulatory mechanisms (16), which can be used to reveal the response mechanisms of *L. lota* to invading viruses. High-throughput sequencing technologies such as RNA sequencing (RNA-seq) have advantages in obtaining complete transcripts of organisms (19), and thus have been successfully applied to analyze the transcriptional responses of a variety of aquatic fishes to viral invasion (20–22). Therefore, RNA-seq can also serve as a useful technique for identifying the transcriptional divergences of *L. lota* associated with viral invasion. Unfortunately, transcriptome studies of *L. lota* have only focused on the response mechanisms of high temperature (16, 23), and the transcriptional regulation mechanisms of *L. lota* in response to viral invasion have not been reported.

Polyriboinosinic polyribocytidylic acid [poly (I:C)] is the viral double-stranded RNA analogue that as an immune adjuvant has been shown to induce viral immune responses in fishes or shellfishes (22, 24–26). In the present study, the liver and spleen of *L. lota* injected with poly (I:C) were obtained and RNA-seq was carried out to explore the genetic regulation mechanisms of *L. lota* on poly (I:C). Furthermore, our results can provide new insights into the immune regulation of *L. lota* against viruses, and provide basic data for viral disease prevention in the *L. lota* intensive culture processes.

2 Materials and methods

2.1 Ethics approval and participation consent

We promise that the present research complies with the applicable international and institutional policies relating to animal experiments. Meanwhile, all experimental methods involved in this study were approved by the Institutional Animal Care and Use Committee of Yantai University and performed in accordance with relevant guidelines and regulations. Additionally, all *L. lota* used in the present study were quickly transported to the laboratory and then were anesthetized with tricaine methanesulfonate (100 mg/L) before dissection.

2.2 *L. lota* collection, maintenance, and poly (I:C) stimulation

L. lota (28.2 ± 1.03 g, 15.6 ± 0.90 cm) were collected from the aquafarm of the Irtysh River, Burqin, Xijiang Province (China) on 29 October 2019. Before poly (I:C) stimulation, all *L. lota* were placed temporarily in the same polyethylene aquariums (volume: 40 L) for a week to acclimatize, and the temperature, pH, ammonia nitrogen, nitrite, nitrate, and dissolved oxygen of water were maintained at 17°C, 7.9, 0.27 mg/L, 0.001 mg/L, 0.05 mg/L, and 5.0 mg/L, respectively. Normal feeding (3% of body weight; at 08:00 and 14:00) was performed throughout the experimental process. Meanwhile, we change the water every morning to ensure the stability of all water factors. After acclimation, all *L. lota* were randomly assigned to two separate aquariums (length × width × height: 72 cm × 53 cm × 44 cm), each of which was assigned 10 individuals (6 were used for subsequent experiments and the remaining 4 were used as backup), and the breeding density of *L. lota* was approximately 1,679.57 g/m^3. We intraperitoneally injected 200 µL of PBS reagent (Beyotime Biotechnology, Shanghai, China) into individual *L. lota* in an aquarium as the control group, and injected 200 µL of poly (I:C) (Beyotime Biotechnology, Shanghai, China) at a concentration of 0.5 mg/mL (dissolved using PBS reagent) into individual *L. lota* in another aquarium as the treatment group. At 12 h and 48 h after injection, *L. lota* in the two groups were sacrificed and dissected to obtain the liver and spleen, and three individuals were randomly collected as biological replicates at each time point in each group. The obtained livers and spleens were immediately frozen with liquid nitrogen and then stored at −80°C. Finally, 24 tissue samples (2 tissues × 2 groups × 2

time nodes × 3 biological replicates) were obtained for subsequent RNA extraction. All experimental groups were named L_{12PBS}, S_{12PBS}, L_{12po}, S_{12po}, L_{48PBS}, S_{48PBS}, $L48_{po}$, and S_{48po}, respectively.

2.3 RNA extraction and detection, library construction, and Illumina sequencing

We used the Trizol Reagent Kit (Vazyme, Nanjing, China) to extract the total RNA of each tissue sample following the manufacturer's protocol. The degradation or contamination degree, purity (OD260/280), concentration, and integrity of RNAs was detected using the agarose gel electrophoresis, Nanodrop (Implen, MUC, Germany), Qubit 2.0 (Thermo Fisher Scientific, MA, USA), and Agilent 2100 (Agilent Technologies, CA, USA), respectively.

The qualified total RNAs were used for library construction. We removed rRNA from the 1 μg of total RNA per sample and purified the remaining mRNA using RNA Purification Beads (Illumina, San Diego, CA, USA), and then cleaned all mRNAs three times using the Beads Binding Buffer (Illumina, San Diego, CA, USA). We used the NEBNext® UltraTM RNA Library Prep Kit for Illumina ® (NEB, USA) to construct 24 sequencing libraries after mRNA fragmentation. Specifically, we first reversely transcribed the mRNA into first-strand cDNA using random hexamers, and then added buffer, dNTPs, and DNA polymerase I to synthesize the second-strand cDNA. The synthesized double-stranded cDNAs were purified using AMPure XP beads (Illumina, San Diego, CA, USA), and terminal repair, A-tail addition, and sequencing connector were then performed. Subsequently, we added A-tails and adapters to the double-stranded cDNAs, respectively. Then, AMPure XP Beads were applied to select the fragment size, and these fragments with appropriate size were amplified by PCR to obtain the cDNA libraries. The constructed cDNA libraries were quantified using Qubit 2.0 (Thermo Fisher Scientific, MA, USA) and then diluted to 1 ng/μL. Finally, the cDNA libraries qualified by the Agilent 2100 (Agilent Technologies, CA, USA) were sequenced on an Illumina HiSeq 2000 platform across one lane with 150 bp paired-end.

2.4 RNA-seq data processing

Trimmomatic software (version 0.36, 27) was used to eliminate low-quality raw RNA-seq reads, mainly referring to these reads that contained sequencing adapters, unknown nucleotides ratio > 10%, and quality scores < 20. Hisat software (version 2.0.4; 28) was used to compare the high-quality clean RNA-seq reads to the published *L. lota* whole genome sequences (29). The regional distribution and density distribution of clean RNA-seq reads on the genome sequences were then analyzed. Meanwhile, we use rMATS (version 3.2.5; 30) software to predict the classification, number, and structure of alternative splicing (AS) events.

2.5 Transcriptional responses of liver and spleen in *L. lota* to the poly (I:C) stimulation

To identify the transcriptional responses of liver and spleen in *L. lota* to the poly (I:C) stimulation, we first quantified the gene expression levels of each sample using the HTSeq (version 2.0; 31) software and described them using FPKM (expected number of Fragments Per Kilobase of transcript sequence per Millions base pairs sequenced). Then, we identified the differentially expressed genes (DEGs) among different experimental groups using DESeq software (version 2.0, 32), and false discovery rate (FDR) adjusted p-value < 0.005 and fold change (FC) ≥ 2 (which corresponds to $|\log_2 FC| \geq 1$) were used as the filtering thresholds. A Venn diagram was applied to visualize the number of DEGs. Furthermore, we determined the clustering relationship of DEG expression level in four experimental groups according to the FPKMs. Finally, we attempted to analyze the biological functions of these DEGs and their products based on the Gene Ontology (GO) and Kyoto Encyclopedia of Genes and Genomes (KEGG) annotation. The hyper-geometric distribution corrected p-value < 0.05 was taken as the criterion of significant enrichment of the GO term and KEGG pathway.

2.6 Quantitative reverse transcription PCR validation

In the present study, quantitative reverse transcription PCR (qRT-PCR) was applied to verify the reliability of transcriptome data. According to the functional annotation information, a total of eight immune-related DEGs (four in the liver and four in the spleen) were randomly selected for qRT-PCR experiments. Meanwhile, Ribosomal protein S29 (*rps29*) and Ribosomal protein L26 (*rpl26*) were used as reference genes for standardization (22). Primer Premier 6.0 was applied to design the reference gene-specific and DEG-specific primers (Table 1). Twenty-four cDNA samples from 12 experimental individuals were diluted 25 times using nuclease-free water according to standard curves and then used as templates for qRT-PCR. The qRT-PCR was conducted on the StepOne Plus Real-Time PCR system (ABI, USA) according to the manufacturer's instructions of the TaKaRa TB Green Premix Ex Taq (Til RAaseH Plus, RR420A). A 20-μL reaction system was formulated, including 2 μL of diluted cDNA template, 0.4 μL of forward primer (10 μM), 0.4 μL of reverse primer (10 μM), 0.4 μL of ROX Reference Dye (50×), and 6.8 μL of RNase-free water. The qRT-PCR cycling conditions were as follows: one cycle of 95 °C for 30 s, followed by 40 cycles of 5 s at 95°C, 30 s at 60°C, and then enter the dissociation stage. Three experimental triplicates were performed for each qRT-PCR cycling condition to ensure the accuracy of qRT-PCR results. The relative expression levels of eight DEGs were calculated by the $2^{-\Delta\Delta CT}$ method ($\Delta CT = CT_{DEG} - CT_{internal\ gene}$, $\Delta\Delta CT = \Delta CT_{treatment\ group} - \Delta CT_{control\ group}$).

TABLE 1 Primer sequences of 2 reference genes and 12 DEGs.

	Gene name	Full gene name	Primer (5′ to 3′)	Product length
Reference genes	*rps29*	Ribosomal protein S29	For_ ACAGCTCTACTGGAGTCAT	146 bp
			Rev_ CGAAGCCGATGTCCTTAG	
	rpl26	Ribosomal protein L26	For_ GCAAGAGGCACTTCAATG	127 bp
			Rev_ ACCTGGACTTCGTCATCT	
DEGs in the liver	*met*	Hepatocyte growth factor	For_GCCACATACAGGTTCTCTT	210 bp
			Rev_ACGACAGCAGACAGGAA	
	casp3	Caspase 3	For_CTGTGCGAGATGCTGAC	143 bp
			Rev_GTGGTGATGGCTGGAATC	
	hsp90a1	Heat shock protein 90 class A member 1	For_CGAGAAGAAGAAGCAGGAT	104 bp
			Rev_GGTTGGAGACGGAGACT	
	lgp2	Laboratory of genetics and physiology 2	For_GGTGGTGGTCCTGGTTA	217 bp
			Rev_AGCGTGTCTGTCCTCAT	
DEGs in the spleen	*pmp22*	Peripheral myelin protein 22	For_TTCTTCTTGGAGTGCTTGT	159 bp
			Rev_CATTGCTGGCTGGTAGG	
	csf1r	Colony stimulating factor 1 receptor	For_CGTGGTGGATGCTAACTT	177 bp
			Rev_TCATTGGTGGAGAGGAGAT	
	ccnd2	Cyclin-D2	For_CTACACAGACAACTCCATCA	128 bp
			Rev_GCAGCCTCCTCACAATG	
	flt3	FMS-like tyrosine kinase 3	For_ACAACGACTCCAACTACG	271 bp
			Rev_CTCCAGCACTTACACATCA	

3 Results

3.1 RNA-seq data of 24 samples

All raw RNA-seq reads have been submitted to the NCBI sequence read archive under the BioProject PRJNA874751. A total of 228.08 Gb of clean RNA-seq reads were captured after removing the low-quality raw RNA-seq reads, and the summary of RNA-seq reads is shown in Supplementary File 1. All clean RNA-seq reads from 24 samples were compared to the reference genome (Supplementary File 2) and results showed that 90.97% of the clean RNA-seq reads can be located on the reference genome. Meanwhile, the percentages of clean RNA-seq reads with multiple mapped locations and uniquely mapped locations on the reference genome are 7.14% and 83.83%, respectively. Furthermore, although many clean RNA-seq reads are mapped to the exon region of reference genome, a small number of reads are mapped to the intergenic region, and a minimal proportion of clean RNA-seq reads were compared to intron regions (Supplementary File 3). Meanwhile, there was a positive correlation between the distribution density of clean RNA-seq reads and chromosome length (Supplementary File 4). Additionally, a total of 20,646 predicted genes were successfully annotated on at least one protein database. Of all annotated predicted genes, 3,432, 14,369, 13,246, 17,187, 20,576, 18,218, 13,388, and 11,282 predicted genes had significantly matched with the sequences in the AnimalTFDB, GO, KEGG, KOG, NR, Pfam, Swiss-Prot, and TrEMBL databases, respectively (Figure 1).

3.2 AS events

A total of 3,347 and 3,361 AS events were predicted based on "junction count only-" and "reads on target and junction counts-" quantitative methods, respectively. Meanwhile, a total of 198 and 202 different AS events were predicted based on "junction count only-" and "reads on target and junction counts-" quantitative methods, respectively. Among the five common AS events (namely, skipped exon [SE], alternative 5′ splice site [A5SS], alternative 3′ splice site [A3SS], mutually exclusive exons [MXE], and retained intron [RI]), SE and MXE were found to be the most abundant AS events (Table 2).

3.3 The number of DEGs of *L. lota* stimulated by poly (I:C)

In the present study, we have identified the poly (I:C)-stimulated DEGs in liver (L_{12po}-vs-L_{12PBS}, L_{48po}-vs-L_{48PBS}) and spleen (S_{12po}-vs-S_{12PBS}, and S_{48po}-vs-S_{48PBS}) of *L. lota* (Supplementary File 5). Results showed that the number of DEGs

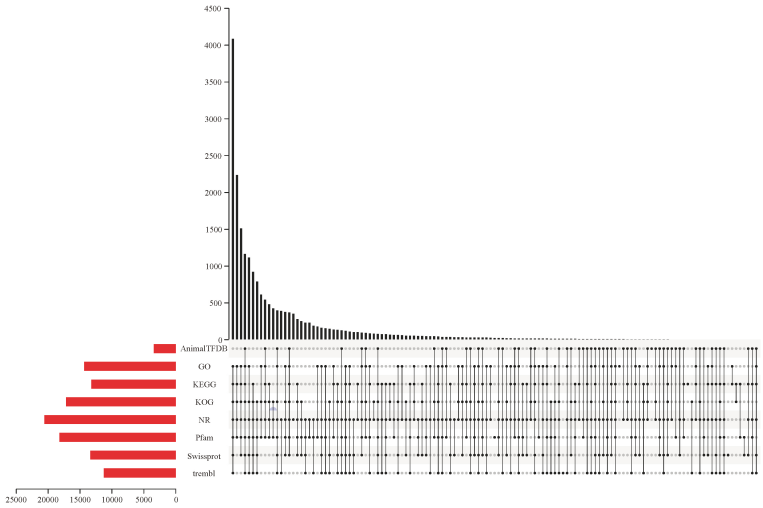

FIGURE 1
The number of genes successfully matched to sequences in the AnimalTFDB, GO, KEGG, KOG, NR, Pfam, Swiss-Prot, and TrEMBL databases, respectively.

TABLE 2 AS classification and quantitative statistics.

	SE	MXE	A5SS	A3SS	RI
Number of ASs based on junction count only	3,161	186	0	0	0
Number of different ASs based on junction count only	178 (81:97)	20 (4:16)	0	0	0
Number of ASs based on reads on target and junction counts	3,175	186	0	0	0
Number of different ASs based on reads on target and junction counts	181 (82:99)	21 (4:17)	0	0	0

increased with the increase in infiltration time of liver (2,186 at 12 h and 3,123 at 48 h; Figure 2A) and spleen (1,542 at 12 h and 2,622 at 48 h; Figure 2B) in poly (I:C). Compared with the PBS treatments, a total of 1,231 (56.31%) and 1,776 (56.87%) upregulated genes were identified from the liver exposed to poly (I:C) at 12 h and 48 h, respectively. Meanwhile, a total of 769 (49.87%) and 1,502 (57.28%) upregulated genes were identified from the spleen exposed to poly (I:C) at 12 h and 48 h, respectively. Additionally, cluster analysis showed that the expression levels of DEGs from the same tissue and the same treatment were similar, and the similarity of DEG expression levels in the same tissue was higher than that between tissues (Figure 3).

We found that a substantial overlap of 300 DEGs existed in four experimental pairs (L_{12po}-vs-L_{12PBS}, L_{48po}-vs-L_{48PBS}, S_{12po}-vs-S_{12PBS}, and S_{48po}-vs-S_{48PBS}) (Figure 4). Considering that these genes contributed more to the responses of *L. lota* to poly (I:C), we obtained annotation information of 300 DEGs (Supplementary File 6). Not unexpectedly, there are abundant immune-related genes (such as Nuclear valosin-containing protein [*NVLp*], Tumor necrosis factor [*TNF*], Zinc-binding protein [*ZBP*], Antigen peptide transporter (*APT*), Calcium/calmodulin-dependent protein kinase type 1G [*Camk1g*], and Interferon regulatory factor 4 [*IRF-4*]) in *L. lota* that were ultimately predicted (the yellow marked part of Supplementary File 6).

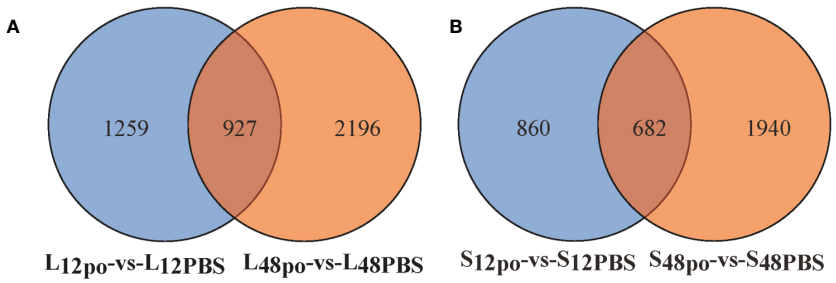

FIGURE 2
The poly (I:C)-stimulated DEGs in liver **(A)** and spleen **(B)** of *L. lota*.

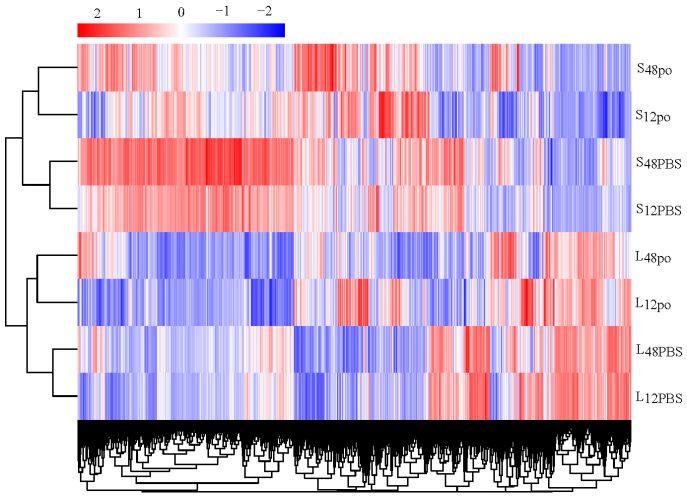

FIGURE 3
The clustering relationship of DEG expression levels of four experimental groups according to the FPKM.

3.4 The biological functions of poly (I:C) response-associated genes in *L. lota*

Unsurprisingly, poly (I:C) injection significantly affected the biological processes of *L. lota*, and this phenomenon had time and tissue specificity. Firstly, we matched the up- and downreg ulated genes in the liver and spleen into the GO database and then obtained the GO annotation information (Supplementary File 7; Figure 5). At 12 h after poly (I:C) injection, upregulated genes in the liver and spleen were significantly enriched in 79 and 156 GO terms (corrected p-value < 0.05), respectively. Meanwhile, downregulated genes in the liver and spleen were significantly enriched in 78 and 74 GO terms (corrected p-value < 0.05), respectively. At 48 h after poly (I:C) injection, upregulated genes in the liver and spleen were significantly enriched in 162 and 73 GO terms (corrected p-value < 0.05), respectively. Meanwhile, downregulation in the liver and spleen were significantly enriched in 12 and 24 GO terms (corrected p-value < 0.05), respectively. The terms of up- or down regulated genes are related to protein regulation, amino acid regulation, energy regulation, cellular homeostasis, immune cell integrity and ion transport.

We recorded the networks of molecular interactions in the cells and the variants specific to *L. lota* by mapping the up- and downreg ulated genes in the liver and spleen to the KEGG database, respectively (Supplementary File 8; Figure 6). At 12 h after poly (I:C) injection, upregulated genes in the liver and spleen were significantly enriched in the 14 (namely, Herpes simplex infection pathway, Proteasome pathway, Apoptosis pathway, Jak-STAT signaling pathway, p53 signaling pathway, RIG-I-like receptor signaling pathway, Toll-like receptor signaling pathway, Cytosolic DNA-sensing pathway, Glycerophospholipid metabolism, Ubiquitin-mediated proteolysis, Ether lipid metabolism pathway, Cytokine–cytokine receptor interaction pathway, alpha-Linolenic acid metabolism pathway, and NOD-like receptor signaling pathway) and 11 (namely, RIG-I-like receptor signaling pathway, Herpes simplex infection pathway, Apoptosis pathway, Toll-like receptor signaling pathway, p53 signaling pathway, NOD-like receptor signaling pathway, Jak-STAT signaling pathway, Cytosolic DNA-

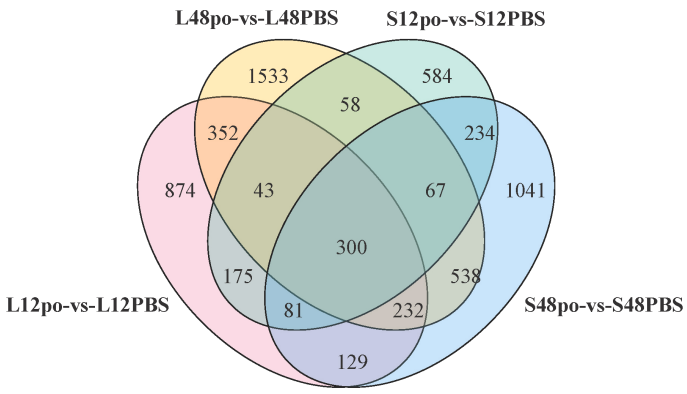

FIGURE 4
The common DEGs among four experimental pairs.

10.3389/fimmu.2023.1272393

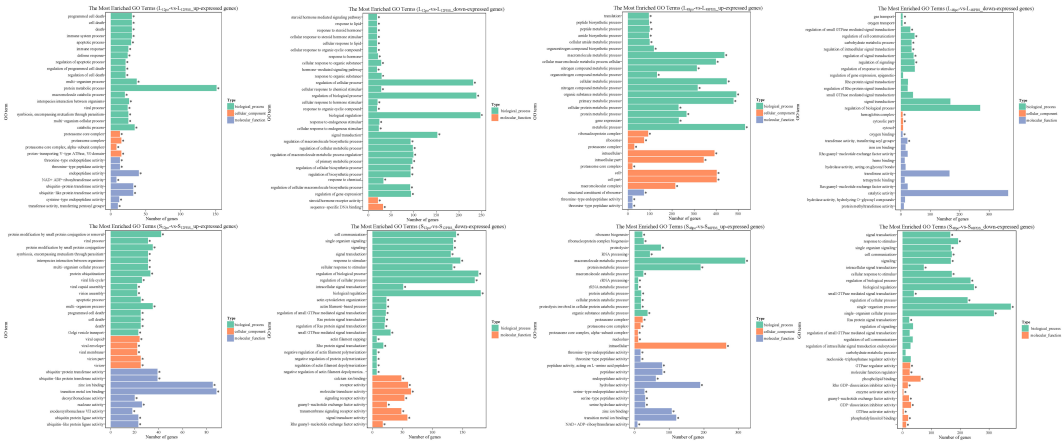

FIGURE 5
The top 30 significantly enriched GO terms of the up- and down regulated genes in the liver and spleen. The vertical coordinate represents the enriched GO terms, and the horizontal coordinate represents the number of DEGs in GO terms. Different colors are used to distinguish biological processes, cellular component, and molecular function. "*" represents the significance of GO terms.

sensing pathway, Cytokine–cytokine receptor interaction pathway, Proteasome pathway, and Drug metabolism - other enzymes pathway) metabolic pathways, respectively (corrected p-value < 0.05). Meanwhile, downregulated genes in the liver and spleen were significantly enriched in the seven (namely, Phosphatidylinositol signaling system pathway, Adherens junction pathway, Focal adhesion pathway, Notch signaling pathway, Glycerolipid metabolism pathway, Inositol phosphate metabolism pathway, and TGF-beta signaling pathway) and five (namely, Focal adhesion pathway, ECM–receptor interaction pathway, Vascular smooth muscle contraction pathway, Regulation of actin cytoskeleton pathway, and Cytokine–cytokine receptor interaction pathway) metabolic pathways, respectively (corrected p-value < 0.05). However, the number and type of metabolic pathways significantly enriched at 48 h of poly (I:C) stimulation varied, which was present in both tissues. Results showed that upregulated genes in the liver and spleen were significantly enriched in the 13 (namely, Ribosome pathway, Proteasome pathway, Spliceosome pathway, Ribosome biogenesis in eukaryotes pathway, Pyrimidine metabolism pathway, RNA transport pathway, DNA replication pathway, Herpes simplex infection pathway, RNA polymerase pathway, Purine metabolism pathway, Cytosolic DNA-sensing pathway, RIG-I-like receptor signaling pathway, and Protein processing in endoplasmic reticulum pathway) and 5 (namely, Proteasome pathway, Ribosome biogenesis in eukaryotes pathway, Herpes simplex infection pathway, RIG-I-like receptor signaling pathway, and Pyrimidine metabolism pathway) metabolic pathways, respectively (corrected p-value < 0.05). Meanwhile, downregulated genes in the liver and spleen were

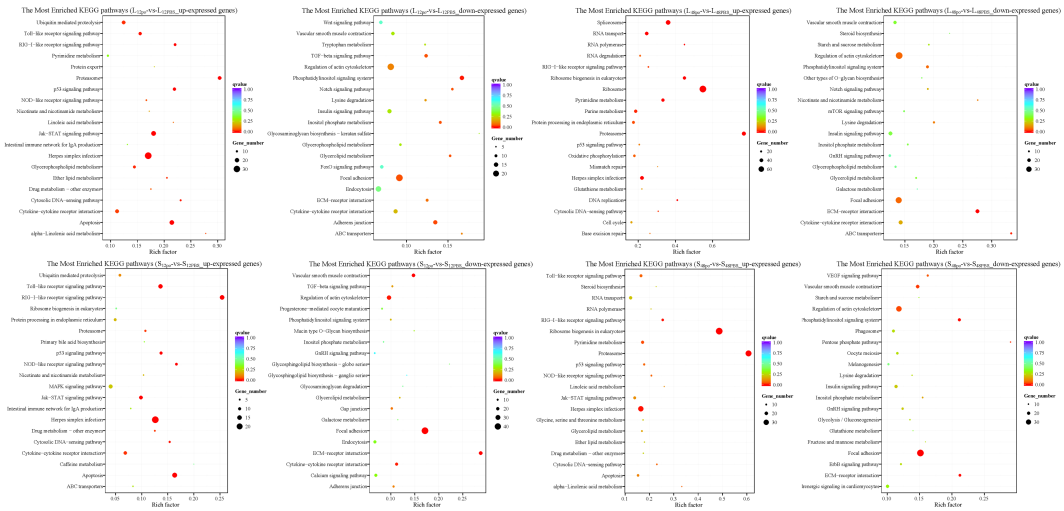

FIGURE 6
The top 20 significantly enriched KEGG pathways of the up- and down regulated genes in the liver and spleen. The vertical coordinate represents the enriched KEGG pathways, and the horizontal coordinate represents the Rich factor. The size of the dots represents the number of DEGs in KEGG pathways, and different colors of dots represent the different q values.3.5 Validation of immune-related gene expression levels.

significantly enriched in the two (namely, ECM–receptor interaction pathway and ABC transporters pathway) and six (included Focal adhesion pathway, Phosphatidylinositol signaling system pathway, ECM–receptor interaction pathway, Pentose phosphate pathway, Vascular smooth muscle contraction pathway, and Regulation of actin cytoskeleton pathway) metabolic pathways, respectively (corrected p-value < 0.05).

The expression trend of eight genes was concordant based on the qRT-PCR data and the RNA-seq data, which meant that the sequencing results were reliable. The different genes showed different expression trends after the poly (I:C) challenge (Figure 7). Detailed *casp3*, *hsp90a1*, and *lgp2* in the liver were upregulated at 12 h and 48 h after poly (I:C) stimulation, while *met* was downregulated. In the spleen, *csf1r*, *ccnd2*, and *flt3* were downregulated at 12 h and 48 h after poly (I:C) stimulation. Meanwhile, *pmp22* in the spleen was downregulated at 12 h after poly (I:C) stimulation, but upregulated at 48 h after poly (I:C) stimulation.

4 Discussion

Disease has been proven to seriously restrict the healthy and sustainable development of aquaculture (33). At present, the use of various chemicals and antibiotics is the essential preventive measure in aquaculture (22, 34, 35). It is worth noting that long-term use of drug in aquaculture may lead to a series of disasters, such as decreased fish immunity, increased pathogen resistance, and drug residues. Immune adjuvants can significantly improve the antigen-specific immune response and vaccine efficacy of fish in a short period of time, so they are gradually applied in the aquaculture (12, 36). For *L. lota* aquaculture, understanding the transcriptional regulatory mechanisms of *L. lota* to immune adjuvants will help to predict the response ability of *L. lota* to viral diseases, and further provide a theoretical basis for exploring disease prevention and control strategies in the *L. lota* aquaculture processes.

4.1 High RNA-seq reads accuracy

The present clean RNA-seq reads covers more than 90% of the *L. lota* genome, and the percentage of clean RNA-seq reads with multiple locations on the genome were less than 10%. This means that our sequenced reads were uncontaminated. Meanwhile, a large proportion of reads could be compared to the exon region and a small proportion to the intergenic region, which provided evidence for the integrity of the *L. lota genome* annotation information. Residues from pre-mRNA and intron retention events during AS processes resulted in a small number of reads being compared to the intron region. Additionally, many protein-coding genes (20,646/21,664; 95.30%; 29) can be functionally annotated in at least one protein database. In conclusion, our sequencing reads can provide a basic resource for studying the regulatory mechanisms of *L. lota* to poly (I:C).

4.2 Genetic regulatory changes in liver and spleen of *L. lota* exposed to poly (I:C)

4.2.1 DEGs

The expression changes of functional genes may contribute to the efficient response of *L. lota* to poly (I:C) challenge. We found that the expression levels of many functional genes in liver and spleen of *L. lota* were changed in response to poly (I:C) stimulation, which also provided evidence for the immune-inducing properties of poly (I:C) (22, 26). Meanwhile, we also found that the number of DEGs and upregulated genes increased with the duration (12 h to 48 h) of poly (I:C) stimulation in both liver and spleen. This may mean that *L. lota* need to activate more efficient gene expression patterns in response to longer periods of poly (I:C) stimulation. The clustering results show similarity in functional gene expression levels, but did not represent exact phylogenetic relationships of functional genes. However, the clustering results may indirectly confirm that the DEGs we acquired are critical functional genes that respond to poly (I:C) stimulation. It is understandable that functionally similar genes derived from the same tissue show similar expression levels in response to similar stimulation, but the expression levels of the same functional genes in response to the same stimulus will show tissue specificity, which may depend on the stimulus reception time and response ability of tissue. In the present study, eight randomly selected immune-related DEGs (namely, *casp3*, *hsp90a1*, *lgp2*, *met*, *csf1r*, *ccnd2*, *flt3*, and *pmp22*) were further verified by qRT-PCR. Upregulated *casp3* in *L. lota* liver exposed for 12 h and 48 h can cleave and inactivate a variety of important proteins in the cytoplasm, resulting in an imbalance of cellular homeostasis and ultimately leading to apoptosis of damaged

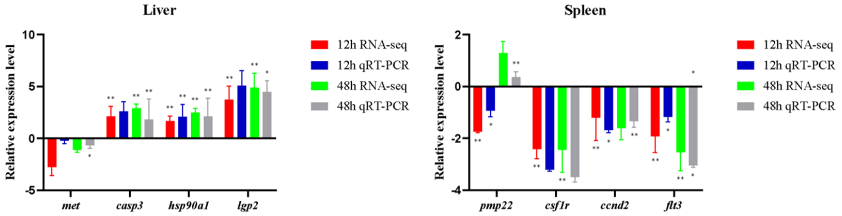

FIGURE 7
Expression levels of immune-related genes obtained based on RNA-seq and qRT-PCR. Asterisks indicate statistical significance (*p < 0.05) or extremely statistical significance (**p < 0.01).

liver cells, which contributes to the maintenance of metabolic capacity, structural integrity, and function of the liver stimulated by poly (I:C) (37). The heat shock proteins (HSPs) encoded by the *HSP90a1* is the core component of HSP90-SGT1-RAR1, which has been proven to be an essential signaling component of immune response (38). Accumulating evidence suggests that *lgp2* is a member of the pathogen recognition receptor family and plays a key role in recognizing the innate immune response induced by viral infection (39). Therefore, we boldly speculated that the upregulation of *HSP90a1* and *lgp2* ensures enhanced liver response to poly (I:C) to ensure a rapid response of liver to the invading virus. Additionally, we also found that the expression of *met* in the liver was downregulated, and *met* has been confirmed to be involved in hepatocyte growth factor receptor, which may imply that poly (I:C) stimulation may lead to liver injury in *L. lota* (40). The inhibition of *met* is essential to avoid excessive cell proliferation and maintain normal biological processes in the liver (41). Three functional genes (namely, *csf1r*, *ccnd2*, and *flt3*) in the spleen were downregulated at 12 h and 48 h after poly (I:C) stimulation. *csf1r* may contribute to the inhibition of macrophages, which has a positive effect on the activation of immune responses in damaged tissues (42). It is not clear why *csf1r* decreases its expression, and this could link inhibition of the macrophage-mediated response to a positive effect on the activation of the immune response in damaged tissues. The *ccnd2* gene can inhibit the growth of DNA-damaged cells by regulating the expression of various transcription factors (43). A previous study has confirmed that loss- of-function mutations in the *flt3* promote the development of blood cells, which are particularly important for immune responses, through a compensatory increase in ligand levels (44). Additionally, we also found that *pmp22* was downregulated at 12 h after poly (I:C) stimulation, but upregulated at 48 h after poly (I:C) stimulation. It is worth noting that *pmp22* is a negative regulator that can precisely regulate the cell cycle, and high expression of *pmp22* can often arrest cells in the G_0/G_1 phase (45). In conclusion, the expression levels of some functional genes in liver and spleen of *L. lota* were changed, thus guaranteeing the normal metabolism, tissue structure, and life state of poly (I:C)-stimulated *L. lota*. We do not deny that there are more critical functional genes that have not attracted our attention or carried out qRT-PCR detection, which is also needed for future research.

4.2.2 Physiological regulation mechanisms

The physiological regulation mechanisms of poly (I:C)-stimulated *L. lota* showed tissue and time specificity (46). The DEGs of *L. lota* exposed to poly (I:C) stimulation were discovered to have protein-regulated functions. Undoubtedly, *L. lota* stimulated by poly (I:C) is energy-consuming (47); thus, changes in protein regulation may have provided energy for cell survival and other life activities (48). A previous study has also confirmed that fishes have a much higher protein requirement than other vertebrates because they are less adept at using lipid and carbohydrate for energy, which may be more pronounced in diseased conditions (48). We also found that some DEGs were involved in the regulation of threonine, which may contribute to the improvement of amino acid utilization (49) and further improve the energy production of *L. lota* stimulated by poly (I:C). Some DEGs have been hypothesized to be associated with cellular homeostasis and immune cell integrity. This may imply that *L. lota* can reduce the toxic effects of poly (I:C) by maintaining the cytoskeletal integrity of liver and spleen (50). We also found that some DEGs were involved in the ion transport and cell death. In fact, toxic substances may require specific carriers (such as organic anions) to enter cells and cause cell death (51), and thus *L. lota* may inhibit the entry of poly (I:C) into cells by these ion transport-related genes.

The upregulated genes in both the liver and spleen were significantly enriched in three poly (I:C) detection and antiviral innate immunity-related pathways, namely, Herpes simplex infection pathway (52), Proteasome pathway (53), and RIG-I-like receptor signaling pathway (54). Except for three shared pathways, upregulated genes were also significantly enriched in the Apoptosis pathway, Toll-like receptor (TLR) signaling pathway, NOD-like receptor (NLR) signaling pathway, p53 signaling pathway, JAK-STAT signaling pathway, and Drug metabolism - other enzymes pathway. Apoptosis is an autonomous and orderly cell suicide process controlled by genes, which is necessary for the regulation of immune function and maintenance of tissue stability (55, 56). The disorder of apoptosis will lead to a series of pathological changes (55, 56). We hypothesized that the *L. lota* stimulated by poly (I:C) activated the apoptosis pathway, and the damaged cells thus entered apoptosis and were eliminated. Pattern recognition receptor (PRR)-related pathways (including the TLR and NLR signaling pathway) have also been annotated. PRRs are the bridge between innate and acquired immunity, and their activators can be used as immunoadjuvants (57–59). Poly (I:C) has been shown to activate the PRR signaling pathway after binding to PRRs and then exerting innate immunity (60). In fact, the activation of the PRR signaling pathways may also contribute to apoptosis of *L. lota*-damaged liver or spleen cells (61). The significant enrichment of upregulated genes in the p53 signaling pathway may also be applied to enable poly (I:C)-damaged cells to perform DNA repair or accelerate apoptosis (62). It is well established that organisms invaded by viruses can regulate cell cycle arrest, DNA repair, and apoptosis by regulating *p53* gene and p53 protein (63, 64). Additionally, the JAK-STAT signaling pathway as an important cytokine-stimulated signal transduction pathway was also activated by poly (I:C) stimulation (65). The JAK-STAT signaling pathway has been confirmed to be involved in the immune regulation, cell proliferation, differentiation, and apoptosis of other teleost fishes [i.e., *Carassius auratus gibelio* (66), *Tachysurus fulvidraco* (67), and *Sebastiscus marmoratus* (68)] stimulated by poly (I:C). Considering that the virus mainly hides in cells and replicates and spreads through cellular metabolism (67), we hypothesized that *L. lota* may initiate the cellular apoptotic process to limit the contagion of poly (I:C) in the liver or spleen (68). Some upregulated genes also significantly enriched the Drug metabolism - other enzymes pathway. It was not difficult to find that poly (I:C) stimulation changed the enzyme catalytic capacity of liver or spleen in

L. lota. Enzymes have been confirmed to be involved in a variety of biological processes in diseased fish, including cell proliferation and death, cell migration, cytoskeleton dynamics, cell cycle regulation, and regulation of numerous signaling pathways (69, 70). Meanwhile, some enzymes, such as proteasome and lysozyme, are immune molecules secreted by immune cells, which can improve and enhance macrophage phagocytosis ability and thus play a critical role in the defense against pathogens in fishes (53, 71–73).

The downregulated genes in both liver and spleen were significantly enriched in the Focal adhesion pathway, ECM–receptor interaction pathway, Vascular smooth muscle contraction pathway, and Regulation of actin cytoskeleton pathway. Focal adhesion kinase (FAK) is a critical enzyme in the Focal adhesion pathway, which can integrate viral signals from outside the cell and regulate the activity of downstream molecules, thereby controlling cell metabolism, proliferation, and even cell fate (74). FAK has also been shown to degrade p53 protein through the ubiquitination pathway and prevent cellular apoptosis (74). Therefore, there is reason to believe that activation of the Focal adhesion pathway may hinder the clearance of *L. lota*-damaged cells. The ECM–receptor interaction pathway, Vascular smooth muscle contraction pathway, and Regulation of actin cytoskeleton pathway were confirmed to be involved in cell migration, which is required for immune surveillance, and tissue repair and regeneration (75, 76). The virus-invaded cell migration drives progression of fish diseases, and thus, we hypothesized that the downregulation of genes related to the three pathways mentioned above may contribute to the reduction of the poly (I:C) invasion of *L. lota* liver or spleen cells. Additionally, the downregulated genes in the liver were also significantly enriched in some specific pathways, including the Phosphatidylinositol (PI) signaling system pathway, Inositol phosphate (IP) metabolism pathway, Notch signaling pathway, Lysine degradation pathway, Cytokine–cytokine receptor interaction pathway, ABC transporters pathway, Glycerolipid metabolism pathway, and Insulin signaling pathway. Previous studies have demonstrated that the PI signaling system pathway and IP metabolism pathway can reduce the proliferation ability and induce apoptosis of DNA-damaged cells by reducing the concentration and activity of IP of PI kinases (77). This is mainly because PI and IP kinases can cause the release of intracellular calcium, which is the regulator of intracellular messenger and cellular activity and is critical for cell survival (78, 79). The Notch signaling pathway can inhibit the inflammatory response of macrophages induced by TLRs (80, 81), and lead to the impairment of M1 type activation of macrophages (82). Therefore, inhibition of the Notch signaling pathway is valuable for the activation of macrophages in *L. lota* liver. Lysine is a non-specific bridging molecule that connects antigens to T cells (83). The lack of lysine reduces cytokine synthesis, thereby inhibiting lymphocyte proliferation and reducing cell-mediated immune response (84). In this study, the downregulation of the Lysine degradation pathway and Cytokine–cytokine receptor interaction pathway may safeguard lysine and cytokine content and ultimately enhance the liver cell-mediated immune response of *L. lota*. ABC transporters perform various physiological functions such as resistance to foreign invasion, antigen presentation, and lipid transport (85). We also found that the downregulated genes in the liver were significantly enriched in the ABC transporter pathway, but the immune response of this pathway is still worth further investigation in future studies. Additionally, the downregulated genes in poly (I:C)-stimulated *L. lota* liver were also significantly enriched in the lipid and glucose metabolism-related pathways (Glycerolipid metabolism pathway and Insulin signaling pathway). Liver is not only an important immune organ, but also a very important metabolic organ, which is very important for the balance of glucose and lipid metabolism and the maintenance of energy homeostasis (86). Meanwhile, it should be noted that the inhibited Insulin signaling pathway can stimulate gluconeogenesis and fatty acid oxidation, which are critical for the release of large amounts of energy, and help to fuel the immune response of *L. lota* liver cells.

In conclusion, functional genes and their products of the liver and spleen exerted their effects to regulate the physiological functions of *L. lota* stimulated by poly (I:C), and finally ensured their survival. According to the inferred potential function of poly (I:C)-stimulated DEGs, we have proposed management measures for *L. lota* attacked by viruses, as follows: the regulation of the breeding environment is the first development, which not only is conducive to eliminating or alleviating the stress response of virus-infected *L. lota*, but also can increase the efficacy of drugs; protein (especially lysine) supplementation in the diet is also necessary because *L. lota* consume energy to deal with the virus; and lysine supplementation will aid in cytokine synthesis and proliferation of lymphocytes required for the immune response.

5 Conclusion

Poly (I:C) as an immune adjuvant can be used to explore the viral immune responses of *L. lota*. In this study, RNA-seq was used for the first time to determine the transcriptome of liver and spleen of *L. lota* stimulated by poly (I:C) to explore the genetic regulatory mechanisms of *L. lota* to immune adjuvant. We found that the liver and spleen of *L. lota* showed different responses to poly (I:C) stimulation, which was manifested at the levels of DEGs and related biological functions. Meanwhile, we suspected that the stress of liver and spleen of *L. lota* is serious with the extension of poly (I:C) stimulation time (12 h to 48 h). Based on the annotation information of DEGs, we hypothesized that *L. lota* could initiate apoptosis of DNA-damaged cells to inhibit poly (I:C) propagation in the liver and spleen. Meanwhile, some enzymes that enhance immune effects and metabolic mechanisms that provide energy have also been found to be necessary for *L. lota* to cope with the poly (I:C) challenge. This study provides basic resources for exploring the regulatory mechanisms of *L. lota* to poly (I:C) and other immune adjuvants. Furthermore, we expect that the present study can provide valuable information for future disease prevention in *L. lota* artificial culture.

Data availability statement

The datasets presented in this study can be found in online repositories. The names of the repository/repositories and accession number(s) can be found in the article/Supplementary Material.

Ethics statement

The animal studies were approved by the Institutional Animal Care and Use Committee of Yantai University. The studies were conducted in accordance with the local legislation and institutional requirements. Written informed consent was obtained from the owners for the participation of their animals in this study.

Author contributions

FL: Data curation, Formal Analysis, Methodology, Software, Writing – original draft. YZ: Investigation, Methodology, Writing – original draft. AX: Data curation, Investigation, Writing – original draft. TG: Conceptualization, Funding acquisition, Resources, Supervision, Visualization, Writing – review & editing.

Funding

The author(s) declare financial support was received for the research, authorship, and/or publication of this article. This research was supported by the Province Key Research and Development Program of Zhejiang (2021C02047).

Acknowledgments

We sincerely thank Dr. Tianyan Yang for assistance in collecting samples and Dr. Yinquan Qu for reviewing our manuscript.

Conflict of interest

The authors declare that the research was conducted in the absence of any commercial or financial relationships that could be construed as a potential conflict of interest.

Publisher's note

Supplementary material

The Supplementary Material for this article can be found online at: https://www.frontiersin.org/articles/10.3389/fimmu.2023.1272393/full#supplementary-material

SUPPLEMENTARY FILE 3
Distribution of RNA-seq reads of each sample in different regions of the reference genome.

SUPPLEMENTARY FILE 4
Density distribution of RNA-seq reads of each sample on chromosome.

SUPPLEMENTARY FILE 5
The DEGs among four experimental pairs (L_{12po}-vs-L_{12PBS}, L_{48po}-vs-L_{48PBS}, S_{12po}-vs-S_{12PBS}, and S_{48po}-vs-S_{48PBS}).

SUPPLEMENTARY FILE 6
The common DEGs among four experimental pairs.

SUPPLEMENTARY FILE 7
The significantly enriched GO terms of the up- and downregulated genes in the liver and spleen.

SUPPLEMENTARY FILE 8
The significantly enriched KEGG pathways of the up- and downregulated genes in the liver and spleen.

References

1. Hanwell D, Hutchinson SA, Collymore C, Ashley EB, Rhain L, Ayoob G, et al. Restrictions on the importation of zebrafish into Canada associated with spring viremia of carp virus. *Zebrafish* (2016) 13:S153–63. doi: 10.1089/zeb.2016.1286

2. Zhang QY, Gui JF. Diversity, evolutionary contribution and ecological roles of aquatic viruses. *Sci China Life Sci* (2018) 61:1486–502. doi: 10.1007/s11427-018-9414-7

3. Kibenge FS. Emerging viruses in aquaculture. *Curr Opin Virol* (2019) 34:97–103. doi: 10.1016/j.coviro.2018.12.008

4. Zhu F. A review on the application of herbal medicines in the disease control of aquatic animals. *Aquaculture* (2020) 526:735422. doi: 10.1016/j.aquaculture.2020.735422

5. Dalmo RA, Ingebrigtsen K, Bøgwald J. Non-specific defence mechanisms in fish, with particular reference to the reticuloendothelial system (RES). *J Fish Dis* (1997) 20:241–73. doi: 10.1046/j.1365-2761.1997.00302.x

6. Seki E, Brenner DA. Toll-like receptors and adaptor molecules in liver disease: update. *Hepatology* (2008) 48:322–35. doi: 10.1002/hep.22306

7. Zapata A, Cooper E. *The immune system: comparative histophysiology*. Chichester: John Wiley and Sons (1990) p. 54–6.

8. Crispe IN. The liver as a lymphoid organ. *Annu Rev Immunol* (2009) 27:147–63. doi: 10.1146/annurev.immunol.021908.132629

9. Racanelli V, Rehermann B. The liver as an immunological organ. *Z Für Gastroenterol* (2011) 49:54–62. doi: 10.1055/s-0029-1245947

10. Qin XB, Gao B. The complement system in liver diseases. *Cell Mol Immunol* (2006) 3:333–40. doi: 10.1016/j.cellimm.2006.05.009

11. Gonzalez SF, Buchmann K, Nielsen ME. Complement expression in common carp (*Cyprinus carpio* L.) during infection with *Ichthyophthirius multifiliis*. *Dev Comp Immunol* (2007) 31:576–86. doi: 10.1016/j.dci.2006.08.010

12. Tafalla C, Bøgwald J, Dalmo RA. Adjuvants and immunostimulants in fish vaccines: current knowledge and future perspectives. *Fish Shellfish Immunol* (2013) 35:1740–50. doi: 10.1016/j.fsi.2013.02.029

13. Ellis AE, Munro AL, Roberts RJ. Defense mechanism in fish. Study of the plice (*Pleuronectes platesa*). *J Fish Biol* (1976) 8:67–78. doi: 10.1111/j.1095-8649.1976.tb03908.x

14. Nikcevic M, Hegedis A, Mickovic B. The burbot (*Lota* L.) in Yugoslavia, habitats and thermal acclimation capacity. *Ichthyologia* (1995) 27:5–11.

15. Qian L, Fan ZM, Hu BL, Wang YX, Ai T. Study on hatching conditions of *Lota*. *Freshw Fish* (2006) 36:57–8.

16. Lou FR, Liu MH, Han ZQ, Gao TX. Comparative transcriptome reveals the thermal stress response differences between Heilongjiang population and Xinjiang population of *Lota*. *Comp Biochem Physiol Part D: Genomics Proteomics* (2022) 42:100960. doi: 10.1016/j.cbd.2022.100960

17. Zhang YQ, Yin JS, Zhang C, Jia ZH, Fan P. Embryonic development of burbot (*Lota lota*) in Heilongjiang River. *Chin J Fish* (2013) 26:24–8. doi: 10.1086/671331

18. Guo S. Epidemic characteristics and classification and prevention case studies of parasitic on *Lota* in Irtysh River. [dissertation/master's thesis]. Urumqi (XJ): Xinjiang Agricultural University (2016). pp12.

19. Wolf JBW. Principles of transcriptome analysis and gene expression quantification: an RNA-seq tutorial. *Mol Ecol Resour* (2013) 13:559–72. doi: 10.1111/1755-0998.12109

20. Qian T, Wang K, Mu Y, Ao J, Chen X. Molecular characterization and expression analysis of TLR 7 and TLR 8 homologs in large yellow croaker (*Pseudosciaena crocea*). *Fish Shellfish Immun* (2013) 35:6713–9. doi: 10.1016/j.fsi.2013.05.019

21. Ye H, Lin QS, Luo H. Applications of transcriptomics and proteomics in understanding fish immunity. *Fish Shellfish Immunol* (2018) 77:319–27. doi: 10.1016/j.fsi.2018.03.046

22. Zhang Y, Wang XY, Shi HL, Song N, Han F, Chai XJ, et al. Comparative transcriptomic analysis of the liver and spleen in marbled rockfish (*Sebastiscus marmoratus*) challenged with polyriboinosinic polyribocytidylic acid (poly(I:C)). *Aquaculture* (2022) 554:738144. doi: 10.1016/j.aquaculture.2022.738144

23. Yang TY, Zhang Y, Meng W, Zhong X, Shan Y, Gao TX. Comparative transcriptomic analysis brings new insights into the response to acute temperature acclimation in burbot (*Lota lota*). *Aquacult Rep* (2021) 20:100657. doi: 10.1016/j.aqrep.2021.100657

24. Zhou ZX, Zhang BC, Sun L. Poly(I:C) induces antiviral immune responses in Japanese flounder (*Paralichthys olivaceus*) that require TLR3 and MDA5 and is negatively regulated by Myd88. *PloS One* (2014) 9:e112918. doi: 10.1371/journal.pone.0112918

25. Lafont M, Vergnes A, Vidal-Dupiol J, de Lorgeril J, Gueguen Y, Haffner P, et al. A sustained immune response supports long-term antiviral immune priming in the Pacific oyster, *Crassostrea gigas*. *mBio* (2020) 11:e02777–19. doi: 10.1128/mBio.02777-19

26. Liu QN, Tang YY, Zhou MJ, Luo S, Li YT, Wang G, et al. Differentially expressed genes involved in immune pathways from yellowhead catfish (*Tachysurus fulvidraco*) after poly (I:C) challenge. *Int J Biol Macromol* (2021) 183:340–5. doi: 10.1016/j.ijbiomac.2021.04.167

27. Bolger AM, Lohse M, Usadel B. Trimmomatic: a flexible trimmer for Illumina sequence data. *Bioinformatics* (2014) 30:2114–20. doi: 10.1093/bioinformatics/btu170

28. Kim D, Langmead B, Salzberg SL. HISAT: a fast spliced aligner with low memory requirements. *Nat Methods* (2015) 12:357–60. doi: 10.1038/nmeth.3317

29. Han ZQ, Liu MH, Liu Q, Zhai H, Xiao SJ, Gao TX. Chromosome-level genome assembly of burbot (*Lota lota*) provides insights into the evolutionary adaptations in freshwater. *Mol Ecol Resour* (2021) 21:2022–33. doi: 10.1111/1755-0998.13382

30. Shen S, Park JW, Lu ZX, Lin L, Henry MD, Wu YN, et al. rMATS: Robust and flexible detection of differential alternative splicing from replicate RNA-Seq data. *Proc Natl Acad Sci United States America* (2014) 111:E5593–5601. doi: 10.1073/pnas.1419161111

31. Putri GH, Anders S, Pyl PT, Pimanda JE, Zanini F. Analysing high-throughput sequencing data in Python with HTSeq 2.0. *Bioinformatics* (2022) 38:2943–5. doi: 10.1093/bioinformatics/btac166

32. Love MI, Huber W, Anders S. Moderated estimation of fold change and dispersion for RNA-seq data with DESeq2. *Genome Biol* (2014) 15:550. doi: 10.1186/s13059-014-0550-8

33. Magnadottir B. Immunological control of fish diseases. *Mar Biotechnol* (2010) 12:361–79. doi: 10.1007/s10126-010-9279-x

34. Plant KP, LaPatra SE. Advances in fish vaccine delivery. *Dev Comp Immunol* (2011) 35:1256–62. doi: 10.1016/j.dci.2011.03.007

35. Shivam S, El-Matbouli M, Kumar G. Development of fish parasite vaccines in the OMICs era: progress and opportunities. *Vaccines* (2021) 9:179. doi: 10.3390/vaccines9020179

36. Wegienka G, Havstad S, Zoratti EM, Kim H, Johnson CC. Association between Vitamin D levels and allergy-related outcomes vary by race and other factors. *J Allergy Clin Immunol* (2015) 136:1309–14. doi: 10.1016/j.jaci.2015.04.017

37. Martínez-Reza I, Díaz L, García-Becerra R. Preclinical and clinical aspects of TNF-α and its receptors TNFR1 and TNFR2 in breast cancer. *J Biomed Sci* (2017) 24:90. doi: 10.1186/s12929-017-0398-9

38. Seo YS, Lee SK, Song MY, Suh JP, Hahn TR, Ronald P, et al. The HSP90-SGT1-RAR1 molecular chaperone complex: A core modulator in plant immunity. *J Plant Biol* (2008) 51:1–10. doi: 10.1007/BF03030734

39. Hei L, Zhong J. Laboratory of genetics and physiology 2 (LGP2) plays an essential role in hepatitis C virus infection-induced interferon responses. *Hepatology* (2017) 65:1478–91. doi: 10.1002/hep.29050

40. Tavian D, De Petro G, Benetti A, Portolani N, Giulini SM, Barlati S. u-PA and c-met mRNA expression is co-ordinately enhanced while hepatocyte growth factor mRNA is down-regulated in human hepatocellular carcinoma. *Int J Cancer* (2000) 87:644–9. doi: 10.1002/1097-0215(20000901)87:5<644::AID-IJC4>3.0.CO;2-W

41. Goździk-Spychalska J, Szyszka-Barth K, Spychalski L, Ramlau K, Wójtowicz J, Batura-Gabryel H, et al. c-MET inhibitors in the treatment of lung cancer. *Curr Treat Options Oncol* (2014) 15:670–82. doi: 10.1007/s11864-014-0313-5

42. Hume DA, MacDonald KPA. Therapeutic applications of macrophage colony-stimulating factor-1 (CSF-1) and antagonists of CSF-1 receptor (CSF-1R) signaling. *Blood* (2012) 119:1810–20. doi: 10.1182/blood-2011-09-379214

43. Zhao WW, Zhu JY, Han YY. Molecular evolution analysis of CCND gene family. *J Med Mol Biol* (2014) 11:144–9.

44. Saevarsdottir S, Olafsdottir TA, Ivarsdottir EV, Halldorsson GH, Gunnarsdottir K, Sigurdsson A, et al. *FLT3* stop mutation increases FLT3 ligand level and risk of autoimmune thyroid disease. *Nature* (2020) 584:619–23. doi: 10.1038/s41586-020-2436-0

45. Roux KJ, Amici SA, Fletcher BS, Notterpek L. Modulation of epithelial morphology, monolayer permeability, and cell migration by growth arrest specific 3/peripheral myelin protein 22. *Mol Biol Cell* (2005) 16:1142–51. doi: 10.1091/mbc.e04-07-0551

46. Liu HJ, Meng FX, Li M, Wang RX, Shi G. Immune response of the *MHC 1α* gene of *Boleophthalmus pectinirostris* to the viral mimetic poly(I:C) under high salinity stress. *J Fish Sci China* (2019) 26:729–37.

47. Chen XM, Guo GL, Sun L, Yang QS, Wang GQ, Zhang DM. Modulatory role of L-carnitine against microcystin-LR-induced immunotoxicity and oxidative stress in common carp. *Fish Physiol Biochem* (2017) 43:1081–93. doi: 10.1007/s10695-017-0354-3

48. Thompson KR, Muzinic LA, Engler LS, Webster CD. Evaluation of practical diets containing different protein levels, with or without fish meal, for juvenile Australian red claw crayfish (*Cherax quadricarinatus*). *Aquaculture* (2005) 244:241–9. doi: 10.1016/j.aquaculture.2004.11.018

49. Dong YW, Jiang WD, Liu Y, Wu P, Jiang J, Kuang SY, et al. Threonine deficiency decreased intestinal immunity and aggravated inflammation associated with NF-κB and target of rapamycin signalling pathways in juvenile grass carp (*Ctenopharyngodon idella*) after infection with *Aeromonas hydrophila*. *Br J Nutr* (2017) 118:92–108. doi: 10.1017/S0007114517001830

50. Li G, Yan W, Qiao Q, Chen J, Cai F, He Y, et al. Global effects of subchronic treatment of microcystin-LR on rat splenetic protein levels. *J Proteomics* (2012) 77:383–93. doi: 10.1016/j.jprot.2012.09.012

51. Fischer WJ, Hitzfeld BC, Tencalla F, Eriksson JE, Mikhailov A, Dietrich DR. Microcystin-LR toxicodynamics, induced pathology, and immunohistochemical localization in livers of blue-green algae exposed rainbow trout (*Oncorhynchus mykiss*). *Toxicol Sci* (2000) 54:365–73. doi: 10.1093/toxsci/54.2.365

52. Cheshenko N, Del Rosario B, Woda C, Marcellino D, Satlin LM, Herold BC. Herpes simplex virus triggers activation of calcium-signaling pathways. *J Cell Biol* (2003) 163:283–93. doi: 10.1083/jcb.200301084

53. Rombout JH, Taverne N, van de Kamp M, Taverne-Thiele AJ. Differences in mucus and serum immunoglobulin of carp (*Cyprinus carpio* L.). *Dev Comp Immunol* (1993) 17:309–17. doi: 10.1016/0145-305X(93)90003-9

54. Kasthuri SR, Wan Q, Whang I, Lim BS, Yeo SY, Choi CY, et al. Functional characterization of the evolutionarily preserved mitochondrial antiviral signaling protein (MAVS) from rock bream, *Oplegnathus fasciatus*. *Fish Shellfish Immunol* (2014) 40:399–406. doi: 10.1016/j.fsi.2014.07.034

55. Evan GI, Vousden KH. Proliferation, cell cycle and apoptosis in cancer. *Nature* (2001) 411:342–8. doi: 10.1038/35077213

56. Guimarães AC, Linden R. Programmed cell deaths, apoptosis and alternative death styles. *Eur J Biochem* (2004) 271:1638–50. doi: 10.1111/j.1432-1033.2004.04084.x

57. Yu L, Chen S. Toll-like receptors expressed in tumor cells: targets for therapy. *Cancer Immunol Immunother* (2008) 57:1271–8. doi: 10.1007/s00262-008-0459-8

58. Fitzgerald KA. The interferon inducible gene: Viperin. *J Interferon Cytokine Res* (2011) 31:131–5. doi: 10.1089/jir.2010.0127

59. Nasirudeen AMA, Wong HH, Thien P, Xu S, Lam KP, Xiang D. RIG-I, MDA5 and TLR3 synergistically play an important role in restriction of dengue virus infection. *PloS Negl Trop Dis* (2011) 5:e926. doi: 10.1371/journal.pntd.0000926

60. Alexopoulou L, Holt AC, Medzhitov R, Flavell RA. Recognition of double-stranded RNA and activation of NF-kappa B by Toll-like receptor 3. *Nature* (2001) 413:732–8. doi: 10.1038/35099560

61. Salaun B, Coste I, Rissoan MC, Lebecque SJ, Renno T. TLR3 can directly trigger apoptosis in human cancer cells. *J Immunol* (2006) 176:4894–901. doi: 10.4049/jimmunol.176.8.4894

62. Cai BL, Ma MT, Chen B, Li ZH, Abdalla BA, Nie QH, et al. MiR-16-5p targets *SESN1* to regulate the *p53* signaling pathway, affecting myoblast proliferation and apoptosis, and is involved in myoblast differentiation. *Cell Death Dis* (2018) 9:367. doi: 10.1038/s41419-018-0403-6

63. May P, May E. Twenty years of p53 research: structural and functional aspects of the p53 protein. *Oncogene* (1999) 18:7621–36. doi: 10.1038/sj.onc.1203285

64. Prives C, Hall PA. The p53 pathway. *J Pathol* (1999) 187:112–26. doi: 10.1002/(SICI)1096-9896(199901)187:1<112::AID-PATH250>3.0.CO;2-3

65. Xin P, Xu XY, Deng CJ, Liu S, Wang YZ, Zhou XG, et al. The role of JAK/STAT signaling pathway and its inhibitors in diseases. *Int Immunopharmacol* (2020) 80:106210. doi: 10.1016/j.intimp.2020.106210

66. Zhang JL, Cui ZY, Hu GY, Jiang XY, Wang J, Qiao G, et al. Transcriptome analysis provides insights into the antiviral response in the spleen of gibel carp (*Carassius auratus gibelio*) after poly I: C treatment. *Fish Shellfish Immunol* (2020) 102:13–9. doi: 10.1016/j.fsi.2020.03.065

67. Tengs T, Rimstad E. Emerging pathogens in the fish farming industry and sequencing-based pathogen discovery. *Dev Comp Immunol* (2017) 75:109–19. doi: 10.1016/j.dci.2017.01.025

68. Kik M, Martel A, Spitzen-van der Sluijs A, Pasmans F, Wohlsein P, Gröne A, et al. Ranavirus-associated mass mortality in wild amphibians, the Netherlands 2010: a first report. *Vet J* (2011) 190:284–6. doi: 10.1016/j.tvjl.2011.08.031

69. Janssens V, Goris J. Protein phosphatase 2A: a highly regulated family of serine/threonine phosphatases implicated in cell growth and signalling. *Biochem J* (2001) 353:417–39. doi: 10.1042/bj3530417

70. Lechward K, Awotunde OS, Swiatek W, Muszyńska G. Protein phosphatase 2A: variety of forms and diversity of functions. *Acta Biochim Polonica* (2001) 48:921–33. doi: 10.18388/abp.2001_3858

71. Alexander JB, Ingram GA. Noncellular nonspecific defence mechanisms of fish. *Annu Rev Fish Dis* (1992) 2:249–79. doi: 10.1016/0959-8030(92)90066-7

72. Liu L, Zhu B, Wu S, Lin L, Zhou Y, Wang W, et al. Spring viraemia of carp virus induces autophagy for necessary viral replication. *Cell Microbiol* (2015) 17:595–605. doi: 10.1111/cmi.12387

73. Espín-Palazón R, Martínez-López A, Roca FJ, López-Muñoz A, Tyrkalska SD, Candel S, et al. TNFα impairs rhabdoviral clearance by inhibiting the host autophagic antiviral response. *PloS Pathogens* (2016) 12:e1005699. doi: 10.1371/journal.ppat.1005699

74. Li SY, Wang ZG. Progress in focal adhesion kinase signaling pathway. *Biotechnol Bull* (2009) 12:6–10.

75. Yamaguchi H, Condeelis J. Regulation of the actin cytoskeleton in cancer cell migration and invasion. *Biochim Biophys Acta* (2007) 1773:642–52. doi: 10.1016/j.bbamcr.2006.07.001

76. Tang X, Hou Y, Yang G, Wang X, Tang S, Du YE, et al. Stromal miR-200s contribute to breast cancer cell invasion through CAF activation and ECM remodeling. *Cell Death Differ* (2016) 23:132–45. doi: 10.1038/cdd.2015.78

77. Herbst RS, Bunn PA. Targeting the epidermal growth factor receptor in non-small cell lung cancer. *Clin Cancer Res* (2003) 9:5813–24. doi: 10.1159/000322214

78. Fischer OM, Hart S, Gschwind A, Ullrich A. EGFR signal transactivation in cancer cells. *Biochem Soc Trans* (2003) 31:1203–8. doi: 10.1042/bst0311203

79. Ma XD, Ma X, Sui YF, Wang WL, Wang CM. Signal transduction of gap junctional genes, connexin32, connexin43 in human hepatocarcinogenesis. *World J Gastroenterol* (2003) 9:946–50. doi: 10.3748/wjg.v9.i5.946

80. Zhang QH, Wang CM, Liu ZL, Liu XG, Han CF, Cao XT, et al. Notch signal suppresses Toll-like receptor-triggered inflammatory responses in macrophages by inhibiting extracellular signal-regulated kinase 1/2-mediated nuclear factor κB activation. *J Biol Chem* (2012) 287:6208–17. doi: 10.1074/jbc.M111.310375

81. Qin G, Zhang Y, Zhang B, Wang X, Yin JP, Lin Q. Seahorse TLR5 gene responses to Vibrio vulnificus infection, which in combination with scuticociliates causes heavy reductions in seahorse aquaculture. *J Fish Dis* (2018) 41:1933–6. doi: 10.1111/jfd.12893

82. Wang YC, He F, Feng F, Liu XW, Han H. Notch signaling determines the M1 versus M2 polarization of macrophages in antitumor immune responses. *Cancer Res* (2010) 70:4840–9. doi: 10.1158/0008-5472.CAN-10-0269

83. Li P, Yin YL, Li DF, Kim SW, Wu GY. Amino acids and immune function. *Br J Nutr* (2007) 98:237–52. doi: 10.1017/S000711450769936X

84. Chen C, Sander JE, Dale NM. The effect of dietary lysine deficiency on the immune response to Newcastle disease vaccination in chickens. *Avian Dis* (2003) 47:1346–51. doi: 10.1637/7008

85. Hou WT, Wang L, Xu D, Chen YX, Zhou CZ. ABC transporters and human diseases. *J Univ Sci Technol China* (2018) 48:853–61.

86. Liu W, Cao HC, Ye C, Chang CJ, Lu MH, Jing YY, et al. Hepatic miR-378 targets p110α and controls glucose and lipid homeostasis by modulating hepatic insulin signaling. *Nat Commun* (2014) 5:5684. doi: 10.1038/ncomms6684

frontiers | Frontiers in Immunology

TYPE Original Research
PUBLISHED 29 January 2024
DOI 10.3389/fimmu.2024.1346512

OPEN ACCESS

EDITED BY
Elena Chaves-Pozo,
Spanish Institute of Oceanography, Spain

REVIEWED BY
Myung-Hwa Jung,
Hanseo University, Republic of Korea
Mehdi Soltani,
Murdoch University, Australia
Carlos Angulo,
Centro de Investigación Biológica del Noroeste (CIBNOR), Mexico

*CORRESPONDENCE
Dušan Palić
d.palic@lmu.de
Sohrab Ahmadivand
Sohrab.ahmadivand@lmu.de

RECEIVED 29 November 2023
ACCEPTED 09 January 2024
PUBLISHED 29 January 2024

CITATION
Ahmadivand S, Krpetic Z, Martínez MM, Garcia-Ordoñez M, Roher N and Palić D (2024) Self-assembling ferritin nanoplatform for the development of infectious hematopoietic necrosis virus vaccine. *Front. Immunol.* 15:1346512. doi: 10.3389/fimmu.2024.1346512

Self-assembling ferritin nanoplatform for the development of infectious hematopoietic necrosis virus vaccine

Sohrab Ahmadivand[1*], Zeljka Krpetic[2], Merce Márquez Martínez[3,4], Marlid Garcia-Ordoñez[3], Nerea Roher[3,4] and Dušan Palić[1*]

[1]Faculty of Veterinary Medicine, Ludwig-Maximilians University Munich, Munich, Germany, [2]Biomedical Research Centre, School of Science Engineering and Environment, University of Salford, Salford, United Kingdom, [3]Institute of Biotechnology and Biomedicine (IBB), Universitat Autònoma de Barcelona, Barcelona, Spain, [4]CIBER de Bioingeniería Biomateriales y Nanomedicina (CIBER-BBN), Barcelona, Spain

Self-assembling protein nanoparticles are used as a novel vaccine design platform to improve the stability and immunogenicity of safe subunit vaccines, while providing broader protection against viral infections. Infectious Hematopoietic Necrosis virus (IHNV) is the causative agent of the WOAH-listed IHN diseases for which there are currently no therapeutic treatments and no globally available commercial vaccine. In this study, by genetically fusing the virus glycoprotein to the H. pylori ferritin as a scaffold, we constructed a self-assembling IHNV nanovaccine (FerritVac). Despite the introduction of an exogenous fragment, the FerritVac NPs show excellent stability same as Ferritin NPs under different storage, pH, and temperature conditions, mimicking the harsh gastrointestinal condition of the virus main host (trout). MTT viability assays showed no cytotoxicity of FerritVac or Ferritin NPs in zebrafish cell culture (ZFL cells) incubated with different doses of up to 100 µg/mL for 14 hours. FerritVac NPs also upregulated expression of innate antiviral immunity, IHNV, and other fish rhabdovirus infection gene markers (mx, vig1, ifit5, and isg-15) in the macrophage cells of the host. In this study, we demonstrate the development of a soluble recombinant glycoprotein of IHNV in the E. coli system using the ferritin self-assembling nanoplatform, as a biocompatible, stable, and effective foundation to rescue and produce soluble protein and enable oral administration and antiviral induction for development of a complete IHNV vaccine. This self-assembling protein nanocages as novel vaccine approach offers significant commercial potential for non-mammalian and enveloped viruses.

KEYWORDS

ferritin nanoparticles, IHNV, self-assembling vaccine, fish viruses, ZFL cells, macrophages, protein stability

1 Introduction

Vaccination strategies to prevent and control viral pathogens and disease outbreaks in aquaculture need to be optimized for efficacy and stress-free administration, with consideration of production and delivery costs, environmental risks, and regulatory compliance (1, 2). The traditional vaccine production and application approach is based on the use of inactivated or attenuated viral vaccines, which are commercially available for some viral diseases (3). Even with the relatively low risk of possible reversion to virulence and spreading of vaccine strain in the environment, such vaccines still offer benefits including induction of a strong immune response when administered via stressful intraperitoneal injection and combined with oil adjuvants (1–3). DNA-based vaccines have recently shown promising results against certain viruses, but they raise safety issues regarding genetically modified organisms (GMO) and, despite the efficacy of some oral formulations, are administered by labor-intensive intramuscular (i.m) injection (4–6). Novartis' APEX-IHN® DNA vaccine is an example, approved for i.m use in Atlantic salmon in Canada, but not elsewhere due to GMO safety concerns (4).

Another vaccine approach is the development of subunit vaccines, including the production of viral antigen proteins in a heterologous expression system. Although safer and more cost-effective to produce, their efficacy is variable and the development of oral subunit vaccines remains challenging due to gastrointestinal barriers (7). Most subunit vaccines require intraperitoneal (IP) injection, which is expensive and difficult to administer to young fish and causes stress and injury to the fish (1).

Infectious hematopoietic necrosis virus (IHNV), the enveloped (-) ss RNA virus of the Rhabdoviridae family, is the major cause of significant losses in the global trout and salmon aquaculture industry, with mortality rates reaching 90%, mainly in small fish. Neither therapeutic treatment nor a safe/mass delivery global commercial IHNV vaccine is currently available (8).

Research on vaccine development against IHNV has been ongoing for over four decades and several vaccine candidates based on inactivated virus, recombinant G protein expressed from prokaryotic and eukaryotic systems, attenuated virus strains, and DNA vectors have been shown to be efficient in eliciting specific and long-lasting protective immunity in fish but none has met all the requirements for commercialization, especially safety and mass delivery to a large number of highly susceptible small fish (9).

Approaches including the production of a recombinant IHNV glycoprotein in *E. coli* (10), yeast (11), and baculovirus/insect cells (12), failed to elicit high levels of protection against homologous virus challenge, although in some cases, neutralizing antibodies were detected in the sera of immunized fish. Furthermore, these low levels of protection were achieved only when recombinant glycoprotein was administered by intraperitoneal injection in combination with an adjuvant (13). Similarly, synthetic peptides representing putative antigenic determinants of the IHNV glycoprotein were poorly immunogenic (14).

Glycoprotein G is the unique target of neutralizing and protective antibodies, and recombinant subunit vaccines have been based on this protein (9–14). However, the complexity of expression and the challenge of producing soluble and functional recombinant glycoprotein to induce protective immunity, as well as the route of administration due to the protein stability issues, remain the main obstacles to the development of an effective IHNV subunit vaccine for mass delivery to fish fry (1, 2).

Displaying structurally defined antigenic epitopes in high copy numbers on the surface of self-assembling nanoparticles (NPs), such as VLPs or protein nanocages, to improve antigen stability and immunogenicity, with targeted delivery and slow release, is one of the novel technologies to address the challenges of subunit vaccines (15).

Although no VLP-based vaccines have yet been licensed for aquaculture, there is considerable experimental evidence of the potential of this type of vaccine for protecting fish against viral diseases such as infectious pancreatic necrosis (IPN) (16), pancreatic disease (PD) (17), and viral nervous necrosis (VNN) (18).

However, in contrast to VLPs of the non-enveloped viruses assembly process with only capsid proteins, enveloped viruses require an additional membrane component for assembly into mature virions, leading to enveloped VLPs not being structurally uniform and therefore difficult to characterize (19). A possible solution for the presentation of target antigens would be to display them to the host on the surfaces of self-assembled protein nanocages, which, in lieu of lipid membranes and matrix proteins, serve as an ideal scaffold for the enveloped viruses such as IHNV.

Ferritin is a major intracellular iron storage protein present in most living organisms, with 24 identical subunits that spontaneously self-assemble and form NPs complexes (20). Ferritin nanocages can enhance the immunogenicity of antigens by displaying them on their outer surface in an orderly manner, similar to the whole organism vaccines, leading to long-lasting immunity, which recently has been proven to work well both *in vitro* and *in vivo* for some mammalian viruses (21–25). The vaccines have been developed using eukaryotic host cells such as human embryonic kidney cells, and prokaryotes (*E. coli*) expression systems, delivered successfully through different routes in animal models (21–25). The use of ferritin NPs as an antigen scaffold can therefore improve the immunogenicity of subunit vaccines, and can also be considered as a promising platform for oral vaccine development due to its unique structure and stability under harsh temperature and pH conditions (20, 26).

This study describes for the first time the use of the self-assembling ferritin nanocages as vaccine platform for a non-mammalian virus. This approach resulted in the successful development of a soluble IHNV glycoprotein on a self-assembled ferritin nanoparticle in a low-cost production system (*E. coli*), which is biocompatible, stable, and effective for antiviral induction.

2 Materials and methods

2.1 Cell cultures

Zebrafish liver (ZFL) cells (CRL-2643, ATCC) were cultured in DMEM 4.5 g/mL glucose (Gibco) supplemented with 0.01 mg/mL

insulin, 50 ng/mL epidermal growth factor, 10% (v/v) heat-inactivated FBS, 5% (v/v) antibiotic/antimycotic, and 0.5% (v/v) heat-inactivated trout serum at 28°C with 5% CO_2 as previously described (27). Adherent rainbow trout head kidney macrophages (RT-HKM) were isolated from the head kidney as described previously (27, 28), and cultured in the same supplemented medium at 15°C with 5% CO_2. After 24 h, the cells were washed in PBS to remove nonadherent cells, and the media was replaced with fresh culture media and then changed every 48 hours for up to 5 days, which were used for immune gene expression assays.

2.2 Vector construction and cloning

The glycoprotein (G) gene fragment (184 aa) (29), from the ectodomain-encoded region of the European standard isolate of IHNV (X89213) fused (GGSSRSS linker) to N-terminal of *Helicobacter pylori* ferritin (WP_000949190) and a His-tag in the C-terminus. Then the construct was synthesized by Invitrogen GeneArt Gene Synthesis (ThermoFisher, DE) and cloned using the pET22b vector with XhoI and BamHI sites in *E. coli* (DH5α) bacteria. The IHNV-G fragment and ferritin control constructs and red fluorescent protein (iRFP-His) non-immunological control protein were similarly designed and cloned (27).

2.3 Protein expression and purification

For protein expression, vector constructs were isolated using the QIAprep Spin Miniprep Kit (Qiagen, USA) and transformed to BL21 *E. coli* strain with XhoI and BamHI enzyme digestion verification. Expression then was performed using BL21(DE3) grown in LB with 100 µg/mL ampicillin and induced with IPTG at 1 mmol/L. The expression temperature was set at 20°C for overnight cultivation. Cells were harvested by centrifugation (5000 g for 15 min at 4°C) and stored at -80°C. Protein expression was confirmed using SDS-PAGE and Western blot using an anti-His-tag antibody. Despite the different expression and purification conditions, the IHNV-G fragment was an insoluble protein (Supplementary Figure 1), while the FerritVac was soluble. After cell lysis, the recombinant proteins were purified by immobilized metal affinity chromatography (IMAC) on an ÄKTA Pure FPLC system. Proteins were eluted with a linear gradient of elution buffer (20 mM Tris HCl (pH 8.0), 50 mM NaCl, 500 mM imidazole) after selective binding to a HisTrap HP 1 mL column (GE Healthcare). Selected protein fractions were dialyzed to remove imidazole in the 20 mM Tris HCl (pH 8.0), 50 mM NaCl buffer. The Ferritin and FerritVac proteins were then also submitted to size exclusion chromatography (SEC) in a HiLoad 16/600 Superdex 200 pg column (Cytiva, Marlborough, MA, USA, ref. GE28-9893-35) with isocratic elution in 20 mM TRIS-HCl pH 8.0. Proteins with different sizes were eluted by monitoring their absorbance at 280 nm. The peaks obtained were compared with known molecular weight marker proteins (GE-Healthcare, USA). Fractions corresponding to monomers and trimers of the proteins were collected separately (Supplementary Figure 2). The final protein concentration was determined using a NanoDrop and Qubit™ Protein Broad Range (BR) Assay Kits (ThermoFisher, DE).

2.4 SDS-PAGE and western blotting

The SDS-polyacrylamide gel electrophoresis (SDS-PAGE) of the proteins was carried out on a 5-12% Bis-Tris gel with Coomassie blue visualization. For Western blotting, briefly after separation by SDS-PAGE, the proteins were electrophoretically transferred to PVDF membranes (Millipore) and then incubated in TTBS containing 10% skim milk for 1 h at room temperature to block non-specific binding during incubation with antibodies. The membranes were incubated overnight at 4°C with 1:10,000 anti-His primary antibody (ThermoFisher, DE) in 20 mL TTBS containing 10% skim milk, washed three times for 10 minutes at 25°C with 0.01% TTBS, and incubated for 1 hour at room temperature with 1:10,000 goat anti-mouse secondary antibody (ThermoFisher, DE) in the same buffer. Then, chemiluminescence visualization was performed using the SuperSignal™ Western Blot Kit (ThermoFisher, DE) and a BioRad ChemiDoc.

2.5 Dynamic light scattering

Dynamic light scattering (DLS) using a Zetasizer Nano ZS (Malvern Instruments, UK) was used to determine the particle size distribution and zeta potential of the protein NPs at 25°C, confirming the colloidal stability. Triplicate measurements were performed on 100 µL of each sample. Prism 9 (GraphPad software) was used to generate volume size distribution (nm) histograms.

2.6 Transmission electron microscopy

For transmission electron microscopy images, 10 µL of the protein samples (Ferritin and FerritVac NPs) were applied to carbon-coated copper grids for 10 min. The grids then were negatively stained with 10 µL of 2% (w/v) uranyl acetate solution and wiped out with filter paper strips after 1 min. The resulting grids were visualized with a JEOL 1400 (JEOL Ltd.) TEM instrument at 120 kV, and images were captured with a CCD GATAN ES1000W Erlangshen camera (Gatan Inc.). Size measurements were performed using ImageJ software (U.S. National Institutes of Health, Bethesda, MD), averaging 50 individual measurements for each protein nanoparticle.

2.7 Stability assays

The stability of FerritVac and ferritin NPs in 100 µL 20 mM Tris-HCl and 50 mM NaCl buffer (pH: 8.0) was measured by DLS under different storage conditions of 4°C and -80°C freeze-thaw after 2 weeks and under the same conditions found in the gastrointestinal tract of trout (pH:8.0 and pH:3.0) at the optimum temperature for trout fry culture and IHNV infection (15°C) for 2

and 4 h (8, 30). The pH of the buffer was adjusted with HCl and then exchanged using Pierce Protein Concentrator columns (ThermoFisher, DE).

2.8 Cytotoxicity assay with ZFL cell line

The MTT assay according to Thwaite et al. (31) was used to determine the cytotoxic effects of NPs on ZFL cells. After 2.5 h on minimal media, cultures were stimulated with NPs at 1, 5, 25, 50, and 100 μg/ml in duplicate wells and plates, and incubated for 14 h at 28°C. Cultures were washed in PBS and 10% MTT substrate (Sigma-Aldrich) was added. Cells without NPs were used as controls. The cells were then further incubated at 28°C for 30 min. The solution was removed and solubilized in DMSO, and the absorbance was read at 550 nm on a Victor 3 plate reader (PerkinElmer). The experiment was repeated three times. Data normalized to control readings set at 100% and analyzed by one-way analysis of variance (ANOVA).

2.9 Expression of antiviral genes in RT-HKM primary cells

The trout head kidney macrophage primary cells were simulated with the different doses of FerritVac NPs (10, 25, and 50 μg/mL) for 14 hours at 15°C, and compared with untreated cells and cells incubated with 25 μg/mL of ferritin and iRFP proteins as controls in triplicate plates. Total RNA was then extracted from the cells using the ReliaPrep™ RNA Cell Miniprep System (Promega), and cDNA was synthesized using the GoScript™ Reverse Transcription System Kit (Promega). The qPCR was performed using Fast SYBR™ Green Master Mix (ThermoFisher, DE) (32),, for gene markers of the innate immune response to viral infection (*mx, vig1, ifit5*, and *isg-15*) (33, 34),. The expression of the target genes has been corrected based on a reference gene (*EF-1 α*) and calculated relative to the control via the $2^{-\Delta\Delta Ct}$ method (35). Primer details are shown in the Supplementary Table 1.

2.10 Statistical analysis

Analyses were performed using SPSS 23 and GraphPad Prism 9 software. A one-way ANOVA was performed with the Duncan test to compare all group means and Dunnett's multiple comparisons test between each treatment and control mean, at a significance level of $p < 0.05$.

3 Results

3.1 Purification and characterization of NPs

For the construction of the nanovaccine, the most immunogenic fragment in the ectodomain of IHNV glycoprotein (29) was linked to the N-terminus of ferritin (Figure 1A), and a nanoparticle displaying the IHNV-G (FerritVac) was generated after the self-assembly of the ferritin. Figure 1B shows a schematic of the FerritVac NPs. The proteins were expressed in *E. coli* and purified by Ni-chelating affinity chromatography. Purified proteins were dialyzed for imidazole removal. While the IHNV glycoprotein alone was insoluble (Supplementary Figure 1), we successfully expressed and purified a soluble ferritin containing the IHNV glycoprotein fragment in the *E. coli* system we successfully expressed and purified a soluble ferritin containing the IHNV glycoprotein fragment in the E. coli system (Figures 1C and 1D). SDS-PAGE revealed 42, 22, 20, and 36 kDa for ferritin, IHNV-G, and iRFP, respectively (Supplementary Figure 1).

After purification, the ferritin and FerritVac proteins were also submitted to size exclusion chromatography (SEC) to differentially elute proteins according to their hydrodynamic volumes. The fractions belonging to peaks 1 and 2 were separately collected and evaluated to remove aggregates and other low molecule impurities (Supplementary Figure 2). Full physicochemical characterization of the protein nanoparticles including stability in buffer solution was performed with Dynamic Light Scattering (DLS) and the morphology of the particles was determined using Transmission Electron Microscopy (TEM). The nanoparticles characterization by TEM is shown in Figures 2A, B and dynamic light scattering (DLS) analysis is shown in Figures 2C, D.

TEM micrographs show spherical Ferritin and FerritVac NPs with a narrow particle size and mean diameters of 15.8 ± 0.52 nm and 20.53 ± 1.13 nm, respectively. DLS analysis revealed a highly monodisperse population of FerritVac NPs with a low polydispersity index (0.29 ± 0.01). The resulting FerriVac NPs resulted in a larger hydrodynamic diameter, compared to ferritin, as expected. There was no significant difference between the diameter of the particles visualized by TEM and the diameter determined by DLS (Table 1).

Zeta potential (ζ-potential) measurements confirmed the colloidal stability of analyzed dispersions (Table 1) with the electric charges of ferritin and FerritVac negatively charged. The ζ-potential for FerritVac NPs was -18.42 ± 1.04, similar to that of Ferritin (-20.46 ± 0.16 mV), indicating a lack of particle aggregation in dispersion.

3.2 The stability of NPs

The stability of FerritVac and Ferritin NPs under different storage conditions was evaluated by DLS (Figures 3A, B). After 2 weeks of storage at 4°C and a freeze-thawing at -80°C, the protein NPs were stable and appeared as a single peak with no significant change in the size of NPs, demonstrating the monodispersity of NP samples under defined storage conditions. However, a slight decrease in particle size was observed at 4°C, which may indicate that proteins begin to disassemble over time. While freezing and thawing stress can cause proteins to denature and aggregate, this Ferritin platform demonstrated stability.

To verify the suitability for oral administration, we evaluated the stability of the NPs at pH:8.0 and pH:3.0 at 15°C, which resemble the gastrointestinal pH conditions of trout at the

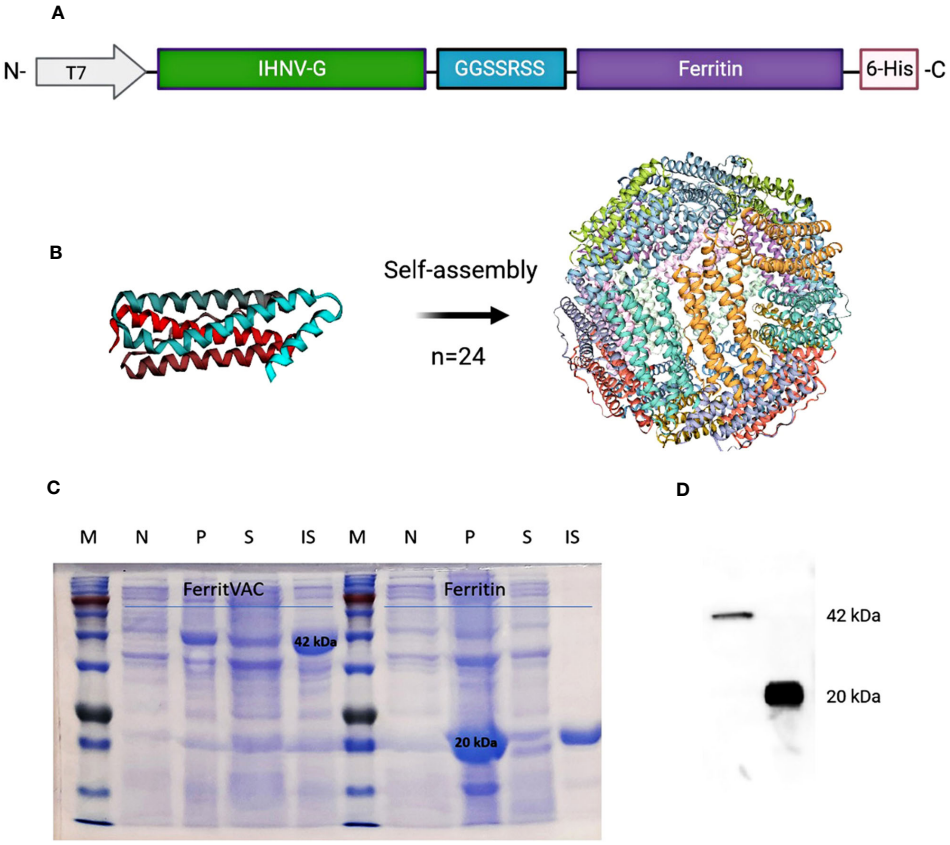

FIGURE 1
Construction and production of IHNV vaccine (FerritVac) using a Ferritin nanocage. **(A)** Construction of the FerritVac fusion protein: The IHNV glycoprotein fragment (aa 270 to 453) protein was linked (GGSSRSS linker) to the N-terminal of the (*H*) *pylori* ferritin with a His-tag in the C-terminus. **(B)** 3D schematic diagram of the ferritin platform. **(C)** SDS-PAGE (12%) of Ferritin and FerritVac protein NPs: Total protein production before (N) and after (P) IPTG induction for the same volume of culture sample. Soluble (S) and insoluble (IS) fractions after IPTG induction (overnight at 20°C) and cell lysis. **(D)** Western blot analysis of FerritVac (42 kDa) and Ferritin (20 kDa).

optimal water temperature for the culture of the species and other salmonids (Figures 3C-F). At pH:8.0 and incubation at 15°C of the samples, DLS analysis showed stable protein NPs after 2 h in solution and a slight increase in particle size of Ferritin NPs after 4h, indicating that the samples began to aggregate. Despite the stability after 2 h, a gradual increase in size and appearance of an aggregation peak with size of 68.9 ± 3.25 and 79.8 ± 2.63 for Ferritin and FerritVac NPs, respectively, were observed after 4 h of incubation at lower pH:3 and temperature of 15°C. Overall, the FerritVac NPs show excellent stability as Ferritin, displaying a similar environmental tolerance pattern.

3.3 Cytotoxicity in ZFL cells

There was no significant difference in survival between the control and any of the treatment groups in the MTT assays in ZFL cells incubated with 1, 5, 25, 50, and 100 µg/mL of each NPs for 14 h, indicating that neither FerritVac nor Ferritin NPs are cytotoxic at these doses (Figure 4). Cell viability values remained above 95% for both FerritVac and Ferritin up to 25 µg/mL after 14 h of exposure. However, a slight decrease with no significant difference was observed in the ZFL cells from 50 µg/mL and above, dropping to about 82% (p =0.25) and 70% (p =0.08) viability at the highest concentration (100 µg/mL) of FerritVac and Ferritin NPs, respectively.

3.4 Expression of antiviral genes in RT-HKM primary cells

To investigate the ability of FerritVac NPs to stimulate the expression of innate antiviral genes in antigen-presenting immune cells, we treated the rainbow trout head kidney macrophage primary cells with the NPs. Untreated cells and cells treated with 25 µg/mL of Ferritin and iRFP were used as controls. Genes tested included *mx, vig1, ifit5*, and *isg-15*, which are relevant markers of innate antiviral immunity, IHNV, and other fish rhabdovirus infections (33, 34). For all genes tested, FerritVac NPs exposure induced up-regulation significantly different from the controls in a dose-dependent manner (Figure 5).

The qPCR analysis revealed a significant increase in the expression of *mx* and *vig1* genes of macrophage cells incubated with 25 or 50 µg/ml dose of FerritVac NPs compared to the control

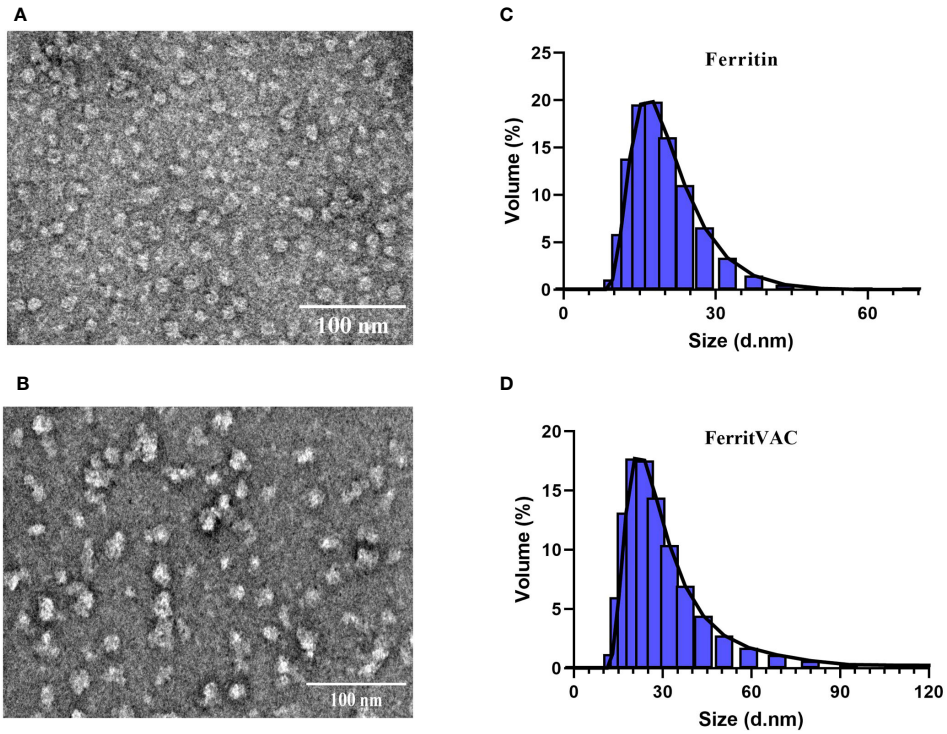

FIGURE 2
Morphological characterization and particle size distribution of Ferritin and FerritVac by TEM and DLS. Transmission electron micrographs (scale bar =100 nm) of negatively stained Ferritin **(A)** and FerritVac **(B)**. The. Size distribution of Ferritin **(C)** and FerritVac **(D)** characterized by DLS. Size distribution analysis of FerritVac nanoparticles *via* DLS showed an average diameter of 20.53 nm, which was larger than the diameter of Ferritin cages (15.8 nm).

groups as well as the lower dose of 10 μg/ml of NPs (Figures 5A, B). While the *ifit5* gene was significantly up-regulated in all dose groups of FerritVac NPs (Figure 5C), the *isg-15* gene was only significantly up-regulated (about 10-fold) in the cells treated with the higher dose of 50 μg/ml of NPs (Figure 5D). No significant differences were observed between cells incubated with 25μg/ml iRFP or ferritin NPs compared to untreated controls (p >0.05).

4 Discussion

Viral diseases in aquaculture are difficult to control due to the lack of approved and affordable antiviral veterinary medical products, as well as challenges in developing effective and safe viral vaccines that can be mass-administered to young fish, especially during early stages of their life cycle characterized with high susceptibility to virus infections (1–3). Gaps in treatment and prevention of viral diseases are associated with periodic disease outbreaks, animal welfare problems, and losses in aquaculture worldwide, threatening the long-term sustainability of the sector (36–38).

Self-assembling protein nanoparticles, such as ferritin, have shown remarkable thermal and pH stability, monodispersity, small uniform size, biodegradable, biocompatible, cost-effective mass production, reversible spontaneous assembly/disassembly, and surface conjugation by genetic or chemical means, addressing the issue of stability and immunogenicity of safe subunit vaccines and providing broader protection against viral infections even through oral administration (20, 26, 38).

Helicobacter pylori self-assembling ferritin has been used for the development of safe subunit nano vaccines, against some human and other mammalian viruses such as Middle East respiratory syndrome-coronavirus (MERS-CoV) (19), Influenza A virus (21), HIV (22), rotavirus A (23), SARS-CoV-2 (24), Canine distemper virus (25), classical swine fever virus (39), foot-and-mouth disease virus (40), hepatitis C virus (41), and Zika Virus (42), which have

TABLE 1 ζ-potential and particle size of purified FerritVac and Ferritin NPs determined by DLS and TEM.

NPs [a]	TEM (nm)	DLS (nm)	PDI	ζ-potential (mV)
Ferritin	16.23 ± 1.34	15.8± 0.52	0.47 ± 0.00	- 20.46 ± 0.16
FerritVac	20.73 ± 2.28	20.53 ± 1.13	0.29 ± 0.01	- 18.42 ± 1.04

[a]The diameter of 50 particles visualized by TEM was determined using ImageJ software [mean ± standard deviation (SD)], and DLS mean size values ± SD were obtained by considering the volume-based distribution. PDI, polydispersity index.

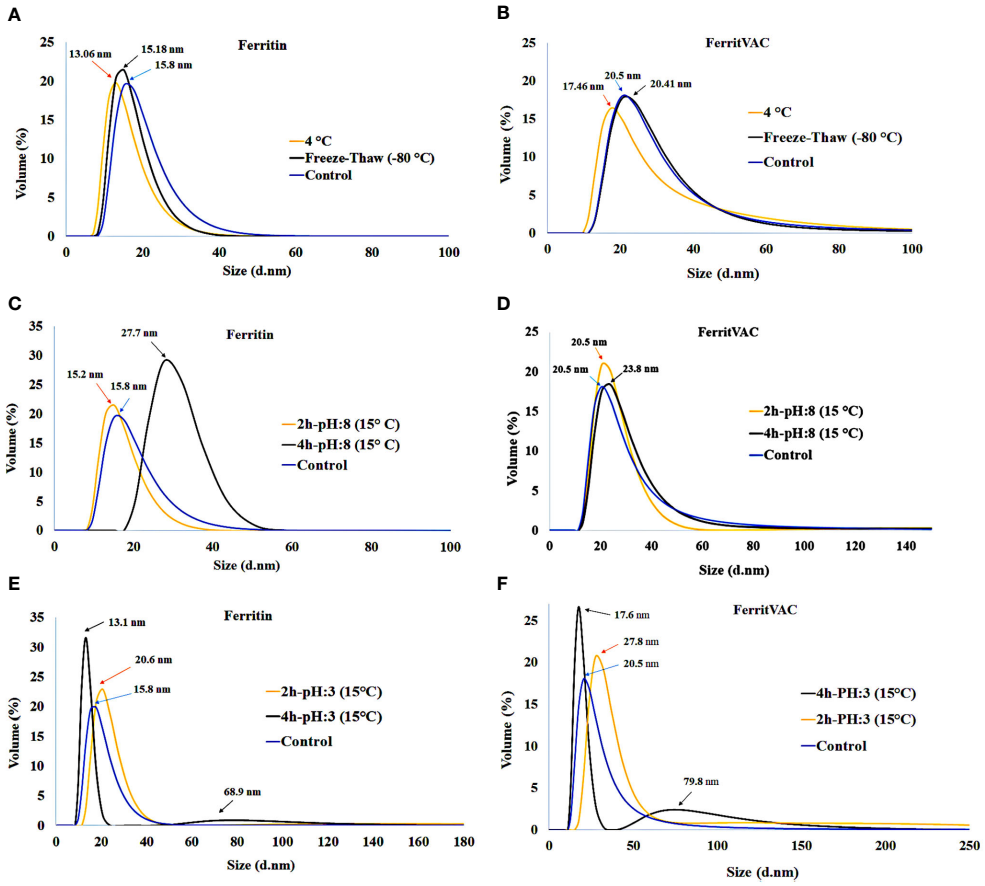

FIGURE 3
Stability of FerritVac and Ferritin NPs assessed by DLS under different storage conditions: 4°C and -80°C freeze-thaw after 2 weeks **(A, B)**, and for 2 h and 4 h at pH:8.0 **(C, D)** and pH:3.0 **(E, F)** at 15°C, which resemble the gastrointestinal pH conditions of trout, the main host of IHNV, at the optimal water temperature for the culture of the species and other salmonids. The data show a high stability of both NPs. However, over time the harsh conditions can gradually lead to disassembly and aggregation, which can be seen as a slight decrease and increase in peak size, respectively.

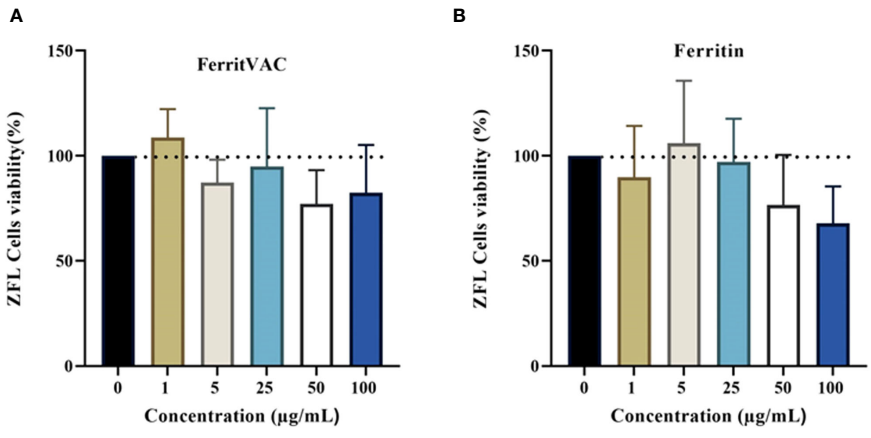

FIGURE 4
MTT assay cytotoxicity of FerritVac and Ferritin NPs in zebrafish liver (ZFL) cells: ZFL were incubated with FerritVac **(A)** and Ferritin **(B)** NPs at 1, 5, 25, 50, 100 µg/mL in duplicate wells and plates (n=4) for 14 h at 28 °C. ZFL cells without NPs incubated were used as control. After MTT treatment, incubation for 30 min, and subsequent solubilization in DMSO, absorbance was measured at 550 nm and data normalized to control readings set at 100%. A one-way analysis of variance (ANOVA) with Dunnett's multiple comparison test was performed between each treatment and control at a significance level of $p<0.05$. None of the treatment groups were significantly different from the control ($p>0.05$).

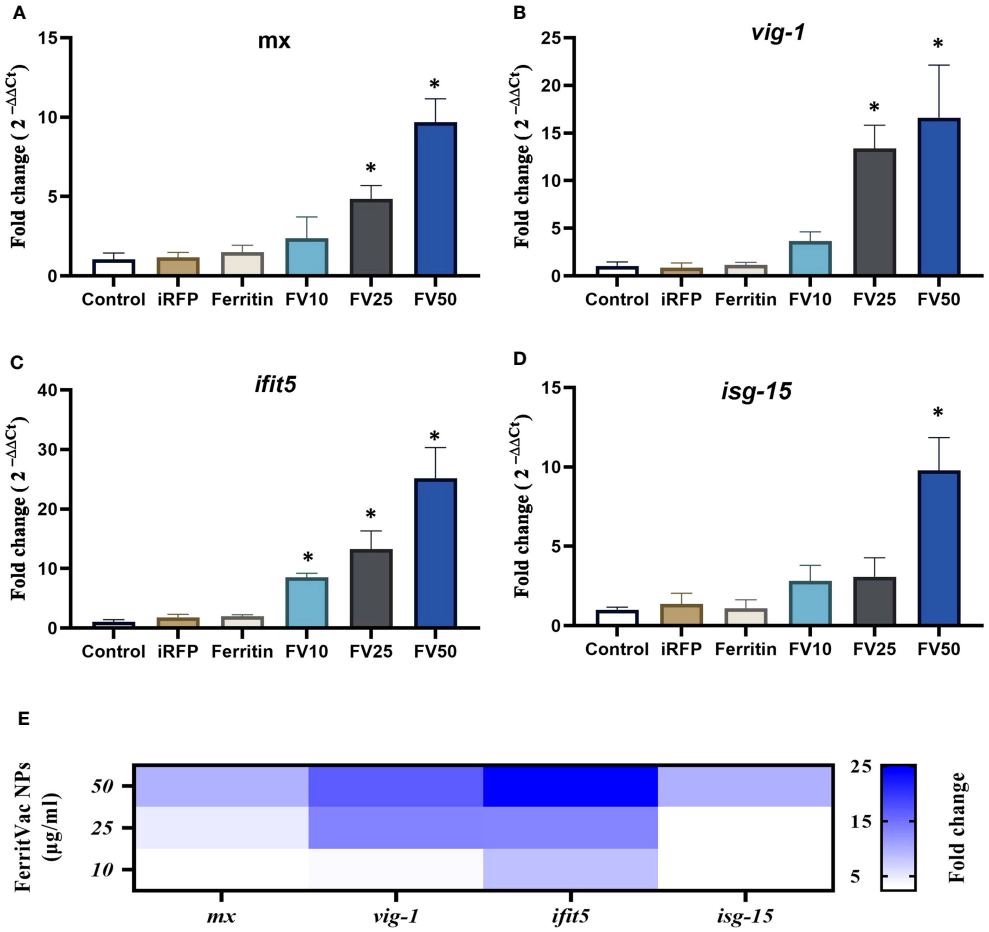

FIGURE 5
Expression of antiviral genes in trout head kidney macrophage primary cells (RT-HKM) incubated with FerritVac and Ferritin NPs. **(A)** *mx*, **(B)** *vig1*, **(C)** *ifit5*, and **(D)** *isg-15* gene expression in the cells incubated for 14 h as follows: unstimulated cells (control), iRFP (25 µg/mL) as an immunogenically irrelevant control, Ferritin (25 µg/mL) and different concentrations of FerritVac NPs 10 µg/mL (FV10), 25 µg/mL (FV25) and 50 µg/mL (FV50). **(E)** Heat map comparing expression changes of analyzed genes in RT-HKM cells incubated with FerritVac NPs. Samples are from three independent experiment plates from three different fish. Data were normalized based on the endogenous *EF-1a* gene and presented as mean fold change relative to unstimulated control cells; $2^{-\Delta\Delta CT}$ method). A one-way ANOVA was performed with Duncan to compare all groups' means, and Dunnett's multiple comparisons test between each treatment and control mean, at a significance level of $p < 0.05$. Asterisks indicate a significant difference compared to the control (* $p < 0.05$).

been produced in bacteria, insects and mammalian cells systems. In this study, we have for the first time used self-assembling ferritin nanocages as a vaccine platform against a non-mammalian viral pathogen (IHNV).

It has been reported that multiple engineered nanoparticle-based vaccines using *E. coli* expression system do not support soluble protein purification and fail to assemble as intended (15). While the IHNV glycoprotein alone was insoluble, we successfully expressed and purified soluble ferritin NPs containing the IHNV glycoprotein fragment in the low-cost *E. coli* production system. This suggests that a ferritin nanocage can be used as a novel vehicle for the rescue and production of soluble proteins that are otherwise difficult to obtain using conventional methods such as the prokaryote system.

The presence of spherical NPs observed under TEM confirmed that the FerritVac (IHNV glycoprotein-Ferritin) monomer that was produced in bacterial cells, maintains its self-assembling properties and is able to form the expected nanostructure. Moreover, the NP size determined by electron microscopy (around 20.73 ± 2.28 nm) was in accordance with the DLS results measurements, and with previously characterized *H. pylori* ferritin-based vaccine candidates, yielding nanoparticles with 20-40 nm diameter after self-assembly (22, 23, 43, 44), the size range ideal for cellular uptake and B-cell activation (45).

The observed increase in diameter of FerritVac compared to that of ferritin alone could be attributed to the presence of the exogenous protein, which may reflect the modification and size of NP cages observed in this study.

We also measured the ζ-potential of Ferritin and FerritVac NPs, indicating negative values and within the range recently reported for a ferritin-based vaccine against the Zika virus by Rong et al. (42). Zeta potential measurements refer to the potential difference between the dispersion medium and the stationary layer of the fluid surrounding the dispersed particle, including the potential difference between the particle surface and surrounding liquid medium, representing the measure of colloidal stability of

nanoparticles in dispersion (46). In our study, the display of IHNV glycoprotein on the Ferritin cage did not affect the stability of the nanoparticles.

The Ferritin protein complex has remarkable thermal and pH stability, withstanding temperatures of up to 80 - 100°C (20, 47). In this study, both the protein FerritVac and the ferritin NPs showed no significant changes after 2 weeks of storage at 4°C and a -80°C freeze-thaw cycle. It is noteworthy that these NPs were stored at 4°C for approximately one week during the process of purification, dialysis, and SEC prior to the stability tests, which indicates an even longer stability of the NPs. We also determined the stability of the NPs at pH:8.0 and pH:3.0 at 15°C, mimicking the pH conditions in the rainbow trout gastrointestinal (GI) tract and optimal water temperatures for the culture of this species and other salmonids in an effort to indicate suitability for oral administration of FerritVac to the rainbow trout juveniles at the age susceptible to IHNV (<6 months) (48). The pH of different sections of the rainbow trout GI tract after feeding remains acidic (pH 3.5) for at least 2h (30). However, in our study, both FerritVac and ferritin showed signs of degradation only at time points after 4 h in the low pH (3.0) conditions, as these conditions gradually lead to disassembly and aggregation, evidenced by the decrease and increase in the NP size, respectively. Similarly, it has been shown that the Ferritin protein shell begins to disassemble at pH below 3.4, but this process is reversible by subsequent elevation to higher pH values, making the platform suitable for antigenic protein delivery as well (26, 49).

The biocompatibility of active protein-based materials is critical for their biomedical use, therefore, zebrafish liver (ZFL) cells were used as a model to investigate the cytotoxicity of the Ferritin-based nanoparticles, which have already been used for some fish viral proteins (27, 31). The results of the MTT assay showed that neither FerritVac nor ferritin NPs significantly reduced ZFL cell viability compared to the control group at any of the concentrations tested after 14 hours of incubation, suggesting that these spherical nanostructures are biocompatible with living cells in an *in vitro* system. Considering zebrafish are a widely accepted biomedical research animal model, the importance of liver hepatocytes in detoxification processes, and no relevant previous studies regarding ferritin/ferritin-protein complex toxicity in this model system, our findings have significance not only for aquatic vertebrates but also for mammalian, including human being, studies.

Our results showed that FerritVac NPs upregulated the expression of innate antiviral and relevant gene markers of IHNV and other fish Rhabdovirus infection, including *mx, vig1, ifit5*, and *isg-15*, in antigen-presenting cells, trout head kidney macrophages (33, 34). Type I IFNs interfere with viral infection through the induction of a vast repertoire of ISGs via the Jak/STAT pathway, some of the ISGs exerting a direct antiviral activity such as mx, viperin/vig1, and isg15 (50), the expression of which can be simulated during IHNV infection (34). While ISGs are intrinsically located downstream of IFN in the antiviral pathways induced by viral infections, a number of them, such as viperin/vig1, are able to up-regulate type I IFNs and are therefore involved in positive feedback regulatory loops (50–52). FerittVac NPs from 25 μg/ml and above induced upregulation of *mx* and *vig1* genes in RT-HKM cells, however, *isg-15* was upregulated only at the highest dose of the NPs. Previous studies showed that over-expression of ISG15 in EPC cells is sufficient to induce antiviral activity against Novirhabdoviruses (IHNV, VHSV), Iridoviruses (EHNV) or Birnaviruses (IPNV) (50),. ISGylation, which targets cellular proteins such as TRIM25 and viral proteins such as the P and NV of IHNV, is required for the inhibition of the virus (52). Further, interferon-induced proteins with tetratricopeptide repeats (IFITs) bind to and regulate the functions of cellular and viral RNAs and proteins, thereby inhibiting viral replication (53). FerritVac NPs upregulated the ifit5 gene at all incubated doses. The ifit5 can be upregulated by type I interferons (IFNs) like IFITs, and the dependency of *ifit5* expression on activation of the Jak/STAT pathway has also been confirmed (54). Since there was no gene induction in the RT-HKM cells incubated with the ferritin-only NPs, these results indicate that immunogenicity and antiviral activity of the IHNV-G fragment was developed via the ferritin platform, most likely through the type I IFN-mediated Jak/STAT signaling pathway.

In conclusion, our study, for the first time, describes the use of the ferritin self-assembling nanocages as a vaccine platform for a non-mammalian viral pathogen. This approach resulted in the successful development of a soluble IHNV glycoprotein on a self-assembled ferritin nanoparticle, combining the advantages of glycoprotein antigen and ferritin nanoplatform to develop an effective and safe oral IHNV vaccine. Here, we also provided an initial dataset about the self-assembling protein nanocages approach with the potential to develop into a novel vaccine platform to be used in the prevention and control of aquaculture viral diseases. Further studies are needed to evaluate adaptive immune responses, safety, and efficacy of the FerritVac *in vivo* and to evaluate the applicability of this platform for other viruses.

Data availability statement

The original contributions presented in the study are included in the article/Supplementary Materials, further inquiries can be directed to the corresponding author/s.

Ethics statement

Ethical approval was not required for the studies on animals in accordance with the local legislation and institutional requirements because only commercially available established cell lines were used.

Author contributions

SA: Conceptualization, Data curation, Formal Analysis, Funding acquisition, Investigation, Methodology, Software, Validation, Visualization, Writing – original draft, Writing – review & editing. ZK: Formal Analysis, Methodology, Writing – review & editing. MM: Formal Analysis, Investigation, Methodology, Writing – review & editing. MG-O: Formal

Analysis, Methodology, Writing – review & editing, Investigation. NR: Conceptualization, Data curation, Formal Analysis, Investigation, Methodology, Resources, Supervision, Validation, Writing – review & editing. DP: Conceptualization, Data curation, Funding acquisition, Methodology, Project administration, Resources, Supervision, Validation, Writing – review & editing, Formal Analysis.

Funding

The author(s) declare financial support was received for the research, authorship, and/or publication of this article. This research was funded by Alexander von Humboldt Foundation No: IRN 1220630 GF-P.

Acknowledgments

We would like to thank Dr. Ehsan Alirahimi (University Hospital of Cologne) for his technical assistance in Bioinformatic analysis, and to Dr. Molood Behbahanipour (Autonomous University of Barcelona) and Dr. Pouria Rafati (University of Salford) for their assistance in characterizing the nanoparticles. Protein purification has been performed by the ICTS "NANBIOSIS", more specifically by the Protein Production Platform of CIBER in Bioengineering, Biomaterials & Nanomedicine (CIBER-BBN)/IBB, at the UAB (http://www.nanbiosis.es/portfolio/u1-protein-production-platform-ppp/).

Conflict of interest

The authors declare that the research was conducted in the absence of any commercial or financial relationships that could be construed as a potential conflict of interest.

Publisher's note

Supplementary material

The Supplementary Material for this article can be found online at: https://www.frontiersin.org/articles/10.3389/fimmu.2024.1346512/full#supplementary-material

References

1. Adams A. Progress, Challenges and opportunities in fish vaccine development. *Fish Shellfish Immunol* (2019) 90:210–4. doi: 10.1016/j.fsi.2019.04.066

2. Ma J, Bruce TJ, Jones EM, Cain KD. A review of fish vaccine development strategies: conventional methods and modern biotechnological approaches. *Microorganisms* (2019) 7:569. doi: 10.3390/microorganisms7110569

3. Dhar AK, Manna SK, Thomas Allnutt FC. Viral vaccines for farmed finfish. *Virus disease.* (2014) 25:1–17. doi: 10.1007/s13337-013-0186-4

4. Evensen and Leong JA. DNA vaccines against viral diseases of farmed fish. *Fish Shellfish Immunol* (2013) 35:1751–8. doi: 10.1016/j.fsi.2013.10.021

5. Ahmadivand S, Soltani M, Behdani M, Evensen Ø, Alirahimi E, Hasanzadeh R, et al. Oral DNA vaccines based on CS-TPP nanoparticles and alginate microparticles confer high protection against infectious pancreatic necrosis virus (IPNV) infection in trout. *Dev Comp Immunol* (2017) 74:178–89. doi: 10.1016/j.dci.2017.05.004

6. Naderi- Samani M, Soltani M, Dadar M, Taheri-mirghaed A, Zargar A, Ahmadivand S, et al. Oral immunization of trout fry with recombinant Lactococcus lactis NZ3900 expressing G gene of viral hemorrhagic septicaemia virus (VHSV). *Fish shellfish Immunol* (2020) 105:62–70. doi: 10.1016/j.fsi.2020.07.007

7. Bill RM. Recombinant protein subunit vaccine synthesis in microbes: a role for yeast? *J Pharm Pharmacol* (2015) 67:319–28. doi: 10.1111/jphp.12353

8. Ahmadivand S, Palić D, Weidmann M. Molecular epidemiology of novirhabdoviruses emerging in Iranian trout farms. *Viruses.* (2021) 13:448. doi: 10.3390/v13030448

9. Yong CY, Ong HK, Tang HC, Yeap SK, Omar AR, Ho KL, et al. Infectious hematopoietic necrosis virus: advances in diagnosis and vaccine development. *PeerJ* (2019) 7:e7151. doi: 10.7717/peerj.7151

10. Gilmore RD, Engelking HM, Manning DS, Leong JA. Expression in Escherichia coli of an epitope of the glycoprotein of infectious hematopoietic necrosis virus protects against viral challenge. *Bio/Technology.* (1988) 6:295–300. doi: 10.1038/nbt0388-295

11. Zhao JZ, Xu LM, Liu M, Cao YS, LaPatra SE, Yin JS, et al. Preliminary study of an oral vaccine against infectious hematopoietic necrosis virus using improved yeast surface display technology. *Mol Immunol* (2017) 85:196–204. doi: 10.1016/j.molimm.2017.03.001

12. Cain KD, LaPatra SE, Shewmaker B, Jones J, Byrne K, Ristow S. Immunogenicity of a recombinant infectious hematopoietic necrosis virus glycoprotein produced in insect cells. *Dis Aquat Org* (1999) 36:67–72. doi: 10.3354/dao036067

13. Hua X, Feng Y, Guan X, Wang Y, Zhou Y, Ren X, et al. Truncated infectious hematopoietic necrosis virus g protein effect on survival, immune response, and disease resistance in rainbow trout. *Dis Aquat Organisms.* (2020) 139:25–33. doi: 10.3354/dao03463

14. Emmenegger E, Landolt M, LaPatra S, Winton J. Immunogenicity of synthetic peptides representing antigenic determinants on the infectious hematopoietic necrosis virus glycoprotein. *Dis Aquat Org* (1997) 28:175–84. doi: 10.3354/dao028175

15. Gregory AE, Titball R, Williamson D. Vaccine delivery using nanoparticles. *Front Cell Infect Microbiol* (2013) 3:13. doi: 10.3389/fcimb.2013.00013

16. Martinez-Alonso S, Vakharia V, Saint-Jean SR, Perez-Prieto S, Tafalla C. Immune responses elicited in rainbow trout through the administration of infectious pancreatic necrosis virus-like particles. *Dev Comp Immunol* (2011) 36:378–84. doi: 10.1016/j.dci.2011.07.010

17. Metz SW, Feenstra F, Villoing S, Hulten MCv, Lent JWv, Koumans J, et al. Low temperature-dependent salmonid alphavirus glycoprotein processing and recombinant virus-like particle formation. *PloS One* (2011) 6:1–10. doi: 10.1371/journal.pone.0025816

18. Lai YX, Jin BL, Xu Y, Huang LJ, Huang RQ, Zhang Y, et al. Immune responses of orange-spotted grouper, Epinephelus coioides, against virus-like particles of betanodavirus produced in Escherichia coli, Vet. Immunol. *Immunopathol.* (2014) 157:87–96. doi: 10.1016/j.vetimm.2013.10.003

19. Kim YS, Son A, Kim J, Kwon SB, Kim MH, Kim P. Chaperna-mediated assembly of ferritin-based middle east respiratory syndrome- coronavirus nanoparticles. *Front Immunol* (2018) 9:1093. doi: 10.3389/fimmu.2018.01093

20. Li CQ, Soistman E, Carter DC. Ferritin nanoparticle technology. A new platform for antigen presentation and vaccine development. *Ind Biotechnol* (2006) 2:143–7. doi: 10.1089/ind.2006.2.143

21. Kanekiyo M, Wei CJ, Yassine HM, Mctamney PM, Boyington JC, Whittle JR, et al. Self-assembling influenza nanoparticle vaccines elicit broadly neutralizing H1N1 antibodies. *Nature.* (2013) 499(7456):102–6. doi: 10.1038/nature12202

22. Sliepen K, Ozorowski G, Burger JA, van Montfort T, Stunnenberg M, LaBranche C, et al. Presenting native-like HIV-1 envelope trimers on ferritin nanoparticles improves their immunogenicity. *Retrovirology* (2015) 12:82. doi: 10.1186/s12977-015-0210-4

23. Li Z, Cui K, Wang H, Liu F, Huang K, Duan Z, et al. A milk-based self-assemble rotavirus VP6-ferritin NPs vaccine elicited protection against the viral infection. *J Nanobiotechnology*. (2019) 17:13. doi: 10.1186/s12951-019-0446-6

24. Joyce MG, King HAD, Elakhal-Naouar I, Ahmed A, Peachman KK, Macedo Cincotta C, et al. A SARS-CoV-2 ferritin nanoparticle vaccine elicits protective immune responses in nonhuman primates. *Sci Transl Med* (2022) 14(632):eabi5735. doi: 10.1126/scitranslmed.abi5735

25. Wang B, Li S, Qiao Y, Fu Y, Nie J, Jiang S, et al. Self-assembling ferritin nanoparticles coupled with linear sequences from canine distemper virus haemagglutinin protein elicit robust immune responses. *J Nanobiotechnol.* (2022) 20:32. doi: 10.1186/s12951-021-01229-0

26. Kim M, Rho Y, Jin KS, Ahn B, Jung S, Kim H, et al. pH-dependent structures of ferritin and apoferritin in solution: disassembly and reassembly. *Biomacromolecules.* (2011) 12:1629–40. doi: 10.1021/bm200026v

27. Torrealba D, Parra D, Seras-Franzoso J, Vallejos-Vidal E, Yero D, Gibert I, et al. Nanostructured recombinant cytokines: a highly stable alternative to short-lived prophylactics. *Biomaterials.* (2016) 107:102–14. doi: 10.1016/j.biomaterials.2016.08.043

28. Smith NC, Umasuthan N, Kumar S, Woldemariam NT, Andreassen R, Christian SL and Rise ML. Transcriptome profiling of atlantic salmon adherent head kidney leukocytes reveals that macrophages are selectively enriched during culture. *Front Immunol* (2021) 12:709910. doi: 10.3389/fimmu.2021.709910

29. Xu L, Mourich DV, Engelking HM, Ristow S, Arnzen J, Leong JC. Epitope mapping and characterization of the infectious hematopoietic necrosis glycoprotein, using fusion proteins synthesized in *Escherichia Coli*. *J Virol* (1991) 65:1611–5. doi: 10.1128/jvi.65.3.1611-1615.1991

30. Sugiura SH. Dietary acidification enhances phosphorus digestibility but decreases Hþ/Kþ-ATPase expression in rainbow trout. *J Exp Biol* (2006) 209:3719–28. doi: 10.1242/jeb.02436

31. Thwaite R, Ji J, Torrealba D, Coll J, Sabés M, Villaverde A and Roher N. Protein nanoparticles made of recombinant viral antigens: A promising biomaterial for oral delivery of fish prophylactics. *Front Immunol* (2018) 9:1652. doi: 10.3389/fimmu.2018.01652

32. Ahmadivand S, Farahmand H, Teimoori-Toolabi L, Mirvaghefi A, Eagderi S, Geerinckx T, et al. Boule gene expression underpins the meiotic arrest in spermatogenesis in male rainbow trout (Oncorhynchus mykiss) exposed to DEHP and butachlor. *Gen Comp Endocrinol* (2016) 225:235–41. doi: 10.1016/j.ygcen.2015.05.011

33. Ortega-Villaizan M, Chico V, Perez L. Fish innate immune response to viral infection-an overview of five major antiviral genes. *Viruses.* (2022) 14:1546. doi: 10.3390/v14071546

34. Shao Y, Zhao J, Ren G, Lu T, Chen X, Xu L. Early or Simultaneous Infection with Infectious Pancreatic Necrosis Virus Inhibits Infectious Hematopoietic Necrosis Virus Replication and Induces a Stronger Antiviral Response during Co-infection in Rainbow Trout (Oncorhynchus mykiss). *Viruses.* (2022) 14:1732. doi: 10.3390/v14081732

35. Livak KJ, Schmittgen TD. Analysis of relative gene expression data using realtime quantitative PCR and the $2^{-\Delta\Delta Ct}$ method. *Methods.* (2001) 25:402–8. doi: 10.1006/meth.2001.1262

36. Ahmadivand S, Soltani K, Shokrpoor S, Rahmati-Holasoo H, El-Matbouli M, Taheri-Mirghaed A. Cyprinid herpesvirus 3 (CyHV-3) transmission and outbreaks in Iran: Detection and characterization in farmed common carp. *Microbial Pathogenesis.* (2020) 149:104321. doi: 10.1016/j.micpath.2020.104321

37. Ahmadivand S, Weidmann M, El-Matbouli M, Rahmati-Holasoo H. Low pathogenic strain of infectious pancreatic necrosis virus (IPNV) associated with recent outbreaks in Iranian trout farms. *Pathogens.* (2020) 9(10):782. doi: 10.3390/pathogens9100782

38. Zhang Q, Ke F, Gui L, Zhao Z. Recent insights into aquatic viruses: Emerging and reemerging pathogens, molecular features, biological effects, and novel investigative approaches. *Water Biol Security.* (2022) 1:100062. doi: 10.1016/j.watbs.2022.100062

39. Zhao Z, Chen X, Chen Y, Li H, Fang K, Chen H, et al. A self-assembling ferritin nanoplatform for designing classical swine fever vaccine: elicitation of potent neutralizing antibody. *Vaccines* (2021) 9:45. doi: 10.3390/vaccines9010045

40. Chen Y, Hu Y, Chen H, Li X, Qian PA. ferritin nanoparticle vaccine for foot-and-mouth disease virus elicited partial protection in mice. *Vaccine* (2020) 38:5647–52. doi: 10.1016/j.vaccine.2020.06.063

41. He L, Cheng Y, Kong L, Azadnia P, Giang E, Kim J, et al. Approaching rational epitope vaccine design for hepatitis C virus with meta-server and multivalent scaffolding. *Sci Rep* (2015) 5:12501. doi: 10.1038/srep12501

42. Pattnaik A, Sahoo BR, Struble LR, Borgstahl GEO, Zhou Y, Franco R, et al. A ferritin nanoparticle-based zika virus vaccine candidate induces robust humoral and cellular immune responses and protects mice from lethal virus challenge. *Vaccines* (2023) 11:821. doi: 10.3390/vaccines11040821

43. Swanson KA, Rainho-Tomko JN, Williams ZP, Lanza L, Peredelchuk M, Kishko M, et al. A respiratory syncytial virus (RSV) F protein nanoparticle vaccine focuses antibody responses to a conserved neutralization domain. *Sci Immunol* (2020) 5: eaba6466. doi: 10.1126/sciimmunol.aba6466

44. Zhang B, Chao CW, Tsybovsky Y, Abiona OM, Hutchinson GB, Moliva JI, et al. A platform incorporating trimeric antigens into self-assembling nanoparticles reveals SARS-CoV-2-spike nanoparticles to elicit substantially higher neutralizing responses than spike alone. *Sci Rep* (2020) 10:18149. doi: 10.1038/s41598-020-74949-2

45. Chaudhuri A, Battaglia G, Golestanian R. The effect of interactions on the cellular uptake of nanoparticles. *Phys Biol* (2011) 8:046002. doi: 10.1088/1478-3975/8/4/046002

46. Rasmussen MK, Pedersen JN, Marie R. Size and surface charge characterization of nanoparticles with a salt gradient. *Nat Commun* (2020) 11:1–8. doi: 10.1038/s41467-020-15889-3

47. Rodrigues MQ, Alves PM, Roldão A. Functionalizing ferritin nanoparticles for vaccine development. *Pharmaceutics*. (2021) 13:1621. doi: 10.3390/pharmaceutics13101621

48. Ahmadivand S, Soltani M, Mardani K, Shokrpoor S, Hassanzadeh R, Rahmati-Holasoo H, et al. Infectious hematopoietic necrosis virus (IHNV) outbreak in farmed rainbow trout in Iran: viral isolation, pathological findings, molecular confirmation, and genetic analysis. *Virus Res* (2017) 229:17–23. doi: 10.1016/j.virusres.2016.12.013

49. Stühn L, Auernhammer J, Dietz C. pH-depended protein shell dis- and reassembly of ferritin nanoparticles revealed by atomic force microscopy. *Sci Rep* (2019) 9:17755. doi: 10.1038/s41598-019-53943-3

50. Langevin C, Aleksejeva E, Passoni G, Palha N, Levraud JP, Bou-dinot P. The antiviral innate immune response in fish: evolution and conservation of the IFN system. *J Mol Biol* (2013) 425:4904–20. doi: 10.1016/j.jmb.2013.09.033

51. Sadler AJ, Williams BRG. Interferon-inducible antiviral effectors. *Nat Rev Immunol* (2008) 8:559–68. doi: 10.1038/nri2314

52. Yoneyama M, Kikuchi M, Natsukawa T, Shinobu N, Imaizumi T, Miyagishi M, et al. The RNA helicase RIG-I has an essential function in double-stranded RNA-induced innate antiviral responses. *Nat Immunol* (2004) 5:730–7. doi: 10.1038/ni1087

53. Langevin C, van der Aa LM, Houel A, Torhy C, Briolat V, Lunazzi A, et al. Zebrafish ISG15 exerts a strong anti-viral activity against RNA and DNA viruses and regulates the interferon response. *J Virol* (2013) 87:10025–36. doi: 10.1128/JVI.01294-12

54. Bela-ong DB, Greiner-Tollersrud L, Andreas van der Wal Y, Jensen I, Seternes OM, Jørgensen JB. Infection and microbial molecular motifs modulate transcription of the interferon-inducible gene ifit5 in a teleost fish. *Dev Comp Immunol* (2020) 111:103746. doi: 10.1016/j.dci.2020.103746

frontiers | Frontiers in Immunology

TYPE Original Research
PUBLISHED 14 February 2024
DOI 10.3389/fimmu.2024.1359552

OPEN ACCESS

EDITED BY
Iddya Karunasagar,
Nitte University, India

REVIEWED BY
Guan-Jun Yang,
Ningbo University, China
Bei Huang,
Jimei University, China

*CORRESPONDENCE
Maria K. Dahle
Maria.dahle@vetinst.no

RECEIVED 21 December 2023
ACCEPTED 23 January 2024
PUBLISHED 14 February 2024

CITATION
Tsoulia T, Sundaram AYM, Braaen S, Jørgensen JB, Rimstad E, Wessel Ø and Dahle MK (2024) Transcriptomics of early responses to purified *Piscine orthoreovirus*-1 in Atlantic salmon (*Salmo salar* L.) red blood cells compared to non-susceptible cell lines. *Front. Immunol.* 15:1359552. doi: 10.3389/fimmu.2024.1359552

Transcriptomics of early responses to purified *Piscine orthoreovirus*-1 in Atlantic salmon (*Salmo salar* L.) red blood cells compared to non-susceptible cell lines

Thomais Tsoulia[1,2], Arvind Y. M. Sundaram[1,3], Stine Braaen[4], Jorunn B. Jørgensen[2], Espen Rimstad[4], Øystein Wessel[4] and Maria K. Dahle[1,2]*

[1]Departments of Aquatic Animal Health and Analysis and Diagnostics, Norwegian Veterinary Institute, Ås, Norway, [2]Department of Biotechnology, Fisheries and Economy, UiT Arctic University of Norway, Tromsø, Norway, [3]Department of Medical Genetics, Oslo University Hospital, Oslo, Norway, [4]Department of Veterinary Medicine, Norwegian University of Life Sciences, Ås, Norway

Piscine red blood cells (RBC) are nucleated and have been characterized as mediators of immune responses in addition to their role in gas exchange. Salmonid RBC are major target cells of Piscine orthoreovirus-1 (PRV-1), the etiological agent of heart and skeletal muscle inflammation (HSMI) in farmed Atlantic salmon (*Salmo salar*). PRV-1 replicates in RBC *ex vivo*, but no viral amplification has been possible in available A. salmon cell lines. To compare RBC basal transcripts and transcriptional responses to PRV-1 in the early phase of infection with non-susceptible cells, we exposed A. salmon RBC, Atlantic salmon kidney cells (ASK) and Salmon head kidney cells (SHK-1) to PRV-1 for 24 h. The RNA-seq analysis of RBC supported their previous characterization as pluripotent cells, as they expressed a wide repertoire of genes encoding pattern recognition receptors (PRRs), cytokine receptors, and genes implicated in antiviral activities. The comparison of RBC to ASK and SHK-1 revealed immune cell features exclusively expressed in RBC, such as genes involved in chemotactic activity in response to inflammation. Differential expression analysis of RBC exposed to PRV-1 showed 46 significantly induced genes (≥ 2-fold upregulation) linked to the antiviral response pathway, including RNA-specific PRRs and interferon (IFN) response factors. In SHK-1, PRV induced a more potent or faster antiviral response (213 genes induced). ASK cells showed a differential response pattern (12 genes induced, 18 suppressed) less characterized by the dsRNA-induced antiviral pathway. Despite these differences, the RIG-I-like receptor 3 (*RLR3*) in the family of cytosolic dsRNA receptors was significantly induced in all PRV-1 exposed cells. IFN regulatory factor 1 (*IRF1*) was significantly induced in RBC only, in contrast to *IRF3/IRF7* induced in SHK-1. Differences in IRF expression and activity may potentially affect viral propagation.

KEYWORDS

piscine orthoreovirus, red blood cell, Atlantic salmon, salmon kidney cell line, transcriptome

1 Introduction

Red blood cells (RBC) are primarily known for their physiological role in respiratory processes, where intracellular heme and hemoglobin molecules regulate the uptake and transport of oxygen and carbon dioxide (1). In addition to this, a diverse range of physiological and immunologic properties have been attributed to vertebrate RBC, including redox homeostasis, hemoglobin antimicrobial activity and pathogen binding (2, 3). While mammalian RBC are enucleated and lack transcription/translation machinery, teleost RBC have retained their nucleus and organelles in the cytoplasm, essential for intracellular signaling, gene expression and protein production in response to stimuli (2, 4, 5). Previous studies of teleost RBC have shown their ability to react by innate immune responses and physiological differentiation in response to viral infections and systemic signals, respectively (2–4, 6–8). Unlike mammalian RBC, where the nucleus and cellular components are extruded during erythropoiesis to ensure efficient gas exchange (3, 9), transcriptome analyses of teleost RBC has revealed the expression of a complex set of genes involved in virus sensing, antiviral defense and antigen presentation (5, 8, 10, 11). However, the scale of RBC contribution to innate and potentially adaptive immunity is not fully understood.

Viral infections represent a major threat for the piscine aquaculture industry, and efficient prevention remains challenging. Heart and skeletal muscle inflammation (HSMI) is one of the most common viral diseases in farmed Atlantic salmon (*Salmo salar* L.) in Norway (12). The disease is characterized by extensive heart and muscle inflammation with infiltration of immune cells in the epi-, endo- and myocardium, myositis and necrosis in the red skeletal muscle (13–15). The causative agent of HSMI is Piscine orthoreovirus-1 genotype (PRV-1) (14, 16), a member of the order *Reovirales*, family *Spinareoviridae*, genus *Orthoreovirus*. This genus also contains the mammalian and avian orthoreoviruses (MRV and ARV, respectively). PRV-1 has a ten-segmented, double stranded RNA (dsRNA) genome packed in a double-layered icosahedral protein capsid, and was the first orthoreovirus reported in fish (14, 17).

Salmonid RBC are the main target cells of PRV-1 in the primary phase of infection (18). Comparative *in silico* studies with MRV indicate that PRV-1 may use the same infection mechanism, and further studies have indicated that the virus replication occurs in globular neo-organelles referred to as viral factories in the cytoplasm (16, 17, 19, 20). During the peak of infection, high loads of viral RNA and protein are produced within the cells and virus is released into plasma (16, 20). The peak in antiviral responses to PRV-1 has been associated with a decrease in plasma viremia and reduction in viral protein production in RBC (6, 16, 20), along with suppression of some RBC functions, such as hemoglobin production, and expression of metabolic genes (16, 21). Even though the impacts of PRV-1 infection on A. salmon RBC gene expression have been partly characterized *in vivo* and *in vitro* (6, 8, 22), the regulation of genes in RBC shortly after PRV-1 encounter has not been explored in detail.

In the present study, we compared the transcriptomic responses of A. salmon RBC to those of two A. salmon kidney cell lines at resting state, and 24 h after PRV-1 exposure. Atlantic salmon kidney cells (ASK) (23) and Salmon head kidney cells (SHK-1) (24) have been screened and characterized as non-supportive for PRV-1 propagation earlier, showing no evidence of virus replication (25). Here, we report the similarities and differences observed between A. salmon RBC, ASK and SHK-1 before and after PRV-1 exposure, focusing on pathways of the innate immune system.

2 Materials and methods

2.1 Blood sampling

Six A. salmon pre-smolts (30-50g) were euthanized using benzocaine chloride (1g/5L water) for 5 min, and peripheral blood from the caudal vein was collected in heparinized vacutainers (Vacutest, Sarstedt). The blood was used for isolation of red blood cells.

2.2 Isolation of RBC

RBC were isolated from the heparinized blood diluted 1:10 in sterile phosphate buffered saline (dPBS) and laid on top of a Percoll (GE healthcare, Uppsala Sweden) gradient (bottom layer 49%; top layer 34%) which was centrifuged (500 x G, 4°C, 20 min), washed with dPBS and collected as previously described (18). The cells were counted, and their viability was assessed using Countess (Invitrogen, Eugene, Oregon, USA) and resuspended to a concentration of 3×10^7 cells/mL in Leibovitz's L15 medium (Life Technologies, Carlsbad, CA, USA) supplemented with fetal calf serum (2%) (Sigma- Aldrich) and gentamicin (50 µg/mL- Lonza Biowhittaker, Walkersville, USA). The isolated RBC were inspected by light microscopy in three areas (approximately 100 cells/area, ≥ 300 cells in total) to ensure a maximum of two cells without typical RBC morphology (99% culture purity) (8) The cultures were placed at 15°C under constant agitation (225 rpm).

2.3 Atlantic salmon cell line cultures

The A. salmon kidney (ASK) cell line and the Salmon head kidney (SHK-1) cell line, were routinely split (1:2) once a week and cultivated at 20°C in Leibovitz's L15 medium supplemented with 4 mM L-glutamine (Life Technologies, Carlsbad, CA, USA), fetal bovine serum (10%) (Sigma- Aldrich), 40 µM 2-mecaptoethanol and gentamicin (50 µg/mL- Lonza Biowhittaker, Walkersville, USA). The cells were kept at 15°C during culturing and experiments.

2.4 Preparation of purified piscine orthoreovirus-1

Purified PRV-1 was used as inoculum in the *ex vivo* stimulation experiment. The virus was a variant of high virulence (NOR2012) (16), that had been purified from a blood cell pellet of infected fish using cesium chloride density gradient as described previously (16) and stored in Dulbecco's PBS with 15% glycerol at -80°C. The copy

number was determined using absolute quantification RT-qPCR as previously described (16).

2.5 *Ex vivo* stimulation

RBC isolated from six fish were plated in NuncTM non-treated 24-well plates with flat bottom (Thermo Fisher) (5×10^6 RBC per well, in 0.5 mL medium). RBC cultures were kept at 15°C under constant agitation (225 rpm) using an Ecotron incubation shaker (Infors HT, Basel Switzerland) to ensure a homogenous suspension. The virus exposure setup included six wells (one per fish) exposed identically to purified PRV-1 (5×10^6 virus particles per well/multiplicity of infection (MOI) of 1) and six control wells (one per fish). Following 24 h of incubation, exposed and control cells were harvested by centrifugation in Eppendorf tubes, media removal and lysis in RT buffer (Qiagen, Hilden, Germany) for RNA isolation.

ASK and SHK-1 experiments were performed at three separate time points (3 parallels). Each time, cells were counted and seeded in 6-well plates with flat bottom (4.5×10^4 cells in 1 mL medium-approx. 80% confluent) (Thermo Fisher) and kept at 15°C in brand incubator. The cultivation setup each time included three wells exposed identically to purified PRV-1 and 3 control wells. Briefly, the cells in the wells were washed three times with dPBS and 4.5×10^5 virus particles (MOI of 10) was added per exposed well. After 24 h of incubation, the cells were washed with dPBS and lysed with RT buffer (Qiagen, Hilden, Germany) for RNA isolation and subsequent RT- qPCR analysis to assess whether PRV-1 was associated with the cells.

2.6 RNA isolation and sequencing

Lysed cells were homogenized using 5 mm steel beads and TissueLyser II (Qiagen). Total RNA was extracted using RNeasy Plus Mini Kit (Qiagen, Hilden, Germany) following the manufacturer's protocol. Isolated RNA was eluted in 50 µL Rnase-free distilled water. RNA was quantified using NanoDrop ND- 1000 spectophotometer (Thermo Fiscer Scientific, Wilmington, DE, USA). RNA quality (RIN >8) was ensured using Agilent 2100 Bioanalyser (Agilent, USA) before being sent for sequencing.

Six biological replicates of the exposed and control RBC (12 samples in total), along with three experimental replicates of the exposed and control kidney cells (6 samples for ASK and 6 samples for SHK-1, respectively) were sent to Norwegian Sequencing Centre (NSC). Library preparation was performed using strand- specific TruSeq RNA Library Prep kit (Illumina, CA, USA). Libraries were subsequently sequenced on Illumina HiSeq to obtain 150 bp paired end reads.

2.7 Bioinformatics and statistics

Fastq files of reads from RNA-seq were cleaned (trim/remove adapter and low quality sequences) using BBDuk tool in BBMap v38.22 suite (parameters: ktrim=r, k=23, mink=11, hdist=1, tbo, tpe, qtrim=r, trimq=15, maq=15, minlen=36, forcetrimright=149) (26). Cleaned reads were further mapped to the A. salmon genome (ENSEMBL ICSASG_v2) using the HISAT2 v.2.2.1 (parameters: –rna-strandness RF) (27). FeatureCounts v.1.4.6-p1 (parameters: -p -s 2) was used for estimating the number of reads and aligning against the reference genes in ENSEMBL r104 GTF annotation (28). Initial data analysis was performed using the Bioconductor packages in R, including DESeq2 v.1.34.0 (29) and the SARTools v.1.7.4 (30). Normalization and differential expression analysis were conducted for the cells exposed to the virus against their unexposed controls using DESeq2. The annotation tables were cleaned using median count reads ≥ 10 as a cut off, to get rid of genes with zero or low counts. Subsequently, adjusted p-value (padj) was calculated using Benjamin- Hochberg (BH) correction and gene with padj below 0.05 were considered as differentially expressed genes (DEGs). ShinyGO v0.77 (31) was used for both gene ontology (GO) and Kyoto Encyclopedia of Genes and Genomes (KEGG) enrichment analysis with FDR cutoff 0.05. Pathview R package was used to draw KEGG pathway maps (32, 33).

3 Results

3.1 Transcriptome analysis of Atlantic salmon RBC and kidney cell lines in resting state

Information on total sequenced reads and alignment rate of mapping of all biological conditions is provided in Supplementary File A, Table 1. Normalized RNA- seq data were compared to identify features that are differentially expressed between RBC and kidney cell lines, ASK and SHK-1, at the unexposed resting state. The variability of the biological conditions within the experiment was assessed with a principal component analysis (PCA) (Supplementary File A, Figure 1). This analysis showed low variability within the biological (RBC) and experimental (ASK, SHK-1) replicates of each cell type, confirming consistency in the data, while the distribution of the clusters against the two first principal components indicated that SHK-1 and ASK are more closely related.

3.2 Transcriptional profiling of Atlantic salmon RBC and kidney cell lines, ASK and SHK-1

The original dataset consisted of 55819 features (genes). After filtering out 16989 genes with zero normalized median count reads, the differences and similarities in the expression profile of RBC, ASK and SHK-1 were assessed using an upset plot, including 38830 features (referred to as analyzed dataset) (Figure 1). A cutoff ≥ 10 counts was applied, and 24962 genes were found transcribed in RBC, 27518 genes in ASK and 27461 in SHK-1. In the three cell types, 24559 common genes were expressed. ASK and SHK-1 were sharing 2769 expressed genes (ASK & SHK-1 cutoff ≥ 10 median

counts, RBC = 0 median counts), verifying their highest level of similarity as indicated by PCA. A subset of 346 genes were exclusively expressed in RBC, while 44 genes were only expressed in RBC and ASK, and 13 genes were only expressed in RBC and SHK-1 (Figure 1).

To identify the processes in which the genes of each subset are involved, Kyoto Encyclopedia of Genes and Genomes (KEGG) pathway enrichment analysis was performed. The lists of gene functional groups found in the enrichment analysis are provided in Supplementary File B. RBC, ASK and SHK-1 appeared to all share genes related to fundamental cellular processes, such as endocytosis, protein processing in ER and ubiquitin mediated proteolysis. Two KEGG pathways associated to cellular responses activated by viral and bacterial invasion, "Herpes simplex virus 1 infection" and "Salmonella infection" respectively, showed the greatest representation of shared genes (456 and 410 genes, respectively) between RBC, ASK and SHK-1. This indicated that RBC possess immune functions similar to ASK and SHK-1 and are able to respond to viral and bacterial pathogens. The KEGG pathways named "Herpes simplex virus 1 infection" and "Salmonella infection" were first described in mammals in response to these pathogens but have also been identified in teleost (33). In this study, the official KEGG nomenclature is used even if they refer to pathogens not relevant for this study.

3.2.1 Gene ontology enrichment analyses for the genes exclusively mapped to RBC

The subset of genes mapped exclusively in RBC consisted of 346 features. To identify biological processes that may be regulated by these genes, gene ontology (GO) enrichment analysis on Biological Process (GO : BP) was performed. Most genes were involved in "Cell surface-" and "G protein-coupled receptor" signaling pathways, whereas only a few appeared to contribute to physiological processes, such as gas transport and respiratory burst. Regarding the immune characteristics of the cells, genes involved in chemotaxis (e.g. C-C chemokine receptor type 9 (*CCR9*) and C-C motif chemokine 4 (*CCL4*) –like), phagocytosis (e.g. coronin-1A-like) and innate immune response pathway [e.g. interferon regulatory factor 4 (*IRF4*) and interleukin-1 receptor type II (*IL1R2*)] were represented. The detailed GO : BP categories along with the list of the 346 genes are provided in Supplementary File B. KEGG pathway enrichment analysis was considered inconclusive for such a small input.

3.3 Identification of differentially expressed genes between Atlantic salmon RBC and kidney cell lines, ASK and SHK-1

Differential gene expression analysis was performed to estimate differences in gene expression patterns between RBC and each kidney cell line (ASK and SHK-1). Filtering out low count genes (cutoff ≥ 10 median counts), the comparison of RBC against ASK and SHK-1 resulted in 14493 and 14397 differentially expressed genes (DEGs), respectively (Supplementary File A, Figure 2). In both comparisons, approximately 7500 DEGs indicated higher expression levels in RBC (thus, lower expression levels in ASK and SHK-1). Accordingly, approximately 6800 DEGs indicated lower expression level in RBC (thus, higher expression levels in ASK and SHK-1). ASK vs SHK-1 resulted in 10018 DEGs, 5041 with higher expression levels in SHK-1 and 4977 with higher expression level in ASK. The lists of DEGs emerging from the comparison of RBC vs SHK-1, RBC vs ASK and ASK vs SHK-1 are provided in Supplementary File C.

To determine the pathways to which DEGs of RBC vs ASK and SHK-1 belonged, KEGG pathway enrichment analysis was performed. The analysis was performed for DEGs with normalized median counts ≥ 10 and fold- change ≤ 0.5 for the

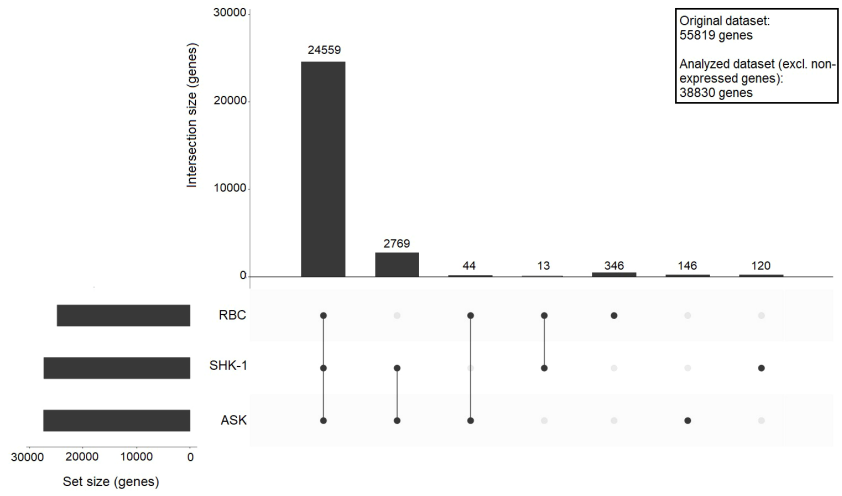

FIGURE 1
Upset plot showing sharing and unique gene expression for ASK, SHK-1, and RBC. A cutoff ≥ 10 counts was applied to define genes as expressed, and 0 counts required to define genes as not expressed in a cell type; The bars show the number of shared expressed genes between the indicated motifs: RBC vs SHK-1, RBC vs ASK and ASK vs SHK-1, or unique for a specific cell type. The analysis was performed using a dataset of 38830 genes (analysed dataset).

downregulated genes in ASK and SHK-1 compared to RBC (i.e "Higher expression compared to RBC" group of genes) and ≥ 2 for the upregulated genes in ASK and SHK-1 compared to RBC (i.e"Lower expression compared to RBC" group of genes). The majority of DEGs with higher expression in RBC compared to both ASK and SHK-1 were involved in innate immune processes related to viral sensing (KEGG nomenclature "Herpes simplex virus 1 infection") (119 and 126 genes, respectively), as shown in Figures 2, 3 in detail. Several genes with significantly higher transcripts in RBC were also involved in pathways associated with cellular functions like "Endocytosis", "Autophagy" and "Ubiquitin mediated proteolysis" (Figure 2). RBC DEGs belonging to KEGG groups, "MTOR-" and "FoXO" signaling pathways were only reported in the comparison of RBC vs ASK (Figure 2A, top), while "Ribosome" and "Basal transcription factors" in RBC vs SHK-1 (Figure 2B, top).

The majority of DEGs with lower expression in RBC were primarily involved in processes of cytoskeleton and paracellular communication ("Reg. of actin cytoskeleton" and "Tight junction") and host defense against bacterial invasion ("Salmonella infection"). Several genes were grouped within KEGG categories related to cellular senescence, metabolism and oxidative phosphorylation (Figure 2). Genes involved in ribosome biogenesis were more highly expressed in SHK-1 compared to RBC, indicating that RBC are less active in protein production (Figure 2B, bottom). Results from RBC vs ASK showed that genes linked to cell cycle events were more highly expressed in ASK (Figure 2A, bottom), which is expected for a continuous cell line.

To better understand the role of RBC in modulating functions of the innate immune system, we focused on signaling pathways involved in viral sensing and infection. These are included in the KEGG category referred to as "Herpes simplex virus 1 infection-sasa05168" pathway that consisted of the largest amount of DEGs with significantly higher expression levels in RBC. Figure 3A was extracted from the original pathway sasa05168 as established by Kanehisa Laboratories (2020). The detailed modified pathway is provided in Supplementary File A, Figure 3.

RBC expressed genes involved in toll-like receptor (TLR) and RIG-I-like receptor (RLR) signaling. Several signaling mediators in these pathways, such as interleukin 1 receptor associated kinase 1

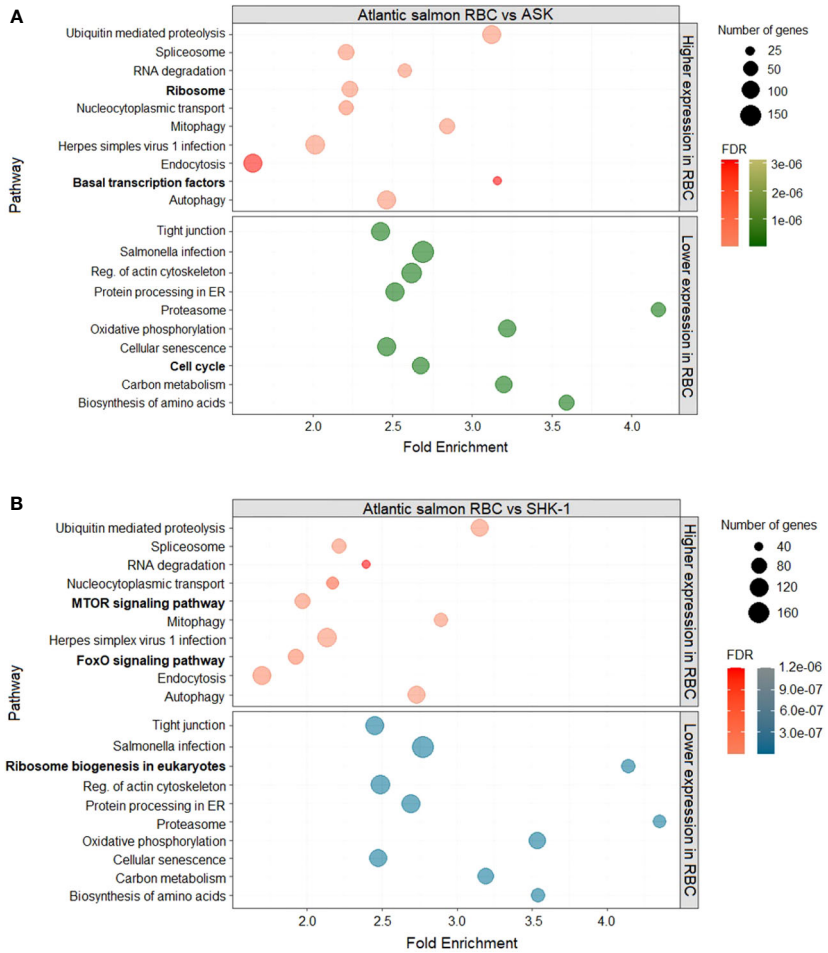

FIGURE 2
DEGs of RBC (red) compared to the kidney cell lines, **(A)** ASK (green) and **(B)** SHK-1 (blue). Kyoto Encyclopedia of Genes and Genomes (KEGG) pathway enrichment analysis was further analysed in ShinyGO 0.76 for FDR cutoff ≤ 0.05 and DEGs with fold-change ≥ 2 and ≤ 0.5.

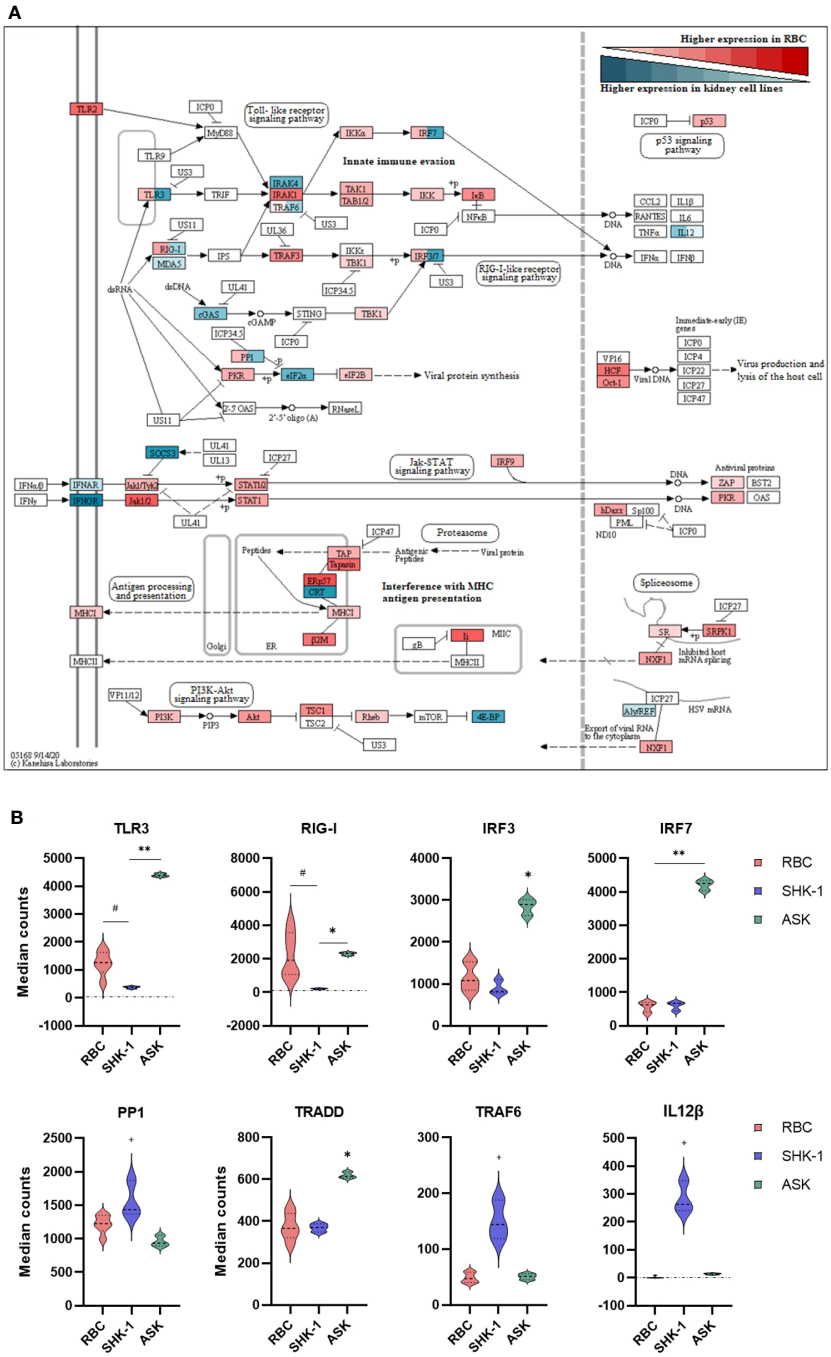

FIGURE 3
Differential expression analysis of selected genes associated with innate immunity in RBC, ASK and SHK-1. **(A)** Signaling pathways triggered by viral invasion. Red: Significantly higher normalized counts in RBC; Cyan: Similar and Significantly higher normalized counts in ASK and SHK-1. Red and cyan: Significantly different expression levels between ASK and SHK-1, and also with RBC were colored in both red and cyan. This figure was modified from the "Herpes simplex virus 1 infection" pathway- sasa05168 in KEGG, to include only immune pathways of interest. **(B)** Selected genes with significantly different expression pattern between the kidney cell lines, ASK and SHK-1, and RBC. $^{\#}p \leq 0.05$ in RBC vs ASK and SHK-1; $^{*}p \leq 0.05$ in ASK vs RBC and SHK-1; $^{**}p \leq 0.05$ in ASK vs RBC and SHK-1; $^{+}p \leq 0.05$ in SHK-1 vs ASK and RBC.

(*IRAK1*) and TNF receptor associated factor 3 (*TRAF3*), showed a higher expression level in RBC compared to ASK and SHK-1 (Figure 3A). However, the basal expression levels of pattern recognition receptors (PRRs), *TLR3*, melanoma differentiation-associated protein 5 (*MDA5*) and *RLR1* (also referred to as *RIG-I or DDX58)*, and interferon regulatory factors (*IRF*) 3 and 7 were significantly higher in ASK. Several components essential to antigen processing and presentation (MHCI pathway), inhibition of viral production (*PKR* regulation and *Jak-STAT* signaling pathway) and regulation of apoptosis and viral propagation (*PI3K- Akt* pathway)

showed significantly higher transcripts in RBC than ASK and SHK-1 (Figure 3A). While ASK and SHK-1 indicated similar expression patterns overall, a few genes related to cell cycle and immune cell differentiation were expressed significantly higher in SHK-1 (Figure 3B).

3.4 Identification of innate immune function genes in Atlantic salmon RBC

RBC have traditionally been characterized exclusively as gas exchangers expressing hemoglobins (3). As expected, several hemoglobin (Hb) subunits were found among the most highly expressed genes in RBC in the dataset (Table 1), also indicating culture purity. Expression levels of iron storage ferritins and mediators of heme biosynthetic pathway (such as *BLVRB* and *ALAS2*), which typically function in blood/RBC (34, 35), were also among the highest expressed genes. Also, MHC class I-related gene protein-like and thymus-specific serine protease (*TSSP*) antigen processing components were among the most highly expressed genes in salmonid RBC (Table 1). To further assess the purity of the RBC culture, transcripts of typical T cells and B cells markers were sought and evaluated. While many were not identified in our datasets, such as *CD3* and *CD34*, a few typical T cell and B cell markers such as *CD4* and *CD8* (36), showed near- zero count reads (Table 1).

To assess the contribution of RBC to innate immunity, we focused on identifying components associated with pathogen recognition, cell-to-cell communication, activation of the innate immune system and host defense. The detection of infectious agents is mainly mediated by (germline-encoded) PRRs. PRRs are highly conserved among vertebrates and the main families described in

TABLE 1 Transcript counts of the 20 most highly expressed genes in A. salmon RBC compared to ASK and SHK-1.

Gene	Description	Ensembl ID	RBCs (counts)	ASK (counts)	SHK-1 (counts)
HBAA2	Hemoglobin subunit alpha-4	*ENSSSAG00000044737*	797987	157	172
-	Ferritin heavy subunit	*ENSSSAG00000049977*	671668	112424	70642
HBB1	Hemoglobin subunit beta-1-like	*ENSSSAG00000044957*	579951	130	137
-	Hyperosmotic glycine rich protein	*ENSSSAG00000068063*	421881	200118	163430
HBA4	Hemoglobin subunit alpha-4	*ENSSSAG00000065254*	321654	89	87
HBB	Hemoglobin subunit beta-like	*ENSSSAG00000045065*	321344	83	92
HBA	Hemoglobin subunit alpha	*ENSSSAG00000065229*	244043	75	68
HSPA8	Heat shock protein 8	*ENSSSAG00000049191*	213336	55203	37017
HBB	Beta globin	*ENSSSAG00000065233*	210828	44	47
HBB1	Hemoglobin subunit beta-1-like	*ENSSSAG00000065315*	187925	106	117
FRIH	Ferritin, heavy polypeptide 1-1	*ENSSSAG00000051567*	156074	32006	99410
HBBA2	Hemoglobin subunit beta-1-like	*ENSSSAG00000065226*	150808	45	44
NRK2	Nicotinamide riboside kinase 2-like	*ENSSSAG00000077245*	142822	9601	2613
TSSP	Thymus-specific serine protease	*ENSSSAG00000053130*	136772	32	38
BLVRB	Biliverdin reductase B	*ENSSSAG00000069097*	117596	965	1314
ALAS2	5'-aminolevulinate synthase 2	*ENSSSAG00000068428*	106223	28	30
-	Major histocompatibility complex class I-related gene protein isof. X1	*ENSSSAG00000077419*	87427	29250	54093
MIBP2	Nicotinamide riboside kinase 2-like	*ENSSSAG00000068654*	79622	4905	3683
WBP4-like	WW domain-binding protein 4-like	*ENSSSAG00000077000*	78270	434	278
5NTC	Cytosolic purine 5-nucleotidase	*ENSSSAG00000045618*	67967	23	21
Cd4	***S. salar* T-cell surface glycoprotein CD4**	***ENSSSAG00000076595***	**1**	**6**	**0**
Cd8a	***CD8- alpha***	***ENSSSAG00000065860***	**0**	**0**	**0**
Cd8b	***CD8- beta***	***ENSSSAG00000045680***	**1**	**0**	**0**
Cd34	***CD34* molecule**	***ENSSSAG00000079346***	**0**	**952**	**589**
MME	**Neprilysin- like**	***ENSSSAG00000042374***	**5**	**0**	**1**

Transcript counts of five distinct T cells and B cells markers (in bold) were also included to assess RBC culture purity. The expression levels of the genes were measured as median normalized count reads (counts). All listed genes indicated significantly higher expression in RBC ($p \leq 0.5$).

fish include toll-like receptors (TLRs), nucleotide oligomerization domains (NOD) -like receptors, retinoid acid-inducible (RIG) -like receptors (RLRs), C-type lectin receptors (CLRs) and scavenger receptors (SRs) (37). A wide repertoire of PRRs from all five families was found in RBC. TLRs, RLRs and NLRs were the most abundant PRRs in the cells and those with the highest transcript levels are listed in Table 2. RLRs, which primarily recognize double- stranded (ds) RNA oligonucleotides, showed collectively the highest expression. *TLR3*, previously identified in salmonid RBC and known to bind dsRNA, was detected in high transcript numbers (8). *TLR8*, which recognizes single- stranded (ss) RNA, showed the highest expression among the TLRs (38, 39). Several NLRs, which primarily have been characterized in mammals as sensors of bacterial components, such as lipopolysaccharides (LPS) and peptidoglycans (PGNs) were identified in RBC. Variants of NLR family CARD domain containing 3- like (*NLRC3L*) showed the highest expression (45). In addition, *NLRC5* and *NOD1/NOD2* were detected. Their role and functionality in teleosts are modestly studied.

The majority of the signaling regulators and effectors which interact with TLRs and RLRs, along with various non-RLR DEAD/DEAH box RNA helicases with diverse roles in innate immunity, were identified in RBC, as shown in Figure 4 (top). Indicatively, *DHX37* showed the highest expression level, however details about its function have not been determined in either fish or mammals. *IRF1* (isoform 2), known to regulate the induction of interferon (*IFN*) and IFN-stimulated genes, and *IRF9*, associated with antiviral immunity (46), were highly expressed in the RBC transcriptome. Several cytokine receptors were found in our dataset, but only a few cytokines (interleukins and chemokines) were expressed in RBC, including interleukin 15 and 34 (*IL15* and *IL34*), and *CCL4- like* chemokine (Figure 4). Common IFN stimulated antiviral effector genes, such as IFN stimulated gene 15 (*ISG15*) like (*UBIL*) and myxovirus resistance (*Mx2*), known to be induced by IFNs, were also identified in RBC in high transcript numbers.

3.5 Differential expression analysis of RBC and kidney cell lines exposed to PRV-1

To identify the antiviral responses in RBC at early PRV-1 exposure (24 h) compared to non- susceptible cell lines, normalized RNA-seq data of the samples exposed to the virus were compared to unexposed controls through differential expression analysis (DESeq2). Information on total sequenced reads and alignment rate of mapping, along with principal component analysis (PCA) are provided in Supplementary File A, Figure 4. Differential expression analysis of RBC exposed to PRV-1 vs the unexposed controls showed a set of 46 significantly induced genes (≥ 2-fold upregulation) and 1 significantly suppressed (≤ 0.5-fold downregulation) gene (Figure 5). In contrast, 213 genes were significantly induced and 10 genes were significantly suppressed in

TABLE 2 Pattern recognition receptors (PRRs) identified in A. salmon RBC.

Gene	Ensembl ID	RBC (counts)	Ligands	Reference in teleost
Toll-like receptors (TLRs)				
TMSB4X (or TLR8)	*ENSSSAG00000076485*	2060	ssRNA	(38)
TLR3	*ENSSSAG00000040910*	1244	dsRNA	(8)
TLR2	*ENSSSAG00000003781*	50	LPS	(39)
TLR19	*ENSSSAG00000042328*	31	Non specified	(39)
Retinoic acid-inducible gene (RIG)-like receptors (RLRs)				
MDA5	*ENSSSAG00000078885*	2264	dsRNA	(40)
DDX58	*ENSSSAG00000045391*	2232	(ds)RNA	(41)
DHX58	*ENSSSAG00000037858*	1824	ssRNA; dsRNA	(40)
Nucleotide oligomerization domains (NOD)-like receptors (NLRs)				
NLRC3L1	*ENSSSAG00000005336*	1461	DNA and RNA oligonucleotides	(42)
	ENSSSAG00000056446	1177		
	ENSSSAG00000046213	1033		
NLRC5	*ENSSSAG00000068298*	233	Bacterial components	(43)
NOD1	*ENSSSAG00000053537*	170	Bacterial PGNs	(44)
NOD2	*ENSSSAG00000076025*	26	Bacterial PGNs	(44)

The majority of mapped PRRs were categorized in 3 major groups: toll-like receptors (TLRs), retinoic acid inducible gene (RIG)- like receptors and nucleotide- oligomerization domain (NOD)-like receptors. The basal expression levels of the genes were measured as median normalized count reads (counts). Only genes with transcripts ≥ 10 (cutoff ≥ 10 median counts) were included in the analysis. LPS, lipopolysaccharides; PGNs, peptidoglycans.

10.3389/fimmu.2024.1359552

Non- RLR DEAD/H box helicases	Counts	Signaling adaptors	Counts	IFN regulatory factors	Counts
DHX37	23590	*IPS* (or *MAVS*)	1026	*IRF9*	5548
DDX46	5431	*TRAF3*	513	*IRF1 (isof. 2)*	4517
DDX3X (isof. X2)	2714	*IKBKγ* (or *IKK*)	316	*IRF3*	1152
DDX6	2552	*TRIM25-like*	242	*IRF7*	574
DDX24	2183	*TBK1*	266	*IRF1*	234
DHX33	1782	*TICAM1*	35	*IRF4*	72

Interleukins & interleukin receptors	Counts	Chemokines & chemokine receptors	Counts	IFN pathway activators & IFN-inducible genes	Counts
IL15	3588	*CCL4- like*	197	*STAT1*	14545
IL6R β (isof. X2)	1500		40	*STAT2*	8350
IL34	152	*CCR9*	598	*JAK1*	1018
IL15Rα	728		294	*EIF2αK2*	42
IL6Rα	177	*CXCR4*	266	*UBIL*	1820
I10R2	172	*CXCR4β*	42	*MX2*	970

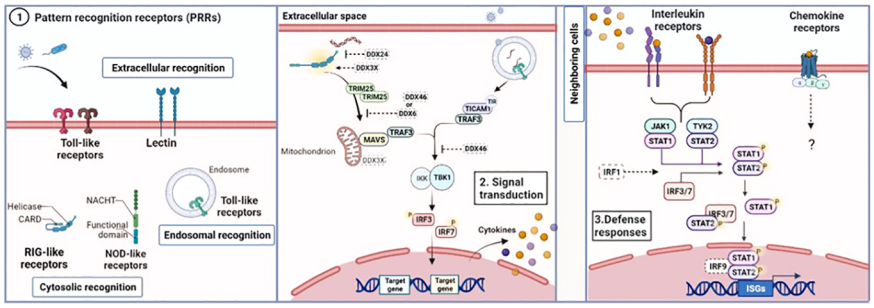

FIGURE 4
Examples of RBC genes involved in innate immune responses identified in A. salmon RBC. Transcripts of non- RLR DEAD/DEAH box helicases, signaling adaptors and interferon regulatory factors (IRFs) (table on top). Transcripts of interleukins (ILs) and interleukin receptors (ILRs), chemokines (C-C and C-X-C motifs) and chemokine receptors and interferon (IFN) pathway activators and IFN- inducible genes (table on bottom). The expression levels of the genes were measured as median normalized count reads (counts) (RBC n= 6). Only genes with transcript reads ≥ 10 (cutoff ≥ 10 median counts) were included in the analysis. Short description of the pathways relevant for genes expressed in RBC and listed in the tables above. Elements drawn in dash have not been characterized in teleost, and their roles were based on mammalian models. Step 1. Pattern recognition receptors (PRRs). Step 2. Signaling mediators and interferon regulatory factors acting downstream of PRR binding, leading to secretion of IFNs and pro-inflammatory cytokines. Step 3. Pathways induced when secreted IFNs and cytokines bind to receptors, leading to expression of several innate immune effectors.

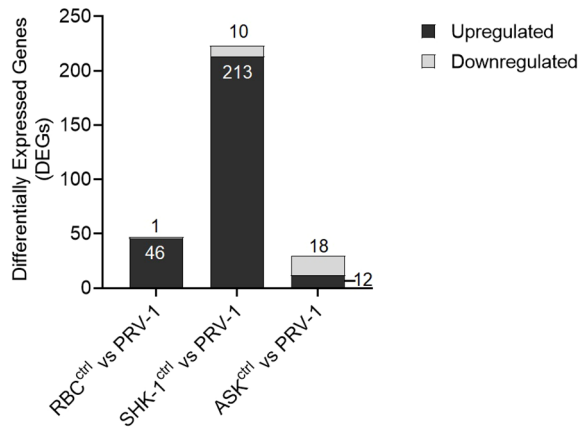

FIGURE 5
Differential gene expression analysis of A. salmon RBC, SHK-1 and ASK exposed to PRV-1 for 24h compared to their unexposed controls (RBC vs PRV-1, SHK-1 vs PRV-1 and ASK vs PRV-1, respectively). The analysis was performed on genes with median counts ≥ 10. Cutoff ≥ 2-fold change for upregulated DEGs and ≤ 0.5-fold change for downregulated DEGs was applied.

SHK-1. In ASK, 12 genes were significantly induced and 18 genes significantly suppressed. Thus, SHK-1 demonstrated the strongest and ASK the weakest responses to PRV-1.

3.6 GO and KEGG enrichment analysis for the DEGs of RBC, ASK and SHK-1 exposed to PRV-1

We performed GO and KEGG pathway enrichment analyses with an FDR (adjusted p value) cutoff of 0.05 for the upregulated DEGs (≥ 2-fold change) in RBC, ASK and SHK-1 to identify biological processes and signaling pathways activated in response to PRV-1 (Figure 6). As the significantly downregulated genes were too few, they were not subjected to these analyses. GO enrichment analysis for Biological Process (GO : BP) resulted in 9 GO terms for RBC, 6 for SHK-1 and 3 for ASK. Genes in RBC were mainly involved in four biological processes: “Response to biotic stimulus”, “Protein modification by small protein conjugation or removal”, “Defense response” and “Immune system process”. GO term “Immune system process” consisted of 6 genes, including *RLR3*

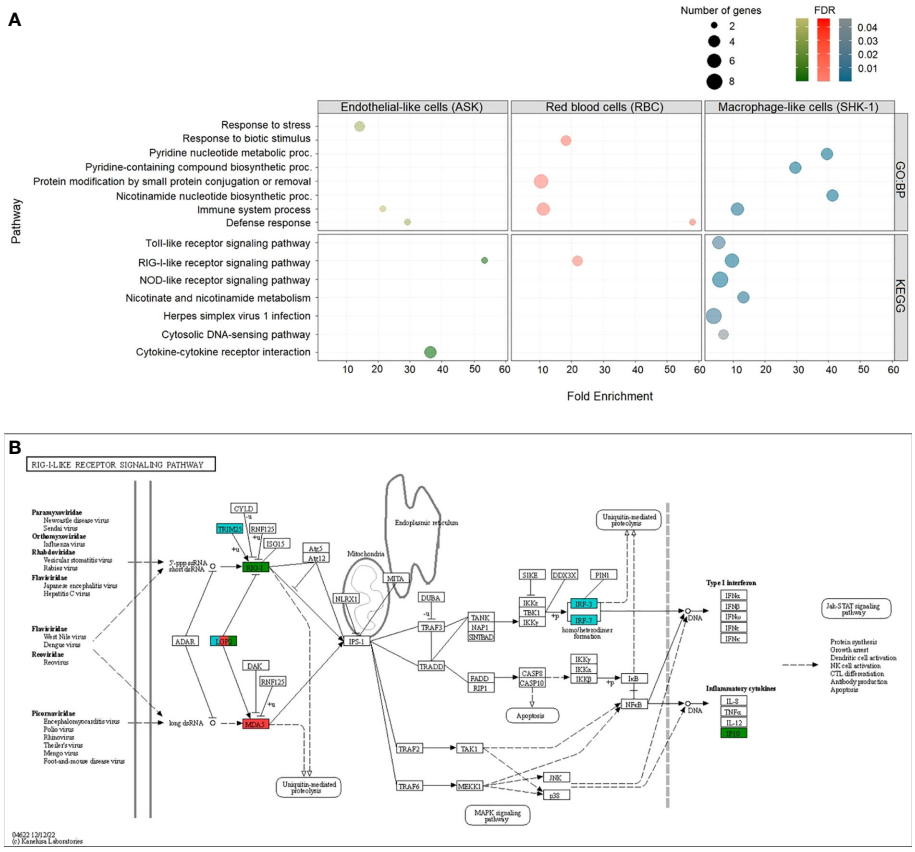

FIGURE 6
Up-regulated DEGs (cutoff ≥ 2-fold change) in ASK, RBC and SHK-1 exposed to PRV-1. Enriched Gene Ontology (GO) terms within the GO category "Biological Process" (GO : BP) and Kyoto Encyclopedia of Genes and Genomes (KEGG) pathways with FDR (adjusted p value) lower than 0.05 were considered significant. **(A)** GO : BP (top) and KEGG pathways (bottom) enriched in ASK (green), RBC (red) and SHK-1 (blue). **(B)** Representation of KEGG pathway:"RIG-I-like receptor signaling pathway"-sasa04622, as significantly enriched in RBC, ASK and SHK-1. Genes involved in pathway and significantly induced in RBC, ASK and SHK-1 exposed to PRV-1 were annotated in red, green and blue, respectively.

[also referred to as laboratory of genetics and physiology 2 (*LGP2*)], melanoma differentiation-associated protein 5 (*MDA5*) and transcription factors involved in *type I IFN*-pathway activation, *IRF1-2* and *IRF1*. From the GO terms that appeared for ASK, biological functions associated with response to stress showed the greatest representation, while groups "Immune system process" and "Defense response" consisted of only two significantly expressed genes, one of which was *RLR3*. Other significantly induced genes in SHK-1 were primarily involved in metabolic functions associated with the formation of nicotinamide-adenine dinucleotide phosphate, such as "Pyridine nucleotide metabolic process", "Pyridine-containing compound" and "Nicotinamide nucleotide" biosynthetic processes. The GO : BP term "Immune system process" was also significantly enriched for SHK-1, including genes such as the dsRNA receptors *RLR3* and *TLR3*, and the antiviral effectors, *UBIL* and *Mx2*. A detailed description of GO terms in RBC, ASK and SHK-1 is provided in Supplementary File D.

KEGG analysis revealed one category, "RIG-I-like receptor signaling pathway"- sasa04622, which was significantly enriched in RBC, ASK and SHK-1. This category consists of genes involved in immune pathways activated upon binding of dsRNA to RLRs, including the *RLR3* gene (referred to as *LGP2* in the pathway). The cytosolic dsRNA receptor *MDA5* gene was induced only in RBC, and the *RLR1* gene was induced only in ASK (Figure 6B). In SHK-1, the tripartite motif-containing protein 25 (*TRIM25*) gene, *IRF3* and *IRF7* in this pathway was also significantly induced (Figure 6B). In contrast to RBC, genes significantly induced in SHK-1 were categorized in five more groups, four of which are involved in innate immunity (such as "Toll like receptor" and "NOD-like receptor" signaling pathways), while significantly induced genes in ASK were categorized in one additional group, associated with cytokine- cytokine interaction (Figure 6A).

Given the outcome of the differential expression analysis, GO and KEGG pathway enrichment analyses, 24 h exposure of RBC to PRV-1 triggered the activation of PRRs that recognize viral dsRNA (*MDA5* and *RLR3* induction) and signaling factors that regulate the secretion of IFNs and pro-inflammatory cytokines. To better understand the immune responses occurring in RBC after PRV-1 exposure, compared to non- susceptible kidney cell lines, we focused on genes typically involved in dsRNA viral recognition, signal transduction, *IFN*-pathway activation, and virus eradication. The comparison of the immune transcriptome responses of RBC to SHK-1 showed that SHK-1 respond more potently to PRV-1 than RBC by significantly inducing the expression of a wider repertoire

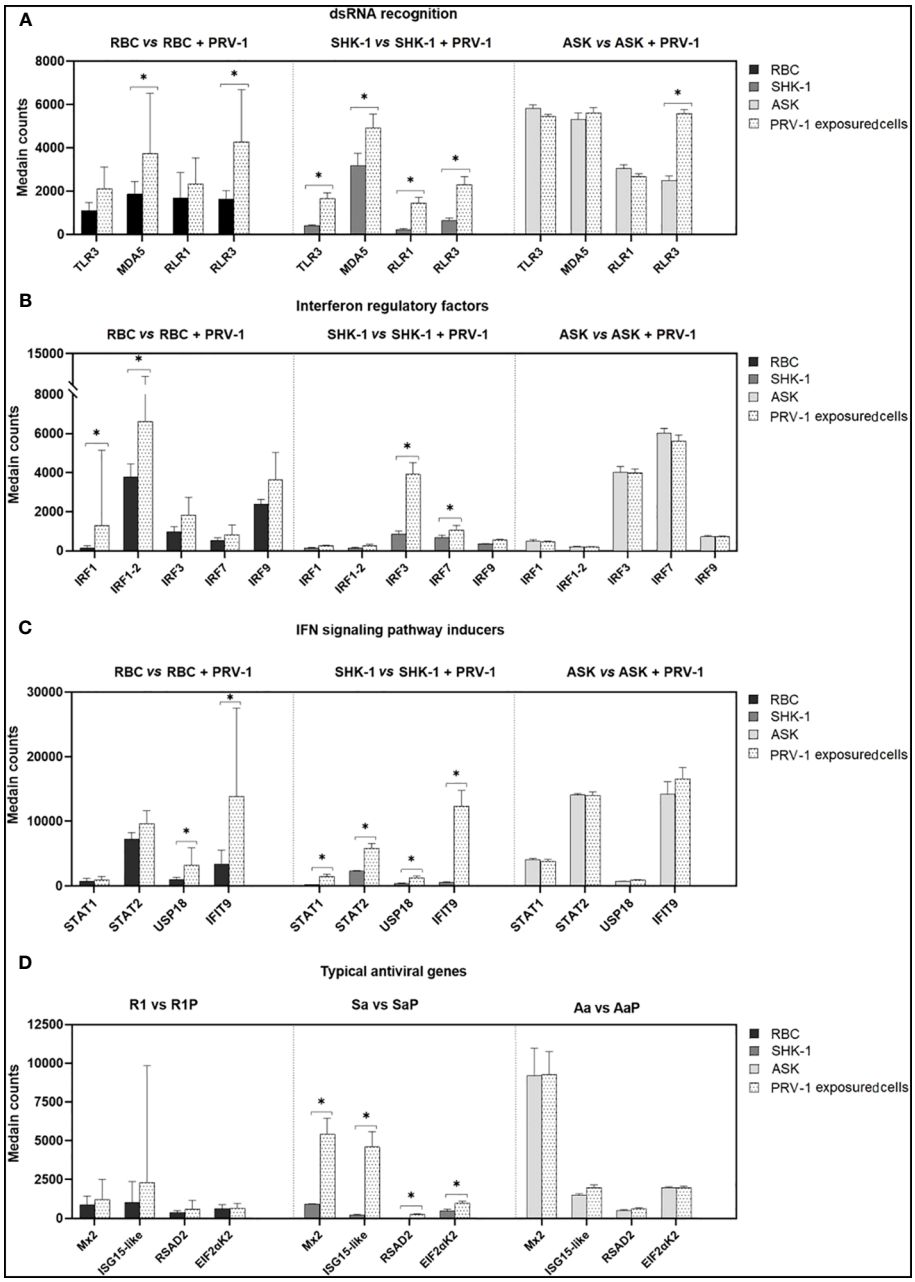

FIGURE 7
Comparison of the transcriptome responses linked to selected innate antiviral genes in RBC, SHK-1 and ASK exposed to PRV-1 (RBC vs RBC + PRV-1, SHK-1 vs SHK-1 + PRV-1 and ASK vs ASK + PRV-1, respectively). Regulation of **(A)** dsRNA pattern recognition receptors, **(B)** interferon regulatory factors, **(C)** genes involved in *IFN*-signaling patway activation and **(D)** IFN-inducible antiviral effectors. RBC vs PRV-1, n=6, SHK-1 vs PRV-1 and ASK vs PRV-1, n=3. *p<0.05.

of dsRNA pattern recognition receptors and typical antiviral genes. On the contrary, the comparison of RBC to ASK showed that ASK induced *RLR3*, while other typical antiviral responses were absent (Figure 7).

4 Discussion

The present transcriptional analysis showed that genes with the highest expression levels in RBC are primarily involved in respiratory processes, including multiple hemoglobins and mediators of heme biosynthesis. This is consistent with the traditional physiological characteristics of RBC as gas exchangers (3). Previous multi-omics analyses of salmonid RBC in response to viral infection revealed the expression of several genes involved in different aspects of immunity, including antigen presentation through MHC I and MHC II (8, 47). Current transcriptomic data indicated exceedingly high basal levels of the MHC I- associated protein- encoding genes, such as *UBA* and *UGA* genes, supporting A. salmon RBC role in innate immunity. Earlier characterization of

UBA and *UGA* genes in rainbow trout leukocytes and lymphoid organs showed induced gene expression in response to viral infection (48). However, this was not the case in A. salmon RBC exposed to PRV-1 for 24 h, for which the short period of exposure to the virus may be a possible explanation.

The number of genes expressed in RBC in resting state was at comparable level as in ASK and SHK-1 cell lines, indicating that RBC are multifunctional. Although sets of genes involved in regulation of cellular homeostasis and survival (e.g. RNA processing and protein biosynthesis) showed similar expression patterns in all three cell types, genes associated with physiological functions which promote intracellular transport (e.g. endocytosis and nucleocytoplasmic transport) and molecule degradation (e.g. ubiquitin mediated proteolysis and autophagy) appeared to be more highly expressed in RBC. In contrast, genes essential for cellular structural integrity and differentiation, such as keratins (type I or II), serpines and cofilins, showed low transcription levels in RBC, while being more prominent in both kidney cell lines. Entry of PRV-1 into RBC have been predicted to occur via receptor-mediated endocytosis through *in silico* comparison of PRV proteins with MRV, for which viral uptake mechanisms are well characterized (49). In this sense, higher expression levels of genes involved in intracellular transport in RBC compared to non-susceptible ASK and SHK-1, may be linked to differences in uptake mechanisms. No genes involved in endocytic processes in RBC were significantly induced in response to 24 h-exposure to PRV-1.

Genes involved in signaling pathways triggered by viral invasion were expressed in RBC as well as ASK and SHK-1, confirming that RBC possess innate immune functions, as previously published (2, 5, 8, 47). Notably, the basal expression of genes associated with antiviral defense was more distinguished in RBC, compared to genes involved in responses to bacteria, indicating that RBC exhibit higher sensitivity to viruses.

Innate immunity represents the first line of host defense against invading pathogens, the recognition of which is mediated by PRRs (36, 50). Interestingly, RBC express a wide repertoire of PRRs, some of which have not been reported in salmonid erythrocytes earlier and that are able to detect pathogen-associated molecular patterns (PAMPs) derived from viruses and other pathogens. *TLR8* and *NLRC3- like* receptor genes appeared among the most highly expressed. Earlier studies on PRR signaling in fish showed that *TLR8* and *NLRC3-like* receptors trigger inflammatory responses through *MyD88-* and *NOD1/RIP2-* dependent signaling pathways upon recognition of synthetic ssRNA oligonucleotides and bacterial cell wall components, respectively (38, 42). The ability of salmonid RBC to manifest innate immune responses has most extensively been studied in response to RNA viruses (8, 47, 51) and there are few reports that demonstrate their immune responses to bacterial and parasites (51, 52). Although the gene expression of microbial-specific PRRs alone should not be considered indicative for their functional role, it may strengthen the notion of RBC as contributors to innate immunity against a broad range of infectious agents.

It is worth noting that various DEAD/H- box RNA helicases, recently characterized for their diverse roles in antiviral immunity in fish and mammals, were largely detected in RBC transcriptome (41, 53). Herein, *MDA5* and *RLR3* are reported in A. salmon RBC for the first time. Together with *RLR1*, these genes belong to the RLR family. Teleost RLRs, like in mammals, bind dsRNA viruses, and subsequently induce the activation of *type I IFN* signaling pathway and secretion of pro-inflammatory cytokines (53, 54). Previous transcriptional studies reported significant upregulation of *RLR1* in PRV-1 infected A. salmon, and *MDA5* and *RLR3* in viral hemorrhagic septicemia virus (VHSV) infected rainbow trout RBC (8, 22, 47).

RBC express multiple transcriptional activators that are essential for dsRNA-PRRs signaling, including several IRFs. For instance, binding of dsRNA to the cytosolic RNA sensors *RLR1* or *MDA5* leads to the activation of interferon promoter stimulating protein- 1 (*IPS* or *MAVS*). This activator, in association with TNF receptor- associated factor 3 (*TRAF3*) and TANK-binding kinase 1 (*TBK-1*), phosphorylates/activates *IRF3/7*, which potentiate the transcription of pro-inflammatory cytokines and IFNs (46, 53, 54). *TLR3*, similar to RLRs, is known to interact with TIR domain-containing adaptor (*TRIF* or *TICAM1*) to regulate the secretion of IFNs through the nuclear factor kappa B (*NF-κB*)- and *IRF3/7* - dependent signaling pathways (55). In general, secreted *IFN* and cytokines, in turn, bind to transmembrane *IFN*/cytokine receptors, and trigger the expression of IFN- stimulated genes by means of recruiting kinases and transcription factors, such as *JAK*, *STAT1/2*, *IRF9* and/or *IRF1* (53–55). The identification of genes corresponding to such complete signaling pathways in RBC transcriptome not only reinforces RBC characterization as immune mediators, but also contributes to our original hypothesis that they regulate multiple immune functions through both well characterized and unexplored signaling pathways in salmonid RBC.

A rather intriguing finding was the expression of several interleukin (IL) and chemokine receptors in A. salmon RBC, but only a few of the corresponding cytokines were expressed. As in mammals, fish cytokines are secreted by many cell types and involved in cell-to-cell communication though an endocrine and/or paracrine manner (56, 57). The expression of pro-inflammatory IL receptor subunits, such as *IL6R* and *IL1R*, may imply immune activation of RBC upon binding to *IL1* and *IL6*, secreted by other immune cells. Fish and mammalian *IL10* and *IL10R* regulate anti-inflammatory functions, a feature that suggests involvement in mechanisms of viral persistence (58). Since RBC express *IL10R*, they may participate in processes related to such mechanism, for example in the persistent phase of PRV-1 infection (59). In contrast to rainbow trout RBC, which were shown to express *IL1β*, *IL8* and *IFNγ* in response to infectious hematopoietic necrosis virus (IHNV) and thermal stress, A. salmon RBC demonstrated high transcript levels of only *IL15* and *IL34* (7, 36). Studies on the characterization of *IL15* in rainbow trout suggested its involvement in CD4+ T cell survival, where it induces *IFNγ* through a *STAT5p*-dependent signaling pathway (60, 61). The function of *IL34* is modestly explored in salmonids. However, in recent studies in fresh water fish species such as Largemouth bass (*Micropterus salmoides*) and grass carp (*Ctenopharyngodon idella*), *IL34* was suggested to be involved in macrophage activation (62, 63).

The comparison of RBC to ASK and SHK-1 revealed sets of genes, which were exclusively expressed in RBC, and involved in

innate/adaptive immune processes and chemotaxis. This supports the multifunctional nature of RBC, while providing insight into their unique immunological features. Indicatively, among the wide assortment of IRFs identified in the total transcriptome, *IRF4* expression appeared only in RBC. Earlier characterization of IRFs in A. salmon showed that *IRF4*, similar to its mammalian counterpart, inhibits *IFN* production (64). Additional immunosuppressive effects on RBC may be mediated by *IL1R2*, which have been shown to compete with *IL1* for binding *IL1Ra* in seabream (*Sparus aurata*) and grass carp (*Ctenopharyngodon idellus*) (65, 66). In mammals, *CCR9* is distributed on the surface of intestine cells where it binds its specific ligand *CCL25*. In both mammals and teleost, upregulation of *CCL25* in gut has been associated with infiltration of *CCR9*- expressing inflammatory cells (67, 68). The expression of *CCR9* in RBC may indicate that, similarly to immature T-lymphocytes, they may migrate into tissues expressing *CCL25* ligand. Mammalian C-C chemokine 4 (*CCL4*) is commonly expressed in different antigen- presenting cells (APC), and *CCL4* regulation has only recently been studied in fish (57, 69, 70). Functional characterization of *CCL4* in orange- spotted grouper (*Epinephelus coioides*) showed that recombinant *CCL4* exhibits chemotactic activity, attracting leukocytes, such as macrophages and NK-cells, and stimulating lymphocyte differentiation (71); thus, the role of *CCL4* was suggested to be conserved in teleost and mammals (69, 71). Since A. salmon RBC express *CCL4*, they may be involved in inflammatory responses by recruiting macrophages and NK-cells and/or triggering lymphocyte differentiation. Although, it is hard to assume the role and involvement of these cytokines and cytokine receptors in the immune functions of RBC, hypotheses regarding the possible migration of RBC into inflammatory tissue like other circulating immune cells could represent an open and interesting field of study.

A few immune genes were significantly induced in RBC 24 h after PRV-1 encounter. Most DEGs are involved in dsRNA recognition and subsequent signal transduction via IRFs, but *type I IFN* and IFN- stimulated genes were not found induced. In contrast, several genes implicated in RNA virus recognition and antiviral defense were significantly expressed in SHK-1, while remaining at basal levels in ASK. Previous transcriptional analysis of ASK cells in response to synthetic dsRNA analogue, poly(I:C), revealed significant induction of the RNA-specific PRRs genes *MDA5* and *RLR3*, and antiviral effectors genes, such as *type I IFN* and *Mx1* and *ISG15*, 12 h post stimulation (72). This suggests that despite the ability of ASK to respond to naked dsRNA, the processes associated with ligand recognition and initiation of immune defense may differ in response to purified virus. To date, recognition of PRV-1 in RBC has primarily been associated with the induction of endosomal *TLR3* and cytosolic *RLR1* (6, 8). Our data, however, showed upregulation of the *MDA5* and *RLR1* genes after 24 h-exposure to the virus. Several putative PRR- genes for RNA viruses were significantly induced in SHK-1, including *TLR3*, *RLR1*, *MDA5* and *RLR3*, whereas only *RLR3* was induced in ASK. PRV-1 propagation is not supported by SHK-1, and the upregulation of many genes involved in a range of different antiviral pathways in response to virus, may be a possible explanation. Interestingly, the *RLR3* gene was significantly induced in all PRV-exposed cells. In contrast to *RLR1* and *MDA5*, the role of *RLR3* in antiviral immunity in fish cells is poorly understood. In mammals, *RLR3* is associated with both positive and negative contribution to antiviral signaling in a concentration- dependent manner. *RLR3*, when at low levels, functions synergistically with *MDA5*, and thereby enhance *MDA5*-mediated antiviral signaling. Oppositely, *RLR3* at high expression levels competes with *RLR1* and *MDA5* for dsRNA viral recognition and suppresses RLR signaling pathway by inhibiting receptor interaction with the *IPS* activator (73). In teleost, *RLR3* has mainly been associated with positive regulation of antiviral signaling; its expression was linked to significant induction of antiviral effectors, such as *Mx*, in rainbow trout, and decrease of grass carp reovirus (GCRV) and spring viremia of carp virus (SVCV) titers in black carp (*Mylopharyngodon Piceus*) *in vitro* (40, 74). In contrast to mammals, functional characterization of *RLR3* in fish did not show suppression or synergy with *MDA5*, but rather a parallel function (40). Relative expression of *RLR3* in A. salmon RBC, ASK and SHK-1 in response to PRV-1 do not provide sufficient evidence for its putative function. However, its significant induction may indicate a pivotal contribution to viral recognition and the following antiviral events in the cell.

As mentioned above, *MDA5* activation is commonly followed by the transcriptional activity of *IRF3* and/or *IRF7* (53, 75). Induction of these IRF genes has previously been reported in salmonid erythrocytes at later stages of PRV-1 infection *in vivo* (8). Here, only *IRF1* was significantly upregulated, whereas there was not significant induction of *IRF3* and *IRF7* in response to PRV-1. *IRF1* has been shown to actively participate in induction of IFN and ISG transcription as a response to RNA viruses in mammals and fish (46, 76). As opposed to RBC, ASK and SHK-1 expressed low levels of *IRF1* both pre- and post- exposure to PRV-1. In contrast, the expression of *IRF3* and *IRF7* was significantly induced in SHK-1 after PRV-1 exposure, while expressed at constitutively high levels in ASK. Previous investigation of IRF involvement in antiviral defense in mammals revealed that *IRF1* may function independently of *IRF3/IRF7* (77). Considering that RBC is the only cell type susceptible to PRV-1, the low activation of *IRF3/7* and strong induction of *IRF1* in RBC could represent a difference associated with antiviral responsiveness to PRV-1.

The entry of PRV into RBC likely occur through endosomal uptake, as its mammalian counterpart MRV (78). This process leads to virion disassembly at late endosomes and release of transcriptionally active viral core particles into the cytoplasm that subsequently produce capped, but not poly- adenylated ssRNA copies (79). Interferon-induced protein with tetratricopeptide repeats 5-like (*IFIT9*, also referred to as IFIT5 in rainbow trout) and ubl carboxyl-terminal hydrolase 18-like (*USP18*) have been implicated in inhibition of VHSV replication and negative regulation of immune responses mediated by type I IFN, respectively (80, 81). Both *IFIT9* and *USP18* were significantly upregulated in RBC, which in correlation with the expression profile of PRRs and IRFs, may be indicative of viral status in the cells. Complementary to this, no induction of typical antiviral genes, such as *Mx*, interferon-stimulated gene 15- like (*UBIL*), *PKR* (referred to as *EIF2aK2*) and viperin-like (*RSAD2*), which have previously been found upregulated in PRV-1 infected RBC *in vivo*, was observed after a 24 h viral stimulation of

RBC (8). In contrast, SHK-1 responded to PRV-1 by inducing the expression of several IFN-inducible genes and their corresponding transcription factors (e.g. *STAT1/2* that regulates *Mx* and *ISG15* transcription) significantly. Typical antiviral response genes highly expressed in SHK-1 but not in RBC, such as *Mx2* and *ISG15-like*, may play a role in the successful eradication of the virus (72, 80, 82, 83). The comparison, however, of RBC to ASK showed that no typical antiviral responses were observed in ASK. Instead, pro-inflammatory cytokines *IL-11* and *CXCL10* were significantly induced. These findings may indicate that ASK cells lack viral uptake and sufficient sensing of viral RNA, whereas SHK-1 cells may take up PRV, respond, but inhibit viral replication more efficiently by strong antiviral responses. The antiviral response in RBC may be delayed compared to the SHK-1 response, which might favor the replication of the virus.

In conclusion, the present transcriptional analysis supports previous characterization of RBC as multifunctional cells with both physiological and immunological properties. In contrast to ASK and SHK-1 cells, RBC showed higher expression levels of genes related to endocytosis and intracellular transport and uniquely expressed *CCL4* and *CCR9* genes, suggesting putative chemotactic activity and an ability to recruit immune cells. Exposure of RBC to PRV-1 for 24 h induced a typical antiviral response of intermediate strength, stronger than in ASK cells, but possibly delayed compared to responses in SHK-1. A difference in IRF gene induction (*IRF1* in RBC, *IRF3/7* in SHK-1 cells) may affect the antiviral response pathway and allow onset of PRV-1 replication in RBC.

Data availability statement

The original contributions presented in the study are publicly available. This data can be found here: NCBI SRA BioProject- PRJNA1028935, https://www.ncbi.nlm.nih.gov/bioproject/PRJNA1028935.

Ethics statement

The animal study was approved by Norwegian Animal Research Authority/Norwegian University of Life Sciences Aquatic facility. The study was conducted in accordance with the local legislation and institutional requirements.

Author contributions

TT: Data curation, Formal Analysis, Investigation, Methodology, Validation, Visualization, Writing – original draft, Writing – review & editing, Software. AYMS: Data curation, Formal Analysis, Methodology, Supervision, Validation, Visualization, Writing – original draft, Writing – review & editing, Software. SB: Formal Analysis, Methodology, Validation, Writing – review & editing. JBJ: Investigation, Supervision, Validation, Visualization, Writing – review & editing. ER: Conceptualization, Funding acquisition, Resources, Supervision, Validation, Writing – review & editing. ØW: Conceptualization, Formal Analysis, Funding acquisition, Investigation, Methodology, Project administration, Resources, Supervision, Validation, Writing – review & editing. MKD: Conceptualization, Data curation, Formal Analysis, Funding acquisition, Investigation, Methodology, Project administration, Resources, Supervision, Validation, Writing – original draft, Writing – review & editing.

Funding

The author(s) declare financial support was received for the research, authorship, and/or publication of this article. The research was financially supported by the Research Council of Norway, project #302551 (RED FLAG), #245286, and #301477. The funders had no role in study design, data collection and analysis, decision to publish, or preparation of the manuscript.

Acknowledgments

We thank Øyvind Haugland at PHARMAQ/Zoetis, leader of NRC project #245286 (HSMI- CMS- Vacc) for facilitating RNAseq planning and Randi Faller for helping with the RNA extraction/quality control. We thank Kanehisa Laboratories for providing permission to modify the KEGG pathways sasa05168 and sasa046221. Figure 4 was created and licensed by BioRender.

Conflict of interest

The authors declare that the research was conducted in the absence of any commercial or financial relationships that could be construed as a potential conflict of interest.

Publisher's note

Supplementary material

The Supplementary Material for this article can be found online at: https://www.frontiersin.org/articles/10.3389/fimmu.2024.1359552/full#supplementary-material

References

1. Jensen FB. Red blood cell pH, the Bohr effect, and other oxygenation-linked phenomena in blood O2 and CO2 transport. *Acta Physiol Scand* (2004) 182(3):215–27. doi: 10.1111/j.1365-201X.2004.01361.x

2. Morera D, MacKenzie SA. Is there a direct role for erythrocytes in the immune response? *Vet Res* (2011) 42(1):1–8. doi: 10.1186/1297-9716-42-89

3. Anderson HL, Brodsky IE, Mangalmurti NS. The evolving erythrocyte: red blood cells as modulators of innate immunity. *J Immunol* (2018) 201(5):1343–51. doi: 10.4049/jimmunol.1800565

4. Zhu W, Su J. Immune functions of phagocytic blood cells in teleost. *Rev Aquac* (2022) 14(2):630–46. doi: 10.1111/raq.12616

5. Morera D, Roher N, Ribas L, Balasch JC, Doñate C, Callol A, et al. Rna-seq reveals an integrated immune response in nucleated erythrocytes. *PloS One* (2011) 6(10): e26998. doi: 10.1371/journal.pone.0026998

6. Wessel Ø, Krasnov A, Timmerhaus G, Rimstad E, Dahle MK. Antiviral responses and biological concequences of Piscine orthoreovirus infection in salmonid erythrocytes. *Front Immunol* (2019) 10(JAN):3182. doi: 10.3389/fimmu.2018.03182

7. Chico V, Puente-Marin S, Nombela I, Ciordia S, Mena MC, Carracedo B, et al. Shape-shifted red blood cells: A novel red blood cell stage? *Cells* (2018) 7(4):31. doi: 10.3390/cells7040031

8. Dahle MK, Wessel Ø, Timmerhaus G, Nyman IB, Jørgensen SM, Rimstad E, et al. Transcriptome analyses of Atlantic salmon (Salmo salar L.) erythrocytes infected with piscine orthoreovirus (PRV). *Fish Shellfish Immunol* (2015) 45(2):780–90. doi: 10.1016/j.fsi.2015.05.049

9. Ji P, Murata-Hori M, Lodish HF. Formation of mammalian erythrocytes: Chromatin condensation and enucleation. *Trends Cell Biol* (2011) 21(7):409–15. doi: 10.1016/j.tcb.2011.04.003

10. Shen Y, Wang D, Zhao J, Chen X. Fish red blood cells express immune genes and responses. *Aquac Fish* (2018) 3(1):14–21. doi: 10.1016/j.aaf.2018.01.001

11. Puente-Marin S, Nombela I, Ciordia S, Mena MC, Chico V, Coll J, et al. In silico functional networks identified in fish nucleated red blood cells by means of transcriptomic and proteomic profiling. *Genes (Basel)* (2018) 9(4):202. doi: 10.3390/genes9040202

12. Sommerset I, Wiik-Nielsen J, Oliveira VHS, Moldal T, Bornø G, Haukaas A, et al. *Norwegian Fish Health Report 2022, Norwegian Veterinary Institute Report, series #5a/2023*, published by the Norwegian Veterinary Institute (2023).

13. Kongtorp RT, Taksdal T, Lyngøy A. Pathology of heart and skeletal muscle inflammation (HSMI) in farmed Atlantic salmon Salmo salar. *Dis Aquat Organ* (2004) 59(3):217–24. doi: 10.3354/dao059217

14. Palacios G, Lovoll M, Tengs T, Hornig M, Hutchison S, Hui J, et al. Heart and skeletal muscle inflammation of farmed salmon is associated with infection with a novel reovirus. *PloS One* (2010) 5(7):3–9. doi: 10.1371/journal.pone.0011487

15. Finstad ØW, Falk K, Løvoll M, Evensen Ø, Rimstad E. Immunohistochemical detection of piscine reovirus (PRV) in hearts of Atlantic salmon coincide with the course of heart and skeletal muscle inflammation (HSMI). *Vet Res* (2012) 43(1):1–11. doi: 10.1186/1297-9716-43-27

16. Wessel Ø, Braaen S, Alarcon M, Haatveit H, Roos N, Markussen T, et al. Infection with purified Piscine orthoreovirus demonstrates a causal relationship with heart and skeletal muscle inflammation in Atlantic salmon. *PloS One* (2017) 12(8): e0183781. doi: 10.1371/journal.pone.0183781

17. Markussen T, Dahle MK, Tengs T, Løvoll M, Finstad ØW, Wiik-Nielsen CR, et al. Sequence analysis of the genome of piscine orthoreovirus (PRV) associated with heart and skeletal muscle inflammation (HSMI) in Atlantic Salmon (Salmo salar). *PloS One* (2013) 8(7):e70075. doi: 10.1371/journal.pone.0070075

18. Finstad ØW, Dahle MK, Lindholm TH, Nyman IB, Løvoll M, Wallace C, et al. Piscine orthoreovirus (PRV) infects Atlantic salmon erythrocytes. *Vet Res* (2014) 45 (1):1–13. doi: 10.1186/1297-9716-45-35

19. Haatveit HM, Nyman IB, Markussen T, Wessel Ø, Dahle MK, Rimstad E. The non-structural protein μnS of piscine orthoreovirus (PRV) forms viral factory-like structures. *Vet Res* (2016) 47(1):1–11. doi: 10.1186/s13567-015-0302-0

20. Haatveit HM, Wessel Ø, Markussen T, Lund M, Thiede B, Berg Nyman I, et al. Viral protein kinetics of piscine orthoreovirus infection in Atlantic Salmon blood cells. *Viruses* (2017) 9(3):49. doi: 10.3390/v9030049

21. Wessel Ø, Hansen EF, Dahle MK, Alarcon M, Vatne NA, Nyman IB, et al. Piscine orthoreovirus-1 isolates differ in their ability to induce heart and skeletal muscle inflammation in atlantic salmon (Salmo salar). *Pathogens* (2020) 9(12):1–22. doi: 10.3390/pathogens9121050

22. Wessel Ø, Olsen CM, Rimstad E, Dahle MK. Piscine orthoreovirus (PRV) replicates in Atlantic salmon (Salmo salar L.) erythrocytes ex vivo. *Veterinary Res* (2015) 46:1–11. doi: 10.1186/s13567-015-0154-7

23. Devold M, Krossøy B, Aspehaug V, Nylund A. Use of RT-PCR for diagnosis of infectious salmon anaemia virus (ISAV) in carrier sea trout Salmo trutta after experimental infection. *Dis Aquat Organ* (2000) 40(1):9–18. doi: 10.3354/dao040009

24. Dannevig BH, Brudeseth BE, Gjøen T, Rode M, Wergeland HI, Evensen, et al. Characterisation of a long-term cell line (SHK-1) developed from the head kidney of Atlantic salmon (Salmo salar L.). *Fish Shellfish Immunol* (1997) 7(4):213–26. doi: 10.1006/fsim.1996.0076

25. Pham PH, Misk E, Papazotos F, Jones G, Polinski MP, Contador E, et al. Screening of fish cell lines for piscine orthoreovirus-1 (PRV-1) amplification: Identification of the non-supportive PRV-1 invitrome. *Pathogens* (2020) 9(10):1–25. doi: 10.3390/pathogens9100833

26. Bushnell B. *BBTools software package*. (2014).

27. Kim D, Paggi JM, Park C, Bennett C, Salzberg SL. Graph-based genome alignment and genotyping with HISAT2 and HISAT-genotype. *Nat Biotechnol* (2019) 37(8):907–15. doi: 10.1038/s41587-019-0201-4

28. Liao Y, Smyth GK, Shi W. FeatureCounts: An efficient general purpose program for assigning sequence reads to genomic features. *Bioinformatics* (2014) 30(7):923–30. doi: 10.1093/bioinformatics/btt656

29. Love MI, Huber W, Anders S. Moderated estimation of fold change and dispersion for RNA-seq data with DESeq2. *Genome Biol* (2014) 15(12):1–21. doi: 10.1186/s13059-014-0550-8

30. Varet H, Brillet-Guéguen L, Coppée JY, Dillies MA. SARTools: A DESeq2- and edgeR-based R pipeline for comprehensive differential analysis of RNA-Seq data. *PloS One* (2016) 11(6):1–8. doi: 10.1371/journal.pone.0157022

31. Ge SX, Jung D, Jung D, Yao R. ShinyGO: A graphical gene-set enrichment tool for animals and plants. *Bioinformatics* (2020) 36(8):2628–9. doi: 10.1093/bioinformatics/btz931

32. Luo W, Brouwer C. Pathview: an R/Bioconductor package for pathway-based data integration and visualization. *Bioinformatics* (2013) 29(14):1830–1. doi: 10.1093/bioinformatics/btt285

33. Kanehisa M, Furumichi M, Sato Y, Ishiguro-Watanabe M, Tanabe M. KEGG: Integrating viruses and cellular organisms. *Nucleic Acids Res* (2021) 49(D1):D545–51. doi: 10.1093/nar/gkaa970

34. Tchaikovskii V, Desnick RJ, Bishop DF. Molecular expression, characterization and mechanism of ALAS2 gain-of-function mutants. *Mol Med* (2019) 25(1):4. doi: 10.1186/s10020-019-0070-9

35. Duff MR, Redzic JS, Ryan LP, Paukovich N, Zhao R, Nix JC, et al. Structure, dynamics and function of the evolutionarily changing biliverdin reductase B family. *J Biochem* (2021) 168(2):191–202. doi: 10.1093/jb/mvaa039

36. Dahle MK, Jørgensen JB. Antiviral defense in salmonids – Mission made possible? *Fish Shellfish Immunol* (2019) 87(October 2018):421–37. doi: 10.1016/j.fsi.2019.01.043

37. Buchmann K, Secombes CJ. Principles of fish immunology. *Principles Fish Immunol* (2022). doi: 10.1007/978-3-030-85420-1

38. Skjaeveland I, Iliev DB, Strandskog G, Jørgensen JB. Identification and characterization of TLR8 and MyD88 homologs in Atlantic salmon (Salmo salar). *Dev Comp Immunol* (2009) 33(9):1011–7. doi: 10.1016/j.dci.2009.04.007

39. Palti Y. Toll-like receptors in bony fish: From genomics to function. *Dev Comp Immunol* (2011) 35(12):1263–72. doi: 10.1016/j.dci.2011.03.006

40. Chang M, Collet B, Nie P, Lester K, Campbell S, Secombes CJ, et al. Expression and functional characterization of the RIG-I-like receptors MDA5 and LGP2 in Rainbow trout (Oncorhynchus mykiss). *J Virol* (2011) 85(16):8403–12. doi: 10.1128/JVI.00445-10

41. Songying PV, Ouyang S. *Diverse roles of DEAD/DEAH- box helicases in innate immunity and deseases*. In *Helicases from All Domains of Life*. Academic Press (2019) pp. 141–171.

42. Chang MX, Xiong F, Wu XM, Hu YW. The expanding and function of NLRC3 or NLRC3-like in teleost fish: Recent advances and novel insights. *Dev Comp Immunol* (2021) 114(August 2020):103859. doi: 10.1016/j.dci.2020.103859

43. Xu C, Evensen Ø, Munang'andu HM. *De novo* assembly and transcriptome analysis of Atlantic salmon macrophage/dendritic-like TO cells following type I IFN treatment and Salmonid alphavirus subtype-3 infection. *BMC Genomics* (2015) 16 (1):1–16. doi: 10.1186/s12864-015-1302-1

44. Fang H, Wu XM, Hu YW, Song YJ, Zhang J, Chang MX. NLRC3-like 1 inhibits NOD1-RIPK2 pathway via targeting RIPK2. *Dev Comp Immunol* (2020) 112 (May):103769. doi: 10.1016/j.dci.2020.103769

45. Magalhaes JG, Sorbara MT, Girardin SE, Philpott DJ. What is new with nods? *Curr Opin Immunol* (2011) 23(1):29–34. doi: 10.1016/j.coi.2010.12.003

46. Bergan V, Kileng Ø, Sun B, Robertsen B. Regulation and function of interferon regulatory factors of Atlantic salmon. *Mol Immunol* (2010) 47(11–12):2005–14. doi: 10.1016/j.molimm.2010.04.015

47. Nombela I, Lopez-Lorigados M, Salvador-Mira ME, Puente-Marin S, Chico V, Ciordia S, et al. Integrated transcriptomic and proteomic analysis of red blood cells from rainbow trout challenged with VHSV point towards novel immunomodulant targets. *Vaccines* (2019) 7(3):63. doi: 10.3390/vaccines7030063

48. Landis ED, Purcell MK, Thorgaard GH, Wheeler PA, Hansen JD. Transcriptional profiling of MHC class I genes in rainbow trout infected with infectious hematopoietic necrosis virus. *Mol Immunol* (2008) 45(6):1646–57. doi: 10.1016/j.molimm.2007.10.003

49. Dahle M, Wessel Ø, Rimstad E. Immune response against piscine orthoreovirus (PRV) in salmonids. In *Principles of Fish Immunology: From Cells and Molecules to Host Protection*. Cham: Springer International Publishing (2022) pp. 445–461.

50. Rebl A, Goldammer T. Under control: The innate immunity of fish from the inhibitors' perspective. *Fish Shellfish Immunol* (2018) 77(February):328–49. doi: 10.1016/j.fsi.2018.04.016

51. Puente-Marin S, Thwaite R, Mercado L, Coll J, Roher N, Ortega-Villaizan MD. Fish red blood cells modulate immune genes in response to bacterial inclusion bodies made of TNFα and a G-VHSV fragment. *Front Immunol* (2019) 10:1055. doi: 10.3389/fimmu.2019.01055

52. Chan JT, Picard-Sanchez A, Majstorović J, Rebl A, Koczan D, Dyčka F, et al. Red blood cells in proliferative kidney disease—rainbow trout (Oncorhynchus mykiss) infected by Tetracapsuloides bryosalmonae harbor IgM+ red blood cells. *Front Immunol* (2023) 14(February):1–15. doi: 10.3389/fimmu.2023.1041325

53. Mojzesz M, Rakus K, Chadzinska M, Nakagami K, Biswas G, Sakai M, et al. Cytosolic sensors for pathogenic viral and bacterial nucleic acids in fish. *Int J Mol Sci* (2020) 21(19):1–33. doi: 10.3390/ijms21197289

54. Chen SN, Zou PF, Nie P. Retinoic acid-inducible gene I (RIG-I)-like receptors (RLRs) in fish: current knowledge and future perspectives. *Immunology* (2017) 151 (1):16–25. doi: 10.1111/imm.12714

55. Alexopoulou L, Holt A, Medzhitov R, Flavell R. Recognition of double-stranded RNA and activation of NF-kappaB by Toll. *Nature* (2001) 413(6857):732–8. doi: 10.1038/35099560

56. Sakai M, Hikima Ji, Kono T. Fish cytokines: current research and applications. *Fish Sci* (2021) 87(1):1–9. doi: 10.1007/s12562-020-01476-4

57. Bird S, Tafalla C. Teleost chemokines and their receptors. *Biol (Basel)* (2015) 4 (4):756–84. doi: 10.3390/biology4040756

58. Wilson EB, Brooks DG. The role of IL-10 in regulating immunity to persistent viral infections. *Curr Topics Microbiol Immunol* (2010) 350:39–65. doi: 10.1007/82_2010_96

59. Kannimuthu D, Roh H, Peñaranda MM, Wessel Ø, Mæhle S, Berhe GD, et al. Long-term persistence of piscine orthoreovirus-1 (PRV-1) infection during the pre-smolt stages of Atlantic salmon in freshwater. *Vet Res* (2023) 54(1):69. doi: 10.1186/s13567-023-01201-w

60. Yamaguchi T, Chang CJ, Karger A, Keller M, Pfaff F, Wangkahart E, et al. Ancient cytokine interleukin 15-like (IL-15L) induces a type 2 immune response. *Front Immunol* (2020) 11(October):1–30. doi: 10.3389/fimmu.2020.549319

61. Maisey K, Montero R, Corripio-Miyar Y, Toro-Ascuy D, Valenzuela B, Reyes-Cerpa S, et al. Isolation and characterization of salmonid CD4+ T cells. *J Immunol* (2016) 196(10):4150–63. doi: 10.4049/jimmunol.1500439

62. Xue Y, Jiang X, Gao J, Li X, Xu J, Wang J, et al. Functional characterisation of interleukin 34 in grass carp Ctenopharyngodon idella. *Fish Shellfish Immunol* (2019) 92 (April):91–100. doi: 10.1016/j.fsi.2019.05.059

63. Hoang HH, Wang PC, Chen SC. Interleukin 34 serves as a novel molecular adjuvant against nocardia seriolae infection in largemouth bass (Micropterus salmoides). *Vaccines* (2020) 8(2):151. doi: 10.3390/vaccines8020151

64. Clark TC, Boudinot P, Collet B. Evolution of the IRF family in salmonids. *Genes (Basel)* (2021) 12(2):1–17. doi: 10.3390/genes12020238

65. López-Castejón G, Sepulcre MP, Roca FJ, Castellana B, Planas JV, Meseguer J, et al. The type II interleukin-1 receptor (IL-1RII) of the bony fish gilthead seabream Sparus aurata is strongly induced after infection and tightly regulated at transcriptional and post-transcriptional levels. *Mol Immunol* (2007) 44(10):2772–80. doi: 10.1016/j.molimm.2006.10.027

66. Yang X, Wang S, Du L, Yang K, Wang X, Zhang A, et al. Molecular and functional characterization of IL-1 receptor type 2 in grass carp: A potent inhibitor of IL-1β signaling in head kidney leukocytes. *Dev Comp Immunol [Internet]* (2013) 41 (4):738–45. doi: 10.1016/j.dci.2013.08.023

67. Wu X, Sun M, Yang Z, Lu C, Wang Q, Wang H, et al. The roles of CCR9/CCL25 in inflammation and inflammation-associated diseases. *Front Cell Dev Biol* (2021) 9 (August):1–11. doi: 10.3389/fcell.2021.686548

68. Galindo-Villegas J, Mulero I, García-Alcazar A, Muñoz I, Peñalver-Mellado M, Streitenberger S, et al. Recombinant TNFα as oral vaccine adjuvant protects European sea bass against vibriosis: Insights into the role of the CCL25/CCR9 axis. *Fish Shellfish Immunol* (2013) 35(4):1260–71. doi: 10.1016/j.fsi.2013.07.046

69. Eslamloo K, Caballero-Solares A, Inkpen SM, Emam M, Kumar S, Bouniot C, et al. Transcriptomic profiling of the adaptive and innate immune responses of Atlantic Salmon to Renibacterium salmoninarum infection. *Front Immunol* (2020) 11:567838. doi: 10.3389/fimmu.2020.567838

70. Zou J, Secombes CJ. The function of fish cytokines. *Biology* (2016) 5(2):23. doi: 10.3390/biology5020023

71. Hsu YJ, Hou CY, Lin SJ, Kuo WC, Lin HT, Lin JHY. The biofunction of orange-spotted grouper (Epinephelus coioides) CC chemokine ligand 4 (CCL4) in innate and adaptive immunity. *Fish Shellfish Immunol* (2013) 35(6):1891–8. doi: 10.1016/j.fsi.2013.09.020

72. Andresen AMS, Boudinot P, Gjøen T. Kinetics of transcriptional response against poly (I:C) and infectious salmon anemia virus (ISAV) in Atlantic salmon kidney (ASK) cell line. *Dev Comp Immunol* (2020) 110(April):103716. doi: 10.1016/j.dci.2020.103716

73. Rodriguez KR, Bruns AM, Horvath CM. MDA5 and LGP2: accomplices and antagonists of antiviral signal transduction. *J Virol* (2014) 88(15):8194–200. doi: 10.1128/JVI.00640-14

74. Xiao J, Yan J, Chen H, Li J, Tian Y, Feng H. LGP2 of black carp plays an important role in the innate immune response against SVCV and GCRV. *Fish Shellfish Immunol* (2016) 57:127–35. doi: 10.1016/j.fsi.2016.08.031

75. Nerbøvik IKG, Solheim MA, Eggestøl H, Rønneseth A, Jakobsen RA, Wergeland HI, et al. Molecular cloning of MDA5, phylogenetic analysis of RIG-I-like receptors (RLRs) and differential gene expression of RLRs, interferons and proinflammatory cytokines after in *vitro* challenge with IPNV, ISAV and SAV in the salmonid cell line TO. *J Fish Dis* (2017) 40(11):1529–44. doi: 10.1111/jfd.12622

76. Feng H, Zhang YB, Gui JF, Lemon SM, Yamane D. Interferon regulatory factor 1 (IRF1) and anti-pathogen innate immune responses. *PloS Pathog* (2021) 17(1):1–22. doi: 10.1371/journal.ppat.1009220

77. Carlin AF, Plummer EM, Vizcarra EA, Glass CK, Diamond MS, Shresta S, et al. An IRF-3-, IRF-5-, and IRF-7-independent pathway of dengue Viral Resistance Utilizes IRF-1 to Stimulate Type I and II Interferon Responses of Dengue Viral Resistance Utilizes IRF-1 to Stimulate Type I and II Interferon Responses. *Cell Rep* (2017) 21 (6):1600–12. doi: 10.1016/j.celrep.2017.10.054

78. Roth AN, Aravamudhan P, Fernández de Castro I, Tenorio R, Risco C, Dermody TS. Ins and outs of reovirus: vesicular trafficking in viral entry and egress. *Trends Microbiol* (2021) 29(4):363–75. doi: 10.1016/j.tim.2020.09.004

79. Lemay G. Synthesis and translation of viral mrna in reovirus-infected cells: Progress and remaining questions. *Viruses* (2018) 10(12):671. doi: 10.3390/v10120671

80. Chico V, Salvador-Mira ME, Nombela I, Puente-Marin S, Ciordia S, Mena MC, et al. IFIT5 participates in the antiviral mechanisms of rainbow trout red blood cells. *Front Immunol* (2019) 10(MAR):1–15. doi: 10.3389/fimmu.2019.00613

81. Hou J, Han L, Zhao Z, Liu H, Zhang L, Ma C, et al. USP18 positively regulates innate antiviral immunity by promoting K63-linked polyubiquitination of MAVS. *Nat Commun* (2021) 12(1):2970. doi: 10.1038/s41467-021-23219-4

82. Huang X, Huang Y, Cai J, Wei S, Ouyang Z, Qin Q. Molecular cloning, expression and functional analysis of ISG15 in orange-spotted grouper, Epinephelus coioides. *Fish Shellfish Immunol* (2013) 34(5):1094–102. doi: 10.1016/j.fsi.2013.01.010

83. Huang Y, Huang X, Cai J, OuYang Z, Wei S, Wei J, et al. Identification of orange-spotted grouper (*Epinephelus coioides*) interferon regulatory factor 3 involved in antiviral immune response against fish RNA virus. *Fish Shellfish Immunol* (2015) 42 (2):345–52. doi: 10.1016/j.fsi.2014.11.025

frontiers | Frontiers in Aquaculture

TYPE Original Research
PUBLISHED 14 March 2024
DOI 10.3389/faquc.2024.1306518

OPEN ACCESS

EDITED BY
Iddya Karunasagar,
Nitte University, India

REVIEWED BY
Norma Estrada,
Centro de Investigación Biológica del Noroeste (CIBNOR), Mexico
Makesh Marappan,
Central Institute of Brackishwater Aquaculture (ICAR), India

*CORRESPONDENCE
Esteban Soto
sotomartinez@ucdavis.edu

†PRESENT ADDRESS
Hali T. Jungers,
Department of Animal Care, Newport Aquarium, Newport, KY, United States

RECEIVED 03 October 2023
ACCEPTED 18 January 2024
PUBLISHED 14 March 2024

CITATION
Quijano Cardé EM, Anenson KM, Yun S, Heckman TI, Jungers HT, Henderson EE, Purcell SL, Fast M and Soto E (2024) Effects of Acipenserid herpesvirus 2 on the outcome of a *Streptococcus iniae* co-infection in white sturgeon (*Acipenser transmontanus*). *Front. Aquac.* 3:1306518. doi: 10.3389/faquc.2024.1306518

Effects of Acipenserid herpesvirus 2 on the outcome of a *Streptococcus iniae* co-infection in white sturgeon (*Acipenser transmontanus*)

Eva Marie Quijano Cardé[1], Kelsey M. Anenson[1], Susan Yun[1], Taylor I. Heckman[1], Hali T. Jungers[1†], Eileen E. Henderson[2], Sara L. Purcell[3], Mark Fast[3] and Esteban Soto[1*]

[1]Department of Medicine and Epidemiology, School of Veterinary Medicine, University of California, Davis, Davis, CA, United States, [2]California Animal Health and Food Safety Laboratory, San Bernardino, CA, United States, [3]Atlantic Veterinary College, University of Prince Edward Island, Charlottetown, PE, Canada

Acipenserid herpesvirus 2 (AciHV-2) is a large double-stranded DNA virus in the family *Alloherpesviridae* that causes catastrophic outbreaks in young naive white sturgeon (*Acipenser transmontanus*) populations, with mortalities of up to 80%. Survivors of these infections are suspected to remain latently infected. The gram-positive zoonotic bacterium *Streptococcus iniae* is another important sturgeon pathogen that causes severe myositis and up to 50% mortality during natural outbreaks. Throughout the last decade, co-infections of AciHV-2 and *S. iniae* have been reported in cultured white sturgeon in California resulting in severe presentations of piscine streptococcosis. This phenomenon of herpesvirus and streptococcus co-infection appears to span multiple taxa since in humans, it is recognized that a Human herpesvirus 3 infection (VZV) is a negative prognostic indicator for pediatric Invasive Group A Streptococcal infections (IGASI). While a decrease in humoral immunity caused by VZV has been hypothesized as a potentially important factor in IGASI cases, no natural animal model exists to study this process. Moreover, no studies have investigated these reported co-infections in white sturgeon. Therefore, the goal of this study was to investigate the effects of a recent AciHV-2 infection on the outcome of a subsequent *S. iniae* challenge in white sturgeon fingerlings. When fish were infected with 10^8 colony forming units (CFU) of *S. iniae* intramuscularly (IM), a statistically significant decrease in survival of 41% was detected in the co-infection group compared to the *S. iniae* group (p-value < 0.001). This difference was not observed when fish were infected with 10^6 CFU of *S. iniae* IM. At this lower infection dose, however, a statistically significant downregulation of *tnfα* was observed in the spleen of fish in the co-infection group compared to the *S. iniae* group (p-value = 0.0098). Analysis of serum from survivors revealed a statistically significant reduction in anti-*S. iniae* serum IgM and serum serotransferrin in fish from the

co-infection group compared to the *S. iniae* group (p-value = 0.0134 and p-value = 0.0183, respectively). Further studies are indicated to determine what interactions lead to the decreased production of pathogen-specific IgM, serotransferrin, and TNFα in the host.

KEYWORDS

WSHV-2, invasive group A streptococcal infection, IGASI, varicella, immunomodulation, latency, aquaculture, streptococcosis

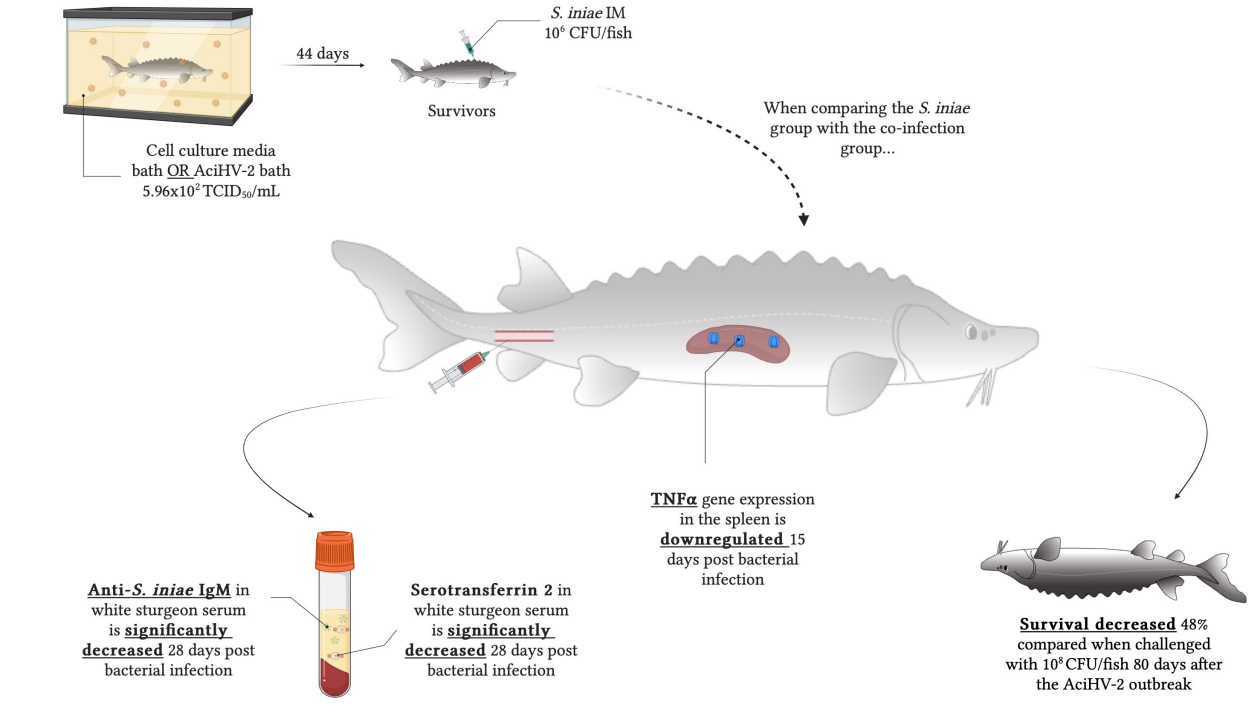

GRAPHICAL ABSTRACT

1 Introduction

The white sturgeon (*Acipenser transmontanus*) is an anadromous fish native to the Pacific Coast of North America (Kelly, 2019) and a central part of the multi-million-dollar aquaculture industry. This species alone accounts for 95% of caviar and sturgeon meat production (Ethier, 2014), and generates an annual revenue of over 200 million dollars in exports for the western region of the United States (Carocci et al., 2004). These aquaculture practices provide substantial returns to producers, generate local employment opportunities, and allow for conservation of wild populations by offering a sustainable alternative to wild-caught fish. Continued expansion of the industry, however, is limited partially by infectious disease.

Acipenserid herpesvirus 2 (AciHV-2, also known as White sturgeon herpesvirus 2 or WSHV-2) is a large double-stranded

DNA virus in the family *Alloherpesviridae* reported to cause epidermal ulceration, lethargy, inappetence, and erratic swimming (Watson et al., 1995; Lepa and Siwicki, 2012) with up to 50% mortality during natural outbreaks (Hanson et al., 2006; Goodwin, 2012; Mugetti et al., 2020). *Streptococcus iniae* (*S. iniae*), a gram-positive, opportunistically zoonotic bacterium that can cause severe myositis and up to 50% mortality during natural outbreaks, is another important pathogen of cultured white sturgeon (Nguyen et al., 2020; Pierezan et al., 2020). In the last decade, co-infections of AciHV-2 and *S. iniae* have been reported in cultured white sturgeon in California, resulting in severe presentations of piscine streptococcosis (Soto et al., 2017). This emerging presentation is particularly intriguing as *S. iniae* infections are typically associated with stress events when causing severe disease in white sturgeon (Nguyen et al., 2020; Pierezan et al., 2020), suggesting that immunomodulation is needed for the bacteria to behave with increased pathogenicity.

This herpesvirus-host-bacteria interaction phenomenon has been described in humans, as it pertains to pediatric Invasive Group A Streptococcal infections (IGASI), which have been increasing in prevalence over the last two decades worldwide (Frère et al., 2016; Suárez-Arrabal et al., 2019). Presentations are varied but serious and include necrotizing fasciitis (Wilson et al., 1995; Sturgeon et al., 2015), endocarditis (Laskey et al., 2000), toxic shock syndrome (Strom et al., 2017), and cellulitis (Oyake et al., 2000). These infections may cause long-term morbidity requiring extended hospitalizations and have a mortality rate of approximately 4% (Laupland et al., 2000; Strom et al., 2017). A known risk factor for a worse prognosis and more severe clinical presentation is a preceding varicella zoster infection, caused by Human herpesvirus 3 (also known as Varicella-Zoster Virus - VZV), which has been detected in 15-30% of IGASI cases in children and increases the risk of acquiring IGASI by 58 fold (Laupland et al., 2000; Sturgeon et al., 2015; Frère et al., 2016). Canada, one of the few countries to enact a universal VZV vaccination program, reported a decrease in IGASI severity, but no significant impact on the annual mean rate or overall mortality rate (Frère et al., 2016). Health disparities and disinformation are factors to consider in the success of vaccine programs (Nicoli and Appay, 2017) and there are countries where VZV vaccines are not available at this time.

While a decrease in humoral immunity of the host caused by VZV has been hypothesized as a potential important factor in IGASI (Laupland et al., 2000), the mechanisms underlying the association between VZV infection and IGASI have not been elucidated. Similarly, while AciHV-2 has been detected in various cases throughout the years, little is known about this virus' pathogenesis and no studies have investigated its potential role in these reported co-infections in white sturgeon.

A particularity about herpesviruses is that they have been described to have a myriad of mechanisms to modulate the host's immune response in order to establish and maintain latency (Speck and Ganem, 2010; Cohen, 2020). In latency, a reversible state achieved after the active outbreak, the full genome of the virus is maintained in the host cell with limited gene expression and no production of viral particles (Speck and Ganem, 2010). Depending on the viral species, herpesviral DNA is maintained as a circular episome (free in the nucleus or tethered to a chromosome) or integrated into the cellular chromosomes near the telomeric junction (Cohen, 2020). Even though the switch to latency severely decreases gene expression, part of the strategy of long-term persistence in the host is to focus efforts on protection from the immune system by immunomodulation, which can be initiated during the active lytic cycle of the virus or throughout the transition to latency. Latency has been extensively studied in mammalian herpesviruses, particularly in those affecting humans (Jarvis and Nelson, 2007; Speck and Ganem, 2010; Cohen, 2020), and continues to be a topic of active research, but little is known about the *Alloherpesviridae* family members including AciHV-2 (Stingley et al., 2003; Eide et al., 2011; Reed et al., 2014). As a member of the *Herpesvirales* order, and based on research done thus far involving other important alloherpesviruses such as Cyprinid Herpesvirus 3 (CyHV-3) (Eide et al., 2011; Reed et al., 2014), it is suspected that AciHV-2 has the potential for latency establishment. While this process may not cause direct mortality or clinical signs, it can have detrimental effects when it comes to the host's ability to clear other pathogens of interest if immunomodulation is indeed occurring. This may be the case in both pediatric IGASI and the reported white sturgeon AciHV-2/*S. iniae* co-infections, where the transcriptional profiles of the herpesviruses may be affecting humoral immunity establishment against the bacteria as well as other unrelated pathways that play a role in protection against streptococcosis.

These natural co-infections in the white sturgeon represent an outstanding opportunity to develop an animal model to study the complex interactions that may be taking place between the herpesvirus, the immune system of the host, and the bacteria (Miller and Neely, 2005). This model would be particularly relevant because previous studies have proposed *S. iniae* as a good candidate for use in animal models in translational research regarding *S. pyogenes, S. agalactiae*, and *S. pneumoniae* due to causing similar clinical presentations and having several homologous virulence factors (Miller and Neely, 2005; Baiano and Barnes, 2009). Finally, the study of this phenomenon using the white sturgeon model simultaneously supports a vital aquaculture industry in the United States.

Therefore, this study aimed to assess the hypothesis that a recent, potentially latent, AciHV-2 infection in white sturgeon increases mortality caused by *S. iniae* and affects the host immune response when compared to single pathogen infections.

2 Materials and methods

2.1 Viral inoculum preparation

White Sturgeon Skin (WSSK-1) cells (Hedrick et al., 1991) were seeded in T75 flasks at approximately 90% confluency in Minimum Essential Media (MEM; Corning Inc, Corning, NY) supplemented with 7.5% Fetal Bovine Serum (FBS; Genesee, El Cajón, CA), L-glutamine (Gibco, Grand Island, NY), and Penicillin/Streptomycin (Gibco, Grand Island, NY) at 20°C.

After 24 hours, these cells were used to propagate AciHV-2 isolate UCD3-30 (Watson et al., 1995) passage number 8 from stock. Ten days post-inoculation, the infected cell cultures were collected and centrifuged at 1900 g for 10 min. A 1 mL aliquot of the supernatant was used to determine the median tissue culture infectious dose of each viral inoculum using the Reed-Muench method (Lei et al., 2021). The remaining supernatant was used in the challenges below.

2.2 Bacterial inoculum preparation

Streptococcus iniae WS-10A (Pierezan et al., 2020) was revived from frozen stock on trypticase soy agar supplemented with 5% sheep's blood (SBA; University of California, Biological Media Services) grown at 30°C for 48 hours. A 0.5 McFarland standard was generated in sterile phosphate-buffered saline (PBS) corresponding to an optical density measurement of 0.15 at 600 nm, read on a UV/Vis photometer (BioPhotometerPlus, Eppendorf AG). The McFarland was diluted 1:10 in sterile PBS.

2.3 Fish screening and acclimation

White sturgeon fry (n = 1000; average weight ~ 1 g) were obtained from a commercial producer and grown in a 259-gallon circular tank for four months with a flow-through system supplied with well water (18 – 20°C) and supplemental aeration maintaining 8 - 9 mg/L of dissolved oxygen. Fish were fed 4% of their body weight daily of a combination of ground and 1 mm salmon sink pellet feed (Skretting: a Nutreco company, Stavanger, Norway) via an automatic feeder. Water temperature was monitored daily and dissolved oxygen was measured weekly.

An arbitrary sample of 12 white sturgeon fry was selected for general health assessment and infectious agent screening. Briefly, fish were euthanized with 1000 mg/L (ppm) buffered tricaine methanesulfonate (MS-222, 1:1 sodium bicarbonate; Syndel USA, Ferndale, WA) and assessed grossly for any external lesions. Skin scrapes and gill clips were evaluated microscopically for evidence of external parasites. Coelomic swabs were plated on tryptic soy agar supplemented with 5% sheep blood (Biological Media Service, University of California-Davis, CA) and incubated at 20°C for 7 days for bacterial assessment. Whole bodies were 1) pooled, 2) diluted 1:5 in MEM supplemented with 2% FBS, L-glutamine, and Penicillin/Streptomycin, 3) processed using a Stomacher 80 Laboratory Blender (Tekmar Company, Cincinnati, OH), 4) brought to a 1:50 final dilution in an antibiotic mixture (FBS, Gentamycin (10 mg/mL; Gemini Bio Products, West Sacramento, CA), Fungizone (amphotericin B 10 mg/mL; Sigma, St. Louis, MO) and HEPES (Mediatech Inc, Manassas, VA), 5) incubated overnight at 10°C, 6) and plated in duplicate onto WSSK-1 and White Sturgeon Spleen (WSS-2) (Hedrick et al., 1991) cells seeded 24 hours in advance at 90% confluency in 12-well plates with MEM supplemented with 2% FBS, L-glutamine, HEPES, and Penicillin/Streptomycin. In addition, the tissue pellet from the virology process was used to screen for AciHV-2 using a recently developed quantitative PCR (Quijano Carde et al., 2024). No external parasites, pathogenic bacteria, or viruses were identified during this screening process. All protocols and procedures using these fish were ethically reviewed and approved by the University of California Institutional Animal Care and Use Committee.

2.4 Laboratory controlled challenges

For the first challenge, henceforth referred to as the "pilot challenge", white sturgeon fingerlings (n = 144; average weight = 10 g) were used. A subgroup of 96 fish was exposed to a 5.1 x 10^2 Median Tissue Culture Infectious Dose ($TCID_{50}$)/mL bath (Lei et al., 2021) of AciHV-2 for 1 hour. The remaining 48 fish were exposed to the same volume of sterile MEM supplemented with 2% FBS, L-glutamine, and Penicillin/Streptomycin for 1 hour and served as negative controls. For purposes of reproducibility, the fish were exposed in 5-gallon tanks. Each tank had 3 L of water, 3 mL of the virus stock or sterile cell culture media, and 12 fish. The virus aliquot used had 5.1x10^5 $TCID_{50}$/mL. Fish were maintained at 18-20°C in 5-gallon circular tanks, fed 1% of their body weight of 1 mm-salmon sink pellet feed once daily, and monitored closely. Mortality was recorded for 80 days and a pectoral fin clip was collected from every mortality (n = 37) to quantify AciHV-2 viral load via qPCR (Quijano Carde et al., 2024). Survivors of each group were then arbitrarily sorted into duplicate 35-gallon rectangular flow-through tanks (23 fish/group) to generate four treatment groups (Negative control, AciHV-2 infected, *S. iniae* infected, and AciHV-2/*S. iniae* co-infected). Fish were allowed to acclimate to their new environment for four days while the temperature was raised 1°C per day until reaching 22-24°C via commercial submersible water heaters (Aqueon, Franklin, WI). Fish in the *S. iniae* infected, and AciHV-2/*S. iniae* co-infected groups were subjected to an *S. iniae* challenge following published protocols using a 10^9 CFU of *S. iniae* per mL suspension (0.1 mL per fish in the epaxial musculature for a final dose of 10^8 CFU per fish) under anesthesia (100 ppm buffered MS-222) after a netting stress event (two 30 sec periods out of the water within a net with 30 sec in the water within the net in between) (Nguyen et al., 2020). Fish in the Negative control, and AciHV-2 infected groups were treated similarly but were injected with 0.1 mL of PBS intramuscularly in the epaxial musculature. During the anesthetic event, a pectoral fin clip sample was collected from each fish for assessment of AciHV-2 pre-bacterial challenge via qPCR (Quijano Carde et al., 2024). Mortality was monitored for 21 days and the cumulative percent mortality (CPM) per treatment was calculated. Pectoral fin clips and spleen samples were collected from each mortality and stored at -80°C for molecular testing via AciHV-2 (Quijano Carde et al., 2024) and *S. iniae* (López-Porras et al., 2019) qPCR, respectively. All survivors were euthanized with 1000 ppm of buffered MS-222. Pectoral fin clips were collected from all survivors for testing of AciHV-2 via qPCR (Quijano Carde et al., 2024).

For the second challenge, henceforth referred to as the "large-scale challenge", white sturgeon fingerlings (n = 720; average weight = 12 g) were used. A subgroup of 360 fish was exposed to a 5.96 x 10^2 $TCID_{50}$/mL bath (Lei et al., 2021) of AciHV-2 for 1 hour. The

remaining 360 fish were exposed to the same volume of sterile MEM supplemented with 2% FBS, L-glutamine, and Penicillin/Streptomycin for 1 hour and served as negative controls. For purposes of reproducibility, the fish were exposed in 35-gallon tanks. Each tank had 26 L of water, 77.5 mL of the virus stock or sterile cell culture media, and 180 fish. The virus aliquot used had $2x10^5$ $TCID_{50}$/mL. Fish were then relocated and maintained at 18-20° C in 259-gallon circular tanks, fed 1% of their body weight of 1 mm-salmon sink pellet feed once daily, and monitored closely. Mortality was recorded for 44 days and a pectoral fin clip was collected from every mortality (n = 180) to quantify AciHV-2 viral load via qPCR (Quijano Carde et al., 2024). Survivors of each group were then arbitrarily sorted into triplicate 35-gallon rectangular flow-through tanks (20 fish/tank) to generate four treatment groups (Negative control, AciHV-2 infected, *S. iniae* infected, and AciHV-2/*S. iniae* co-infected; 60 fish/group). Fish were allowed to acclimate to their new environment for four days while the temperature was raised 1°C per day until reaching 22-24°C via commercial submersible water heaters (Aqueon, Franklin, WI). Fish in the *S. iniae* infected, and AciHV-2/*S. iniae* co-infected groups were subjected to an *S. iniae* challenge following published protocols using a 10^7 CFU of *S. iniae* per mL suspension (0.1 mL per fish in the epaxial musculature for a final dose of 10^6 CFU per fish) under anesthesia (100 ppm buffered MS-222) after a netting stress event (two 30 sec periods out of the water within a net with 30 sec in the water within the net in between) (Nguyen et al., 2020). This bacterial concentration was lower than the one used in the pilot challenge discussed above in order to reduce mortalities and thus have enough fish for immune response assessment sampling. Fish in the Negative control, and AciHV-2 infected groups were treated similarly, but were injected with 0.1 mL of PBS intramuscularly in the epaxial musculature. Mortality was monitored for 28 days and the cumulative percent mortality (CPM) per treatment was calculated. Pectoral fin clips and spleen samples were collected from each mortality and stored at -80°C for molecular testing via AciHV-2 (Quijano Carde et al., 2024) and *S. iniae* (López-Porras et al., 2019) qPCR, respectively. Two fish per tank were euthanized with 1000 ppm buffered MS-222 on day 15 post-injection. The spleen of each euthanized fish was collected aseptically and incubated individually in 0.5 mL of RNA*later* (Thermofisher Scientific, Waltham, MA) overnight at 4°C before being transferred to -80°C for storage until reverse-transcription qPCR (RT-qPCR) analysis. In addition, a pectoral fin clip and spleen sample were collected from each euthanized fish for molecular testing via AciHV-2 (Quijano Carde et al., 2024) and *S. iniae* (López-Porras et al., 2019) qPCR, respectively. At least five moribund individuals per group were euthanized throughout the study and submitted for histological analysis in 10% neutral-buffered formalin (pH 7.2) after fixing for a minimum of 24 hours. Representative tissues (skin, skeletal muscle, gastrointestinal tract, oral cavity, brain, eyes, heart, gills, liver, kidney, spleen, and reproductive tract) were processed routinely, embedded in paraffin, sectioned at 4 µm, and stained with hematoxylin and eosin (H&E) or Gram stain. Slides were scored based on four categories: "degree of erosion/ulceration", "distribution of erosion/ulceration", "percentage of section affected", and "muscle necrosis". At 28 days post-injection, all survivors were euthanized with 1000 ppm of buffered MS-222. Ten euthanized individuals per group of this time point were used for the collection of blood, fin clip samples, spleen samples, and swabs as described in the remainder of this paragraph. At least 0.8 mL of blood was collected individually in microcentrifuge tubes (with no anticoagulant) from the caudal vein. Clotted blood was then centrifuged at 10,000 *g* for 5 min and the serum was stored individually at -20°C until enzyme-linked immunosorbent assay (ELISA) and Western Blot analysis. Re-isolation of bacteria from the posterior kidney and brain swabs was performed in SBA. Pectoral fin clips and spleen samples were collected for molecular testing via AciHV-2 (Quijano Carde et al., 2024) and *S. iniae* (López-Porras et al., 2019) qPCR, respectively. A spleen sample was also collected aseptically and immersed in 0.5 mL of RNA*later* (Thermofisher Scientific, Waltham, MA) overnight at 4°C before being transferred to -80°C for storage until reverse-transcription qPCR (RT-qPCR) analysis. A graphical representation of the timeline of the large-scale challenge can be found in Supplementary Figure 1.

2.5 Pathogen quantification and gene expression assay

Genomic DNA from fin and spleen samples was isolated using the DNeasy Blood & Tissue kit (QIAGEN, Hilden, Germany) with the following modifications: tissues were incubated with ATL buffer and proteinase K at 56°C for 1 hour and samples were incubated with AL buffer at 56°C for 10 minutes. Isolated DNA was stored at -20°C until analysis using the recently developed AciHV-2 qPCR (Quijano Carde et al., 2024) and the previously published *S. iniae* qPCR (López-Porras et al., 2019). Positive controls were included in each assay, consisting of purified genomic DNA extracted from the original inoculums described above in sections 2.1 and 2.2 (10^7 copies/reaction). The DNA concentration and quality of each sample and control were assessed spectrophotometrically (Nanodrop; Thermofisher Scientific, Waltham, MA) and all samples and controls were diluted in sterile water to 50 ng/µL before being used in the qPCR reactions, for a total of 250 ng of DNA per 12 µL reaction. All samples and controls were run in triplicate while using the TaqMan Environmental Master Mix on the QuantStudio3 Real-Time PCR System (Thermofisher Scientific, Waltham, MA).

Total RNA from spleen samples, as well as genomic DNA, were isolated using the AllPrep DNA and RNA Mini Kit (QIAGEN, Hilden, Germany). The DNA and RNA concentration and quality of each sample were assessed spectrophotometrically (Nanodrop). The DNA samples were used for qPCR as described above. The RNA samples were reversed transcribed to cDNA using the High-capacity RNA-to-cDNA kit (Thermofisher Scientific, Waltham, MA). The cDNA samples were diluted 1:2 in sterile water and used to quantify transcript abundance of cytokines, acute-phase proteins, and other molecules involved in various immune pathways from the innate and adaptive responses (Serum Amyloid A - *saa*, Major Histocompatibility Complex Class II - *mhc*II, Interleukin 17 - *il17*, Interferon Regulatory Factor 8 - *irf*8, and Tumor Necrosis Factor alpha - *tnf*α) via previously published reverse-transcription qPCR (RT-qPCR) (Soto et al., 2021; Soto

et al., 2022) protocols. The expression of the Elongation Factor and Beta Actin genes was used to normalize the gene expression data and all samples were run in duplicate. The primer sequences used in this study can be found in Supplementary Table 1.

2.6 Detection of serum anti-*S. iniae* IgM in challenge survivors

An indirect enzyme-linked immunosorbent assay (ELISA) was performed following previously published protocols (Heckman et al., 2022) with modifications. Briefly, *S. iniae* (isolate WS-10A) was grown from stock on SBA at 28°C for 48 hours. The bacteria was resuspended in coating buffer (1% poly-L-lysine in carbonate-bicarbonate) to an optical density (OD) of 0.245 at 600 nm. Immulon 2HB Flat Bottom Microtiter 96-well plates (Thermofisher Scientific, Waltham, MA) were coated with 100 µL of bacterial suspension per well and incubated overnight at 4°C.

The plates were washed three times with low-salt wash buffer (LSWB; 0.02 M Trizma base, 0.38 M NaCl, 0.05% Tween-20, pH 7.3) and a 250 µL suspension of blocking buffer (5% skim milk powder in double-distilled water) added to each well before incubation at room temperature for 3 hours. Following incubation, the plates were washed again three times with LSWB. The white sturgeon serum samples collected at the end of the challenge were diluted 1:200 in LSWB containing 1% bovine serum albumin (BSA; Sigma) and 100 µL of the diluted serum or sterile PBS was added to respective plate wells in duplicate. Plates were then incubated overnight at 4°C.

The plates were washed five times with high-salt wash buffer (HSWB; 0.02 M Trizma base, 0.5 M NaCl, 0.01% Tween-20, pH 7.7), including a 5 min soak on the last wash. Mouse anti-sturgeon IgM monoclonal antibodies (Aquatic Diagnostics Ltd, UK) were diluted 1:75 in PBS and 100 µL added to each well. The plates were incubated at room temperature for 1 hour before washing five times with HSWB, including a 5 min soak. Goat anti-mouse IgG with conjugated horseradish peroxidase (Sigma-Aldrich, St. Louis, MO) was diluted 1:3000 in LSWB with 1% BSA and 100 µL was added to each well. The plates were incubated at room temperature for 1 hour and then washed with HSWB five times, including a 5 min soak on the last wash. Each well received 100 µL of substrate solution (ABTS 1-component microwell peroxidase substrate kit; SeraCare Life Sciences, Milford, MA) and the plates were incubated at room temperature for 30 min. The reaction was terminated by adding 100 µL of stop solution (0.01% Sodium Dodecyl Sulfate in distilled water) to each well. Absorbance at 410 nm was measured using a Cytation 5 Cell Imaging Multimode Reader (BioTek, Winooski, VT) and standardized against the PBS controls.

2.7 Detection of serum serotransferrin in challenge survivors

Serum serotransferrin (STF-2) levels were determined following previously published protocols (Soto et al., 2022). Briefly, the protein concentration in each serum sample was determined using the Pierce BCA Protein Assay Kit (Thermofisher Scientific, Waltham, MA). An aliquot of 25 µg of total protein per sample was denatured in Laemmli buffer (Bio-Rad Laboratories, Hercules, CA) for 5 min at 95°C. Samples were loaded into Mini-PROTEAN® TGX Stain-Free™ 4–15% gels (Bio-Rad Laboratories, Hercules, CA) and separated using the Mini-PROTEAN® Tetra Cell gel apparatus (Bio-Rad Laboratories, Hercules, CA) for 50 min at 150 v. Total protein per sample was imaged using the stain-free application on the ChemiDoc MP imager (Bio-Rad Laboratories, Hercules, CA). Gels were then activated and transferred onto 0.22 µm nitrocellulose (STF) membranes (Azure Biosystems, Dublin, CA) using the Trans-Blot® Turbo™ Mini-size Transfer Stacks and the Trans-Blot® Turbo™ Transfer System (Bio-Rad Laboratories, Hercules, CA) for 3 min. Total protein per sample was imaged again as described above. Membranes were immediately transferred to the blocking buffer of 5% non-fat dry milk in PBS with Tween (PBSTW; 1.37 M NaCl, 27 mM KCl, 100 mM Na_2HPO_4, 18 mM KH_2PO_4, pH 7.4, 0.1% (w/v) Tween 20) and incubated with gentle agitation for 2 h at room temperature. Each blot was then incubated with the following primary/secondary antibody combination: 1) chicken anti-sturgeon serotransferrin (1:500, Somru BioScience Inc., Charlottetown, PE, CA) and 2) donkey anti-chicken IgY^{++}(IgG) (H + L) (1:10,000 Jackson ImmunoResearch Laboratories, Inc.). The primary antibody was diluted in its blocking buffer (5% non-fat dry milk in PBS with Tween) and incubated for 18 hours at 4°C with gentle agitation, while the secondary antibody was diluted in its blocking buffer (5% non-fat dry milk in PBS with Tween) and incubated for 1 h at room temperature with gentle agitation. All protein bands were visualized using Clarity™ Western ECL Substrate Chemiluminescent Detection Reagent (Bio-Rad Laboratories, Hercules, CA) prior to image acquisition and visualized using a ChemiDoc MP Imaging System (Bio-Rad Laboratories, Hercules, CA). Image analysis was performed using Image Lab™ Software (Bio-Rad Laboratories, Hercules, CA). The data is presented as the ratio of protein of interest expressed as a "fold difference" to the loading control, normalized to total protein levels.

2.8 Statistical analysis

The CPM was assessed using Kaplan-Meier survival analysis with a Mantel-Cox test. All data, except survival data, was assessed for normality with a D'Agostino-Pearson omnibus K2 test. Differences between groups for the viral and bacterial loads were determined using unpaired t-tests and Mann-Whitney tests as appropriate for the desired comparison. The significance of differences in relative gene expression levels between treatments was calculated using a one-way ANOVA or a Kruskal-Wallis test as appropriate followed by a Holm-Sídák's multiple comparison test (with a single pooled variance) or a Dunn's multiple comparison test, respectively. The IgM quantification between groups was assessed with a one-way ANOVA and a Sídák's multiple comparison test (with a single pooled variance). The STF-2 quantification between groups was assessed with a Kruskal-Wallis test and a Dunn's multiple comparison test. The histopathologist was not blinded as to treatment group identity and the

histopathological scores were compared via one-way ANOVA and a Sídak's multiple comparison test (with a single pooled variance). All results were considered significant at p-values ≤ 0.05.

3 Results

3.1 Challenge

During the AciHV-2 portion of both challenges, the sturgeon in the AciHV-2 infected group began showing clinical signs seven days post-immersion. Clinical signs included erythema (Figure 1A), lethargy, splenomegaly (Figure 1B), decreased feed intake, buoyancy abnormalities, epidermal ulcerations (Figure 1C), and acute mortality. In addition, it was common to find moderate to severe colonization of the mouth and opercular cavities by oomycetes (Figure 1D) in fish displaying severe clinical signs. The experimental group experienced a decrease in survival of 40% (pilot) and 50% (large-scale) compared to the negative control, with mortalities starting 18 days post-infection (pilot challenge, Figure 2A) and eight days post-infection (large-scale challenge, Figure 3A). Survivors had no overt clinical signs 52 days (pilot challenge) and 40 days (large-scale challenge) post-immersion, with only sporadic mortalities observed in the following days before the bacterial co-infection (Figures 2A, 3A, respectively). When assessing viral load in the mortalities, 89% in the pilot challenge (Figure 2C) and 94% in the large-scale challenge (Figure 3C) tested positive via qPCR with a mean viral load of 10^6 copies in the pilot challenge (Figure 2B) and $10^{5.4}$ copies (large-scale challenge, Figure 3B) per µg of total DNA. Two fish in the negative control group died during the large-scale challenge and they both tested negative for AciHV-2 via qPCR (Figure 3C). Finally, a screening of AciHV-2 via qPCR was performed in the pilot challenge prior to the bacterial infection and only 0.06% of fish tested positive for AciHV-2 (Figure 2D).

During the co-infection portion, the sturgeon infected with *S. iniae* began developing clinical signs 24 hours post-injection in both the pilot and the large-scale challenges (Figure 4A). Clinical signs included lethargy, inappetence or anorexia, injection site ulceration (Figures 4B–D), and acute mortality. In the pilot challenge, the co-infection group had a statistically significant decrease in survival of 41% compared to the *S. iniae* group and 36% compared to AciHV-2 group (Figure 5A). The trends in mortality in the large-scale challenge were consistent with the pilot challenge, with the co-infected group showing a decrease in survival of 7.8% compared to the *S. iniae* group and 9.1% compared to the AciHV-2 group, but this was only statistically significantly different when compared with the AciHV-2 group and not when compared to the *S. iniae* group (Figure 6A). In addition, mortalities started in the co-infection group 24 hours earlier than in the *S. iniae* group during both the pilot and large-scale challenges (Figures 5A, 6A, respectively). In terms of viral and bacterial loads of the challenge mortalities, there was no statistical difference in loads between groups (Figures 5B, C, 6B, C). During the pilot challenge, only four individuals tested positive for AciHV-2 and there was no statistical difference in viral load between groups (p-value = 0.5538, Figure 5D). During the large-scale challenge, all euthanized individuals for gene expression sampling tested negative for AciHV-2 and *S. iniae* via qPCR (n = 6 per group

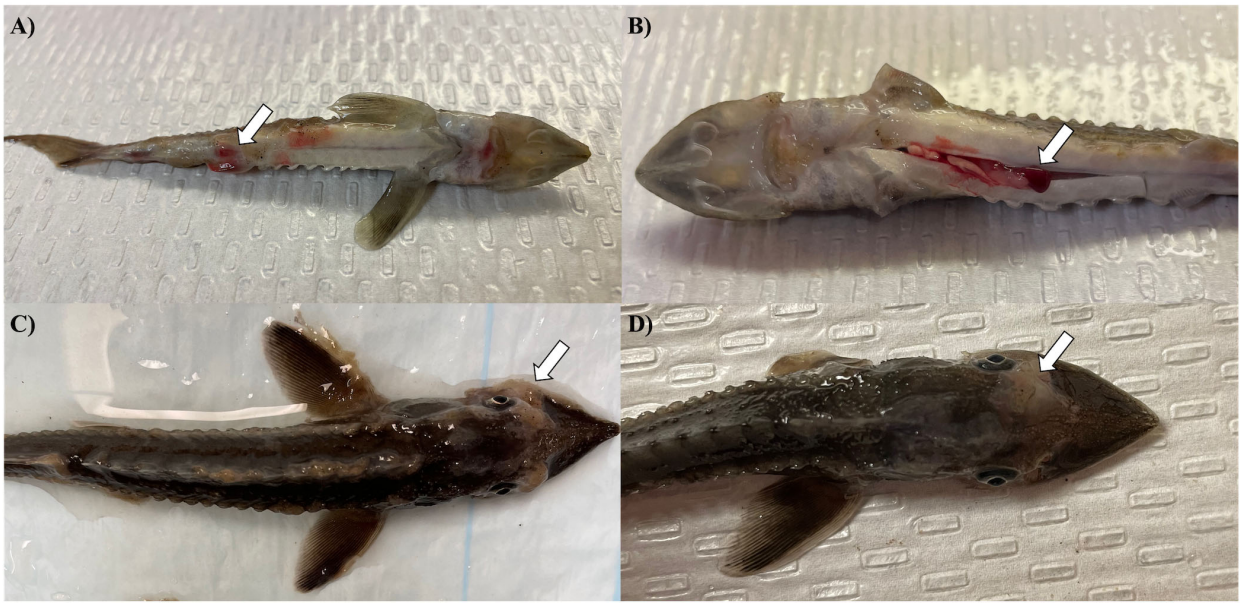

FIGURE 1
Clinical signs in white sturgeon during AciHV-2 challenge. White sturgeon fingerlings were exposed to a $5.1x10^2$ $TCID_{50}$/mL (pilot challenge) or a $5.96x10^2$ $TCID_{50}$/mL (large-scale challenge) bath for 1 hour. Morbidity and mortality were monitored for 44 (large-scale challenge) to 80 (pilot challenge) days after immersion. These are representative images of clinical signs and gross changes observed in both challenges during the AciHV-2 outbreak portion of the experiments. **(A)** Erythema surrounding pelvic fins in a fresh mortality. **(B)** Splenomegaly in a fresh mortality. Pectoral fins had been clipped for diagnostic purposes post-mortem. **(C)** oomycetes colonization in an euthanized fish. **(D)** Epidermal ulceration medial to the left eye in a fresh mortality. The white arrows point towards the lesions described.

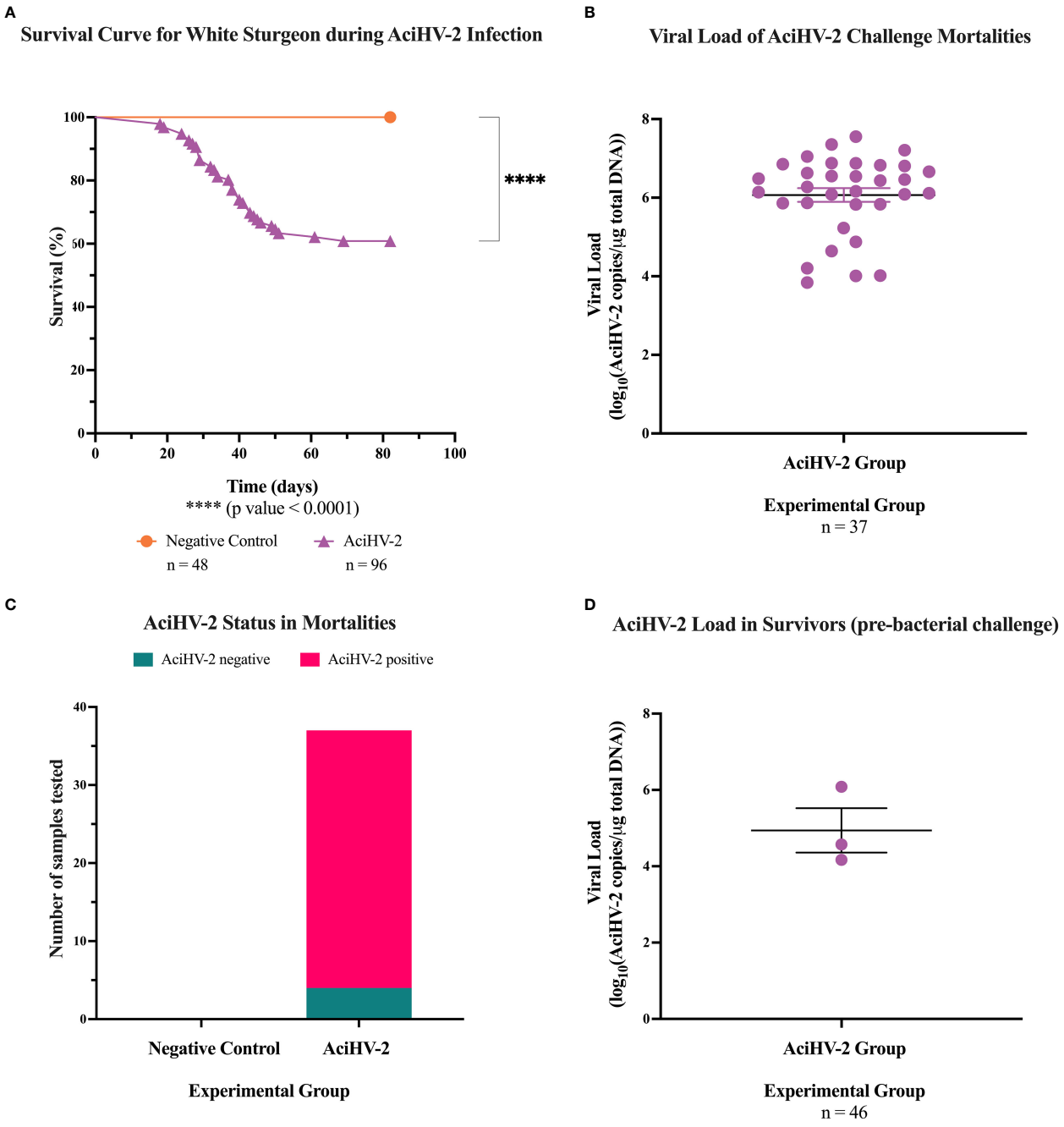

FIGURE 2
Acipenserid Herpesvirus 2 (AciHV-2) challenge during pilot challenge. A 1- hour static immersion challenge with $5.1x10^2$ $TCID_{50}$/mL) of Acipenserid Herpesvirus 2 (AciHV-2) was performed (n=96). A negative control group was treated similarly but sterile cell culture media was used instead of virus suspension (n=48). Mortality was monitored for 80 days and mortalities were tested for AciHV-2 via qPCR of pectoral fin DNA. Survivors were tested for AciHV-2 via quantitative polymerase chain reaction (qPCR) of DNA extracted from the pectoral fin of each fish. **(A)** The solid shapes represent the mean cumulative mortality at each day. The different experimental groups are color-coded. A statistically significant reduction in survival is seen in the AciHV-2 exposed group when compared with the negative control group. **(B)** The solid dots represent the mean viral load of sampled mortalities, with the standard error of the mean plotted. Four mortalities in the AciHV-2 group had undetermined Ct values and are not displayed in this graph. The mean viral load among mortalities was 10^6 copies/ug total DNA. **(C)** The bars represent the number of samples tested for AciHV-2 via qPCR, color-coded by qPCR result. This shows that 89% of the mortalities in the AciHV-2 group tested positive for AciHV-2 via qPCR. **(D)** The solid dots represent the mean viral load of sampled survivors, with the standard error of the mean plotted. Only three individuals tested positive with a mean viral load of $10^{4.9}$ copies/ug total DNA.

at 15 days post-bacterial infection and n = 10 per group at 28 days post-bacterial infection).

Histopathological analysis of at least five moribund or fresh mortalities per group during the large-scale challenge revealed that erosion and ulceration scores were only statistically significantly increased in the groups infected with AciHV-2 (Figures 7A–C, p-value < 0.0001). In addition, while lesions in fish exposed to *S. iniae* were most often characterized by muscle necrosis, none of the

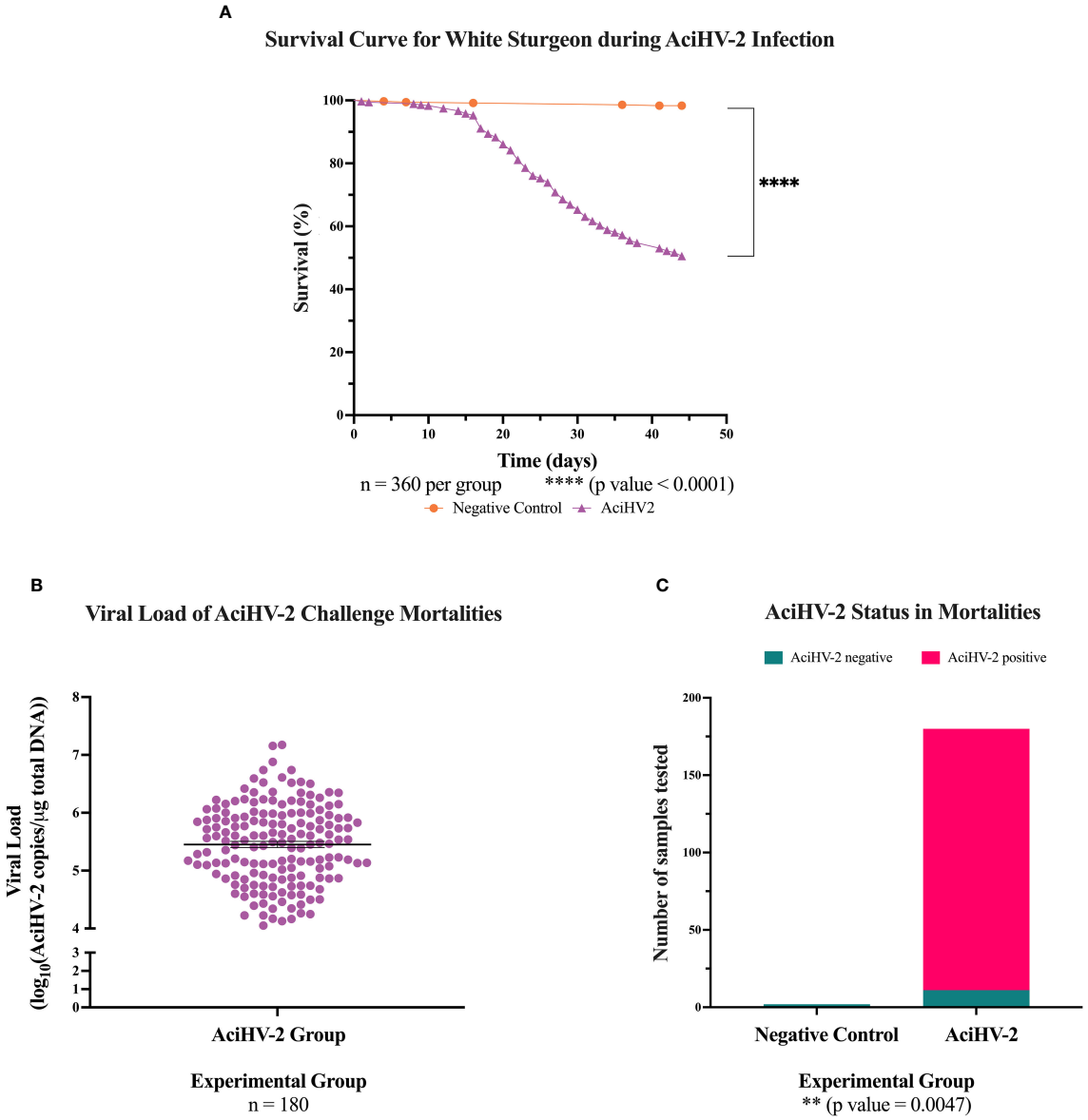

FIGURE 3
Acipenserid Herpesvirus 2 (AciHV-2) challenge during large-scale challenge. An immersion challenge model was performed by exposing white sturgeon fingerlings to a 5.96x10^2 $TCID_{50}$/mL bath or a sterile cell culture media bath for 1 hour. Mortality was monitored for 44 days after immersion and mortalities tested for AciHV-2 via quantitative polymerase chain reaction (qPCR). Survivors were weighed at the end of the challenge. **(A)** The solid shapes represent the mean cumulative mortality at each day. The different experimental groups are color-coded. A statistically significant reduction in survival is seen in the AciHV-2 exposed group when compared with the negative control group. **(B)** The solid dots represent the mean viral load of sampled mortalities, with the standard error of the mean plotted. Both mortalities in the negative control group and 11 mortalities in the AciHV-2 group had undetermined Ct values and are not displayed in this graph. The mean viral load among mortalities was $10^{5.4}$ copies/ug total DNA. **(C)** The bars represent the number of samples tested for AciHV-2 via qPCR, color-coded by qPCR result. This shows that 94% of the mortalities in the AciHV-2 group tested positive for AciHV-2 via qPCR, while none of the mortalities in the negative control group tested positive for AciHV-2 via qPCR. There is a strong association between an AciHV-2 positive status and the experimental group.

infected groups had statistically significant muscle necrosis scores present in the sections analyzed when compared to the negative control (Figure 7D). However, it is important to note that the injection site may have been absent in certain slides evaluated, affecting the overall score per group. Representative images of the lesions used for histopathological scoring can be found in Supplementary Figure 2. In fish infected with AciHV-2, lesions were often centered on the epithelium (skin and oral mucosa) and were characterized by areas of erosion and ulceration (Figures 8C, D, G). Secondary colonization of these areas of ulceration by bacteria (Figures 8D, G) and/or oomycetes (Figure 8C) was common. In fish infected with *S. iniae*, lesions were most pronounced at the injection site and were characterized by degeneration and necrosis of the myocytes surrounding the injection site, as well as large numbers of coccoid bacteria (Figures 8E, H). There also appeared to be large numbers of intravascular coccoid bacteria, consistent with septicemia. Fish infected with both AciHV-2 and S. *iniae* typically exhibited epithelial lesions and/or injection site lesions.

10.3389/faquc.2024.1306518

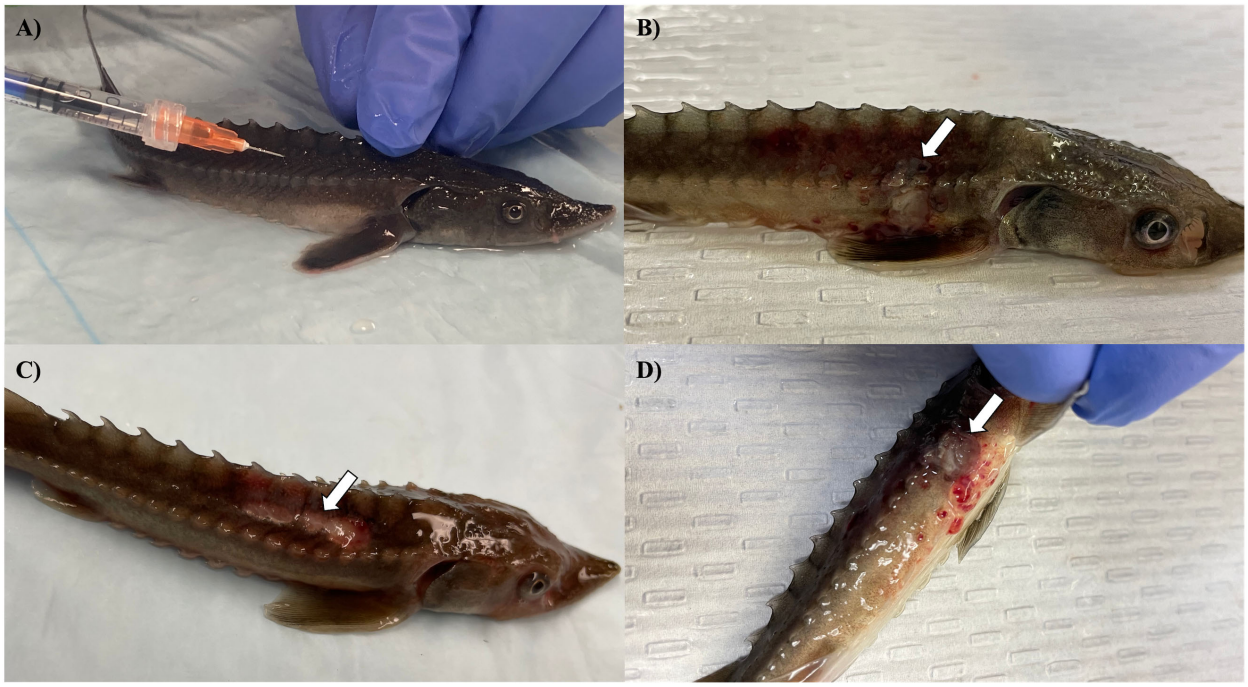

FIGURE 4
Clinical signs and gross changes in white sturgeon during AciHV-2 and *S. iniae* co-infection challenge. White sturgeon fingerlings were exposed to a $5.1x10^2$ $TCID_{50}$/mL (pilot challenge) or a $5.96x10^2$ $TCID_{50}$/mL (large-scale challenge) bath for 1 hour or an equivalent volume of sterile cell culture media. Survivors were then injected with 10^6 CFU *S. iniae* per fish or 0.1 mL of sterile Phosphate Buffered Saline. Clinical signs and mortality were monitored for 28 days. **(A)** Injection site for the *S. iniae* intramuscular challenge in an anesthetized white sturgeon fingerling. **(B)** Mild cutaneous ulceration at the injection site in a fresh mortality. **(C)** Moderate to severe ulceration at the injection site in a fresh mortality. **(D)** Moderate to severe ulceration at the injection site with subdermal hemorrhage. The white arrows point towards the lesions described.

3.2 Immune-related gene expression assessment

At 15 days post-bacterial infection during the large-scale challenge, there was a statistically significant downregulation of *tnf-α* transcripts in the spleen of fish in the co-infection group compared to both single pathogen groups (Figure 9A, p-value = 0.0098). In addition, there was a statistically significant downregulation of *irf8* transcripts in the co-infection group compared to the negative control group (Figure 9B, p-value = 0.0374). Finally, there was a statistically significant downregulation of *saa* transcripts in all infected groups compared to the negative control group (Figure 9D, p-value 0.0472). These changes were not present at 28 days, but there was a statistically significant downregulation of *saa* transcripts in the groups infected with *S. iniae* compared to the AciHV-2 group (Figure 10D, p-value 0.0323).

3.3 Humoral immunity assessment

Assessment of anti-*S. iniae* IgM present in the serum of challenged fish revealed a statistically significant reduction in anti-*S.iniae* serum IgM in fish from the coinfection group compared to fish in the *S. iniae* group (Figure 11, p-value = 0.0134).

3.4 Acute-phase protein analysis

Assessment of acute phase proteins in the serum of survivors of the co-infection challenge revealed a statistically significant decrease in serum serotransferrin 2 in the groups previously exposed to AciHV-2 compared to the negative control and *S. iniae* groups (Figure 12).

4 Discussion

The *Herpesvirales* order is characterized by the ability to establish latency, and this process can lead to changes to the immunocompetence of the host (Cohen, 2020). While this has not been explored for AciHV-2, reports of co-infections in white sturgeon (Soto et al., 2017) similar to human pediatric IGASI (Laupland et al., 2000) suggest there is an interaction between the infectious agents and the host that impacts disease outcome. Neither of these presentations across taxa has been investigated in a controlled environment and the study of this co-infection scenario in white sturgeon may inform future studies regarding human pediatric IGASI. Therefore, our initial studies aimed to perform a pilot challenge to assess the hypothesis that a recent, potentially latent, AciHV-2 infection in white sturgeon fingerlings would increase mortalities by a subsequent *S. iniae* infection. Results revealed that the co-infection group had a

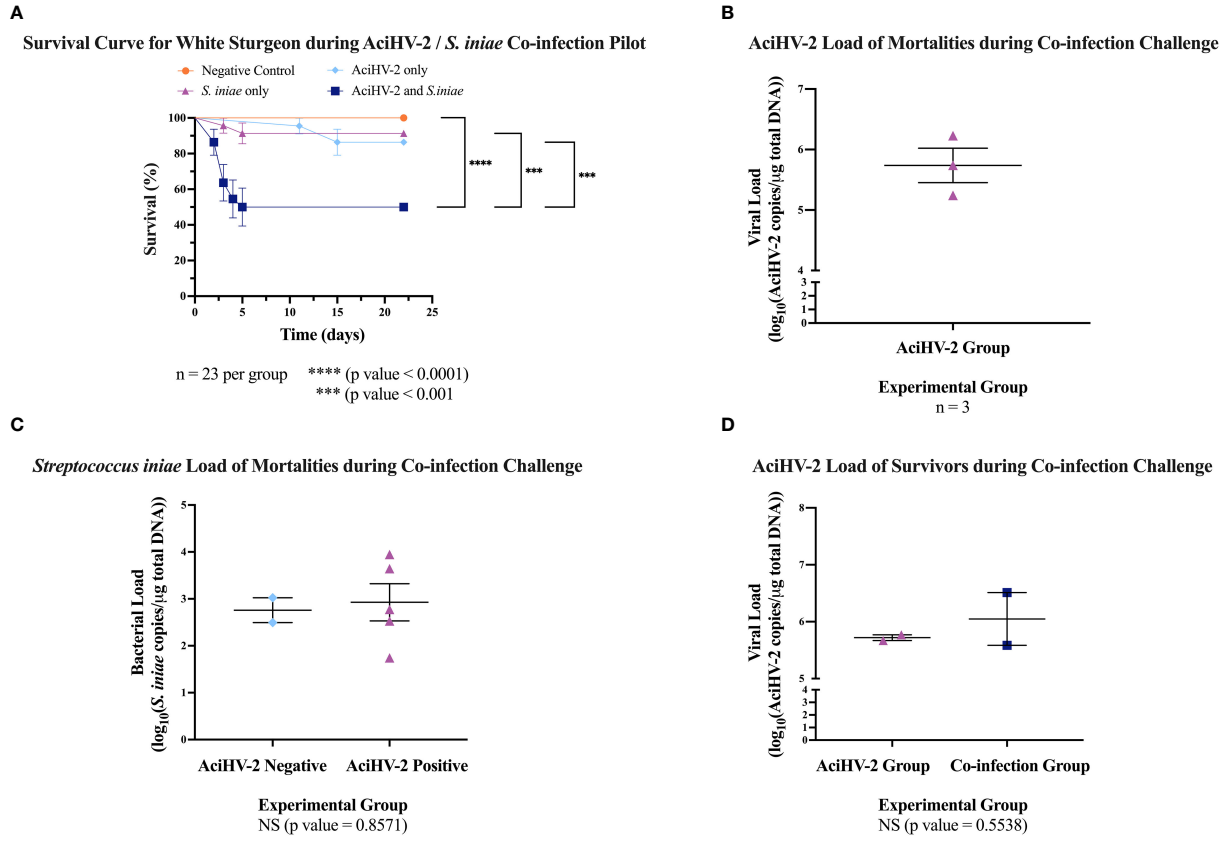

FIGURE 5
Acipenserid Herpesvirus 2 (AciHV-2) and *Streptococcus iniae* (*S. iniae*) co-infection pilot challenge. An immersion challenge model was performed by exposing white sturgeon fingerlings to a $5.1x10^2$ $TCID_{50}$/mL AciHV-2 bath or a sterile cell culture media bath for 1 hour. Survivors of this challenge at 80 days were re-sorted into groups of 23 fish per treatment. Fish received either 10^8 CFU of *S. iniae* or sterile Phosphate Buffered Saline in the epaxial musculature. Mortality was monitored for 21 days after injection and mortalities were tested for AciHV-2 and *S. iniae* via quantitative polymerase chain reaction (qPCR). **(A)** The solid shapes represent the mean cumulative mortality at each day, with standard error of the mean plotted. The different experimental groups are color-coded. The black stars indicate statistical significance between the bracketed groups and p values are stated below. Results reveal that the *S. iniae* group that was previously infected with AciHV-2 had a statistically significant decrease in survival of 41% compared to *S. iniae* alone and of 36% compared to AciHV-2 alone. **(B)** The solid dots represent the mean viral load of sampled mortalities, with the standard error of the mean plotted. Only the AciHV-2 group mortalities tested positive for AciHV-2 via qPCR. **(C)** The solid dots represent the mean bacterial load of sampled mortalities, with the standard error of the mean plotted. There was no statistical difference in bacterial loads between groups. This also shows that 100% and 45% of the mortalities in the *S. iniae* and in the co-infection groups, respectively, tested positive for *S. iniae*. There is a strong association between an *S. iniae* positive status and the experimental group (p value ≤ 0.0001). **(D)** The solid dots represent the mean viral load of sampled survivors, with the standard error of the mean plotted. Experimental groups are color-coded. There was no statistical difference in viral load between groups.

statistically significant decrease in survival of 41% compared to the *S. iniae* group and of 36% compared to AciHV-2 group (Figure 5A). This provided proof of concept that a recent, potentially latent, AciHV-2 infection has a profound impact on the outcome of a subsequent *S. iniae* infection in white sturgeon. While it was hypothesized that this was going to be the case based on natural cases of piscine streptococcosis in white sturgeon that also had AciHV-2 (Soto et al., 2017), these results are consistent with additional reports on *S. iniae*-virus co-infections in other fish species. For example, Japanese flounder (*Paralichthys olivaceus*) experiences statistically increased mortality when infected with *S. iniae* 1 week after an aquabirnavirus (ABV) infection compared with fish infected with *S. iniae* alone (Pakingking et al., 2003). To the authors' knowledge, however, our study is the first to investigate it in the context of a herpesvirus infection in sturgeon during what is suspected to be the latent phase (80 days post-infection, 30 days past the last mortality of the active outbreak, with no AciHV-2 detectable in fin tissue of the majority of survivors – Figures 3A, D).

A large-scale challenge was then performed to investigate aspects of the immune system potentially affected by AciHV-2 and leading to altered interactions between the host and *S. iniae*. For the large-scale challenge presented here, while following similar trends to the pilot challenge (Figure 5A), there was no significant difference in survival between the co-infection group and the *S. iniae* group (Figure 6A). The primary differences between the pilot and large-scale challenge experiments were time between viral and bacterial infection (80 *vs* 44 dpi, respectively) and bacterial dose (10^8 *vs* 10^6 CFU/fish, respectively). While the overall lower mortality rate may preclude statistical significance, this still raises interesting questions into the effect of timing and bacterial infectious dose in co-infections, and these concepts have been investigated before for *S. iniae* in other co-infections.

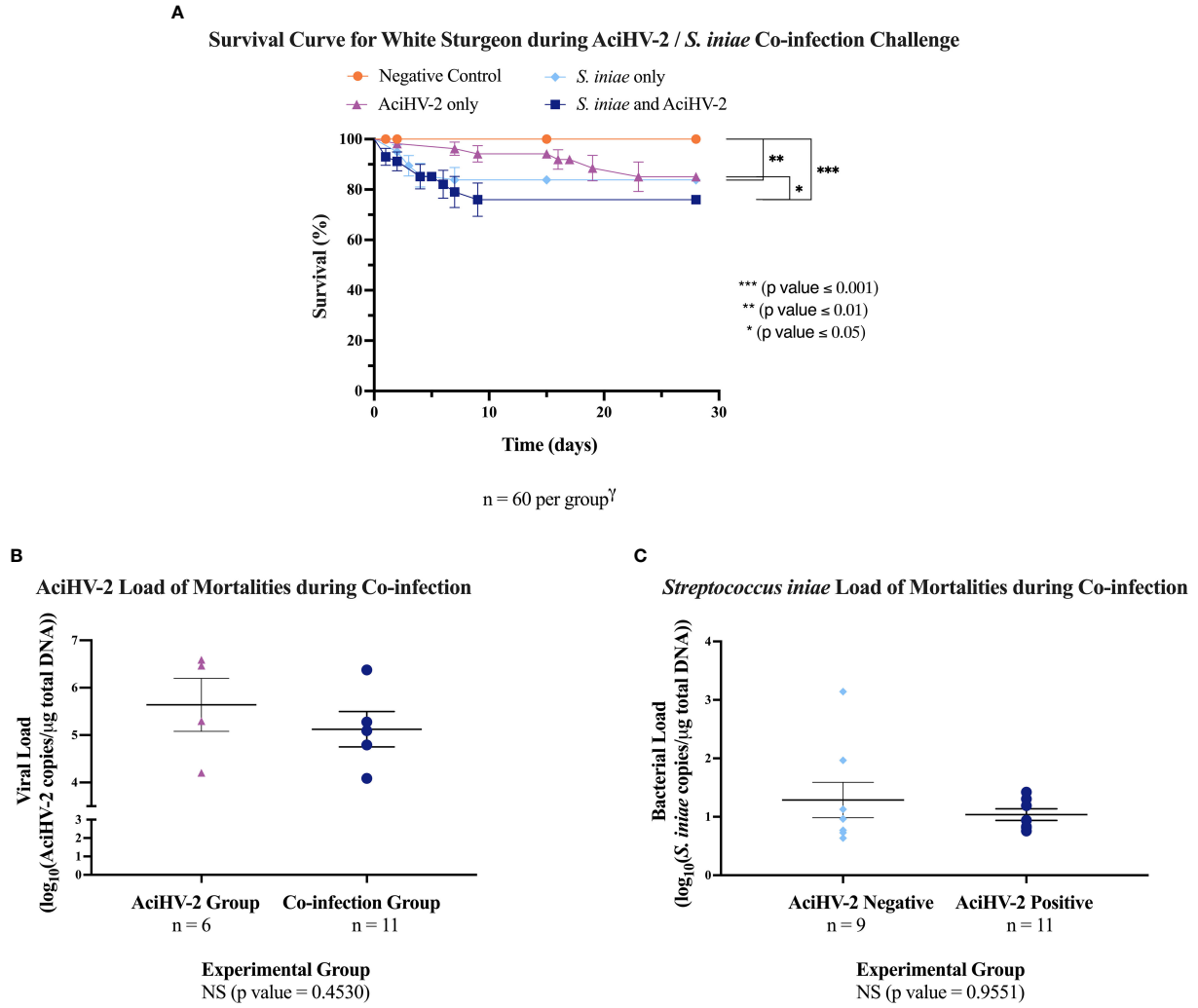

FIGURE 6
Acipenserid Herpesvirus 2 (AciHV-2) and *Streptococcus iniae* (*S. iniae*) co-infection large-scale challenge. An immersion challenge model was performed by exposing white sturgeon fingerlings to a 5.96x10^2 $TCID_{50}$/mL AciHV-2 bath or a sterile cell culture media bath for 1 hour. Survivors of this challenge at 44 days were re-sorted into groups of 60 fish (triplicate tanks of 20 fish each) per treatment. Fish received either 10^6 CFU of *S. iniae* or sterile Phosphate Buffered Saline in the epaxial musculature. Mortality was monitored for 28 days after injection and mortalities tested for AciHV-2 and *S. iniae* via quantitative polymerase chain reaction (qPCR). **(A)** The solid shapes represent the mean cumulative mortality at each day, with standard error of the mean plotted. The different experimental groups are color coded. A statistically significant reduction in survival is seen in all infected groups when compared to the negative control, except for the AciHV-2 group. When comparing infected groups among themselves, the co-infection group has the lowest survival, showing a statistically significant reduction compared to the AciHV-2 group. **(B)** The solid dots represent the mean viral load of sampled mortalities, with the standard error of the mean plotted. There was no statistical difference in viral loads between groups. This also shows that 67% and 45% of the mortalities in the AciHV-2 and in the co-infection groups, respectively, tested positive for AciHV-2. There is a strong association between an AciHV-2 positive status and the experimental group (p value = 0.0027). **(C)** The solid dots represent the mean bacterial load of sampled mortalities, with the standard error of the mean plotted. There was no statistical difference in bacterial loads between groups. This also shows that 89% and 45% of the mortalities in the *S. iniae* and in the co-infection groups, respectively, tested positive for *S. iniae*. There is a strong association between an *S. iniae* positive status and the experimental group (p value ≤ 0.0001).

In terms of the bacterial infection dose, a study assessing *S. iniae* infections in tilapia (*Oreochromis niloticus*) showed that infection dose had an impact on the mortality rate observed only if high-density conditions were present (Shoemaker et al., 2000). High-density environments have been associated with immunosuppression in fish due to eliciting a physiologic stress response (Aidos et al., 2020). Our two studies combined seem to support that both factors (high bacterial infection dose and immunomodulation) must be present in order to impact mortality in a statistically significant manner.

In terms of the timing of the infection, in the ABV-*S. iniae* study using Japanese flounder mentioned above, the authors observed that if they infected the flounder with *S. iniae* 3 weeks post ABV infection rather than 1-week, no difference in mortality was observed between co-infection and single pathogen groups (Pakingking et al., 2003). The authors suggest that active replication of ABV, which happens during early infection, may be required to induce immunosuppression and worsen the outcome of the *S. iniae* infection. In our large-scale challenge, fish were infected

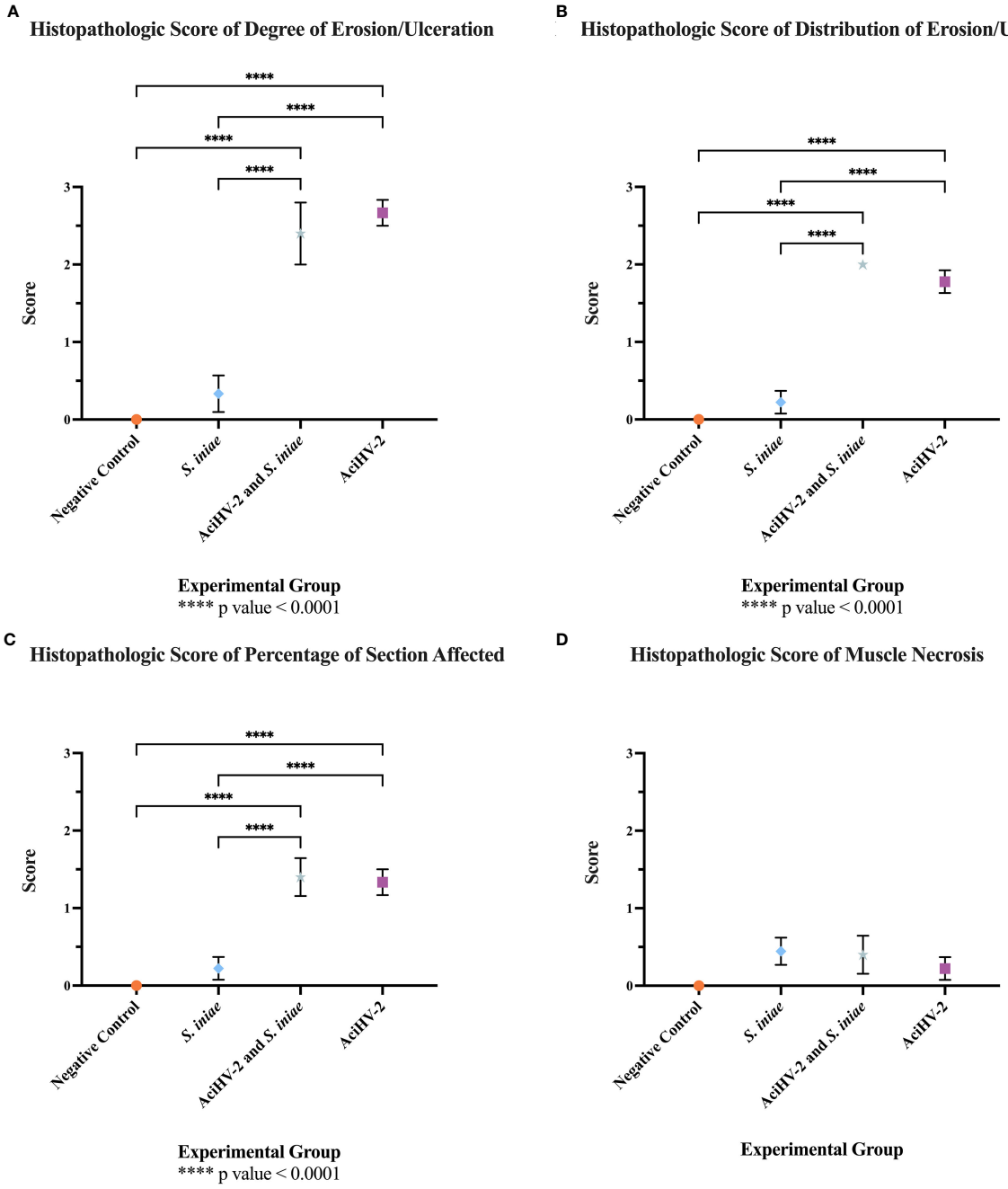

FIGURE 7
Histopathologic evaluation of tissues from mortalities of the co-infection challenge. An immersion challenge model was performed by exposing white sturgeon fingerlings to a 5.96x10^2 $TCID_{50}$/mL Acipenserid herpesvirus 2 (AciHV-2) bath or a sterile cell culture media bath for 1 hour. Survivors of this challenge at 44 days were re-sorted into groups of 60 fish (triplicates of 20 fish) per treatment. Fish received either 10^6 CFU of *S. iniae* or sterile Phosphate Buffered Saline in the epaxial musculature. Mortality was monitored for 28 days after injection and at least 5 mortalities from each challenged group (*S. iniae* group and AciHV-2 group: n = 9 each; co-infection group: n = 5) were submitted for histopathologic analysis. The negative control representatives (n = 10) were submitted as euthanized survivors at the end of the study. **(A)** The "degree of erosion/ulceration" category was scored from 0-3 per slide where 0 represented no erosion or ulceration, 1 represented loss of superficial epithelial cells (erosion), 2 represented loss of epidermis/mucosal epithelium (ulceration), and 3 represented loss of dermis/underlying connective tissue. **(B)** The "distribution of erosion/ulceration" category was scored from 1-2 per slide where 0 represented no erosion or ulceration, 1 represented focal erosion or ulceration, and 2 represented multifocal erosion or ulceration. **(C)** The "percentage of section affected" category was scored from 0-4 per slide where 0 represented no erosion or ulceration, 1 represented less than 25% of the section affected, 2 represented between 25% and 50% of the section affected, 3 represented between 51% and 75% of the section affected, and 4 represented more than 75% of the section affected. **(D)** The "muscle necrosis" category was scored from 0-1 per slide where 0 represented no muscle necrosis present, and 1 represented muscle necrosis present. Results reveal that the degree of, distribution of, and percentage of section affected with erosion/ulceration appears to be driven by the AciHV-2 infection. In addition, none of the infected groups had significant muscle necrosis present in the sections analyzed. Values represent mean with standard error of the mean plotted.

10.3389/faquc.2024.1306518

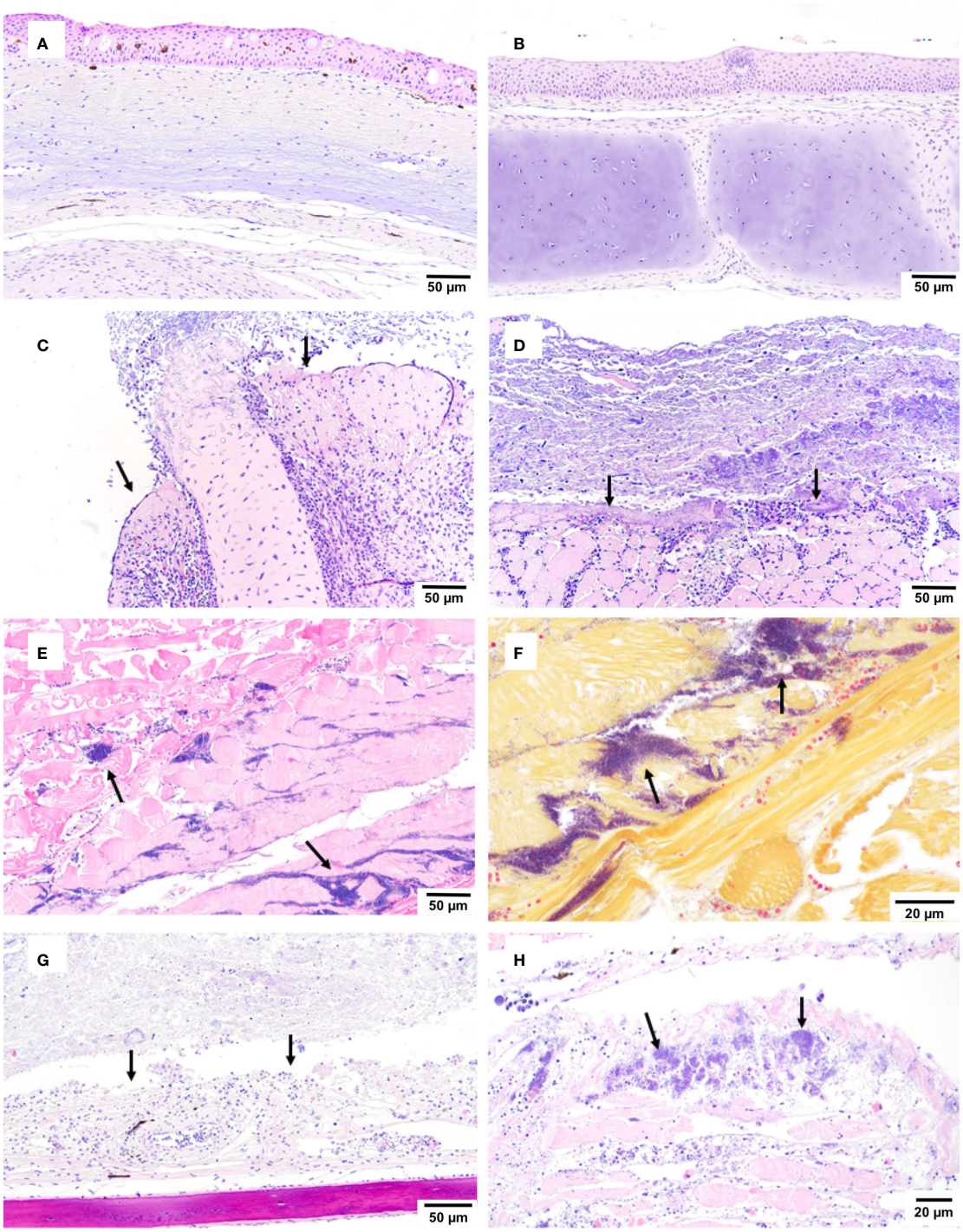

FIGURE 8
Histopathological findings during co-infection challenge. An immersion challenge model was performed by exposing white sturgeon fingerlings to a 5.96x10^2 $TCID_{50}$/mL Acipenserid herpesvirus 2 (AciHV-2) bath or a sterile cell culture media bath for 1 hour. Survivors of this challenge at 44 days were re-sorted into groups of 60 fish (triplicates of 20 fish) per treatment. Fish received either 10^6 CFU of *S. iniae* or sterile Phosphate Buffered Saline in the epaxial musculature. Mortality was monitored for 28 days after injection and at least 5 mortalities from each challenged group (*S. iniae* group and AciHV-2 group: n = 9 each; co-infection group: n = 5) were submitted for histopathologic analysis. The negative control representatives (n = 10) were submitted as euthanized survivors at the end of the study. **(A, B)** the negative control showed no overt pathology (H&E). **(C, D)** the AciHV-2 group showed ulceration - loss of epithelium, and exposure of underlying connective tissue/cartilage **(C)** or skeletal muscle **(D)** with secondary oomycete **(C)** or bacterial **(D)** colonization (H&E). **(E)** the *S. iniae* group showed regionally extensive rhabdomyonecrosis with large numbers of intralesional coccoid bacteria (H&E). **(F)** the *S. iniae* group showed regionally extensive rhabdomyonecrosis with large numbers of intralesional Gram-positive bacteria (Gram stain). **(G)** the co-infection group showed ulceration - loss of epidermis, and exposure of underlying connective tissue/cartilage with secondary colonization by bacteria (H&E). **(H)** the co-infection group showed regionally extensive rhabdomyonecrosis with large numbers of intralesional coccoid bacteria (H&E). The black arrows point towards the lesions described.

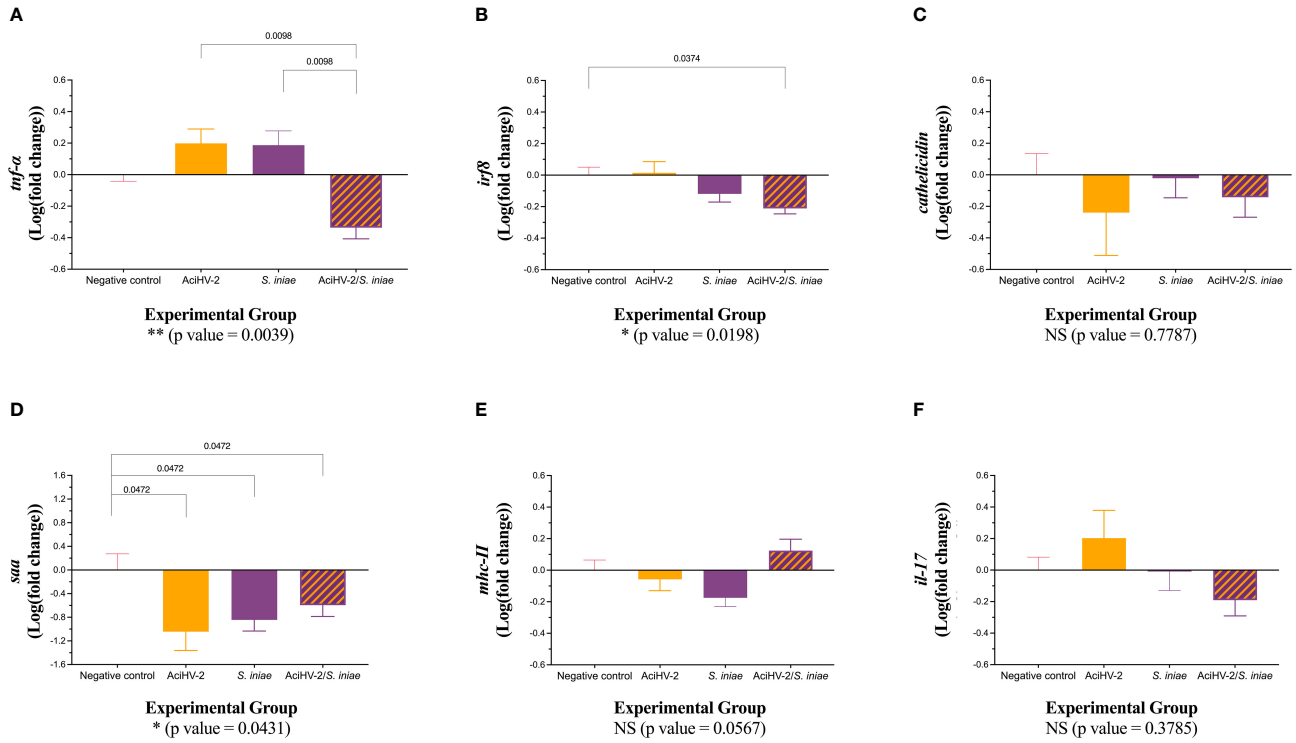

FIGURE 9
Gene expression at 15 days post co-infection challenge. An immersion challenge model was performed by exposing white sturgeon fingerlings to a 5.96x10^2 $TCID_{50}$/mL bath or a sterile cell culture media bath for 1 hour. Survivors of this challenge at 44 days were re-sorted into groups of 60 fish (triplicates of 20 fish) per treatment. Fish received either 10^6 CFU of *S. iniae* or sterile Phosphate Buffered Saline in the epaxial musculature. Mortality was monitored for 28 days after injection. Two fish per tank (six fish per group) were euthanized at 15 days post-injection and spleens were collected for reverse transcription quantitative polymerase chain reaction (RT-qPCR) of important players in the immune response, using elongation factor and beta-actin as housekeeping genes. Results are plotted as the mean and standard error of the mean. Results reveal a statistically significant transcriptional downregulation of *tumor necrosis factor alpha* (*tnfα* - **A)** in the coinfection group compared to the single pathogen groups, as well as some differential transcription of *interferon regulatory factor 8* (*irf8* - **B)** and *serum amyloid a* (*saa* - **D)** when compared to the negative control. **A** is for tumor necrosis factor alpha, **B** is for interferon regulatory factor 8, **C** is for cathelicidin, **D** is for serum amyloid A, **E** is for major histocompatibility complex II, and **F** is for interleukin 17.

with *S. iniae* 44 days after the AciHV-2 immersion compared to 80 days post-immersion in the pilot challenge. It is possible that the transcriptional profile of AciHV-2 is different this early after the active outbreak and the immunomodulatory effects are thus distinct from later in its life cycle, which has been described for multiple herpesviruses of mammals (Ye et al., 2011; Rozman et al., 2022). Further comparative studies are warranted to tease apart the contribution to mortality of bacterial infectious dose and of bacterial infection timing in relation to viral infection during this co-infection scenario.

It is well described that latency is not a static, but rather a dynamic state where the virus is mostly dormant, yet the transcriptional profile is not fixed. For example, low levels of lytic gene expression have been detected in cells harboring Herpes Simplex Virus 1 (HSV-1) in the absence of any other evidence of reactivation (Bloom, 2016). Furthermore, studies have also shown that within a population of cells latently infected with HSV-1, a sub-population of those cells can go through transient reactivation while the remaining cells still lack detectable infectious virus or viral lytic transcripts (Bloom, 2016). Given this information, the term latency is applicable only at the cellular level rather than the tissue level. This is important to consider when we assess the effects of the viral population on the immune system of the host. In theory, at any time after the initial outbreak, herpesviruses have the capacity to benefit from the immunomodulation obtained through the expression of specific latency-associated transcripts while going through reactivation events that ensure passing progeny to new hosts. In this study, our main hypothesis suggests that the potentially latent AciHV-2 interacts with the immune system of the white sturgeon in a way that changes the fish's interaction with *S. iniae*. In the pilot challenge, fin clips were collected from all survivors prior to the bacterial infection (Figure 2D), from all mortalities after the bacterial infection (Figure 5B), and from all survivors after the bacterial infection (Figure 5D) to test AciHV-2 detection via qPCR as a marker of reactivation. When assessing the distribution of positive fish throughout the tanks, it is most notably observed that for the co-infection group there is one fish in Tank 1 that was positive during the pre-bacterial infection timepoint that is not detected positive again (Supplementary Figure 3, Tank 1 of the co-infection group) and two fish in Tank 2 that test negative during the pre-bacterial infection timepoint but positive during the survivor timepoint (Supplementary Figure 3, Tank 2 of the co-infection group). These results are evidence of the population undergoing some level of herpesviral reactivation. Further studies are needed to

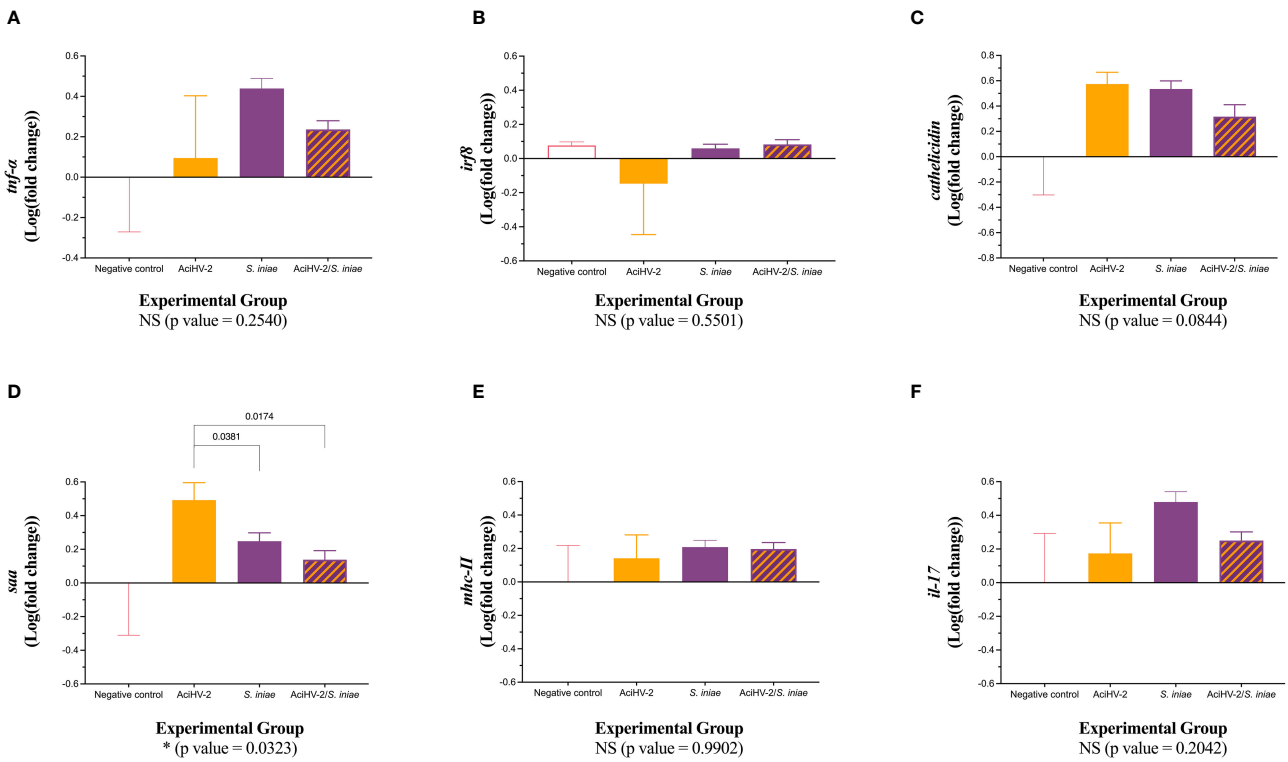

FIGURE 10
Gene expression at 28 days post co-infection challenge. An immersion challenge model was performed by exposing white sturgeon fingerlings to a 5.96x10^2 $TCID_{50}$/mL bath or a sterile cell culture media bath for 1 hour. Survivors of this challenge at 44 days were re-sorted into groups of 60 fish (triplicates of 20 fish) per treatment. Fish received either 10^6 CFU of *S. iniae* or sterile Phosphate Buffered Saline in the epaxial musculature. Mortality was monitored for 28 days after injection. Ten fish per group were euthanized at 28 days post-injection and spleens were collected for reverse transcription quantitative polymerase chain reaction (RT-qPCR) of important players in the immune response, using elongation factor and beta actin as housekeeping genes. Results are plotted as the mean and standard error of the mean. Results reveal a statistically significant transcriptional downregulation of *serum amyloid a* (*saa* - **D)** in the groups infected with bacteria when compared to the AciHV-2 group. **A** is for tumor necrosis factor alpha, **B** is for interferon regulatory factor 8, **C** is for cathelicidin, **D** is for serum amyloid A, **E** is for major histocompatibility complex II, and **F** is for interleukin 17.

show that AciHV-2 achieves latency in a cell population and then to evaluate if latency is maintained in a subpopulation of cells while these reactivation events occur.

It is established that mammalian herpesviruses have multiple pathways for regulating host cellular immune competency, resulting in immune system evasion (Alcami, 2003; Alibek et al., 2014; Crow et al., 2016). The potential for this has also been demonstrated to a lesser extent for certain herpesviruses that affect fish (Piazzon et al., 2015; Lu et al., 2021; Zhou et al., 2021). The evasion mechanisms are diverse, including complement activation inhibition, impaired antigen presentation via numerous pathways, apoptosis and natural killer cell inhibition, interferon signaling interference, and others (Chang et al., 2004; Sehrawat et al., 2018). From the host side, results revealed a significant transcriptional downregulation of *tnfα* at 15 days post-bacterial infection in the co-infection group compared to the *S. iniae* group (Figure 9A). This transcriptional downregulation is not maintained at 28 days post-bacterial infection (Figure 10A). The cytokine TNFα, a potent inflammatory modulator reported to have a prominent pro-inflammatory role while also participating in regulating the extent and duration of the immune response, is mainly produced by activated macrophages, T lymphocytes, and natural killer cells, but it is also expressed at lower levels by various other cells, including fibroblasts, smooth muscle cells, and even tumor cells. Some studies have specifically looked at the augmenting effects of TNFα on B cell proliferation and immunoglobulin production (Pasparaki et al., 1996), which suggests that the transcriptional downregulation of *tnfα* in the spleen at 15 days post-bacterial infection in this study could be having an impact on antibody response. This was supported by the significant decrease in serum anti-*S. iniae* IgM in fish from the co-infection group compared to fish in the single-pathogen group (Figure 11) as had been suggested for pediatric IGASI (Laupland et al., 2000). While a decrease in humoral immunity could be playing a role in this co-infection during the late stages of the disease, and it is most concerning for survivors of the co-infection that were to encounter *S. iniae* again as older fish in the caviar production pipeline, it is unclear at this time if this would be significant in the acute onset of disease where most mortalities were detected during the challenges in this study (first 10 days post-bacterial infection, Figures 5A, 6A). It is important to note though that teleost B cells have been shown to have phagocytic and intracellular killing capacity (Ye and Li, 2020), which may play a role in early immune response against *S. iniae*. More studies are warranted to determine which B cell populations are being affected during these co-infection scenarios and to describe the timeline of humoral immunity development in white sturgeon against *S. iniae*.

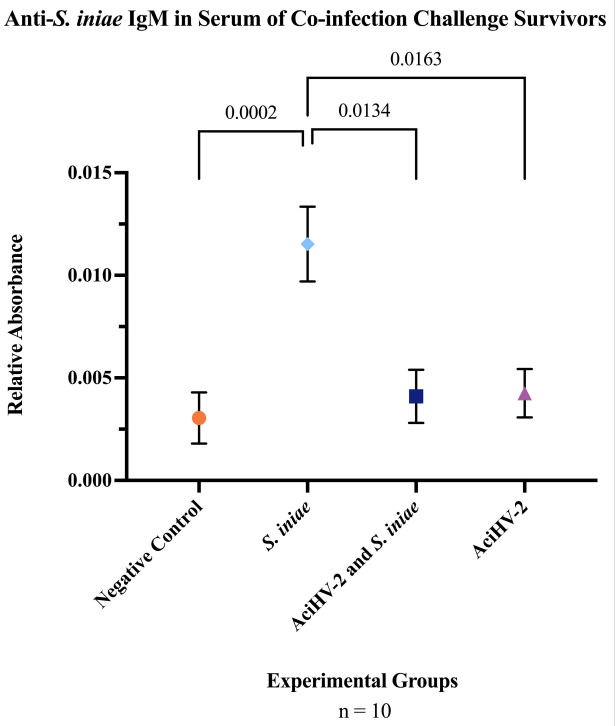

FIGURE 11
Detection of Serum Anti-*S. iniae* IgM in Survivors of Co-infection Challenge. An immersion challenge model was performed by exposing white sturgeon fingerlings to a 5.96x10^2 $TCID_{50}$/mL bath or a sterile cell culture media bath for 1 hour. Survivors of this challenge at 44 days were re-sorted into groups of 60 fish (triplicates of 20 fish) per treatment. Fish received either 10^6 CFU of *S. iniae* or sterile Phosphate Buffered Saline in the epaxial musculature. Mortality was monitored for 28 days after injection and whole blood was collected from the caudal vein of 10 survivors per group. Serum was obtained from the whole blood samples and an indirect enzyme-linked immunosorbent assay (ELISA) was performed to detect anti-*S. iniae* IgM. The solid shapes represent the mean relative absorbance using an $OD_{405\text{-}410}$, with standard error of the mean. The p values calculated between groups is stated in each comparison bracket. Results reveal that the *S. iniae* group that was previously infected with AciHV-2 had a statistically significant decrease in serum anti-*S. iniae* IgM levels compared to the group that received *S. iniae* alone.

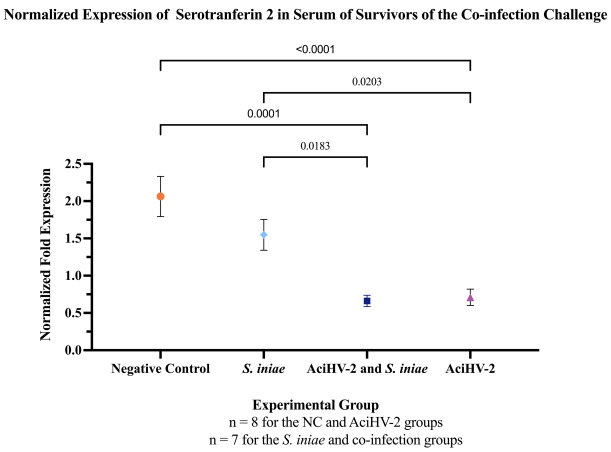

FIGURE 12
Detection of Serum Serotransferrin in Survivors of Co-infection Challenge. An immersion challenge model was performed by exposing white sturgeon fingerlings to a 5.96x10^2 $TCID_{50}$/mL bath or a sterile cell culture media bath for 1 hour. Survivors of this challenge at 44 days were re-sorted into groups of 60 fish (triplicates of 20 fish) per treatment. Fish received either 10^6 CFU of *S. iniae* or sterile Phosphate Buffered Saline in the epaxial musculature. Mortality was monitored for 28 days after injection and whole blood was collected from the caudal vein of 10 survivors per group. Serum was obtained from the whole blood samples and Western Blotting was performed to identify Serotransferrin 2 (STF-2) in the samples. The solid shapes represent the mean normalized fold expression, with standard error the mean plotted. The p values calculated between groups are stated in each comparison bracket. Results reveal that the co-infection and AciHV-2 groups had a statistically significant decrease in serum STF-2 levels compared to the group that received *S. iniae* alone and the negative control.

Recently, sequencing of the full genome of AciHV-2 demonstrated that one of the open reading frames of AciHV-2, ORF 101, has the TNFRSF14_teleost conserved domain (Quijano Carde et al., 2024). This is present in members of the TNF Receptor superfamily, which are common targets for viral manipulation due to their important roles in the regulation of immune responses as well as viral entry (Tiwari et al., 2005; Rakus et al., 2017). While further characterization of ORF 101 in AciHV-2 is needed to understand its expression patterns and effects on the host, other teleost herpesviruses have been shown to influence *tnfα* expression. For example, Cyprinid Herpesvirus 3 (CyHV-3) has been shown to encode two TNFR homologs, of which one causes upregulation of *tnfα* (Zhou et al., 2021). To our knowledge, AciHV-2 alone has not been shown to change expression patterns of *tnfα* in the spleen, but this changes during the co-infection state. Further studies are indicated to determine what interactions lead to the decreased transcript abundance of *tnfα* and of pathogen-specific IgM in the host, and to understand the temporal transcriptional patterns of the host and AciHV-2, particularly as it pertains to the expression of *tnfα* and ORF 101. Assessing translation to determine if these gene expression changes lead to effects at the protein level is also warranted.

The impact of co-infection on the production of the acute-phase protein serotransferrin 2 (STF-2), which has been shown to play a role in the inflammatory response during certain infections in white sturgeon (Soto et al., 2021), was also assessed. Fish exposed to AciHV-2 (both single pathogen and co-infection) had a significant decrease in STF-2 serum levels compared to the Negative control and *S. iniae* groups (Figure 12) at 28 days post-bacterial infection. This finding provides an alternate or perhaps complementary hypothesis on the mechanism behind the decreased anti-*S. iniae* IgM levels in the serum of fish in the co-infection group (Figure 11). Serotransferrin 2 is a protein in the transferrin family, which is known for its iron transportation role. Because of its ability to bind iron, serotransferrin is considered part of the immune response where it creates an iron-limited environment that is not conducive to pathogen replication, including *S. iniae* (Stafford and Belosevic, 2003). This function alone has been identified as a mechanism against herpesvirus as well (Maffettone et al., 2008). Nonetheless, even though this direct mechanism could explain the worsened disease state observed in the co-infection group, serotransferrin has an additional function related to immunity against herpesviruses as it has been described to be a primary activator of fish macrophages, an important antigen-presenting cell to CD4+ T cells in fish (Stafford and Belosevic, 2003).

Evidence indicating that CD4+ T cells are vital for herpesvirus control continues to emerge (Walton et al., 2013). This is particularly highlighted in both susceptibility to and reactivation of herpesviruses when human host has a CD4+ T cell deficiency (Komanduri et al., 2001). CD4+ T cells play a role in herpesvirus control not only by using helper functions, but also by using direct effector functions that impact viral replication via secreted interferon (IFN) gamma and TNFα (Casazza et al., 2006). Finally, CD4+ T cells are also involved in a robust and appropriate humoral response, being shown to be necessary for the generation of plasma and memory B cells, as well as germinal center establishment and responses (Elong Ngono et al., 2019). Given the importance of CD4+ T cell response in the control of herpesviral infections, both during the lytic and latent stages, it has been described that herpesviruses have a variety of strategies to manipulate CD4+ T cell responses (Walton et al., 2013). A potential mechanism by which AciHV-2 – white sturgeon – *S. iniae* interactions lead to an inferior antibody response against *S. iniae* during a co-infection may involve the potential effects of AciHV-2 on the general CD4+ T cell population via a decrease in serotransferrin. Affected CD4+ T cells have been reported to have decreased production of TNFα as well as inhibited cytotoxic effector functions in human and murine cytomegalovirus infections (Walton et al., 2013). This may indicate that the downregulation of TNFα may be related to the poor activation of both fish macrophages and CD4+ T cells.

The results from this study support an altered immune response in the co-infection group, including the hypothesized impaired humoral immunity against *S. iniae* and additional impacts to important players of the innate immune response. Further studies are indicated to determine what interactions lead to the decreased production of pathogen-specific IgM in the host. Piscine streptococcosis is a significant emerging disease of white sturgeon with the capacity to cause outstanding losses in white sturgeon aquaculture, particularly considering its effect on subadult populations. Our understanding of the circumstances under which *S. iniae* causes significant disease and the mechanisms responsible for creating the ideal scenario for this to occur will focus prevention and therapeutic programs in aquaculture farms.

Data availability statement

The raw data supporting the conclusions of this article will be made available by the authors, without undue reservation.

Ethics statement

The animal study was approved by the University of California Institutional Animal Care and Use Committee. The study was conducted in accordance with the local legislation and institutional requirements.

Author contributions

EQC: Conceptualization, Data curation, Formal analysis, Funding acquisition, Investigation, Methodology, Validation, Writing – original draft, Writing – review & editing. KA: Investigation, Writing – review & editing. SY: Formal analysis, Investigation, Methodology, Writing – review & editing. TH: Investigation, Methodology, Writing – review & editing. HJ: Investigation, Writing – review & editing. EH: Formal analysis, Investigation, Methodology, Visualization, Writing – review & editing. SP: Data curation, Formal analysis, Investigation, Methodology, Writing – review & editing. MF: Conceptualization, Formal analysis, Funding acquisition, Investigation, Methodology, Project administration, Resources, Supervision, Validation, Visualization, Writing – review & editing. ES: Conceptualization, Funding acquisition, Investigation, Methodology, Project administration, Resources, Supervision, Validation, Visualization, Writing – review & editing.

Funding

The author(s) declare financial support was received for the research, authorship, and/or publication of this article. This work was supported in part by the Comparative Medical Science Training Program NIH T-32 OD011147 (EMQC) and the USDA National Institute of Food and Agriculture (Animal Health project CACALV-AH-410).

Acknowledgments

The authors wish to thank the team of the Center for Aquatic Biology and Aquaculture at UC Davis for their constant support with the housing and care of the fish used in this project and to Dr. Eric Littman for his assistance with fish care during the pilot study.

Conflict of interest

The authors declare that the research was conducted in the absence of any commercial or financial relationships that could be construed as a potential conflict of interest.

Publisher's note

Supplementary material

The Supplementary Material for this article can be found online at: https://www.frontiersin.org/articles/10.3389/faquc.2024.1306518/full#supplementary-material

References

Aidos, L., Cafiso, A., Serra, V., Vasconi, M., Bertotto, D., Bazzocchi, C., et al. (2020). How different stocking densities affect growth and stress status of acipenser baerii early stage larvae. *Animals.* 10 (8), 1289. doi: 10.3390/ani10081289

Alcami, A. (2003). Viral mimicry of cytokines, chemokines and their receptors. *Nat. Rev. Immunol.* 3 (1), 36–50. doi: 10.1038/nri980

Alibek, K., Baiken, Y., Kakpenova, A., Mussabekova, A., Zhussupbekova, S., Akan, M., et al. (2014). Implication of human herpesviruses in oncogenesis through immune evasion and supression. *Infect. Agent Cancer.* 9 (1), 3. doi: 10.1186/1750-9378-9-3

Baiano, J. C. F., and Barnes, A. C. (2009). Towards control of *streptococcus iniae*. *Emerg. Infect. Dis.* 15 (12), 1891–1896. doi: 10.3201/eid1512.090232

Bloom, D. C. (2016). "Chapter two - alphaherpesvirus latency: A dynamic state of transcription and reactivation," in *Advances in virus research* (Cambridge, MA; San Diego, CA, United States; Kidlington, Oxford, London: Academic Press), 53–80. Available at: https://linkinghub.elsevier.com/retrieve/pii/S0065352715000901.

Carocci, F., Lagrange, C., Levavasseur, V., and Yakimushkin, A. (2004). *Sturgeons (Acipenseriformes)* (Rome, Italy: Food and Agriculture Organization of the United Nations). Available at: https://www.fao.org/3/Y5261E/y5261e06.htm.

Casazza, J. P., Betts, M. R., Price, D. A., Precopio, M. L., Ruff, L. E., Brenchley, J. M., et al. (2006). Acquisition of direct antiviral effector functions by CMV-specific CD4+ T lymphocytes with cellular maturation. *J. Exp. Med.* 203 (13), 2865–2877. doi: 10.1084/jem.20052246

Chang, W. L. W., Baumgarth, N., Yu, D., and Barry, P. A. (2004). Human cytomegalovirus-encoded interleukin-10 homolog inhibits maturation of dendritic cells and alters their functionality. *J. Virol.* 78 (16), 8720–8731. doi: 10.1128/JVI.78.16.8720-8731.2004

Cohen, J. I. (2020). Herpesvirus latency. *J. Clin. Invest.* 130 (7), 3361–3369. doi: 10.1172/JCI136225

Crow, M. S., Lum, K. K., Sheng, X., Song, B., and Cristea, I. M. (2016). Diverse mechanisms evolved by DNA viruses to inhibit early host defenses. *Crit. Rev. Biochem. Mol. Biol.* 51 (6), 452–481. doi: 10.1080/10409238.2016.1226250

Eide, K. E., Miller-Morgan, T., Heidel, J. R., Kent, M. L., Bildfell, R. J., LaPatra, S., et al. (2011). Investigation of koi herpesvirus latency in koi. *J. Virol.* 85 (10), 4954–4962. doi: 10.1128/JVI.01384-10

Elong Ngono, A., Young, M. P., Bunz, M., Xu, Z., Hattakam, S., Vizcarra, E., et al. (2019). CD4+ T cells promote humoral immunity and viral control during Zika virus infection. *PloS Pathog.* 15 (1), e1007474. Fernandez-Sesma A. doi: 10.4049/jimmunol.202.Supp.140.15

Ethier, V. (2014). *Farmed sturgeon* (Monterey, CA, United States: Monterey Bay Aquarium Seafood Watch). Available at: https://seafood.ocean.org/wp-content/uploads/2016/10/Sturgeon-Farmed-US.pdf.

Frère, J., Bidet, P., Tapiéro, B., Rallu, F., Minodier, P., Bonacorsi, S., et al. (2016). Clinical and microbiological characteristics of invasive group A streptococcal infections before and after implementation of a universal varicella vaccine program: table 1. *Clin. Infect. Dis.* 62 (1), 75–77. doi: 10.1093/cid/civ793

Goodwin, A. (2012). *Herpesviruses in fish* (Stoneville, MS, United States: Southern Regional Aquaculture Center).

Hanson, L. A., Rudis, M. R., Vasquez-Lee, M., and Montgomery, R. D. (2006). A broadly applicable method to characterize large DNA viruses and adenoviruses based on the DNA polymerase gene. *Virol. J.* 3 (1), 28. doi: 10.1186/1743-422X-3-28

Heckman, T. I., Shahin, K., Henderson, E. E., Griffin, M. J., and Soto, E. (2022). Development and efficacy of *Streptococcus iniae* live-attenuated vaccines in Nile tilapia, Oreochromis niloticus. *Fish Shellfish Immunol.* 121, 152–162. doi: 10.1016/j.fsi.2021.12.043

Hedrick, R., McDowell, T., Groff, J., Yun, S., and Wingfield, W. (1991). Isolation of an epitheliotropic herpesvirus from white sturgeon *Acipenser transmontanus*. *Dis. Aquat Organ.* 11, 49–56. doi: 10.3354/dao011049

Hedrick, R. P., McDowell, T. S., Rosemark, R., Aronstein, D., and Lannan, C. N. (1991). Two cell lines from white sturgeon. *Trans. Am. Fish Soc* 120 (4), 528–534. doi: 10.1577/1548-8659(1991)120<0528:TCLFWS>2.3.CO;2

Jarvis, M. A., and Nelson, J. A. (2007). "Chapter 42: Molecular basis of persistence and latency," in *Human herpesviruses: biology, therapy, and immunoprophylaxis* (Cambridge: Cambridge University Press). Available at: https://www.ncbi.nlm.nih.gov/books/NBK47414/?report=reader#_NBK47414_pubdet_.

Kelly, J. (2019). *White sturgeon* (West Sacramento, CA, United States: California Department of Fish and Wildlife). Available at: https://wildlife.ca.gov/Conservation/Fishes/Sturgeon/White-Sturgeon.

Komanduri, K. V., Feinberg, J., Hutchins, R. K., Frame, R. D., Schmidt, D. K., Viswanathan, M. N., et al. (2001). Loss of cytomegalovirus-specific CD4 $^{+}$ T cell responses in human immunodeficiency virus type 1–infected patients with high CD4 $^{+}$ T cell counts and recurrent retinitis. *J. Infect. Dis.* 183 (8), 1285–1289. doi: 10.1086/319683

Laskey, A. L., Johnson, T. R., Dagartzikas, M. I., and Tobias, J. D. (2000). Endocarditis attributable to group A hemolytic streptococcus after uncomplicated varicella in a vaccinated child. *PEDIATRICS.* 106 (3), 4. doi: 10.1542/peds.106.3.e40

Laupland, K. B., Davies, H. D., Low, D. E., Schwartz, B., Green, K.the Ontario Group A Streptococcal Study Group, et al. (2000). Invasive group A streptococcal disease in children and association with varicella-zoster virus infection. *Pediatrics* 105 (5). doi: 10.1542/peds.105.5.e60

Lei, C., Yang, J., Hu, J., and Sun, X. (2021). On the calculation of TCID50 for quantitation of virus infectivity. *Virol. Sin.* 36 (1), 141–144. doi: 10.1007/s12250-020-00230-5

Lepa, A., and Siwicki, A. K. (2012). Fish herpesvirus diseases: a short review of current knowledge. *Acta Vet. Brno.* 81 (4), 383–389. doi: 10.2754/avb201281040383

López-Porras, A., Elizondo, C., Chaves, A. J., Camus, A. C., Griffin, M. J., Kenelty, K., et al. (2019). Application of multiplex quantitative polymerase chain reaction methods to detect common bacterial fish pathogens in Nile tilapia, *Oreochromis niloticus* , hatcheries in Costa Rica. *J. World Aquac Soc* 50 (3), 645–658. doi: 10.1111/jwas.12576

Lu, J. F., Jin, T. C., Zhou, T., Lu, X. J., Chen, J. P., and Chen, J. (2021). Identification and characterization of a tumor necrosis factor receptor like protein encoded by Cyprinid Herpesvirus 2. *Dev. Comp. Immunol.* 116, 103930. doi: 10.1016/j.dci.2020.103930

Maffettone, C., De Martino, L., Irace, C., Santamaria, R., Pagnini, U., Iovane, G., et al. (2008). Expression of iron-related proteins during infection by bovine herpes virus type-1. *J. Cell Biochem.* 104 (1), 213–223. doi: 10.1002/jcb.21618

Miller, J. D., and Neely, M. N. (2005). Large-scale screen highlights the importance of capsule for virulence in the zoonotic pathogen *streptococcus iniae*. *Infect. Immun.* 73 (2), 921–934. doi: 10.1128/IAI.73.2.921-934.2005

Mugetti, D., Pastorino, P., Menconi, V., Pedron, C., and Prearo, M. (2020). The old and the new on viral diseases in sturgeon. *Pathogens.* 9 (2), 146. doi: 10.3390/pathogens9020146

Nguyen, D. T., Marancik, D., and Soto, E. (2020). Intracoelomic- and intramuscular-injection challenge model of piscine streptococcosis in white sturgeon fingerlings. *J. Aquat Anim. Health* 32 (3), 133–138. doi: 10.1002/aah.10112

Nicoli, F., and Appay, V. (2017). Immunological considerations regarding parental concerns on pediatric immunizations. *Vaccine.* 35 (23), 3012–3019. doi: 10.1016/j.vaccine.2017.04.030

Oyake, S., Ohi, T., and Koga, M. (2000). A case of varicella complicated by cellulitis and scarlet fever due to *streptococcus pyogenes*. *J. Dermatol.* 27 (11), 750–752. doi: 10.1111/j.1346-8138.2000.tb02272.x

Pakingking, R., Takano, R., Nishizawa, T., Mori, K., Iida, Y., Arimoto, M., et al. (2003). Experimental Coinfection with Aquabirnavirus and Viral Hemorrhagic Septicemia Virus (VHSV), *Edwardsiella tarda* or *Streptococcus iniae* in Japanese Flounder Paralichthys olivaceus. *Fish Pathol.* 38 (1), 15–21. doi: 10.3147/jsfp.38.15

Pasparaki, M., Alexopoulou, L., Episkopou, V., and Kollias, G. (1996). Immune and inflammatory responses in TNF~-deficient mice: A critical requirement for TNFoL in the formation of primary B cell follicles, follicular dendritic cell networks and germinal centers, and in the maturation of the humoral immune response. *J. Exp. Med.* 184, 1397–1411. doi: 10.1084/jem.184.4.1397

Piazzon, M. C., Wentzel, A. S., Tijhaar, E. J., Rakus, K. Ł., Vanderplasschen, A., Wiegertjes, G. F., et al. (2015). Cyprinid herpesvirus 3 Il10 inhibits inflammatory activities of carp macrophages and promotes proliferation of Igm $^{+}$ B cells and memory T cells in a manner similar to carp Il10. *J. Immunol.* 195 (8), 3694–3704. doi: 10.4049/jimmunol.1500926

Pierezan, F., Shahin, K., Heckman, T. I., Ang, J., Byrne, B. A., and Soto, E. (2020). Outbreaks of severe myositis in cultured white sturgeon (*Acipenser transmontanus* L.) associated with *Streptococcus iniae*. *J. Fish Dis.* 43 (4), 485–490. doi: 10.1111/jfd.13145

Quijano Carde, E. M., Anenson, K., Waldbieser, G., Brown, C. T., Griffin, M., Henserson, E., et al. (2024). Acipenserid herpesvirus 2 genome and partial validation of a qPCR for its detection in white sturgeon Acipenser transmontanus. *Dis. Aquat. Org.* 157, 45-59. doi: 10.3354/dao03768

Rakus, K., Ronsmans, M., Forlenza, M., Boutier, M., Piazzon, M. C., Jazowiecka-Rakus, J., et al. (2017). Conserved fever pathways across vertebrates: A herpesvirus expressed decoy TNF-α Receptor delays behavioral fever in fish. *Cell Host Microbe* 21 (2), 244–253. doi: 10.1016/j.chom.2017.01.010

Reed, A. N., Izume, S., Dolan, B. P., LaPatra, S., Kent, M., Dong, J., et al. (2014). Identification of B cells as a major site for cyprinid herpesvirus 3 latency. *J. Virol.* 88 (16), 9297–9309. doi: 10.1128/JVI.00990-14

Rozman, B., Nachshon, A., Levi Samia, R., Lavi, M., Schwartz, M., and Stern-Ginossar, N. (2022). Temporal dynamics of HCMV gene expression in lytic and latent infections. *Cell Rep.* 39 (2), 110653. doi: 10.1016/j.celrep.2022.110653

Sehrawat, S., Kumar, D., and Rouse, B. T. (2018). Herpesviruses: harmonious pathogens but relevant cofactors in other diseases? *Front. Cell Infect. Microbiol.* 8, 177. doi: 10.3389/fcimb.2018.00177

Shoemaker, C. A., Evans, J. J., and Klesius, P. H. (2000). Density and dose: factors affecting mortality of *Streptococcus iniae* infected tilapia žOreochromis niloticus/. *Aquaculture.* 188, 229–235. doi: 10.1016/S0044-8486(00)00346-X

Soto, E., Coleman, D., Yazdi, Z., Purcell, S. L., Camus, A., and Fast, M. D. (2021). Analysis of the white sturgeon (*Acipenser transmontanus*) immune response during immunostimulation and *Veronaea botryosa* infection. *Comp. Biochem. Physiol. Part D Genomics Proteomics.* 40, 100879. doi: 10.1016/j.cbd.2021.100879

Soto, E., Fast, M. D., Purcell, S. L., Denver Coleman, D., Yazdi, Z., Kenelty, K., et al. (2022). Expression of immune markers of white sturgeon (*Acipenser transmontanus*) during Veronaea botryosa infection at different temperatures. *Comp. Biochem. Physiol. Part D Genomics Proteomics.* 41, 100950. doi: 10.1016/j.cbd.2021.100950

Soto, E., Richey, C., Stevens, B., Yun, S., Kenelty, K., Reichley, S., et al. (2017). Co-infection of Acipenserid herpesvirus 2 (AciHV-2) and *Streptococcus iniae* in cultured white sturgeon *Acipenser transmontanus*. *Dis. Aquat Organ.* 124 (1), 11–20. doi: 10.3354/dao03108

Speck, S. H., and Ganem, D. (2010). Viral latency and its regulation: lessons from the gammaherpesviruses. *Cell Host Microbe* 8 (1), 100–115. doi: 10.1016/j.chom.2010.06.014

Stafford, J. L., and Belosevic, M. (2003). Transferrin and the innate immune response of fish: identification of a novel mechanism of macrophage activation. *Dev. Comp. Immunol.* 27 (6–7), 539–554. doi: 10.1016/S0145-305X(02)00138-6

Stingley, R. L., Griffin, B. R., and Gray, W. L. (2003). Channel catfish virus gene expression in experimentally infected channel catfish, *Ictalurus punctatus* (Rafinesque). *J. Fish Dis.* 26 (8), 487–493. doi: 10.1046/j.1365-2761.2003.00484.x

Strom, M. A., Hsu, D. Y., and Silverberg, J. I. (2017). Prevalence, comorbidities and mortality of toxic shock syndrome in children and adults in the USA: Epidemiology of Toxic Shock Syndrome. *Microbiol. Immunol.* 61 (11), 463–473. doi: 10.1111/1348-0421.12539

Sturgeon, J. P., Segal, L., and Verma, A. (2015). Going out on a limb: do not delay diagnosis of necrotizing fasciitis in varicella infection. *Pediatr. Emerg. Care* 31 (7), 503–507. doi: 10.1097/PEC.0000000000000255

Suárez-Arrabal, M. C., Sánchez Cámara, L. A., Navarro Gómez, M. L., Santos Sebastián M del, M., Hernández-Sampelayo, T., Cercenado Mansilla, E., et al. (2019). Enfermedad invasiva por *Streptococcus pyogenes*: cambios en la incidencia y factores pronósticos. *Pediatría.* 91 (5), 286–295. doi: 10.1016/j.anpedi.2018.12.017

Tiwari, V., Clement, C., Scanlan, P. M., Kowlessur, D., Yue, B. Y. J. T., and Shukla, D. (2005). A role for herpesvirus entry mediator as the receptor for herpes simplex virus 1 entry into primary human trabecular meshwork cells. *J. Virol.* 79 (20), 13173–13179. doi: 10.1128/JVI.79.20.13173-13179.2005

Walton, S., Mandaric, S., and Oxenius, A. (2013). CD4 T cell responses in latent and chronic viral infections. *Front. Immunol.* 4. doi: 10.3389/fimmu.2013.00105/abstract

Watson, L., Yun, S., Groff, J., and Hedrick, R. (1995). Characteristics and pathogenicity of a novel herpesvirus isolated from adult and subadult white sturgeon *Acipenser transmontanus*. *Dis. Aquat Organ.* 22, 199–210. doi: 10.3354/dao022199

Wilson, G. J., Talkington, D. F., Gruber, W., Edwards, K., and Dermody, T. S. (1995). Group A streptococcal necrotizing fasciitis following varicella in children: case reports and review. *Clin. Infect. Dis.* 20 (5), 1333–1338. doi: 10.1093/clinids/20.5.1333

Ye, F., Lei, X., and Gao, S. J. (2011). Mechanisms of kaposi's sarcoma-associated herpesvirus latency and reactivation. *Adv. Virol.* 2011, 1–19. doi: 10.1155/2011/193860

Wu, L., Qin, Z., Liu, H., Lin, L., Ye, J., and Li, J. (2020). Recent advances on phagocytic B cells in teleost fish. *Front. Immunol. Dis. Aquat. Org.* 157, 45-59. doi: 10.3389/fimmu.2020.00824

Zhou, Y., Ouyang, P., Tao, Y., Yin, L., Wang, K., Geng, Y., et al. (2021). Comparison the function of Cyprinid herpesvirus 3 encoded two viral tumor necrosis factor receptors. *Aquac Rep.* 21, 100878. doi: 10.1016/j.aqrep.2021.100878

frontiers | Frontiers in Immunology

TYPE Original Research
PUBLISHED 12 June 2024
DOI 10.3389/fimmu.2024.1304603

OPEN ACCESS

EDITED BY
Isabel Bandín,
University of Santiago de Compostela, Spain

REVIEWED BY
Marina Machado,
University of Porto, Portugal
Marco Albano,
University of Messina, Italy

*CORRESPONDENCE
Elena Chaves-Pozo
elena.chaves@ieo.csic.es

RECEIVED 29 September 2023
ACCEPTED 13 May 2024
PUBLISHED 12 June 2024

CITATION
García-Beltrán JM, Johnstone C, Arizcun M, Cuesta A, Pérez M and Chaves-Pozo E (2024) The susceptibility of shi drum juveniles to betanodavirus increases with rearing densities in a process mediated by neuroactive ligand–receptor interaction.
Front. Immunol. 15:1304603.
doi: 10.3389/fimmu.2024.1304603

The susceptibility of shi drum juveniles to betanodavirus increases with rearing densities in a process mediated by neuroactive ligand–receptor interaction

José María García-Beltrán[1,2], Carolina Johnstone[3], Marta Arizcun[1], Alberto Cuesta[2], Montse Pérez[4] and Elena Chaves-Pozo[1]*

[1]Physiology and Welfare of Marine Species Group (PHYSIS), Centro Oceanográfico de Murcia, Instituto Español de Oceanografía (COMU-IEO), Consejo Superior de Investigaciones Científicas (CSIC), Murcia, Spain, [2]Immunobiology for Aquaculture Group, Department of Cell Biology and Histology, Faculty of Biology, University of Murcia, Murcia, Spain, [3]Physiology and Welfare of Marine Species Group (PHYSIS), Centro Oceanográfico de Málaga, Instituto Español de Oceanografía (COMA-IEO), Consejo Superior de Investigaciones Científicas (CSIC), Málaga, Spain, [4]Centro Oceanográfico de Vigo, Instituto Español de Oceanografía (COV-IEO), Consejo Superior de Investigaciones Científicas (CSIC), Vigo, Spain

Nervous necrosis virus (NNV) is one of the greatest threats to Mediterranean aquaculture, infecting more than 170 fish species and causing mortalities up to 100% in larvae and juveniles of susceptible species. Intensive aquaculture implies stressed conditions that affect the welfare of fish and their ability to fight against infections. In fact, a higher susceptibility to NNV has been related to poor welfare conditions. In order to analyze the physiological link between stressed conditions and increased susceptibility to NNV, as well as its possible role in the pathogenesis of this disease, we reared shi drum (*Umbrina cirrosa*) juveniles (30.7 $\pm$ 3.10 g body weight), which are expected to be asymptomatic upon NNV infection, at three stocking densities (2, 15, and 30 kg/m^3) for 27 days and subsequently challenged them with NNV. We firstly characterized the stressed conditions of the specimens before and after infection and recorded the mortalities, demonstrating that stressed specimens reared at 30 kg/m^3 suffered mortalities. However, the viral loads in different tissues were similar in all experimental groups, allowing horizontal and vertical transmission of the virus from asymptomatic specimens. All of these data suggest that shi drum tolerates wide ranges of culture densities, although high densities might be a setback for controlling NNV outbreaks in this species. In an attempt to understand the molecular pathways orchestrating this susceptibility change in stressed conditions, we performed a transcriptomic analysis of four tissues under mock- and NNV-infected conditions. In addition to the modification of the exceptive pathways such as cell adhesion, leukocyte migration, cytokine interaction, cell proliferation and survival, and autophagy, we also observed a heavy

alteration of the neuroactive ligand–receptor pathway in three of the four tissues analyzed. Our data also point to some of the receptors of this pathway as potential candidates for future pharmacological treatment to avoid the exacerbated immune response that could trigger fish mortalities upon NNV infection.

KEYWORDS

Umbrina cirrosa, nodavirus, welfare, immune response, stocking densities, pathogenesis, immune-neuroendocrine interactions

1 Introduction

Aquaculture is one of the world's fastest growing food sectors and the main fish supplier to the world's population (1). For this reason, the diversification of aquaculture species with economic potential favors the sustainability of aquaculture and is becoming increasingly important in the development of this production sector (2, 3). Among the new fish species, shi drum (*Umbrina cirrosa*) is an ideal candidate with high economic and nutritional value, particularly in the Mediterranean area (4, 5). Thus, shi drum presents high growth rate, elevated market value, good meat quality, and great adaptability to culture conditions (4–6), being a promising candidate for Mediterranean aquaculture diversification. However, and with regard to the FAO annual reports, shi drum was cultivated in low quantities in Italy in 2013 (7) and, according to some publications, in Greece in the 1990s (8). The fact that the industrial culture of shi drum has not been consolidated yet could be due to some gaps on the knowledge about its biology, to technical problems, or to inadequate market promotion policies that dissuade enterprises to produce this species, among others (3). Although several aspects of shi drum biology have been studied since the 1990s, such as its reproduction, digestive system development, dietary requirements, and growth performance (9), its immunity or stress has only recently started to be assessed (9–11).

Stocking density is one of the main factors that lead to chronic stress responses in fish (12). In this sense, high stocking densities typically have adverse effects on the growth, health, and general welfare of fish (13, 14), while low stocking densities could reduce feed competition, resulting in a decrease in feed intake and growth (14). In aquaculture facilities, chronic stress could be identified through the study of operational welfare indicators (OWIs), which are parameters specific to each species and farming system, related to health from the functional approach to wellbeing, and include both observational measures and water quality and biological parameters (15). The identification of chronic stress is mandatory as it can cause the development of diseases (16). In particular, stress can trigger infectious diseases (17). At present, the infectious diseases with the highest threat to aquaculture are those caused by viruses (17). Among them, the nervous necrosis virus (NNV; family Nodaviridae, genus *Betanodavirus*) is one of the most important marine fish viruses, causing the viral encephalopathy and retinopathy (VER) disease (18, 19). NNV is a non-enveloped virus with a spherical shape and icosahedral symmetry and a genome composed of two single-stranded, positive-sense RNA molecules (20) showing horizontal and vertical transmission (18, 19, 21). Betanodaviruses are classified into four genotypes: RGNNV (red-spotted grouper nervous necrosis virus), SJNNV (striped jack nervous necrosis virus), BFNNV (barfin flounder nervous necrosis virus), and TPNNV (tiger puffer nervous necrosis virus) (21). They are capable of infecting more than 170 marine species, including some of great commercial value (21). Shi drum is susceptible to NNV as severe natural outbreaks of RGNNV have been reported in the Mediterranean Sea in both wild and farmed specimens (5, 22–24). To our knowledge, only the viral isolate It/24/Sdr, which corresponds to the RGNNV genotype, was obtained from a wild shi drum specimen captured in Italian marine areas in 1995 (25). In the Adriatic Sea, however, wild shi drum specimens have been included in a multiple species test, but none of them resulted positive, although other fish species did (26). The rest of the reports that detected NNV in shi drum analyzed farmed specimens (5, 8, 27).

Under experimental conditions, shi drum juveniles of 10 g body weight (bw) were found susceptible to all NNV genotypes (RGNNV, SJNNV, BFNNV, and TPNNV), although the signs of the disease and lesions varied depending on the genotype (9). In general, VER disease is characterized by neurological abnormalities (e.g., erratic swimming and spiral movements with the belly up) and a distinct vacuolization of the nerve tissue (brain and retina) (19, 28). VER disease has been detected in larval and early juvenile stages in most of the species (29), although chronic subclinical infections occurred directly proportionally to the age and weight of the fish (18, 19, 21, 30). In addition to host age or weight, other factors related to stressed conditions, such as suboptimal feed, water quality, or crowding, have been reported to influence NNV infection, leading to mortalities in the case of subclinical infection or increasing mortalities in acute infections (30).

The integration of all the physiological functions upon infection is orchestrated by the immune–neuroendocrine system, which determines either the survival of the specimen or the appearance of the disease, as well as the subsequent mortality in different host and external conditions (31). However, in fish, this system is not completely understood in part due to its great complexity, amplified

by genome duplication events occurring during fish evolution, but also due to epigenomic reprogramming that has been linked to environmental clues in marine fish (32). In order to design efficient tools to combat NNV infection, it is important to understand the epidemiology and the pathogenic mechanism of the virus and its association with host physiology and welfare. The stress status in fish can be evaluated through hormones (cortisol), secondary metabolites (glucose and lactate), and the imbalance in the physiological responses such as growth performance, key humoral innate immune activities, or the antioxidant system (33) in different tissues such as the serum, skin mucus, brain, head kidney, spleen, or liver (34, 35). During stress conditions, there is an imbalance in the production of reactive oxygen species (ROS) and its elimination by the antioxidant system, resulting in high concentrations of ROS that can lead to oxidative stress and make fish susceptible to physiological and metabolic diseases (36). Taking all of these into account, the aim of the study was to assess the physiological status of fish reared at three different densities and the association of crowding and stress with susceptibility to NNV. The stress and the welfare status of the fish were characterized using well-known stress parameters and innate immune responses in the serum and skin mucus. The skin mucus is considered a noninvasive sampling tissue and is continuously produced, with functions including the prevention of the adherence of pathogens to underlying tissues and the provision of a medium in which antimicrobial mechanisms can act (37). In addition, the levels of cortisol in water were included in order to evaluate this new noninvasive stress indicator. Upon infection, the stress indicators were analyzed, as well as the mortality rates and the persistence of the virus in different tissues of surviving fish. In the acute viral infection phase, differential gene expression was assessed using a transcriptomic approach in four tissues: the viral target tissue, the brain (and also the first step in most endocrine regulatory axes) (38), and three immune-related tissues—the spleen, the head kidney, and the liver—to explore the immune–neuroendocrine interactions that might link stress with NNV susceptibility in order to identify potential pharmacological targets for further treatment development.

2 Materials and methods

2.1 Animals

Healthy juveniles of shi drum (*U. cirrosa*) (30.7 ± 3.10 g bw) obtained from natural spawns of culture broodstock (39) were bred at the facilities of the Centro Oceanográfico de Murcia, Instituto Español de Oceanografía (COMU-IEO), CSIC, as described elsewhere (4). Fish were reared with an open-flow natural seawater system (38‰ salinity), suitable aeration to maintain dissolved oxygen above 6.5 mg/L, filtration systems, natural temperature (21.47 ± 1.09°C) and photoperiod, and a culture density of 9 kg/m^3. Ammonia (<0.1 mg/L), nitrite (<0.2 mg/L), and nitrate (<50 mg/L) were determined once weekly.

Handling of the specimens was always performed under the Guidelines of the European Union Council (2010/63/UE) and the Bioethical Committees of the IEO (REGA code ES300261040017) and with approval of the Ministry of Water, Agriculture and Environment of the Autonomous Community Region of Murcia (permit no. A13211203).

2.2 Experimental design and sample collection

Based on the aim of this study, fish reared at 9 kg/m^3 were randomly assigned and divided into nine tanks of 0.25 m^3 capacity with an initial density of 2 kg/m^3 (n = 15 fish/tank), 15 kg/m^3(n = 118 fish/tank), or 30 kg/m^3 (n = 235 fish/tank) at the beginning of the experiment and a final density of 1 kg/m^3 (n = 6 fish/tank), 17 kg/m^3 (n = 109 fish/tank), or 35 kg/m^3 (n = 226 fish/tank) at the end of the experiment. Each condition was performed in triplicate tanks. The fish were fed *ad libitum* with a commercial pellet diet (Skretting, Stavanger, Norway), with a maximum intake of 2.8% of their biomass for 27 days. After 7, 21, and 27 days from the start of the experiment, three fish from each tank (n = 9 fish/experimental group) were sampled. Before starting the collection of specimens, water samples from each tank (100mL/tank) were obtained at each sampling time and stored at −80°C until use. Thereafter, fish (n = 3 fish/tank) were captured and placed in an anesthesia bath with 40 µL/L of clove oil. Once the fish reached the loss of reflex reactivity stage of anesthesia, skin mucus samples were collected using a method previously described (40). The skin mucus was vigorously shaken and centrifuged (400 × g, 10 min at 4°C). The supernatant was then collected and stored at −80°C until use. After measuring the bw and length of each fish, they were completely bled. The blood samples were left to clot at 4°C for 4 h. Subsequently, the serum was obtained after centrifugation (10,000 × g, 10 min at 4°C) and stored at −80°C until use.

On day 27, 10 fish from each tank (n = 30 fish/experimental group) were relocated in the infection facilities in 200-L tanks in a close recirculated seawater flux (38‰ salinity), with a 12-h light/12-h dark photoperiod and 27 ± 1°C controlled temperature for NNV challenge. The animals were fed *ad libitum* daily with a commercial pellet diet (Skretting). A control group was established with fish of the 30-kg/m^3 group, which were mock-infected. Infected fish (n = 6/experimental group) were sampled 4 and 18 days post-infection (dpi). The specimens were anesthetized as described previously. Samples of the eye, brain, liver, spleen, and head kidney were collected at 4 dpi and those of the brain and gonad at 18 dpi. The tissue samples were immersed on a DNA/RNA shield (Zymo Research, Irvine, CA, USA) and stored at −80°C until further processing for gene expression analysis.

2.3 Nodavirus infection

NNV (genotype RGNNV, strain It/411/96) was propagated in the E-11 cell line [17]. NNV stocks were titrated and the viral dilution infecting 50% of the cell cultures ($TCID_{50}$) calculated (41). For NNV infection, fish from all experimental groups were intramuscularly injected with 100 µL of the viral suspension (5.6×10^6 $TCID_{50}$/mL) or with phosphate-buffered saline (PBS) in the case of the mock-infected

group (control). The mortality and clinical signs of infection were recorded daily and the percentage of survival determined. Surviving fish were considered as those fish without any signs of disease during the infection trial or those able to overcome signs of disease within 3 days. In contrast, susceptible fish were those that died during the trial or showed signs of disease for three consecutive days, which were then humanely euthanized using baths containing 40 µL/L of clove oil according to the guidelines on the care and use of fish (42).

2.4 Growth performance

Growth was monitored by obtaining the specific growth rate (SGR), which was calculated as: [(ln final weight – ln initial weight)/number days] × 100. Moreover, the condition factor (CF) following Fulton's *K*-index was calculated as: (bw – lenght^3) × 100.

2.5 Plasmatic and skin mucus analysis

The total protein concentration in skin mucus samples was determined using the dye binding method of Bradford (43).

Peroxidase activity was measured as the ability of the samples to oxidate the substrate 3,3′,5,5′-tetramethylbenzidine hydrochloride (TMB; Sigma, St. Louis, MO, USA) in the presence of hydrogen peroxide according to a protocol previously described (44) using 5 µL of serum or 10 µL of skin mucus. Wells with buffer but not samples were used as blanks. One unit was defined as the amount of activity producing an absorbance change of 1, and the activity was expressed as units per milliliter of serum or units per microgram protein of skin mucus samples.

Protease activity was determined as the percentage of hydrolysis of azocasein (Sigma) using a modified protocol previously described (45) and 10 µL of serum or 30 µL of skin mucus. Proteinase K (2 mg/mL; AppliChem, Darmstadt, Germany) or PBS instead of samples was used as a positive control (100% of activity) or a negative control (0% of activity), respectively. The percentage of protease activity for each sample was calculated as the percentage of activity of the positive control. The results were expressed as percent of activity.

The antiprotease activity in 10 µL of serum or 30 µL of skin mucus was determined as the ability of the samples to inhibit the activity of proteinase K using a modified protocol previously described (46). The blank was prepared by replacing the samples and proteinase K (2 mg/mL) for PBS (no protease activity), while PBS instead of samples was used as the negative control (100% of activity). The percentage of inhibition of proteinase K activity for each sample was calculated as: [100 – (% of protease activity)]. The results were expressed as percent of activity.

Lysozyme activity in 100 µL of serum (diluted 1:2) or 100 µL of skin mucus samples was measured using a modified turbidimetric method previously described (47) and was based on the lysis of 0.3 mg/mL of freeze-dried *Micrococcus lysodeikticus* (Sigma). Changes in the absorbance at 450 nm were measured immediately every 30 s for 30 min at 25°C in a plate reader (MultiskanGo; Thermo Fisher Scientific, Waltham, MA, USA). One unit of lysozyme activity was defined as a reduction in the absorbance of 0.001/min. The lysozyme units were obtained from a standard curve ranging from 20 to 0 µg/mL made with hen egg white lysozyme (HEWL; Sigma). The results were expressed as international units per milliliter of serum or international units per milligram protein of skin mucus samples.

The bactericidal activity of 10 µL of serum or 20 µL of skin mucus samples was determined by evaluating the bacterial growth curves of *Vibrio harveyi* (strain Lg 16/100) using a method previously described (48). The samples replacing bacteria by culture medium were used as negative controls (0% growth and 0% bactericidal activity), while the samples replacing the serum or skin mucus by culture medium were used as positive controls (100% growth or 0% antibacterial activity). Bactericidal activity was calculated as: [100 – (% of bacterial growth)]. The results were corrected using the absorbance measured in each sample at the initial time point and were expressed as percent of activity.

The glucose levels in 4 µL of skin mucus samples were determined using the Glucose-HK enzymatic kit (Spinreact, Girona, Spain) following the manufacturer's instructions. The positive control was established using 4 µL of glucose standard (100 mg/dL) instead of samples, while wells containing only buffer were used as blanks. The results were expressed as milligrams per deciliter.

The lactate levels in 4 µL of skin mucus samples were determined using the Lactate LO-POD enzymatic kit (Spinreact) following the manufacturer's instructions. Positive controls were prepared using 4 µL of lactate standard (10 mg/dL) instead of samples, while wells containing only buffer were used as blanks. The results were expressed as milligrams per deciliter.

The cortisol from the water samples was extracted using a modified protocol previously described (49). Briefly, frozen water samples were thawed and filtered (F1091–130F). The samples were run through extraction cartridge C18 (SEP-PAK; Waters, Milford, MA, USA) following the manufacturer's instructions. Steroids were eluted with 5 mL of 100% methanol. Methanol was evaporated by incubation at 35°C and the steroids reconstituted in 1 mL reaction buffer (RB) [0.1 M phosphate–potassium buffer (PPB), 0.1% bovine serum albumin (BSA), 1 mM ethylenediaminetetraaceticacid (EDTA), 0.4 M NaCl, and 1.5 mM sodium azide (NaN_3), pH 7.4].

The cortisol levels in 5 µL of serum and 20 µL of skin mucus samples or extracted water samples were determined using the cortisol competitive human ELISA kit (Invitrogen, Carlsbad, CA, USA) following the manufacturer's instructions. A cortisol standard curve from 3,200 to 50 pg/mL serial dilutions was established, and the samples and standards were analyzed in duplicate. Wells with assay buffer instead of sample and without the cortisol antibody were used as blanks. The results were expressed as nanograms per milliliter.

The total antioxidant activity of the skin mucus samples was analyzed using the 2,2′-azino-bis-3-(ethylbenzothiazoline-6-sulfonic acid) (ABTS) method previously described (50), which was based on the ability of the antioxidants in the sample to reduce the radical cation of ABTS, as determined by the decoloration of ABTS+, and by measuring the quenching of the absorbance at 730 nm. Wells containing only PBS were used as blanks. This activity was calculated by comparing the values of the sample with a

standard curve of ascorbic acid and was expressed as ascorbic acid equivalents (in millimoles) per milligram protein.

2.6 Viral gene expression in NNV-infected shi drum tissues

Total RNA was isolated from fragments of frozen tissues (the brain from 4 and 18 dpi fish; the eye, liver, spleen, and head kidney from 4 dpi fish; and the gonad from 18 dpi fish) preserved in DNA/RNA Shield™ (Zymo Research) using the Quick-RNA™ MiniPrepPlus Kit (Zymo Research) following the manufacturer's instructions. The SensiFast™ cDNA synthesis kit (Bioline Meridian Life Science, Memphis, TN, USA) was used to synthesize cDNA by mRNA reverse transcription according to the manufacturer's instructions. Subsequent real-time PCR was performed with the AriaMx real-time PCR system (Agilent, Santa Clara, CA, USA) using the PowerUp™ SYBR™ Green Master Mix (Applied Biosystems, Foster City, CA, USA) and viral NNV coat protein (CP) specific primers (Supplementary Table S1). The reaction mixtures were incubated for 10 min at 95°C, followed by 40 cycles of 15 s at 95°C, 1 min at 60°C, and a final 15 s at 95°C, 1 min at 60°C, and 15 s at 95°C. For each mRNA, gene expression was corrected by the expression of the *beta-actin* (*actb*) gene in each sample and was expressed as $2^{-\Delta Ct}$, where ΔC_t was determined by subtracting the C_t value of *actb* from that of the target (51).

2.7 RNA isolation, library construction, and sequencing

We next analyzed the transcriptome of the viral target tissue (brain) and the immune-related tissues (spleen, head kidney, and liver) of the mock- and NNV-infected fish groups, in which higher mortalities were recorded (reared at 30 kg/m^3 prior to infection). Total RNA was extracted from each sample using the Trizol reagent (Invitrogen) according to the manufacturer's specifications. The preparation of RNA libraries and transcriptome sequencing were conducted by Novogene Co., Ltd. (Cambridge, UK). mRNA was purified from total RNA using poly-T oligo-attached magnetic beads. After fragmentation, the first-strand DNA was synthesized using random hexamer primers, followed by the second-strand cDNA synthesis. Libraries were ready after end repair, A-tailing, adapter ligation, size selection, amplification, and purification. Thereafter, the libraries were checked with Qubit and real-time PCR for quantification and bioanalyzer to determine the size distribution. Quantified libraries were sequenced on the Illumina platform (Instrument HWI-ST1276). The original raw data from the Illumina platform were transformed to sequenced reads through base calling and were recorded in a FASTQ file (52). In this case, in the absence of a reference genome, clean reads were assembled using Trinity (53). Subsequently, the CORSET software (54) was used to remove the redundancies from the Trinity results. Finally, BUSCO was used to attempt to provide a quantitative assessment of completeness in terms of the expected gene content of the transcriptome.

2.8 Bioinformatics analysis of transcriptome data

2.8.1 Gene functional annotation

In order to obtain a comprehensive gene functional annotation, seven databases were used: NCBI non-redundant protein sequences (Nr), NCBI nucleotide sequences (Nt), Protein family (Pfam), Cluster of Orthologous Groups of Protein/Eukaryotic Orthologous Groups (KOG/COG), Swiss-Prot, Kyoto Encyclopedia of Genes and Genomes (KEGG), and Gene Ontology (GO). CDS prediction was performed in two steps. Firstly, BLAST was used to align the unigene sequences to NR and Swiss-Prot; if matched, the CDS was translated into peptide sequences. If there was no match, TransDecoder was used to predict the coding regions and to determine the sequence direction. The AnimalTFDB database was used to perform the transcription factor analysis.

2.8.2 Gene expression analysis

As the reference transcriptome, the *de novo* shi drum filtered by Corset was used. RSEM (55) was used to quantify the expression levels. The read count for each sample was converted into FPKM (fragments per kilobase of transcript per million mapped reads) values. To compare the gene expression levels under different conditions, the FPKM distribution diagram was used. To reveal differences in the gene expression between samples and the repeatability of the experiments (by comparison of replicates), the square of Pearson's correlation coefficient was calculated.

2.8.3 Differential expression analysis

Read counts from the gene expression level analysis were normalized with DESeq2 (56). A negative binomial distribution was used as a model for the estimation of *p*-values; for calculation of the false discovery rate (FDR), the Benjamini–Hochberg (BH) method was applied [log2(FoldChange), $p_{adj} < 0.05$]. Cluster analysis was performed to discover genes with similar expression patterns under various experimental conditions.

2.8.4 GO enrichment analysis

In order to determine which biological functions or pathways are significantly associated with differentially expressed genes (DEGs), GO enrichment analysis was performed with GOseq and topGO ACG plotting was done with topGO. KEGG annotates a gene to the pathway level and was applied using KOBAS, while protein–protein interaction analysis was performed with the NCBI BLAST 29.0 software.

2.9 Quantitative real-time PCR validation for mRNA expression

The sequences of four potential reference genes were retrieved from transcriptome data and were used to design specific primers using the NCBI Primer-BLAST software (Supplementary Table S1). Real-time PCR reactions were run as described above. To confirm the specificity of each primer pair, melting curve analysis of the

amplified products was performed. Negative controls with no template were always included in all the reactions.

2.10 Statistical analyses

The results from the growth performance rates and plasmatic and skin mucus analysis, as well as the gene expression, were expressed as the mean ± SEM. Normality of the variables was confirmed with the Shapiro–Wilk test, while homogeneity of variance was assessed using the Levene test. Two-way ANOVA was performed to determine differences between rearing densities and time point. Upon infection, differences between the mock-infected and infected specimens were analyzed according to the Student's *t*-test. Survival was determined by the Kaplan–Meier method, and statistical differences were studied using a log-rank (Mantel–Cox) test. The significance level was 95% in all cases ($p \leq 0.05$). All data were analyzed using SPSS for Windows ® (version 15.0; SPSS Inc., Chicago, IL, USA). Some of the figures were drawn using the freely available SRplot web server (https://www.bioinformatics.com.cn).

3 Results

3.1 Increasing the rearing density altered the shi drum stress parameters while scarcely affecting growth performance

Scarce differences were observed in growth performance when fish reared at different densities were compared at the same time point. After 27 days of culture, the fish farmed at 2 kg/m^3 showed higher SGR than those farmed at 15 kg/m^3 (Table 1). The opposite results were observed for the stress parameters (Table 2). Thus, the serum cortisol levels were higher at all time points in fish reared at 15 and 30 kg/m^3 than in those reared at 2 kg/m^3. The same pattern was observed in the skin mucus cortisol levels on days 7 and 27 and in skin mucus glucose on day 27 (Table 2). Interestingly, when fish reared at the same density were compared through time, statistically significant differences were observed in the glucose levels of skin mucus from 21 days onwards at all rearing densities. Moreover, increases in the ABTS activity through time were observed at the rearing densities of 15 and 2 kg/m^3 (Table 2). The skin color of fish reared at 15 and 30 kg/m^3 was dark at the end of the experiment (Figure 1A). Interestingly, the bactericidal and lysozyme activities and the cortisol levels from the serum and skin mucus were positively correlated, as well as glucose and cortisol or glucose and lactate from the skin mucus. In contrast, a negative correlation was observed between the skin mucus glucose and the ABTS levels (Table 3).

3.2 Antiprotease and lysozyme activities showed differences at different rearing densities and through time

No differences were observed in the serum or skin mucus peroxidase, protease, and bactericidal activities, nor in the serum lysozyme activity of fish farmed at different densities at any assayed time (Table 4).

In the case of antiprotease activity, fish reared at 2 kg/m^3 for 27 days showed higher serum levels than fish reared at higher densities, which was significantly lower in fish reared at 15 kg/m^3. In addition, fish reared at 30 kg/m^3 for 21 days showed lower levels than the same group at 7 and 27 days (Table 4). In the skin mucus, the antiprotease activity levels of fish reared at 2 kg/m^3 for 7 days were lower than those of fish reared at 30 kg/m^3 for 7 days (Table 4). Interestingly, the antiprotease activity in the skin mucus decreased through time in fish reared at 15 and 30 kg/m^3. With regard to the lysozyme activity in the skin mucus, fish farmed at 2 kg/m^3 showed lower or higher levels at 21 or 27 days, respectively, than those farmed at higher densities, which was significantly lower in fish reared at 15 kg/m^3 for 21 days and in fish reared at 15 and 30 kg/m^3 for 27 days. In fact, differences in this activity through time were observed in fish reared at 30 kg/m^3 (Table 4).

3.3 Mortalities from NNV infection only occurred in fish reared at the highest density

After 27 days of rearing at different densities, the fish were infected with NNV to ascertain any association between rearing densities, stress, and mortalities. As darkness of the skin is an external sign of stress and was observed in fish reared at 30 kg/m^3 (Figure 1A), we used fish from this condition as the mock-infected control in order to exclude any unspecific mortalities due to poor welfare of the fish. After NNV challenge (Figure 1B), statistically significant mortalities were only recorded in fish reared at 30 kg/m^3, although some mortalities also occurred in fish reared at 15 kg/m^3 ($n = 5$ in 30 kg/m^3 vs. $n = 2$ in 15 kg/m^3). In contrast, no mortalities occurred at the lowest density (2 kg/m^3) or in the control group

TABLE 1 Growth performance data.

	7 days			21 days			27 days		
	2 kg/m^3	15 kg/m^3	30 kg/m^3	2 kg/m^3	15 kg/m^3	30 kg/m^3	2 kg/m^3	15 kg/m^3	30 kg/m^3
SGR (%)	0.94 ± 1.04	−0.65 ± 1.08	1.34 ± 1.29	1.32 ± 0.35	0.28 ± 0.27	0.28 ± 0.45	1.19 ± 0.24a	0.46 ± 0.16b	0.68 ± 0.26ab
CF (%)	1.24 ± 0.02	1.30 ± 0.03	1.33 ± 0.05	1.20 ± 0.01	1.30 ± 0.04	1.29 ± 0.03	1.20 ± 0.03	1.32 ± 0.03	1.34 ± 0.04

Shown are the specific growth rate (SGR) and condition factor (CF) of shi drum specimens reared at 2, 15, and 30 kg/m^3 for 7, 21, and 27 days. Lowercase letters denote statistically significant differences between different rearing densities at the same time point ($p \leq 0.05$).

TABLE 2 Data of the serum and skin mucus stress parameters of shi drum specimens reared at 2, 15, and 30 kg/m^3 for 7, 21, and 27 days.

	7 days			21 days			27 days		
	2 kg/m^3	15 kg/m^3	30 kg/m^3	2 kg/m^3	15 kg/m^3	30 kg/m^3	2 kg/m^3	15 kg/m^3	30 kg/m^3
Water cortisol	0.49 ± 0.10	0.55 ± 0.02	0.90 ± 0.55	0.70 ± 0.19	0.72 ± 0.17	0.51 ± 0.14			
Serum cortisol	6.06 ± 3.03a	20.08 ± 7.78b	26.00 ± 15.68b	2.50 ± 1.00a	9.44 ± 2.55b	28.81 ± 14.47b	3.36 ± 0.83a	8.64 ± 2.24b	13.06 ± 7.81b
Skin mucus cortisol	1.31 ± 0.39a	3.08 ± 0.58b	3.51 ± 0.96b	2.01 ± 0.32	1.33 ± 0.50*	2.88 ± 0.89	0.65 ± 0.06a	1.59 ± 0.40b	2.13 ± 0.79b
Skin mucus glucose	12.42 ± 1.46	12.46 ± 1.46	12.62 ± 1.27	7.08 ± 0.53*	6.38 ± 0.44*	6.91 ± 0.94*	5.47 ± 0.66a*	9.00 ± 1.00b*	8.97 ± 1.25b*
Skin mucus lactate	1.02 ± 0.21	1.24 ± 0.18	1.39 ± 0.20	0.77 ± 0.15	0.90 ± 0.23	1.09 ± 0.22	0.68 ± 0.28	0.87 ± 0.18	1.35 ± 0.26
Skin mucus ABTS	3.63 ± 0.23	2.64 ± 0.14	3.32 ± 0.48	4.57 ± 0.82	8.59 ± 2.02*	4.94 ± 1.13	6.44 ± 0.89*	5.11 ± 0.56	4.24 ± 0.37

Lowercase letters denote statistically significant differences between different rearing densities at the same time point. Asterisk denotes statistically significant differences between time points at the same rearing condition ($p \leq 0.05$).

(Figure 1B). Interestingly, all mortalities occurred within the first 5 days of infection (Figure 1B), and then the infection appeared to be overcome. Analysis of the transcription levels of the viral CP gene (Figure 1C) found no statistically significant differences between fish reared at different densities, either at 4 dpi or at 18 dpi, in any of the tissues analyzed (the brain at 4 and 18 dpi; the eyes, liver, spleen, and head kidney at 4 dpi; and the gonad at 18 dpi). When comparing tissues, lower levels were observed in the liver, spleen, head kidney, and gonad, while the brain and eyes showed more than 100- or 10-fold higher levels at 4 or 18 dpi, respectively (Figure 1C).

3.4 NNV scarcely alters the stress parameters, but increases the bactericidal activity

With regard to the serum and mucus stress parameters after infection (Table 5), only the lactate levels of the skin mucus were significantly increased in the 15-kg/m^3 infected fish compared with the mock-infected fish. No differences were observed in the peroxidase, protease, and lysozyme activities of the serum or skin mucus after NNV infection at any rearing density (Table 6). Interestingly, an inversely proportional relationship between the rearing density and skin mucus antiprotease activity was observed in fish infected with NNV, although only the fish reared at 30 kg/m^3 showed a statistically significant decrease of this activity when compared with the mock-infected fish (Table 6). The bactericidal activity showed significant increases upon infection (Table 6). Thus, this activity increased in the skin mucus of fish reared at 2 kg/m^3 and in the serum and skin mucus of fish reared at 30 kg/m^3 when compared with the mock-infected fish (Table 6).

3.5 The neuroactive ligand–receptor pathway is systemically affected by NNV

The response on day 4 of NNV infection in four tissues of fish reared at 30 kg/m^3 density was subsequently explored through a transcriptomic study in order to clarify the coordinated response of the viral target tissue (the brain) and the three immune tissues: the head kidney, the spleen, and the liver. As genetic data from shi drum are extremely limited, we firstly performed *de novo* transcriptomic profiling for this species, obtaining a mean of 39,392,132.3 ± 6,007,761.71 clean reads for each sample and a total annotated unigenes of 157,126 (Supplementary Figures S1–S3). Almost half of these (41.3%) were homologous to *Larimichthys crocea*, a Sciaenidae fish similar to shi drum (Figure 2A). We next compared the identified genes in each tissue in the mock-infected (Figure 2B) and NNV-infected (Figure 2C) conditions and found that all tissues co-expressed the same number of genes in both conditions, with 15,957 and 15,963, respectively. However, the genes specifically expressed in each tissue were altered upon infection depending on the tissue. Thus, the genes specifically expressed in the head kidney and liver increased when those expressed in the spleen and brain decreased (Figures 2B, C). Interestingly, the genes co-expressed in the spleen and brain and in the liver and brain decreased, while the genes co-expressed in the spleen and liver, the spleen and head kidney, the brain and head kidney, and the liver and head kidney increased upon infection (Figures 2B, C). Analysis of the DEGs in the tissues between the mock-infected (control) and NNV-infected conditions observed that the number of upregulated genes was higher in all comparisons than the downregulated genes, with the exception of the mock- vs. NNV-infected brain (C-Br vs. NNV-Br) and the NNV-infected brain vs. NNV-infected head kidney (NNV-Br vs. NNV-HK) in which the number of downregulated genes was higher (Figure 2D). Looking at the expression profiles and comparing the mock- and NNV-infected profiles in each tissue and in all four tissues analyzed together, the expression profiles of the head kidney, spleen, and brain and the general profiles of the control and infected fish were clustered together, while the liver had a different profile (Figure 2E). In general, there were gene expression differences between the mock-infected and infected conditions, but to a lesser extent than between tissues at the same condition (Figures 2D, E).

Focusing on the functions of the DEGs, in the head kidney (Figure 3A), only three KEGG pathways were significantly modified

10.3389/fimmu.2024.1304603

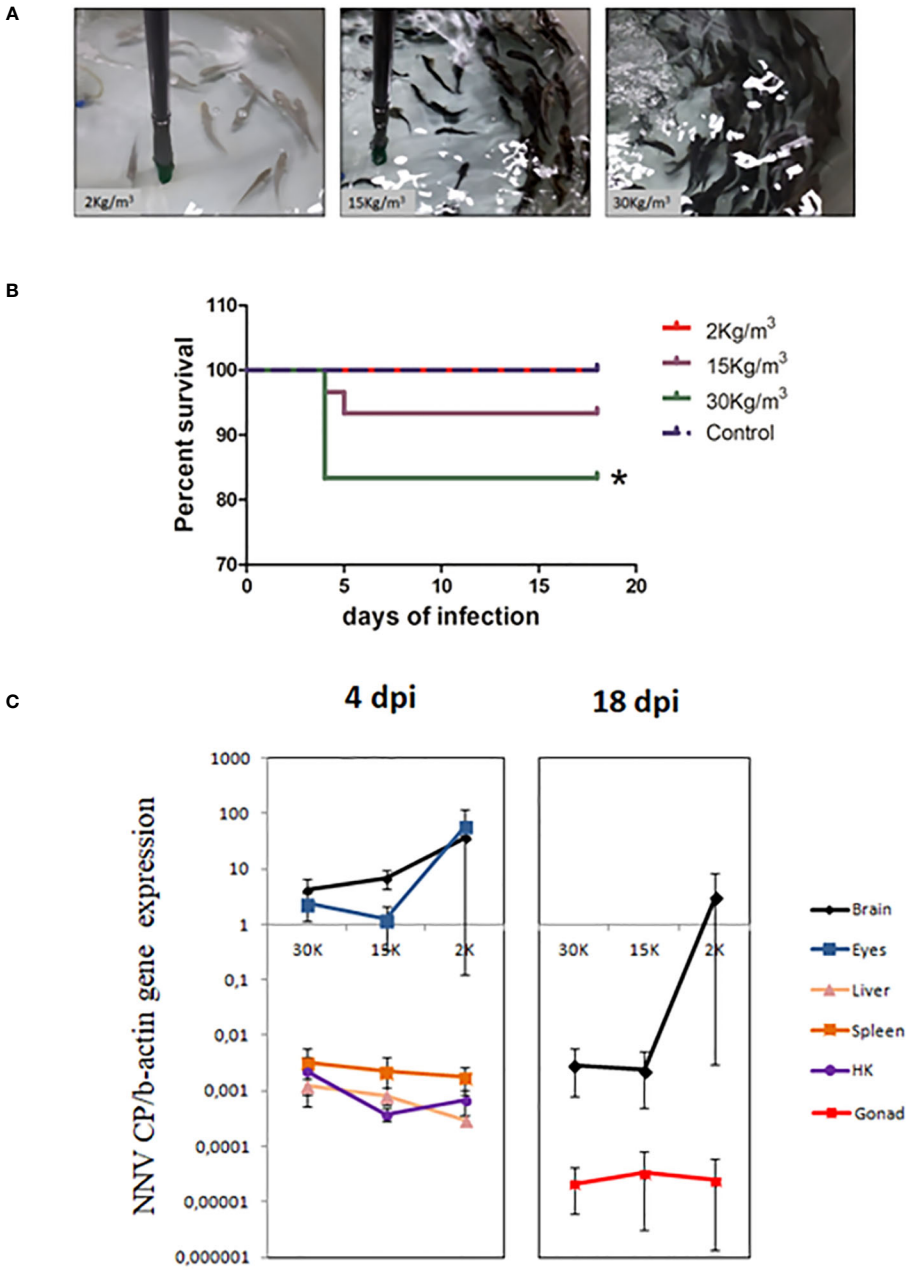

FIGURE 1
Juvenile shi drum specimens became susceptible to nervous necrosis virus (NNV) under stressed conditions. **(A)** Photographs showing the skin color of shi drum juveniles reared at 2, 15, or 30 kg/m^3 density. **(B)** Survival percentage of shi drum juveniles reared at 2, 15, or 30 kg/m^3 density for 27 days and then infected with 5.6 × 10^5 $TCID_{50}$/mL of NNV. **(C)** Relative expression of the viral capsid protein gene in several tissues of shi drum juveniles reared at different densities for 27 days and then infected with NNV. *dpi*, days post-infection. Asterisks denote statistically significant differences between control and infected groups accordingly with a Log-ranked (Mantel-Cox) test.

upon infection (the neuroactive ligand–receptor interaction, the synaptic vesicle cycle, and the insulin secretion pathways), while in the liver (Figure 3B), there were 12 pathways related to autophagy, phagosome, cholesterol and lipid metabolism, cell cycle and renewal, and innate acute response through complement pathways. In the spleen, 62 pathways were modified, while there were 84 in the brain, the target tissue of NNV (Supplementary Data 1). In the spleen (Figure 3C), the top 20 pathways significantly modified were related to autophagy and the main spleen function as a secondary immune tissue, such as cytokine–cytokine interaction, hematopoietic cell linage, antigen processing and presentation, migration and cell adhesion, and different signaling pathways. In the brain (Figure 3D), however, the top 20 pathways significantly modified were related to cell adhesion, synapses, and hormone signaling (Figure 3D). Interestingly, a unique pathway was observed to be modified upon infection in the head kidney, spleen, and brain: the neuroactive ligand–receptor interaction pathway. This pathway was highly modified in the head kidney (29 of the 281 expressed genes

10.3389/fimmu.2024.1304603

TABLE 3 Correlation observed in the serum and skin mucus immune and stress parameters.

	Serum lysozyme	Serum bactericidal	Serum cortisol	Skin mucus peroxidase	Skin mucus lysozyme	Skin mucus bactericidal	Skin mucus cortisol	Skin mucus glucose	Skin mucus lactate	Skin mucus ABTS
Serum lysozyme	1.000	−0.044	−0.138	0.120	**0.830**	−0.111	−0.204	−0.153	−0.369	0.187
		0.789	0.429	0.463	**0.000**	0.515	0.319	0.352	0.021	0.331
Serum bactericidal		1.000	−0.292	−0.100	0.017	**0.484**	−0.277	−0.120	0.054	−0.006
			0.035	0.384	0.909	**0.000**	0.045	0.292	0.639	0.963
Serum cortisol			1.000	0.129	−0.077	−0.311	**0.606**	0.189	0.275	−0.185
				0.351	0.668	0.025	**0.000**	0.171	0.044	0.266
Skin mucus peroxidase				1.000	−0.031	−0.006	−0.049	−0.162	−0.136	**0.692**
					0.834	0.959	0.712	0.137	0.216	**0.000**
Skin mucus lysozyme					1.000	−0.048	−0.114	−0.001	−0.189	−0.030
						0.748	0.488	0.994	0.188	0.865
Skin mucus bactericidal						1.000	−0.218	−0.133	0.019	0.221
							0.101	0.233	0.868	0.098
Skin mucus cortisol							1.000	**0.467**	0.356	−0.257
								0.000	0.005	0.088
Skin mucus glucose								1.000	**0.564**	**−0.507**
									0.000	**0.000**
Skin mucus lactate									1.000	−0.406
										0.001
Skin mucus ABTS										1.000

The number located in the first row of each analyzed activity corresponds to Pearson's correlation coefficient and the number locate in the second row to significant differences (p-value). Values in bold are the parameters that showed correlation. The parameters that did not show any significant correlation were not included.
ABTS, 2,2′-azino-bis-3-(ethylbenzothiazoline-6-sulfonic acid).

were modified, 10%) and, to a lesser extent, in the spleen (54 of the 933 expressed genes were modified, 0.05%) and the brain (117 of the 2,087 expressed genes were modified, 0.05%). Focusing on this pathway (Figure 4, Supplementary Data 2), most of the receptors altered are involved in neurological disorders and inflammation; however, some of them regulate the vascular system, the feeding behavior and energy consumption, the renewal of cells, and the stress response. The receptors altered in the three tissues were the muscarinic acetylcholine receptor (CHRM), adrenergic receptor (ADR), serotonin receptor (HTR), muscarinic glutamate receptor (GRM), and leptin receptor (LEPR), while the ligands included endothelin and different ligands of the proteinase-activated like receptor (Figure 4). Interestingly, multiple receptors of each type with different isoforms in some cases were present in shi drum tissues and were regulated in a tissue-specific manner upon NNV infection at stressed conditions induced by high rearing densities (Figure 5).

4 Discussion

VER disease is caused by NNV infection, but the clinical signs and susceptibility observed for each species depend on the biological cycle stage and the physiological status of the specimen (21). On the one hand, acute or chronic stress has been associated with higher mortalities during NNV outbreaks (29). On the other hand, there is evidence demonstrating that the mortalities from NNV infection are directly related to the intensity of the inflammatory response associated with the infection (58–61) and inversely to the bw (18, 19, 21, 30). However, and differently from mammals, antiviral treatments that help overcome the exacerbated immune responses and that lead to mortalities upon virus infection have not been developed in fish aquaculture as palliative treatments. This could be due to the lack of knowledge on the immune–neurocrine interactions that orchestrate these effects upon infection. In this framework, we analyzed the growth, immune status, and stress response of juvenile shi drum specimens (30.7 ± 3.10 g bw) under three stocking densities (2, 15, and 30 kg/m^3) for 27 days and subsequently challenged them with NNV. The main aim was to demonstrate the association of poor welfare and stressed conditions with high NNV susceptibility, as well as the molecular pathways involved.

The optimal density for shi drum culture is unknown as, to our knowledge, this species is not farmed and human consumption is only locally appreciated, but is based on wild fisheries. We routinely rear shi

10.3389/fimmu.2024.1304603

TABLE 4 Data of the serum and skin mucus innate immune parameters of shi drum specimens reared at 2, 15, and 30 kg/m^3 for 7, 21, and 27 days.

	7 days			21 days			27 days		
	2 kg/m^3	15 kg/m^3	30 kg/m^3	2 kg/m^3	15 kg/m^3	30 kg/m^3	2 kg/m^3	15 kg/m^3	30 kg/m^3
Serum peroxidase	153.00 ± 16.15	186.31 ± 27.94	152.28 ± 30.26	198.65 ± 40.02	149.18 ± 23.79	189.30 ± 31.79	108.27 ± 20.10	149.70 ± 21.83	107.79 ± 18.40
Skin mucus peroxidase	10.83 ± 0.48	11.46 ± 0.97	13.39 ± 1.40	10.03 ± 0.77	14.84 ± 2.26	13.60 ± 1.72	13.86 ± 1.95	14.89 ± 1.13	13.50 ± 1.15
Serum protease	0.86 ± 0.14	1.18 ± 0.13	0.86 ± 0.21	0.82 ± 0.11	1.15 ± 0.17	0.95 ± 0.19	0.79 ± 0.15	0.38 ± 0.13	0.67 ± 0.10
Skin mucus protease	0.12 ± 0.03	0.39 ± 0.20	0.18 ± 0.05	0.21 ± 0.06	0.12 ± 0.02	0.36 ± 0.24	0.14 ± 0.04	0.54 ± 0.29	0.34 ± 0.16
Serum antiprotease	12.20 ± 0.93	9.97 ± 0.75	11.60 ± 0.80	10.08 ± 0.82	10.70 ± 1.30	8.55 ± 1.01*	11.91 ± 0.82a	8.68 ± 1.07b	9.90 ± 0.52ab
Skin mucus antiprotease	2.07 ± 0.27a	2.98 ± 0.29ab	3.30 ± 0.33b	2.32 ± 0.20	2.20 ± 0.22*	2.38 ± 0.21*	1.85 ± 0.33	1.86 ± 0.22*	1.89 ± 0.31*
Serum lysozyme	1,018.42 ± 48.32	1,210.83 ± 183.28	1,164.10 ± 103.27	968.28 ± 72.19	1,190.50 ± 78.37	1,230.77 ± 82.93	1,001.42 ± 70.92	1,036.09 ± 215.57	974.36 ± 87.00
Skin mucus lysozyme	15.67 ± 6.22	6.54 ± 3.04	27.65 ± 7.73	26.70 ± 7.87a	129.29 ± 37.60b	45.22 ± 8.90ab*	56.81 ± 6.55a*	23.31 ± 5.15b*	21.61 ± 6.64b*
Serum bactericidal	17.38 ± 3.06	16.70 ± 3.74	10.78 ± 3.04	13.87 ± 2.18	12.94 ± 2.37	9.95 ± 2.20	17.35 ± 2.13	11.65 ± 3.73	13.89 ± 2.65
Skin mucus bactericidal	8.74 ± 1.45	10.04 ± 2.55	10.02 ± 1.73	12.29 ± 1.81	14.92 ± 1.80	10.34 ± 2.14	11.56 ± 1.97	10.77 ± 2.73	12.72 ± 3.39

Lowercase letters denote statistically significant differences between different rearing densities at the same time point. Asterisk denotes statistically significant differences between time points at the same rearing condition ($p \leq 0.05$).

drum at 9–15 kg/m^3 because it does not show unbalanced behavior and the industrial rearing densities for other Mediterranean fish species are normally around 15 kg/m^3. Three stocking densities—one very low (2 kg/m^3), one medium (15 kg/m^3), and one close to our typical culture density, a high one (30 kg/m^3)—were tested in order to compare them and to assess whether the stocking density could be a factor that triggers sudden outbreaks. Firstly, we determined by direct observation that shi drum specimens reared at 15 and 30 kg/m^3 display dark skin and a more nervous behavior than those reared at 2 kg/m^3, which showed a clear gray color similar to the color of the tank. Interestingly, at medium and high densities, all fish showed a darker coloration, probably due to the fact that they imitate each other instead of the tank. Hence, the density appeared to affect the mimicry of the fishes, changing from a protective resemblance (fish adopt the color of the tank) to a social mimicry (they mime the color of each other), as reviewed (62). In any case, skin color regulation has been known to be linked to stress hormones such as somatolactin, cortisol, and prolactin or thyroid hormones and is a clear sign of stress (63–66). In fact, those fish with dark skin showed the highest levels of serum cortisol from day 7 onwards. Similar to our results, other fish species reared at high densities showed higher levels of cortisol than those reared at a low density (14, 36, 67–75). Taking into account that the study and standardization of a large number of OWIs will allow better monitoring of the health and welfare of fish (21), and that our

TABLE 5 Data of the serum and skin mucus stress parameters of shi drum specimens reared at 2, 15, and 30 kg/m^3 for 27 days and after nervous necrosis virus (NNV) infection.

	Mock-infected	NNV-infected		
	30 kg/m^3	2 kg/m^3	15Kg/m^3	30 kg/m^3
Serum cortisol	4.35 ± 0.66	4.87 ± 0.70	3.84 ± 0.52	3.44 ± 0.86
Skin mucus cortisol	0.62 ± 0.16	1.64 ± 0.50	2.08 ± 0.67	1.28 ± 0.58
Serum glucose	73.65 ± 20.41	61.95 ± 4.41	111.32 ± 9.70	82.49 ± 12.37
Skin mucus glucose	6.67 ± 0.64	5.56 ± 0.39	6.48 ± 0.63	6.11 ± 0.41
Serum lactate	29.04 ± 8.18	33.12 ± 1.93	37.61 ± 1.64	32.17 ± 3.48
Skin mucus lactate	0.55 ± 0.06	0.74 ± 0.12	1.05 ± 0.17*	1.01 ± 0.31
Skin mucus ABTS	1.64 ± 0.19	1.37 ± 0.13	1.82 ± 0.20	1.57 ± 0.16

Asterisk denotes statistically significant differences between mock-infected and infected specimens ($p \leq 0.05$).

10.3389/fimmu.2024.1304603

TABLE 6 Data of the serum and skin mucus immune parameters of shi drum specimens reared at 2, 15, and 30 kg/m^3 for 27 days and after nervous necrosis virus (NNV) infection.

	Mock-infected	NNV-infected		
	30 kg/m^3	2 kg/m^3	15Kg/m^3	30 kg/m^3
Serum peroxidase	122.06 ± 11.67	137.75 ± 14.51	133.48 ± 24.71	138.23 ± 25.51
Skin mucus peroxidase	1.52 ± 0.19	1.26 ± 0.20	1.16 ± 0.22	1.22 ± 0.20
Serum protease	0.88 ± 0.14	1.01 ± 0.11	0.95 ± 0.13	0.93 ± 0.29
Skin mucus protease	0.07 ± 0.02	0.11 ± 0.04	0.16 ± 0.10	0.08 ± 0.04
Serum antiprotease	7.89 ± 0.54	6.37 ± 0.86	7.49 ± 2.07	6.43 ± 1.30
Skin mucus antiprotease	3.25 ± 0.5	2.70 ± 0.44	2.51 ± 0.16	1.70 ± 0.31*
Serum lysozyme	6.44 ± 2.02	12.15 ± 2.77	12.73 ± 3.57	8.65 ± 2.00
Skin mucus lysozyme	38.25 ± 11.14	86.47 ± 20.16	113.16 ± 36.13	66.81 ± 14.62
Serum bactericidal	18.19 ± 3.34	25.25 ± 4.19	25.18 ± 5.17	32.13 ± 5.06*
Skin mucus bactericidal	1.88 ± 1.02	7.93 ± 1.40*	6.97 ± 2.29	9.44 ± 3.17*

Asterisk denotes statistically significant differences between mock-infected and infected specimens ($p \leq 0.05$).

serum data provided evidence that shi drum specimens show signs of a stress response when reared at densities of 15 and 30 kg/m^3, we next explored the possibility of identifying noninvasive OWIs by analyzing the levels of cortisol in the water and skin mucus and the levels of glucose and lactate and the total antioxidant activity (ABTS levels) in the skin mucus. For water cortisol, we succeeded in detecting it, but failed to observe differences on day 7 or day 21, contrary to what has been described in rainbow trout where the water cortisol levels

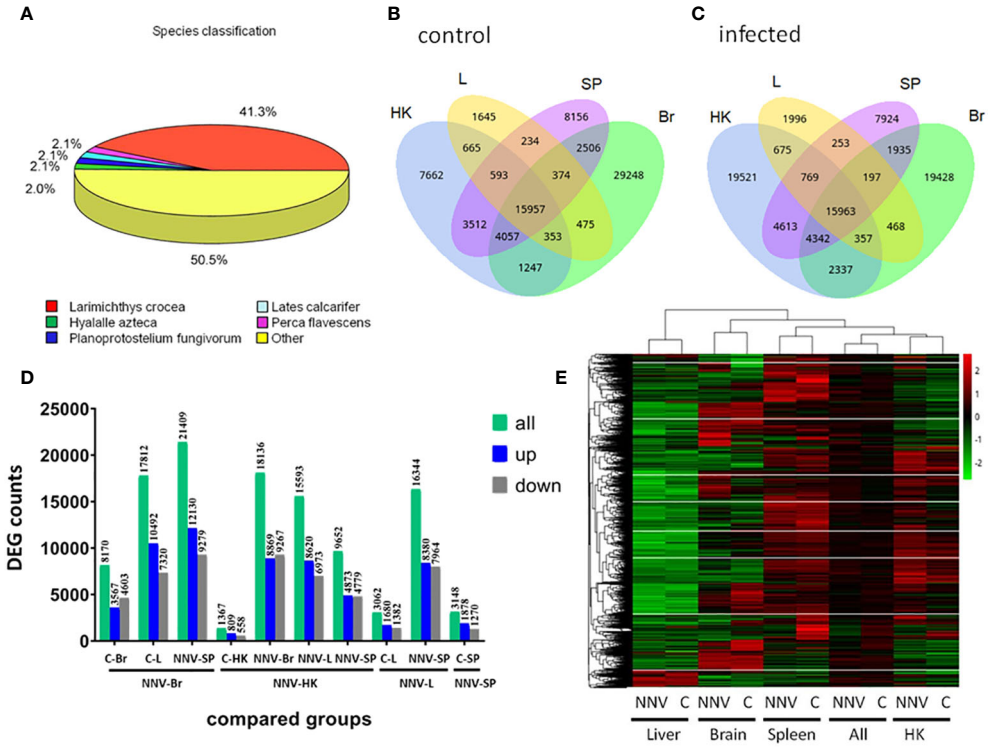

FIGURE 2
Gene identification and differential expression analysis in mock- and nervous necrosis virus (NNV)-infected head kidney (*HK*), liver (*L*), spleen (*SP*), and brain (*Br*) from shi drum juveniles reared at 30 kg/m^3 density for 27 days prior to infection. **(A)** Species classification of the unigenes annotated in the *de novo* transcriptome. **(B)** Venn diagram of the expressed genes in HK, L, SP, and Br of mock-infected shi drum juveniles. **(C)**. Venn diagram of the expressed genes in HK, L, SP, and Br of the NNV-infected shi drum juveniles. **(D)** Number of differentially expressed genes (DEGs) in different comparisons performed between mock- and NNV-infected tissues. **(E)** Heatmap showing the cluster analysis of the DEGs in the different tissues analyzed (L, Br, S, and HK) under the mock-infected **(C)** and NNV-infected (*NNV*) conditions. (All) columns represent the expression added in the four tissues analyzed under the mock- and NNV-infected conditions.

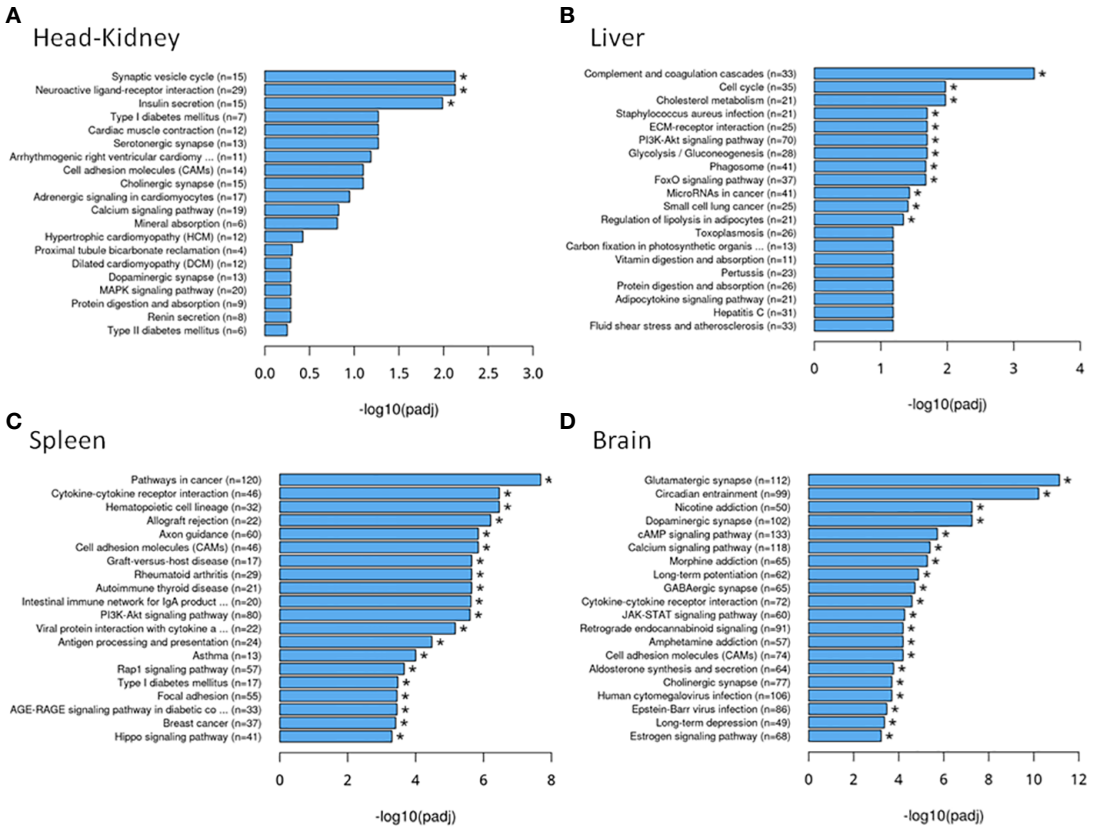

FIGURE 3
Top 20 Kyoto Encyclopedia of Genes and Genomes (KEGG) pathways associated with the differentially expressed genes in each tissue: **(A)** Head kidney. **(B)** Liver. **(C)** Spleen. **(D)** Brain. * Asterisks denote KEGG pathways significantly modified upon infection.

significantly changed depending on the density culture conditions (69). Glucose and lactate levels are indicators of stress and are frequently used to evaluate the welfare of farmed fish (14, 36, 70). Thus, in the skin mucus, the cortisol and glucose levels increased in the fish reared at medium and high densities on days 7 and 27 or on day 27, respectively, but no differences were observed on day 21. Although further studies are needed, our data point to the feasible use of stress-related parameters in the skin mucus as OWIs for shi drum. On the other hand, the exceptive negative relationship between stress and growth described in other fish species (76) was partially observed in shi drum. Thus, the SGR index decreased in the fish reared at medium and high densities, but all specimens showed similar use of feed, as revealed by the similar CF values. All of these data demonstrate that mainly fish at 15 and 30 kg/m^3 showed a poor welfare status, although the effect of the stressed conditions was not excessively substantial. Taking into account that high stocking densities can negatively affect the general welfare of fish (13, 14, 36) by reducing the immune functions (70), we next determined whether the innate immune responses were unbalanced in our stressed fish by analyzing the innate activities in the serum and skin mucus. The fish skin mucus is one of the most important components of the first line of defense against a broad spectrum of pathogens (37, 40, 77) and acts as a barrier between fish and their environment (77), protecting them against microbial infections (37). In this study, no differences were observed in the serum or skin mucus peroxidase, protease, or total bactericidal activity of fish farmed at different stocking densities at any assayed time. However, in the case of antiprotease activity in the serum, fish farmed at medium and high densities for 27 days showed a decrease compared to those farmed at the lowest density; in the skin mucus, the opposite results were observed on day 7. Similarly to the serum antiprotease, the skin mucus lysozyme activity of fish farmed at medium and high densities for 27 days showed a decrease compared with fish farmed at the lowest density. In contrast to other fish species previously studied (73, 78–81), the shi drum specimens reared at different densities did not show differences in the serum lysozyme activity. Taken together, these data suggest that the shi drum skin mucus could reflect more rapidly the immunosuppression triggered by the stress response than the serum, although further studies are needed to clarify this issue. In conclusion, all of the stress parameter and immune data obtained in this study suggested that shi drum specimens reared at 15 and 30 kg/m^3 display stress responses at the moment of infection (27 days) and that their innate immune responses are not highly unbalanced, at least at naive conditions.

Taking into account the observed susceptibility of shi drum to NNV and the previously described relationship between stress and increased NNV susceptibility observed in other fish species (30), we subsequently studied the effect of NNV infection on shi drum specimens farmed at different stocking densities. Therefore, after

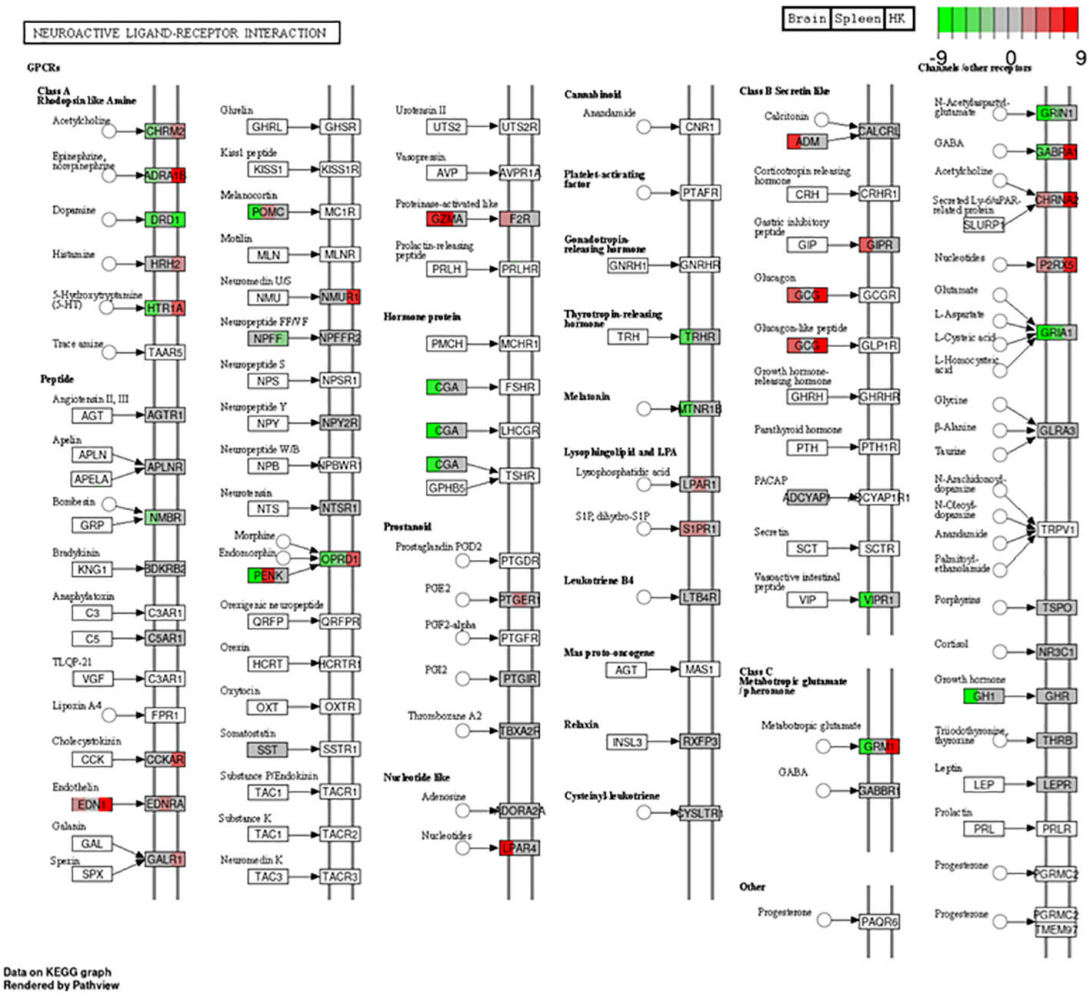

FIGURE 4
Differentially expressed genes in the neuroactive ligand–receptor interaction pathway (hsa04080) plotted using Pathview (57). Each *gene square* was divided into three parts corresponding to the brain, spleen, and head kidney expression from left to right. Red represents upregulated genes, while green represents downregulated genes.

being reared at different stocking densities for 27 days, we challenged the fish from each experimental group with the RGNNV genotype (the most common genotype in the Mediterranean area). A group of fish from the highest density group were mock-infected (control group), but no mortalities due to the handling conditions were observed despite the fish having a poor welfare status. In the infected groups, however, only the fish reared at 15 and 30 kg/m^3 suffered mortalities upon infection, with the mortalities observed in the group reared at the highest density being statistically significant. In addition, this group also recorded the highest cortisol levels and the lowest glucose levels prior to infection. Interestingly, when analyzing the serum and skin mucus parameters of all fish on day 4 of infection by comparing them with the levels displayed by mock-infected fish, no statistically significant differences were observed in all of the parameters analyzed in the group recording no mortalities (2 kg/m^3). Therefore, in shi drum and under our experimental conditions, we were not able to identify any serum or skin mucus parameter that might be useful in the prediction of the stress occurring upon NNV infection in asymptomatic specimens.

Interestingly, shi drum specimens at the larval stage or with a low bw are very susceptible to RGNNV (5, 9); however, in this study, fish with a bw of 30 g and were reared at low density (2 kg/m^3) became asymptomatic, even after demonstrating infection, as shown by the expression of the viral CP in their tissues. The inverse relationship between susceptibility to NNV and bw observed in this work has already been described in many species (18). However, to our knowledge, this study is the first to demonstrate the link between stressed conditions and the appearance of VER disease, as well as mortalities in fish with a bw at which they should be asymptomatic.

Shi drum specimens reared at the lowest density (2 kg/m^3) and infected with NNV showed a high variability in the CP transcription levels in the viral target tissues (the brain and eyes) at both time points analyzed. This variability was strikingly higher for fish reared at 2 kg/m^3 when compared with those at 15 or 30 kg/m^3 rearing conditions. Interestingly, although they showed higher variable viral levels, they were asymptomatic and were able to control the disease. It has been recently proposed that an exacerbated inflammatory response leads to mortalities upon NNV infection (58–61). Thus, it

10.3389/fimmu.2024.1304603

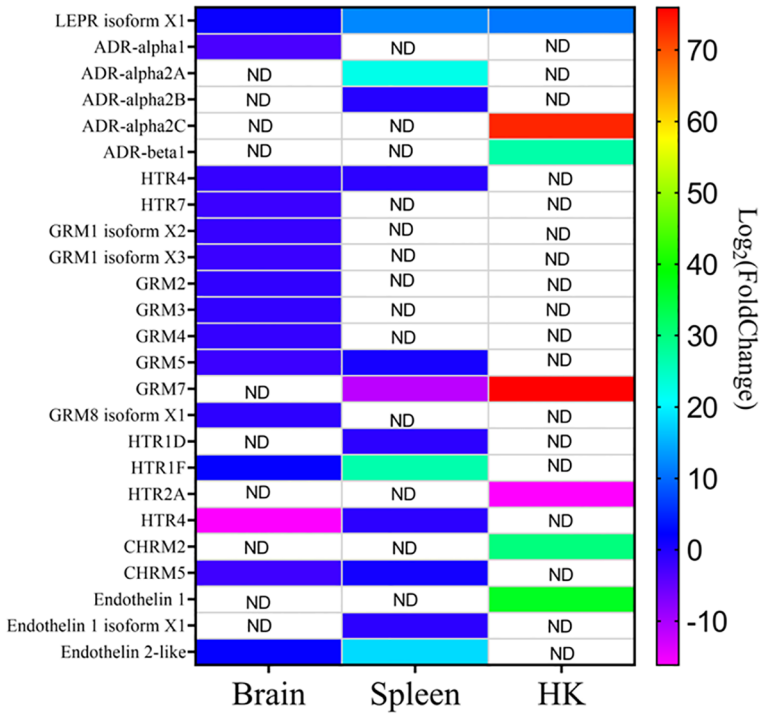

FIGURE 5
Heatmap showing the different expression of CHRM (muscarinic acetylcholine receptor), HTR (serotonin receptor), GRM (muscarinic glutamate receptor), and LEPR (leptin receptor), endothelin, and their isoforms in the different tissues upon nervous necrosis virus (NNV) infection at stressed conditions. ND, not detected.

is possible that the shi drum specimens at low densities show lower clinical signs and mortalities due to a low inflammatory response, which will likely depend on their physiological welfare. In contrast, the fish reared at high densities might display a high inflammatory response due to their stressed condition. Although further studies are necessary to clarify this issue, our transcriptomic data supported this hypothesis as the pathways related to cytokine and chemokine signaling and inflammation were upregulated in the brain and spleen of the NNV-infected specimens reared at 30 kg/m^3 (the highest density). In fact, for the immune response, the transcriptomic profile of the spleen showed altered related pathways such as autophagy, antigen processing and presentation, and cytokine interaction, as previously described in an NNV-infected larva transcriptome (82). In addition, the profile observed in the brain resembles similarities to that in a transcriptomic study performed in a brain-derived cell line infected with NNV (83). Interestingly, in the shi drum brain, the estrogen signaling pathway was altered upon infection, as also occurred in European sea bass (84). However, and in contrast to that in European sea bass (85), in the shi drum brain, none of the kisspeptin-regulated genes were altered, nor the gonadotrophin-releasing hormone genes. As these genes belong to the hypothalamic–pituitary–gonadal (HPG) axis, the differences observed between species might modify their capabilities of vertically transmitting the virus. In fact, NNV colonized the gonad of the European sea bass and gilthead seabream specimens upon infection, but it is extremely difficult to detect the virus at 15 dpi as viral gene expression is under the qPCR detection limit, as previously demonstrated (84). However, in shi drum, the expression of the CP gene at 18 dpi was low, but was easily detected in the gonad in all experimental groups (both in fish that showed VER clinical signs and those that did not) using qPCR, as demonstrated in this study. These data led to considering the possibility of developing a methodology to detect NNV in asymptomatic shi drum through gonad biopsies. Nevertheless, further studies are required to clarify the kinetics of the viral transcription rates in surviving fish through time and the relationship between the CP transcription levels in the gonad and the regulation of the HPG axis. This knowledge would be of great importance in combating vertical and horizontal transmission from asymptomatic fish.

In contrast to previous transcriptomic studies that focused on immune responses (82, 83, 86), this work also attempted to understand the molecular pathways involved in the association between stressed or poor welfare conditions and the exacerbated inflammatory response that triggered higher mortalities. In that sense, this work identified for the first time several receptors and ligands belonging to the neuroactive ligand–receptor pathway that were heavily regulated in a systemic way, as their expression was modified in three of the four tissues analyzed. According to our data, the molecules regulated in the three tissues were CHRM, ADR, HTR, GRM, and LEPR. All of these are neurotransmitter receptors in the brain, but are also present in different types of immune cells and other tissues as they belong to the endocrine system (16, 87–91). Therefore, they are a direct link between neurological disorder, endocrine regulation, and immune response. Our data revealed that shi drum expressed all these receptors in multiple isoforms and that

they were differentially regulated upon NNV infection in stressed conditions depending on the receptor type, the isoform, and the tissue. The presence of multiple genes that produce an array of receptors differentially expressed in different cells or tissues is expected due to the multiple genome duplications that have occurred during teleost fish evolution (92). However, the complexity observed in the regulation in multiple tissues of these receptors upon NNV infection at stressed conditions points to their importance in orchestrating the imbalance that leads to mortalities upon infection and highlights these receptors as potent targets for pharmacological treatment. Thus, further studies focusing on the neuroactive ligand–receptor pathway are needed to understand the pathology of NNV and its link to poor welfare culture conditions.

5 Conclusions

This work is the first study in which the effect of a combination of stocking densities and viral infection in shi drum has been analyzed. In this study, juvenile shi drum specimens (30.7 ± 3.10 g bw) tolerated high rearing densities, even with a poor welfare status. Despite the serum and skin mucus innate immune responses and the antioxidant system being almost unaffected by the poor welfare status and the fish being big enough to be asymptomatic, mortalities occurred upon NNV infection. These data demonstrate that chronic stress due to a high stocking density is a key factor in the pathogenesis of NNV in shi drum juveniles. In addition, our data showed that the skin mucus might reflect more rapidly the immunosuppression triggered by stress response than the serum in shi drum juveniles. Further studies are needed in this sense to clarify its potential for noninvasive sampling to detect stress. Regarding the molecular pathways orchestrating the link between stressed conditions and NNV susceptibility, it was found that, in general, the immune–neuroendocrine system might be crucial and that, in particular, the receptors CHRM, ADR, HTH, and LEPR might be involved in a systemic regulation that could lead to an exacerbated inflammatory response upon NNV infection, causing mortalities at an unexpected fish weight.

Data availability statement

The data presented in the study are deposited in the NCBI's BioProject repository, accession number ID 1033413 (https://www.ncbi.nlm.nih.gov/bioproject/PRJNA1033413).

Ethics statement

The animal study was approved by The Bioethical Committees of the IEO (REGA code ES300261040017) and the approval of the Ministry of Water, Agriculture and Environment of the Autonomous Community Region of Murcia (Permit Number A13211203). The study was conducted in accordance with the local legislation and institutional requirements.

Author contributions

JG-B: Formal analysis, Investigation, Methodology, Visualization, Writing – original draft. CJ: Data curation, Formal analysis, Investigation, Methodology, Validation, Visualization, Writing – review & editing. MA: Conceptualization, Investigation, Methodology, Resources, Writing – review & editing. AC: Investigation, Methodology, Writing – review & editing. MP: Conceptualization, Funding acquisition, Project administration, Supervision, Visualization, Writing – review & editing. EC-P: Conceptualization, Formal analysis, Investigation, Methodology, Project administration, Resources, Supervision, Visualization, Writing – original draft, Writing – review & editing.

Funding

The author(s) declare financial support was received for the research, authorship, and/or publication of this article. This work was financed by the OWI TWO project co-financed by the European Maritime and Fisheries Fund (EMFF) and the IEO-CSIC, by the European Union NextGenerationEU/PRTR, MCIN/AEI10.13039/501100011033 and Fundación Séneca (ThinkInAzulprogramme: PRTR-C17.I1) and by the Ministry of Universities through subsidies to public universities for the requalification of the Spanish university system, Margarita Salas Grants, managed by the University of Murcia.

Acknowledgments

We thank the staff of the COMU-IEO, CSIC for their technical assistance in fish management.

Conflict of interest

The authors declare that the research was conducted in the absence of any commercial or financial relationships that could be construed as a potential conflict of interest.

The author(s) declared that they were an editorial board member of Frontiers, at the time of submission. This had no impact on the peer review process and the final decision.

Publisher's note

Supplementary material

The Supplementary Material for this article can be found online at: https://www.frontiersin.org/articles/10.3389/fimmu.2024.1304603/full#supplementary-material

References

1. FAO. *The State of World Fisheries and Aquaculture*. Rome, Italy: FAO (2022). doi: 10.4060/CC0461EN

2. Kim DY, Shinde SK, Kadam AA, Saratale RG, Saratale GD, Kumar M, et al. Advantage of species diversification to facilitate sustainable development of aquaculture sector. *Biol*. (2022) 11:368. doi: 10.3390/BIOLOGY11030368

3. Basurco B, Abellán E. Marine finfish species diversification : current situation and prospects in Mediterranean aquaculture (1999). CIHEAM. Available online at: http://agris.fao.org/agris-search/search.do?recordID=QC1999000183 (Accessed October 5, 2018).

4. Chaves-Pozo E, Abellán E, Baixauli P, Arizcun M. An overview of the reproductive cycle of cultured specimens of a potential candidate for Mediterranean aquaculture, *Umbrina cirrosa*. *Aquaculture*. (2019) 505:137–49. doi: 10.1016/j.aquaculture.2019.02.039

5. Katharios P, Tsigenopoulos CS. First report of nodavirus outbreak in cultured juvenile shi drum, *Umbrina cirrosa* L., in Greece. *Aquac Res*. (2010) 42:147–52. doi: 10.1111/are.2010.42.issue-1

6. Arizcun M, Abellán E, García-Alcázar A. *Primeros estudios sobre reproducción y cultivo larvario de verrugato* (Umbrina cirrosa *L.)*. Zaragoza, Spain: XII Congreso Nacional de Acuicultura (2009) p. 518–9

7. Italy - National Aquaculture Sector Overview . Available online at: https://www.fao.org/fishery/en/countrysector/it/en (Accessed April 22, 2024).

8. Bitchava K, Chassalevris T, Lampou E, Athanassopoulou F, Economou V, Dovas CI. Occurrence and molecular characterization of betanodaviruses in fish and invertebrates of the Greek territorial waters. *J Fish Dis*. (2019) 42:1773–83. doi: 10.1111/JFD.13098

9. Chaves-Pozo E, Arizcun M, Cuesta A. Betanodavirus genotypes produce clinical signs and mortality in the shi drum (*Umbrina cirrosa*), and infective particles are isolated from the damaged brain. *Aquaculture*. (2021) 541:736777. doi: 10.1016/j.aquaculture.2021.736777

10. Henry M, Fountoulaki E. Optimal dietary protein/lipid ratio for improved immune status of a newly cultivated Mediterranean fish species, the shi drum *Umbrina cirrosa*, L. *Fish Shellfish Immunol*. (2014) 37:215–9. doi: 10.1016/J.FSI.2014.02.005

11. Hidalgo MC, Morales AE, Arizcun M, Abellán E, Cardenete G. Regional asymmetry of metabolic and antioxidant profile in the sciaenid fish shi drum (*Umbrina cirrosa*) white muscle. Response to starvation and refeeding. *Redox Biol*. (2017) 11:682–7. doi: 10.1016/J.REDOX.2017.01.022

12. Pérez-Sánchez T, Mora-Sánchez B, Balcázar JL. Biological approaches for disease control in aquaculture: advantages, limitations and challenges. *Trends Microbiol*. (2018) 26:896–903. doi: 10.1016/j.tim.2018.05.002

13. Baldwin L. The effects of stocking density on fish welfare. *Plymouth Student Sci*. (2011) 4:372–83

14. Seo J, Park J. Does stocking density affect growth performance and hematological parameters of juvenile olive flounder *paralichthys olivaceus* in a recirculating aquaculture system? *Anim*. (2022) 13:44. doi: 10.3390/ANI13010044

15. Segner H, Sundh H, Buchmann K, Douxfils J, Sundell KS, Mathieu C, et al. Health of farmed fish: Its relation to fish welfare and its utility as welfare indicator. *Fish Physiol Biochem*. (2012) 38:85–105. doi: 10.1007/s10695-011-9517-9

16. Nardocci G, Navarro C, Cortés PP, Imarai M, Montoya M, Valenzuela B, et al. Neuroendocrine mechanisms for immune system regulation during stress in fish. *Fish Shellfish Immunol*. (2014) 40:531–8. doi: 10.1016/J.FSI.2014.08.001

17. Kibenge FS. Emerging viruses in aquaculture. *Curr Opin Virol*. (2019) 34:97–103. doi: 10.1016/J.COVIRO.2018.12.008

18. Munday BL, Kwang J, Moody N. Betanodavirus infections of teleost fish : a review. *J Fish Dis*. (2002) 25:127–42. doi: 10.1046/j.1365-2761.2002.00350.x

19. OIE. "Viral encephalopathy and retinopathy.,". In: *Manual of Diagnostic Tests for Aquatic Animals* Europe in Paris: World organization for animal health (2016). p. 1–20

20. Yong CY, Yeap SK, Omar AR, Tan WS. Advances in the study of nodavirus. *PeerJ*. (2017) 5:e3841. doi: 10.7717/peerj.3841

21. Bandín I, Souto S. Betanodavirus and VER disease: A 30-year research review. *Pathog*. (2020) 9:106. doi: 10.3390/PATHOGENS9020106

22. Dalla Valle L, Negrisolo E, Patarnello P, Zanella L, Maltese C, Bovo G, et al. Sequence comparison and phylogenetic analysis of fish nodaviruses based on the coat protein gene. *Arch Virol*. (2001) 146:1125–37. doi: 10.1007/s007050170110

23. Pavoletti E, Prearo M, Ghittino M, Ghittino C. Casi di encefaloretinopatia in ombrina (*Umbrina cirrosa*) con descrizione della sintomatologia clinica e del quadro anatomoistopatologico. *Boll Soc Patol Ittica*. (1998) 23:24–33

24. Comps M, Trindade M, Delsert C. Investigation of fish encephalitis viruses (FEV) expression in marine fishes using DIG-labelled probes. *Aquaculture*. (1996) 143:113–21. doi: 10.1016/0044–8486(96)01264–1

25. Skliris GP, Krondiris JV, Sideris DC, Shinn AP, Starkey WG, Richards RH. Phylogenetic and antigenic characterization of new fish nodavirus isolates from Europe and Asia. *Virus Res*. (2001) 75:59–67. doi: 10.1016/S0168–1702(01)00225–8

26. Ciulli S, Galletti E, Grodzki M, Alessi A, Battilani M, Prosperi S. Isolation and genetic characterization of Betanodavirus from wild marine fish from the Adriatic Sea. *Vet Res Commun*. (2007) 31:221–4. doi: 10.1007/s11259-007-0010-y

27. Dalla Valle L, Zanella L, Patarnello P, Paolucci L, Belvedere P, Colombo L. Development of a sensitive diagnostic assay for fish nervous necrosis virus based on RT-PCR plus nested PCR. *J Fish Dis*. (2000) 23:321–7. doi: 10.1046/j.1365-2761.2000.00255.x

28. Costa JZ, Thompson KD. Understanding the interaction between Betanodavirus and its host for the development of prophylactic measures for viral encephalopathy and retinopathy. *Fish Shellfish Immunol*. (2016) 53:35–49. doi: 10.1016/j.fsi.2016.03.033

29. Johansen R. Nodavirus Infection of Farmed Marine Fish with Emphasis on Subclinical and Persisent Infection (2004). Uitgever niet vastgesteld. Available online at: https://www.researchgate.net/profile/Renate-Johansen-2/publication/264991834_Nodavirus_infection_of_farmed_marine_fish_with_emphasis_on_subclinical_and_persistent_infection/links/53fb07820cf20a4549703835/Nodavirus-infection-of-farmed-marine-fish-with-emph (Accessed September 27, 2023).

30. Shetty M, Maiti B, Shivakumar Santhosh K, Venugopal MN, Karunasagar I. Betanodavirus of marine and freshwater fish: Distribution, genomic organization, diagnosis and control measures. *Indian J Virol*. (2012) 23:114–23. doi: 10.1007/s13337-012-0088-x

31. Blom JMC, Ottaviani E. Immune-neuroendocrine interactions: evolution, ecology, and susceptibility to illness. *Med Sci Monit Basic Res*. (2017) 23:362. doi: 10.12659/MSMBR.907637

32. Metzger DCH, Schulte PM. Epigenomics in marine fishes. *Mar Genomics*. (2016) 30:43–54. doi: 10.1016/J.MARGEN.2016.01.004

33. Schreck CB, Tort L. The concept of stress in fish. *Fish Physiol*. (2016) 35:1–34. doi: 10.1016/B978–0-12–802728–8.00001–1

34. Bruslé J, Gonzàlez i Anadon G. The structure and function of fish liver. *Fish Morphol*. (2017), 77–93. doi: 10.1201/9780203755990–6

35. Tort L. Stress and immune modulation in fish. *Dev Comp Immunol*. (2011) 35:1366–75. doi: 10.1016/J.DCI.2011.07.002

36. Onxayvieng K, Piria M, Fuka MM, Gavrilović A, Liang X, Liu L, et al. High stocking density alters growth performance, blood biochemical profiles, and hepatic antioxidative capacity in gibel carp (*Carassius gibelio*). *Fish Physiol Biochem*. (2021) 47:203–12. doi: 10.1007/s10695-020-00905-6

37. Koshio S. Immunotherapies targeting fish mucosal immunity - Current knowledge and future perspectives. *Front Immunol*. (2016) 6:643/BIBTEX. doi: 10.3389/fimmu.2015.00643

38. Janz DM. Endocrine system. *Lab Fish*. (2000), 189–217. doi: 10.1016/B978–012529650–2/50016–0

39. Arizcun M, García-Alcázar A, Abellán E. *Completion of the shi drum (*Umbrina cirrosa*) life cycle*. European aquaculture 14 abstract book. Ostend, Belgium: European Aquaculture society (2014). pp. 78–9

40. Guardiola FA, Cuesta A, Arizcun M, Meseguer J, Esteban MA. Comparative skin mucus and serum humoral defence mechanisms in the teleost gilthead seabream (*Sparus aurata*). *Fish Shellfish Immunol*. (2014) 36:545–51. doi: 10.1016/J.FSI.2014.01.001

41. Reed LJ, Müench H. A simple method of estimating fifty per cent endpoints. *Am J Epidemiol*. (1938) 27:493–7. doi: 10.1093/oxfordjournals.aje.a118408

42. Batt J, Bennett-Steward K, Couturier C, Hammell L, Harvey-Clark C, Kreiberg H, et al. CCAC guidelines on: The care and use of fish in research, teaching, and testing | IslandScholar. Canadian Council on Animal Care 1510–130 Albert Street Ottawa ON CANADA K1P 5G4 (2005). Available online at: https://www.islandscholar.ca/islandora/object/ir:21280 (Accessed January 13, 2021).

43. Bradford M. A rapid and sensitive method for quantification of microgram quantities of protein using the principle of protein dye binding. *Anal Biochem*. (1976) 72:248–54. doi: 10.1006/abio.1976.9999

44. Quade MJ, Roth JA. A rapid, direct assay to measure degranulation of bovine neutrophil primary granules. *Vet Immunol Immunopathol*. (1997) 58:239–48. doi: 10.1016/S0165–2427(97)00048–2

45. Charney J, Tomarelli RM. A colorimetric method for the determination of the proteolytic activity of duodenal juice. *J Biol Chem*. (1947) 171:501–5. doi: 10.1016/S0021-9258(17)41059-3

46. Ellis AE. "Serum antiproteases in fish.,". In: Stolen JS, Fletcher TC, Anderson DP, Roberson BS, van Muiswinkel WB, editors. *Techniques in fish immunology*. New Jersey: Fair Haven, N.J. SOS Publications (1990). p. 95–9

47. Parry RM, Chandan RC, Shahani KM. A rapid and sensitive assay of muramidase. *Proc Soc Exp Biol Med*. (1965) 119:384–6. doi: 10.3181/00379727-119-30188

48. Sunyer JO, Tort L. Natural hemolytic and bactericidal activities of sea bream *Sparus aurata* serum are effected by the alternative complement pathway. *Vet Immunol Immunopathol.* (1995) 45:333–45. doi: 10.1016/0165-2427(94)05430-Z

49. Ruane NM, Komen H. Measuring cortisol in the water as an indicator of stress caused by increased loading density in common carp (*Cyprinus carpio*). *Aquaculture.* (2003) 218:685–93. doi: 10.1016/S0044–8486(02)00422–2

50. Arnao MB, Cano A, Acosta M, Ano AI, Osta MA. Methods to measure the antioxidant activity in plant material. A comparative discussion. *Free Radic Res.* (2016) 3:589–96. doi: 10.1080/10715769900301371

51. Pfaffl MW. "Relative quantification.,", in: *Real-time PCR* (2007). Taylor & Francis Group. Available online at: https://www.gene-quantification.de/pfaffl-rel-quan-book-ch3.pdf (Accessed July 18, 2019).

52. Cock PJA, Fields CJ, Goto N, Heuer ML, Rice PM. The Sanger FASTQ file format for sequences with quality scores, and the Solexa/Illumina FASTQ variants. *Nucleic Acids Res.* (2010) 38:1767–71. doi: 10.1093/NAR/GKP1137

53. Grabherr MG, Haas BJ, Yassour M, Levin JZ, Thompson DA, Amit I, et al. Full-length transcriptome assembly from RNA-Seq data without a reference genome. *Nat Biotechnol.* (2011) 29:644–52. doi: 10.1038/nbt.1883

54. Davidson NM, Oshlack A. Corset: Enabling differential gene expression analysis for *de novo* assembled transcriptomes. *Genome Biol.* (2014) 15:1–14. doi: 10.1186/s13059-014-0410-6

55. Li B, Dewey CN. RSEM: Accurate transcript quantification from RNA-Seq data with or without a reference genome. *BMC Bioinf.* (2011) 12:1–16. doi: 10.1186/1471-2105-12-323

56. Love MI, Huber W, Anders S. Moderated estimation of fold change and dispersion for RNA-seq data with DESeq2. *Genome Biol.* (2014) 15:1–21. doi: 10.1186/s13059-014-0550-8

57. Tang D, Chen M, Huang X, Zhang G, Zeng L, Zhang G, et al. SRplot: A free online platform for data visualization and graphing. *PloS One.* (2023) 18:18–26. doi: 10.1371/JOURNAL.PONE.0294236

58. Montes A, Figueras A, Novoa B. Nodavirus encephalopathy in turbot (*Scophthalmus maximus*): Inflammation, nitric oxide production and effect of anti-inflammatory compounds. *Fish Shellfish Immunol.* (2010) 28:281–8. doi: 10.1016/J.FSI.2009.11.002

59. Chiang YH, Wu YC, Chi SC. Interleukin-1β secreted from betanodavirus-infected microglia caused the death of neurons in giant grouper brains. *Dev Comp Immunol.* (2017) 70:19–26. doi: 10.1016/J.DCI.2017.01.002

60. Poisa-Beiro L, Dios S, Montes A, Aranguren R, Figueras A, Novoa B. Nodavirus increases the expression of Mx and inflammatory cytokines in fish brain. *Mol Immunol.* (2008) 45:218–25. doi: 10.1016/J.MOLIMM.2007.04.016

61. Cervera L, González-Fernández C, Cano D, Esteban MÁ, Mercado L, Chaves-Pozo E, et al. Immunity elicited by AMP-encoding plasmids fails to increase the protection of European sea bass against nodavirus. *Fish Shellfish Immunol.* (2023) 132:108507. doi: 10.1016/J.FSI.2022.108507

62. Randal JE. A review of mimicry in marine fishes. *Zool Stud.* (2005) 44:299–328.

63. Wendelaar Bonga SE. The stress response in fish. *Physiol Rev.* (1997) 77:591–625. doi: 10.1152/physrev.1997.77.3.591

64. Peter MCS. The role of thyroid hormones in stress response of fish. *Gen Comp Endocrinol.* (2011) 172:198–210. doi: 10.1016/J.YGCEN.2011.02.023

65. Kaneko T. Cell biology of somatolactin. *Int Rev Cytol.* (1996) 169:1–24. doi: 10.1016/S0074-7696(08)61983-X

66. Vissio PG, Darias MJ, Di Yorio MP, Pérez Sirkin DI, Delgadin TH. Fish skin pigmentation in aquaculture: The influence of rearing conditions and its neuroendocrine regulation. *Gen Comp Endocrinol.* (2021) 301:113662. doi: 10.1016/J.YGCEN.2020.113662

67. Belo MAA, Schalch SHC, Moraes FR, Soares VE, Otoboni AMMB, Moraes JER. Effect of dietary supplementation with vitamin E and stocking density on macrophage recruitment and giant cell formation in the teleost fish, *piaractus mesopotamicus*. *J Comp Pathol.* (2005) 133:146–54. doi: 10.1016/J.JCPA.2005.04.004

68. Palermo F, Nabissi M, Cardinaletti G, Tibaldi E, Mosconi G, Polzonetti-Magni AM. Cloning of sole proopiomelanocortin (POMC) cDNA and the effects of stocking density on POMC mRNA and growth rate in sole, *Solea solea*. *Gen Comp Endocrinol.* (2008) 155:227–33. doi: 10.1016/J.YGCEN.2007.05.003

69. Klug JJ, Treuting PM, Sanders GE, Winton JR, Kurath G. Effects of stocking density on stress response and susceptibility to infectious hematopoietic necrosis virus in rainbow trout. *J Am Assoc Lab Anim Sci.* (2021) 60:637–45. doi: 10.30802/AALAS-JAALAS-21–000003

70. Jia R, Wang L, Hou Y, Feng W, Li B, Zhu J. Effects of stocking density on the growth performance, physiological parameters, redox status and lipid metabolism of micropterus salmoides in integrated rice–fish farming systems. *Antioxidants.* (2022) 11:1215. doi: 10.3390/antiox11071215

71. Swain HS, Das BK, Upadhyay A, Ramteke MH, Kumar V, Meena DK, et al. Stocking density mediated stress modulates growth attributes in cage reared *Labeo rohita* (Hamilton) using multifarious biomarker approach. *Sci Rep.* (2022) 12:1–14. doi: 10.1038/s41598-022-13570-x

72. Li D, Liu Z, Xie C. Effect of stocking density on growth and serum concentrations of thyroid hormones and cortisol in Amur sturgeon, *Acipenser schrenckii*. *Fish Physiol Biochem.* (2012) 38:511–20. doi: 10.1007/s10695-011-9531-y

73. Long L, Zhang H, Ni Q, Liu H, Wu F, Wang X. Effects of stocking density on growth, stress, and immune responses of juvenile Chinese sturgeon (*Acipenser sinensis*) in a recirculating aquaculture system. *Comp Biochem Physiol Part C Toxicol Pharmacol.* (2019) 219:25–34. doi: 10.1016/J.CBPC.2019.02.002

74. Lee JW, Min BH, Lee B, Kim K, Yoon M. Effects of stocking density on stress, hematological responses, and growth of black rockfish *sebastes schlegelii*. *J Aquat Anim Health.* (2022) 34:82–91. doi: 10.1002/AAH.10151

75. Salas-Leiton E, Anguis V, Martín-Antonio B, Crespo D, Planas JV, Infante C, et al. Effects of stocking density and feed ration on growth and gene expression in the Senegalese sole (*Solea Senegalensis*): Potential effects on the immune response. *Fish Shellfish Immunol.* (2010) 28:296–302. doi: 10.1016/J.FSI.2009.11.006

76. Pickering AD. Growth and stress in fish production. *Genet Aquac.* (1993) 111:51–63. doi: 10.1016/B978–0-444–81527-9.50010–5

77. Dash S, Das SK, Samal J, Thatoi HN. Epidermal mucus, a major determinant in fish health: a review. *Iran J Vet Res.* (2018) 19:72. doi: 10.22099/ijvr.2018.4849

78. Liu G, Ye Z, Liu D, Zhao J, Sivaramasamy E, Deng Y, et al. Influence of stocking density on growth, digestive enzyme activities, immune responses, antioxidant of *Oreochromis niloticus* fingerlings in biofloc systems. *Fish Shellfish Immunol.* (2018) 81:416–22. doi: 10.1016/J.FSI.2018.07.047

79. Telli GS, Ranzani-Paiva MJT, Dias D de C, Sussel FR, Ishikawa CM, Tachibana L. Dietary administration of Bacillus subtilis on hematology and non-specific immunity of Nile tilapia *Oreochromis niloticus* raised at different stocking densities. *Fish Shellfish Immunol.* (2014) 39:305–11. doi: 10.1016/J.FSI.2014.05.025

80. Lin W, Li L, Chen J, Li D, Hou J, Guo H, et al. Long-term crowding stress causes compromised nonspecific immunity and increases apoptosis of spleen in grass carp (*Ctenopharyngodon idella*). *Fish Shellfish Immunol.* (2018) 80:540–5. doi: 10.1016/J.FSI.2018.06.050

81. Sadhu N, Sharma SRK, Joseph S, Dube P, Philipose KK. Chronic stress due to high stocking density in open sea cage farming induces variation in biochemical and immunological functions in Asian seabass (*Lates calcarifer*, Bloch). *Fish Physiol Biochem.* (2014) 40:1105–13. doi: 10.1007/s10695-014-9909-8

82. Peruzza L, Pascoli F, Dalla Rovere G, Franch R, Ferraresso S, Babbucci M, et al. Transcriptome analysis reveals a complex response to the RGNNV/SJNNV reassortant Nervous Necrosis Virus strain in sea bream larvae. *Fish Shellfish Immunol.* (2021) 114:282–92. doi: 10.1016/J.FSI.2021.04.021

83. Chaves-Pozo E, Bandin I, Olveira JG, Esteve-Codina A, Gómez-Garrido J, Dabad M, et al. European sea bass brain DLB-1 cell line is susceptible to nodavirus: A transcriptomic study. *Fish Shellfish Immunol.* (2019) 86:14–24. doi: 10.1016/J.FSI.2018.11.024

84. Valero Y, Arizcun M, Esteban MÁ, Bandín I, Olveira JG, Patel S, et al. Nodavirus colonizes and replicates in the testis of gilthead seabream and european sea bass modulating its immune and reproductive functions. *PloS One.* (2015) 10:e0145131. doi: 10.1371/journal.pone.0145131

85. Valero Y, Cuesta A, Cammarata M, Esteban M, Chaves-Pozo E. Immune-endocrine interactions in the fish gonad during infection: an open door to vertical transmission. *Fishes.* (2018) 3:24. doi: 10.3390/FISHES3020024

86. Chaves-Pozo E, Valero Y, Esteve-Codina A, Gómez-Garrido J, Dabad M, Alioto T, et al. Innate cell-mediated cytotoxic activity of european sea bass leucocytes against nodavirus-infected cells: A functional and RNA-seq study. *Sci Rep.* (2017) 7:15396. doi: 10.1038/s41598–017-15629–6

87. Prokop JW, Duff RJ, Ball HC, Copeland DL, Londraville RL. Leptin and leptin receptor: Analysis of a structure to function relationship in interaction and evolution from humans to fish. *Peptides.* (2012) 38:326–36. doi: 10.1016/J.PEPTIDES.2012.10.002

88. Covantes-Rosales CE, Toledo-Ibarra GA, Díaz-Resendíz KJG, Ventura-Ramón GH, Girón-Pérez MI. Muscarinic acetylcholine receptor expression in brain and immune cells of. *Oreochromis niloticus J Neuroimmunol.* (2019) 328:105–7. doi: 10.1016/J.JNEUROIM.2019.01.012

89. Kawashima K, Fujii T, Moriwaki Y, Misawa H. Critical roles of acetylcholine and the muscarinic and nicotinic acetylcholine receptors in the regulation of immune function. *Life Sci.* (2012) 91:1027–32. doi: 10.1016/J.LFS.2012.05.006

90. Herr N, Bode C, Duerschmied D. The effects of serotonin in immune cells. *Front Cardiovasc Med.* (2017) 4:48/BIBTEX. doi: 10.3389/fcvm.2017.00048

91. Khan NA, Deschaux P. Role of serotonin in fish immunomodulation. *J Exp Biol.* (1997) 200:1833–8. doi: 10.1242/JEB.200.13.1833

92. Leggatt RA, Iwama GK. Occurrence of polyploidy in the fishes. *Rev Fish Biol Fish.* (2003) 13:237–46. doi: 10.1023/B:RFBF.0000033049.00668.fe

frontiers | Frontiers in Immunology

TYPE Original Research
PUBLISHED 14 June 2024
DOI 10.3389/fimmu.2024.1410150

OPEN ACCESS

EDITED BY
Elena Chaves-Pozo,
Spanish Institute of Oceanography, Spain

REVIEWED BY
Guan-Jun Yang,
Ningbo University, China
Mahmoud Tanekhy,
Alexandria University, Egypt

*CORRESPONDENCE
Neeraj Kumar
neeraj_journal@live.in

RECEIVED 31 March 2024
ACCEPTED 23 May 2024
PUBLISHED 14 June 2024

CITATION
Kumar N, Thorat ST, Gunaware MA, Kumar P and Reddy KS (2024) Unraveling gene regulation mechanisms in fish: insights into multistress responses and mitigation through iron nanoparticles. *Front. Immunol.* 15:1410150. doi: 10.3389/fimmu.2024.1410150

Unraveling gene regulation mechanisms in fish: insights into multistress responses and mitigation through iron nanoparticles

Neeraj Kumar*, Supriya Tukaram Thorat, Meghana Ajit Gunaware, Paritosh Kumar and Kotha Sammi Reddy

School of Edaphic Stress Management (SESM), ICAR-National Institute of Abiotic Stress Management, Baramati, India

The recent trend of global warming poses a significant threat to ecosystems worldwide. This global climate change has also impacted the pollution levels in aquatic ecosystems, subsequently affecting human health. To address these issues, an experiment was conducted to investigate the mitigating effects of iron nanoparticles (Fe-NPs) on arsenic and ammonia toxicity as well as high temperature stress (As+NH_3+T). Fe-NPs were biologically synthesized using fish waste and incorporated into feed formulations at 10, 15, and 20 mg kg^{-1} diet. A total of 12 treatments were designed in triplicate following a completely randomized design involving 540 fish. Fe-NPs at 15 mg kg^{-1} diet notably reduced the cortisol levels in fish exposed to multiple stressors. The gene expressions of *HSP 70*, *DNA* damage-inducible protein (*DDIP*), and DNA damage were upregulated by stressors (As+NH_3+T) and downregulated by Fe-NPs. Apoptotic genes (*Cas 3a* and *3b*) and detoxifying genes (*CYP 450*), metallothionein (*MT*), and inducible nitric oxide synthase (*iNOS*) were downregulated by Fe-NPs at 15 mg kg^{-1} diet in fish subjected to As+NH_3+T stress. Immune-related genes such as tumor necrosis factor (*TNFα*), immunoglobulin (*Ig*), and interleukin (*IL*) were upregulated by Fe-NPs, indicating enhanced immunity in fish under As+NH*3*+T stress. Conversely, Toll-like receptor (*TLR*) expression was notably downregulated by Fe-NPs at 15 mg kg^{-1} diet in fish under As+NH_3+T stress. Immunological attributes such as nitro blue tetrazolium chloride, total protein, albumin, globulin, A:G ratio, and myeloperoxidase (MPO) were improved by dietary Fe-NPs at 15 mg kg^{-1} diet in fish, regardless of stressors. The antioxidant genes (*CAT*, *SOD*, and *GPx*) were also strengthened by Fe-NPs in fish. Genes associated with growth performance, such as growth hormone regulator (*GHR1* and *GHRβ*), growth hormone (*GH*), and insulin-like growth factor (*IGF 1X* and *IGF 2X*), were upregulated, enhancing fish growth under stress, while *SMT* and *MYST* were downregulated by Fe-NPs in the diet. Various growth performance indicators were improved by dietary Fe-NPs at 15 mg kg^{-1} diet. Notably, Fe-NPs also

enhanced arsenic detoxification and reduced the cumulative mortality after a bacterial infection. In conclusion, this study highlights that dietary Fe-NPs can effectively mitigate arsenic and ammonia toxicity as well as high temperature stress by modulating gene expression in fish.

KEYWORDS

iron nanoparticles, toxicity, gene regulation, detoxification, fish

1 Introduction

The recent dramatic change in ecosystems has been witnessed to affect all living organisms, including humans, animals, and fish. Climate change, pollution, and degraded water quality are affecting the aquatic systems, resulting in the species extinction of aquatic organisms including fish (1, 2). With fish reared under a degraded environment, this results in changes at the gene and cellular levels. The contamination reaches up to cellular level of the aquatic organism, and the final product is contaminated, which increases the chances of deadly diseases occurring in consumers such as humans. Climate change and pollution can also lead to occurrences of diseases in all ecosystems. While climate change and pollution are distinct factors, they often work together to degrade the food chain and web. In aquatic systems like aquaculture and fisheries, ammonia emerges as a critical abiotic factor affecting the production and survival of aquatic animals, including fish (1). The adverse effect of abiotic factors such as arsenic (As), ammonia (NH_3), and high temperature has weakened the immunity of aquatic organisms, which results in decreases in the efficiency of gene regulations involved in the detoxification of contamination. Moreover, arsenic pollution broadly covers the globe, including Asia, America, Europe, African countries, etc. Asian countries such as Bangladesh and the northeastern parts of India and China are also badly affected. Almost 200 million people are at a high risk (3, 4), of which 43,000 people die annually in Bangladesh due to arsenic pollution (4). As per the International Agency for Research on Cancer (IARC), it is also considered a class I carcinogenic (5). Arsenic is widely used for agriculture, veterinary drugs, medicines, metal alloy manufacturing, microelectronics, glassware, and wood preservatives (6, 7). Furthermore, the toxicity of ammonia (NH_3) in aquatic ecosystems is crucial, resulting in mass mortality in fish. NH_3 mainly originates from high fish protein diet, fish waste, and metabolic process of the aquatic organism, resulting in NH_3 toxicity in aquatic systems (8, 9). The breakdown of amino acids, pyrimidines, and purines also generates ammonia (10), which exists in two forms: unionized ammonia (NH_3) and ionized ammonium (NH_4^+) (11). Ammonia toxicity can lead to noticeable reductions in growth performance (12), immunity, tissue erosion, neurotoxicity, and oxidative stress and ultimately result in high mortality (13). Similarly, elevated temperature also alters the fish physiology as fish are poikilothermic animals.

Iron (Fe) is an essential nutrient which has an important role in oxygen transport and cellular respiration in fish (14). Moreover, the fish can absorb Fe using its gills and intestinal mucosa (14). In this study, multiple abiotic factors (As, NH_3, and high temperature—T) were employed for stress which induces a weakened immunity in fish, resulting in alterations of the gene regulations involved in the immunity of fish, although immunity has been indicated and reflected from primary stress response to tertiary stress response. In the case of weak immunity, the natural kappa factor (NFkB) signaling pathway is inhibited due to multiple abiotic factor stress. Moreover, the dietary iron nanoparticles (Fe-NPs) improve the immunity of the fish using the NFkB signaling pathway (15, 16). The nano-form of iron sulfate is highly bioavailable to fish compared to other forms of iron (17). Therefore, the supplementation of Fe-NPs diet can be maximized as enhancer of immunity, anti-oxidant status, and the growth performance of the fish (18). The gene responsible for apoptosis and programmed cell death, cytokines, NF-κB pathway, immune genes, and anti-oxidant defense genes are important for regulatory mechanism (19, 20), although cytokines are vital signaling molecules released during various conditions, modulating inflammatory responses and maintaining barrier integrity (21). Therefore, Fe-NPs control the gene regulation involved in the abovementioned process.

Abbreviations: Fe-NPs, Iron nanoparticles; As, Arsenic; NH_3,Ammonia; T, High temperature; NFkB, Nuclear factor kappa B; iNOS, Inducible nitric oxide synthase; HSP70, Heat shock protein; MT, Metallothionine; CAT, Catalase; SOD, Superoxide dismutase; GPx, Glutathione peroxidase; CAS 3a, Caspase 3a; TNFα, Tumor necrosis factor; IL, Interleukin; TLR, Toll-like receptors; GH, Growth hormone; GHR1; GHRβ, Growth hormone regulator 1 and β; MYST, Myostatin; SMT, Somatostatin; NFkB, Natural kappa factor; IARC, International Agency for Research on Cancer; T, High temperature; IPCC, Intergovernmental Panel on Climate Change; TAN, Total ammonia nitrogen; RAC, Research Advisory Committee; PME, Prioritization, Monitoring and Evaluation; LC_{50}, Lethal concentration; CMC, Carboxymethyl cellulose; CP, Crude protein; EE, Ether extract; FEC, Feed conversion efficiency; SGR, Specific growth rate; PER, Protein efficiency ratio; DGI, Daily growth index; TGC, Thermal growth coefficient; RFI, Relative feed intake; ICPMS, Inductively coupled plasma mass spectrometry.

Neurotoxicity using acetylcholine esterase (AChE) was also inhibited using multiple abiotic stresses, although the dietary Fe-NPs enhanced the AChE activities (22). Fe-NPs supplementation could enhance the growth performance in the fish. It has advantage over bulk Fe as Fe-NPs have higher bioavailability and better absorption, which can promote fish growth (18). The Fe-NPs also decrease alanine amino transferase (ALT) and aspartate amino transferase (AST) and promote good fish health (18).

A mechanistic study of multiple stresses is required to understand the gene regulation involved in such process. However, *Pangasianodon hypophthalmus* is the fish species best suited to study the impact of multiple stresses and different gene regulation pathways (23, 24). *P. hypophthalmus* has high demand due to its medicinal and taste characteristics, and it has potential for diversification as an aquaculture species (25). The aims of the present study are dealt with by two major objectives, namely (1): to understand the mechanistic role of Fe-NPs in mitigating multiple stresses (abiotic and biotic) and (2) to elucidate the role of gene regulation involved in the response to multiple stress, such as a low dose of arsenic and ammonia toxicity as well as high temperature in *P. hypophthalmus*.

2 Materials and methods

2.1 Ethics statement

The institute aquaculture wet lab facilities were registered under the Committee for the Purpose of Control and Supervision of Experiments on Animals (CCSEA)—2190/GO/RReBi/SL/2022/CCSEA. The study was approved by institute PME as 7–1(PME) 2024–04. This study was in compliance with Animal Research: Reporting of *In Vivo* Experiments (ARRIVE) guidelines.

2.2 Experimental animals and design

The fish were taken from the National Institute of Abiotic Stress Management's Farm Pond. The fish weighed an average of 6.02 ± 0.24 g and measured 5.12 ± 0.18 cm in size. The fish were kept in a 150-L rectangular plastic aquarium. The fish were placed in quarantine with potassium permanganate ($KMnO_4$) and a 1% dip salt solution. A total of 12 treatments were designed for this experiment: iron nanoparticles supplied to the group at 10, 15, and 20 mg kg^{-1} diet with or without stressors: arsenic (As); ammonia (NH_3); arsenic and ammonia (As+NH_3); and arsenic, ammonia, and high temperature (As+NH_3+T). Table 1 presents the details of the treatments.

Fe-NPs diet was fed to the fish twice a day, at 9:00 AM and 5:00 PM. Every day, the uneaten food and excrement were removed by siphoning. The APHA method (26) was used to periodically analyze the water quality parameters, and the results were recorded within the typical range for this fish's culture (27). Every other day, the water was physically changed (2/3rd of water), and arsenic (sodium arsenite, $NaAsO_2$) and $(NH_4)_2SO_4$ were added as sources of ammonia toxicity (NH_3) and to provide constant aeration using a compressed air pump. The As, As+NH_3, As+NH_3+T, and NH_3 stressor groups were kept together by ammonium sulfate [1/10th of LC_{50} 2.0 mg L^{-1} of $(NH_4)_2SO_4$] (12) and arsenic (1/10th of LC_{50} 2.68 mg L^{-1}) (28) and high temperature (34°C) maintained with thermostatic heaters. Four experimental diets of iso-nitrogenous (35% crude protein) and iso-caloric type were prepared. Different feed ingredients were used, such as fish meal, groundnut meal, soybean meal, wheat flour, carboxymethyl cellulose (CMC), cod liver oil, lecithin, and vitamin C. The Fe-NPs free mineral mixture was prepared manually for inclusion in the diets. The heat-labile ingredients were mixed after heating the feed ingredient. In terms of proximate analysis of the diets, these were analyzed using the method of AOAC (29). Crude protein was analyzed using nitrogen content, ether extract (EE) using solvent extraction, and ash estimation using muffle furnace (550°C) (Table 2). Total carbohydrate % was calculated by using the following equation:

$$\text{Total carbohydrate \%} = 100 - (\text{CP \%} + \text{EE \%} + \text{Ash \%} + \text{Moisture \%})$$

The gross energy of the diets was calculated using the method described by Halver (30).

TABLE 1 Experimental design of the present investigation.

S. no.	Details of the treatments	Notation
1	Control	Ctr
2	Arsenic exposure and fed with control diet	As
3	Ammonia exposure and fed with control diet	NH_3
4	Concurrent exposure to arsenic and ammonia and fed with control diet	As+NH_3
6	Concurrent exposure to arsenic, ammonia, and high temperature and fed with control diet	As+NH_3+T
7	Fed with iron nanoparticles at 10 mg kg^{-1} diet	Fe-NPs at 10 mg kg^{-1} diet
8	Fed with iron nanoparticles at 15 mg kg^{-1} diet	Fe-NPs at 15 mg kg^{-1} diet
9	Fed with iron nanoparticles at 20 mg kg^{-1} diet	Fe-NPs at 20 mg kg^{-1} diet
10	Concurrent exposure to arsenic, ammonia, and high temperature and fed with iron nanoparticles at 10 mg kg^{-1} diet	Fe-NPs at 10 mg kg^{-1} diet+As +NH_3+T
11	Concurrent exposure to arsenic, ammonia, and high temperature and fed with iron nanoparticles at 10 mg kg^{-1} diet	Fe-NPs at 15 mg kg^{-1} diet+As +NH_3+T
12	Concurrent exposure to arsenic, ammonia, and high temperature and fed with iron nanoparticles at 10 mg kg^{-1} diet	Fe-NPs at 20 mg kg^{-1} diet+As +NH_3+T

TABLE 2 Ingredient composition and proximate analysis of experimental diets (% dry matter) of iron nanoparticles (Fe-NPs) fed to *Pangasianodon hypophthalmus* for 90 days.

Feed ingredients	Fe-NPs—0 mg kg^{-1} diet	Fe-NPs—10 mg kg^{-1} diet	Fe-NPs—15 mg kg^{-1} diet	Fe-NPs—20 mg kg^{-1} diet
Soybean meal[a]	35.5	35.5	35.5	35.5
Fish meal[a]	25	25	25	25
Groundnut meal[a]	10	10	10	10
Wheat flour[a]	17.47	17.46	17.455	17.45
Sunflower oil[a]	4.5	4.5	4.5	4.5
Cod liver oil[a]	1.5	1.5	1.5	1.5
CMC[b]	2	2	2	2
Vitamin and mineral mix[c]	2	2	2	2
Vitamin C[d]	0.03	0.03	0.03	0.03
Lecithin[b]	2	2	2	2
Fe-NPs	0	0.01	0.015	0.02
Proximate composition of the diets				
Crude protein (CP)	35.22 ± 0.28	35.28 ± 0.03	35.05 ± 0.09	35.12 ± 0.03
Ether extract (EE)	9.29 ± 0.04	9.54 ± 0.12	9.57 ± 0.16	9.56 ± 0.12
Total carbohydrate (TC)	37.69 ± 0.18	37.19 ± 0.35	36.72 ± 0.45	37.45 ± 0.10
Organic matter (OM)	90.75 ± 0.04	90.19 ± 0.49	90.29 ± 0.54	90.40 ± 0.14
Dry matter (DM)	91.44 ± 0.20	91.82 ± 0.43	91.05 ± 0.18	91.73 ± 0.17
Digestible energy (DE)	356.62 ± 0.82	356.67 ± 1.21	354.05 ± 1.69	357.19 ± 1.22
Iron (Fe, mg kg^{-1})	2.62 ± 0.13	13.81 ± 0.32	19.48 ± 0.60	23.73 ± 0.97

Digestible energy (DE) (kcal/100 g) = (% CP × 4) + (% EE × 9) + (TC × 4). Data are expressed as mean ± SE; n = 3.
[a]Procured from the local market.
[b]Himedia Ltd.
[c]Manually prepared vitamin mineral mixture—composition of the vitamin mineral mix (quantity/250 g starch powder): vitamin A—55,00,00 IU; vitamin D3—11,00.00 IU; vitamin B1—20 mg; vitamin E—75 mg; vitamin K—1.00 mg; vitamin B12—0.6 mcg; calcium pantothenate—2.50 mg; nicotinamide—1,000 mg; pyridoxine—100 mg; Zn—500 mg; I—1.00 mg; Mn—100 mg; Cu—200 mg; Co—45 mg; Ca—50 g; P—30 g; Se—2 ppm.
[d]SD Fine Chemicals Ltd., India.

2.3 Synthesis of iron nanoparticles using the green approach

2.3.1 Preparation of fish tissue extract

Fish waste (gill tissue) was used to synthesize Fe-NPs. The tissues were cut open, and blood and dust were washed away with running water. After tissue homogenization (SCILOGEX D160, Serial number-DA198AB0000585; 1275 Cromwell Ave., Suite 122; Rocky Hill, CT, USA), the supernatant was recovered by centrifuging (Thermoscientific, SORVALL, Legend MICRO 21 R) at 5,000–6,000 rpm. Whatman paper (0.45-µm pore size) was then used as filter to get the gill extract (31, 32).

2.3.2 Preparation and characterization of iron nanoparticles

Ferrous sulfate (0.4 M) was combined with the gill extract. After that, this was stirred at room temperature for 30 min. After that, the magnetic stirrer was maintained at 60 °C for 2.5–4 h while gradually adding 0.8 M NaOH drop by drop until a reddish-brown solution is achieved. Following the acquisition of a reddish-brown hue in the solution, a spectrophotometer [UV1900i; Shimadzu (Asia Pacific) Pte Ltd., Cintech IV, Science Park I, Singapore 118264] was used to measure the peak value at (216–600 nm), where a high absorption peak was found at 250 nm. After centrifuging it and washing it three times in distilled water, pellet was obtained. The pellet was then

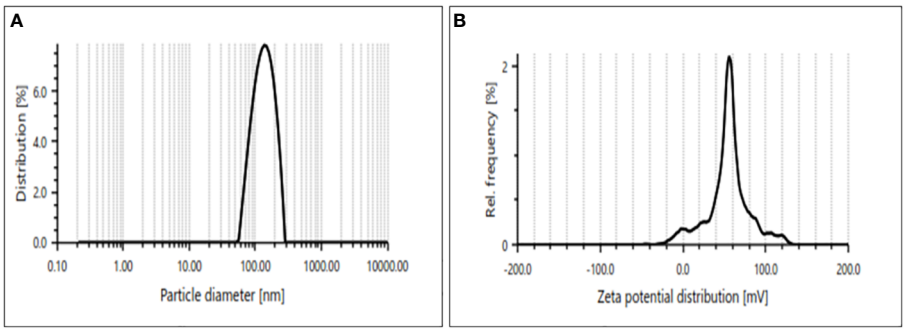

FIGURE 1
(A, B) Size of iron nanoparticles (Fe-NPs) 130nm and Zeta potential 53.7 mV.

allowed to dry in the concentrator. Iron nanoparticles (Fe-NPs) are obtained as a reddish-brown powder after drying. Additionally, the synthesized Fe-NP formulations were combined with Milli-Q water and subjected to particle size characterization (Particle Analyser, Litesizer 500, Anton Paar, Austria). The mean size and zeta potential were obtained as 130.17 nm and 53.3 mV, respectively (Figures 1A, B).

2.4 RNA isolation and quantification

Total RNA was isolated from *P. hypophthalmus* liver and muscle tissues using the TRIzol technique. The liver and muscle (*MYST* and *SMT*) tissues were homogenized using liquid nitrogen. After adding chloroform to the homogenized samples for phase separation, they were incubated for 5 min. Following centrifugation, the RNA-containing aqueous phase was separated into a 1.5-mL tube, and isopropanol was used to precipitate the RNA. After air-drying the RNA pellet, it was dissolved in RNAse-free water after the precipitated RNA had been cleaned with 75% ethanol. For later use, RNA was kept in storage at -80°C. Furthermore, 1.0% agarose gel was used to confirm the integrity of the RNA. It was made by melting agarose in 1X TAE buffer to the necessary amount. A gel documentation system (ChemiDocTM MP imaging system, Bio-Rad) was used to visualize the RNA bands. The RNA was quantified using a nano-drop spectrophotometer (Thermo-scientific).

2.5 cDNA synthesis and quantitative PCR

Revert Aid First Strand cDNA synthesis kit (Thermo-scientific) was used to synthesize cDNA from total extracted RNA. Prior to the creation of cDNA, trace quantities of DNA were eliminated using DNase I. A volume of 12 µL contained the reaction mixture, including 15 pmol of oligo dT primers and 100 ng of RNA. In the PCR, the reaction mixture was heated to 65°C for 5 min before being cooled on ice. With that, the chilled mixture was centrifuged for a brief period of time with the addition of 1 µL Ribo Lock RNase Inhibitor (20 U/µL), 1.0 µL of reverse transcriptase enzyme, 5X reaction buffer (4.0 µL), and 2 µL dNTP Mix (10 mM). Subsequently, the mixture was

TABLE 3 Details of the primer for relative quantitative real-time PCR.

Gene	Primer sequence (5′ –3′)	Accession number
SOD	F-GTCCATCTTACCCGGTGCCC R-CGAGAGAAGACCCGGAACGC	XM_034299545.1
CAT	F-AGCAGGCGGAGAAGTACCCA R-GCTGCTCCACCTCAGCGAAA	XM_026919141.2
GPx	F- GTCACTGCAGGATGCAACAC R- TTGGAATTCCGCTCATTGAT	XM_026947312.2
HSP 70	F- CTCCTCCTAAACCCCGAGTC R- CCACCAGCACGTTAAACACA	XM_026934573.2
iNOS	F-ACACCACGGAGTGTGTTCGT R-GGATGCATGGGACGTTGCTG	XM_026931613.2
DNA damage inducible protein	F-CACCTTCGCCCTCGAAGTCT R-GCTCGGGTGAGGTCTCTCAG	XM_026938137.2
TNFα	F-TGGAGTTCTGCTTGCCGTGG R-GCAGCCTTTGCAGTCTCGGA	XM_026942329.2
TLR	F: TCACCACGAACGAGACTTCATCC R: GACAGCACGAAGACACAGCATC	XM_026916808.2
Ghr1	FTATTGGCTACAGCTCGCCGC R-AATCACCCCGACTGTGCTGC	XM_034306157.1
Ghrb	F-TTGAGCTTTGGGACTCGGAC R-CGTCGATCTTCTCGGTGAGG	XM_026942987.2
IGF-1X1	F-GCAACGGCACACAGACACGC R-CAGACGTTCCCTCACCATCCTCT	XM_034313382.2
IGF-1X2	F-CGAGAGCAACGGCACACAGA R-TTCTGATGGACCTCCTTAC AAGATG	XM_034313383.2
IL	F- AGCAGGATCCATCAAAGTGG R- GTGCTCCAGCTCTCTGGGTA	XM_026918084.2
Ig	F- GGCCAGTAATCGTACCTCCA R- CTTCGTAAGGTCCCCACTGA	XM_026923540.2
MYST	F-GGGAAAGACCTGGCCGTGAC R-TCGAGGCCGGATTCTCGTCT	XM_026910492.2
SMT	F- CTCTGGGTGGCAGAATGAAT R- AACATGAAGAGAACGTTTTCCAG	XM_026921272.2

(Continued)

TABLE 3 Continued

Gene	Primer sequence (5′ –3′)	Accession number
GH	F-CCCAGCAAGAACCTCGGCAA R-GCGGAGCCAGAGAGTCGTTC	GQ859589.1
CYP P450	F-GATTCGGCATCCGTGCGTGC R-GATGTGGCTGGGACGAGCA	NC_047599.1
MT	F-CACGGCTTTTCCTGTCCGCT R-AACAGCGCCCCCAGGTGTC	AF087935.1
Cas 3a	F-CGGCATGAACCAGCGCAAC R-TCCACCGCACCATCTGTCCC	NC_047622.1
Cas3b	F-AGCTTTCCGTGAGCTGGGCT R-TGGCTGACTTGCTGTGGTCCT	NC_047601.1
Na^+K^+ATPase	F-AACTACAAGCCCACGTACCA R-CTTGCCAGCCTTAAAGCCAA	XM_026923907.3
β-actin	F-CAGCAAGCAGGAGTACGATG R-TGTGTGGTGTGTGGTTGTTTTG	XM_031749543.1

SOD, superoxide dismutase; CAT, catalase; GPx, glutathione peroxidase; HSP, heat shock protein; iNOS, nitric oxide synthase; TNFα, tumor necrosis factor; TLR, Toll-like receptor; Ghr, growth hormone receptor; IL, interleukin; Ig, immunoglobulin; MYST, myostatin; SMT, somatostatin; CYP P450, cytochrome P450; MT, metallothionine; Cas 3a and 3b, caspase 3; GH, growth hormone; IGF1 and 2, insulin-like growth factor.

incubated for 42 min at 60°C and for 5 min at 70°C. Through the use of β-actin PCR, the generated cDNA was verified. Quantitative PCR (real-time PCR) was conducted using gene-specific primers and the SYBR green PCA master mix (Bio-Rad). SYBR Green Master Mix (1X), primer (1 μL), and 1 μL of cDNA were included in the quantification samples. The reaction cycle was set up as follows: 10 min of initial denaturation at 95°C, 39 cycles of cDNA amplification, followed by 15 s of denaturation at 95°C and 1 min of annealing at 60° C (33). Table 3 has the primers' specifics listed.

2.6 Growth performance

The study examined the growth performance parameters, including relative feed intake (RFI), weight gain (%), feed conversion ratio (FCR), specific growth rate, thermal growth coefficient (TGC), protein efficiency ratio (PER), and daily growth index (DGI). For a total of 90 days, the fish's weight was recorded every 15 days.

$$\text{FCR} = \text{Total dry feed intake(g)}/\text{Wet weight gain(g)}$$

$$\text{SGR} = 100(\ln \text{FBW} - \ln \text{IBW})/\text{number of days}$$

$$\text{Weight gain}(\%) = \text{Final body weight (FBW)} - \text{Initial body weight (IBW)}/\text{Initial body weight (IBW)} \times 100$$

$$\text{Relative feed intake (FI)}\ (\%/\text{day}) = 100 \times (\text{TFI}/\text{IBW})$$

$$\text{PER} = \text{Total wet weight gain (g)}/\text{crude protein intake (g)}$$

Thermal growth coefficient (TGC)

$$= (\text{FBW}^{1/3} - \text{IBW}^{1/3}) \times (\Sigma D0)^{-1},$$

where ΣD0 is the thermal sum (feeding days × average temperature, ° C)

$$\text{Daily growth index, DGI}\ (\%) = (\text{FBW}^{1/3} - \text{IBW}^{1/3})/\text{days} \times 100$$

2.7 Gene study

The different genes were investigated in liver tissues in this study, viz., superoxide dismutase (*SOD*), catalase (*CAT*), glutathione-s-transferase (*GST*), heat shock protein (*HSP 70*), nitric oxide synthase (*iNOS*), cytochrome P450 (*CYP 450*), caspase 3a (*CAS 3a* and *3b*), metallothionine (*MT*), tumor necrosis factor (*TNFα*), Toll-like receptor (*TLR*), growth hormone receptor (*Ghr1* and *Ghrb*), interleukin (*IL*), immunoglobulin (*Ig*), growth hormone (*GH*), and insulin like growth factor 1 and 2 (*IGF1* and *IGF 2*), and in muscle tissue, somatostatin (*SMT*) and myostatin (*MYST*) were studied for real-time quantification.

2.8 Cortisol

Cortisol was determined using ELISA kit (commercially available Cortisol EIA kit, catalog no. 500360, Cayman Chemicals, USA). The assay was performed as per the instruction provided with the kit. The final reading was obtained using an ELISA plate reader (Biotek India Pvt. Ltd.).

2.9 Arsenic and iron analysis from fish tissues, feed, and experimental water

To measure the levels of arsenic, samples were taken from the kidney, brain, gills, liver, and muscle. On the other hand, the concentration of Fe was determined in the fish muscle and diet. Using inductively coupled plasma mass spectrometry (ICP-MS) (Agilent 7700 series, Agilent Technologies, USA) in a microwave digestion system (Microwave Reaction System, Multiwave PRO, Anton Paar GmbH, Austria, Europe), the tissues and diets were processed in accordance with the method of Kumar et al. (31, 34).

2.10 Alkaline single-cell gel electrophoresis/comet assay

With a slight modification (32), the alkaline single-cell gel electrophoresis/comet assay of Ali et al. (35) was used to assess DNA damage in kidney tissue. The kidney tissue (50 mg) was placed in an ice-cold homogenization buffer [20 mM EDTA; 1-X Hanks' balanced salt solution; 10% dimethyl sulfoxide (DMSO), pH

7.0–7.5] after having been cleaned twice with chilled phosphate buffer saline (Ca^{2+}- and Mg^{2+}-free). The tissue was used to create a single-cell suspension, which was then suspended in phosphate saline buffer after having been centrifuged for 5 min at 4°C and 3,000 rpm to extract the cell pellets. Trypan Blue Exclusion Test was also utilized for the cell viability test (35). After coating the glass slide with 200 µL of 1% regular agarose, it was combined with 85 µL of 0.5% low melting point agarose which was added to 15 µL of cell suspension (about 20,000 cells), which was then covered with a coverslip. Furthermore, following the removal of the cover slip, 100 µL of low melting point agarose was once more applied to the slides. The slides were then left in the lysing solution (100 mM Na^2 EDTA, 2.5 M NaCl, 10 mM Tris, pH 10, with fresh additions of 1% Triton X-100 and 10% DMSO) for an entire night at 4°C. After that, the slides were put in a horizontal gel electrophoresis unit using electrophoresis buffer (1 Mm Na^2EDTA, 300 mM NaOH, and 0.2% DMSO, pH >13.5), and the electrophoresis unit was run for 20 min at 4°C using 15 V (0.8 V cm^{-1}) and 300 mA. After that, the slides were cleaned three times using 0.4 in neutralizing buffer using Tris buffer, pH 7.5, at 0.4 M. To visualize the DNA damage, 75 µL of ethidium bromide (20 µg mL^{-1}) was applied to the slides for 5 min. After that, the slides were examined under a fluorescence microscope (Leica Microsystems Ltd., DM 2000, Heerbrugg, Switzerland), and pictures were taken and examined using an Open Comet image analysis system. According to the software calculated, the metric chosen for quantifying DNA damage was percent tail DNA (i.e., % tail DNA = 100% head DNA).

2.11 Challenge study with *Aeromonas hydrophila*

After 90 days of feeding trial, nine fishes per replicate (total of three replicates, 27 fish per treatment) were challenged with virulent *A. hydrophila* (Hi-Media, Mumbai, India, lot no. 637–51-5 and Ref 0637 P), grown in nutrient broth for 24 h at 37°C in a BOD incubator, and harvested by centrifuging the culture broth at 10,000 rpm for 10 min at 4°C. The cells were then washed thrice in sterile PBS (pH 7.2), and the final concentration was maintained at 10^8 CFU mL^{-1}. The fishes were intraperitoneally injected with 0.15 mL of bacterial suspension in each treatment group. The fish mortality in each treatment group was recorded up to 7 days of the challenge study. The tissues were dissected out from dead fish for confirmation of *A. hydrophila* as a causative agent of death.

2.12 Statistics

The Statistical Package for the Social Sciences (SPSS) version 16 program has been used to process the statistical analysis of the experimental data. Using Duncan's multiple-range tests and a one-way ANOVA (analysis of variance), the significance and treatment impact have been examined. After analysis, the data was determined to be significant at $p<0.05$.

3 Results

3.1 Cortisol

The results of the serum cortisol levels in *P. hypophthalmus* reared under ammonia and arsenic toxicity as well as high temperature stress are illustrated in Figure 2A. The serum cortisol level exhibited a noticeable elevation (p = 0.0017) when exposed concurrently to ammonia and arsenic toxicity along with high temperature stress. This elevation was followed by concurrent exposure to ammonia and arsenic toxicity alone and then by exposure to ammonia and arsenic alone when compared to control and Fe-NP-supplemented groups. Additionally, dietary supplementation of Fe-NPs at 15 mg kg^{-1} diet, with or without stressors (As+NH_3+T) and subsequent supplementation at 10 mg kg^{-1} diet, significantly reduced the cortisol levels compared to the control and other experimental groups.

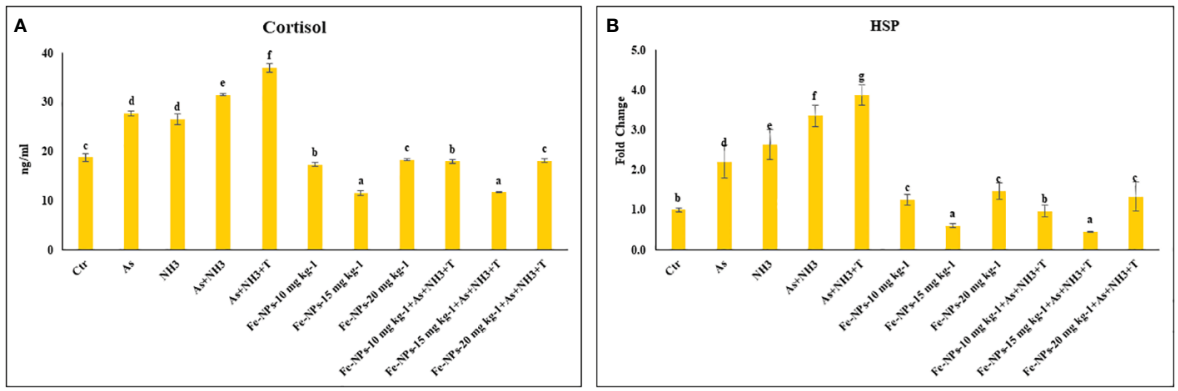

FIGURE 2
(A, B) Effect of dietary iron nanoparticles (Fe-NPs) on cortisol and *HSP 70* against multiple stress in fish. Within endpoints and groups, bars with different superscripts differ significantly (a-g). Data expressed as Mean ± SE (n=3).

3.2 Heat shock protein (*HSP 70*)

The expression of the *HSP 70* gene in liver tissue was significantly upregulated (p = 0.0022) by concurrent exposure to ammonia and arsenic toxicity, followed by exposure to arsenic combined with ammonia, ammonia alone, and arsenic alone, when compared to the control and other experimental groups. Interestingly, dietary supplementation of Fe-NPs at 15 mg kg^{-1} diet, with or without stressors, notably downregulated the expression of the *HSP 70* gene compared to the control and other experimental groups. Moreover, groups fed with Fe-NPs at 10 and 20 mg kg^{-1} diet, with or without stressors, showed a significantly lower expression of the *HSP 70* gene compared to all groups exposed to stressors (As, NH_3, As+NH_3, and As+NH_3+T) (Figure 2B).

3.3 DNA damage inducible protein and DNA damage

The gene expression of DNA damage inducible protein (*DDIP*) was notably upregulated (p = 0.0013) by concurrent exposure to ammonia and arsenic toxicity as well as high temperature stress, followed by exposure to arsenic combined with ammonia, ammonia alone, and arsenic alone, when compared to the control and Fe-NP-supplemented groups. Moreover, the gene expression of *DDIP* was significantly downregulated in the group fed with Fe-NPs at 15 mg kg^{-1} diet, with or without stressors (As+NH_3+T), compared to the control and other experimental groups. Groups fed with Fe-NPs at 10 and 20 mg kg^{-1} diet, without stressors, exhibited lower gene regulation of *DDIP* compared to groups exposed to stressors (arsenic, ammonia, arsenic combined with ammonia, and arsenic combined with ammonia and high temperature) (Figure 3A).

Furthermore, the results of DNA damage (comet) in the form of tail DNA % and head DNA % in the gill tissue of *P. hypophthalmus* are shown in Figure 3B. Head DNA (%) was notably lowered (p = 0.016), whereas tail DNA (%) was notably higher (p = 0.025) in the group exposed to concurrent arsenic, ammonia, and high temperature, followed by arsenic and ammonia, ammonia alone, and arsenic alone, compared to the control and other experimental groups. The group fed with dietary Fe-NPs at 15 mg kg^{-1} diet exhibited noticeably lower tail DNA (%) and higher head DNA (%), with or without stressors, compared to the control and other experimental groups.

3.4 Caspase, metallothionine, and cytochrome p450

In the present study, the gene expression of *Cas 3a* and *3b*, *MT*, and *CYP 450*, respectively, was investigated in the liver tissue of *P. hypophthalmus* reared under multiple stress conditions (As, NH_3, As+NH_3, and As+NH_3+T), and the results are presented in Figures 4A, B. *Cas 3a* gene expression was significantly upregulated (p = 0.017) by exposure to arsenic alone, followed by As+NH_3+T, As+NH_3, and NH_3-alone groups. Conversely, *Cas 3b* expression was significantly upregulated (p = 0.0012) by concurrent exposure to arsenic, ammonia, and high temperature stress, followed by As+NH_3, arsenic alone, and ammonia alone groups, compared to the control and other experimental groups. However, both *Cas 3a* and *3b* were downregulated by Fe-NPs at 1.5 mg kg^{-1} diet, with or without stressors, compared to the control and other experimental groups (Figure 4A). *MT* gene expression was substantially upregulated (p = 0.0031) by As+NH_3+T, followed by arsenic, ammonia, and As+NH_3 exposure in *P. hypophthalmus*, compared to the control and Fe-NP-supplemented groups (Fe-NPs 10 and 15 mg kg^{-1} diet). Conversely, *CYP 450* gene expression was notably (p = 0.016) highly upregulated by exposure to arsenic alone, followed by As+NH_3+T, ammonia alone, and As+NH_3 exposure, compared to the control and other experimental groups. Interestingly, *MT* and *CYP 450* gene expressions were significantly downregulated by dietary Fe-NPs at 15 mg kg^{-1} diet compared to the control and other experimental groups (Figure 4B).

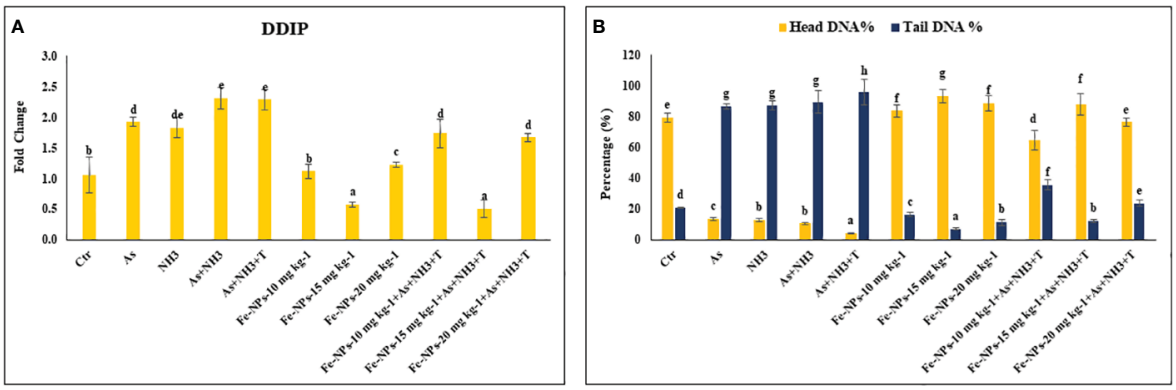

FIGURE 3
(A, B) Effect of dietary iron nanoparticles (Fe-NPs) on gene expression of DNA damage inducible protein (*DDIP*) and DNA damage against multiple stress in fish. Within endpoints and groups, bars with different superscripts differ significantly (a-g). Data expressed as Mean ± SE (n=3).

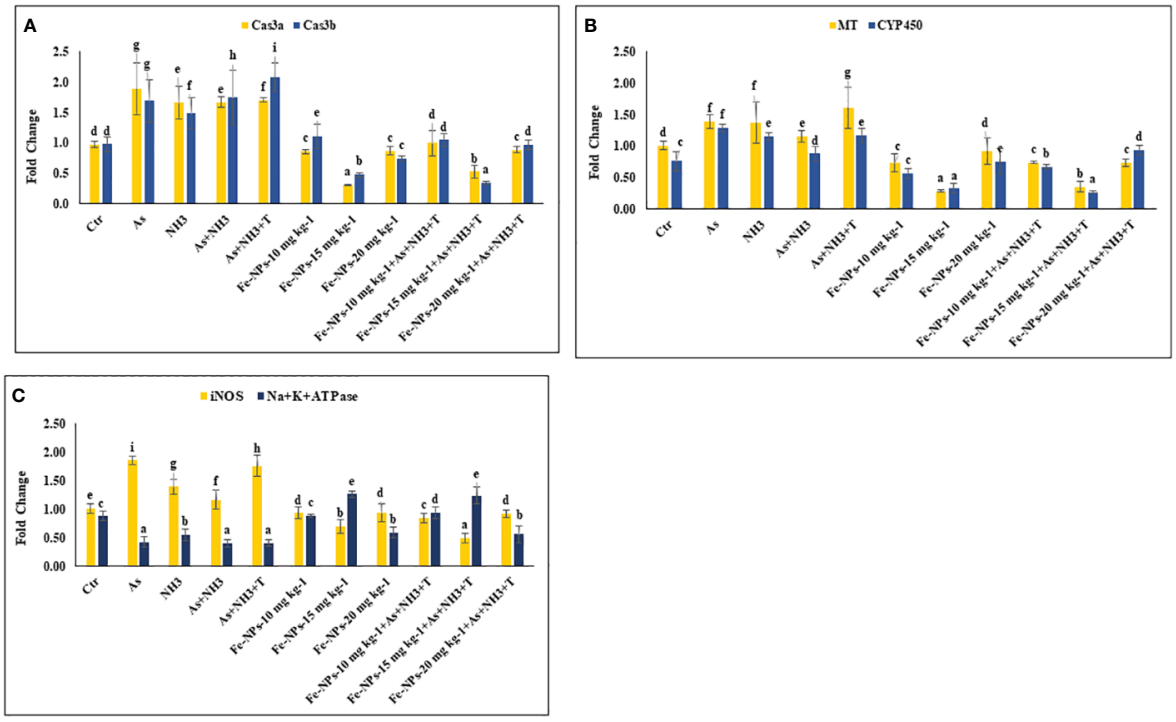

FIGURE 4
(A–C) Effect of dietary iron nanoparticles (Fe-NPs) on gene expression of Caspase 3a and 3b, metallothionine (*MT*), cytochrome P450 (*CYP 450*), inducible nitric oxide synthase (*iNOS*) and *Na+K+ATPase* against multiple stress in fish. Within endpoints and groups, bars with different superscripts differ significantly (a-g). Data expressed as Mean ± SE (n=3).

3.5 Inducible nitric oxide synthase and *Na$^+$K$^+$ATPase*

The gene expression of inducible nitric oxide synthase (*iNOS*) and *Na$^+$K$^+$ATPase* in the liver tissue of *P. hypophthalmus* reared under multiple stresses is depicted in Figure 4C. *iNOS* gene was substantially upregulated ($p = 0.0071$) by arsenic exposure, followed by As+NH_3+T, ammonia alone, and As+NH_3 exposure, compared to the control and Fe-NP-supplemented groups. Notably, the *iNOS* gene was significantly downregulated with Fe-NPs at 15 mg kg^{-1} diet, with or without stressors (As+NH_3+T), followed by Fe-NPs at 10 and 20 mg kg^{-1} diet, with or without stressors, in comparison to the control and stressor-exposed groups. Furthermore, *Na$^+$K$^+$ATPase* gene expression was noticeably ($p = 0.019$) highly upregulated with dietary Fe-NPs at 15 mg kg^{-1} diet, with or without stressors, compared to the control and other experimental groups. Conversely, *Na$^+$K$^+$ATPase* was significantly downregulated with As+NH_3+T, As+NH_3, arsenic-alone, and ammonia-alone exposures, compared to the control and Fe-NP-supplemented groups (Figure 4C).

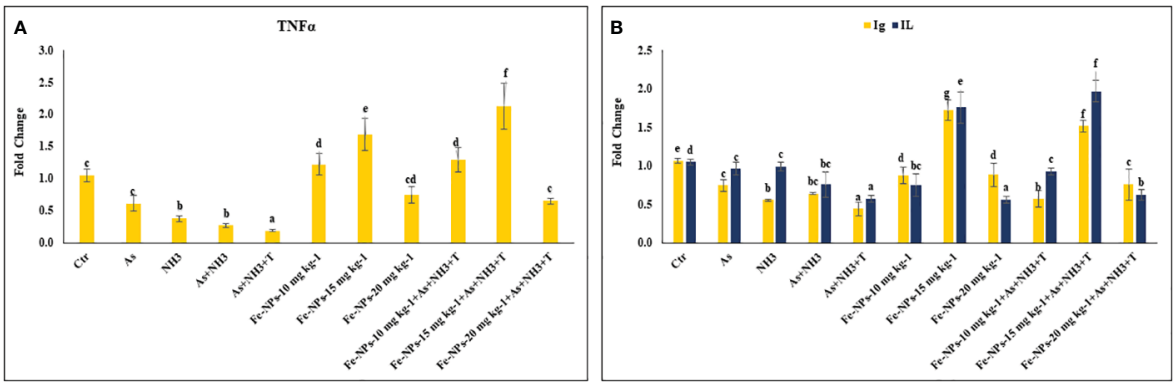

FIGURE 5
(A, B) Effect of dietary iron nanoparticles (Fe-NPs) on gene expression of tumor necrosis factor (*TNFa*), immunoglobin (*Ig*) and interleukin (*IL*) against multiple stress in fish. Within endpoints and groups, bars with different superscripts differ significantly (a-g). Data expressed as Mean ± SE (n=3).

3.6 Cytokines and immunological genes: tumor necrosis factor, interleukin, immunoglobulin, and toll-like receptor

The gene expression of tumor necrosis factor (*TNFα*), interleukin (*IL*), and immunoglobulin (*Ig*), respectively, were determined in the liver tissue of *P. hypophthalmus* subjected to multiple stressors, and the results are presented in Figures 5A, B. *TNFα* gene expression was significantly downregulated ($p = 0.0018$) by As+NH_3+T, followed by As+NH_3, NH_3, and As exposure, compared to the control and other experimental groups. Conversely, *TNFα* was noticeably upregulated by dietary Fe-NPs at 15 mg kg^{-1} diet, with or without stressors, followed by Fe-NPs at 10 and 20 mg kg^{-1} diet, compared to the control and other experimental groups (Figure 5A). Similarly, *IL* ($p = 0.01$) and *Ig* ($p = 0.016$) gene expressions were substantially downregulated by concurrent exposure to arsenic, ammonia, and high temperature, followed by As+NH_3, NH_3, and As, compared to the control and diet-supplemented groups. Conversely, both *IL* and *Ig* gene expression were significantly upregulated by dietary Fe-NPs at 15 mg kg^{-1} diet, with or without stressors, compared to the control, Fe-NP-fed groups (10 and 20 mg kg^{-1} diet), and stressor-exposed groups (Figure 5B). Furthermore, Toll-like receptor (*TLR*) gene expression was substantially upregulated by As+NH_3, followed by As+NH_3+T, NH_3, and As-alone exposure, compared to the control and other experimental groups. Moreover, Fe-NPs at 15 mg kg^{-1} diet, with or without stressors, significantly downregulated *TLR* gene expression compared to the control and stressor-exposed groups. Dietary Fe-NPs at 10 and 20 mg kg^{-1} diet supplements were less effective in mitigating multiple stressors in fish (Figure 6A).

3.7 Immunological attributes

The immunological attributes, such as nitroblue tetrazolium (NBT), blood glucose, total protein (TP), albumin (A), globulin (G), A:G ratio, and myeloperoxidase (MPO), were determined in *P. hypophthalmus* subjected to multiple stressors. The data are presented in Table 4. The NBT ($p = 0.016$), TP ($p = 0.012$), and globulin ($p = 0.0022$) levels were significantly decreased by concurrent exposure to arsenic, ammonia, and high temperature, followed by As+NH_3, NH_3, and As groups, compared to the control and Fe-NP-supplemented groups. Moreover, NBT, TP, and globulin levels were significantly elevated with dietary supplementation of Fe-NPs at 15 mg kg^{-1} diet, with or without stressors, compared to the control and other experimental groups. Furthermore, blood glucose was noticeably ($p = 0.0027$) elevated by stressors (As+NH_3+T, As+NH_3, NH_3, and As) compared to the control and dietary Fe-NP-supplemented groups. Conversely, dietary Fe-NPs at 15 mg kg^{-1} diet significantly reduced the blood glucose levels in fish under both control and stressor conditions. Moreover, the A:G ratio showed similar trends to blood glucose levels, as Fe-NP supplementation improved the A:G ratio. Additionally, concurrent exposure to arsenic, ammonia, and high temperature significantly lowered the MPO levels, followed by NH_3-alone and As-alone exposures. Interestingly, dietary Fe-NPs at 15 mg kg^{-1} diet noticeably enhanced ($p = 0.0013$) the MPO levels. The other supplemented groups of Fe-NPs at 10 and 20 mg kg^{-1} diet showed similar MPO levels to the control.

3.8 Gene related to anti-oxidative status

The gene expression of *GPx*, *SOD*, and *CAT* in the liver tissue of *P. hypophthalmus* subjected to multiple stressors is documented in Figures 6A, B. Exposure to As+NH_3+T, NH_3, As+NH_3, and As significantly upregulated the gene expression of GPx ($p = 0.011$), SOD ($p = 0.002$), and CAT ($p = 0.001$) compared to the control and other experimental groups. Interestingly, dietary Fe-NPs at 15 mg kg^{-1} diet were effective in downregulating the gene expression of *GPx*, *SOD*, and *CAT* compared to the control and other experimental groups. The dietary supplementation of Fe-NPs at 10 and 20 mg kg^{-1} diet showed similar gene expression levels of *GPx*, *SOD*, and *CAT* as the control group.

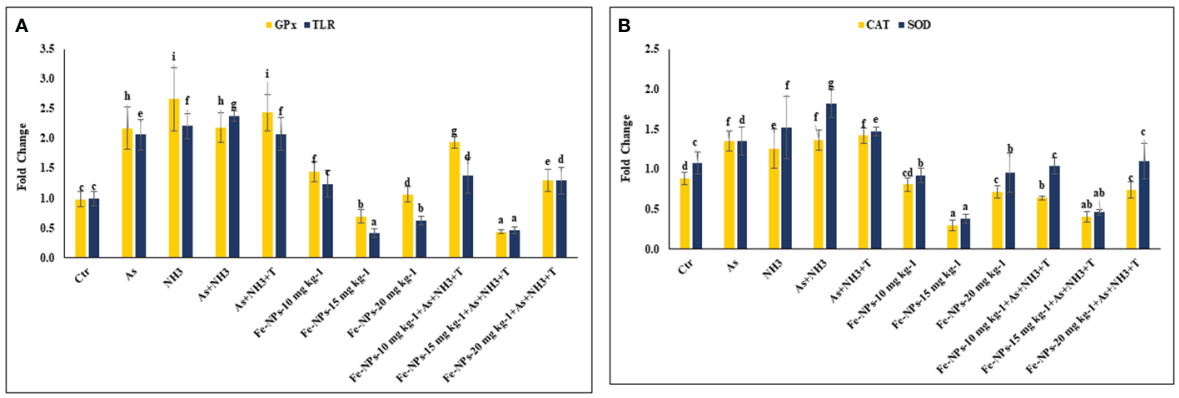

FIGURE 6
(A, B) Effect of dietary iron nanoparticles (Fe-NPs) on gene expression of *GPx*, toll like receptor (*TLR*), catalase (*CAT*) and superoxide dismutase (*SOD*) against multiple stress in fish. Within endpoints and groups, bars with different superscripts differ significantly (a-g). Data expressed as Mean ± SE (n=3).

10.3389/fimmu.2024.1410150

TABLE 4 Effect of dietary iron nanoparticles (Fe-NPs) on NBT, BG, total protein, albumin, globulin, A:G ratio, and MPO against multiple stress in fish.

Exposure/diets (mg kg^{-1})	NBT	BG	Total protein	Albumin	Globulin	A:G ratio	MPO
Ctr/Ctr	0.57 ± 0.03^{d}	100.86 ± 3.20^{c}	1.05 ± 0.07^{d}	0.22 ± 0.01	0.83 ± 0.07^{c}	0.27 ± 0.02^{c}	0.38 ± 0.02^{c}
As/Ctr	0.46 ± 0.01^{c}	121.30 ± 3.11^{d}	0.52 ± 0.03^{c}	0.17 ± 0.02	0.36 ± 0.02^{bc}	0.48 ± 0.11^{d}	0.24 ± 0.01^{b}
NH_3/Ctr	0.37 ± 0.02^{b}	127.19 ± 0.30^{e}	0.38 ± 0.01^{b}	0.13 ± 0.01	0.25 ± 0.01^{b}	0.52 ± 0.07^{d}	0.26 ± 0.02^{b}
As+NH_3/Ctr	0.32 ± 0.01^{b}	132.35 ± 2.26^{f}	0.25 ± 0.01^{a}	0.12 ± 0.01	0.13 ± 0.02^{a}	1.02 ± 0.30^{e}	0.19 ± 0.01^{a}
As+T+NH_3/Ctr	0.21 ± 0.01^{a}	148.61 ± 2.32^{g}	0.24 ± 0.02^{a}	0.13 ± 0.03	0.11 ± 0.01^{a}	1.28 ± 0.17^{f}	0.17 ± 0.01^{a}
Fe-NPs-10	0.57 ± 0.03^{d}	95.32 ± 2.71^{b}	1.09 ± 0.02^{d}	0.09 ± 0.02	1.00 ± 0.12^{d}	0.09 ± 0.01^{a}	0.35 ± 0.02^{c}
Fe-NPs-15	0.74 ± 0.05^{e}	79.83 ± 1.65^{a}	1.47 ± 0.11^{e}	0.15 ± 0.01	1.31 ± 0.02^{e}	0.12 ± 0.01^{ab}	0.47 ± 0.03^{d}
Fe-NPs-20	0.56 ± 0.02^{d}	103.30 ± 0.58^{cd}	1.00 ± 0.04^{d}	0.12 ± 0.01	0.89 ± 0.03^{c}	0.13 ± 0.01^{ab}	0.38 ± 0.02^{c}
As+T+NH_3/Fe-NPs-10	0.56 ± 0.01^{d}	105.05 ± 0.74^{d}	0.44 ± 0.03^{bc}	0.11 ± 0.01	0.33 ± 0.02^{bc}	0.33 ± 0.07^{c}	0.32 ± 0.02^{c}
As+T+NH_3/Fe-NPs-15	0.74 ± 0.02^{e}	79.45 ± 0.65^{a}	1.83 ± 0.17^{f}	0.19 ± 0.05	1.64 ± 0.06^{f}	0.12 ± 0.03^{ab}	0.46 ± 0.03^{d}
As+T+NH_3/Fe-NPs-20	0.53 ± 0.04^{d}	104.23 ± 1.30^{cd}	0.98 ± 0.02^{d}	0.15 ± 0.02	0.83 ± 0.03^{c}	0.18 ± 0.02^{b}	0.38 ± 0.02^{c}
P-value	0.016	0.0027	0.012	0.18	0.0022	0.0019	0.0013

Values in the same row with different superscript letters (a, b, c, d, e) differ significantly. Total protein, albumin, globulin: g dL^{-1} blood glucose: mg dL^{-1}. Data expressed as mean ± SE (n = 3).

3.9 Growth-related gene expression

Figures 7A, B display the results of *MYST* and *SMT* gene regulation in the muscle tissue of *P. hypophthalmus* subjected to multiple stresses. *MYST* (p = 0.0065) and *SMT* (p = 0.0037) were substantially upregulated by concurrent exposure to As+NH_3+T, followed by arsenic alone, As+NH_3, and NH_3 exposure, compared to the control and Fe-NP-supplemented groups. Moreover, *MYST* gene regulation was significantly downregulated by dietary Fe-NP at 15 mg kg^{-1} diet, with or without stressors, followed by Fe-NPs at 20 mg kg^{-1} diet, with or without stressors, and Fe-NPs at 10 mg kg^{-1} diet, compared to the control and other experimental groups. Similarly, *SMT* gene expression was significantly downregulated with Fe-NPs at 15 mg kg^{-1} diet, with or without stressors, followed by Fe-NPs at 10 mg kg^{-1} diet, with or without stressors, and Fe-NPs at 20 mg kg^{-1} diet without stressors, compared to the control and other experimental groups.

3.10 Growth hormone regulator 1 and growth hormone regulator β

GHR1 (p = 0.0017) and *GHR β* (p = 0.0042) gene regulations were significantly downregulated in response to stressors (As+NH_3+T, As+NH_3, NH_3, and As) compared to the control and other experimental groups. The *GHR1* gene expression was significantly

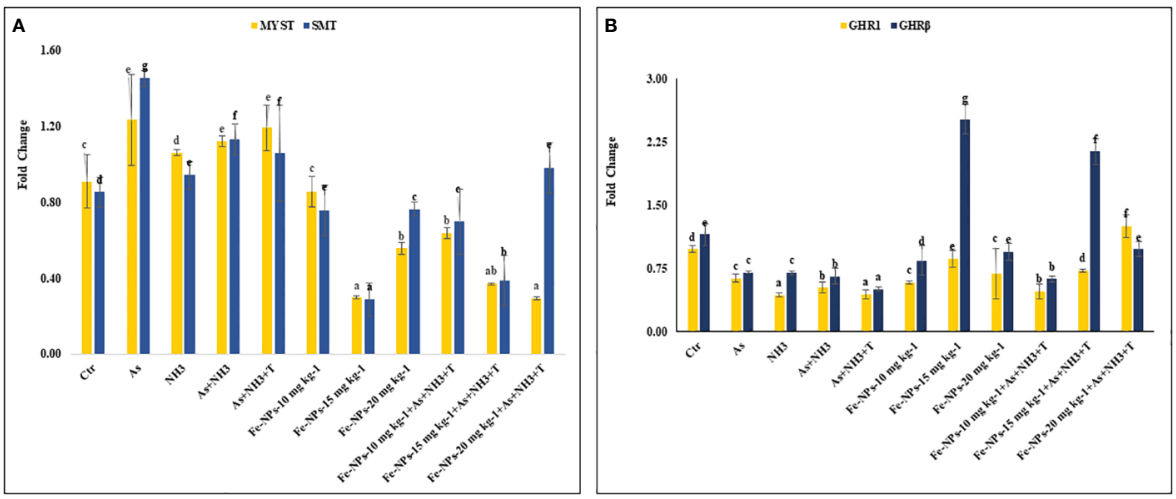

FIGURE 7
(A, B) Effect of dietary iron nanoparticles (Fe-NPs) on gene expression of myostatin (*MYST*), somatostatin (*SMT*), and growth hormone regulator (*GHR1* and *GHRβ*) against multiple stress in fish. Within endpoints and groups, bars with different superscripts differ significantly (a-g). Data expressed as Mean ± SE (n=3).

upregulated by Fe-NPs at 20 mg kg^{-1} diet with stressors, followed by Fe-NPs at 15 mg kg^{-1} diet without stressors, compared to the control and other experimental groups. Similarly, *GHR β* was significantly upregulated by Fe-NPs at 15 mg kg^{-1} diet, with or without stressors, compared to the control and other experimental groups (Figure 7B).

3.11 Growth hormone and insulin-like growth factors (*IGF1X* and *IGF2X*)

The gene regulations of *GH*, *IGF1X*, and *IGF2X* in the liver tissue of *P. hypophthalmus* subjected to stressors are presented in Figures 8A, B. GH was substantially upregulated (p = 0.018) by dietary Fe-NPs at 15 mg kg^{-1} diet, with or without stressors, compared to the control and stressor-exposed groups. Conversely, *GH* gene expression was significantly downregulated by As+NH_3+T, followed by As+NH_3, NH_3, and As exposures, compared to the control and supplemented-diet groups. Furthermore, *IGF1X* and *IGF2X* gene regulations were noticeably downregulated by concurrent exposure to As+NH_3+T, followed by As+NH_3, NH_3, and As-alone groups, compared to the control and Fe-NP-supplemented groups. Dietary Fe-NPs at 15 mg kg^{-1} diet, with or without stressors, substantially upregulated the *IGF1X* and *IGF2X* genes compared to the control and stressor-exposed groups. Additionally, other dietary groups, such as Fe-NPs at 10 and 20 mg kg^{-1} diet, were also efficient in upregulating *IGF1X* and *IGF2X* gene regulation against arsenic, ammonia, and high temperature stress (Figure 8B).

3.12 Growth performance

Table 5 summarizes the results of growth performance indicators such as final weight gain %, food conversion ratio (FCR), specific growth rate (SGR), protein efficiency ratio (PER), daily growth index (DGI), and relative feed intake (RFI) of *P. hypophthalmus* reared under different stress conditions. The final weight gain % was noticeably enhanced by dietary Fe-NPs at 15 mg kg^{-1} diet, with (160%) or without stressors (162%), followed by Fe-NPs with (137%) or without stressors (147%), compared to the control and stressor-exposed groups. Conversely, the final weight gain % was significantly reduced by concurrent exposure to As +NH_3+T (60%), As+NH_3 (68%), NH_3 (68%), and As (72%), compared to the control and Fe-NP-supplemented groups. Similarly, SGR, PER, DGI, and RFI followed the same pattern and were enhanced with dietary Fe-NPs at 15 mg kg^{-1} diet.

3.13 Detoxification of arsenic by Fe-NPs diet

The arsenic concentration in the experimental water varied as follows: control (0.02 mg kg^{-1} diet), As group (1931 μg L^{-1}), NH_3 group (0.01 μg L^{-1}), As+NH_3 (2160 μg L^{-1}), As+NH_3+T (2324 μg L^{-1}), Fe-NPs at 10, 15, and 20 mg kg^{-1} diet (below detection limit), and Fe-NPs with As+NH_3+T at 10 mg kg^{-1} diet (1730 μg L^{-1}), 15 mg kg^{-1} diet (507 μg L^{-1}), and 20 mg kg^{-1} diet (1925 μg L^{-1}). However, the results showed that dietary Fe-NPs at 15 mg kg^{-1} diet with stressors (As+NH_3+T) exhibited the lowest arsenic concentration. Moreover, the highest bioaccumulation was observed in the kidney, followed by the liver, gill, muscle, and brain in the group exposed to As+NH_3+T. Dietary Fe-NPs at 15 mg kg^{-1} diet showed the highest detoxification of arsenic in all tissues (Table 6).

3.14 Challenging test

The cumulative mortality and relative percentage survival were determined after a 90-day experimental trial. Cumulative mortality rates were observed as follows: 44%, 61%, 61%, 63.9%, 61%, 69%, 44%, 27%, 55%, 50%, and 38.9% in the control, As alone, NH_3 alone, As+NH_3, As+NH_3+T, and Fe-NPs at 10, 15, and 20 mg kg^{-1}

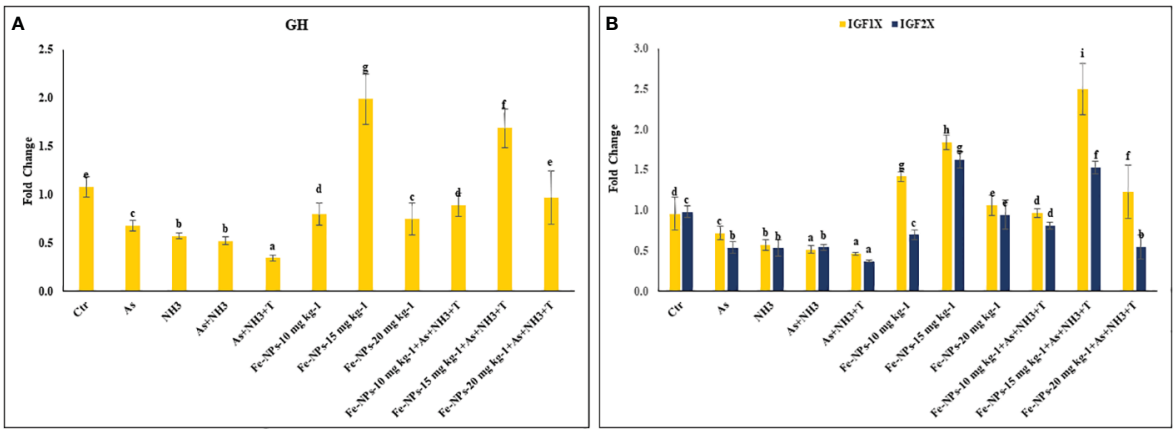

FIGURE 8
(A, B) Effect of dietary iron nanoparticles (Fe-NPs) on gene expression of growth hormone (*GH*), insulin like growth factor (*IGF IX* and *IGF 2X*) against multiple stress in fish. Within endpoints and groups, bars with different superscripts differ significantly (a-g). Data expressed as Mean ± SE (n=3).

TABLE 5 Effect of dietary iron nano-particles (Fe-NPs) on growth performance, viz., final body weight gain (%), FCR, SGR, PER, DGI (%), TGC, and RFI against multiple stress in fish.

Exposure/diets (mg kg^{-1})	Final body weight gain, %	FCR	SGR	PER	DGI (%)	RFI
Ctr/Ctr	96.15 ± 5.54^{d}	3.15 ± 0.15^{c}	0.75 ± 0.03^{c}	0.91 ± 0.03^{b}	1.08 ± 0.04^{c}	300.92 ± 2.84^{d}
As/Ctr	72.78 ± 4.70^{c}	3.80 ± 0.18^{d}	0.61 ± 0.02^{b}	0.76 ± 0.06^{a}	0.84 ± 0.02^{b}	274.85 ± 4.10^{c}
NH_3/Ctr	68.02 ± 5.83^{b}	3.99 ± 0.27^{de}	0.58 ± 0.04^{ab}	0.72 ± 0.04^{a}	0.80 ± 003^{b}	268.40 ± 3.52^{bc}
As+NH_3/Ctr	68.81 ± 4.33^{b}	3.87 ± 0.22^{de}	0.58 ± 0.03^{ab}	0.76 ± 0.02^{a}	0.83 ± 0.05^{b}	264.32 ± 2.15^{b}
As+T+NH_3/Ctr	60.03 ± 0.97^{a}	4.27 ± 0.05^{e}	0.52 ± 0.01^{a}	0.73 ± 0.04^{a}	0.76 ± 0.04^{a}	256.26 ± 1.59^{a}
Fe-NPs-10	102.24 ± 2.93^{e}	3.07 ± 0.07^{c}	0.78 ± 0.02^{c}	1.01 ± 0.01^{b}	1.17 ± 0.02^{d}	313.34 ± 2.55^{f}
Fe-NPs-15	162.10 ± 1.88^{h}	2.23 ± 0.03^{b}	1.07 ± 0.01^{d}	1.52 ± 0.10^{e}	1.59 ± 0.02^{e}	361.70 ± 1.46^{i}
Fe-NPs-20	147.68 ± 9.01^{g}	2.15 ± 0.15^{a}	1.01 ± 0.04^{d}	1.39 ± 0.04^{d}	1.57 ± 0.09^{e}	315.28 ± 2.77^{f}
As+T+NH_3/Fe-NPs-10	101.55 ± 7.34^{e}	3.04 ± 0.18^{c}	0.78 ± 0.04^{c}	0.95 ± 0.08^{b}	1.12 ± 0.06^{d}	305.75 ± 4.21^{e}
As+T+NH_3/Fe-NPs-15	160.06 ± 0.31^{h}	2.18 ± 0.01^{a}	1.06 ± 0.03^{d}	1.35 ± 0.03^{d}	1.68 ± 0.11^{f}	349.30 ± 1.85^{h}
As+T+NH_3/Fe-NPs-20	137.51 ± 6.46^{f}	2.34 ± 0.09^{b}	0.96 ± 0.05^{d}	1.26 ± 0.07^{c}	1.49 ± 0.06^{e}	321.05 ± 4.32^{g}
P-value	0.0028	0.001	0.001	0.0025	0.014	0.0011

Values in the same row with different superscript letters (a, b, c, d, e) differ significantly. Data expressed as mean ± SE (n = 3).
FCR, feed conversion ratio; SGR, specific growth rate; PER, protein efficiency ratio; DGI, daily growth index; TGC, thermal growth coefficient; RFI, relative feed intake.

diet without stressors and with stressors, respectively. Similarly, the relative percentage survival varied as (–) 17% (–), 17% (–), 35% (–), 41%, 11%, 41%, 17%, 0%, 35%, and (–) 5.9% in the corresponding groups: control, As alone, NH_3 alone, As+NH_3, As+NH_3+T, and Fe-NPs at 10, 15, and 20 mg kg^{-1} diet without stressors and with stressors, respectively (Figure 9).

4 Discussion

The present investigation highlights the critical role of dietary Fe-NPs in mitigating various stressors such as arsenic, ammonia, and high temperature (34°C) in *P. hypophthalmus*. The study primarily elucidates the mechanistic role of different gene regulations involved

TABLE 6 Effect of dietary iron nanoparticles (Fe-NPs) on detoxification of arsenic in different fish tissues reared under control and multiple stress conditions.

Exposure/diets (mg kg^{-1})	Water (μg L^{-1})	Liver (mg kg^{-1})	Kidney (mg kg^{-1})	Gill (mg kg^{-1})	Muscle (mg kg^{-1})	Brain (mg kg^{-1})	Fe-muscle (mg kg^{-1})
Ctr/Ctr	0.02 ± 0.00	BDL	0.03 ± 0.0	BDL	BDL	BDL	1.27 ± 0.03
As/Ctr	1,931.02 ± 32.88	6.65 ± 0.16	7.91 ± 0.16	3.26 ± 0.09	3.85 ± 0.23	0.52 ± 0.02	1.84 ± 0.09
NH_3/Ctr	0.01 ± 0.0	BDL	0.14 ± 0.01	BDL	BDL	BDL	1.03 ± 0.02
As+NH_3/Ctr	2,160.14 ± 16.22	6.84 ± 0.09	7.31 ± 0.11	2.23 ± 0.05	1.00 ± 0.02	0.83 ± 0.03	0.92 ± 0.06
As+T+NH_3/Ctr	2,324.64 ± 25.92	8.39 ± 0.61	9.32 ± 0.02	3.49 ± 0.24	3.47 ± 0.58	0.94 ± 0.02	1.00 ± 0.16
Fe-NPs-10	BDL	BDL	BDL	BDL	BDL	BDL	4.73 ± 0.42
Fe-NPs-15	BDL	BDL	BDL	BDL	BDL	BDL	6.49 ± 0.56
Fe-NPs-20	BDL	BDL	BDL	BDL	BDL	BDL	8.95 ± 0.30
As+T+NH_3/Fe-NPs-10	1,730.81 ± 36.43	2.96 ± 0.42	3.58 ± 0.35	2.39 ± 0.24	1.47 ± 0.16	0.86 ± 0.06	7.13 ± 0.29
As+T+NH_3/Fe-NPs-15	507.72 ± 44.88	0.38 ± 0.08	0.47 ± 0.02	0.15 ± 0.02	0.01 ± 0.0	0.10 ± 0.01	7.32 ± 0.38
As+T+NH_3/Fe-NPs-20	1,925.31 ± 25.91	3.99 ± 0.18	2.23 ± 0.38	1.17 ± 0.08	0.66 ± 0.06	0.80 ± 0.09	9.46 ± 0.15

Data expressed as mean ± SE (n = 3).

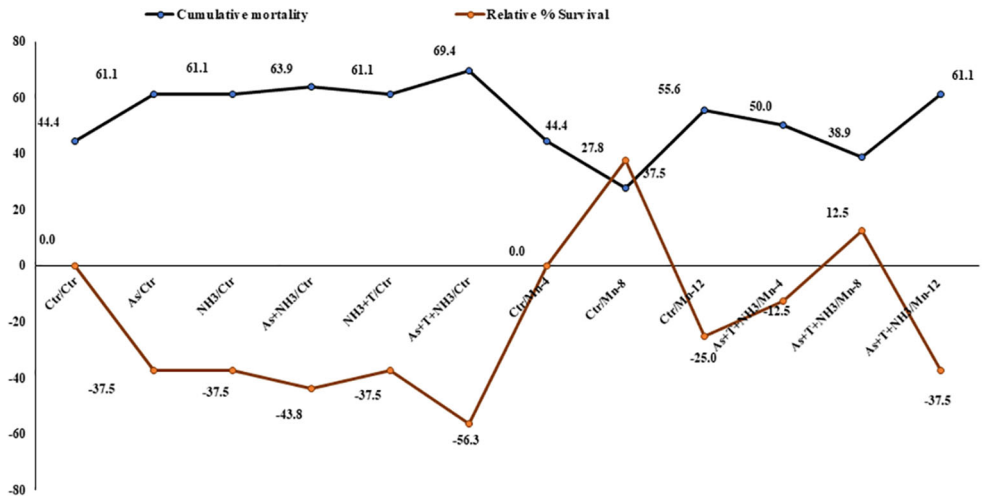

FIGURE 9
Effect of dietary iron nanoparticles (Fe-NPs) on cumulative mortality and relative percentage survival of fish reared under multiple stress after infected with pathogenic bacteria. Within endpoints and groups, bars with different superscripts differ significantly (a-g). Data expressed as Mean ± SE (n = 3).

in immunity, antioxidative status, apoptosis, genotoxicity, growth performance, and more. It demonstrates that dietary Fe-NPs strengthen fish immunity through various gene regulations. In this study, Fe-NPs at 15 mg kg^{-1} diet substantially decreased the cortisol levels in fish reared under both control and stressor conditions. This reduction could be attributed to Fe-NPs' activation of the hypothalamus–pituitary–interrenal (HPI) axis to control the stimulating cortisol synthesis in interrenal kidney tissue (36, 37).

Interestingly, dietary Fe-NPs reduced the cortisol levels possibly by suppressing the gene expression of *CYP 450* in fish exposed to arsenic, ammonia toxicity, and high temperature stress (38). It is also plausible that non-heme proteins containing iron, present in the adrenal cortex and involved in cortisol synthesis, play a role (39). It was also found that deficiency and overdose of iron supplementation can lead to CYP impairment. Such report has been reflected in our study (40).

The expression of the *HSP 70* gene significantly increased under stressors (As, NH_3, As+NH_3, and As+NH_3+T), leading to diminished protein protection from oxidative damage, enhanced ROS production, protein misfolding, and exacerbated oxidative stress (23). Conversely, dietary Fe-NPs at 15 mg kg^{-1} diet downregulated HSP 70 gene expression, protecting against proteasomal degradation (41), promoting proper protein folding, preventing protein aggregation, degrading denatured proteins, and folding misfolded proteins (42). Surprisingly, dietary Fe-NPs downregulated the *HSP 70* gene expression, and this could be due to activation of the HSP transcription factor, which reduces the binding activity of heat shock elements (35, 43).

Furthermore, dietary Fe-NPs at 15 mg kg^{-1} diet protected against DNA damage and downregulated DDIP gene expression. Even slight changes in the dose of dietary Fe-NPs induced genotoxicity, as demonstrated in the present study, although stressors (As, NH_3, As +NH_3, and As+NH_3+T) induced a higher generation of reactive oxygen species, dysregulation of cell proliferation, apoptosis, diminished DNA repair, and aberrations in histone post-translational modification and DNA methylation (44).

The gene expression of *Cas 3a* and *3b* was regulated by dietary Fe-NPs at 15 mg kg^{-1} diet, whereas stressors (As, NH_3, As+NH_3, and As +NH_3+T) upregulated *Cas 3a* and *3b* (45). Iron nanoparticles (Fe-NPs) possess the protein disulfide isomerase (PDI) multifunctional enzyme systems, which control apoptosis via *Cas 3a* and *3b* (46, 47). The isomerization and rearrangement of disulfide bonds are the major functions of PDI, which has two active sites of thiol groups. It also has the capacity to bind zinc and copper at active thiol sites (48, 49).

The toxicity induced by arsenic, ammonia, and high temperature stress significantly upregulated *MT* gene expression. *MT* gene expression is commonly induced by metal toxicity and various environmental stressors in fish (50, 51). This upregulation might be mediated by the metal-responsive transcription factor 1 (MTF-1), a major activator of *MT* gene expression (52) primarily regulated by phosphorylation (53). It was reported that protein kinases such as c-Jun N-terminal kinase (JNK), phosphoinositide 3-kinase (PI3K), and protein kinase C (PKC) play roles in modifying the MTF-1 signaling pathway (53). Interestingly, dietary Fe-NPs at 15 mg kg^{-1} diet noticeably controlled and downregulated *MT* gene expression, potentially due to the essential role of iron in the erythropoietic system and the production of reticulocytes or other young cells with a basal level of MT-I much higher than that in mature erythrocytes (54).

Cytochrome P450 (*CYP 450*) is an important heme-thiolate protein involved in detoxifying xenobiotics, drugs, carcinogens, and other toxic substances (55). In this investigation, arsenic, ammonia, and high temperature stress upregulated *CYP 450* gene expression in the liver tissue of *P. hypophthalmus*. This upregulation might be attributed to reactive oxygen species generated by stressors, leading to lipid peroxidation, cellular toxicity, and, ultimately, cell death. Additionally, it is involved in apoptosis and upregulation of the transcription of bcl2-associated X (Bax) (56), an important cell death-promoting gene in fish that induces the release of cytochrome

c, leading to caspase activation (57). Interestingly, dietary Fe-NPs at 15 mg kg^{-1} diet controlled the gene expression of *CYP 450* in the liver tissue of *P. hypophthalmus*.

The iNOS gene expression was significantly upregulated by stressors (As+NH_3+T, As+NH_3, NH_3, and As). *iNOS* gene expression mainly depends on ammonia toxicity as it accumulates in tissues. Ammonia is converted into urea via the ornithine–urea cycle (OUC) and then into glutamine via glutamine synthetase, including non-essential amino acids (58). Similarly, blood carrying high ammonia concentrations affects the liver tissue (59). Moreover, nitric oxide provides protection to the cellular system against oxidative stress (59). Interestingly, dietary Fe-NPs at 15 mg kg^{-1} diet substantially downregulated iNOS gene expression. The interrelationship between iron and iNOS gene expression is profound, as iron nanoparticles prevent the accumulation of higher oxygen radicals through a NOS-dependent mechanism (60). Iron also triggers hypertrophy, inducing the expression of antiapoptotic proteins such as Bcl-2 and survivin and hypertrophic agents endothelin (ET-1) and leukemia inhibitory factor (LIF), thus decreasing H_2O_2-induced necrosis (61, 62). Furthermore, during stress conditions, the organism requires more energy in the form of ATPase; therefore, the gene expression of *Na^+K^+ATPase* was highly upregulated. Notably, Fe-NPs at 15 mg kg^{-1} diet aid in the formation of more ATPase and supply it to the fish reared under multiple stress conditions.

Furthermore, dietary Fe-NPs regulate the expression of cytokine genes such as *TNFα*. This regulation could be attributed to the role of iron in the regulation of ferritin levels in macrophages, enhancing the gene regulation of *TNFα* (63). In the present study, *TNFα* was substantially downregulated by stressors (As+NH_3+T, As+NH_3, NH_3, and As). *TNFα* is also associated with the activation of B-cell-activating factor (BAFF), which aids in NFkB regulation (64). *TNFα* and *IL* are inflammation-related cytokines upregulated after exposure to ammonia, arsenic, and high temperature stress (65). *IL* promotes T-cell-induced inflammatory responses and releases pro-inflammatory cytokines for amplification. It binds to receptors and plays an important biological role using the nuclear factor kappa-B (NF-κB) and MAP kinase pathway (66). Additionally, TNFα is involved in apoptosis, inflammation, and cell proliferation, stimulating the immune system and activating the NF-κB pathway (67). Hence, exposure to ammonia, arsenic, and high temperature stress increases these gene regulations in fish. Moreover, dietary Fe-NPs at 15 mg kg^{-1} diet improve *IL* gene expression and upregulate its expression. This could be due to the potential of Fe-NPs to stimulate the production of hepcidin (68). The iron storage protein ferritin has two units, H-subunits (H-mRNA) and light subunits (L-mRNA), which remain unchanged, indicating that *IL* is regulated by translational mechanisms during infection and stress (69).

Furthermore, the expression of *TLR* genes was upregulated by arsenic, ammonia, and high temperature stress, whereas dietary Fe-NPs at 15 mg kg^{-1} diet downregulated *TLR* gene expression. These results could be due to heme and iron sequestration in response to inflammatory/infectious stimuli during stress (70). *TLR* also plays an important role in activating signaling pathways that enhance fish immunity and reduce stress using the NF-κB pathway. Interestingly, dietary Fe-NPs upregulated *Ig* gene expression in fish reared under control and stressor conditions (As, NH_3, and high temperature). This strengthening of fish immunity via the upregulation of *Ig* gene expression by Fe-NPs diet could be due to enhanced immunoglobulin and T-cell levels in fish under control and stressor conditions (71, 72).

NBT, BG, total protein, albumin, globulin, A:G ratio, and MPO are also important immunological attributes whose levels indicate fish immunity. These immunological attributes were noticeably affected by exposure to arsenic, ammonia, and high temperature, leading to reduced immunity (23). This reduction could be attributed to the higher energy requirements of fish during stress conditions, resulting in significant decreases in these parameters (73). Albumin, crucial for transporting biomolecules such as drugs, hormones, vitamins, and bilirubin, also supports the regulation of hormones and fat metabolism (74). MPO produces hypochlorous acid through respiratory burst via hydrogen peroxide, exhibiting cytotoxic effects on mammals and bacteria (75). Despite higher NBT levels typically indicating better immunity, the present study observed a noticeable reduction in NBT levels under stressors (As, NH_3, and T), reflecting compromised immunity in the fish. Surprisingly, dietary Fe-NPs at 15 mg kg^{-1} diet enhance fish immunity using these immunological attributes (71, 72). Dietary Fe-NPs help activate dendritic cells and enhance interleukin and cytokine production, accelerating the enhancement of fish immunity (76, 77).

Fe-NPs are essential nutrients for antioxidant enzymatic systems as they strengthen antioxidant gene regulation and enzymatic systems such as CAT, SOD, and GPx. In the present investigation, arsenic, ammonia, and high temperature stress substantially upregulated the gene regulation of SOD, CAT, and GPx in fish liver tissue (23). However, dietary Fe-NPs at 15 mg kg^{-1} noticeably downregulated the gene expression of SOD, CAT, and GPx, reducing reactive oxygen species (78, 79). This could be attributed to the role of Fe-NPs in maintaining oxidative stress by reducing reactive oxygen species (ROS) and acting as oxygen carrier proteins that regulate the antioxidant status of the fish (80). It is important to note that the antioxidant defense system is crucial to maintain overall health by safeguarding cells and tissues from oxidative stress damage caused by excessive hydroxyl radicals and reactive oxygen species (ROS) through scavenging them (81, 82). Moreover, Fe-NPs have many biological functions, including serving as an antioxidant defense system in fish by utilizing superoxide dismutase and glutathione peroxidase to prevent free radical production and lipid peroxidation (83). Interestingly, CAT, known as a heme-containing enzyme, acts together with SOD to counterbalance cellular ROS and improve the antioxidative status (83).

Growth performance indicators such as weight gain %, specific growth rate (SGR), protein efficiency ratio (PER), daily growth index (DGI), and relative feed intake (RFI) were noticeably reduced, and the feed conversion ratio (FCR) was enhanced with stressors (As, NH_3, and high temperature). Conversely, dietary Fe-NPs improved the growth performance of the fish. Iron plays an important role in maintaining organismal iron homeostasis and enhances growth performance. Supplementation of Fe-NP diets enhances growth performance, possibly due to the nutrient ability of iron oxide nanoparticles and the enhancement of feed utilization in fish reared under control and stressor conditions (As, NH_3, As+NH_3, and As +NH_3+T) (84). Additionally, Fe-NPs have smaller sizes and are

efficiently utilized in dietary form (84). Fe-NPs diets also enhance digestive activities and increase physiological processes, which help in enhancing growth performance (85). Fe-NP diets also have higher bioavailability and better absorption, which enhances growth performance in fish reared under control and adverse conditions (86). Furthermore, genes related to growth performance such as *MYST*, *SMT*, *GHR1*, *GHRβ*, *GH*, *IGF1X*, and *IGF2X* were also altered by arsenic, ammonia, and high temperature stress. These genes were noticeably upregulated (*GHR1*, *GHRβ*, *GH*, *IGF1X*, and *IGF2X*) by dietary Fe-NPs at 15 mg kg^{-1}. Dietary Fe-NPs at 15 mg kg^{-1} diet substantially downregulated MYST and SMT, possibly due to the role of *MYST* in decreasing myoblasts, resulting in terminal differentiation and fiber enlargement (87). Moreover, gene regulation of *IGF1X1* and *IGF1X2* is important for biomolecular regulation via lipid, carbohydrate, protein, and mineral metabolism and differentiation and proliferation of cells, ultimately influencing growth (18). As GH binds to the receptor in liver cells to stimulate the release and synthesis of IGF gene expression, dietary Fe-NPs aid in this process. Fe-NPs diet is responsible for growth enhancement and biomolecular function in the cells of aquatic organisms. Interestingly, Fe has a close relationship with the secretion and regulation of *IGF*, which directly affects growth performance using the central nervous system of fish reared under control and stressor conditions (88, 89). Ghrelin is also important for stimulating growth hormone from the pituitary gland, which controls the regulation of *GH*. It also stimulates the growth hormone (*GH*) releasing hormone and somatostatin axis, resulting in increased production of *IGF-I* in the liver (90).

Furthermore, the bioaccumulation of arsenic in the liver, kidney, gill, muscle, and brain was determined. The highest bioaccumulation of arsenic was observed in the kidney and liver tissues of the group concurrently exposed to arsenic, ammonia, and high temperature stress. Interestingly, in the group fed with Fe-NPs at 15 mg kg^{-1} diet with stressors, the arsenic levels were notably reduced. Arsenic levels below the detection limit were observed in the groups fed with Fe-NPs at 10, 15, and 20 mg kg^{-1} diet without stressors. These results could be attributed to the role of Fe-NPs in enhancing the detoxification of arsenic in kidney and liver tissues through *CYP 450* gene expression, as shown in the results.

Moreover, the survival rate of the fish was higher in the groups fed with Fe-NPs at 10, 15, and 20 mg kg^{-1} diet with or without stressors after bacterial challenge. Dietary Fe-NPs possess strong antibacterial and phagocytic capacities, which enhance the immunity of the fish and reduce mortality after bacterial infection. Moreover, in the present study, the immunity-related genes have been improved by dietary Fe-NPs diet. Genes such as TNFα, TLR, Ig, and IL strongly support the immunity during stress conditions, especially during infection condition (12). Fe-NPs also enhance the fluidity of membranes of antibacterial compounds like lysozyme and reduce lipid peroxidation (91–93).

5 Conclusions

The present investigation revealed that nano-nutrients in the form of iron nanoparticles (Fe-NPs) mitigate multiple abiotic stresses such as ammonia and arsenic toxicity as well as high temperature stress in fish. Moreover, it is the first to report the mechanistic role of Fe-NPs in mitigating arsenic and ammonia toxicity as well as high temperature stress in fish. Fe-NPs regulate genes involved in growth performance, immunity, antioxidative capacity, genotoxicity, and stress responses in *P. hypophthalmus*. Additionally, Fe-NPs lead to the positive modulation of gene expression related to cortisol regulation, *HSP 70* production, apoptosis inhibition, and genotoxicity prevention. Interestingly, Fe-NPs at 15 mg kg^{-1} diet enhance the detoxification of arsenic in fish tissues. Fe-NPs have also improved immunity against pathogenic bacteria and enhanced fish survival under multiple stresses. Importantly, these findings highlight the potential of Fe-NPs at 15 mg kg^{-1} in enhancing the wellbeing of fish species in the face of contemporary challenges posed by climate change and pollution.

Data availability statement

The datasets for this article are not publicly available due to concerns regarding participant/patient anonymity. Requests to access the datasets should be directed to the corresponding author.

Ethics statement

The animal study was approved by Prioritization, Monitoring and Evaluation (PME). The study was conducted in accordance with the local legislation and institutional requirements.

Author contributions

NK: Writing – review & editing, Writing – original draft, Visualization, Validation, Supervision, Software, Resources, Project administration, Methodology, Investigation, Funding acquisition, Formal analysis, Data curation, Conceptualization. ST: Writing – review & editing, Methodology, Formal analysis. MG: Writing – review & editing, Methodology. PK: Writing – review & editing, Validation, Methodology, Data curation. KR: Writing – review & editing, Supervision.

Funding

The author(s) declare financial support was received for the research, authorship, and/or publication of this article. The present work was supported by the Indian Council of Agricultural Research (ICAR), New Delhi, India, under institute project #IXX15014.

Acknowledgments

The authors sincerely acknowledge the director of ICAR-NIASM for providing the research facilities for this work.

Conflict of interest

The authors declare that the research was conducted in the absence of any commercial or financial relationships that could be construed as a potential conflict of interest.

Publisher's note

References

1. Kumar N, Chandan NK, Bhushan S, Singh DK, Kumar S. Health risk assessment and metal contamination in fish, water and soil sediments in the East Kolkata Wetlands, India, Ramsar site. *Sci Rep*. (2023) 13:1546. doi: 10.1038/s41598-023-28801-y

2. Kumar N, Krishnani KK, Singh NP. Oxidative and cellular stress as bioindicators for metals contamination in freshwater mollusk *Lamellidens marginalis*. *Environ Sci pollut Res*. (2017) 24:16137–47. doi: 10.1007/s11356-017-9266-0

3. Ye Y, Gaugler B, Mohty M, Malard F. Old dog, new trick: trivalent arsenic as an immunomodulatory drug. *Br J Pharmacol*. (2020) 177:2199–214. doi: 10.1111/bph.15011

4. Shaji E, Santosh M, Sarath KV, Prakash P, Deepchand V, Divya BV. Arsenic contamination of groundwater: a global synopsis with focus on the Indian Peninsula. *Geosci Front*. (2021) 12:101079. doi: 10.1016/j.gsf.2020.08.015

5. IARC International Agency for Research on Cancer. *IARC monographs on the evaluation of carcinogenic risks to humans: a review of human carcinogens: arsenic, metals, fibres, and dusts* Vol. 100C. . Lyon, France: World Health Organization (2012).

6. Mohanty B.P. T, Ganguly S, Sarkar SD, Mahanty A. Curcumin has protective effect on the eye lens against arsenic toxicity, Biol. *Trace Elem Res*. (2020) 199(9):3354–59. doi: 10.1007/s12011–020-02448–6

7. Okoye E.A. B, Ruggieri F, Ezejiofor AN, Nwaogazie IL, Frazzoli C, Orish E, et al. Arsenic and toxic metals in meat and fish consumed in Niger delta, Nigeria: Employing the margin of exposure approach in human health risk assessment, Food and Chem. *Toxicol*. (2022) 159:112767. doi: 10.1016/j.fct.2021.112767

8. Ip YK, Ammonia production SF. excretion, toxicity, and defence in fish: a review. *Front Physiol*. (2010) 1:134. doi: 10.3389/fphys.2010.00134

9. YSI. *Understanding ammonia in aquaculture ponds* (2010). Available online at: http://www.ysi.com/media/pdfs/A585-Understanding-Ammonia-in-Aquaculture-Ponds.pdf.

10. Ruyet PLJ, Chartois H, Quemener L. Comparative acute ammonia toxicity in marine fish and plasma ammonia response. *Aquaculture*. (1995) 136:181–94. doi: 10.1016/0044-8486(95)01026-2

11. Randall DJ, Tsui TKN. Ammonia toxicity in fish. *Mar pollut Bull*. (2002) 45:17–23. doi: 10.1016/S0025-326X(02)00227-8

12. Kumar N, Kumar S, Singh AK, Gite A, Patole PB, Thorat ST. Exploring mitigating role of zinc nanoparticles on arsenic, ammonia and temperature stress using molecular signature in fish. *J Trace Elements Med Biol*. (2022) 74:127076. doi: 10.1016/j.jtemb.2022.127076

13. Li M, Yu N, Qin JG, Li E, Du Z, Chen L. Effects of ammonia stress, dietary linseed oil and *Edwardsiella ictaluri* challenge on juvenile darkbarbel catfish Pelteobagrus vachelli. *Fish Shellfish Immunol*. (2014) 38:158–65. doi: 10.1016/j.fsi.2014.03.015

14. National Research Council (NRC). *Nutrient requirements of fish and shrimp*. Washington, DC: National Academy Press (2011).

15. Guo Y.-L, Wu P, Jiang W-D, Liu Y, Kuang S-Y, Jiang J, et al. The impaired immune function and structural integrity by dietary iron deficiency or excess in gill of fish after infection with Flavobacterium columnare: regulation of NF-κB, TOR, JNK, p38MAPK, Nrf2 and MLCK signalling. *Fish Shellfish Immunol*. (2018) 74:593–608. doi: 10.1016/j.fsi.2018.01.027

16. Guo Y-L, Jiang W-D, Wu P, Liu Y, Zhou X-Q, Kuang S-Y, et al. The decreased growth performance and impaired immune function and structural integrity by dietary iron deficiency or excess are associated with TOR, NF-κB, p38MAPK, Nrf2 and MLCK signaling in head kidney, spleen and skin of grass carp (Ctenopharyngodon idella). *Fish Shellfish Immunol*. (2017) 65:145–68. doi: 10.1016/j.fsi.2017.04.009

17. Behera T, Swain P, Rangacharulu PV, Samanta M. Nano-Fe as feed additive improves the hematological and immunological parameters of fish, Labeo rohita H. *Appl Nanosci*. (2014) 4:687–94. doi: 10.1007/s13204-013-0251-8

18. Afshari A, Sourinejad I, Gharaei A, Johari SA, Ghasemi Z. The effects of diet supplementation with inorganic and nanoparticulate iron and copper on growth performance, blood biochemical parameters, antioxidant response and immune function of snow trout Schizothorax zarudnyi (Nikolskii, 1897). *Aquaculture*. (2021) 539:736638. doi: 10.1016/j.aquaculture.2021.736638

19. Zhang T, Ma C, Zhang Z, Zhang H, Hu H. NF-κB signaling in inflammation and cancer. *Med Commun*. (2020) 2:618–53. doi: 10.1002/mco2.104

20. Qian S, Wei Z, Yang W, Huang J, Yang Y, Jinghui Wang J. The role of BCL-2 family proteins in regulating apoptosis and cancer therapy. *Front Oncol*. (2022) 12:985363. doi: 10.3389/fonc.2022.985363

21. Christian F, Smith EL, Carmody RJ. The regulation of NF-κB subunits by phosphorylation. *Cells*. (2016) 5:12. doi: 10.3390/cells5010012

22. Zafar S, Faisal S, Jan H, Ullah R, Rizwan M, Abdullah, et al. Development of iron nanoparticles (FeNPs) using biomass of enterobacter: its characterization, antimicrobial, anti-alzheimer's, and enzyme inhibition potential. *Micromachines (Basel)*. (2022) 13:1259. doi: 10.3390/mi13081259

23. Kumar N, Thorat ST, Chavhan S, Reddy KS. Understanding the molecular mechanism of arsenic and ammonia toxicity and high-temperature stress in *Pangasianodon hypophthalmus*. *Environ Sci Pollut Res*. (2024) 31:15821–36. doi: 10.1007/s11356–024-32093–8

24. Kumar N, Thorat ST, Kochewad SA, Reddy KS. Manganese nutrient mitigates ammonia, arsenic toxicity and high temperature stress using gene regulation via NFkB mechanism in fish. *Sci Rep*. (2024) 14:1273. doi: 10.1038/s41598–024-51740–1

25. Singh AK, Lakra WS. Culture of Pangasianodon hypophthalmus in India: Impacts and present scenario. *Pak J Biol Sci*. (2012) 15:19–26. doi: 10.3923/pjbs.2012.19.26

26. APHA-AWWA-WEF. *Standard methods for the estimation of water and waste water. 20th edn*. Clesceri LS, Greenberg AE, Eaton AD, editors. Washington, DC: American Public Health Association, American Water Works Association, Water Environment Federation (1998).

27. Kumar N, Krishnani KK, Singh NP. Effect of dietary zinc-nanoparticles on growth performance, anti-oxidative and immunological status of fish reared under multiple stressors. *Biol Trace Elem Res*. (2018) 186:267–78. doi: 10.1007/s12011-018-1285-2

28. Kumar N, Gupta SK, Bhushan S, Singh NP. Impacts of acute toxicity of arsenic (III) alone and with high temperature on stress biomarkers, immunological status and cellular metabolism in fish. *Aquat. Toxicol*. (2019) 4:105233. doi: 10.1016/j.aquatox.2019.105233

29. AOAC. *Official methods of analysis of the association of official analytical chemists. 16th edn*. Arlington: AOAC International (1995) p. 31–65.

30. Halver JE. The nutritional requirements of cultivated warm water and cold water fish species. In Report of the FAO Technical Conference on Aquaculture, Kyoto, Japan, 26 May–2 June 1976. FAO Fisheries Report No. 188 FI/ R188 (En), p 9 (1976).

31. Kumar N, Chandan NK, Wakchaure GC, Singh NP. Synergistic effect of zinc nanoparticles and temperature on acute toxicity with response to biochemical markers and histopathological attributes in fish. *Comp Biochem Physiol Part- C: Toxicol Pharmacol*. (2020) 229:108678. doi: 10.1016/j.cbpc.2019.108678

32. Kumar N, Thorat ST, Gite A, Patole PB. Nano-copper enhances gene regulation of non-specific immunity and antioxidative status of fish reared under multiple stresses. *Biol Trace Elem Res*. (2023) 201:4926–50. doi: 10.1007/s12011-023-03575-6

33. Pfaf MW. A new mathematical model for relative quantification in real-time RT-PCR, Nucl. *Acids Res*. (2001) 29:e45. doi: 10.1093/nar/29.9.e45

34. Kumar N, Krishnani KK, Meena KK, Gupta SK, Singh NP. Oxidative and cellular metabolic stress of Oreochromis mossambicus as biomarkers indicators of trace element contaminants. *Chemosphere*. (2017) 171:265–74. doi: 10.1016/j.chemosphere.2016.12.066

35. Ali A, Bharadwaj S, O'Carroll R, Ovsenek N. HSP90 interacts with and regulates the activity of heat shock factor 1 in *Xenopus oocytes*. *Mol Cell Biol*. (1998) 18:4949–60. doi: 10.1128/MCB.18.9.4949

36. Hajirezaee S, Mohammadi G, Naserabad SS. The protective effects of vitamin C on common carp (Cyprinus carpio) exposed to titanium oxide nanoparticles (TiO2-NPs). *Aquaculture*. (2020) 518:734734. doi: 10.1016/j.aquaculture.2019.734734

37. Khoei AJ. Evaluation of potential immunotoxic effects of iron oxide nanoparticles (IONPs) on antioxidant capacity, immune responses and tissue bioaccumulation in common carp (*Cyprinus carpio*). *Comp Biochem Physiol C Toxicol Pharmacol*. (2021) 244:109005. doi: 10.1016/j.cbpc.2021.109005

38. Saad MJA, Morais SM, T.O. Saad STO. Reduced cortisol secretion in patients with iron deficiency. *Ann Nutr Metab*. (1991) 35(2):111–5. doi: 10.1159/000177633

39. Simpson ER, Mason JI. Molecular aspects of the biosynthesis of adrenal steroids. *Pharmacol Ther Part B: Gen Systemat Pharmacol*. (1976) 2:339–69. doi: 10.1016/S0306-039X(76)80012-8

40. Voss L, Yilmaz K, Burkard L, Vidmar J, Stock V, Hofmann U, et al. Impact of iron oxide nanoparticles on xenobiotic metabolism in Hepa RG cells. *Arch Toxicol*. (2020) 94:4023–35. doi: 10.1007/s00204-020-02904-1

41. Vos MJ, Hageman J, Carra S, Kampinga HH. Structural and functional diversities between members of the human HSPB, HSPH, HSPA, and DNAJ chaperone families. *Biochemistry*. (2008) 47:7001–11. doi: 10.1021/bi800639z

42. Desai NS, Agarwal AA, Uplap SS. HSP: evolved and conserved proteins, structure and sequence studies. *Int J Bioinform Res*. (2010) 2:67–87. doi: 10.9735/0975-3087

43. Zou J, Guo Y, Guettouche T, Smith DF, Voellmy R. Repression of heat shock transcription factor HSF1 by HSP90 (HSP90 complex) that forms a stress sensitive complex with HSF1. *Cell*. (1998) 94:471–80. doi: 10.1016/S0092-8674(00)81588-3

44. Hughes MF. Arsenic toxicity and potential mechanisms of action. *Toxicol Lett*. (2002) 133:1–16. doi: 10.1016/S0378-4274(02)00084-X

45. Kumar N, Singh DK, Chandan NK, Thorat ST, Patole PB, Gite A, et al. Nano–zinc enhances gene regulation of non–specific immunity and antioxidative status to mitigate multiple stresses in fish. *Sci Rep*. (2023) 13:5015. doi: 10.1038/s41598-023-32296-y

46. Ferrari DM, Soling HD. The protein disulphide-isomerase family: unravelling a string of folds. *Biochem J*. (1999) 339:1–10. doi: 10.1042/bj3390001

47. Wroblewski VJ, Masnyk M, Khambatta SS, Becker GW. Mechanisms involved in degradation of human insulin by cytosolic fractions of human, monkey, and rat liver. *Diabetes*. (1992) 41:539–47. doi: 10.2337/diabetes.41.4.539

48. Solovyov A, Gilbert HF. Zinc-dependent dimerization of the folding catalyst, protein disulfide isomerase. *Protein Sci*. (2004) 13:1902–7. doi: 10.1110/ps.04716104

49. Narindrasorasak S, Yao P, Sarkar B. Protein disulfide isomerase, a multifunctional protein chaperone, shows copper-binding activity. *BBRC*. (2003) 33:405–14. doi: 10.1016/j.bbrc.2003.09.226

50. Kumar N, Thorat ST, Chavhan S. Multifunctional role of dietary copper to regulate stress-responsive gene for mitigation of multiple stresses in *Pangasianodon hypophthalmus*. *Sci Rep*. (2024) 14:2252. doi: 10.1038/s41598-024-51170-z

51. Kumar N, Thorata ST, Gite A, Patole P. Synergistic effect of nickel and temperature on gene expression, multiple stress markers, and depuration: an acute toxicity in fish. *Environ Sci pollut Res*. (2023) 30:123729–50. doi: 10.1007/s11356–023-30996–6

52. Andrews GK. Regulation of metallothionein gene expression by oxidative stress and metal ions. *Biochem Pharmacol*. (2000) 59:95–104. doi: 10.1016/S0006-2952(99)00301-9

53. Saydam N, Adams TK, Steiner F, Schaffner W, Freedman JH. Regulation of metallothionein transcription by the metal-responsive transcription factor MTF-1: identification of signal transduction cascades that control metal-inducible transcription. *J Biol Chem*. (2002) 277:20438–45. doi: 10.1074/jbc.M110631200

54. Aileen R, James NM, Anne MW, Ian B. Effects of iron deficiency on metallothionein-I concentrations in blood and tissues of rats. *J Nutr*. (1989) 119:439–45. doi: 10.1093/jn/119.3.439

55. Zangar RC, Davydov DR, Verma S. Mechanisms that regulate the production of reactive oxygen species by cytochrome P450. *Toxicol Appl Pharmacol*. (2004) 199:316–31. doi: 10.1016/j.taap.2004.01.018

56. Zeng C, Sun H, Xie P, Wang J, Zhang G, Chen N, et al. The role of apoptosis in MCLR-induced developmental toxicity in zebrafish embryos. *Gig. Sanit*. (2014) 149:25–32. doi: 10.1016/j.aquatox.2014.01.021

57. Wei MC, Zong W, Cheng EH, Lindsten T, Panoutsakopoulou V, Ross AJ, et al. Proapoptotic BAX and BAK: a requisite gateway to mitochondrial dysfunction and death. *Science*. (2001) 292:727–30. doi: 10.1126/science.1059108

58. Banerjee B, Bhuyan G, Koner D, Saha N. Differential expression of multiple glutamine synthetase genes in airbreathing magur catfish, Clarias magur and their induction under hyper-ammonia stress. *Gene*. (2018) 671:85–95. doi: 10.1016/j.gene.2018.05.111

59. Vile GF, Tanew-Ilitschew A, Tyrrell RM. Activation of NFkappa B in human skin fibroblasts by the oxidative stress generated by UVA radiation. *Photochem Photobiol*. (1995) 62:463–8. doi: 10.1111/j.1751-1097.1995.tb02369.x

60. Dendorfer A, Heidbreder M, Hellwig-Burgel T, Johren O, Qadri F, Dominiak P. Deferoxamine induces prolonged cardiac preconditioning via accumulation of oxygen radicals. *Free Radic Biol Med*. (2005) 38:117–24. doi: 10.1016/j.freeradbiomed.2004.10.015

61. Hahn JY, Cho HJ, Bae JW, Yuk HS, Kim K, Park KW, et al. beta-Catenin overexpression reduces myocardial infarct size through differential effects on cardiomyocytes and cardiac fibroblasts. *J Biol Chem*. (2006) 281:30979–89. doi: 10.1074/jbc.M603916200

62. Zhao XS, Pan W, Bekeredjian R, Shohet RV. Endogenous endothelin-1 is required for cardiomyocyte survival *in vivo*. *Circulation*. (2006) 114:830–7. doi: 10.1161/CIRCULATIONAHA.105.577288

63. Laskar A, Eilertsen J, Li W, Yuan X-M. SPION primes THP1 derived M2 macrophages towards M1-like macrophages. *Biochem Biophys Res Commun*. (2013) 441:737–42. doi: 10.1016/j.bbrc.2013.10.115

64. Ai XG, Shen YF, Min C, Pang SY, Zhang JX, Zhang SQ, et al. Molecular structure, expression and bioactivity characterization of TNF13B (BAFF) gene in mefugu Takifugu obscurus. *Fish Shellfish Immunol*. (2011) 30:1265–74. doi: 10.1016/j.fsi.2011.03.020

65. Zhang TX, Yan ZG, Zheng X, Wang SP, Fan JT, Liu ZT. Effects of acute ammonia toxicity on oxidative stress, DNA damage and apoptosis in digestive gland and gill of Asian clam (Corbicula fluminea). *Fish Shellfish Immunol*. (2020) 99:514–25. doi: 10.1016/j.fsi.2020.02.046

66. Ding Y. J, Chen X. Comparative study of interleukin-17C (IL-17C) and IL-17D in large yellow croaker Larimichthys crocea reveals their similar but differential functional activity. *Dev Comp Immunol*. (2017) 76:34–44. doi: 10.1016/j.dci.2017.05.014

67. Lam W.S. SY, Lin SJ, Lin CC, Chen YM, Wang HC, Chen TY, et al. The expression of two novel orange-spotted grouper (Epinephelus coioides) TNF genes in peripheral blood leukocytes, various organs, and fish larvae. *fish shellfish Immunol*. (2011) 30:618–29. doi: 10.1016/j.fsi.2010.12.011

68. Nemeth E, Roetto A, Garozzo G, Ganz T, Camaschella C. Hepcidin is decreased in TFR2 hemochromatosis. *Blood*. (2005) 105:1803–6. doi: 10.1182/blood-2004-08-3042

69. Rogers JT. Ferritin translation by interleukin-1and interleukin-6: the role of sequences upstream of the start codons of the heavy and light subunit genes. *Blood*. (1996) 87:2525–37. doi: 10.1182/blood.V87.6.2525.bloodjournal8762525

70. Recalcati S, Locati M, Marini A, Santambrogio P, Zaninotto F, De Pizzol M, et al. Differential regulation of iron homeostasis during human macrophage polarized activation. *Eur J Immunol*. (2010) 40:824–35. doi: 10.1002/eji.200939889

71. Abdel Rahman AN, MansourDA, Abd El-Rahman GI, Elseddawy NM, Zaglool AW, et al. Imidacloprid toxicity in Clarias gariepinus: protective role of dietary Hyphaene thebaica against biochemical and histopathological disruption, oxidative stress, immune genes expressions, and Aeromonas sobria infection. *Aquaculture*. (2022) 555:738170. doi: 10.1016/j.aquaculture.2022.738170

72. Elabd H, Youssuf H, Mahboub HH, Salem SMR, Husseiny WA, Khalid A, et al. Growth, hemato-biochemical, immune-antioxidant response, and gene expression in Nile tilapia (Oreochromis niloticus) received nano iron oxide-incorporated diets. *Fish Shellfish Immunol*. (2022) 128:574–81. doi: 10.1016/j.fsi.2022.07.051

73. Zhang YL, Wang GY, Zhang ZH, Xie YY, Jin H, Dong ZR. Partial amino acid metabolism and glutamine synthesis as the ammonia defensive strategies during aerial exposure in Chinese loach Paramisgurnus dabryanus. *Front Physiol*. (2019) 10:10–3389. doi: 10.3389/fphys.2019.00014

74. Uribe C, Folch H, Enriquez R, Moran G. Innate and adaptive immunity in teleost fish: A review. *Vet Med*. (2011) 56:486–503. doi: 10.17221/3294-VETMED

75. Beutler B. Innate immunity: An overview. *Mol Immunol*. (2004) 40:845–59. doi: 10.1016/j.molimm.2003.10.005

76. Chen P-J, Chih-Hsiang S, Chi-Yen T, Shih-Wei T, Chiung-Hsiang C. Toxicity assessments of nanoscale zerovalent iron and its oxidation products in medaka (Oryzias latipes) fish. *Mar pollut Bull*. (2011) 63:339–46. doi: 10.1016/j.marpolbul.2011.02.045

77. Goya GF, Marcos-Campos I, Fernandez-Pacheco R, Saez B, Godino J, As L, et al. Dendritic cell uptake of iron-based magnetic nanoparticles. *Cell Bio Int*. (2008) 32:1001–5. doi: 10.1016/j.cellbi.2008.04.001

78. He K, Huang R, Cheng L, Liu Q, Zhang Y, Yan H, et al. Effects of dietary nano-iron on growth, hematological parameters, immune antioxidant response, and hypoxic tolerance in juvenile Largemouth Bass (*Micropterus salmoides*). *Aquacul Rep*. (2023) 33:101759. doi: 10.1016/j.aqrep.2023.101759

79. Kripli B, Solyom B, Speier G, Kaizer J. Stability and catalase-like activity of a mononuclear non-heme oxoiron (IV) complex in aqueous solution. *Molecules*. (2019) 24:3236. doi: 10.3390/molecules24183236

80. Finazzi D, Arosio P. Biology of ferritin in mammals: an update on iron storage, oxidative damage and neurodegeneration. *Arch Toxicol*. (2014) 88:1787–802. doi: 10.1007/s00204-014-1329-0

81. Ismail M, Al-Naqeep G, Chan KW. Nigella sativa thymoquinone-rich fraction greatly improves plasma antioxidant capacity and expression of antioxidant genes in hypercholesterolemic rats. *Free Radic Biol Med*. (2010) 48:664–72. doi: 10.1016/j.freeradbiomed.2009.12.002

82. Nalage RR, Thorata ST, Chandramore K, Reddy KS, Kumar N. Dietary manganese nano-particles improves gene regulation and biochemical attributes for mitigation of lead and ammonia toxicity in fish. *Comp Biochem Physiol Part C*. (2023) 276:109818. doi: 10.1016/j.cbpc.2023.109818

83. Kumar N, Gupta S, Chandan NK, Aklakur Md, Pal AK, Jadhao SB. Lipotropes protect against pathogen-aggravated stress and mortality in low dose pesticide-exposed fish. *PloS One*. (2014) 9:e93499. doi: 10.1371/journal.pone.0093499

84. Behera T, Swain P, Rangacharulu PV, Samanta M. Nano-Fe as feed additive improves the hematological and immunological parameters of fish, Labeo rohita H. *Appl Nanosci*. (2014) 4:687–94. doi: 10.1007/s13204-013-0251-8

85. Vetrano AM, Heck DE, Mariano TM, Mishin V, Laskin DL, Laskin JD. Characterization of the oxidase activity in mammalian catalase. *J Biol Chem*. (2005) 280:35372–81. doi: 10.1074/jbc.M503991200

86. Thangapandiyan S, Alisha ASA, Anidha K. Growth performance, hematological and biochemical effects of iron oxide nanoparticles in Labeo rohita. *Biocatalysis Agric Biotechnol*. (2020) 25:101582. doi: 10.1016/j.bcab.2020.101582

87. Uzo-God OC, Agarwal A, Singh NB. Effects of dietary nano and macro iron oxide (Fe2O3) on the growth, biochemical, and hematological profiles of African catfish (Clarias gariepinus) fingerlings. *J Appl Aquac*. (2018) 31(2):153–71. doi: 10.1080/10454438.2018.1534704

88. Bass J, Oldham J, Sharma M, Kambadur R. Growth factors controlling muscle development, Domest. *Anim. Endocrinol*. (1999) 17:191–7. doi: 10.1016/S0739-7240(99)00036-3

89. Moriyama S, Ayson FG, Kawauchi H. Growth regulation by insulin-like growth factor-I in fish. *Biosci Biotechnol Biochem*. (2000) 64:1553–62. doi: 10.1271/bbb.64.1553

90. Prodanović R, Kirovski D, Vujanac I, Dodovski P, Jovanović L, Šamanc H. Relationship between serum iron and insulin-like growth factor-I concentrations in 10-day-old calves. *Acta Vet Brno*. (2014) 83:133–7. doi: 10.2754/avb201483020133

91. González EM, Contreras I, Estrada JA. Effect of iron deficiency on the expression of insulin-like growth factor-II and its receptor in neuronal and glial cells. *Neurología (English Edition)*. (2014) 29:408–15. doi: 10.1016/j.nrleng.2013.10.017

92. Hashizume T, Horiuchi M, Tate N, Nonaka S, Mikami U, Kojima M. Effects of ghrelin on growth hormone secretion from cultured adenohypophysial cells in pigs. *Domest. Anim. Endocrinol.* (2003) 24:209–18. doi: 10.1016/S0739-7240(02)00240-0

93. Van Asbeck BS, Verbrugh HA, van Oost BA, Marx J, Imhof HW, Verhoef J. Listeria monocytogenes meningitis and decreased phagocytosis associated with iron overload. *Br Med J.* (1982) 284:542–4. doi: 10.1136/bmj.284.6315.542

frontiers | Frontiers in Immunology

TYPE Original Research
PUBLISHED 15 August 2024
DOI 10.3389/fimmu.2024.1439465

OPEN ACCESS

EDITED BY
Iddya Karunasagar,
Nitte University, India

REVIEWED BY
Rahul Krishnan,
Kerala University of Fisheries and Ocean Studies, India
Xiuzhen Sheng,
Ocean University of China, China

*CORRESPONDENCE
Mohamed Emam
melsayedemam@mun.ca
Matthew L. Rise
mrise@mun.ca

†These authors have contributed equally to this work

RECEIVED 28 May 2024
ACCEPTED 08 July 2024
PUBLISHED 15 August 2024

CITATION
Emam M, Kumar S, Eslamloo K, Caballero-Solares A, Hall JR, Xue X, Paradis H, Gendron RL, Santander J and Rise ML (2024) Transcriptomic response of lumpfish (*Cyclopterus lumpus*) head kidney to viral mimic, with a focus on the *interferon regulatory factor* family. *Front. Immunol.* 15:1439465. doi: 10.3389/fimmu.2024.1439465

Transcriptomic response of lumpfish (*Cyclopterus lumpus*) head kidney to viral mimic, with a focus on the *interferon regulatory factor* family

Mohamed Emam[1*], Surendra Kumar[1†], Khalil Eslamloo[1,2†], Albert Caballero-Solares[1], Jennifer R. Hall[3], Xi Xue[1], Hélène Paradis[4], Robert L. Gendron[4], Javier Santander[5] and Matthew L. Rise[1*]

[1]Department of Ocean Sciences, Memorial University of Newfoundland, St. John's, NL, Canada, [2]Centre for Marine Applied Research, Dartmouth, NS, Canada, [3]Aquatic Research Cluster, Core Research Equipment and Instrument Training (CREAIT) Network, Ocean Sciences Centre, Memorial University of Newfoundland, St. John's, NL, Canada, [4]Faculty of Medicine, Memorial University of Newfoundland, St. John's, NL, Canada, [5]Marine Microbial Pathogenesis and Vaccinology Laboratory, Department of Ocean Sciences, Memorial University of Newfoundland, St. John's, NL, Canada

The economic importance of lumpfish (*Cyclopterus lumpus*) is increasing, but several aspects of its immune responses are not well understood. To discover genes and mechanisms involved in the lumpfish antiviral response, fish were intraperitoneally injected with either the viral mimic polyinosinic:polycytidylic acid [poly(I:C)] or phosphate-buffered saline (PBS; vehicle control), and head kidneys were sampled 24 hours post-injection (hpi) for transcriptomic analyses. RNA sequencing (RNA-Seq) (adjusted p-value <0.05) identified 4,499 upregulated and 3,952 downregulated transcripts in the poly(I:C)-injected fish compared to the PBS-injected fish. Eighteen genes identified as differentially expressed by RNA-Seq were included in a qPCR study that confirmed the upregulation of genes encoding proteins with antiviral immune response functions (e.g., *rsad2*) and the downregulation of genes (e.g., *jarid2b*) with potential cellular process functions. In addition, transcript expression levels of 12 members of the interferon regulatory factor (IRF) family [seven of which were identified as poly(I:C)-responsive in this RNA-Seq study] were analyzed using qPCR. Levels of *irf1a*, *irf1b*, *irf2*, *irf3*, *irf4b*, *irf7*, *irf8*, *irf9*, and *irf10* were significantly higher and levels of *irf4a* and *irf5* were significantly lower in the poly(I:C)-injected fish compared to the PBS-injected fish. This research and associated new genomic resources enhance our understanding of the genes and molecular mechanisms underlying the lumpfish response to viral mimic stimulation and help identify possible therapeutic targets and biomarkers for viral infections in this species.

KEYWORDS

antiviral, lumpfish (*Cyclopterus lumpus*), IRF, RNA seq, qPCR

Introduction

Lumpfish (*Cyclopterus lumpus*) are commonly used as an environmentally friendly solution for sea lice control (e.g., *Lepeophtheirus salmonis*) in Atlantic salmon (*Salmo salar*) farms in the North Atlantic region (1–3). Sea lice infestations lead to decreased fish health, growth, and, consequently, market value (4). Additionally, lumpfish as a biological method to control sea lice help reduce the reliance on chemical treatments, which contribute to environmental pollution. However, lumpfish farming faces several challenges. For example, lumpfish are susceptible to several infectious diseases, which can be transferred to other aquatic hosts such as Atlantic salmon (2, 5). Atlantic salmon and lumpfish can both be infected with pathogens such as the bacterium *Renibacterium salmoninarum* and the viral hemorrhagic septicemia (VHS) virus (2, 6). While lumpfish may be infected by viral pathogens (e.g., Supplementary Table S1), the development of vaccines for farmed lumpfish has thus far focused on bacterial pathogens (7–12) rather than viruses. The development of vaccines for the protection of lumpfish against viral infection is a priority (7).

Polyinosinic:polycytidylic acid [poly(I:C)] is a synthetic analog of double-stranded RNA (dsRNA) that can mimic viral infections (i.e., elicit a potent antiviral-like response) in several species including teleosts and is commonly used as an immune stimulant in aquaculture research (13–15). Poly(I:C) was previously used in several studies to evaluate the antiviral response of zebrafish (*Danio rerio*), Chinook salmon (*Oncorhynchus tshawytscha*), seven-band grouper (*Epinephelus septemfasciatus*), and Atlantic salmon, as it mimics RNA viral pathogens of fish (15–19). For example, positive-sense single-stranded RNA (ssRNA) viruses such as nodaviruses and flaviviruses form dsRNA intermediates during their replication cycle (20–22). Also, it has been reported that lumpfish can be infected with dsRNA viruses (Supplementary Table S1), such as *C. lumpus* toti-like virus (CLuTLV) (23), and ssRNA viruses that likely produce dsRNA during their replication cycle including *C. lumpus* virus (CLuV) (24) and nervous necrosis virus (NNV) (25).

RNA sequencing (RNA-Seq) is a highly robust method for assessing global gene expression responses, as it generates accurate and reproducible results (26). Transcriptomic studies may be used to identify genes and pathways that respond to immune challenges. As examples, the transcriptomic responses to viral infection [e.g., infectious salmon anemia virus (ISAV) and infectious pancreatic necrosis virus (IPNV)] and/or poly(I:C) were previously explored in Atlantic salmon, rainbow trout (*Oncorhynchus mykiss*) (27), red-spotted grouper (*Epinephelus akaara*) (28), yellowhead catfish (*Tachysurus fulvidraco*) (29), ya-fish (*Schizothorax prenanti*) (30), and yellow catfish (*Pelteobagrus fulvidraco*) (31). To our knowledge, the lumpfish transcriptomic response to a viral pathogen has not been studied. While lumpfish primary leukocytes' transcript expression responses to poly(I:C) have been studied recently (32, 33), the lumpfish systemic immune antiviral transcriptomic response [e.g., response of immune tissue/organ such as head kidney to *in vivo* stimulation with poly(I:C)] had not been characterized prior to the current study. Characterization of the lumpfish head kidney transcriptomic response to poly(I:C) will provide a foundation for understanding the mechanisms underlying the lumpfish immune response to viral infections, thereby aiding in the development of vaccines and the improvement of aquaculture practices.

In addition to the transcriptomic response to poly(I:C), several aspects of lumpfish antiviral mechanisms remain uncharacterized. Interferon regulatory factor (IRF) family members are key elements of fish immune responses (34). Transcript expression levels of several members of the IRF family (e.g., IRF3, 5, and 7) are upregulated following viral infections (34). IRFs are transcription factors, and their activation leads to the induced expression of interferons (IFNs) and IFN-stimulated genes (ISGs), which play crucial roles in antiviral responses. Additionally, *irf* expression is dysregulated in response to several stressors such as viral and bacterial infections, heat shock, and toxins (35–37). Moreover, while members of the IRF family are suggested to be highly conserved in their structure across vertebrate species, they also play some species-dependent roles (38–40). Several members of the IRF family were characterized in teleost species such as common carp (*Cyprinus carpio* L.) (41), Japanese flounder (*Paralichthys olivaceus*) (42), turbot (*Scophthalmus maximus*) (43, 44), Japanese seabass (*Lateolabrax japonicus*) and Atlantic cod (*Gadus morhua*) (45–47). However, the antiviral response of the lumpfish *irf* family members remained unknown prior to this study. In addition to transcriptomic profiling, in this study, we focused on evolutionary aspects and poly(I:C) responses of *irf* family members to investigate if these genes play conserved roles in lumpfish.

In the current study, we analyzed the transcriptomic response of lumpfish head kidney to intraperitoneal (IP) injection with poly(I:C) using RNA-Seq. Real-time quantitative polymerase chain reaction (qPCR) analyses were then utilized to assess expression levels of selected transcripts (e.g., representing hub genes in pathway analyses and well-known antiviral biomarkers) to confirm the results of the RNA-Seq analyses and, specifically, to elucidate the expression profiles of the 12 members of the lumpfish *irf* family in response to poly(I:C). Also, we investigated the molecular phylogeny of IRF members from lumpfish and three other teleost species representing different superorders to improve our understanding of the evolutionary history of the IRF family across Teleostei. The results of the current study enhance our knowledge of the genes and molecular pathways involved in the antiviral immune responses of fishes.

Materials and methods

Animals, experimental design, and sample collection

Juvenile lumpfish were raised at the Dr. Joe Brown Aquatic Research Building (JBARB), Ocean Sciences Centre, Memorial University of Newfoundland, Canada (48). At 300 days post-hatch, 18 fish (average weight ± standard deviation = 85.4 ± 14.6 g) were randomly selected and distributed into three 500-L tanks. The fish were held in 8–10°C filtered and UV-treated seawater, with a flow rate of 7.5 L/min, and the oxygen level was maintained at a saturation range of 95%–110%. The photoperiod was 12-h light and 12-h dark. The fish were fed a commercial diet (Marine grower diet, Zeigler Bros., Inc., Gardners, PA, USA) at 0.5% of the average body weight per day.

After 1 month, the poly(I:C) challenge study was conducted. Briefly, the fish were fasted for 24 h and then lightly anesthetized with MS-222 (50 mg/L, Syndel Laboratories, Vancouver, BC, Canada). Three individuals per tank were intraperitoneally injected with either poly(I:C) [2 µg/g fish, dissolved in phosphate-buffered saline (PBS)] or PBS (sham-injection/vehicle control). Immediately after injection, each fish was stitched with nylon surgical thread on one fin [the left pectoral fin for poly(I:C) or the right pectoral fin for PBS] and then returned to the same tank. At 24 hours post-injection (hpi), fish were euthanized using MS-222 (400 mg/L), and the head kidneys were collected. The samples were flash-frozen in liquid nitrogen and stored at −80°C until RNA extraction. All procedures in this experiment were performed following the Canadian Council of Animal Care guidelines (Memorial University of Newfoundland Animal Care Protocol, 17–03-RG and 18–01-MR) and in accordance with ARRIVE guidelines (https://arriveguidelines.org). Figure 1A depicts an overview of the workflow in this study.

Total RNA sample preparation

The RNA extractions were performed as described in Emam et al. (49). Briefly, the head kidney samples were homogenized in TRIzol Reagent (Invitrogen/Thermo Fisher Scientific, Burlington, ON, Canada) using stainless steel beads (5 mm; QIAGEN, Mississauga, ON, Canada) and a TissueLyser (QIAGEN), and the total RNA extractions were then completed following the manufacturer's instructions. Total RNA samples (~25 µg) were treated with 6.8 Kunitz units of DNaseI (RNase-Free DNase Set, QIAGEN) for 10 min at room temperature and then purified using the RNeasy MinElute Cleanup kit (QIAGEN) following the manufacturer's instructions. The integrity and the purity of the purified RNA were evaluated using 1% agarose gel electrophoresis and NanoDrop spectrophotometry (NSW-1000), respectively. The RNA samples used in this study showed high integrity (i.e., tight 28S and 18S ribosomal RNA bands at a ratio of ~2:1) and purity (i.e., A260/280 and A260/230 ratios above 1.9 and 2.0, respectively).

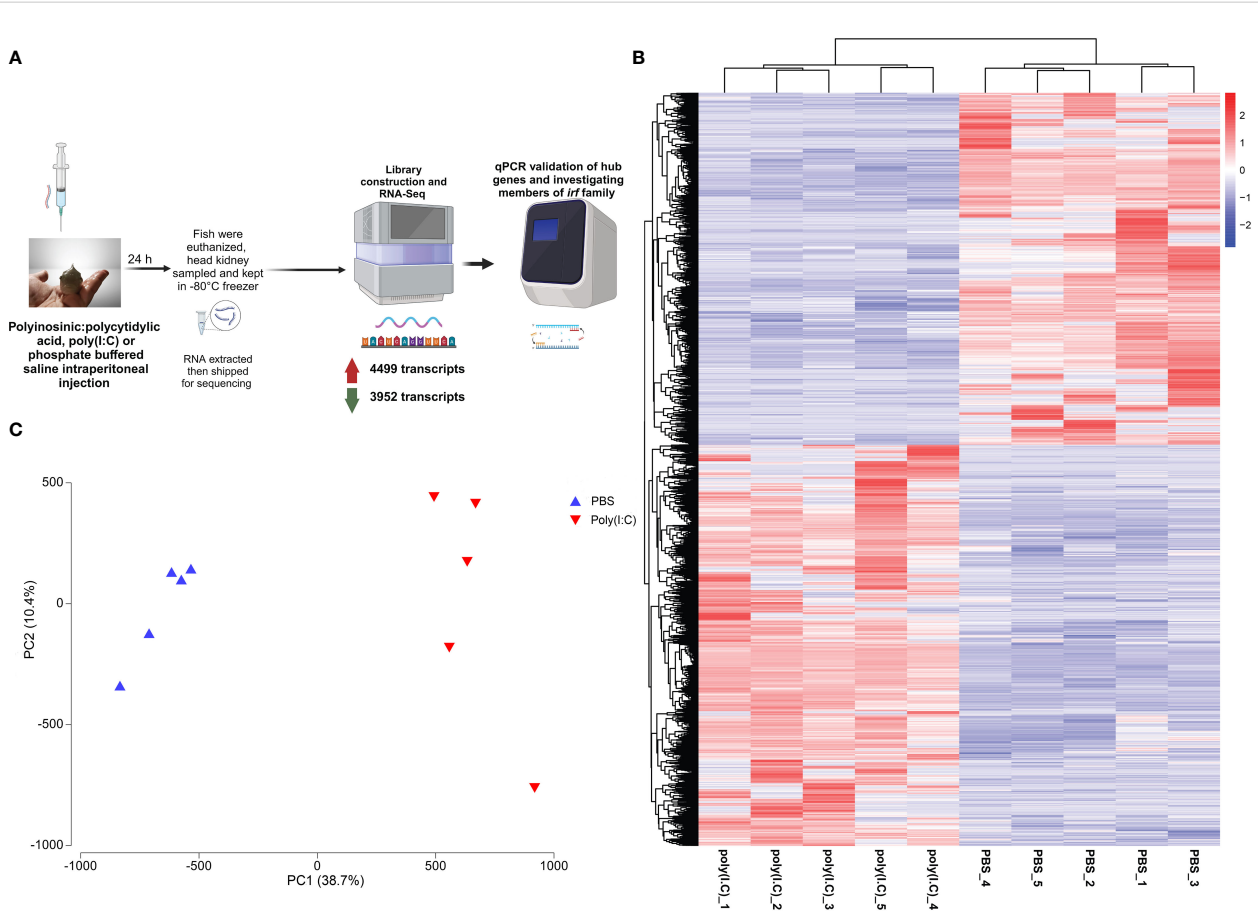

FIGURE 1
(A) Overview of the methods used in the current study. This figure was generated using Biorender.com. **(B)** Heatmap and hierarchical clustering of polyinosinic:polycytidylic acid [poly(I:C)]-responsive transcripts [i.e., differentially expressed transcripts (DETs)]. The transcripts per million (TPM; $\log_2$ transformed) values for each DET are clustered along the vertical axis, the ID of the sample subjected to RNA-Seq is shown on the base of the figure, and the sample cluster is plotted on the top of the map. **(C)** Principal component analysis of DET of all the samples used in sequencing using TPMs.

RNA–seq analysis

Library construction and RNA-Seq services were performed at the Centre d'expertise et de services (CES), Génome Québec, Montréal, QC, Canada. Prior to library construction, RNA quality was further evaluated using the Bioanalyzer 2100 (Agilent, Santa Clara, CA, USA), and all samples were of high integrity (i.e., with RNA Integrity Numbers of 9.8–10). Ten libraries (i.e., for head kidney RNA samples from five of the nine poly(I:C)-injected fish and five of the nine PBS-injected fish) were constructed using the NEBNext mRNA Library Prep Reagent Set for Illumina (New England Biolabs, Whitby, ON, Canada) following the manufacturer's instructions. Sequencing was performed on the Illumina NovaSeq 6000 [S2] with paired-end 100 bp (PE100) and at least 50 million reads per library. A summary of the RNA-Seq and library construction can be found in Supplementary Table S2.

RNA-seq data processing

The quality control, trimming, and filtering of low-quality reads were performed using FastQC version 0.11.8 and Trimmomatic version 0.3971. The sequencing reads were aligned to the lumpfish genome [*C. lumpus* (assembly fCycLum1.pri), ID: 86363] using HISAT2 version 2.1.0. StringTie version 2.0 was used to assemble and calculate the expression levels of all transcripts using reference gene models provided in the form of Gene Transfer Format (GTF) annotation files that are distributed with the lumpfish genome. StringTie was also used to assemble and quantify novel genes and transcripts. The accuracy of transcript assembly was evaluated using gffcompare version 0.11.2. The read count data used for differential expression analysis were obtained from the python script "prepDE.py" provided by the StringTie authors. The differential expression analysis was performed using DESeq2 version 1.28.1 in the Bioconductor package at an adjusted p-value (padj) threshold of <0.05, $|\log_2$ fold change$| > 1$, and filtering for transcripts with expression transcripts per million (TPMs) greater than 1 in at least two replicates in each group.

A heatmap with the TPM values ($\log_2$ transformed) of all differentially expressed transcripts (DETs) was generated using the "heatmap3" function of the "gplots" package in R (2023.03.1; Figure 1B). A principal component analysis (PCA; Figure 1C) was performed using the standardized TPMs of all of the identified DETs. A volcano plot was used to show significance ($-\log_{10}$ padj) against the expression $\log_2$ fold change (LFC). Gene Ontology (GO) term enrichment analysis was conducted using the ClueGO (50) plugin of Cytoscape (51) version 3.5 and using the *C. lumpus* ontology database. The enrichment analyses considered biological process, cellular component, and molecular function. The distribution of up- and downregulated transcripts within each leading GO term were plotted by LFC using density plots (Figure 2B). Leading GO terms were then manually classified based on related function into 1) intracellular processes and regulation of gene expression; 2) immune system, movement, cell structure, and apoptosis; and 3) cell signaling and response to stimuli (Figure 2). A circular bar plot was used to show GO terms with the highest percentage of DETs, after removing redundant GO terms, using library(tidyverse). The standard lumpfish gene symbols for all transcripts in our RNA-Seq dataset were used as references for the enrichment analyses, which were performed at the transcript level since ClueGO conducts the analyses using standard symbols. The heatmap and hierarchical clustering of DETs (using TPMs; $\log_2$ transformed) that participated in enriching "response to virus", "regulation of retinoic acid receptor signaling pathway", and "response to lipid" were generated using TBtools software (52).

qPCR overview

To confirm the results of the RNA-Seq analyses, transcript expression levels of 18 genes (either hub genes or known antiviral biomarkers) that were identified as differentially expressed were also assessed using qPCR. In addition, expression levels of the 12 members of the lumpfish *irf* family [seven of which were also identified as poly(I:C)-responsive by RNA-Seq] were assessed to elucidate the response of this gene family to poly(I:C). Levels were assessed in all of the 18 study samples (i.e., head kidney samples from the poly(I:C)- and PBS-injected fish at 24 hpi; n = 9 per group).

cDNA synthesis and qPCR parameters

First-strand cDNA templates for qPCR were synthesized in 20-µL reactions from 1 µg of DNaseI-treated, column-purified total RNA using random primers (250 ng; Invitrogen), dNTPs (0.5 mM final concentration; Invitrogen), and M-MLV reverse transcriptase (200 U; Invitrogen) with the manufacturer's first-strand buffer (1× final concentration) and DTT (10 mM final concentration) at 37°C for 50 min.

The qPCR amplifications were performed in 13 µL reactions containing 1× Power SYBR Green PCR Master Mix (Applied Biosystems, Foster City, CA, USA), 50 nM of both the forward and reverse primers, and the indicated cDNA quantity. All reactions were performed in triplicate and included no-template controls (NTCs). Amplifications were performed using either the ViiA 7 Real-Time PCR system or the QuantStudio 6 Flex Real-Time PCR system (384-well format) (Applied Biosystems). The qPCR analysis program included 1 cycle of 50°C for 2 min, 1 cycle of 95°C for 10 min, and 40 cycles of 95°C for 15 s and 60°C for 1 min, with fluorescence detection at the end of each 60°C step, and was followed by dissociation curve analysis.

Primer design and quality assurance testing

Previously published (2) and newly designed qPCR primers were used in this study. For the 25 qPCR-analyzed genes that were identified as differentially expressed in the RNA-Seq analyses, a BLASTn search of the non-redundant nucleotide (nr/nt) sequence database of the National Center for Biotechnology Information (NCBI) [*C. lumpus* (taxid: 8103) sequences only] was performed to

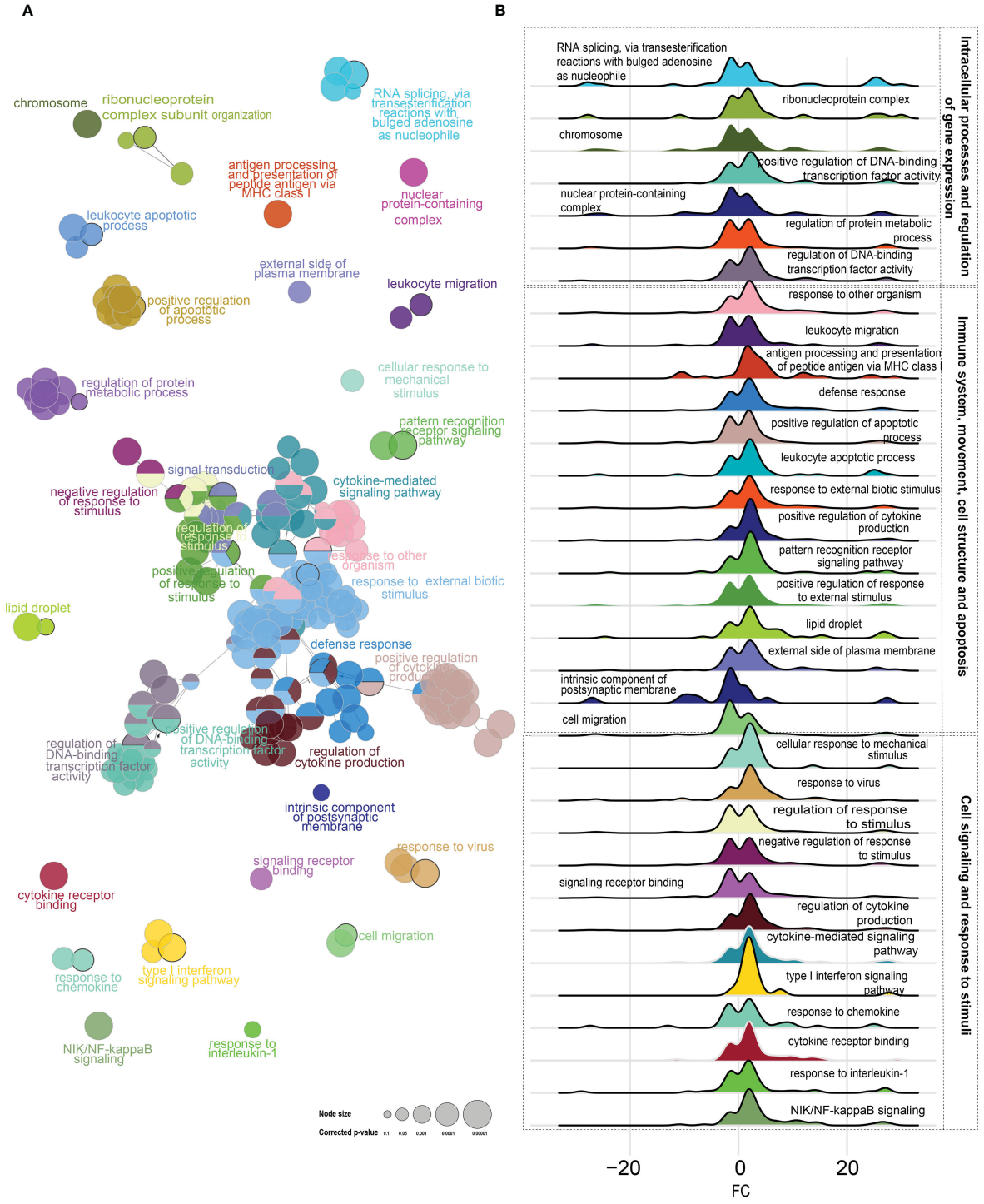

FIGURE 2
(A) Gene Ontology (GO) term enrichment and pathway term network analysis of differentially expressed transcripts (DETs). The GO term enrichment analysis was performed using ClueGO plugin in Cytoscape. The p-value was adjusted at 0.05, kappa score level was ≥0.4 on ClueGO, and Benjamini–Hochberg correction was used. Biological process, cellular component, and molecular function were the selected ontologies on ClueGO. Nodes represent enriched GO terms. A complete list of the enriched GO terms is found in Supplementary Table S4, while the leading GO terms are also labeled in the figure. **(B)** Density plots of the fold change for the leading GO terms, showing the upregulated and downregulated genes in each GO term.

identify annotated sequences corresponding to the transcript sequence generated herein [i.e., transcript of interest (TOI)]. This search also determined if gene paralogues/isoforms were present; the additional five *irf* family members were identified using BLASTn. A database of the sequences obtained from GenBank was compiled using Vector NTI (Vector NTI Advance 11.5.4, Life Technologies, Carlsbad, CA, USA). For a given gene, if paralogues/isoforms were present, multiple sequence alignments were

performed using AlignX (Vector NTI Advance 11.5.4) to identify regions where paralogue/isoform-specific qPCR primers for the TOI could be designed (i.e., in an area with ≥3-bp difference between them). However, if sequences for transcript variants were present, primers were designed in a region that was conserved among the variants and generated identical amplicons. Most primers were designed using either PrimerQuest (www.idtdna.com/Primerquest/Home/Index) or Primer3 (53, 54) however, some were manually designed in paralogue/isoform-specific areas to ensure specificity. All primers had a melting temperature (T_m) of 60°C and were located in the CDS.

The qPCR primers utilized herein were subjected to quality control testing as described previously (55). All showed single-product amplification and the absence of primer dimer in the NTC using dissociation curve analysis. Amplification efficiencies were calculated for two cDNA pools generated from all individuals in the PBS group and from all individuals in the poly(I:C) group. Standard curves were generated using a 5-point 1:3-fold dilution series starting with cDNA representing 10 ng of input total RNA. The reported efficiencies are an average of the two values. The sequences, amplicon sizes, and efficiencies for all primer pairs used in the qPCR analyses are presented in Table 1.

Endogenous control (normalizer) selection

Transcript expression levels of each gene of interest (GOI) were normalized to expression levels of two endogenous control genes. These endogenous controls were selected from five candidate normalizers [*ribosomal protein lateral stalk subunit p1* (*rplp1*), *ribosomal protein l32* (*rpl32*), *poly(A) binding protein cytoplasmic 1b* (*papbc1b*), *eukaryotic translation initiation factor 3 subunit d* (*eif3d*), *eukaryotic translation elongation factor 1 alpha 2a* (*ef1a2a*)]. Briefly, the fluorescence threshold cycle (C_T) values for all 18 samples were measured for each of these transcripts using cDNA representing 5 ng of input total RNA and then analyzed using geNorm (qBase plus, Biogazelle NV, Zwijnaarde, Belgium) (56). This analysis identified *rpl32* and *ef1a2a* as the most stably expressed normalizers, with geNorm M-values of 0.20 and 0.21, respectively.

Experimental qPCR and data analyses

The qPCR analyses were conducted according to MIQE guidelines (57). cDNA representing 5 ng of input total RNA was used as a template in the PCRs. The relative quantity (RQ) of each GOI in each of the 18 samples was then determined using the qBase relative quantification framework (58, 59). This was performed using the C_T values measured for each GOI, with normalization to both *rpl32* and *ef1a2a* and with the amplification efficiencies incorporated. For each GOI, the sample with the lowest normalized expression was used as the internal calibrator (i.e., assigned an RQ value = 1.0). The RQ values are presented as mean ± SE (Figures 4, 5).

Phylogenetic tree analysis of putative IRF orthologues

Putative orthologous amino acid (AA) sequences for IRF family members from a fish representing each of the four teleost superorders, namely, Protacanthopterygii (Atlantic salmon), Acanthopterygii (lumpfish), Paracanthopterygii (Atlantic cod), and Ostariophysi (zebrafish; *D. rerio*), were collected from the NCBI GenBank non-redundant (nr) protein database (59 in total). The GenBank accession numbers and AA sequences are provided in Supplementary Table S5. The sequences were subjected to BLASTP analyses to help identify all of the IRF isoforms/paralogues for each species and to ensure that all sequences used in the tree were unique (i.e., the tree did not include transcript variants; if present, the best representative sequence was selected). Phylogenetic and molecular evolutionary analyses were conducted using MEGA 11 (v.11.0.13) (60). Briefly, a multiple sequence alignment was performed using the ClustalW algorithm. The phylogenetic tree was then constructed using the Neighbor-Joining method with the Poisson correction; the bootstrap test of phylogeny was performed with 10,000 replicates.

Statistical analysis

All of the residuals were tested for homoscedasticity and normality (i.e., Levene's and Shapiro–Wilk tests). Significant ($p < 0.05$) differences in transcript expression levels between the PBS- and poly(I:C)-injected groups were assessed using either Student's t-test or the Mann–Whitney U test (for genes that failed the normality test). These analyses were performed using SPSS (IBM SPSS Statistics, Version 25, Armonk, NY, USA). PCA (Figure 1C) was performed using PRIMER 7 (PRIMER-E Ltd., Auckland, New Zealand). The scatter plot for the LFC (Supplementary Figure S2) was generated using the function "ggscatter" for the library "ggpubr".

Results

Lumpfish head kidney transcriptome assemblies and RNA-Seq analyses

Transcriptome sequencing and assemblies

In this study, RNA-Seq was used to profile the responses of lumpfish to viral mimic, poly(I:C). Supplementary Table S2 summarizes the RNA-Seq read quality control for the 10 samples. The average number of raw reads across all samples was 79.7 M (range, ~62M to 92M). On average, 98% of the read pairs (across all samples) survived the trimming process (range, 97.8% to 98.2%). The average percentage of reads that dropped during trimming was 0.4% (range, 0.3% to 0.5%). Overall, the results show that most reads were successfully trimmed and kept. Both uniquely and multi-mapped reads were used for transcript assembly. Overall, ~94%–

10.3389/fimmu.2024.1439465

TABLE 1 Primers used in qPCR analysis.

Gene name	Symbol	GenBank accession number	[a]E (%)	[b]Nucleotide sequence (5′–3′)	Amplicon size (bp)	Reference
Activating transcription factor 3	*atf3*	XM_034528323	97.6	F:AGGAGCTGAAGCAGCAGAAG	135	This study
				R:TGCTCTCCTTGATGTGTTGC		
ADAM metallopeptidase domain 22	*adam22*	XM_034553371	96.8	F:CCAGTGTCCAACAAATGTGC	143	This study
				R:AGAACTTGTCAGCCGCTGTT		
ADAM metallopeptidase with thrombospondin type 1 motif, 15a	*adamts15a*	XM_034550916	92.9	F:GACCAGCCTCAGAAACCGTT	120	This study
				R:TGGCTGCATAAAGGGACAGG		
ATP-dependent RNA helicase lgp2	*dhx58 (lgp2)*	XM_034539875.1	95.2	F:GCAACCTGGTGGTACGCTAT	104	(2)
				R:CTCGGCGACCACTGAATACT		
Adenosine monophosphate deaminase 2b	*ampd2b*	XM_034537011	80.6	F:CACGTTGTGGGTTTTGACAG	100	This study
				R:TGTGCTCCTCTGTCCAGTTG		
Cholesterol 25-hydroxylase like 3	*ch25hl3*	XM_034540810	89.9	F:GCTCTCTGGAGCTGCTGTCT	103	This study
				R:CAGCTGTTGATGAGGTGGAA		
E3 ubiquitin/ISG15 ligase TRIM25-like	*trim25*	XM_034531793	91.8	F:CTCCTTCCTCTGTGTGTTTATGG	80	This study
				R:TCCTGCAGATGAATATGAGTTCAG		
Interferon-induced GTP-binding protein Mx-like	*mx1*	XM_034531951	90	F:TGCACAGACTCAAGCAGAGC	144	(2)
				R:CCACACTTGAGCTCCTCTCC		
Interferon alpha/beta receptor 2-like	*ifnar2*	XM_034560853	90.6	F:ACATGGAGCACACACTGAGC	80	This study
				R:CGGCTGTCAGTTTCAAACAA		
Interleukin-1 beta-like	*il1b*	XM_034542525	104	F:ATTGTGTTCGAGCTCGGTTC	98	(2)
				R:CGAACTATGGTCCGCTTCTC		
Jumonji, AT rich interactive domain 2b	*jarid2b*	XM_034544699	100	F:CTGGTGTACTTGGATGCGGT	111	This study
				R:AAAACGCATCTCCTCGCTCA		
PHD finger protein 8	*phf8*	XM_034538118	96.4	F:AGTAATGGTGCAGGAAGGGC	103	This study
				R:GGGTTTCGTCAATCTGCAGC		
Radical S-adenosyl methionine domain containing 2	*rsad2*	XM_034563028	92	F:AGGAGAGGGTGAAGGGAGAG	133	(2)
				R:ATCCAGAGGCAGGACAAATG		
Sacsin	*sacs*	XM_034549198	82.9	F:CCAGATTGGTACTGCCTGGT	102	This study
				R:GTCCGAGTTGTCCATGTGTG		
Sacsin-like	*sacs-like*	XM_034562115	90.3	F:CAGACGATGCTAAAGCCACA	111	This study
				R:CGTAGAGAGCAGGACCTTGG		
Toll-like receptor 7	*tlr7*	XM_034560839	92.1	F:GGCAAACTGGAAGAATTGGA	100	(2)
				R:GAAGGGATTTGAGGGAGGAG		
Tripartite motif-containing protein 16-like	*trim16*	XM_034532965.1	97.9	F:GGAGTCGACTAAACATCCAGCA	209	This study
				R:TCGACTCACTTCAGTTCTCTGC		
Vesicle-associated membrane protein 8 (endobrevin)	*vamp8*	XM_034541982	92.8	F:GGTGGCTGGAGTGAAAGACA	144	This study
				R:CGAGCCACTTTCTGAGACGT		
[c]*Interferon regulatory factor 1a*	*irf1a*	XM_034527913	89.6	F:CAAGCCAGATCCCAAGACAT	100	This study
				R:GCTGCCTCTCTTCTTGCTGT		

(Continued)

10.3389/fimmu.2024.1439465

TABLE 1 Continued

Gene name	Symbol	GenBank accession number	[a]E (%)	[b]Nucleotide sequence (5′–3′)	Amplicon size (bp)	Reference
Interferon regulatory factor 1b	*irf1b*	XM_034551153	101	F:CCGGCTTCTCAAACAACTTC	112	This study
				R:GAGTCTTTCTCCGGTTGCTG		
Interferon regulatory factor 2	*irf2*	XM_034543211	101	F:GCTTCCCACGTGTCCTCTAC	110	This study
				R:CGGTGTGGTAGCTGATGAGA		
Interferon regulatory factor 3	*irf3*	XM_034559314	91	F:TCATTGAGGGGAGAAACTGC	118	This study
				R:GTCAGGACCACCTCCACTGT		
Interferon regulatory factor 4a	*irf4a*	XM_034554744	97.5	F:TCAGGAGAGAAGGGACTGGA	120	This study
				R:AACGGTGACGGATAGTGGAG		
Interferon regulatory factor 4b	*irf4b*	XM_034529934	97.5	F:CAGGGAGGACTGTCCCAGTA	108	This study
				R:CCCGTAGCTCTGGATTTCTG		
Interferon regulatory factor 5	*irf5*	XM_034526472	97.5	F:GTCCAGGTTGTTCCTGTCGT	130	This study
				R:TGAACTGCTCCACTGTCTGG		
Interferon regulatory factor 6	*irf6*	XM_034533756	110	F:CTTCGGGCCAGTGAACTTAG	125	This study
				R:AGGCCTCTGTCCATCACATC		
Interferon regulatory factor 7	*irf7*	XM_034535915	104	F:GAATTCGGACGACCCTCATA	140	This study
				R:CTGAGGGGAAGCACTCTACG		
Interferon regulatory factor 8	*irf8*	XM_034528338	99.9	F:CAGCCCTGCAGAGATAGAGG	109	This study
				R:CCTGATGCAGATGAAAAGCA		
Interferon regulatory factor 9	*irf9*	XM_034560118	84.9	F:AGTTCACGGAGGTGATGGAG	119	This study
				R:CTTCGCTCTGGGCTTCTTCT		
Interferon regulatory factor 10	*irf10*	XM_034537944	100	F:TGATCCAGGCTCTGAGGTCT	111	This study
				R:CATCGGGCAACGTCTTTACT		
60S ribosomal protein L32	*rpl32*	XP_034392188.1	100	F:GTAAGCCCAGGGGTATCGAC	107	(2)
				R:GGGCAGCATGTACTTGGTCT		
Elongation factor 1-alpha	*ef1a2a*	XM_034545962.1	98.1	F:GAGAAGATGGGCTGGTTCAAG	87	This study
				R:GGCATCCAGAGCCTCCA		

[a]E, efficiency.
[b]F, forward; R, reverse.
[c]Both *irf1a* (named on NCBI as *irf1-like*) and *irf4b* (named on NCBI as *irf4-like*) were re-named based on that of the closest orthologues in the phylogenetic tree (Figure 3).

96% of the processed reads in each sample were mapped to the lumpfish genome (Supplementary Table S2).

Poly(I:C)-responsive transcripts in lumpfish head kidney

We identified 4,499 upregulated and 3,952 downregulated transcripts by poly(I:C) in the head kidney of lumpfish (Supplementary Table S3, Figures 1B, 6). All of the samples belonging to a given group (i.e., PBS- or poly(I:C)-injected) clustered together based on the expression of all of the identified DETs. In addition, the PBS- and poly(I:C)-injected fish were clearly segregated in the PCA space. PC1 explained 38.7% of the variability, and PC2 explained 10.4% of the variability (Figure 1C).

There were 311 GO terms enriched in the poly(I:C)-induced transcript list including 248 biological processes, five cellular components, and seven molecular functions. The most enriched biological process GO terms were related to "defense response", "cytokine-mediated signaling pathway", and "response to other organisms" (Figure 2). Enriched molecular function GO terms included "immune receptor activity", "cytokine receptor binding", and "interleukin-1 binding". Enriched cellular component GO terms included "chromosome", "nuclear protein-containing complex", and "lipid droplet" (Supplementary Table S4). GO terms with the highest percentage of DETs included "regulation of retinoic acid receptor signaling pathway" (Supplementary Figure S1).

The TPMs of the genes represented by the enriched GO term "response to virus" were used to generate the heatmap plotted in

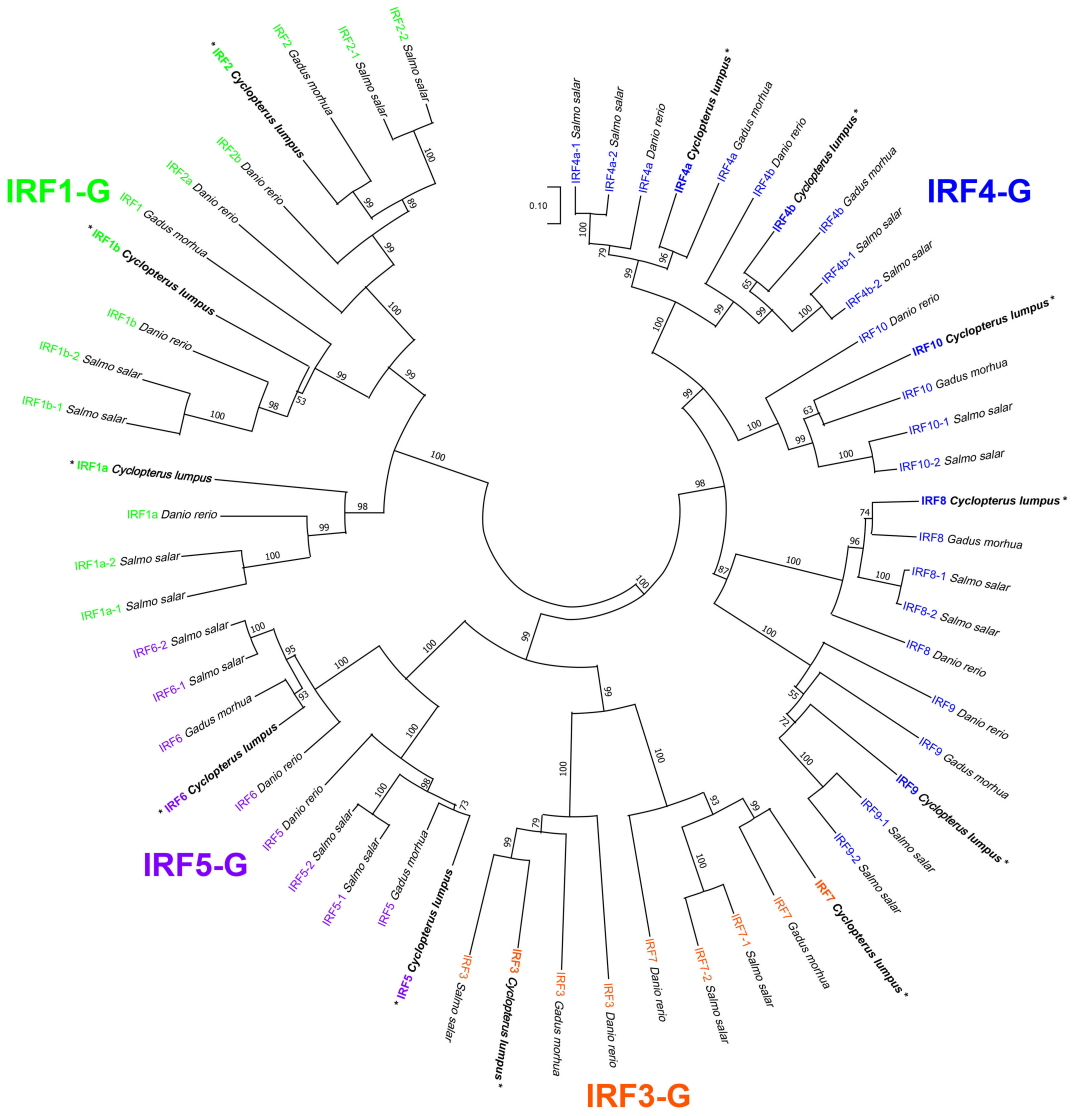

FIGURE 3
Phylogenetic tree analysis of putative interferon regulatory factor (IRF) orthologues across the four teleost superorders. Putative IRF amino acid sequences from a fish representing each of the four teleost superorders, namely, Protacanthopterygii [*Salmo salar* (Atlantic salmon)], Acanthopterygii [*Cyclopterus lumpus* (lumpfish)], Paracanthopterygii [*Gadus morhua* (Atlantic cod)], and Ostariophysi [*Danio rerio* (zebrafish)] were collected from the National Center for Biotechnology Information (NCBI) non-redundant protein database (see Supplementary Table S5). The 59 amino acid sequences were aligned using ClustalW, and the tree was constructed using the Neighbor-Joining method with Poisson correction; the bootstrap test of phylogeny was performed with 10,000 replicates in the MEGA 11 (v.11.0.13) (60) software. The numbers at the branch points represent the bootstrap values, and branch lengths are proportional to calculated evolutionary distances. The scale represents the number of amino acid substitutions per site. The Atlantic salmon IRF paralogues were named as suggested in Clark et al. (2021), with the exceptions being IRF2–1 and IRF2–2, which were named as in Crossman et al. (2023); IRF1a (alias IRF11). The four subgroups—IRF1-G (IRF1 and IRF2), IRF3-G (IRF3 and IRF7), IRF4-G (IRF4, IRF8, IRF9, and IRF10), and IRF5-G (IRF5 and IRF6)—are shown in different colors. Corresponding proteins to transcripts explored using qPCR in the current study are marked by "*".

Figure 7. It showed upregulation of transcripts including *lysosomal trafficking regulator* (*lyst*), *complement component 1, q subcomponent binding protein* (*c1qbp*), *DEAD-box helicase 3 X-linked a* (*ddx3xa*), *interleukin-12 subunit beta* (*il12b*), *stimulator of interferon response cGAMP Interactor 1* (*sting1*), *toll-like receptor 7* (*tlr7*), *cholesterol 25-hydroxylase A* (*ch25ha*), *mitochondrial antiviral signaling protein* (*mavs*), *BCL2 apoptosis regulator B* (*bcl2b*), and *irf2* with poly(I:C) challenge. Also, it showed downregulation of several genes, for example, *vesicle-associated membrane protein 8* (*vamp8*), *spondin2a*, and *scavenger receptor cysteine-rich type 1 protein M130-like.*

To investigate dysregulation in metabolism during a viral mimic challenge, we plotted a heatmap for DETs representing the enriched GO terms "regulation of retinoic acid receptor signaling pathway" and "response to lipid" GO terms (Figures 8A, B). The GO term regulation of the retinoic acid receptor signaling pathway was one of the GO terms with the highest percentage of DETs. Figure 8A shows the upregulation of different transcripts including *tripartite motif*

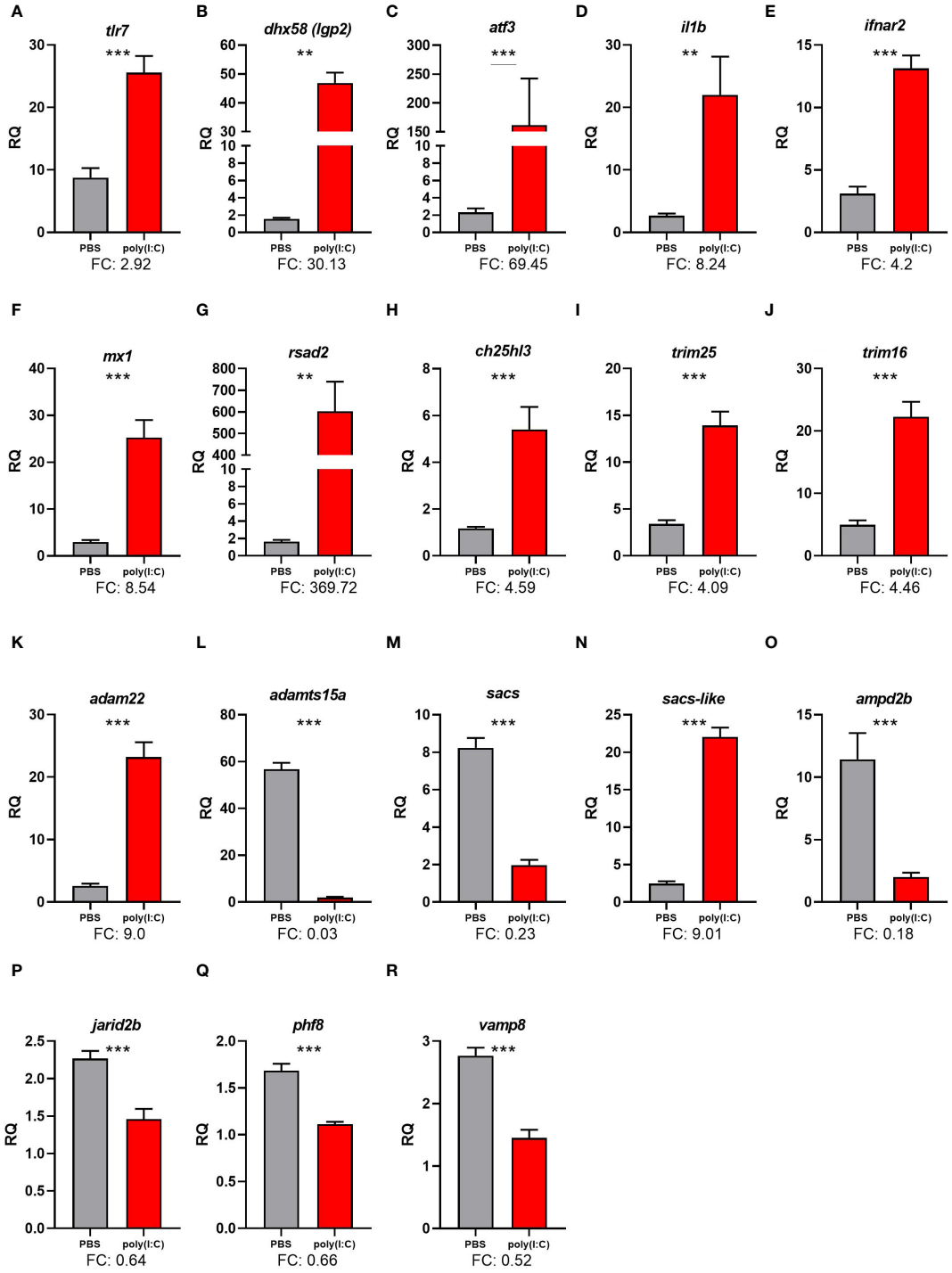

FIGURE 4
qPCR results of selected transcripts that were identified as differentially expressed in response to polyinosinic:polycytidylic acid [poly(I:C)] in RNA-Seq analyses. Transcript levels are presented as mean ± SE relative quantity (RQ) values (i.e., values for the transcript of interest were normalized to both *rpl32* and *ef1a2a* transcript levels and were calibrated to the individual with the lowest normalized expression level of that given transcript). For transcripts exhibiting homogeneity of variance across samples, significance was assessed using t-tests and is denoted with asterisks. For transcripts with unequal variance across samples, significance was assessed using the Mann–Whitney U test and is denoted with underlined asterisks. For both methods, significance levels are "**" for $p \leq 0.01$, and "***" for $p \leq 0.001$. FC, fold-change [mean RQ values for poly(I:C)/mean RQ values for phosphate-buffered saline (PBS)]. The plotted transcripts represent **(A)** *Toll-like receptor 7 (tlr7)*, **(B)** *ATP-dependent RNA helicase lgp2* (*dhx58*), **(C)** *activating transcription factor 3* (*atf3*), **(D)** *Interleukin-1 beta-like* (*il1b*), **(E)** *Interferon alpha/beta receptor 2-like* (*ifnar2*), **(F)** *Interferon-induced GTPbinding protein Mx-like* (*mx1*), **(G)** *Radical S-adenosyl methionine domain containing 2* (*rsad2*), **(H)** *Cholesterol 25-hydroxylase like 3* (*ch25hl3*), *E3 ubiquitin/ISG15 ligase*, **(I)** *TRIM25-like* (*trim25*), **(J)** *Tripartite motif-containing protein 16-like* (*trim16*), **(K)** *ADAM metallopeptidase domain 22* (*adam22*), **(L)** *ADAM metallopeptidase with thrombospondin type 1 motif, 15a* (*adamts15a*), **(M)** *Sacsin* (*sacs*), **(N)** *Sacsin-like* (*sacs-like*), **(O)** *Adenosine monophosphate deaminase 2b* (*ampd2b*), **(P)** *Jumonji, AT rich interactive domain 2b* (*jarid2b*), **(Q)** *PHD finger protein 8* (*phf8*), **(R)** *Vesicle-associated membrane protein 8* (*endobrevin*), vamp8.

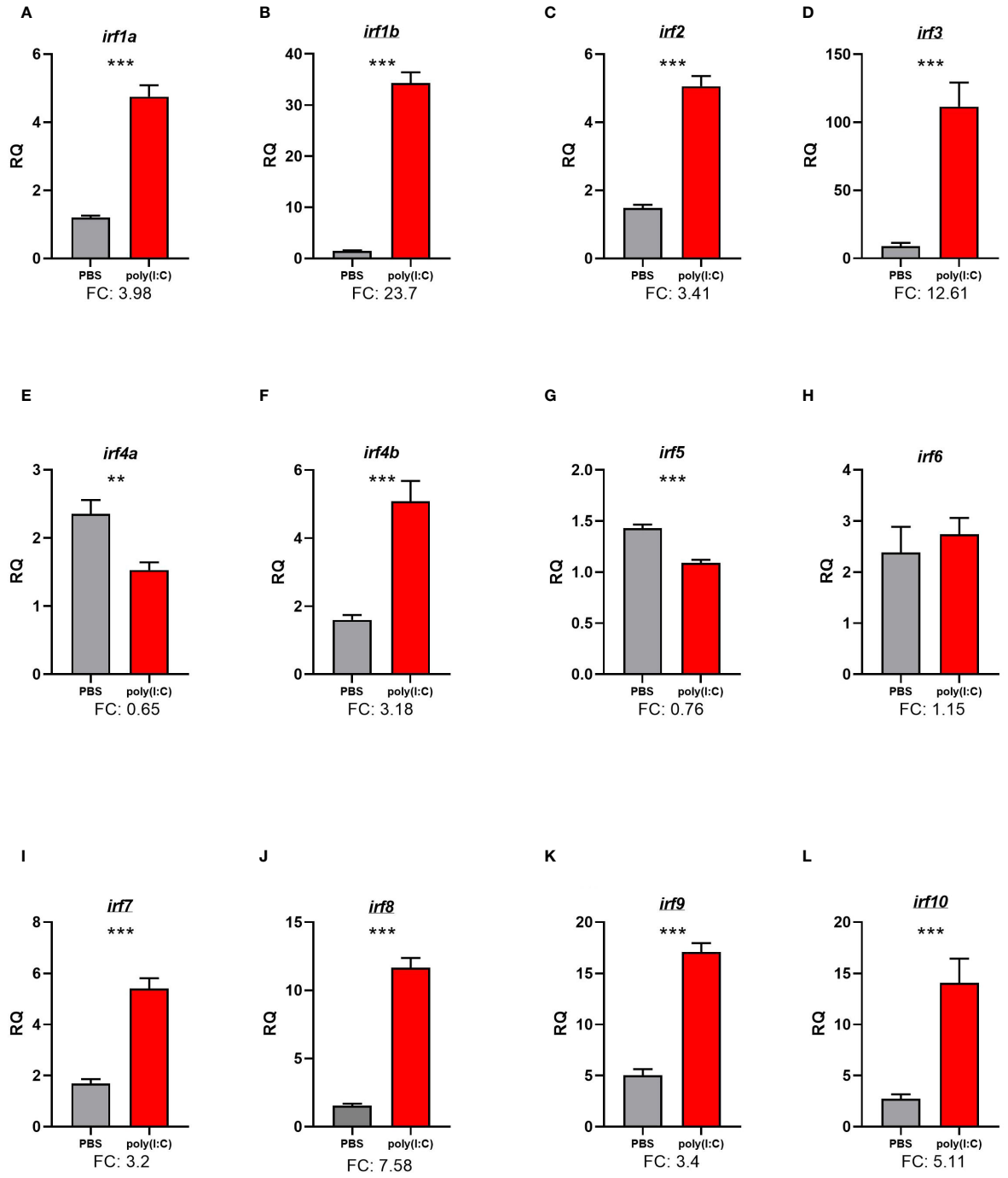

FIGURE 5
qPCR analysis of the response of the 12 *irf* family members in lumpfish to intraperitoneal (IP) challenge with polyinosinic:polycytidylic acid [poly(I:C)]. Transcript levels are presented as mean ± SE relative quantity (RQ) values (i.e., values for the transcript of interest were normalized to both *rpl32* and *ef1a2a* transcript levels and were calibrated to the individual with the lowest normalized expression level of that given transcript). Significance was assessed using t-tests and is denoted with asterisks ("**" for $p \leq 0.01$, and "***" for $p \leq 0.001$). FC, fold-change [mean RQ values for poly(I:C)/mean RQ values for phosphate-buffered saline (PBS)]. The *irf*s with underlined gene symbols were identified as differentially expressed in the RNA-Seq analysis and were validated using qPCR. The *irf*s with non-underlined symbols were not differentially expressed in the RNA-Seq analysis using the preidentified cutoff criteria. Both *irf1a* [named in National Center for Biotechnology Information (NCBI) as *irf1-like*] and *irf4b* (named in NCBI as *irf4-like*) were named based on the closest orthologues in the phylogenetic tree (Figure 3). **(A)** *interferon regulatory factor 1a (irf1a)*, **(B)** *Interferon regulatory factor 1b (irf1b)*, **(C)** *Interferon regulatory factor 2 (irf2)*, **(D)** *Interferon regulatory factor 3 (irf3)*, **(E)** *Interferon regulatory factor 4a (irf4a)*, **(F)** Interferon regulatory factor 4b (irf4a), **(G)** *Interferon regulatory factor 5 (irf5)*, **(H)** *Interferon regulatory factor 6 (irf6)*, **(I)** *Interferon regulatory factor 7 (irf7)*, **(J)** *Interferon regulatory factor 8 (irf8)*, **(K)** *Interferon regulatory factor 9 (irf9)*, **(L)** *interferon regulatory factor 10. (irf10)*.

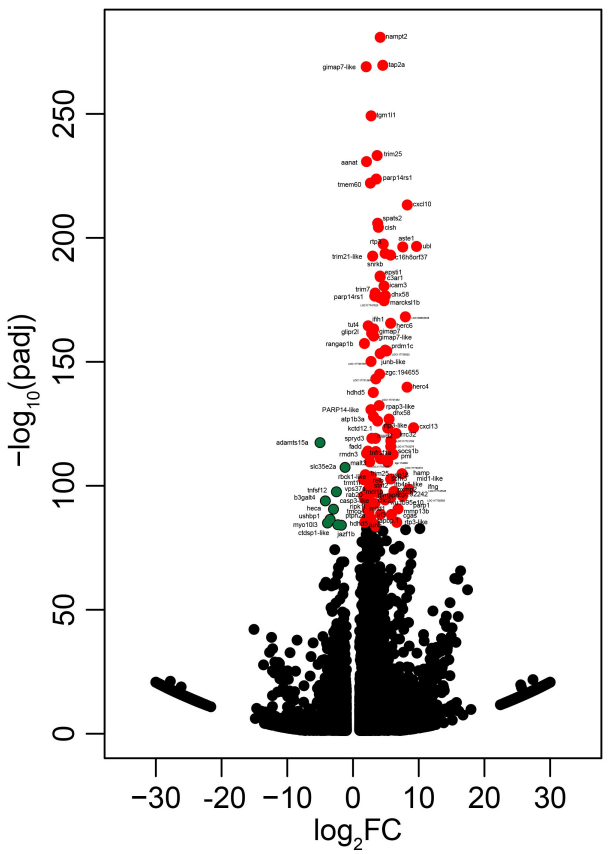

FIGURE 6
Volcano plot reporting $-\log_{10}$ adjusted p-values (padj) against $\log_2$ fold-changes. Dots represent differentially expressed transcripts. The colored dots represent the most significant transcripts from the upregulated and downregulated probes (red and green, respectively) (Supplementary Table S3). Dots are labeled with the gene symbols of the putative human orthologues, and one uncharacterized is labeled with the locus annotation.

containing 16-like (*trim16-like*) and *tripartite motif containing 25-like* (*trim25-like*). Also, it shows downregulation of genes including *dehydrogenase/reductase 3B* (*dhrs3b*), *kruppel-like factor 17* (*klf17*), *c-terminal binding protein 2a* (*ctbp2a*), and others representing *mitogen-activated protein kinase 11-like*, *vesicle-associated membrane protein 8* and *fibroleukin* with poly(I:C) injection.

The GO term "response to lipid" was enriched with a mixture of upregulated and downregulated genes (Figure 8B). For example, *mucosa-associated lymphoid tissue lymphoma translocation protein 1* (*malt1*), *NLR family CARD domain containing 3-like* (*nlrc3l*), and *B-cell lymphoma 2 B* (*bcl2b*) were upregulated with poly(I:C). While *frizzled class receptor 4* (*fzd4*), *annexin a2 receptor* (*anxa2r*), *prostaglandin E receptor 2* (*ptger2a*), *peroxisome proliferator-activated receptor alpha B* (*pparab*), and *peroxisome proliferator-activated receptor gamma coactivator 1 alpha* (*ppargc1a*) were downregulated with poly(I:C) stimulation.

qPCR validation

The qPCR results confirmed the RNA-Seq results for all of the selected transcripts (Supplementary Figure S2). There was a significant correlation ($p = 0.007$; Pearson's coefficient = 0.61) between the qPCR and the RNA-Seq results (Supplementary Figure S2).

The qPCR analysis confirmed the poly(I:C) induction of *tlr7*, *ATP-dependent RNA helicase lgp2* (*dhx58*), *activating transcription factor 3* (*atf3*), *interleukin 1 beta* (*il1b*), *interferon alpha/beta receptor 2* (*ifnar2*), *interferon-induced GTP-binding protein Mx-like* (*mx1*), *radical S-adenosyl methionine domain containing 2* (*rsad2*), *ch25ha*, *trim25*, *trim16*, *ADAM metallopeptidase domain 22* (*adam22*), and *spastic ataxia of Charlevoix-Saguenay* (*sacsin*)-*like* (*sacs-like*) (Figure 4).

The qPCR analysis confirmed the poly(I:C) repression of *ADAM metallopeptidase with thrombospondin type 1 motif 15* (*adamts15a*), *sacs*, *adenosine monophosphate deaminase 2b* (*ampd2b*), *jumonji and at-rich interaction domain containing 2* (*jarid2b*), *histone lysine demethylase phf8* (*phf8*), and *vamp8* (Figure 4).

Lumpfish *irf* family qPCR and phylogenetic analysis

To characterize the response of the 12 *irf* family members in lumpfish stimulated with poly(I:C), their transcript expression levels were assessed using qPCR. Seven members, i.e., *irf1b*, *irf2*, *irf3*, *irf7*, *irf8*, *irf9*, and *irf10*, were identified as dysregulated with poly(I:C) challenge in the RNA-Seq analyses, whereas *irf1a*, *irf4a*, *irf4b*, *irf5*, and *irf6* were not detected as differentially expressed using a cutoff level of LFC = 1.0. With the exception of *irf6*, all *irf* family members subjected to qPCR analysis were found to be poly(I:C)-responsive. The transcript levels of *irf1a*, *irf1b*, *irf2*, *irf3*, *irf7*, *irf8*, *irf9*, and *irf10* were upregulated with poly(I:C) injection when compared with the PBS-injected group. The levels of *irf4a* and *irf5* were suppressed in response to poly(I:C) injection. The levels of *irf6* were not significantly different between the poly(I:C)- and PBS-injected groups (Figure 5).

A total of 59 IRF family members in species representing the four teleost superorders (lumpfish, Acanthopterygii; Atlantic salmon, Protacanthopterygii; zebrafish, Ostariophysi; and Atlantic cod Paracanthopterygii), identified in the GenBank nr protein database, were used to build a phylogenetic tree (Figure 3). As anticipated, the teleost IRF sequences cluster into the four previously defined subgroups: IRF1-G (IRF1 and IRF2), IRF3-G (IRF3 and IRF7), IRF4-G (IRF4, IRF8, IRF9, and IRF10), and IRF5-G (IRF5 and IRF6) (61). The phylogenetic tree shows that lumpfish IRF2, IRF4a, IRF4b, IRF5, IRF6, IRF7, IRF8, and IRF10 are evolutionarily more closely related to the Atlantic cod compared with the Atlantic salmon or zebrafish putative orthologues (Figure 3). However, the tree also reveals that lumpfish IRF3 is most closely related to Atlantic salmon IRF3 (i.e., sharing a branch point); likewise, lumpfish IRF9 is more closely related to Atlantic salmon IRF9 paralogues (IRF9–1 and IRF9–2, arising from duplication in the salmonid lineage) than to Atlantic cod or zebrafish IRF9 sequences (Figure 3). Finally, for IRF1a and IRF1b, zebrafish and Atlantic salmon sequences are more closely related to each other than either are to the lumpfish putative orthologous sequences.

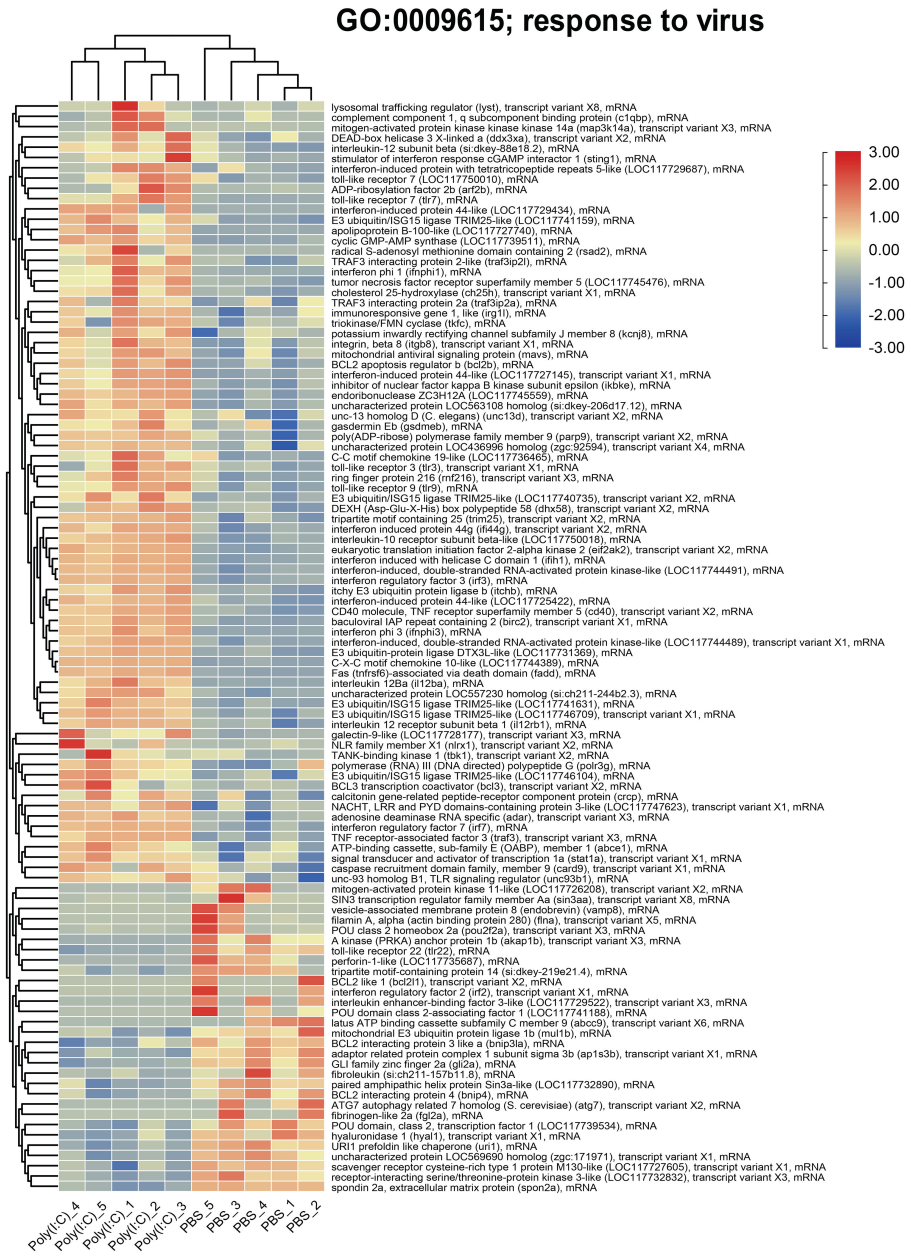

FIGURE 7
Heatmap and hierarchical clustering of differentially expressed transcripts (DETs) associated with "response to virus" using transcripts per million (TPMs; log_2 transformed).

Discussion

The current RNA-Seq results detected an extensive global gene expression response (i.e., 4,499 upregulated and 3,952 downregulated DETs) in the head kidney of poly(I:C)-challenged lumpfish, shedding light on the molecular mechanisms and immune pathways involved in response to this viral mimic. GO term analyses identified enriched immune-related GO terms consistent with an immune response to a viral challenge based on the current knowledge about molecular antiviral responses in teleost fish (13, 14). Several leading immune-related GO terms (e.g., "antigen processing and presentation of peptide antigen via MHC class I", "leukocyte apoptotic process", "pattern recognition receptor signaling pathway", "response to virus", "type I interferon signaling pathway", and "NIK/NF-kappaB signaling") were primarily represented by poly(I:C)-induced DETs compared with downregulated ones (Figure 2B). Many of the leading GO terms within cellular component and biological process categories (e.g., "RNA splicing, via transesterification reactions with bulged adenosine as nucleophile", "chromosome", "nuclear protein-containing complex", and "cell migration") were represented by a higher number of downregulated DETs compared with upregulated

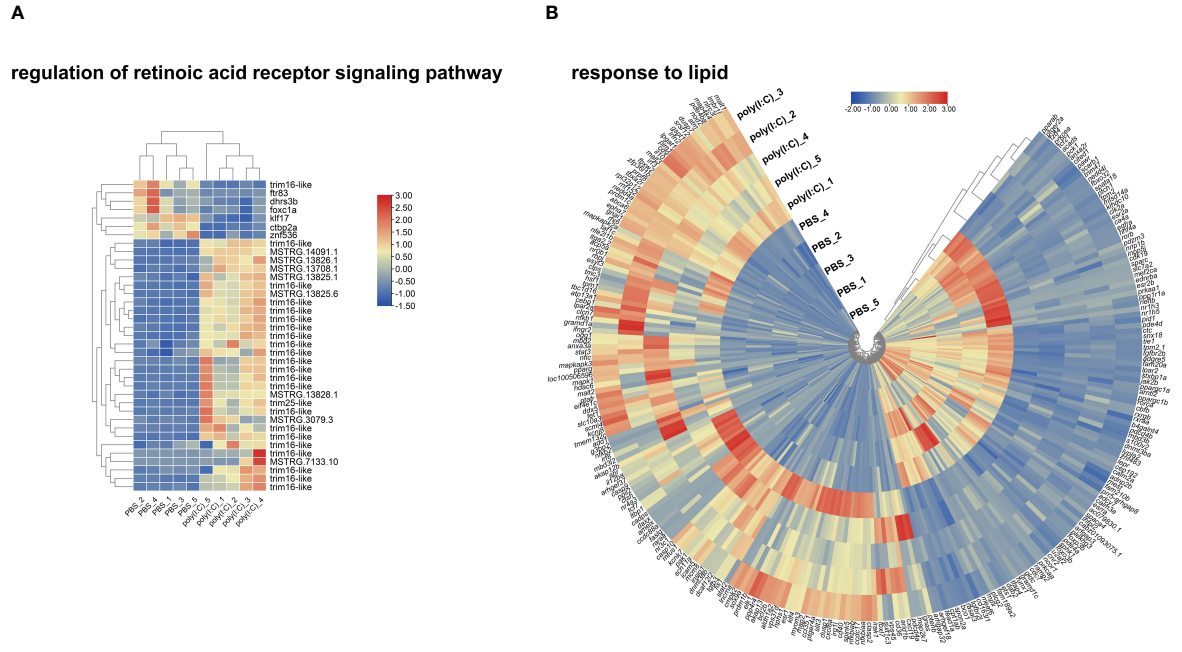

FIGURE 8
Heatmap and hierarchical clustering of differentially expressed transcripts (DETs) that participated in enriching "regulation of retinoic acid receptor signaling pathway" in panel **(A)** and "response to lipid" in panel **(B)** using transcripts per million (TPM; $\log_2$ transformed).

DETs. These results suggest a possible shift in cellular activity toward fighting infection, highlighting gene expression regulation patterns toward the induction of immune-relevant genes.

Our GO term enrichment results generally agreed with those of a recent *in vitro* study (32) investigating the effects of poly(I:C) on the transcriptome of lumpfish primary leukocytes after 24 h of exposure, especially in terms of general immune-relevant GO terms such as "cytokine receptor binding" and "response to virus". However, the present study identified a more varied suite of enriched biological processes, including GO terms related to cell migration (e.g., "leukocyte migration"), apoptosis (e.g., "leukocyte apoptotic process"), and adaptive immunity (e.g., "antigen processing and presentation of peptide antigen via MHC class I"), which may be a consequence of analyzing transcriptome changes in head kidney samples as opposed to primary leukocytes. Notably, in Rao et al. (32), biological processes associated with the metabolism of nitrogen-containing compounds (e.g., "peptide metabolic process") were dominant. Our analyses also identified enriched GO terms related to retinoic acid (e.g., "regulation of retinoic acid receptor signaling pathway") like in Rao et al. (32) but also other terms associated with lipids (e.g., "lipid droplet" and "response to lipid"). We anticipate that single-cell RNA-Seq in lumpfish will likely allow the assignment of transcript expression changes to specific cells within the head kidney, elucidating GO terms enriched in each type of cell.

During viral infection, the host's metabolism undergoes various changes to combat the virus and support the immune response. This may be evidenced in the current study by enrichment in GO terms relevant to metabolism (e.g., GO terms related to lipid and retinoic acid metabolism; Supplementary Table S3, Figures 2A, B). In mammals, lipid droplets (62, 63) and retinoic acid (64) are key players in the viral infection mechanisms and the inflammatory processes they trigger. The GO term "regulation of retinoic acid receptor signaling pathway" was one of the GO terms with the highest percentage of DETs (Supplementary Figure S1). The heatmap for "regulation of retinoic acid receptor signaling pathway" (Figure 8A) shows that several *trim16-like* transcripts were upregulated by poly(I:C), except for one downregulated transcript (accession number: XM_034555257.1). The heatmap also showed decreased transcript levels for *ftr83* (*tripartite motif-containing protein 11*), *dhrs3b*, *foxc1a* (*forkhead box C1a*), *klf17* (*krüppel-like factor 17*), *ctbp2a* (*C-terminal binding protein 2a*), and *znf536* (*zinc finger protein 536*) in the poly(I:C)-injected fish (Figure 8A). These poly(I:C)-responsive genes encode proteins involved in regulating the retinoid metabolic process (*dhrs3b*), regulation of cell proliferation (*foxc1a*), differentiation (*klf17*), and response to external stress (e.g., *ctbp2a* and *znf536*) (65–68). Their regulation may be instrumental to mounting the immune response to the viral mimic challenge in lumpfish and highlights the role of vitamin A (retinoic acid) during viral infection in lumpfish. However, vitamin A modulation of the immune response during viral infection requires further research.

Several upregulated and downregulated genes by poly(I:C) identified herein contributed to enriching the GO term "response to lipid" (Figure 8B). For example, transcripts encoding receptors (e.g., *fzd4*, *anxa2r*, and *ptger2a*) and transcription factors involved in metabolism, energy homeostasis, and immunomodulation (69) (e.g., *pparab* and *ppargc1a*) were found downregulated by the viral mimic challenge (Figure 8B). Others were found to be upregulated, for example, transcripts encoding proteins involved in the

activation of the transcription factor NF-κB (i.e., *malt1*), intracellular pattern recognition receptors previously suggested to regulated innate immune response (70) (e.g., *nlrc3l*), and apoptosis (e.g., *bcl2b*) (71). Overall, the enrichment of "response to lipid" and other lipid-related GO terms may highlight the role of lipids during viral infection (62, 72–74), emphasizing the potential of dietary lipids to modulate the antiviral fish immune response.

The enriched GO term "response to virus" was predominantly represented by upregulated transcripts involved in antiviral immune defense [e.g., *mavs*, and *signal transducer and activator of transcription 1a* (*stat1a*)] (75), inflammation (e.g., *ch25h*, *tumor necrosis factor-alpha*, and *il6*) (76), oxidative stress (e.g., *c1qbp*) (77), and apoptosis regulation (e.g., *bcl2b*) (78). Although to a lesser extent, this GO term was also represented by poly(I:C)-repressed genes related to various cellular process, like vesicle trafficking (e.g., *vamp8*) (79) and autophagy (e.g., *autophagy related 7 homolog* and *atg7*) (80) as well as deubiquitination and protein metabolism (e.g., *mitochondrial E3 ubiquitin protein ligase 1b* and *mul1b*) (81). The dysregulated transcripts representing this GO term indicate the involvement of genes with diverse functions in the antiviral immune response.

qPCR results of lumpfish response to poly (I:C)

In the current study, all of the 18 genes used in the qPCR validated the RNA-Seq, indicating the reliability of the RNA-Seq results (Supplementary Figure S1). In the qPCR study, two pattern recognition receptor (PRR)-encoding genes, *tlr7* and *dhx58*, were found to be upregulated by poly(I:C). *Tlr7* contributed to 59 enriched GO terms, including "NIK/NF-kappaB signaling", "pattern recognition receptor signaling pathway", "response to virus", and "regulation of cytokine production". Similarly, *dhx58* contributed to enriching 83 GO terms, including "response to virus", "positive regulation of intracellular signal transduction", and "regulation of response to stimulus" (Supplementary Table S3). PRRs detect conserved pathogen-associated molecular patterns (PAMPs) and consequently activate the innate immune response (82). Upon recognition of viral single-stranded RNA molecules, TLR7 triggers the production of type I IFNs and pro-inflammatory cytokines, which are critical for the host's antiviral response (83–85). DHX58 is a member of the RLR family and an ATP-dependent RNA helicase, also known as LGP2 or RIG-I-like receptor 1 (RLR1), and has several antiviral roles such as regulation of TLRs and RLRs (86). *Dhx58* was also found to be upregulated in Atlantic cod spleen and brain after IP injection with poly(I:C) in the brains of nodavirus-positive Atlantic cod (87, 88) and lumpfish infected with *R. salmoninarum* (2). *Dhx58* was upregulated in lumpfish larvae after oral immunization against *Vibrio anguillarum* (8); also, it was highly upregulated in lumpfish leukocytes after stimulation with poly(I:C) (32). The results of previous and current studies suggest that DHX58 plays a role in both the antibacterial and antiviral immune responses of lumpfish, whereas TLR7 dysregulation occurs following the activation of its antiviral responses.

In the current study, the transcript levels of *atf3* were strongly upregulated (over 69-fold) in the head kidneys of lumpfish stimulated with poly(I:C), as it was previously reported for Atlantic salmon macrophages (13) and Atlantic cod spleen (89). Mammalian ATF3 is activated by cellular stress response pathways and plays a role in the host's immune response to viral infections (89, 90). ATF3 upregulation during viral infections promotes a stronger immune response and increased resistance in various mammalian species including mice and humans (91–93). Additionally, human ATF3 can directly inhibit the replication of some viruses by suppressing their transcription (93) and regulating the expression of the host's immune-related genes such as IFN-induced and pro-inflammatory cytokines (94). While our results indicate the involvement of *atf3* in lumpfish's antiviral immune response, its viral inhibitory and regulatory functions are yet to be investigated in this species.

Two lumpfish transcripts encoding proteins classified as cytokines and cytokine receptors (i.e., *il1b* and *ifnar2*) were found to be over fourfold upregulated by poly(I:C). Several ILs contributed to enriching key GO terms, including "response to interleukin-1", "signaling receptor binding", "leukocyte migration", and "defense response to other organism" (Supplementary Table S3). IL1B is a pro-inflammatory cytokine mediating the immune response of fish to viral and bacterial infection (95, 96). The production of IL1B by immune cells such as macrophages is triggered by the detection of viral nucleic acid by PRRs, such as TLRs (97). Previous studies showed *il1b* induction in the kidney of Sockeye salmon (*Oncorhynchus nerka*) infected with infectious hematopoietic necrosis virus (IHNV) (95, 96). Type I interferons, including IFNA, are produced following viral detection (98) and can activate cellular antiviral immune mechanisms (e.g., the expression of IFN-stimulated genes) and the recruitment of immune cells such as natural killer cells and T cells (98). It was previously reported that IFNA inhibited Salmonid Alphavirus Subtype 3 replication in a salmon cell line (i.e., TO cells originated from head kidney leukocytes) (99). Additionally, *ifna* was found upregulated in the head kidney of Atlantic salmon with New Piscine Orthomyxovirus (POMV) infection (100). These results collectively emphasize the conserved roles of IL1B and IFNA in the antiviral responses of lumpfish as in other teleost fishes.

Antiviral markers *mx1*, *rsad2* (alias *viperin*), and *ch25hl3* were found upregulated by poly(I:C) stimulation. *Rsad2* and *ch25hl3* contributed to enriching several GO terms, e.g., "response to virus" (Figure 7) and "defense response to other organism" (Supplementary Table S3). Atlantic salmon *mx* and *rsad2* showed strong upregulation in ISAV-infected TO cells (101), poly(I:C)-stimulated macrophages (13), and the head kidney of poly(I:C)-injected fish (55). MX1 plays a role in the salmon immune response to viral infections, notably myxoviruses such as ISAV (102), and spring viraemia of carp virus (SVCV) (103). The poly(I:C)-induced *mx1* can enhance resistance to viral infections in salmonids (104). RLR-activated RSAD2 (105) regulates the RLR signaling pathway through phosphorylation of downstream targets, e.g., MAVS (mitochondrial antiviral-signaling protein) and IRF3 [interferon regulatory factor 3; one of the top upregulated transcripts in the

current study], leading to amplified antiviral response (106). CH25H plays a role in the immune response of salmon to bacterial infections (e.g., *Renibacterium salmoninarum* and *Piscirickettsia salmonis*) (49, 107, 108). Viral infections can lead to increased expression of *ch25h* in salmon (109). Additionally, it has been found that fish CH25H can directly inhibit the replication of some viruses (110). Altogether, *mx1*, *rsad2*, and *ch25hl3* responses seen herein reflect the activation of antiviral agents by poly(I:C) in lumpfish and suggest these transcripts as potential antiviral biomarkers for this species.

The mRNA levels of *trim16* and *trim25*, which play roles as immune regulators, were upregulated by poly(I:C) in lumpfish. TRIM25 shared in enriching several GO terms, such as "signaling receptor binding", "response to virus", "regulation of cytokine production", and "response to lipid" (Supplementary Table S3). TRIM16 and TRIM25 are E3 ubiquitin ligases that play key roles in the host's immune response to viral infections (111). Lumpfish leukocytes stimulated with poly(I:C) showed higher levels of *trim25* from 6 to 24 h post-challenge (32). In Atlantic salmon TO cells, *trim16* and *trim25* were strongly upregulated by ISAV infection (101). The literature regards TRIM16L as a negative regulator of IFN-mediated antiviral responses in fish. However, the role of this protein in antiviral immune responses may be cell type-dependent, based on the available gene expression regulation data from fish and human cells exposed to viral infection (65, 112, 113). Human TRIM25 is reported to be able to target and degrade viral proteins (e.g., influenza A virus), thereby inhibiting viral replication (114). The conserved induction of *trim16* and *trim25* found in the current study highlights the importance of these factors in the antiviral response of lumpfish and suggests their role in the regulatory mechanism by which lumpfish respond to viral pathogens.

Adam22 was found upregulated with poly(I:C) stimulation and contributed to enriching "organonitrogen compound metabolic process" GO term (Supplementary Table S3). In a similar direction to our results, transcript levels of *adam22* were previously found upregulated in the brain of Atlantic cod injected with poly(I:C) (88). Human ADAM22 has been shown to mediate the entry of the human rhinovirus (HRV) (115). However, the role of ADAM22 during antiviral immune response remains to be elucidated in lumpfish.

Lumpfish *sacs-like* (accession number: XM_034562115) was upregulated by poly(I:C) stimulation, whereas its paralogue (XM_034549198) was poly(I:C)-suppressed (Figure 4, Supplementary Table S3). The levels of Atlantic cod *sacs* have been reported to increase in the brain of nodavirus carrier fish (88) and Atlantic cod macrophages stimulated with poly(I:C) (14). It was also found upregulated in the brain of sockeye salmon infected with IHNV (116). The current study results may indicate paralogue-specific functions for lumpfish *sacs* genes. Opposite transcriptional regulation was previously reported for some paralogues in zebrafish and salmon (117, 118). However, further research is needed to understand the implications of the different *sacs* regulation patterns in lumpfish antiviral immune responses.

We identified several immune-related genes downregulated in poly(I:C)-stimulated lumpfish. The transcript levels of *ampd2b* were found to be downregulated by poly(I:C) and contributed to enriching the "GTP metabolic process" GO term. AMPD2 is an enzyme involved in the regulation of cellular energy levels, i.e., purine metabolism by converting adenosine monophosphate (AMP) to inosine monophosphate (IMP) (119). Therefore, the downregulation of *ampd2b* may indicate a decrease in energy production or utilization in the head kidney cells of the lumpfish, which could be part of the response to the stress caused by the viral mimic. Transcripts encoding proteins that are involved in epigenetic regulation and histone modification, such as *jarid2b* (120) and *phf8* (121), were suppressed (qPCR and RNA-Seq results) in the head kidney of the poly(I:C)-injected fish (Figure 4, Supplementary Table S3). *Jarid2b* contributed to enriching several GO terms, including "regulation of cellular protein metabolic process", and *phf8* contributed to enriching different GO terms including "immune system development" (Supplementary Table S4). Although histone modifications were found to play a protective role in the body's defense against viral infections (122), the functions of *jarid2b* and *phf8* in epigenetic interaction and immune response of teleost fish require further study. The transcript levels of *vamp8* were downregulated in both the RNA-Seq and qPCR results (Figure 4, Supplementary Table S3). Also, they shared in enriching several GO terms, e.g., "regulation of cell activation" and "positive regulation of multicellular organismal process" (Supplementary Table S4). VAMP8 plays several roles in intracellular membrane trafficking and fusion (123). VAMP8 may also be implicated in the release of cytokine and the inhibition of phagocytosis (124). The downregulation of *vamp8* may be part of the above-hypothesized inhibited cellular function or the immune response regulation.

Different members of *irf* family response to poly(I:C)

IRFs are a family of transcription factors that play a key role in the host's immune response to viral infections, especially in regulating IFN and interferon-stimulated genes (125). In the current study, the qPCR results showed that *irf1a*, *irf1b*, *irf2*, *irf3*, *irf4b*, *irf7*, *irf8*, *irf9*, and *irf10* were significantly and strongly upregulated (FC range, 3.2 for *irf4b* and *irf7* to 23.7 for *irf1b*) by poly(I:C) injection (Figure 5). Similar to qPCR results, the RNA-Seq also identified significant induction of *irf1b*, *irf2*, *irf3*, *irf7*, *irf8*, *irf9*, and *irf10* by poly(I:C) (Supplementary Table S3, Figure 5). Various *irf*s (e.g., *irf1*, *irf2*, *irf3*, *irf4b*, *irf7*, *irf9*, and *irf10*) (46) were previously found upregulated with poly(I:C) or viral infection in teleost species (13, 126–129). The *irf* family members (i.e., *irf1*, *irf2*, *irf3*, *irf7*, *irf8*, and *irf10*) detected in our transcriptomic analysis contributed to enriching various GO terms, for example, "pattern recognition receptor signaling pathway", "response to type I interferon", "regulation of signaling", and "cytokine production". In contrast, *irf9* was only involved in enriching "cytokine production". These IRFs have been shown to play several roles in the activation of innate immunity and the production of type I interferons, which are important in the defense against viral infections (46, 47). IRF1 is a negative regulator of cytokine-

induced cell proliferation in mammals (130). It has been reported that *irf2* positively regulates the antiviral responses of large yellow croaker (*Larimichthys crocea*) (129). IRF7 and IRF3, key family members involved in antiviral responses, are activated downstream of the RLR and RLR pathways and enhance the expression of several immune genes such as IFNs (131). Human IRF8 supports the rapid expansion of virus-specific natural killer cells by enhancing the expression of genes involved in the cell cycle (132). IRF9 mediates the type I interferon responses, resulting in the production of IFN-induced genes (133). Zebrafish IRF 2, 4b, and 10 were suggested to be negative regulators of IFN (134), indicating that their role in the host's antiviral response may be different among species. The induction of *irf* genes by poly(I:C), alongside dysregulation of several genes involved in TLR, RLR, and IFN pathways seen herein, highlights the importance of these transcription factors in antiviral responses of lumpfish. However, despite conserved structure, IRF family members may have species-specific regulatory functions (135, 136); further studies are needed to functionally characterize the lumpfish IRFs.

Unlike other lumpfish *irf*s studied here, *irf4a* and *irf5* were significantly downregulated (less than twofold) in response to poly(I:C). IRF4 was previously reported to play a role in the differentiation of immune cells and the regulation of the immune response (137–139). In agreement with these findings, seabream *irf5* was found to be downregulated with NNV at 12 h post-infection (140). Poly(I:C)-dependent *irf4a* and *irf5* downregulation seen herein suggest their potential role in the regulation of antiviral responses in lumpfish.

The phylogenetic analysis of IRF sequences from lumpfish, Atlantic salmon, Atlantic cod, and zebrafish was used to examine the evolutionary history of IRF family members in lumpfish in the current study. The majority of lumpfish IRF family members (e.g., IRF2, IRF4a, IRF4b, IRF5, IRF6, IRF7, and IRF10) were grouped with the corresponding Atlantic cod orthologues. Overall, the phylogenetic tree suggests a high degree of similarity and evolutionary conservation between the IRF family members in lumpfish and their orthologues in other species. The observed grouping supports the notion that these specific IRF genes have been conserved over evolutionary time in teleost fishes, highlighting their functional importance across species, e.g., lumpfish and Atlantic cod. This finding contributes to our understanding of the evolutionary relationships and conservation of IRF genes in lumpfish.

Conclusion

Our findings suggest that poly(I:C) injection dysregulated diverse pathways associated with the antiviral immune system, cellular differentiation, cytokine production and response, NF-κB signaling, response to retinoic acid and lipids, and cell migration in the lumpfish head kidney. The leading GO terms related to cellular processes were enriched with more downregulated transcripts than the upregulated ones (e.g., "chromosome"). In contrast, GO terms with immune-relevant enriched pathways were dominated by upregulated genes. Our qPCR results validated the upregulation of genes involved in innate immunity and antiviral defense mechanisms and the downregulation of those with putative roles in cellular processes (e.g., histone modification: *jarid2b* and *phf8*).

The regulation of several lumpfish *irf* family members with poly (I:C) injections suggests their involvement in the host's antiviral response. However, the functional characterization of IRF family members in lumpfish requires additional investigation. The results of the current study provide valuable insight into the underlying mechanisms of the induction of the innate immune system using poly(I:C) and suggest potential targets for developing therapeutic strategies and evaluating vaccine efficacy in lumpfish.

Data availability statement

The datasets presented in this study can be found in online repositories. The names of the repository/repositories and accession number(s) can be found below: PRJNA1082277 (SRA).

Ethics statement

All procedures in the present study were approved (Protocol numbers: 17-03-RG and 18-01-MR) by the Animal Care Committee of Memorial University, following the guidelines of the Canadian Council on Animal Care and in accordance with ARRIVE guidelines (https://arriveguidelines.org). The study was conducted in accordance with the local legislation and institutional requirements.

Author contributions

ME: Conceptualization, Data curation, Formal analysis, Funding acquisition, Investigation, Methodology, Project administration, Resources, Software, Supervision, Validation, Visualization, Writing – original draft, Writing – review & editing. SK: Formal analysis, Writing – review & editing. KE: Writing – original draft, Investigation, Writing – review & editing. AC-S: Investigation, Writing – review & editing. JH: Writing – original draft, Writing – review & editing. XX: Writing – original draft, Writing – review & editing. HP: Writing – original draft, Writing – review & editing. RG: Writing – original draft, Writing – review & editing. JS: Writing – original draft, Writing – review & editing. MR: Conceptualization, Data curation, Formal analysis, Funding acquisition, Investigation, Methodology, Project administration, Resources, Software, Supervision, Validation, Visualization, Writing – original draft, Writing – review & editing.

Funding

The author(s) declare financial support was received for the research, authorship, and/or publication of this article. This study was funded by a Natural Sciences and Engineering Research Council of Canada (NSERC) Discovery Grant to MLR (2020–04519) and an Ocean Frontier Institute Vitamin Research Fund award to RLG and HP.

Acknowledgments

We would like to thank the JBARB team for helping with rearing the fish. We want to thank the Atlantic Computational Excellence Network (ACENET) and Compute Canada for facilitating the computational resources for the RNA-Seq data bioinformatics analyses.

Conflict of interest

The authors declare that the research was conducted in the absence of any commercial or financial relationships that could be construed as a potential conflict of interest.

Publisher's note

All claims expressed in this article are solely those of the authors and do not necessarily represent those of their affiliated organizations, or those of the publisher, the editors and the reviewers. Any product that may be evaluated in this article, or claim that may be made by its manufacturer, is not guaranteed or endorsed by the publisher.

Supplementary material

The Supplementary Material for this article can be found online at: https://www.frontiersin.org/articles/10.3389/fimmu.2024.1439465/full#supplementary-material

References

1. Gendron RL, Hyde T, Paradis H, Cao T, Machimbirike VI, Segovia C, et al. CD45 in ocular tissues during larval and juvenile stages and early stages of *V. Anguillarum* infection in young lumpfish (*Cyclopterus lumpus*). *Fish Shellfish Immunol.* (2022) 128:523–35. doi: 10.1016/j.fsi.2022.08.023

2. Gnanagobal H, Cao T, Hossain A, Dang M, Hall JR, Kumar S, et al. Lumpfish (*Cyclopterus lumpus*) is susceptible to *Renibacterium Salmoninarum* infection and induces cell-mediated immunity in the chronic stage. *Front Immunol.* (2021) 12:733266. doi: 10.3389/fimmu.2021.733266

3. Powell A, Treasurer JW, Pooley CL, Keay AJ, Lloyd R, Imsland AK, et al. Use of lumpfish for sea-lice control in salmon farming: challenges and opportunities. *Rev Aquac.* (2018) 10:683–702. doi: 10.1111/raq.12194

4. Torrissen O, Jones S, Asche F, Guttormsen A, Skilbrei OT, Nilsen F, et al. Salmon lice – impact on wild salmonids and salmon aquaculture. *J Fish Dis.* (2013) 36:171–94. doi: 10.1111/jfd.12061

5. Snieszko SF. "9 - NUTRITIONAL FISH DISEASES." In: Halver JE, editor. *Fish Nutrition*. Academic Press (1972). p. 403–37. doi: 10.1016/B978-0-12-319650-7.50014-6

6. Guðmundsdóttir S, Vendramin N, Cuenca A, Sigurðardóttir H, Kristmundsson A, Iburg TM, et al. Outbreak of viral haemorrhagic septicaemia (VHS) in lumpfish (*Cyclopterus lumpus*) in Iceland caused by VHS virus genotype IV. *J Fish Dis.* (2019) 42:47–62. doi: 10.1111/jfd.12910

7. Tollaksvik T. (2023). The University of Bergen. Available online at: https://bora.uib.no/bora-xmlui/handle/11250/3085928 (Accessed December 1, 2023).

8. Dang M, Cao T, Vasquez I, Hossain A, Gnanagobal H, Kumar S, et al. Oral Immunization of Larvae and Juvenile of Lumpfish (*Cyclopterus lumpus*) against Vibrio Anguillarum Does Not Influence Systemic Immunity. *Vaccines (Basel).* (2021) 9:819. doi: 10.3390/vaccines9080819

9. Erkinharju T, Dalmo RA, Hansen M, Seternes T. Cleaner fish in aquaculture: review on diseases and vaccination. *Rev Aquac.* (2021) 13:189–237. doi: 10.1111/raq.12470

10. Erkinharju T, Strandskog G, Vågnes Ø, Hordvik I, Dalmo RA, Seternes T. Intramuscular vaccination of Atlantic lumpfish (*Cyclopterus lumpus* L.) induces inflammatory reactions and local immunoglobulin M production at the vaccine administration site. *J Fish Dis.* (2019) 42:1731–43. doi: 10.1111/jfd.13101

11. Erkinharju T, Lundberg MR, Isdal E, Hordvik I, Dalmo RA, Seternes T. Studies on the antibody response and side effects after intramuscular and intraperitoneal injection of Atlantic lumpfish (*Cyclopterus lumpus* L.) with different oil-based vaccines. *J Fish Dis.* (2017) 40:1805–13. doi: 10.1111/jfd.12649

12. Erkinharju T, Dalmo RA, Vågsnes Ø, Hordvik I, Seternes T. Vaccination of Atlantic lumpfish (*Cyclopterus lumpus* L.) at a low temperature leads to a low antibody response against *Aeromonas salmonicida*. *J Fish Dis.* (2018) 41:613–23. doi: 10.1111/jfd.12760

13. Eslamloo K, Xue X, Hall JR, Smith NC, Caballero-Solares A, Parrish CC, et al. Transcriptome profiling of antiviral immune and dietary fatty acid dependent responses of Atlantic salmon macrophage-like cells. *BMC Genomics*. (2017) 18:706. doi: 10.1186/s12864-017-4099-2

14. Eslamloo K, Xue X, Booman M, Smith NC, Rise ML. Transcriptome profiling of the antiviral immune response in Atlantic cod macrophages. *Dev Comp Immunol.* (2016) 63:187–205. doi: 10.1016/j.dci.2016.05.021

15. Ruyra A, Torrealba D, Morera D, Tort L, MacKenzie S, Roher N. Zebrafish liver (ZFL) cells are able to mount an anti-viral response after stimulation with Poly (I:C). *Comp Biochem Physiol B Biochem Mol Biol.* (2015) 182:55–63. doi: 10.1016/j.cbpb.2014.12.002

16. Lulijwa R, Alfaro AC, Merien F, Burdass M, Meyer J, Venter L, et al. Metabolic and immune responses of Chinook salmon (*Oncorhynchus tshawytscha*) smolts to a short-term poly (I:C) challenge. *J Fish Biol.* (2020) 96:731–46. doi: 10.1111/jfb.14266

17. Jensen I, Albuquerque A, Sommer A-I, Robertsen B. Effect of poly I:C on the expression of Mx proteins and resistance against infection by infectious salmon anaemia virus in Atlantic salmon. *Fish Shellfish Immunol.* (2002) 13:311–26. doi: 10.1006/fsim.2001.0406

18. Andresen AMS, Gjøen T. Chitosan nanoparticle formulation attenuates poly (I:C) induced innate immune responses against inactivated virus vaccine in Atlantic salmon (*Salmo salar*). *Comp Biochem Physiol D Genomics Proteomics*. (2021) 40:100915. doi: 10.1016/j.cbd.2021.100915

19. Nishizawa T, Takami I, Yoshimizu M, Oh M-J. Required dose of fish nervous necrosis virus (NNV) for Poly(I:C) immunization of sevenband grouper *Epinephelus septemfasciatus*. *Aquaculture*. (2011) 311:100–4. doi: 10.1016/j.aquaculture.2010.12.009

20. Nishikiori M, den Boon JA, Unchwaniwala N, Ahlquist P. Crowning touches in positive-strand RNA virus genome replication complex structure and function. *Annu Rev Virol.* (2022) 9:193–212. doi: 10.1146/annurev-virology-092920-021307

21. Wu SX, Ahlquist P, Kaesberg P. Active complete *in vitro* replication of nodavirus RNA requires glycerophospholipid. *Proc Natl Acad Sci U.S.A.* (1992) 89:11136–40. doi: 10.1073/pnas.89.23.11136

22. Bandín I, Souto S. Betanodavirus and VER disease: A 30-year research review. *Pathogens*. (2020) 9:106. doi: 10.3390/pathogens9020106

23. Sandlund L, Mor SK, Singh VK, Padhi SK, Phelps NBD, Nylund S, et al. Comparative molecular characterization of novel and known piscine toti-like viruses. *Viruses*. (2021) 13:1063. doi: 10.3390/v13061063

24. Edwards M, Bignell JP, Papadopoulou A, Trani E, Savage J, Joseph AW, et al. First detection of *Cyclopterus lumpus* virus in England, following a mortality event in farmed cleaner fish. *Bull EAFP*. (2022) 43:28–37. doi: 10.48045/001c.56559

25. Toffan A, De Salvador M, Scholz F, Pretto T, Buratin A, Rodger HD, et al. Lumpfish (*Cyclopterus lumpus*, Linnaeus) is susceptible to viral nervous necrosis: Result of an experimental infection with different genotypes of Betanodavirus. *J Fish Dis.* (2019) 42:1667–76. doi: 10.1111/jfd.13088

26. Kukurba KR, Montgomery SB. RNA sequencing and analysis. *Cold Spring Harb Protoc.* (2015) 2015:951–69. doi: 10.1101/pdb.top084970

27. Aedo JE, Aravena-Canales D, Dettleff P, Fuentes-Valenzuela M, Zuloaga R, Rivas-Aravena A, et al. RNA-seq analysis reveals the dynamic regulation of proteasomal and autophagic degradation systems of rainbow trout (*Oncorhynchus mykiss*) skeletal muscle challenged with infectious pancreatic necrosis virus (IPNV). *Aquaculture*. (2022) 552:738000. doi: 10.1016/j.aquaculture.2022.738000

28. Sandamalika WMG, Liyanage DS, Lim C, Yang H, Lee S, Jeong T, et al. Differential gene expression of red-spotted grouper (*Epinephelus akaara*) in response to lipopolysaccharide, poly I:C, and nervous necrosis virus revealed by RNA-seq data. *Fish Shellfish Immunol.* (2022) 131:939–44. doi: 10.1016/j.fsi.2022.11.006

29. Liu Q-N, Tang Y-Y, Zhou M-J, Luo S, Li Y-T, Wang G, et al. Differentially expressed genes involved in immune pathways from yellowhead catfish (*Tachysurus fulvidraco*) after poly (I:C) challenge. *Int J Biol Macromolecules*. (2021) 183:340–5. doi: 10.1016/j.ijbiomac.2021.04.167

30. Du X, Li Y, Li D, Lian F, Yang S, Wu J, et al. Transcriptome profiling of spleen provides insights into the antiviral mechanism in *Schizothorax prenanti* after poly (I: C) challenge. *Fish Shellfish Immunol.* (2017) 62:13–23. doi: 10.1016/j.fsi.2017.01.004

31. Liu Y, Xin Z-Z, Zhang D-Z, Wang Z-F, Zhu X-Y, Tang B-P, et al. Transcriptome analysis of yellow catfish (*Pelteobagrus fulvidraco*) liver challenged with polyriboinosinic polyribocytidylic acid (poly I:C). *Fish Shellfish Immunol.* (2017) 68:395–403. doi: 10.1016/j.fsi.2017.07.030

32. Rao SS, Lunde HS, Dolan DWP, Fond AK, Petersen K, Haugland GT. Transcriptome-wide analyses of early immune responses in lumpfish leukocytes upon stimulation with poly(I:C). *Front Immunol.* (2023) 14:1198211. doi: 10.3389/fimmu.2023.1198211

33. Rao SS, Nelson PA, Lunde HS, Haugland GT. Evolutionary, comparative, and functional analyses of STATs and regulation of the JAK-STAT pathway in lumpfish upon bacterial and poly(I:C) exposure. *Front Cell Infect Microbiol.* (2023) 13:1252744. doi: 10.3389/fcimb.2023.1252744

34. Jefferies CA. Regulating IRFs in IFN driven disease. *Front Immunol.* (2019) 10:325. doi: 10.3389/fimmu.2019.00325

35. Yan R, van Meurs M, Popa ER, Jongman RM, Zwiers PJ, Niemarkt AE, et al. Endothelial interferon regulatory factor 1 regulates lipopolysaccharide-induced VCAM-1 expression independent of NFκB. *J Innate Immun.* (2017) 9:546–60. doi: 10.1159/000477211

36. Lai CF, Wang T-Y, Yeh M-I, Chen T-Y. Characterization of orange-spotted grouper (*Epinephelus coioides*) interferon regulatory factor 4 regulated by heat shock factor 1 during heat stress in response to antiviral immunity. *Fish Shellfish Immunol.* (2020) 106:755–67. doi: 10.1016/j.fsi.2020.08.033

37. Han C, Huang W, Peng S, Zhou J, Zhan H, Li W, et al. Characterization and expression analysis of the interferon regulatory factor (IRF) gene family in zig-zag eel (*Mastacembelus armatus*) against *Aeromonas veronii* infection. *Dev Comp Immunol.* (2023) 140:104622. doi: 10.1016/j.dci.2022.104622

38. Yanai H, Negishi H, Taniguchi T. The IRF family of transcription factors. *Oncoimmunology*. (2012) 1:1376–86. doi: 10.4161/onci.22475

39. Li W, Zhao G, Jiao Z, Xiang C, Liang Y, Huang W, et al. Nuclear import of IRF11 via the importin α/β pathway is essential for its antiviral activity. *Dev Comp Immunol.* (2023) 141:104649. doi: 10.1016/j.dci.2023.104649

40. Langevin C, Aleksejeva E, Passoni G, Palha N, Levraud J-P, Boudinot P. The antiviral innate immune response in fish: evolution and conservation of the IFN system. *Journal of Molecular Biology* (2013) 425:4904–20. doi: 10.1016/j.jmb.2013.09.033

41. Zhu Y, Qi C, Shan S, Zhang F, Li H, An L, et al. Characterization of common carp (*Cyprinus carpio* L.) interferon regulatory factor 5 (IRF5) and its expression in response to viral and bacterial challenges. *BMC Vet Res.* (2016) 12:127. doi: 10.1186/s12917-016-0750-4

42. Hu G-B, Lou H-M, Dong X-Z, Liu Q-M, Zhang S-C. Characteristics of the interferon regulatory factor 5 (IRF5) and its expression in response to LCDV and poly I: C challenges in Japanese flounder, *Paralichthys olivaceus*. *Dev Comp Immunol.* (2012) 38:377–82. doi: 10.1016/j.dci.2012.06.001

43. Zhang J, Sun L. Transcriptome analysis reveals temperature-regulated antiviral response in turbot *Scophthalmus maximus*. *Fish Shellfish Immunol.* (2017) 68:359–67. doi: 10.1016/j.fsi.2017.07.038

44. Hu G, Xia J, Lou H, Liu Q, Lin J, Yin X, et al. Cloning and expression analysis of interferon regulatory factor 7 (IRF-7) in turbot, *Scophthalmus maximus*. *Dev Comp Immunol.* (2011) 35:416–20. doi: 10.1016/j.dci.2010.12.004

45. Dong X, Xu H, Mai K, Xu W, Zhang Y, Ai Q. Cloning and characterization of SREBP-1 and PPAR-α in Japanese seabass *Lateolabrax japonicus*, and their gene expressions in response to different dietary fatty acid profiles. *Comp Biochem Physiol B Biochem Mol Biol.* (2015) 180:48–56. doi: 10.1016/j.cbpb.2014.10.001

46. Inkpen SM, Solbakken MH, Jentoft S, Eslamloo K, Rise ML. Full characterization and transcript expression profiling of the interferon regulatory factor (IRF) gene family in Atlantic cod (*Gadus morhua*). *Dev Comp Immunol.* (2019) 98:166–80. doi: 10.1016/j.dci.2019.03.015

47. Inkpen SM, Hori TS, Gamperl AK, Nash GW, Rise ML. Characterization and expression analyses of five interferon regulatory factor transcripts (Irf4a, Irf4b, Irf7, Irf8, Irf10) in Atlantic cod (*Gadus morhua*). *Fish Shellfish Immunol.* (2015) 44:365–81. doi: 10.1016/j.fsi.2015.02.032

48. Deering MJ, Paradis H, Ahmad R, Al-Mehiawi AS, Gendron RL. The role of dietary vitamin A in mechanisms of cataract development in the teleost lumpfish (*Cyclopterus lumpus* L). *J Fish Dis.* doi: 10.1111/jfd.13899

49. Emam M, Eslamloo K, Caballero-Solares A, Lorenz EK, Xue X, Umasuthan N, et al. Nutritional immunomodulation of Atlantic salmon response to *Renibacterium salmoninarum* bacterin. *Front Mol Biosci.* (2022) 9:931548. doi: 10.3389/fmolb.2022.931548

50. Bindea G, Mlecnik B, Hackl H, Charoentong P, Tosolini M, Kirilovsky A, et al. ClueGO: a Cytoscape plug-in to decipher functionally grouped gene ontology and pathway annotation networks. *Bioinformatics.* (2009) 25:1091–3. doi: 10.1093/bioinformatics/btp101

51. Shannon P, Markiel A, Ozier O, Baliga NS, Wang JT, Ramage D, et al. Cytoscape: a software environment for integrated models of biomolecular interaction networks. *Genome Res.* (2003) 13:2498–504. doi: 10.1101/gr.1239303

52. Chen C, Chen H, Zhang Y, Thomas HR, Frank MH, He Y, et al. TBtools: an integrative toolkit developed for interactive analyses of big biological data. *Mol Plant.* (2020) 13:1194–202. doi: 10.1016/j.molp.2020.06.009

53. Koressaar T, Remm M. Enhancements and modifications of primer design program Primer3. *Bioinformatics.* (2007) 23:1289–91. doi: 10.1093/bioinformatics/btm091

54. Kõressaar T, Lepamets M, Kaplinski L, Raime K, Andreson R, Remm M. Primer3_masker: integrating masking of template sequence with primer design software. *Bioinformatics.* (2018) 34:1937–8. doi: 10.1093/bioinformatics/bty036

55. Caballero-Solares A, Hall JR, Xue X, Eslamloo K, Taylor RG, Parrish CC, et al. The dietary replacement of marine ingredients by terrestrial animal and plant alternatives modulates the antiviral immune response of Atlantic salmon (*Salmo salar*). *Fish Shellfish Immunol.* (2017) 64:24–38. doi: 10.1016/j.fsi.2017.02.040

56. Vandesompele J, De Preter K, Pattyn F, Poppe B, Van Roy N, De Paepe A, et al. Accurate normalization of real-time quantitative RT-PCR data by geometric averaging of multiple internal control genes. *Genome Biol.* (2002) 3:research0034.1. doi: 10.1186/gb-2002-3-7-research0034

57. Bustin SA, Benes V, Garson JA, Hellemans J, Huggett J, Kubista M, et al. The MIQE guidelines: minimum information for publication of quantitative real-time PCR experiments. *Clin Chem.* (2009) 55:611–22. doi: 10.1373/clinchem.2008.112797

58. Livak KJ, Schmittgen TD. Analysis of relative gene expression data using real-time quantitative PCR and the 2−ΔΔCT method. *Methods.* (2001) 25:402–8. doi: 10.1006/meth.2001.1262

59. Pfaffl MW. A new mathematical model for relative quantification in real-time RT–PCR. *Nucleic Acids Res.* (2001) 29:e45–5. doi: 10.1093/nar/29.9.e45

60. Tamura K, Stecher G, Kumar S. MEGA11: molecular evolutionary genetics analysis version 11. *Mol Biol Evol.* (2021) 38:3022–7. doi: 10.1093/molbev/msab120

61. Nehyba J, Hrdlicková R, Bose HR. Dynamic evolution of immune system regulators: the history of the interferon regulatory factor family. *Mol Biol Evol.* (2009) 26:2539–50. doi: 10.1093/molbev/msp167

62. Zhou Y, Pu J, Wu Y. The role of lipid metabolism in influenza A virus infection. *Pathogens.* (2021) 10:303. doi: 10.3390/pathogens10030303

63. Farías MA, Diethelm-Varela B, Navarro AJ, Kalergis AM, González PA. Interplay between lipid metabolism, lipid droplets, and DNA virus infections. *Cells.* (2022) 11:2224. doi: 10.3390/cells11142224

64. Sarohan AR. COVID-19: endogenous retinoic acid theory and retinoic acid depletion syndrome. *Med Hypotheses.* (2020) 144:110250. doi: 10.1016/j.mehy.2020.110250

65. Langevin C, Aleksejeva E, Houel A, Briolat V, Torhy C, Lunazzi A, et al. FTR83, a member of the large fish-specific finTRIM family, triggers IFN pathway and counters viral infection. *Front Immunol.* (2017) 8:617. doi: 10.3389/fimmu.2017.00617

66. Qin Z, Ren F, Xu X, Ren Y, Li H, Wang Y, et al. ZNF536, a novel zinc finger protein specifically expressed in the brain, negatively regulates neuron differentiation by repressing retinoic acid-induced gene transcription. *Mol Cell Biol.* (2009) 29:3633–43. doi: 10.1128/MCB.00362-09

67. Bin L, Deng L, Yang H, Zhu L, Wang X, Edwards MG, et al. Forkhead box C1 regulates human primary keratinocyte terminal differentiation. *PloS One.* (2016) 11:e0167392. doi: 10.1371/journal.pone.0167392

68. McConnell BB, Yang VW. Mammalian krüppel-like factors in health and diseases. *Physiol Rev.* (2010) 90:1337–81. doi: 10.1152/physrev.00058.2009

69. Yang Q, Xie Y, Alexson SEH, Dean Nelson B, DePierre JW. Involvement of the peroxisome proliferator-activated receptor alpha in the immunomodulation caused by peroxisome proliferators in mice. *Biochem Pharmacol.* (2002) 63:1893–900. doi: 10.1016/S0006-2952(02)00923-1

70. Li S, Chen X, Hao G, Geng X, Zhan W, Sun J. Identification and characterization of a novel NOD-like receptor family CARD domain containing 3 gene in response to extracellular ATP stimulation and its role in regulating LPS-induced innate immune response in Japanese flounder (*Paralichthys olivaceus*) head kidney macrophages. *Fish Shellfish Immunol.* (2016) 50:79–90. doi: 10.1016/j.fsi.2016.01.029

71. Deng H, Yue JK, Zusman BE, Nwachuku EL, Abou-Al-Shaar H, Upadhyayula PS, et al. B-cell lymphoma 2 (Bcl-2) and regulation of apoptosis after traumatic brain injury: A clinical perspective. *Medicina (Kaunas).* (2020) 56:300. doi: 10.3390/medicina56060300

72. Jármay K, Karácsony G, Nagy A, Schaff Z. Changes in lipid metabolism in chronic hepatitis C. *World J Gastroenterol.* (2005) 11:6422–8. doi: 10.3748/wjg.v11.i41.6422

73. Grunfeld C, Feingold KR. Regulation of lipid metabolism bycytokines during host defense. *Nutrition.* (1996) 12:S24–6. doi: 10.1016/0899-9007(95)00073-9

74. Abu-Farha M, Thanaraj TA, Qaddoumi MG, Hashem A, Abubaker J, Al-Mulla F. The role of lipid metabolism in COVID-19 virus infection and as a drug target. *Int J Mol Sci.* (2020) 21:3544. doi: 10.3390/ijms21103544

75. Ren Z, Ding T, Zuo Z, Xu Z, Deng J, Wei Z. Regulation of MAVS expression and signaling function in the antiviral innate immune response. *Front Immunol.* (2020) 11:1030. doi: 10.3389/fimmu.2020.01030

76. Magoro T, Dandekar A, Jennelle LT, Bajaj R, Lipkowitz G, Angelucci AR, et al. IL-1β/TNF-α/IL-6 inflammatory cytokines promote STAT1-dependent induction of CH25H in Zika virus–infected human macrophages. *J Biol Chem.* (2019) 294:14591–602. doi: 10.1074/jbc.RA119.007555

77. Wang J, Huang CL-H, Zhang Y. Complement C1q binding protein (C1QBP): physiological functions, mutation-associated mitochondrial cardiomyopathy and current disease models. *Front Cardiovasc Med.* (2022) 9:843853. doi: 10.3389/fcvm.2022.843853

78. Singh R, Letai A, Sarosiek K. Regulation of apoptosis in health and disease: the balancing act of BCL-2 family proteins. *Nat Rev Mol Cell Biol*. (2019) 20:175–93. doi: 10.1038/s41580-018-0089-8

79. Behrendorff N, Dolai S, Hong W, Gaisano HY, Thorn P. Vesicle-associated membrane protein 8 (VAMP8) is a SNARE (Soluble N-ethylmaleimide-sensitive factor attachment protein receptor) selectively required for sequential granule-to-granule fusion. *J Biol Chem*. (2011) 286:29627–34. doi: 10.1074/jbc.M111.265199

80. Sebti S, Prébois C, Pérez-Gracia E, Bauvy C, Desmots F, Pirot N, et al. BAT3 modulates p300-dependent acetylation of p53 and autophagy-related protein 7 (ATG7) during autophagy. *Proc Natl Acad Sci USA*. (2014) 111:4115–20. doi: 10.1073/pnas.1313618111

81. Calle X, Garrido-Moreno V, Lopez-Gallardo E, Norambuena-Soto I, Martínez D, Peñaloza-Otárola A, et al. Mitochondrial E3 ubiquitin ligase 1 (MUL1) as a novel therapeutic target for diseases associated with mitochondrial dysfunction. *IUBMB Life*. (2022) 74:850–65. doi: 10.1002/iub.2657

82. Carty M, Bowie AG. Recent insights into the role of Toll-like receptors in viral infection. *Clin Exp Immunol*. (2010) 161:397–406. doi: 10.1111/j.1365-2249.2010.04196.x

83. Ali S, Mann-Nüttel R, Schulze A, Richter L, Alferink J, Scheu S. Sources of type I interferons in infectious immunity: plasmacytoid dendritic cells not always in the driver's seat. *Front Immunol*. (2019) 10:778. doi: 10.3389/fimmu.2019.00778

84. Kawai T, Sato S, Ishii KJ, Coban C, Hemmi H, Yamamoto M, et al. Interferon-α induction through Toll-like receptors involves a direct interaction of IRF7 with MyD88 and TRAF6. *Nat Immunol*. (2004) 5:1061–8. doi: 10.1038/ni1118

85. Blasius AL, Beutler B. Intracellular toll-like receptors. *Immunity*. (2010) 32:305–15. doi: 10.1016/j.immuni.2010.03.012

86. Su C, Tang Y, Zheng C. DExD/H-box helicases: multifunctional regulators in antiviral innate immunity. *Cell Mol Life Sci*. (2022) 79:2. doi: 10.1007/s00018-021-04072-6

87. Rise ML, Hall J, Rise M, Hori T, Gamperl AK, Kimball J, et al. Functional genomic analysis of the response of Atlantic cod (*Gadus morhua*) spleen to the viral mimic polyriboinosinic polyribocytidylic acid (pIC). *Dev Comp Immunol*. (2008) 32:916–31. doi: 10.1016/j.dci.2008.01.002

88. Rise ML, Hall JR, Rise M, Hori TS, Browne MJ, Gamperl AK, et al. Impact of asymptomatic nodavirus carrier state and intraperitoneal viral mimic injection on brain transcript expression in Atlantic cod (*Gadus morhua*). *Physiol Genomics*. (2010) 42:266–80. doi: 10.1152/physiolgenomics.00168.2009

89. Feng CY, Rise ML. Identification and molecular cloning of Atlantic cod (*Gadus morhua*) activating transcription factor 3 (ATF3) transcript and its induction in spleen following intraperitoneal polyriboinosinic polyribocytidylic acid injection. *Fish Shellfish Immunol*. (2011) 31:475–81. doi: 10.1016/j.fsi.2011.06.002

90. Shu M, Du T, Zhou G, Roizman B. Role of activating transcription factor 3 in the synthesis of latency-associated transcript and maintenance of herpes simplex virus 1 in latent state in ganglia. *Proc Natl Acad Sci U.S.A*. (2015) 112:E5420–5426. doi: 10.1073/pnas.1515369112

91. Sood V, Sharma KB, Gupta V, Saha D, Dhapola P, Sharma M, et al. ATF3 negatively regulates cellular antiviral signaling and autophagy in the absence of type I interferons. *Sci Rep*. (2017) 7:8789. doi: 10.1038/s41598-017-08584-9

92. Rosenberger CM, Clark AE, Treuting PM, Johnson CD, Aderem A. ATF3 regulates MCMV infection in mice by modulating IFN-γ expression in natural killer cells. *Proc Natl Acad Sci*. (2008) 105:2544–9. doi: 10.1073/pnas.0712182105

93. Hai T, Wolford CC, Chang Y-S. ATF3, a hub of the cellular adaptive-response network, in the pathogenesis of diseases: is modulation of inflammation a unifying component? *Gene Expr*. (2010) 15:1–11. doi: 10.3727/105221610X12819686555015

94. Labzin LI, Schmidt SV, Masters SL, Beyer M, Krebs W, Klee K, et al. ATF3 is a key regulator of macrophage IFN responses. *J Immunol*. (2015) 195:4446–55. doi: 10.4049/jimmunol.1500204

95. Polinski MP, Bradshaw JC, Rise ML, Johnson SC, Garver KA. Sockeye salmon demonstrate robust yet distinct transcriptomic kidney responses to rhabdovirus (IHNV) exposure and infection. *Fish Shellfish Immunol*. (2019) 94:525–38. doi: 10.1016/j.fsi.2019.09.042

96. Polinski MP, Bradshaw JC, Inkpen SM, Richard J, Fritsvold C, Poppe TT, et al. *De novo* assembly of Sockeye salmon kidney transcriptomes reveal a limited early response to piscine reovirus with or without infectious hematopoietic necrosis virus superinfection. *BMC Genomics*. (2016) 17:848. doi: 10.1186/s12864-016-3196-y

97. Takeuchi O, Akira S. Pattern recognition receptors and inflammation. *Cell*. (2010) 140:805–20. doi: 10.1016/j.cell.2010.01.022

98. McNab F, Mayer-Barber K, Sher A, Wack A, O'Garra A. Type I interferons in infectious disease. *Nat Rev Immunol*. (2015) 15:87–103. doi: 10.1038/nri3787

99. Xu C, Guo T-C, Mutoloki S, Haugland Ø, Marjara IS, Evensen Ø. Alpha interferon and not gamma interferon inhibits salmonid alphavirus subtype 3 replication *in vitro*. *J Virol*. (2010) 84:8903. doi: 10.1128/JVI.00851-10

100. Samsing F, Alexandre P, Rigby M, Taylor RS, Chong R, Wynne JW. Transcriptome response of atlantic salmon (*Salmo salar*) to a new piscine orthomyxovirus. *Pathogens*. (2020) 9:807. doi: 10.3390/pathogens9100807

101. Workenhe ST, Hori TS, Rise ML, Kibenge MJT, Kibenge FSB. Infectious salmon anaemia virus (ISAV) isolates induce distinct gene expression responses in the Atlantic salmon (*Salmo salar*) macrophage/dendritic-like cell line TO, assessed using genomic techniques. *Mol Immunol*. (2009) 46:2955–74. doi: 10.1016/j.molimm.2009.06.015

102. Valenzuela-Miranda D, Boltaña S, Cabrejos ME, Yáñez JM, Gallardo-Escárate C. High-throughput transcriptome analysis of ISAV-infected Atlantic *salmon Salmo* salar unravels divergent immune responses associated to head-kidney, liver and gills tissues. *Fish Shellfish Immunol*. (2015) 45:367–77. doi: 10.1016/j.fsi.2015.04.003

103. Wei X, Li XZ, Zheng X, Jia P, Wang J, Yang X, et al. Toll-like receptors and interferon associated immune factors responses to spring viraemia of carp virus infection in common carp (*Cyprinus carpio*). *Fish Shellfish Immunol*. (2016) 55:568–76. doi: 10.1016/j.fsi.2016.05.043

104. Saint-Jean SR, Pérez-Prieto SI. Effects of salmonid fish viruses on Mx gene expression and resistance to single or dual viral infections. *Fish Shellfish Immunol*. (2007) 23:390–400. doi: 10.1016/j.fsi.2006.11.012

105. Zhang X, Yang F, Li K, Cao W, Ru Y, Chen S, et al. The insufficient activation of RIG-I–like signaling pathway contributes to highly efficient replication of porcine picornaviruses in IBRS-2 cells. *Mol Cell Proteomics : MCP*. (2021) 20:100147. doi: 10.1016/j.mcpro.2021.100147

106. Rustagi A, Gale M. Innate antiviral immune signaling, viral evasion and modulation by HIV-1. *J Mol Biol*. (2014) 426:1161–77. doi: 10.1016/j.jmb.2013.12.003

107. Eslamloo K, Caballero-Solares A, Inkpen SM, Emam M, Kumar S, Bouniot C, et al. Transcriptomic profiling of the adaptive and innate immune responses of Atlantic salmon to *Renibacterium salmoninarum* infection. *Front Immunol*. (2020) 11:567838. doi: 10.3389/fimmu.2020.567838

108. Xue X, Caballero-Solares A, Hall JR, Umasuthan N, Kumar S, Jakob E, et al. Transcriptome profiling of Atlantic salmon (*Salmo salar*) parr with higher and lower pathogen loads following *Piscirickettsia salmonis* infection. *Front Immunol*. (2021) 12:789465. doi: 10.3389/fimmu.2021.789465

109. Adamek M, Davies J, Beck A, Jordan L, Becker AM, Mojzesz M, et al. Antiviral actions of 25-hydroxycholesterol in fish vary with the virus-host combination. *Front Immunol*. (2021) 12:581786. doi: 10.3389/fimmu.2021.581786

110. Zhang Y, Wang L, Huang X, Wang S, Huang Y, Qin Q. Fish cholesterol 25-hydroxylase inhibits virus replication via regulating interferon immune response or affecting virus entry. *Front Immunol*. (2019) 10:322. doi: 10.3389/fimmu.2019.00322

111. van Gent M, Sparrer KMJ, Gack MU. TRIM proteins and their roles in antiviral host defenses. *Annu Rev Virol*. (2018) 5:385–405. doi: 10.1146/annurev-virology-092917-043323

112. Yu Y, Huang X, Zhang J, Liu J, Hu Y, Yang Y, et al. Fish TRIM16L exerts negative regulation on antiviral immune response against grouper iridoviruses. *Fish Shellfish Immunol*. (2016) 59:256–67. doi: 10.1016/j.fsi.2016.10.044

113. Cho JY, Kim J, Kim J-W, Lee D, Kim D-G, Kim Y-S, et al. Characterization of TRIM16, a member of the fish-specific finTRIM family, in olive flounder *Paralichthys olivaceus*. *Fish Shellfish Immunol*. (2022) 127:666–71. doi: 10.1016/j.fsi.2022.07.003

114. Choudhury NR, Trus I, Heikel G, Wolczyk M, Szymanski J, Bolembach A, et al. TRIM25 inhibits influenza A virus infection, destabilizes viral mRNA, but is redundant for activating the RIG-I pathway. *Nucleic Acids Res*. (2022) 50:7097–114. doi: 10.1093/nar/gkac512

115. Marschall M, Strojan H, Kiener R, Wangen C, Sonntag E, Müller R, et al. Differential upregulation of host cell protein kinases by the replication of α-, β- and γ-herpesviruses provides a signature of virus-specific signalling. *J Gen Virol*. (2020) 101:284–9. doi: 10.1099/jgv.0.001370

116. Müller A, Sutherland BJG, Koop BF, Johnson SC, Garver KA. Infectious hematopoietic necrosis virus (IHNV) persistence in Sockeye Salmon: influence on brain transcriptome and subsequent response to the viral mimic poly(I:C). *BMC Genomics*. (2015) 16:634. doi: 10.1186/s12864-015-1759-y

117. Eslamloo K, Kumar S, Xue X, Parrish KS, Purcell SL, Fast MD, et al. Global gene expression responses of Atlantic salmon skin to *Moritella viscosa*. *Sci Rep*. (2022) 12:4622. doi: 10.1038/s41598-022-08341-7

118. Sommer F, Torraca V, Kamel SM, Lombardi A, Meijer AH. Frontline Science: Antagonism between regular and atypical Cxcr3 receptors regulates macrophage migration during infection and injury in zebrafish. *J Leukocyte Biol*. (2020) 107:185–203. doi: 10.1002/JLB.2HI0119-006R

119. Tomczyk M, Glaser T, Slominska EM, Ulrich H, Smolenski RT. Purine nucleotides metabolism and signaling in huntington's disease: search for a target for novel therapies. *Int J Mol Sci*. (2021) 22:6545. doi: 10.3390/ijms22126545

120. Zhou M, Yao Z, Zhao M, Fang Q, Ji X, Chen H, et al. Molecular cloning and expression responses of jarid2b to high-temperature treatment in nile tilapia (*Oreochromis niloticus*). *Genes (Basel)*. (2022) 13:1719. doi: 10.3390/genes13101719

121. Loenarz C, Ge W, Coleman ML, Rose NR, Cooper CDO, Klose RJ, et al. PHF8, a gene associated with cleft lip/palate and mental retardation, encodes for an Nε-dimethyl lysine demethylase. *Hum Mol Genet*. (2010) 19:217–22. doi: 10.1093/hmg/ddp480

122. Tsai K, Cullen BR. Epigenetic and epitranscriptomic regulation of viral replication. *Nat Rev Microbiol*. (2020) 18:559–70. doi: 10.1038/s41579-020-0382-3

123. Jahn R, Scheller RH. SNAREs — engines for membrane fusion. *Nat Rev Mol Cell Biol*. (2006) 7:631–43. doi: 10.1038/nrm2002

124. Verboogen DRJ, González Mancha N, ter Beest M, van den Bogaart G. Fluorescence Lifetime Imaging Microscopy reveals rerouting of SNARE trafficking driving dendritic cell activation. *eLife*. (2017) 6:e23525. doi: 10.7554/eLife.23525

125. Clark TC, Boudinot P, Collet B. Evolution of the IRF family in salmonids. *Genes (Basel)*. (2021) 12:238. doi: 10.3390/genes12020238

126. Bergan V, Kileng Ø, Sun B, Robertsen B. Regulation and function of interferon regulatory factors of Atlantic salmon. *Mol Immunol.* (2010) 47:2005–14. doi: 10.1016/j.molimm.2010.04.015

127. Sun F, Zhang Y-B, Liu T-K, Gan L, Yu F-F, Liu Y, et al. Characterization of fish IRF3 as an IFN-inducible protein reveals evolving regulation of IFN response in vertebrates. *J Immunol.* (2010) 185:7573–82. doi: 10.4049/jimmunol.1002401

128. Ai K, Luo K, Xia L, Gao W, Hu W, Qi Z, et al. Functional characterization of interferon regulatory factor 5 and its role in the innate antiviral immune response. *Fish Shellfish Immunol.* (2018) 72:31–6. doi: 10.1016/j.fsi.2017.10.042

129. Chen X, Guan Y, Li K, Luo T, Mu Y, Chen X. IRF1 and IRF2 act as positive regulators in antiviral response of large yellow croaker (*Larimichthys crocea*) by induction of distinct subgroups of type I IFNs. *Dev Comp Immunol.* (2021) 118:103996. doi: 10.1016/j.dci.2021.103996

130. Romeo G, Fiorucci G, Chiantore MV, Percario ZA, Vannucchi S, Affabris E. Review: IRF-1 as a negative regulator of cell proliferation. *J Interferon Cytokine Res.* (2002) 22:39–47. doi: 10.1089/107999002753452647

131. Bonjardim CA, Ferreira PCP, Kroon EG. Interferons: signaling, antiviral and viral evasion. *Immunol Lett.* (2009) 122:1–11. doi: 10.1016/j.imlet.2008.11.002

132. Adams NM, Lau CM, Fan X, Rapp M, Geary CD, Weizman O-E, et al. Transcription factor IRF8 orchestrates the adaptive natural killer cell response. *Immunity.* (2018) 48:1172–1182.e6. doi: 10.1016/j.immuni.2018.04.018

133. Paul A, Tang TH, Ng SK. Interferon regulatory factor 9 structure and regulation. *Front Immunol.* (2018) 9:1831. doi: 10.3389/fimmu.2018.01831

134. An L-L, Zhao X, Gong X-Y, Li Y-L, Qu Z-L, Sun H-Y, et al. Promoter binding and nuclear retention features of zebrafish IRF family members in IFN response. *Front Immunol.* (2022) 13:861262. doi: 10.3389/fimmu.2022.861262

135. Huang B, Qi ZT, Xu Z, Nie P. Global characterization of interferon regulatory factor (IRF) genes in vertebrates: Glimpse of the diversification in evolution. *BMC Immunol.* (2010) 11:22. doi: 10.1186/1471-2172-11-22

136. Stein C, Caccamo M, Laird G, Leptin M. Conservation and divergence of gene families encoding components of innate immune response systems in zebrafish. *Genome Biol.* (2007) 8:R251. doi: 10.1186/gb-2007-8-11-r251

137. Tussiwand R, Everts B, Grajales-Reyes GE, Kretzer NM, Iwata A, Bagaitkar J, et al. Klf4 expression in conventional dendritic cells is required for T helper 2 cell responses. *Immunity.* (2015) 42:916–28. doi: 10.1016/j.immuni.2015.04.017

138. Rengarajan J, Mowen KA, McBride KD, Smith ED, Singh H, Glimcher LH. Interferon regulatory factor 4 (IRF4) interacts with NFATc2 to modulate interleukin 4 gene expression. *J Exp Med.* (2002) 195:1003–12. doi: 10.1084/jem.20011128

139. Klein U, Casola S, Cattoretti G, Shen Q, Lia M, Mo T, et al. Transcription factor IRF4 controls plasma cell differentiation and class-switch recombination. *Nat Immunol.* (2006) 7:773–82. doi: 10.1038/ni1357

140. Peruzza L, Pascoli F, Dalla Rovere G, Franch R, Ferraresso S, Babbucci M, et al. Transcriptome analysis reveals a complex response to the RGNNV/SJNNV reassortant Nervous Necrosis Virus strain in sea bream larvae. *Fish Shellfish Immunol.* (2021) 114:282–92. doi: 10.1016/j.fsi.2021.04.021

Frontiers in Immunology

Explores novel approaches and diagnoses to treat immune disorders.

The official journal of the International Union of Immunological Societies (IUIS) and the most cited in its field, leading the way for research across basic, translational and clinical immunology.

Discover the latest Research Topics

See more →

Frontiers

Avenue du Tribunal-Fédéral 34
1005 Lausanne, Switzerland
frontiersin.org

Contact us

+41 (0)21 510 17 00
frontiersin.org/about/contact